Modelling Neoplastic Progression in Epithelial Ovarian Cancer

Kate Lawrenson
University College London

November 2009

Declaration

I, Kate Lawrenson, confirm that the work presented in this thesis is my own. Where information has been derived from other sources, I confirm that this has been indicated in the thesis.

Abstract

A national screening programme could significantly reduce mortality from epithelial ovarian cancer (EOC). The biological events that occur in the early stages of development of EOCs remain poorly understood, thus hindering the discovery of biomarkers of early disease. This thesis describes the development of a three-dimensional heterotypic genetic model of neoplastic transformation of normal ovarian surface epithelial (NOSE) cells.

hTERT, *C-MYC*, *KRAS* and *BRAF* are genes that are commonly mutated or overexpressed in EOCs. Ectopic expression of *hTERT* increased *in vitro* lifespan of NOSE cells without inducing neoplastic transformation. Subsequent overexpression of *CMYC* +/- $KRAS^{G12V}$/$BRAF^{V600E}$ in immortalised NOSE (IOSE) cells induced a significant increase in anchorage-independent growth and invasive ability. In *in vitro* assays and gene expression microarrays, phenotypic and molecular heterogeneity was associated with differential oncogene expression. Physiological and biological features of NOSE cells grown in 3D more closely resembled characteristics of NOSE cells *in vivo* than when grown by classical two-dimensional (2D) approaches. 3D models of oncogene-expressing clones revealed characteristics of malignant cells *in vivo* that could not be detected in 2D monolayer cultures.

Gene expression microarrrays profiles of ∼25,000 genes were generated to identify novel genes that are altered synergistically with the oncogenes that were introduced. A panel of genes has been identified that provides novel candidates for detecting ovarian carcinomas at the earliest, most treatable, stages of disease.

Finally, a role for ageing fibroblasts in the initiation of EOC development was explored. In 2D and 3D *in vitro* co-culture assays, pre-senescent and senescent ovarian fibroblasts differentially affected proliferation, anchorage-independent growth, migration and invasion of $IOSE^{CMYC}$ cell lines but not of IOSE cells. These data provide *in vitro* evidence that the ageing microenvironment can promote transformation of ovarian epithelial cells, and that this is conditional upon mutation in the OSE.

Acknowledgements

Firstly, I would like to thank my principal supervisor, Dr Simon Gayther, for making it possible for me to carry out this Ph.D, for his help in guiding my research, and for his inspiring enthusiasm for and dedication to the field of ovarian cancer research. Many thanks to Simon also for guidance in the writing of this thesis and in preparing papers for publication. I would also like to thank every member, past and present, of his team at the Gynaecological Cancer Research Laboratories: thanks to Dr Dimitra Dafou for a great introduction to cell biology at the start of my Ph.D; thanks also to: Dr Susan Ramus, Dr Chris Jones, Jeremy Ford, Eva Wozniak, Tanya Lebi, Mark Cox, Kate Thornton; with special thanks to my fellow Ph.D students: James Morris, Maria Notoridou, Lydia Quaye, Ken Choi, Kate McAllister, Sheetal Dyall, Raquel Perez-Rubio. I would particularly like to thank Barbara Grun, for numerous invaluable scientific discussions, for sharing a common aim, and for being a wonderful colleague and friend.

I would also like to thank Professor Ian Jacobs, Director of UCL's Institute for Women's Health (at the time of writing), Director of the Eve Appeal and Head of the the Department of Gynaecological Oncology; Dr John Timms and his team at the Cancer Proteomics Laboratory; Dr Elizabeth Benjamin for guidance with histopathological analysis; and Dr Duncan Sproul for advice with the gene expression microarray analyses. Thanks to Phillipa Munsen at University College Hospital Advanced Diagnostic Laboratory for histology services, Mark Cox for sequencing services and Kerra Pearce at the UCL Genomics Facility for array services.

I am also exceedingly grateful to the patients who kindly agree to donate samples for research, and to the surgeons and staff at UCLH for their assistance and cooperation with setting up the tissue collection.

This work has been supported by an MRC studentship, and would not have been possible without the support of the Eve Appeal Gynaecology Cancer Research Fund and the Rosetrees Trust.

This thesis is dedicated to my wonderful family, partner and friends.

Contents

List of Figures

List of Tables

List of Abbreviations

2D two-dimensional

3D three-dimensional

BRAF V-raf murine sarcoma viral oncogene homolog B1

BRCA1/2 breast-cancer gene 1/2

BST borderline serous tumour

cDNA complimentary RNA

DNA deoxyribonucleic acid

ECM extracellular matrix

EDTA ethylenediaminetetaacetic acid

EGF epidermal growth factor

ERK extracellular signal regulated kinase

FBS foetal bovine serum

FACS fluorescence activated cell sorting

FC fold-change (in mRNA/protein expression)

H&E hematoxylin and eosin

HGSC high-grade serous carcinoma

INOF immortalised normal ovarian fibroblast

IOSE immortalised ovarian surface epithelium

KRAS V-Ki-ras2 Kirsten rat sarcoma viral oncogene homolog

LMP low-malignant potential

LOH loss of heterozygosity

mRNA messenger RNA

MCS multicellular spheroid

MMLV murine molony leukaemia virus

NOF normal ovarian fibroblasts

NOSE normal ovarian surface epithelium

NOSE-CM NOSE-complete medium

PI3K phosphatidylinositol 3-kinase

PIK3CA phosphatidylinositol 3-kinase catalytic alpha polypeptide

PBS phosphate-buffered saline

PCR polymerase chain reaction

PH-MCS polyHEMA multicellular spheroids

RT-PCR reverse transcription-polymerase chain reaction

RFLP-PCR restriction fragment length polymorpism - polymerase chain reaction

RNA ribonucleic acid

RCCS-MCS rotary cell culture system multicellular spheroids

RCCS rotary cell culture system

SA-β-gal senescence-associated-β-galactosidase

SFM serum-free medium

SOF senescent ovarian fibroblast

SEM scanning electron microscopy

SNP single nucleotide polymorphism

SV40 simian virus 40

TEM transmission electron microscopy

1

Introduction

1.1 Epithelial Ovarian Cancer

Survival rates from epithelial ovarian cancer (EOC) have improved very little over the last four decades. The majority of ovarian cancer are diagnosed at an advanced stage (Stage III or IV) and 5-year survival rates are under 30% (Figure 1.1). This is largely due to the fact that EOCs are a complex group of tumours in terms of histology, molecular characteristics, prognoses and clinicopathological features (Table 1.1). Early stage tumours are characteristically asymptomatic, or any symptoms that are present are vague and non-specific to the disease, and therefore do not aid early diagnosis. Consequently, researchers have little access to early-stage tumour specimens, thus there is a genuine need for robust *in vitro* models of EOC initiation and progression to increase our understanding of early ovarian tumourigenesis. Futhermore, such models could be used to aid the development of novel biomarkers that could be used to detect EOCs at the earliest, most treatable stages.

1.1.1 Subtypes of Epithelial Ovarian Cancer

Arguably, the one common feature of EOCs is their site of diagnosis. Epithelial ovarian cancers show striking histological variability, and each of the subtypes is associated with distinct molecular features, diverse biomarker profiles and distinct subtype-specific clinical behaviour, as summarised in Table 1.1. As the need for rigorous subtyping of EOCs has become more apparent, improved protocols for tumour classification have been developed [Shih and Kurman, 2004]; [Koebel et al., 2008]. Standardised tumour subtyping approaches between pathologists and across hospitals and indeed countries greatly improves

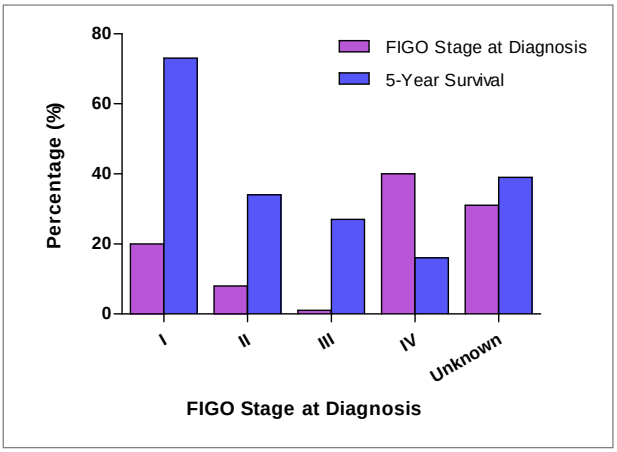

Figure 1.1: Stage at diagnosis and 5-year survival rates for epithelial ovarian cancer. Data shown are for patients registered on the Thames Cancer Registry, diagnosed between 1992 and 1996.

the ability to study EOC subtypes effectively with larger, collaborative studies, such as the recent genome-wide association study which identified a new EOC susceptibility locus on chromosome 9 [Song et al., 2009].

Epithelial ovarian tumours are described in terms of the epithelia of the genito-urinary organs which they resemble (Table 1.1):

High-grade serous carcinomas (HGSCs)

HGSCs resemble the histopathology of the fallopian tube epithelium, and are the most common type of malignant epithelial ovarian tumour. Patients with serous cystadenocarcinomas identified at Stage 1, when tumour growth is limited to the ovaries, have overall survival rates of over 90%. However, the vast majority of HGSCs are detected when the cancer has already progressed to FIGO Stage III/IV and disease has spread from either one or both ovaries to form peritoneal metastases and involvement of the retroperitoneal or inguinal lymph nodes.

Molecular analyses indicate that low-grade and high-grade serous tumours arise via distinct pathways. Mutation/loss of heterozygosity in *BRCA1/2* and mutations in *TP53* are common genetic abberations in ovarian HGSCs but rarely occur in borderline tumours [Russell et al., 2000]. HGSCs commonly express the cancer antigen 125 (CA125), oestrogen receptor (ER) and Wilms tumor 1 (WT1) biomarkers.

Subtype (frequency %)	Origin & Precursor Lesion(s)	Genetic Alterations	Biomarkers	Clinical Behaviour	Typical Histology (100x)
High grade serous **39% of EOCs**	Ovarian/Fimbrial fallopian tube epithelium Ovarian cortical inclusion cyst/ endosalpingiosis	*BRCA1/2* *TP53* *KRAS* *p16*	WT1 Mesothelin CA125 ER TP53	Late stage presentation, peritoneal metastases	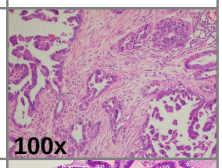
Borderline/ LMP serous **13% of EOCs**	Ovarian epithelium	*BRAF* *KRAS* *PIK3CA*	WT1 Mesothelin CA125 ER	Better prognosis than HGS	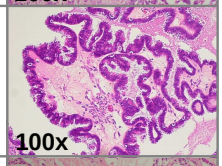
Mucinous **11% of EOCs**	Ovarian epithelium	*KRAS* *HOXA11*	Matripase	Early stage presentation, intracystic	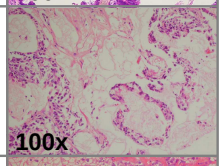
Clear Cell **9% of EOCs**	Ovarian epithelium Endometriosis	*PTEN* MMR pathway	None yet identified	Localised High fq of chemoresistance	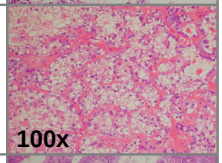
Endometrioid **20% of EOCs**	Ovarian epithelium Endometriosis	*PTEN* MMR pathway *HOXA10*	ER PR CA125	Peritoneal metastases	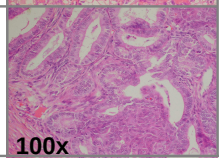

Table 1.1: Epithelial ovarian cancer subtypes are diverse in terms of cellular origins, known genetic alterations, biomarkers and clinical characteristics. Distribution in the UK of histotypes are indicated. Typical histological appearance are shown by representative H&E sections. MMR = mismatch repair, LMP = low malignant potential. Biomarker data are summarised from [Koebel et al., 2008].

Borderline serous tumours (BSTs)

Although histologically similar to HGSCs and with a similar panel of associated biomarkers, borderline serous (or low-malignant potential, LMP) ovarian tumours have more favourable prognosis than the high-grade counterparts. The molecular features of BSTs are distinct from HGSCs. Analysis of borderline serous tumours (BSTs) and neighbouring non-transformed epithelial cystadenoma (which are cytologically normal) identified identical *KRAS* and *BRAF* mutations in both areas [Ho et al., 2004]. This suggests that (i) BSTs may evolve from a normal lesion in which cells are harbouring *KRAS*/*BRAF* mutations; and (ii) mutations in these genes are early events in ovarian tumourigenesis of low-grade serous lesions [Shih and Kurman, 2005].

Mucinous cystadenocarcinomas

Mucinous EOC resemble the glanduar epithelium of the endocervix or gastrointestinal tract. These tumours generally have favourable prognoses, since a significant proportion of patients present with the disease at Stage I or Stage II when the disease is still confined to the ovaries. Mucinous tumours contain a large amount of mucus-like material, produced by goblet cells that resemble cells lining the normal intestine. *KRAS* mutations are found in frequencies of 40-60% in benign, borderline and malignant mucinous tumour subtypes, with the highest frequencies observed in the latter [Gemignani et al., 2003]; [Jordan et al., 2006]; [Heinzelmann-Schwarz et al., 2006]. Mucinous tumours are thought to arise in an adenoma → cystadenoma → carcinoma model [Russell and McCluggage, 2004]. This model is also supported by histological studies. EOC samples that consist of invasive tissue with areas of benign or borderline histologies are more likely to be invasive mucinous than the invasive serous subtype [Mayr et al., 2006]. A biomarker commonly expressed is Matripase; notably absent is expression of CA125 and WT1.

Endometrioid and clear cell carcinomas

Endometrioid and clear cell tumours resemble the epithelium of the endometrium. The vast majority of these tumours present at Stage III or Stage IV, where the disease has metastasised to distant organs of the body. These two subtypes have similar genetic alternations (loss of *PTEN* function and defects in the mismatch repair pathway) and origins. A recent study of EOC biomarkers by Huntsman and colleagues (summarised within Figure 1.1) has demonstrated that endometrioid and clear cell tumours may be distinguished by oestrogen/progesterone receptor (ER/PR) expression (absent in clear cell) [Koebel et al., 2008].

Undifferentiated tumours

These occur at low frequencies and are usually high-grade. Very little is known about the molecular features and biomarkers of undifferentiated tumours, but some are thought to be misdiagnosed serous or endometrioid tumours.

1.1.2 Diverse Cellular Origins of Epithelial Ovarian Cancers

It is apparent that EOCs arise from diverse cellular origins; predominantly from the ovarian surface epithelium (OSE), but also from endometrial epithelia, fallopian tube epithelia, and perhaps also endocervical epithelia, ectopically transported to the ovary as endometrioisis, endosalpingiosis, and endocervicosis (Figure 1.2).

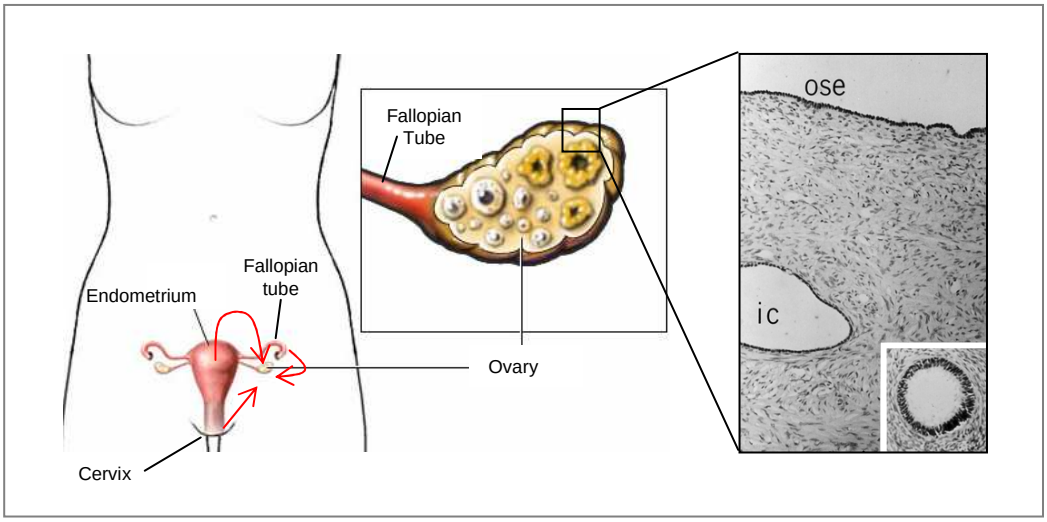

Figure 1.2: Diverse cellular origins for EOCs. Current theory suggests that the majority of epithelial ovarian carcinomas originate from epithelial cells of the ovary (ovarian surface epithelium, OSE on the surface of the ovary or within inclusion cysts, IC); an as yet unquanitifed proportion of high-grade serous EOCs are thought to arise in the epithelia at the distal end of the fallopian tube, or from fallopian tube epithelial cells relocated to the ovary (endosalpingiosis). Endometrial and clear cell tumours may arise from epithelium of the endometrium ectopically transported to the ovary (endometriosis). Red arrows show hypothesised cell movements from different organ sites to the ovary, prior to ovarian cancer development. Diagram adapted from www.myhealth.ucsd.edu and [Auersperg et al., 2001]

The Ovarian Surface Epithelium

Human ovaries are covered with a monolayer of flat/cuboidal mesothelial-type epithelial cells referred to as the ovarian surface epithelium (OSE) (Figure 1.2). These cells are widely considered to be the origin of a large proportion of epithelial ovarian cancers [Auersperg et al., 2001]; [Okamura and Katabuchi, 2001]. Primary normal OSE (NOSE) cell cultures show considerable phenotypic plasticity and can exhibit both epithelial (presence of desmosomes; collagen IV, laminin and cytokeratin production) and mesenchymal characteristics (no expression of E-cadherin; collagen I, collagen III and vimentin pro-

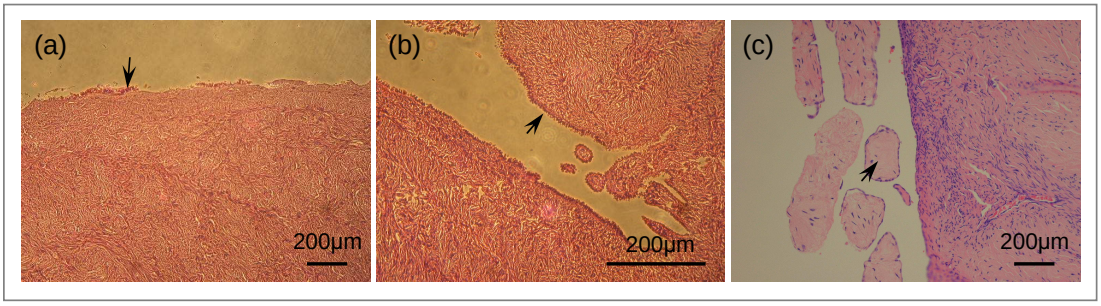

Figure 1.3: The ovarian surface epithelium *in vivo*. (a) Normal OSE cells on the surface of the ovary (arrow). Surface epithelial cells are loosely attached, and some epithelia have been lost from this sample during processing into paraffin. (b) Epithelial invagination into the ovarian stroma brings OSE cells into the ovarian cortex (arrow). These structures are thought to arise following follicular rupture, and can lead to inclusion cyst formation if the invagination closes up at the surface of the ovary. (c) Complex papillary structures (arrow) observed on the surface of an ovary from a patient with a family history of ovarian cancer.

duction) [Auersperg et al., 1994]; [Dyck et al., 1996]. NOSE and immortalised OSE cell lines also have an elongated, mesenchymal morphology *in vitro*, that resembles the 'epithelial scattering' phenotype observed when classic epithelial cells undergo an epithelial-to-mesenchymal transition. *In vitro* culture of these cells was first achieved by Auerperg and collegues in 1984, and is described in Chapter 3 [Auersperg et al., 1984].

Neoplastic changes within ovarian cortical inclusion cysts (ICs) (p53 signatures) suggests that the high-grade serous carcinoma subtype can originate within these relatively common structures. The term 'cortical inclusion cyst' describes cystic structures within the ovarian stroma (see Figure 1.2) that are below 100mm in diameter and are lined with epithelium. ICs form from the invagination of the OSE during ovulation, or from papillary structures commonly seen on the surface of ovaries (see Figure 1.3).

Inclusion cysts have a different microenvironment to the surface of the ovary. When trapped within inclusion cysts, ovarian epithelial cells are physically closer to the mitogenic hormonal environment of the ovarian stroma. A basement membrane consisting of collagen IV and laminin plus a thick collageous layer termed the *tunica albuginea*, separates normal ovarian surface epithelial cells from the underlying stroma [Auersperg et al., 2001]. Basement membranes are present in all tissues as a sheet of fibrillous matrix protiens underlying epithelial or endothelial monolayers. The function of the basement membrane is to anchor the epithelial/endothelial cells to the connective tissue below through cell-matrix adhesions. Basement membranes also act as a physical barrier during the earliest stages of neoplastic transformation. However, during the process of ovarian inclusion

cyst formation, the basement membrane/*tunica albuginea* matrix layer is lost, and thus the barrier separating the ovarian epithelial cells from the mitogenic stromal environment no longer exists [Auersperg et al., 2001]. It is likely that the close proximity of OSE trapped within ICs to bioactive molecules (e.g. hormones and mitogens) in the stromal milieu contributes to the rapid growth of these tumours. Elevated levels of oestrogen or growth factors in the ovarian stroma may be required for this effect to be significant [Wong and Auersperg, 2003].

Interestingly, *BRCA1/2* mutation carriers and families with a history of breast and ovarian cancer (groups with increased risk of EOC) have a higher frequency of inclusion cysts [Werness et al., 2000]. One study analysed histopathological atypia along with expression of a number of cell cycle regulatory proteins in 94 prophylactically removed ovaries of 50 Ashkenazi Jewish women carrying *BRCA1* or *BRCA2* mutations. Mutation carriers had significantly more atypical features of the OSE and also a higher frequency of inclusion cysts compared to controls. Furthermore, TP53 expression in the cortical inclusions within ovaries of *BRCA1/2* mutation carriers was found to be significantly elevated compared to controls [Kerner et al., 2005]. This suggests that, in mutation carriers at least, pre-neoplastic areas of ovarian ICs have identifiable molecular features, and these biomarkers could reveal the histological features and molecular profile of the subsequent tumour (*BRCA1/2* tumours are mostly serous and TP53 mutations are very common in this subtype).

Lessons from the Microenvironment and Developmental Biology

The cellular origins of EOCs have been extensively disputed in the literature over the last several years. If all ovarian cancers do arise from the OSE, then this would indeed require differentation of the uncommitted OSE cell. At most other organ sites, epithelial cell tumours are characterised by a loss of tissue organisation and of features of differentiation; the inverse is true for EOCs. EOCs are more differentiated than their proposed cell of origin, and unlike other epithelia which become more mesenchymal with transformation, the OSE has mesenchymal characteristics which are lost during the process of oncogenesis. Expression of the E-Cadherin adhesion molecule illustrates this paradox - most epithelia express E-Cadherin and this molecule is important for cell polarity and the formation of glandular epithelial stuctures, such as breast acini. Typically, loss of E-Cadherin expression is associated with loss of tissue organisation and progression from a quiescent, organised tissue to a hyperproliferative, disorganised structure (Figure 1.4). The OSE somewhat unusually, does not express E-Cadherin, and E-Cadherin expression is often acquired during EOC development, thus EOCs are more differentiated and demon-

strate a higher level of tissue organisation than the precursor cell [Sundfeldt et al., 1997]. E-Cadherin expression is found in 27-100% serous, 40% mucinous and 22% of clear-cell EOCs, suggesting that maintenance of E-Cadherin expression occurs in all of the major EOC histotypes [Sundfeldt et al., 1997]; [Faleiro-Rodrigues et al., 2004].

In vitro, SV40-immortalised OSE cell expressing E-Cadherin undergo a mesenchymal to epithelial transition [Auersperg et al., 1999]. An interesting observation is that the epithelia lining inclusion cysts express E-Cadherin and CA125 [Sundfeldt et al., 1997]; [Miotti et al., 2005]; reviewed in [Auersperg et al., 2001]. Therefore, OSE lining ICs becomes more committed to an epithelial phenotype, thus displaying features of EOCs. This suggests that the ovarian stromal-epithelial interactions may play a key role during EOC initiation. The microenvironmental cues that may be responsible for this are not yet known, though age-related changes may have a role, and are explored in Chapter 5 of this thesis.

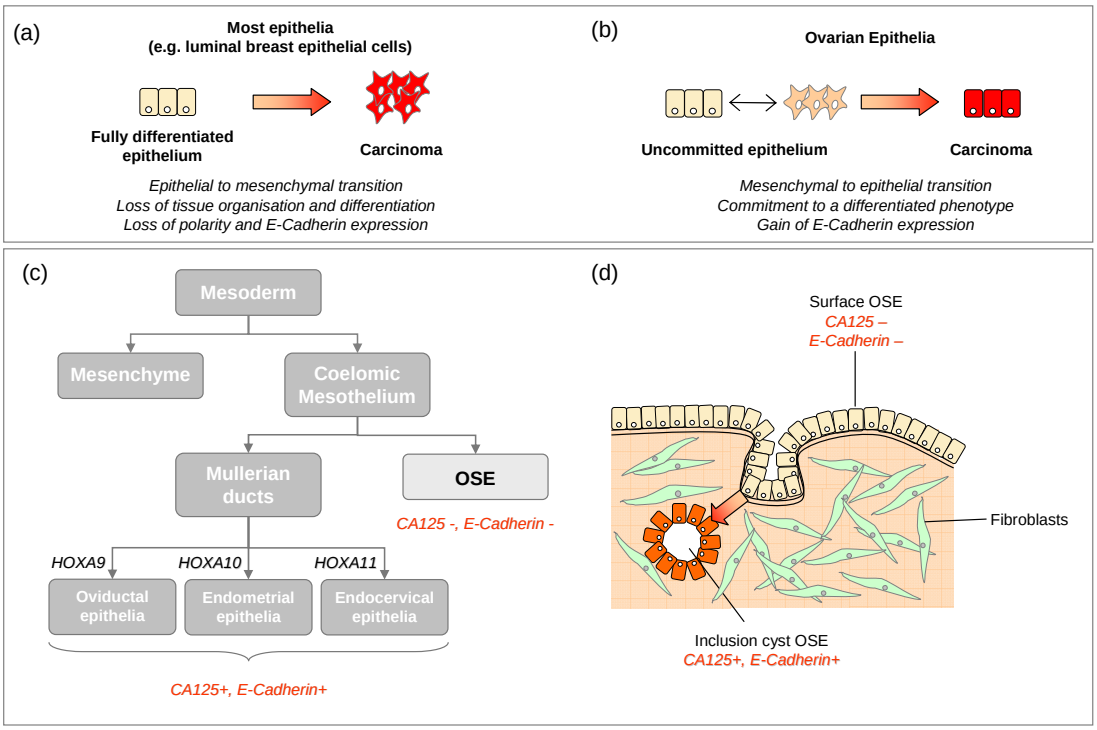

Figure 1.4: EOC genesis: development gone awry? (a, b) Most other epithelia in the body loose tissue organisation and features of differentiation when transformed (e.g. E-Cadherin expression, polarity). The inverse is true for EOCs. (c, d) Common developmental origins of the OSE and Müllerian-derived epithelia suggest a role for the ovarian stroma in stimulating a Müllerian-type differentiation of the OSE within inclusion cysts.

The issue of the transdifferentiation from uncommitted epithelial monolayer to differen-

tiated epithelial cells by the OSE is often used as an argument against an OSE origin for EOCs. This is backed up the the fact that EOCs resemble epithelia from the other organs of the reproductive tract, as described above, leading some researchers to hypothesise that all EOCs derive from ectopically located Müllerian epithelia [Dubeau, 1999]. Ovarian and Müllerian epithelia derive from the same embryological origins (the coelomic mesothelium). During the development, the cells which will form Müllerian duct-derived epithelia migrate into the mesenchyme, gaining expression of CA125 (a differentiation marker of normal Müllerian-derived epithelia; also frequently expressed at high levels in EOCs). The same coelomic mesothelium gives rise to the OSE, which does not undergo migration but forms the cellular monolayer that covers the surface of the ovary. It is hypothesised that OSE trapped in the ovarian stroma undergoes a Müllerian differentiation that mimics differentiation of other gynaecological epithelia during embryogenesis, and that this is reflected by CA125 and E-Cadherin expression often observed in OSE trapped in the ovarian cortex (Figure 1.4) [Roskelley and Bissell, 2002].

The approach to EOCs as 'development gone awry' is an attractive model for EOC genesis, since it would answer many of the unresolved questions regarding origins of the disease. Naora and collegues have modelled the effects of inappropriate HOX gene expression in mouse ovarian surface epithelial (mOSE) cells and demonstrated that ectopic expression of *HOXA9*, *HOXA10*, *HOXA11* in tumourigenic mOSE induces growth of papillary, endometrioid and mucinous tumours respectively (Figure 1.4) [Cheng et al., 2005]. Temporal expression of HOX genes follows location of the genes in the genome, and also the frequencies of each associated tumour subtype.

Other Cellular Origins

Emerging evidence suggests that not all epithelial ovarian cancers originate from ovarian surface epithelial cells, as shown in Table 1.1 and Figure 1.2. More recently, histopathologic analyses and gene expression profiling have provided evidence that a proportion of high-grade serous tumours arise from the fallopian tube epithelium [Marquez et al., 2005]; [Jarboe et al., 2008]. It is well established that over a third of endometrioid and clear cell EOCs are associated with endometriosis (a benign condition in which endometrial cells become hyperproliferative and are found ectopically located throughout the pelvis and other parts of the body) [de la Cuesta et al., 1996].

Detailed histopathological examinations of fallopian tube tissue from prophylactic oophorectomy procedures have found a high proportion of occult *in situ* carcinomas that are of the serous subtype [Callahan et al., 2007]; [Jarboe et al., 2008]. These occult tumours are

morphologically very similar to high-grade serous ovarian cancers (the most common EOC subtype), which has lead to a shift in opinion in the field. Many researchers now consider the fallopian tube epithelia (FTE) to be the site of origin of the majority of the majority of EOCs. Studies to date have used samples from women who have a high risk of EOC, so it has yet to be established whether or not this is true for sporadic tumours. Evidence to support this statement does not rule out a role for the OSE, and taken together, the data suggest dual origins for high-grade serous carcinomas (HGSCs) (Table 1.2).

Observation	Interpretation - non-OSE origin	Interpretation - OSE origin
EOCs are histologically diverse	❖ Most EOCs originate from non-ovarian cells (from the fallopian tube, endometrium, endocervix) ❖ Müllerian-type epithelia within inclusion cysts are ectopically located endometrial, cervical and fallopian tube epithelia	❖ The OSE demonstrates considerable phenotypic plasticity *in vitro* and *in vivo*, and commitment to a differentiated phenotype is a hallmark of transformation of these cells ❖ Many other epithelia give rise to histologically diverse tumours (salivary gland carcinomas arising from a single epithelia have around 20 different histotypes) ❖ Ovarian stromal cues initiate a Müllerian transdifferentation of OSE trapped within inclusion cysts ❖ Ectopic expression of *HOX* genes triggers metamorphosis of the OSE into differentiated Müllerian-type epithelia
Tubal ligation and hysteroscopy decreases EOC risk	❖ Blocks retrograde transport of endometrial epithelial cells to the ovary	❖ Reduces blood flow/affects hormonal milieu of the ovary to create a microenvironment which is less mitogenic
In situ carcinomas in prophylactically removed fallopian tubes	❖ High-grade serous carcinomas originate at the distal portion of the fallopian tube	❖ Area of epithelial differentiation are prone to transformation. Frequency of OSE to FT/FTE to ovarian movement in this area is unknown

Table 1.2: An OSE or FTE origin of EOCs? Different interpretations of the evidence.

1.1.3 Risk Factors for Epithelial Ovarian Cancer

The relative risks for ovarian cancer are summarised in Table 1.3. The most significant risk factor for epithelial ovarian cancer is a mutation in either the *BRCA1* or *BRCA2* gene (Table 1.3). After *BRCA1/2* mutation, the two main risk factors for epithelial ovarian cancer are (i) increased age: the highest incidence of EOC is in women over 75; and (ii) family history (although over 90% of cases are sporadic). Other factors that can alter a women's risk of developing EOC include talcum powder use (increases risk), prophylactic oophorectomy (reduces risk) and tubal ligation (also reduces risk) (references listed in Table 1.3). Some of these epidemiological risk factors have also been modelled *in vitro* - for example OSE from women with a family history show neoplastic features and talc can increase proliferation of OSE cells [Auersperg et al., 1995]; [Buz'Zard and Lau, 2007].

Parity has a protective effect against the development of EOCs: one full term preg-

Epidemiological observation	Change in risk	*In vivo* evidence & Hypothesised mechanism	*In vitro* evidence	Suggested origin	References
Reduced risk with oral contraceptive pill use Reduced risk with pregnancy	⇩50% for 5 years OCP use ⇩40% for 1st pregnancy, 10% for subsequent births	Incessant ovulation hypothesis: reduced number of ovulations reduces (i) opportunity for mutation accumulation in the OSE and (ii) exposure to mitogens in the ovarian stroma	OSE cells transformed *in vitro* form tumours in mice resembling human EOCs (express CA125, cytokeratin). Oestrogen is mitogenic to OSE *in vitro*	OSE	Fathalla 1971 Risch *et al.*, 1996 Modugno *et al.*, 2001 Syed *et al.*, 2001 Lui *et al.*, 2004 Sasaki *et al.*, 2009
Increased risk with talcum powder use	⇧ RR = 1.4-2.08	Stimulation of inflammatory, wound-healing response	Talcum powder induces inflammation and is a known irritant. Talc can also increase proliferation of OSE	OSE	Cramer *et al.*, 1999 Gertig *et al.*, 2000 BuzZard & Lau 2007 Wu *et al.*, 2009
BRCA1/2 mutation	⇧ RR = 16-44	TP53 signatures, early neoplastic features (e.g. E-cadherin expression, metaplasia) observed in OSE, inclusion cysts and fallopian tube fimbrae	FH-OSE cells exhibit features of tumourigenesis (notably, markers of EECs and FTE)	OSE FTE	Jarboe *et al.*, 2007 Wong *et al.*, 1999
Family history of EOC/BC (without BRCA1/2 mutation)	⇧ RR = 3.1-4.6	Low/moderate-risk genes with lower penetrance and yet to be identified are responsible for the non-BRCA/HNPCC related cancers	FH-OSE are more committed to an epithelial phenotype (e.g. maintain expression of CA125)	OSE	Lux *et al.*, 2006 Auersperg *et al.*, 1995
Risk-reducing oophorectomy does not completely abrogate EOC risk	⇩ HR = 0.2 (BRCA mutation carriers)	Primary carcinomas found in the peritoneum following oophorectomy in BRCA1/2 mutation carriers and non-carriers	N/A	OSE FTE PE	Finch *et al.*, 2006
Reduced risk with tubal ligation and hysterectomy	⇩ RR = 0.66 for tubal ligation	Both prevent retrograde transport of EECs. Could also reduce blood flow to the ovary and alter the hormonal microenvironment of the ovary	N/A	EECs OSE	Tworoger *et al.*, 2007 Nagle *et al.*, 2008
Increased EOC risk with advanced age, most cases occur after menopause	⇧ RR = 3 - 7.1 †	Age-related changes in the ovarian stroma promote transformation, in synergy with oncogenic mutation in the epithelium. Gross morphological changes in the ovary increase with advancing age (e.g. number of inclusion cysts)	Senescent fibroblasts promote features of transformation in partially transformed OSE.	OSE	Cai *et al.*, 2006 Lux *et al.*, 2006 Herbig *et al.*, 2006 Lawrenson *et al.*, *submitted to Neoplasia*

Table 1.3: Genetic and epidemiological evidence and the origin of epithelial ovarian cancers. OSE = ovarian surface epithelium; EEC = endometrial epithelial cell; FTE = fallopian tube epithelium; PE = peritoneal epithelium; OCP = oral contraceptive pill; EOC = epithelial ovarian cancer; BC = breast cancer, FH = family history, RR = relative risk, HR = hazard ratio. †Calculated from the cancer statistic registrations, Office for National Statistics: relative risk of malignant ovarian neoplasm (C56) in the 60-over 85 age group compared to in the 20-49 age group.

nancy confers a 40% reduction in the risk of developing EOC, with a further 10% reduction in risk for each successive birth (reviewed in [Elmasry and Gayther, 2006] and [Edmondson and Monaghan, 2001]). The reduced risk of EOC taking the oral contraceptive pill (OCP) has been found in numerous epidemiological studies. This protective effect may apply to all histological subtypes of the disease, with the possible exception of mucinous tumours, where some studies have observed a protective effect and others do not [Modugno et al., 2001]; [Risch et al., 1996]. The protective effect is increased when OCP use is over longer periods of time, and up to a 50% reduced risk of EOC is typically observed after 5 years of OCP use. The reduced risk effect continues even after use of OCP has stopped [Whittemore et al., 1992]. For *BRCA1/2* mutation carriers, the risk of developing EOC is also significantly reduced with long term OCP use [Whittemore et al., 2004].

The Incessant Ovulation Hypothesis

The protective effect of pregnancy and the oral contraceptive pill is likely to be due to the cessation of ovulation which stops the continual cycle of rupture, repair and regrowth of the OSE (applicable to EOCs that originate from ovarian epithelial cells). The incessant ovulation hypothesis for ovarian tumourigenesis was first proposed by Fathalla in 1971, and links the frequency of ovulation and incidence of EOC [Fathalla, 1971]. This theory was modelled in domestic fowl, which represent a natural model of spontaneous ovarian cancer [Blackmore, 1966]; [Goodchild, 1969]. In Fathalla's experiment, the egg production of birds was maximised by artificially maintaining 12-hour days, and this resulted in ovarian adenocarcinomas arising in 17 out of 19 birds. Control hens kept with normal seasonal variation in lighting did not develop ovarian tumours. In combination with epidemiological observations, such as the higher incidence of ovarian neoplasms in nulliparous women, it was inferred that frequent trauma to the OSE caused by ovulation plus repeated exposure to the mitogenic environment within the ovarian stroma is likely to play a role in tumourigenesis of ovarian surface epithelial cells [Fathalla, 1971]. It has subsequently been shown that oestrogen is mitogenic to OSE cells *in vitro* [Syed et al., 2001].

Ageing and Cancer

The risk of developing ovarian carcinoma increases with age (Figure 1.5). Over 80% of all epithelial ovarian cancers are diagnosed in postmenopausal women [Yancik, 1993]; [Smith and Xu, 2008]. The strongest epidemiological data for EOC, (protective effect of OCP use and pregnancy), links EOC risk to pre-menopausal events [Pike et al., 2004]. However, high-grade serous tumours, the most common histopathological subtype of the

disease, are rarely discovered at an early stage, suggesting that these tumours progress rapidly. Thus, this model requires that pre-neoplastic biological and molecular changes are induced in a precursor cell/lesion before the menopause and lie dormant, often for over 10 years, before tumourigenesis begins. Thus, if the beginnings of tumour growth precedes menopause in the majority of cases, this suggests there may be microenvironmental triggers (such as senescent stromal cells) that initiate proliferation of a dormant epithelial cell harbouring somatic mutation(s).

There are many links between epithelial tumourigenesis and ageing. There is a striking increase in the proportion of all epithelial carcinomas with advancing age - under 10% of tumours diagnosed in children are epithelial compared to up to 85% of tumours diagnosed in adults over the age of 40 [Wu et al., 2005]. Mathematical modelling suggests that accumulated spontaneous mutations alone are insufficient for cancer development (reviewed in [DePinho, 2000]). One hypothesis is that normal rates of senescence in local stromal fibroblast cells may create a microenvironment that promotes epithelial tumour development. In this thesis I explore the hypothesis that age-related changes in the ovarian stromal micrs in the epithelium to promote development of epithelial ovarian cancers. This is discussed in more detail in Chapter 5.

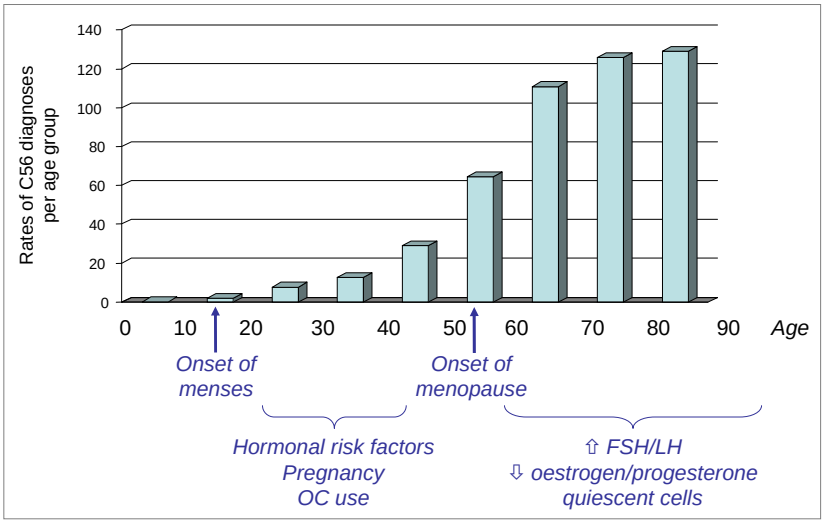

Figure 1.5: Analysis of the incidence of EOCs within different age groups suggests there may be a role for ageing related cellular changes in EOC development. Age related incidence of EOC was calculated from the Thames Cancer Registry 2006. Known hormonal risk factors are pre-menopausal hormonal exposures, yet most EOC incidences occur >10 years after the menopause. C56 = diagnosis of cancer of the ovary

1.2 Genetic Pathways Commonly Dysregulated in EOCs

For the majority of known cancer associated genes, the mechanisms of somatic alteration include: (1) Chromosomal alterations (e.g. translocations, interstitial chromosome deletions and rearrangements and chromosome ploidy); (2) DNA alterations of specific genes (e.g. coding sequence mutations, genomic deletions, rearrangements and amplifications); (3) Gene expression changes resulting from transcript instability, splice-site mutation or aberrant methylation of promoter sequences. (4) Alterations that affect protein expression or protein interactions and stability. As there are multiple mechanisms by which genes or biological pathways can be interrupted, it has been difficult to obtain accurate estimates of the frequency with which specific genes are altered in epithelial ovarian cancers.

There are now several databases cataloguing the genes that are frequently involved in cancer, such as the catalogue of somatic mutations in cancer (COSMIC [1]) [Forbes et al., 2006]. Gene specific databases also exist, such as the IARC TP53 database [Petitjean et al., 2007]. Current data suggest that the genes most commonly mutated in ovarian cancers are *p53*, *KRAS*, *CTNNB1*, *CDKN2A*, *PTEN*, *PIK3CA* and *BRAF*. Tumour suppressor genes that commonly show loss of expression in ovarian cancers, include *BRCA1/2*, *RB1*, *ARH1* (*NOEY2*), *GATA4*, *RNASET2*, *LOT1*, *DCC* and *FHIT*. Oncogenes that are reportedly amplified or overexpressed in ovarian cancers include *CMYC*, *ERBB2, HRAS, CSF1R, ECCF1, EGFR, P13K/AKT2, PTEN/MMAC1, FGF3, MDM2, BCL2,* and also *EGFR* [Fujita et al., 2003]; [Cvetkovic et al., 2004] [Lawrenson et al., 2009b].

From what is known of the genes that are somatically altered in ovarian cancers, it has been possible to build up a picture of the molecular pathways that are critical in ovarian cancer development. The most significant pathways appear to be: (1) The DNA double stranded break (DSB) repair pathway, particularly alterations in the *BRCA1* and *BRCA2* genes: (2) The DNA mismatch repair (MMR) pathway, particularly alterations in MMR genes, including *MSH2* and *MSH6*; (3) The mitogen-activated protein kinase (MAPK) pathway, particularly alterations in the *KRAS* and *BRAF* proto-oncogenes; (4) The phosphatidylinositol 3-kinase (PI3K) pathway, particularly alterations in the *PTEN* tumour suppressor gene and the proto-oncogene *PI3K*.

1.2.1 The DNA Double Stranded Break Repair Pathway

A strong family history of breast and ovarian cancer is the most significant risk factor for the disease, and up to 10% of EOC case are thought to be inherited [Auersperg et al., 2001].

[1] http://www.sanger.ac.uk/genetics/CGP/cosmic/

BRCA1 and *BRCA2* are the only genes to be currently identified as highly penetrant ovarian cancer susceptibility genes [Gayther et al., 1999]. *BRCA1* and *BRCA2*, on chromosomes 17q21 and 13q12-13 respectively, behave as classic tumour suppressor genes (TSGs) and loss of function of these genes occurs in sporadic and inherited tumours. *BRCA1/2* have roles in the repair of double-strand DNA breaks, and in normal cells with mutations in these genes, the accumulation of DNA abberations induces a *p53*-dependent growth arrest. However, in tumour cells with loss of functional *BRCA1/2*, growth arrest is avoided (often by loss of function of *p53*) and DNA damage is repaired by alternative, more error prone mechanisms such as non-homologous end joining and single-strand annealing (Figure 1.6).

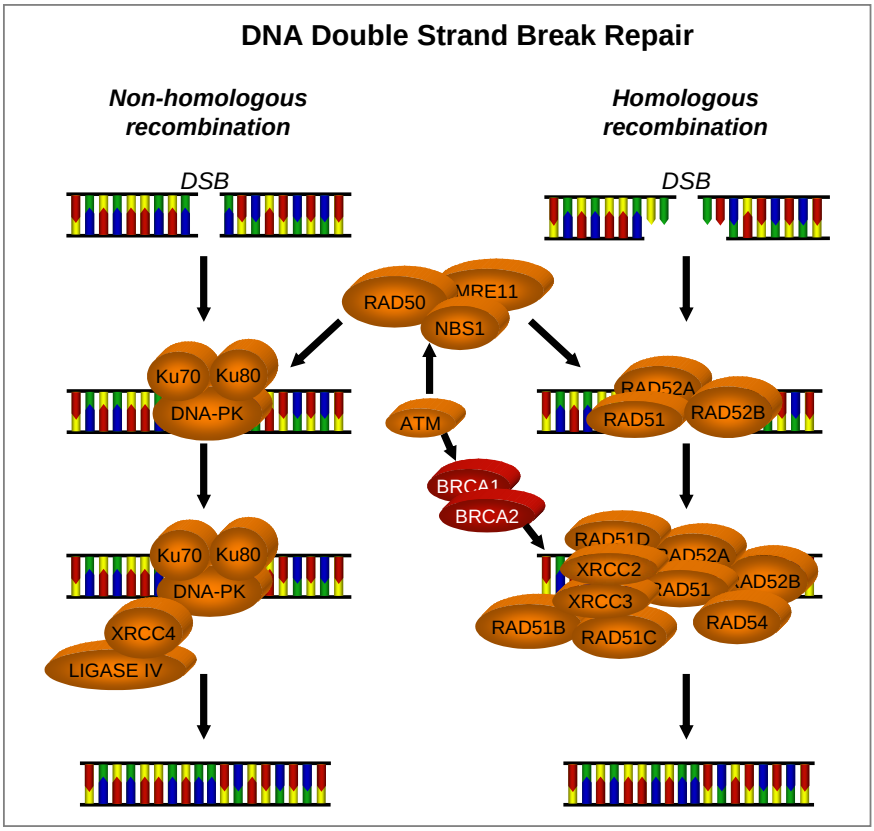

Figure 1.6: Illustration of the DNA double-stranded break repair pathways. In absence of functional *BRCA1/2*, all DNA repair occurs via the non-homologous recombination pathway, which is intrinsically more error-prone than homologous recombination repair of double-stranded DNA breaks.

BRCA1 and *BRCA2* mutation carriers show frequent loss of heterozygosity of the wild-type allele at the *BRCA1/2* loci [Ramus et al., 2003]. In ovarian cancer, the presence of a *BRCA1/2* mutation or a family history of breast/ovarian cancer affects the pro-

file of somatic genetic alterations that occur during tumourigenesis, suggesting there are different pathways for tumour development between these groups [Ramus et al., 2003]; [Israeli et al., 2003]. *BRCA1/2*-associated tumours also have distinct clinical features. This group of tumours are more likely to be high-grade serous or poorly-differentiated, and *BRCA1/2* mutation carriers may also have a better survival that non-mutation carriers [Ramus and Gayther, 2009].

Sporadic tumours often have expression profiles similar to that of either *BRCA1* or *BRCA2* tumours (even though these proteins are rarely somatically mutated in sporadic cases). This suggests either (i) hypermethylation/ other means of inactivation of the *BRCA1/2* gene, mRNA or protein is common in sporadic cases (for example, aberrant intra-cellular localisation), or (ii) there are common pathways involved in the majority of EOC cases [Ramus et al., 2003]; [Wong and Auersperg, 2003]. *BRCA1* and *BRCA2* mutations may cause the ovarian surface epithelium to be more susceptible to transformation. The normal phenotype of *BRCA1/2* mutation-positive OSE cells *in vitro* differs from that of non-mutation carrying cells. Seemingly normal OSE cells from women with a strong family history of breast and ovarian cancer have been found to have characteristics normally associated with ovarian cancer cell lines (e.g. E-Cadherin expression) [Auersperg et al., 2002]. Additionally, the OSE of prophylactially removed ovaries from *BRCA* mutation carriers show higher expression of TP53 and MIB1 (proliferation marker) when compared to ovaries removed from non-mutation-carriers [Schlosshauer et al., 2003]. Despite a significantly elevated risk of breast and ovarian cancer, not every woman with mutations in these genes will develop gynaecological cancers, and greater understanding of the functional role of the various *BRCA1/2* mutations and interactions of these proteins within the cell may give us insight into biological explanations for this.

BRCA1/2 mutations predispose to cancer in a tissue specific manner (mutation carriers have a high risk of breast and ovarian cancer). Menstrual cycle hormones and the hormonal environment within the ovary are likely to play an important role in EOC and may interact in some way with *BRCA1/2* as a predisposing factor to gynaecological cancers. Since *BRCA1/2* mutations cause a defect in DNA damage repair, mutations can accumulate in *BRCA1/2*-mutant cells that may eventually lead to tumour formation. Oestrogen levels in the ovarian stroma are one hundred times greater than in the blood and oestrogen is mitogenic to OSE cell cultures *in vitro* [Syed et al., 2001]; [Wong and Auersperg, 2003]; [Sowter and Ashworth, 2005]. Hence, oestrogenic stimulation of a cell with mutant *BRCA1/2* could trigger to mitosis before DNA damage is fully repaired.

BRCA1 (17q21)

BRCA1 coding mutations have been found in ∼3% of ovarian cancers; but *BRCA1* alteration occurring by a combination of gene deletion (detected as LOH), loss of gene expression (by promoter methylation) or loss of protein expression have been reported in the majority of ovarian cancers [Russell et al., 2000]; [Welcsh and King, 2001]; [Wang et al., 2004].

BRCA1 mutations predispose to breast and ovarian cancers (as well as cancer of the fallopian tube and peritoneum). Around 40% of women who inherit a mutated copy of *BRCA1* will develop EOC by the time they reach age 70 [Edmondson and Monaghan, 2001]. Although the precise functions of *BRCA1* are yet to be fully understood, it is known that this protein plays a role in DNA repair as part of the *BRCA1* associated genome surveillance complex (BASC). Downregulation of *BRCA1* halts the cell cycle at the G2 to M transition (a *p53*-dependant cell cycle checkpoint; this leads to apoptotic cell death or cell cycle arrest [Edmondson and Monaghan, 2001], probably due to defects in the repair of DNA damage. Knockout of this gene is embryonic lethal in mice [Gowen et al., 1996].

BRCA1 can also indirectly affect the development of epithelial ovarian cancer, acting via sex steroids that are secreted from ovarian granulosa cells. Chodankar and colleagues used a Cre-loxP system to knockout *BRCA1* alleles in the ovarian granulosa cells of mice and found that over two-thirds of the homozygous mutant mice developed epithelial ovarian cysts and uterine cysts. The cysts reportedly resembled human serous cystadenomas [Chodankar et al., 2005]. The tumours did not have mutant forms of *BRCA1.* Chodankar *et al* hypothesised that inactivation of *BRCA1* in granulosa cells caused a difference in the steroid hormones produced by these cells. Investigating the roles of hormonal variation in the initiation and development of epithelial ovarian tumours is likely to give insight into the complex interactions that occur in ovarian tumourigenesis.

BRCA2 (13q12-13)

Somatic mutations in the coding region of *BRCA1* occur in only ∼2% of ovarian tumours; but 30-50% of tumours show LOH and decreased expression [Welcsh and King, 2001]. *BRCA2* has numerous putative functions including roles in transcriptional control and in maintenance of genomic stability during mitotic replication. *BRCA2* is also important for the repair of double-stranded breaks by homologous recombination. In *BRCA2*-deficient cells, chromosomal abnormalities (often gross chromosomal rearrangements such as translocations and large deletions) accumulate during mitotic replication, illustrating a role for *BRCA2* in maintenance of chromosomal stability during DNA replication

[Shivji and Venkitaraman, 2004].

TP53

The *p53* tumour suppressor gene is arguably the most important cancer-associated gene discovered to date. This protein plays a fundamental role in cell cycle control, apoptosis, and acts to maintain the integrity of the genome. *p53* also interacts with *BRCA1* as the two proteins co-immunoprecipitate *in vitro* and *in vivo*. When a cell sustains DNA damage, TP53 levels rapidly increase. The protein binds to DNA, inducing expression of *p21* and preventing the cell from entering S phase of the cell cycle until damage is repaired. If the damage to the cells genome is too extensive to be repaired, TP53 will push the cell towards an apoptotic pathway. It is therefore unsurprising that *p53* is mutated in around half of all cancers, and in cancers where elevated TP53 is observed, the protein is mutated and ineffective. Mutations in TP53 are more common in tumours with *BRCA1* and *BRCA2* mutations than without [Ramus et al., 1999].

1.2.2 The DNA Mismatch Repair Pathway

Most cases of hereditary non-polyposis colorectal cancer (HNPCC) syndrome are caused by germline mutations in one of the mismatch repair (MMR) genes, *MLH1*, *MSH2* and *MSH6*. Mutations in one of these genes causes an 80% risk of colorectal cancer in carriers, also increases susceptibility to gynaecological cancers; the lifetime risk of endometrial cancer has been estimated as 40-60% and the risk of ovarian cancer, around 12% [Watson and Lynch, 2001]. This is thought to account for about 2% of all ovarian cancer cases, and the age at diagnosis is considerably lower than it is for sporadic ovarian cancer [Crijnen et al., 2005]; [Malander et al., 2006]. In a normal cell, mismatch repair proteins play crucial roles in the repair of mismatched bases, insertions and deletions (Figure 1.7). An error is identified by either hMutSα (a heterodimer that consists of MSH2:MSH6) or hMutSβ (which consists of MSH2:MSH3). These assemble at the DNA mismatch and recruit hMutLa (MLH1:PMS2 heterodimer), along with other proteins, to the site of damage, and repair takes place. In a cell with MMR deficiency, errors are not repaired and are replicated at mitosis. Consequently, both silent and potentially oncogenic DNA mutations accumulate in the cell.

Microsatellite instability (MSI), a marker of MMR deficiency, has been identified in $\sim$15% of ovarian tumours, although frequencies vary between studies (0-39%) [Allen et al., 2000], [Buller et al., 2001]; [Helleman et al., 2006]. The most plausible explanation for this vari-

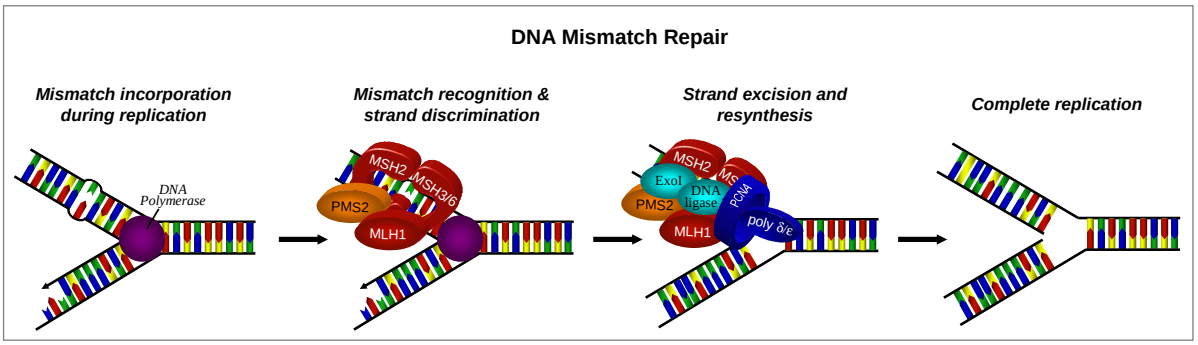

Figure 1.7: Illustration of the mismatch repair pathway. In a normal cell, components of the MMR pathway recognise and repair mismatched bases, insertions and deletions.

ability is the reported correlation between the occurence of MSI and the ovarian cancer phenotype. MSI is commonly found in endometrioid ovarian cancers, relatively frequently in clear cell tumours and tumours of mixed histology, but is rare in serous or mucinous tumours [Fujita et al., 2003]; [Gras et al., 2001]; [Catass et al., 2004]. That MSI is associated directly with genes in the mismatch repair pathway has been suggested from the analysis of *hMLH1*; loss of hMLH1 expression due to promoter hypermethylation has been found in around half of all MSI positive tumours, although somatic coding mutations of the gene are rare [Strathdee et al., 1999]; [Geisler et al., 2003]; [Son et al., 2004].

There is evidence to suggest that MMR status could influence the effectiveness of chemotherapeutic treatments for ovarian cancer. MLH1 or MSH6 deficient ovarian cancer cell lines show increased resistance to some platinum-based therapies, such as cisplatin. The MMR pathway has a role in the recognition and repair of DNA adducts caused by external agents, such as the cisplatin-induced cross-links between adjacent guanine residues. Defects in MMR are associated with increased resistance to platinum-based chemotherapies, as cells deficient in MMR function can divide without pausing to repair drug-induced DNA damage [Brown et al., 1997]; [Vaisman et al., 1998]; [Strathdee et al., 1999]. However, clinical data examining the relationships between MMR defects, patient survival and resistance to platinum-based chemotherapy for ovarian cancer are sparse and contradictory. One study found that whilst loss of hMLH1 was observed in over 50% of 34 Stage III/IV ovarian cancers, loss of this protein was linked to improved survival in this sample set [Scartozzi et al., 2003]. In contrast, Crijnen et al. found that ovarian cancer cases from HNPCC families showed no difference in survival compared to sporadic cases [Crijnen et al., 2005]. However, loss of hMLH expression has been shown to be significantly higher in ovarian tumours post-chemotherapy compared to untreated tumours, suggesting that exposure to chemotherapy induces positive selection for MMR deficient

tumour cells *in vivo* [Brown et al., 1997].

1.2.3 The Mitogen-Activated Protein Kinase Signalling Pathway

In EOCs genetic abberations of genes in the mitogen-activated protein kinase (MAPK) signalling pathway occur in a subtype-specific manner, as summarised in Table 1.4. This thesis looks in detail at the MAPK pathway and the differential effects of $KRAS^{G12V}$ and $BRAF^{V600E}$ in an *in vitro* model of EOC development. Mutations in *RAS* or *RAF* are the most common mechanism by which the MAPK pathway becomes inappropriately activated in tumours.

	Frequency of mutation (%)					
Histological Subtype	***KRAS***	***BRAF***	***PTEN***	**PIK3CA**	**CTNNB1**	**CDKN2A**
Borderline serous	27-36	33-50				
High-grade serous	0-12	0 [α]	3	2	0	6
Mucinous	33-86 *	0	16	6	2	10
Endometrioid	17	0	25	15	27	16
Clear cell	0	0	2	25	0	21

Table 1.4: Subtypes of epithelial ovarian cancer have distinct molecular profiles. [α] 0% signifies mutations have not yet been identified in these subtypes. *Similar frequencies of mutations found in benign, borderline and malignant tissue within same neoplasm. Adapted from [Lawrenson et al., 2009b]

The mitogen-activated protein kinase pathway ($RAS/RAF/MEK/MAPK$) is a key pathway in the transduction of a external mitogenic signal into the nucleus (Figure 1.8). When a mitogen binds to a receptor tyrosine kinase (RTK, such as EGFR or ERBB2) on the cell membrane, the external mitogenic signal is transduced into the nucleus via the mitogen-activated protein kinase pathway. Activation of this pathway induces proliferation and differentiation of a cell, and so unsurprisingly, components of this pathway are frequently mutated in many types of cancer, including melanoma and colorectal carcinoma. Oncogenic mutations activate the pathway in the absence of a mitogenic signal, causing the cell to enter the S phase of mitosis and begin to divide without control. If cells divide before any DNA damage is repaired, consequently, the daughter cells will contain mutations. Should these mutations confer a growth advantage, for example by enabling the cell to bypass apoptotic signals, growth of these cells will be selected for in that population.

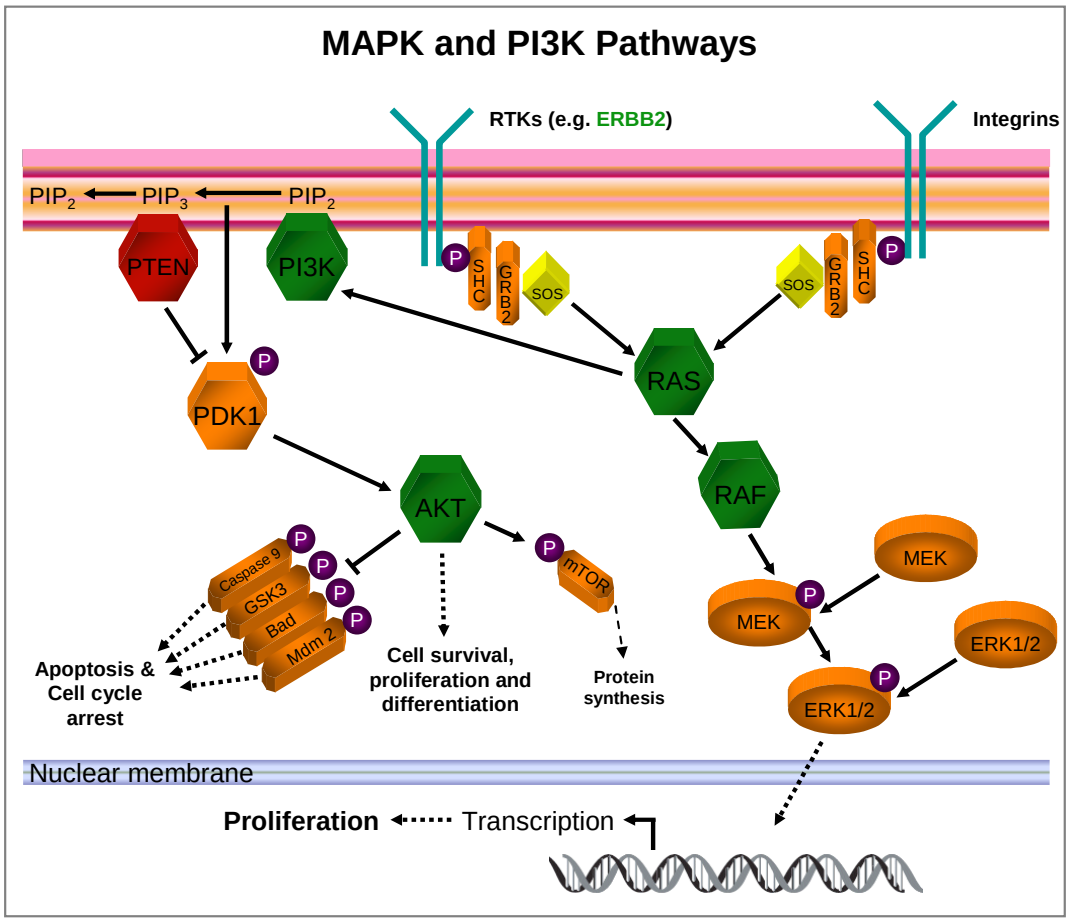

Figure 1.8: Illustration of the mitogen-activated protein kinase and phosphatidylinositol 3-kinase pathways. The mitogen-activated protein kinase (MAPK) and the phosphatidylinositol 3-kinase (PI3K) pathways are frequently activated in ovarian and other cancers, either by loss of tumour suppressor genes, such as phosphatase and tensin homologue (*PTEN*) in the PI3K pathway, or activation of oncogenes such as *KRAS* or *BRAF* in the MAPK pathway. Proto-oncogenes are shown in green, tumour suppressor genes in red.

KRAS

A mutant copy of the *RAS* gene was the first oncogene to be isolated and sequenced. The *RAS* family of proto-oncogenes are small GTPases located on the cytoplasmic aspect of the plasma membrane, and play an important role in transducing extracellular signals for proliferation and differentiation. RAS proteins are guanine nucleotide-binding glycoproteins and to become active, the normal RAS protein must undergo a change in tertiary conformation, triggered by the binding of a GTP molecule, transferred following dimerisation of two receptor tyrosine kinases. Thus, *Ras* acts as a molecular switch, active

when GTP is bound, inactive when GDP is bound. GTP-bound RAS molecules mediate cellular signalling through the hydrolysis of GTP into GDP by their intrinsic GTPase activity, when stimulated by a GTPase activating protien (GAP). RasGAP protiens include p21. In the case of RAS, *son of sevenless*, or *SOS* is a guanine exchange factor that stimulates the release of the bound nucleotide (e.g. GDP) (Figure 1.8). Once GDP is released the RAS protien is free to bind a fresh GTP from the cytosol. Hyperactive mutated forms of RAS proteins are permanently in an active conformation, even in the absence of an extracellular signal. When a RAS molecule is constitutively active, a signal is continuously transduced to the nucleus, inducing the transcription of genes involved in division or differentiation.

There are three *RAS* isoforms: *HRAS*, *NRAS* and *KRAS*, and often, mutations of one isoform is associated with a particular cancer. Activating mutations in a *RAS* gene are thought to be found in around one-quarter of all cancers [Schulze et al., 2004]. In EOCs, *KRAS* mutations are present in approximately two-thirds of mucinous tumours and one-third of low-grade and borderline serous ovarian tumours [Shih and Kurman, 2004]. Mutations in *HRAS* or *NRAS* have not been detected in ovarian tumours to date. *KRAS* mutations are also found in around 17% of endometrioid carcinomas, specifically in the low-grade tumours [Geyer et al., 2009]. The majority of these mutations are a substitution at position 12 in the amino acid sequence replacing glycine with arginine (V12G). This mutation leads to the constitutive binding of GTP, and thus constitutive sigalling by the mutated *Ras* molecule.

BRAF

RAF is the first protein kinase in the MAPK pathway. RAF proteins are serine/threonine kinases that act downstream of RAS. RAF molecules transduce signals down the MAPK/ERK pathway from RAS by phosphorylating serine or threonine residues on downstream effector molecules, namely MEK1 and MEK2. RAF proteins only bind GTP-bound RAS, which recruits RAF to the membrane and activates the RAF molecule. *BRAF* mutations cluster in or near the activation domain of the BRAF molecule and cause the activation domain to be permanently in an active conformation, thus stimulating enhanced kinase activity towards MEK1/2 substrates.

There are three *RAF* isoforms: *ARAF*, *BRAF* and *CRAF*, and (as with *RAS*) mutations in each are associated with different cancers, for example, *BRAF* mutations are common in melanoma [Michaloglou et al., 2005]. Activating mutations in *BRAF* are also found in around one-third of low-grade serous ovarian neoplasms, and interestingly, unlike *KRAS*

mutations, several studies have reported that *BRAF* mutations are rare/absent in all other subtypes of EOC [Mayr et al., 2006]; [Russell and McCluggage, 2004]; [Gemignani et al., 2003]. This is surprising, considering activation of the MAPK pathway is found in other ovarian tumour histotypes, and adds to evidence that different histological subtypes may arise from distinct genetic pathways and that somatic genetic alterations determine the molecular features and aetiology of the tumour.

C-MYC

C-MYC is one of the most well characterised proto-oncogenes. The family of *MYC* transcription factors play critical roles in cell growth through the control of the transcription of a broad range of genes involved in fundamental cellular processes, such as cell cycle control, apoptosis, and DNA and protein synthesis. Like *RAS*, *C-MYC* has been implicated in tumourigenesis of many different tissues, which is unsurprising considering its role in cellular proliferation and differentiation. *C-MYC* expression directly affects levels of cyclins and cyclin-CDK complexes to push the cell cycle forwards and induce proliferation. *C-MYC* interacts with the *p21* tumour suppressor gene, removing the protective cell senescence response and forcing the cell to stay in the cell cycle [Nasi et al., 2001]. In a quiescent cell, forced expression of *C-MYC* causes the cell to re-enter the cell cycle. Furthermore *C-MYC*-overexpression, in combination with *OCT4*, *SOX2* and *KLF4* induces pluirpotency in differentiated cells [Takahashi et al., 2007]; [Aasen et al., 2008]. Finally, *C-MYC* interacts with the TP53 and retinoblastoma tumour suppressor pathways, and can remove inhibition of cell division imposed by these two tumour suppressor pathways. Hence, *C-MYC* can play a role in tumourigenesis through its interactions in one or multiple pathways critical in cell growth and differentiation. Analysis of EOC tumour samples has detected amplification or overexpression of the *C-MYC* gene at frequencies of around 35-76% [Nasi et al., 2001]; [Dimova et al., 2006].

v-myc is a viral homologue of *CMYC*, and is encoded in many retroviruses (e.g. MC29, FTT, OK10) that are capable of transforming mammalian cell lines [Lee and Reddy, 1999]. *v-myc* differs to *CMYC* in that it contains substitutions and deletions, mostly at the N- and C-terminal regions. These mutations make the *v-myc* gene a more potent inducer of neoplastic transformation than its human homologue [Lee and Reddy, 1999]. *v-myc* is often used in *in vitro* models of transformation, but is not absolutely required, as overexpression of human *CMYC*, as commonly detected in human tumours, is often sufficent to transform human cells *in vitro*.

The role of ERBB2

The epidermal growth factor receptor *ERBB2* (*Her-2/neu*) gene is a member of the receptor tyrosine kinase (RTK) superfamily of cell surface receptors. Ligand-binding induces dimerisation of the ERBB2 receptor, and the resulting signal can activate various pathways including the MAPK, PI3K, PLC and STAT pathways. In ovarian cancer, *ERBB2* overexpression occurs in about 10-20% of ovarian tumours but not in early stage (Stage I and II) or borderline tumours. Increased *ERBB2* gene copy number or elevated protein expression may be associated with poorer prognoses [Hogdall et al., 2003]; [Wu et al., 2004]; [Nakayama et al., 2006]. Lassus *et al.* also suggest that *ERBB2* amplification may correlate to TP53 mutation status [Nakayama et al., 2006]. Finally, it appears that mutations of *ERBB2*, *KRAS* and *BRAF* may occur mutually exclusively, suggesting that oncogenic mutation of any one of these genes has equivalent or saturating downstream effects [Tanner et al., 1998].

1.2.4 The Phosphatidylinositol 3-Kinase (PI3K) Signalling Pathway

Perturbations in normal PI3K pathway signalling are also common in cancers. This pathway transduces extracellular signals associated with cellular growth, proliferation and apoptosis. Phosphatase and tensin homologue (*PTEN*) negatively regulates the PI3K pathway, through the dephosphorylation of a membrane-associated phospholipid - phosphatidylinositol (3,4,5)-trisphosphate (PtdIns(3,4,5)P3). PTEN acts in opposition to PI3K, which generates this tri-phosphate. In this way, PTEN and PI3K indirectly regulate AKT, a downstream serine/threonine-specific protein kinase. Loss of PTEN function causes PtdIns(3,4,5)P3 to accumulate and renders the pathway constitutively active.

The *PIK3CA* proto-oncogene encodes p110α, the catalytic subunit of PI3Ks. This protein is amplified or mutated in a number of cancers, including breast, stomach, brain and lung cancers. Most *PIK3CA* somatic missense mutations detected in advanced stage ovarian carcinomas cluster at codon 545, a mutational 'hotspot' which lies within the helical domain of the protein. These mutations substitute a negatively charged glutamic acid for a positively charged lysine or hydrophobic glycine or alanine residue, and are thought to affect interactions between PIK3CA and other molecules, including lipid substrates [Levine et al., 2005]. These activating mutations generate PI3K proteins with increased catalytic activity, PtdIns(3,4,5)P3 is produced faster than it is degraded and signalling, through the AKT and other downstream effectors, increases. *PIK3CA* mutations occur at the highest frequencies in mucinous and endometrioid tumours (Table 1.4).

AKT2 is amplified in ovarian cancer cell lines and tumours [Cheng et al., 1992]. Downstream effectors of AKT play roles in apoptosis and DNA repair (Mdm2, Bad, Caspase 9), cell survival (NF-$\kappa\beta$), growth and protein synthesis (mTOR) and the cell cycle (GSK3α) [Liang and Slingerland, 2003]; [Richardson et al., 2004]. Ovarian cancer cells with activated AKT signalling will apoptose when treated with a PI3K inhibitor (LY294002) suggesting that, once activated, this pathway is critical for cancer cell survival. Furthermore, pre-treatment with LY294002 enhanced the effect of cisplatin treatment in cell lines with activated AKT signalling [Altomare et al., 2004]. Inhibition of mTOR, a downstream effector of AKT, has equivalent but not additive effects to LY294002 (suggesting perturbed signalling at either mTOR or AKT saturates downstream signalling). Furthermore, inhibition of mTOR significantly increases the effectiveness of cisplatin and tamoxifen in ovarian cancer cells with activated AKT signalling *in vitro* and *in vivo* [Treeck et al., 2006]; [Mabuchi et al., 2007]. AKT and mTOR phosphorylation are closely related in ovarian cancers, as phosphorylation of mTOR results in protein synthesis and ultimately is essential for progression through the cell cycle [Altomare et al., 2004]; [Pullen and Thomas, 1997]. Since AKT has a role in many critically important processes in the organism (such as glucose metabolism), mTOR inhibitors are less likely have toxic side effects and therefore may have therapeutic role in ovarian cancers with elevated AKT signalling.

1.3 A Dualistic Model to Classify EOCs

It is now clear that ovarian cancer subtypes develop through the disruption of distinct genetic and biological pathways. A current popular model to categorize EOCs has been developed by Shih and Kurman, and divides ovarian tumours into Type I and Type II tumours [Shih and Kurman, 2004]. In this model, low-grade serous, mucinous, endometrioid, clear cell and malignant Brenner tumours are grouped together as one subclass of ovarian cancers ('Type I' tumours); high-grade serous carcinomas, undifferentiated carcinomas and malignant mixed mesodermal tumours represent another subclass (Type II tumours). The features of each group are summarised in Table 1.5.

1.3.1 Type I Tumours

Type I tumours are typically slow growing, more often identified at lower grade, and evolve from identifiable precursor lesions [Shih and Kurman, 2004]. This model is reminiscent of the model for colorectal cancer (CRC) development, which represents the paradigm for

TYPE/SUBTYPE	CLINICAL FEATURES
TYPE I TUMOURS	
Low-grade serous Endometrioid Mucinous Clear cell Malignant Brenner	Large size Slow growth Growth is usually restricted to the ovary Identifiable precursor lesions
TYPE II TUMOURS	
High-grade serous Undifferentiated	Aggressive growth Rarely present with identifiable precursor lesion Usually have metastasised by time of diagnosis

Table 1.5: Type I and Type II Tumours have distinct clinical features

the linking of histological observations and genetics. A genetic model for CRC development has been defined within a phenotypic framework, starting with normal tissue which accumulates somatic mutations in a stepwise manner, frequently in the *KRAS*, *p53* and *APC* genes [Fearon and Vogelstein, 1990]. Clinically, premalignant polyps are observed which are known to have a high risk of developing into a malignant lesion [Bates and Mercurio, 2005]; [Castagnola and Giaretti, 2005].

Low-grade serous carcinoma/serous borderline tumours

Low-grade and borderline serous ovarian cancers are remarkably similar in their molecular features. 13% of serous carcinomas are classified as borderline serous tumours (BSTs) and approximately two-thirds of low-grade serous carcinoma will contain areas of borderline tumour tissue. BSTs show some phenotypic characteristics of high-grade serous carcinomas, including metastatic potential and increased nuclear atypia, compared to classical low-grade serous tumours [Malpica et al., 2004]. However, molecular analyses suggest BSTs are unrelated to high-grade serous carcinomas; and clinicopatholgical data indicate that they are much less aggressive, and associated with considerably better prognoses than SCs [Singer et al., 2005]; [Bonome et al., 2005]. BSTs rarely harbour *p53* mutations; but *KRAS/BRAF* mutations are frequent, occurring in 60% of tumours [Gemignani et al., 2003]; [Russell and McCluggage, 2004]; [Singer et al., 2005].

Interestingly, unlike *KRAS* mutations, several studies have reported that *BRAF* mutations are rarely found in many subtypes of ovarian cancer [Gemignani et al., 2003]; [Russell and McCluggage, 2004]; [Mayr et al., 2006]. This is surprising, given that activation of the MAPK pathway is found in other ovarian tumour subtypes, and supports the hypothesis that different histological subtypes of ovarian cancer have distinct molec-

ular fingerprints. *BRAF* mutations appear to be limited to the low-grade serous subtype [Singer et al., 2003]; [Mayr et al., 2006].

Mucinous Tumours

The molecular data point to the development of mucinous tumours from a benign lesion evolving into a borderline and then an invasive tumour with *KRAS* mutation often an early event in tumourigenesis. Also, mucinous tumours can be clearly distinguished from other subtypes by their gene expression profiles; unsurprisingly, it is common for genes associated with mucin production to be upregulated in this subgroup, including *MUC2*, *MUC3* and *MUC16*. Mucinous ovarian cancers show molecular similarities with mucinous carcinomas from other organs, such as the intestine [Heinzelmann-Schwarz et al., 2006].

Endometrioid & Clear Cell Carcinomas

A large proportion of endometrioid and clear cell ovarian carcinomas appear to originate in a benign endometriotic lesion. In endometriosis, the uterine lining can be found outside of the womb, often within the abdominal cavity, on the ovaries and fallopian tubes. Epidemiological studies estimate that endometriosis affects up to 8% of women of reproductive age [Eskenazi and Warner, 1997]. Only a small proportion of women with endometriosis go on to develop endometrioid ovarian cancer; but up to 40% of women diagnosed with Stage I endometrioid or clear cell carcinoma present with synchronous endometriosis and around one-third of these tumours arise from within an endometriotic lesion [de la Cuesta et al., 1996]; [Willner et al., 2007]. The transformation of endometriotic lesions involves genes and pathways known to be disrupted in endometrioid and clear cell carcinoma of the ovary and endometrium. Microsatellite instability is a feature of around 9-16% of all endometrioid and clear cell ovarian carcinomas [Gras et al., 2001]. *hMLH1* promoter methylation occurs in around 50% of these tumours and is often accompanied by the loss of expression of a second MMR gene, in particular *hMSH2* [Geisler et al., 2003]. Microsatellite instability and *hMLH1* promoter hypermethylation are found in regions of endometrial hyperplasia within the uterus [Esteller et al., 1998].

Endometrioid tumours frequently display dysregulation of the PI3K pathway. Loss of heterozygosity at the *PTEN* locus on chromosome 10q23 is typically found in 31-42% of endometrioid tumours; somatic mutation of *PTEN* also occurs 20% of this tumour subtype [Obata et al., 1998]; [Sato et al., 2000]; [Willner et al., 2007]. Somatic mutations in the *PTEN* gene have been observed in 15-20% of benign endometrial cysts and en-

dometriosis, suggesting that inactivation of this gene is an early event [Sato et al., 2000]; [Martini et al., 2002]. Mutations in the PI3K pathway, in the *PIK3CA* gene, are relatively common in endometrioid and clear cell carcinomas (12% and 25% respectively), but are rarely found in other EOC subtypes [Campbell et al., 2004]; [Nakayama et al., 2006]; [Willner et al., 2007]. Mutations in the Wnt signalling pathway are also found in around one third of endometrioid ovarian cancers, with high frequencies observed in borderline endometrioid tumours [Oliva et al., 2006]. Interestingly, aberrant signalling of the Wnt or PI3K pathway does not appear to co-exist in a tumour with *p53* mutation. However, high-grade endometrioid ovarian cancers are characterised by mutation of *p53* [Kolasa et al., 2006]; [Wu et al., 2007]. Recently, is has been suggested that a subset of high-grade endometrioid tumours would be more appropriately classified with high-grade serous EOCs, due to similarities in tumour aetiologies, mutational events and biomarkers [Geyer et al., 2009]. Low-grade endometrioid tumours are characterised by β-catenin and *KRAS* mutations - these alterations have not been identified in high-grade endometrial carcinomas [Geyer et al., 2009]. In high-grade endometrioid, *KRAS* and β-catenin mutations are rare, *p53* mutations are often found instead, suggesting high-grade andometrioid and high-grade serous tumours may arise by common molecular pathways [Kolasa et al., 2006].

Malignant Brenner tumours

Malignant Brenner tumours are also known as transitional cell tumours. Identifiable molecular features for malignant Brenner tumours have not yet been identified, probably because these tumours are rare and have not been studied in sufficient detail. The available histopathological evidence suggests that benign Brenner tumours progress to proliferating (or borderline) and then malignant Brenner tumours in a stepwise manner [Monaghan and Williams, 2003].

1.3.2 Type II Tumours

Type II tumours include high-grade serous carcinoma, undifferentiated carcinoma and malignant mixed mesodermal tumours. Features associated with Type II tumours include a poorer prognoses in patients, rapid growth and early metastasis. It has been hypothesised that these tumours arise *de novo* from the surface epithelium or within ovarian inclusion cysts [Scully, 1995]; [Singer et al., 2005]; [Okamura and Katabuchi, 2001].

High-grade serous carcinomas

There is little evidence to suggest that Type I tumours can give rise to Type II tumours. The distinct pathways by which low-grade/borderline and high-grade serous tumours arise is reflected in the expression profiles and somatic mutations that are characteristic of each group. Mutations in *KRAS/BRAF* are rare in high-grade serous carcinoma (HGSC). This suggests that low-grade serous tumours are not precursors of high-grade serous carcinomas and that aberrant MAPK signaling doesn't play a significant role in high-grade tumours [Catass et al., 2004]; [Singer et al., 2003]. Rarely do these high-grade lesions contain benign tissue adjacent to areas of neoplastic cells, possibly because the tumour growth has taken over what remains of the precursor lesion [Jordan et al., 2006]. Mutations in *p53* in HGSCs occur at frequencies of 50-80% and *AKT2* overexpression, or p16 promotor methylation/mutation/gene deletion in 10-20% of tumours. However, it cannot be completely ruled out that some high-grade serous carcinomas arise from low-grade or borderline tumours since there have been incidental findings showing that high-grade and low-grade tumours can co-exist. One study reported identical *KRAS* mutations in a borderline tumour co-existing with a serous carcinoma which may suggest that a subset of high-grade serous tumours evolve from atypical borderline tumours and low-grade micropapillary serous carcinoma [Dehari et al., 2007].

Unlike in low-grade and borderline SCs, the PI3K pathway appears to play a role in the development of a large proportion of high-grade serous carcinomas. Mutations in the *AKT2* kinase domain are not present in this tumour type (nor in SBTs), but *AKT2* does appear to be amplified in about 18% of high-grade SCs [Cheng et al., 1992]. Similarly, mutation of the *PIK3CA* gene; or amplification and polyploidy associated with the *PIK3CA* locus has been found in up to a third of HGSCs but is absent in normal ovaries and BSTs [Wang et al., 2005]; [Nakayama et al., 2006].

Undifferentiated carcinoma and malignant mixed mesodermal tumours

These tumours are rare. Consequently, little is known about their molecular features. Both types of tumours are aggressive and associated with poor long-term survival. At least 90% of ovarian malignant mixed mesodermal tumours harbour mutations in *p53* [Shih and Kurman, 2004]; [Gourley et al., 2002].

1.4 *In vivo* Approaches to Modelling Epithelial Ovarian Cancer

In general, the earliest models of EOC and cellular transformation looked at the disease in rodent cells, both *in vitro* and *in vivo*. A major advantage of rodent models is that they enable the study of disease within a living mammal. Earliest models of EOC predominantly xenografted ovarian cancer cells lines into immuno-compromised rats and mice. It was observed that whilst some cell lines efficiently form tumours that resemble the original tumour, other cancer cell lines that grow well *in vitro* failed to form differentiated tumours when injected into rodents, (reviewed in [Garson et al., 2005]).

1.4.1 Murine Models of Epithelial Ovarian Cancer

Tissue-specific promotors can been used to generate animal models with targeted, organ-specific expression/knock-down of a gene or genes. The discovery of the ovary-specific Müllerian inhibiting substance receptor type II (MISIIR; also known as the Müllerian Inhibitory Factor Receptor 2, MIFR2) lead to the generation of transgenic mice expressing the SV40 early region only in their ovarian surface epithelial cells (mOSE) [Connolly et al., 2003]. Within 13 weeks around half of the transgenic mice developed epithelial ovarian tumours. However, this model provides little information about early stages of EOC since newborn mice expressing SV40-T under the control of the MISIIR promotor are found to have ovarian tumours: disease in this model is early onset, unlike human epithelial ovarian cancer which typically arises in post-menopausal women. Early ovarian neoplastic changes have been modelled in a transgenic mouse model in which activated *PIK3CA* was expressed under the control of MISIIR. Ovarian hyperplasia developed in the mice but no malignant transformation of OSE was observed *in vivo* [Liang et al., 2009]. However, the applicabilty of the MISIIR promotor to the study of EOC origins may be limited as this promotor may not specifically drive gene expression in the ovarian surface epithelium also in the endometrium and fallopian tube epithelium (L.Dubeau, personal communication).

Cre-loxP systems are a popular technique for generating conditional genes knockouts and transgenic organisms harbouring tissue specific deletions. Dinulescu and collegues created a mouse model of early stages of ovarian neoplastic transformation by creating transgenic mice harbouring a floxed $KRAS^{mut}$ 'stop' sequence as well as parts of the *PTEN* gene. By targetting expression of these oncogenic elements to the ovary they were able to initiate endometrioisis and endometrioid ovarian tumours in mice [Dinulescu et al., 2005].

1.4.2 Rat Models of Epithelial Ovarian Cancer

In 2004, Stewart and colleagues created the first rat model of the early stages of epithelial ovarian cancer by exposing the animals to low doses of 7,12-dimethylbenz(a)anthracene (DMBA) in combination with cycles of gonadotrophin treatments which were designed to initiate cycles of proliferation reminiscent of the proliferation observed naturally in the ovary during ovulatory cycles [Stewart et al., 2004]. After 6 to 12 months of the treatment, ovarian carcinomas were observed in the group which received both DMBA and hormone treatment, with early pre-neoplastic lesions detected at months 5-6. One criticism of earlier models has been that the tumours seen in the animals do not reflect the histopathological diversity of human epithelial ovarian tumours and so it is of note that in this study, the tumours that developed were of varying histopathological subtypes. Furthermore, 25% of the pre-neoplastic lesions and one out of the three tumours observed harboured a cancer associated mutation in the *Ki-RAS* gene [Stewart et al., 2004]. *KRAS* mutations are relatively common in epithelial ovarian cancers (discussed above).

Molecular comparison of malignant and non-malignant rat epithelial surface epithelium (rOSE) lead to the discovery of the *lot1* tumour suppressor gene, the human homologue of which, *ZAC1*, was subsequently demonstrated to be downregulated in a large proportion of human epithelial ovarian cancers [Abdollahi et al., 1997a]; [Abdollahi et al., 1997b]; [Cvetkovic et al., 2004]. Loss of function of *ZAC1* occurs early in ovarian cancer development, through epigenetic mechanisms including loss of heterozygosity at 6q24 or hypermethylation at this locus [Cvetkovic et al., 2004]. Expression of *ZAC1* in ovarian cancer cells reduces the rate of cellular proliferation and and increases the rates of apoptotic cell death [Cvetkovic et al., 2004].

Limitations of Animal Models of Disease

Although rat and mouse models have been valuable tools in expanding our knowledge of gene function in EOC, rodent models have so far only lead to the identification of this one gene, *ZAC1*, now known to be involved in human ovarian cancer. This is due in part to the various limitations of using rodents as models of human disease. Fundamental differences exist in the biology of a rodent and a human ovary, as well as in cellular physiology. A bursal membrane that surrounds rodent ovaries is absent in humans and significantly affects the process of metastasis [Garson et al., 2005]. There is also a marked difference in telomere biology of human and rodent cells: normal rodent calls have longer telomeres and telomere length does not appear to limit cellular life-span [Auersperg et al., 2001]. In contrast, in normal human somatic cells, telomerase activity is downregulated and telomere

shortening limits the replicative potential of normal human cells. Immortalisation, or the bypass of senescence, is a crucial step in tumour development. A significant proportion of rodent cells immortalise spontaneously following repeated passageing in culture, but this phenomenon is extremely rare when culturing human cells [Godwin et al., 1992].

Human cells also have more natural barriers to transformation than their rodent counterparts. In murine fibroblasts, inactivation of TP53 is sufficient for the cell to bypass senescence, and expression of one oncogene such as $KRAS^{G12V}$ or *C-MYC* in an immortalised rodent cell is sufficient for the cells to display oncogenic characteristics [Orsulic et al., 2002]. However, in human cells, telomere length must be maintained for the cell to bypass senescence (by the expression of telomerase or activation of the alternative lengthening of telomeres pathway). Subsequent expression of oncogenes, such as $KRAS^{G12V}$ or $BRAF^{V600E}$, usually induce senescence in the absence of additional oncogenic signals [Michaloglou et al., 2005]; [Wei et al., 1999].

1.5 *In vitro* Models of Transformation

In vitro cell biology models are an alternative approach to modelling of disease. *In vitro* models can be performed on human cells, and offer a controlled system for the study of complex pathways. The advantages and disadvantages of *in vitro* and *in vivo* modelling are summarised in Table 1.6.

	In vivo	*In vitro*
Advantages	❖ Enable study of disease in a mammalian system ❖ Interactions with other cell types, e.g immune cells, fibroblasts, are intact ❖ Can study metastasis, invasion and stromal recruitment in a living organism	❖ Disease can be studied in human cells ❖ Cheaper than *in vivo* studies, thus large scale studies and many variations can be tested ❖ More flexible than living systems, model can be tightly controlled ❖ Heterotypic and 3D modelling tools offer more biologically relevant *in vitro* tools
Disadvantages	❖ Limitations on number of and type of alterations that can be introduced e.g. strong tissue specific promoter is needed ❖ Experiments are usually more expensive and long-term	❖ No immune system, number of cell types is limited ❖ 2D tissue culture imposes unnatural growing conditions and different selective pressures compared to cells growing *in vivo*

Table 1.6: Comparison of the advantages and disadvantages *in vitro* and *in vivo* approaches to modelling human diseases

A major hurdle is the establishment of primary cell cultures. Established cell lines of many normal and tumourigenic cell types are commercially available, although it is then impossible to know what alterations may have been introduced through routine tissue culture. Some cell types, including normal ovarian epithelial and fibroblast cultures, are not readily available and so have to be established *in vitro* as primary cultures, fully characterised and then immortalised before further studies can be performed.

1.5.1 Cell Culture and Immortalisation

Non-tumourigenic cells have a limited lifespan *in vivo* and *in vitro* and eventually become growth arrested and senescent [Hayflick, 1965]. Senescence is induced by multiple stimuli including a reduction in telomere length to below a critical threshold (replicative senescence) and expression of mutated *RAS* or *RAF* (oncogene-induced senescence) [Bond et al., 2004]; [Takahashi et al., 2006]; [Drayton et al., 2003]. Senescent cells typically become enlarged and stop dividing, but are able to remain metabolically active over quite large periods of time. Classic senescence markers include expression of senescence-associated β-galactosidase (SA-β-gal), expression of p16 and p21 Cdk inhibitors, and up-regulation of plasminogen activator inhibitor type 1 [Dimri et al., 1995]; [Wei et al., 1999].

Expression of the catalytic subunit of the human telomerase holoenzyme (*hTERT*) as a means to enable primary cell lines to bypass replicative senescence was first demonstrated in retinal pigment epithelial (RPE) cells and foreskin (BJ) fibroblasts [Bodnar et al., 1998]. Although immortalisation is a crucial step in tumourigenesis, cells expressing *hTERT* do not acquire other cancer associated characteristics. Cells immortalised by the expression of *hTERT* do not grow in anchorage-independent growth assays or form tumours in mice [Morales et al., 1999]; [Jiang et al., 1999]. Furthermore, there are no significant differences in the responses of primary cells and their *hTERT* immortalised counterparts to serum deprivation, cell density and treatment with hydroxyurea, (which induces p53-independent arrest during early S-phase), or a combination of thymidine and aphidicolin, (which induce cell cycle arrest at the G1/S transition) [Bodnar et al., 1998]; [Jiang et al., 1999]; [Morales et al., 1999].

However, not all cells can be immortalised by the ectopic expression of *hTERT* in the absence of other genetic alterations [Haga et al., 2007]. It has previously been suggested that OSE cells also could not be immortalised by the expression *hTERT* alone, but in this laboratory and others, it has been demonstrated that primary NOSE cells can be immortalised by introducing *hTERT* alone, or through expression of *hTERT* in combination with an siRNA targetting *pRb* or *p53* [Davies et al., 2003]; [Li et al., 2007]; [Yang et al., 2007a];

[Yang et al., 2007b]. NOSE cells immortalised by ectopic expression of *hTERT* in combination with siRNA targetted knockdown of *pRb* or *p53* mRNA expression do not demonstrate features of a neoplastic phenotype *in vitro* or *in vivo*. Yet, while cells do not form tumours in nude mice or demonstrate an ability to form colonies in anchorage-independent growth, in these models, cells do demonstrate diminished responses to γ-irradiation as well as altered levels of cell cycle proteins and proteins of the *p53* and *pRb* pathways. This is unsurprising when these pathways have been disrupted by siRNA; however, the reduced response to irradiation suggests that the immortalised cells are less capable of responding to and therefore repairing DNA damage. Though these cells are non-tumourigenic, activation of *hTERT* in combination with perturbations in the *p53* and *pRb* tumour suppressor pathways are frequent abberations in EOC speciments, thus, these cells represent a model of pre-neoplastic changes in the OSE [Yang et al., 2007a]; [Yang et al., 2007b].

1.5.2 *In vitro* Assays for a Transformed Phenotype

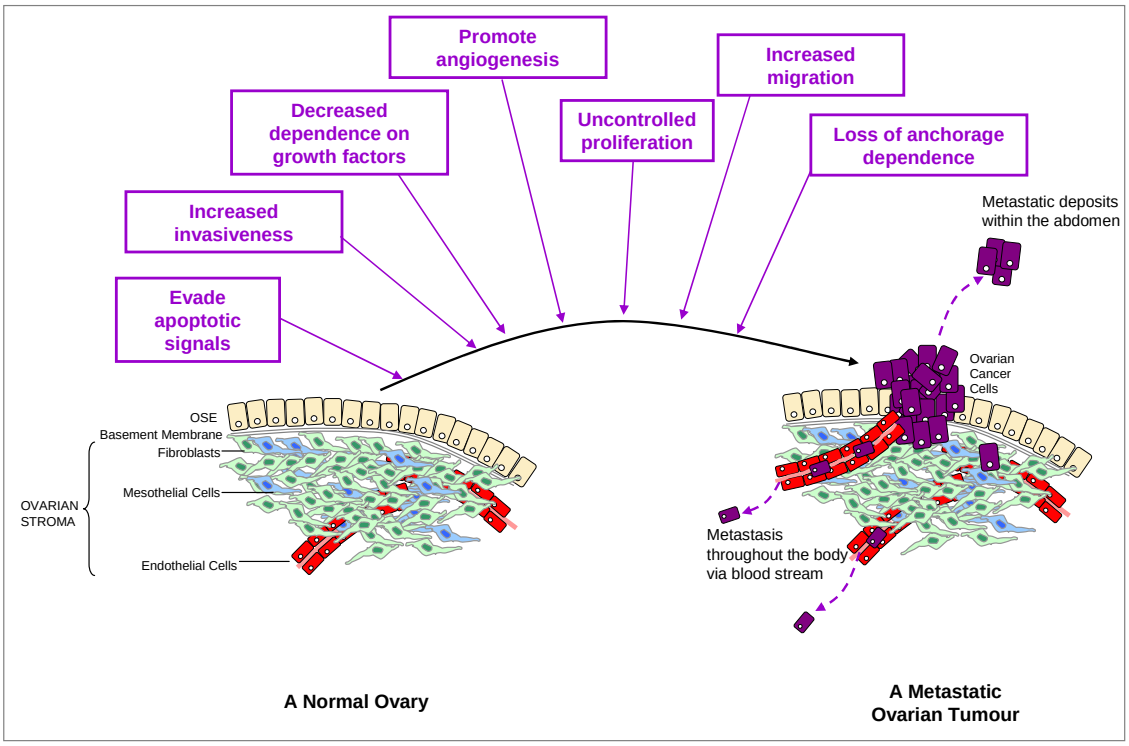

Figure 1.9: Schematic representation of *in vitro* and *in vivo* phenotypic changes that are characteristic of neoplastic and malignant transformation. All of these changes can be monitored *in vitro* many can also be assayed *in vivo*

During the process of *in vitro* or *in vivo* malignant transformation, cells undergo a spec-

trum of phenotypic changes including independence from apoptotic signals and growth factors; anchorage-independent growth; enhanced proliferation, invasiveness and migration. Cells begin to exploit the local microenvironment by evading immune recognition and promoting neovascularisation and development of a tumour stroma (Figure 1.9). These changes can be monitored *in vitro*. The assays typically performed to test for a transformed phenotype include:

Anchorage-Independent Growth Assays assess the ability of a cell line to grow in an anchorage-independent manner, with the loss of a normal contact inhibition response. Cell lines that readily form colonies in anchorage-independent growth assays are showing tumourigenic characteristics.

Invasion Assays demonstrate the invasive ability of a cell line. In transwell invasion assays, cells are placed atop a membrane which is coated with extracellular matrix (ECM) protein, such as Matrigel. Cell lines must degrade the ECM to invade towards a chemoattractant placed in the lower chamber. This assay is considered to be an *in vitro* demonstration of the invasive potential of the cell line.

Migration Assays assess migrative ability of a cell line. Such assays may be transwell assays (as above, but without coating of matrix protein on the membrane), or wound healing assays (which assesses the ability of a cell line to migrate horizontally).

Proliferation/ Anchorage-Dependent Growth Assays Plating a known number of cells, and then passaging and counting cells at regular intervals can be used to determine the population doubling time of a cell line and thus compare proliferative rates or *in vitro* lifespan of cultures. Incubating cells with compounds such as thiazolyl blue tetrazolium bromide (MTT) or Alamar Blue enables more sensitive detection of proliferative rate within a defined time period, and both represent higher-throughput approaches to measuring cell proliferation. Other assays, such as measurement of BrdU incorporation, enable the measurement of cell cycle distribution within a cell population at a given time. Different proliferation assays provide different information about the cell culture of interest. For example, with an MTT assay, the number of viable cells at the endpoint is assayed, by the yellow tetrazole reagent being reduced to a purple formazan product by intracellular reductase enzymes. Higher rates of conversion to formazan in a test cell line compared to controls, could result from increased proliferation, reduced cell death, or higher cell density (e.g. due to loss of contact inhibition of proliferation).

Heterotypic Assaya can be performed to monitor the effect of transformed cells on co-cultured endothelial, immune cells or other stromal cells. These assays can be used

to test if any pro-angiogenic factors are being produced, for example. Tests can also be performed to measure the ability of a cell line to illicit an immune response or recruit stromal cells. Synthesis of specific molecules can also be measured by Western blot or PCR ELISA.

Tumour Formation in Mice Cell lines can be injected into immuno-compromised mice to assay tumour formation efficienies *in vivo*. Xenograft injections can be into a specific organ, the mammary fat pad, the peritoneum or a subcutaneous site. The latency period, histopathology, metastatic activity and aggressiveness of the tumour will give further insight into the characteristics of the *in vivo* transformed phenotype of that cell line.

1.5.3 Transformation with Oncoproteins

Early *in vitro* models of cellular transformation treated cells with radiation and chemical carcinogens to damage DNA and induce neoplastic transformation. Such techniques cause widespread, non-specific damage to the genome. Hahn and collegues produced the first model of cell transformation using specific genetic elements in 1999 by expressing *hTERT* in human epithelial and fibroblast cell lines in combination with the SV40 large T antigen and an oncogenic *HRAS* allele [Hahn et al., 1999].

The use of viral oncoproteins, such as SV40 polyoma virus small and large T and E6/E7 proteins from HPV16 virus have been used extensively in studies of transformation. The E6 and E7 oncoproteins inactivate *p53* and *pRb*, though without conferring the ability of the cell to grow in an anchorage-independent fashion. The SV40 large T antigen (SV40-T) also exerts an oncogenic effect through the binding and inactivation of *p53* and *pRb*. The small t antigen (SV40-t) perturbs the PI3K pathway through protein phosphatase 2A (PP2A). PP2A is a serine/threonine phosphatase that plays a role in the PI3K signalling pathway and stability of *C-MYC* [Arroyo and Hahn, 2005]; [Boehm et al., 2005]. The entire SV40 early region is required for transformation, and it has since been demonstrated that inactivation of *pRB* and *PTEN* using shRNAs will have an equivalent effect as the introduction of SV40 T/t into BJ fibroblasts expressing *hTERT*, *C-MYC* and activated *RAS* in the presence of inactivated TP53 [Boehm et al., 2005].

Hahns model of transformation has since been applied to a variety of cell types, including human mammary epithelial cells (HMECs) and NOSE cells [Elenbaas et al., 2001]; [Kusakari et al., 2003]; [Liu et al., 2004]. In HMECs expressing SV40-T, *hTERT* and $HRAS^{mut}$, the tumourigenicity of the cells was directly proportional to the expression level of oncogenic *HRAS*. Cells with >12-fold overexpression of mutant *HRAS* form tu-

mours in nude mice at high frequencies. A threshold level of *HRAS* overexpression was required for *in vivo* growth, cells with only 3.5-fold *HRAS* overexpression failed to form tumours in mice [Elenbaas et al., 2001].

NOSE cells expressing both *hTERT*, SV40-T and either oncogenic *HRAS* or *ERBB2* grew in soft agar and form undifferentiated tumours in mice at frequencies of 40% and 50% respectively [Kusakari et al., 2003]. In NOSE cells which have been immortalised by co-expression of *hTERT* and SV40T/t, expression of a mutated *KRAS* or *HRAS* generates highly tumourigenic cells that form large tumours when injected into nude mice. The resulting tumours showed many characteristics of human ovarian epithelial cancers [Liu et al., 2004].

1.5.4 Transformation with Defined Genetic Elements

p53 and *pRB* have been identified as crucial targets of SV40T/t for tumourigenesis, but these oncoproteins do have additional effects within the cell [Arroyo and Hahn, 2005]. Thus, this study aimed to create genetic models of NOSE cell transformation through the expression of oncogenes that are known to be involved in EOC, with an aim of mimicking *in vitro*, early tumourigenesis of the ovarian surface epithelium through genetic events that could feasibly occur *in vivo*.

This study will also identify the minimal number of genetic alterations required to induce features of transformation in a phenotypically normal ovarian surface epithelial cells. In Leiden cells, which are *p16*-deficient, expression of *hTERT*, plus mutant *HRAS* or *C-MYC* confers an ability to grow in an anchorage-independent manner. Leiden cells expressing *hTERT*, $HRAS^{G12V}$ plus *C-MYC* form tumours in nude mice [Drayton et al., 2004].

A recent study by Sasaki and collegues has investigated the role of different cellular oncogenes in transformation of the OSE [Sasaki et al., 2009]. Their results are summarised in Table 1.7. They observed that one cell line was more susceptible to transformation than the other, suggesting that genetic background plays an important role in neoplastic development. A dominant negative *p53* allele (DNp53) and $KRAS^{G12V}$ was sufficient to confer *in vivo* growth of immortalised NOSE cells, cells in this study were immortalised with *hTERT*, Cdk4 and cyclinD1). The other cell line needed either additional expression of mutant *Akt*, or mutant *C-MYC* and *Bcl-2* overexpression in order to grow *in vivo*.

Genetic Alterations	*Comments*	*Anchorage-independent growth*	*Growth in vivo - subcut*	*Growth in vivo – i.p.*
HOSE2C				
+ $KRAS^{G12V}$	*Extensive cell death*	*N.R*	*N.R*	*N.R*
+ Dnp53 + $KRAS^{G12V}$	*⇧proliferation*	+	0/4	0/9
+ Dnp53 + $KRAS^{G12V}$ + $CMYC^{mut}$	*⇧ proliferation; small, rounded cell morphology*	+++	0/3	0/10
+ Dnp53 + $KRAS^{G12V}$ + myr-Akt1	*Fibroblastic cell morphology*	++	3/3	($1x10^6$) 10/16 ($1x10^7$) 3/3
+ Dnp53 + $KRAS^{G12V}$ + $PIK3CA^{mut}$	*⇧ proliferation; small, rounded cell morphology*	++	0/3	0/3
+ Dnp53 + $KRAS^{G12V}$ + shRNA.PTEN	*No change in morphology*	+	0/3	0/3
+ Dnp53 + $KRAS^{G12V}$ + $CMYC^{mut}$ + Bcl2	*⇩ apoptosis*	+++	*N.R*	($1x10^6$) 9/9 ($1x10^7$) 3/3
HOSE1C				
+ Dnp53 + $KRAS^{G12V}$	*Small tumours*	*N.R*	*N.R*	2/6
+ Dnp53 + $KRAS^{G12V}$ + $CMYC^{mut}$ + Bcl2	*Extensive dissemination throughout peritoneum*	*N.R*	*N.R*	($1x10^6$) 6/6 ($1x10^7$) 3/3
+ $KRAS^{G12V}$ + $CMYC^{mut}$ + Bcl2	*Intact p53 function*	+++	12/12	*N.R*

Table 1.7: Transformation of the OSE with defined cellular oncogenes, results from Sasaki *et al.* 2009. N.R=not reported. The mutant *C-MYC* allele is more stable than wild-type *C-MYC*, thus *C-MYC* protein accumulates in the cell. The mutant *PIK3CA* allele used in this study contains a mutation commonly found in EOC. subcut = subcutaneous injection of cells, i.p. = intra-peritoneal injection of cells. Numbers of xenografted cells are indicated in brackets.

1.6 Whole Transcriptome Profiling

Although nuclear DNA encoder the entire genome of the organism, only a portion of the total gene complement is actively transcribed in each cell. A small number of housekeeping genes, (e.g. *GAPDH* or *18S* rRNA), are expressed in all cell types. However, the majority of genes are expressed in a tissue-specific, cell-type specific or temporal-specific manner. Many genes are only expressed transiently, in response to intra- or extracellular stimuli. The complexity is compounded by the fact that during tumourigenesis, the gene expression profile of cells evolves as the tumour develops. Profiling the transcriptomic changes with expression microarrays has become a common tool used by scientists to create molecular descriptions of tumours and tumour subtypes. By identifying differentially expressed genes many new potential cancer biomarkers have been identified. Additionally, markers or profile signatures have been identified that can predict patient outcome or therapeutic responses.

1.6.1 Gene Expression Microarray Technologies

There are a number of different microarray platforms available for performing transcrptomic analyses. Some are based on Cy3/Cy5 labelling of test and reference samples that are then co-hybridised to the same array chip and the relative intensities of each dye are analysed. Due to the different stability of the two dyes it is often necessary to perform dye-swap experiments. Other platforms technologies do not use a reference sample, and the signal intensity of each probe indicates transcript abundance.

Robust experimental design of gene expression microarray studies is key to obtaining reliable data. At every stage there are important considerations:

Samples

What is the biological question being asked and how can this be modelled experimentally? What comparisons will be made and which biological and technical controls must be included?
Does this require human or animal tissues to be used?
Primarily it is important that all RNA samples are be collected, harvested and quantified following an consistent protocol, to ensure that any differentially expressed genes identified have not been due to differences in sample collection, harvesting or processing. Samples with low RNA concentrations may require additional amplification steps, if so it is important to ensure consistency of pre-hybridization processing of the RNA samples within an experiment.

Array Platform

The choice of array platform will be determined by the samples, the aim of the experiment and the budget. The Affymetrix U133A platforms are a widely used platform, and if meta-analyses are to be performed it may be preferable to use this platform. Specialised arrays are available to analyse expression of different transcript isoforms, these arrays would be ideal for profiling in detail the transcriptional effects of a single gene.

The Illumina HT12 arrays used in this study are considerably cheaper that the Affymetrix U133A arrays but still have good coverage of the genome whilst enabling higher numbers of replicates to be performed. By using the highest number of biological replicates possible, the researcher increases the reliability of gene lists obtained. Furthermore, the Illumina

BeadChips have been demonstrated to outperform other arrays in a number of technical measurements [Consortium et al., 2006].

The Illumina HT12 arrays have a unique 'bead-array' design. 50-mer oligos are synthesized that are complementary to specific gene targets. The probe sequences are selected using a bioinformatic algorithm that considers many factors, including similarity to other genes, sequence complexity and EST coverage, to ensure that probes are gene-specific and match to multiple EST and cDNA databases. These carefully designed oligos are then immobilized onto 3μm silica beads, and the beads are pooled. The beads are then loaded onto a 'BeadArray'. Each bead is found on the array at least 30 times, equating to a high level of sequence redundancy and thus the ability to calculate average signal and variance per gene. Other microarray platforms typically contain each probe only once. Replicate beads are located throughout the BeadChip, thus reducing the chance of spatial effects distorting gene expression information.

Data pre-processing

Once arrays have been run, the extracted data must first be subjected to a number of pre-processing steps. Firstly, quality control (QC) analysis of the array data is performed to check that across the whole experiment, the arrays have consistent values for labelling controls, signal/noise ratios, hybridization controls, washing stringency controls and negative controls. Many array platforms spike the test RNA sample with control RNA that is co-hybridized to the array along with the sample and acts as internal controls for this QC step.

Pre-processing of microarray data prepares the data for gene-expression analyses by performing background subtraction, transformation and normalisation steps. This is to ensure that any changes in gene expression fold-change are not due to spatial effects, hybridisation artefacts or local background signal. Background correction is used to remove any non-specific signal present on the array, prior to any analysis steps being performed. A variance-stabalizing transformation (VST) step, is a logarithmic transformation algorithm which utilises the variance across the techical replicates within each array (i.e. replicate beads) to predict the confidence intervals of the data. This step is most critical when calculating the significance of differentially expressed genes, in particular high fold-change in the low expression range. Transformed data is then normalised to normalise data across all chips in the experiment. There are many different approaches to data normalisation, including quantile normalisation, simple scaling normalisation and loess normalisation. Robust spline normalisation (RSN) combines features of quantile and loess normalisation

algorithms and was developed with some of the limitations of each technique in mind. For example, loess transformation assumes that the majority of genes are not differentially expressed and that the data are symmetrically distributed, but assumptions may not be applicable to all array datasets. With RSN normalistion, data are first normalised using a quantile normalisation algorithm; secondly a fold-change value is calculated for each probe. Each method has basic assumptions which may make that technique more or less appropriate to a specific experiment and so the researcher must decide which is appropriate to each specific experiment, though, as with all steps of data analysis there is no agreement in the field regarding which method is 'correct'.

Data analysis

Firstly, to analyse and visualise the data from a microarray experiment, clustering of the samples enables groups of data to be organised into hierarchical dendogram trees, in which more closely related samples cluster together. Supervised clustering can also be performed, in which prior knowledge or a training dataset may be used to intelligently cluster the data. Clustering analyses are often employed to group tumour profiles, to look for relatedness between samples and perhaps identify new molecular subgroups.

Secondly, normalised data from a microarray experiment can then be analysed to create gene lists of differentially expressed genes. Ideally, the gene lists across biological replicates can then be compared to create lists of interesting candidate genes that are common across biological replicates. As with data normalisation there are many different approaches to the analysis of differentially expressed genes from microarray experiments. Genes lists can be generated, detailing the most statistically significant changes in gene expression. Alternatively, genes can be ranked by fold-change in gene expression. Typically, change in gene expression of a test sample is calculated relative to a control sample. A fold-change cut-off may be applied - usually a two-fold increase or decrease in gene expression between the test and control sample. With this approach it is extremely important to have appropriate controls for each test sample. It is also important to have technical and biological replicates to reduce frequency of false-negative and false-positives hits that occur by chance in each array. In platforms that do not return absolute values of gene expression for each gene, it is important to have an appropriate biological control and consistent labelling and hybridisation efficiencies to identify statistically different changes in gene expression across different arrays. This is the approach required for the Illumina HT12 platform. Other array platforms enable the co-hybridisation of two samples, by co-hybridising a common control RNA sample across a set of arrays it is possible to calculate absolute measurements of gene expression. Many packages are available for the analysis of

microarray data and the generation of lists of differentially expressed genes in a microarray experiment. A popular choice is the Linear Models of Microarray' or 'limma' package which can be used in 'R' [Smyth, 2004]. Limma enables the simultaneous analysis of many RNA targets across arrays, data are corrected for multiple testing and the resulting expression data matrix can then be used to either identify the top differentially expressed genes or perform clustering analyses.

1.6.2 Functional follow-up of candidate biomarkers

The gene expression profile of a cell contains a wealth of information that correlates to cell behaviour and phenotype, yet understanding the function of individual genes remains immensely challenging. The Human Genome Project has annotated the whole human genome, yet the function of only a minority of the encoded genes and DNA sequences is understood. Understanding the functional biology of a specific gene is usually laborious, technically challenging, and requires lengthy *in vitro* and *in vivo* experimentation. The scientist is often challenged by different mRNA or protein isoforms of that gene, the differential regulation of transcription or protein activity, by protein-protein interactions and by cell type or cell context dependent changes in gene function. Gene expression patterns are controlled by many genetic enhancers, which themselves may be active only in specific contexts. Thus, many projects now aim to use bioinformatic tools to identify molecular fingerprints of tumours that indicate the tumour origin, stage, differentiation, histotype, or clinical behaviour. Such approaches reiterate the fact that that mRNA profiles represent many complex interacting biological pathways that co-ordinate to ultimately determine cellular phenotype and, in the case of tumours, tumour features and behaviour. When working with *in vitro* models, this approach is dependent on good collaborations between bench scientists and expert bioinfomaticians who, importantly, need to be working with a common goal in mind.

1.7 The Role of the Microenvironment

In vitro models of human disease are limited by the restricted ability of the scientist to reproduce *in vivo* environments within the laboratory. Changes in cell shape, tissue geometry, matrix proteins, oxygen and nutrient gradients and the absence of other cell types will all alter cellular phenotype and therefore may interfere with the study of a biological process. Three-dimensional (3D) and heterotypic models aim to restore *in vitro* some features of the tissue *in vivo* that may be lost under rountine 2D culture conditions.

1.7.1 Three-dimensional Cell Culture Models

In vivo, cells are surrounded by a complex extracellular matrix (ECM). Cells contact and communicate with a host of different cell types through receptors distributed throughout the entire cell surface. However, a 2D monoculture consists of clonally derived cells that only communicate along a small proportion of their membrane. This is a major limitation, and so 3D culturing techniques can be employed to try to re-create tissue features and geometry and thus improve the biological relevance of *in vitro* models. There is now substantial evidence to suggest that 3D cultures more closely resemble the *in vivo* microenvironment than 2D cultures, and that culturing cells in 3D can cause phenotypic and molecular changes that reflect the *in vivo* biology of the cell more closely than 2D cultures [Knuechel et al., 1990]; [Zietarska et al., 2007]; [Ghosh et al., 2005]. Additionally, cells that are traditionally difficult to culture in 2D, such as primary hepatocytes, can often be maintained *in vitro* for longer periods when grown in 3D [Khaoustov et al., 1999].

The precedent for modelling the microenvironment was set by Mina Bissell and collegues in the 1990s. Human mammary epithelial cells (HMECs) grown in laminin rich Matrigel formed polarised, growth arrested structures with a central lumen, structures that were closely reminiscent of breast acini [Petersen et al., 1992]; [Weaver et al., 1995]; [Howlett et al., 1995]; [Weaver et al., 1997]. Initially, growing cells in 3D was considered to be costly and time-consuming, without inferring a significant advantage over conventional 2D culturing techniques. Yet Bissell and many other groups have now demonstrated that growing breast epithelial cells in 3D cultures restores functional differentiation of cells. HMECs in 3D express milk proteins (caseins) [Weir et al., 2006]. Caseins are never expressed by these cells when in 2D culture, but expression of these proteins are characteristic of HMECs *in vivo*. Many cell types have now been shown to restore expression of functionally relevant proteins when transferred from a 2D to a 3D modelling system.

Several different approaches can been used to establish 3D cell culture models. The most well described is the growth of cells in 3D using ECM protein gel scaffolds (such as collagen gels or Matrigel). Synthetic scaffolds can also be used, plus other techniques which prevent cell adherence to tissue culture plastics and hence encourage cells to adhere to each other and form multicellular aggregates. Such systems include the rotary cell culture system (RCCS) or polyHEMA coating tissue culture plastics. Reports of culturing ovarian cancer cells in 3D focus on the tumour cell aggregates found in ascitic fluid which have been used to model EOC metastasis *in vitro* [Burleson et al., 2004a]; [Burleson et al., 2004b]; [Burleson et al., 2006] [Zietarska et al., 2007]. 3D culturing of normal ovarian epithelial cells has also been described [Kwong et al., 2009]; [Lawrenson et al., 2009a] (Table 1.8).

		Cell shape/ Architecture of culture	Advantages	Disadvantages	References – normal/malignant ovarian cells
2D Monolayer		Flattened, altered morphology, polarity lost	Cheap, simple to use and manipulate	Limited ECM Unnatural geometry	Many. OSE: first published by Auersperg *et al*., 1984
3D Culture Technique	ECM Gels	Polarity and other biological functions restored (breast epithelium) Signalling interactions with ECM restored	Can be transplanted in vivo Developed to emulate ECM in vivo	Pre-defined ECM components may not reflect tissue of origin	Ohtake *et al*., 1999 Kwong *et al.,* 2009
	RCCS	Cell line dependent size of spheroid Restored features of in vivo tissue	Reduced shear forces compared to spinner flasks Simulated microgravity Cells provide ECM	Expensive, limiting size of vessels and number of docks May induce cell damage in some cell lines	Grun *et al*. 2009 Lawrenson *et al*. 2009
	polyHEMA coated plastics	Cell line dependent size of spheroid Restored epithelial features of in vivo tissue	Cheap, simple to establish and manipulate Can grow in large scale Cells allowed form cultures of un-prescribed architecture and lay down the ECM	Some cell types will not form spontaneous multi-cellular spheroids In large-scale cultures, there is a variety of sized spheroids	Lawrenson *et al*. 2009 Sonoda *et al*., 2003
	Scaffolds	Controlled size of multicellular structure Supportive matrix	Can be transplanted in vivo Can be tailored to resemble tissue *	Expensive, vary in their ability to resemble different tissues	

Table 1.8: Three-dimensional cell culture techniques, advantages and disadvantages ∗ Reviewed in [Lee et al., 2008]. Published 3D models of ovarian epithelia (normal or malignant) are summarised.

Different 3D culture techniques are not equivalent in their effectiveness. In one study, Ghosh *et al.* cultured melanoma cells in collagen gels and found gene expression profiles were similar to that of cells in 2D; and yet when cells were grown on polyHEMA coated plates, they observed the differential expression of >150 genes. Many of the genes upregulated in polyHEMA 3D cultures were consistent with their upregulation *in vivo* [Ghosh et al., 2005]. Thus, in this present study, two 3D culture techniques were compared as models of primary NOSE cells *in vitro* [Lawrenson et al., 2009a]. The purpose of this approach was to evaluate the biological effects of two different 3D culturing techniques on the culture of primary normal ovarian surface epithelial cells, and to establish a 3D model of NOSE cells that could be used to study the earliest stages of neoplastic transformation in epithelial ovarian cancer. The optimisation of 3D modelling techniques is described in Chapter 3 and applications of the 3D models in Chapters 4 & 5.

1.7.2 A Role for Senescent Fibroblasts in Ovarian Epithelial Tumourigenesis?

3D cultures aim to restore tissue geometry. An alternative tool that cell biologists use to improve conventional 2D *in vitro* monoculture models is heterotypic culturing. In heterotypic cultures, it is hypothesised that the different cell types surrounding the cell of interest can affect the target cell phenotype and may be important for normal functional

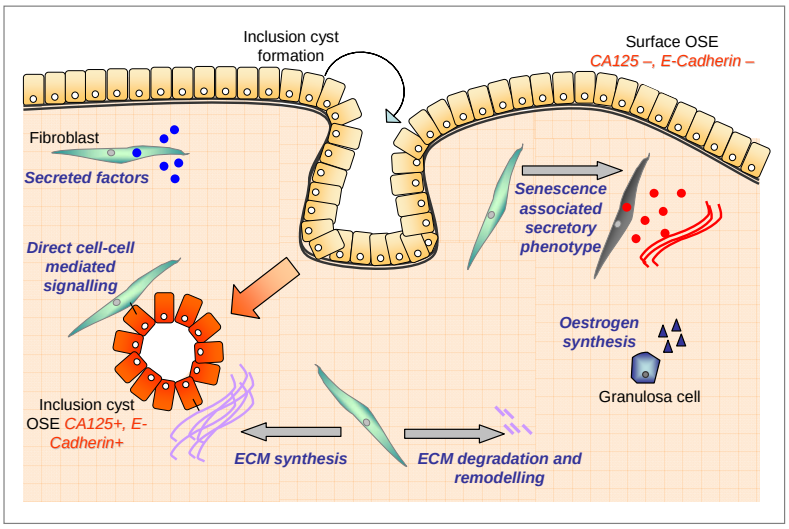

Figure 1.10: Stromal extracellular matrix proteins (ECMs) and molecules secreted by stromal cells (e.g. fibroblasts and granulocytes) can affect epithelial phenotype. Such molecules include hormones (e.g. oestrogen) and a myriad of proteins sythesised by fibroblasts. Upon senescence, fibroblasts become increasingly secretory (the "senescence-associated secretory phenotype" [Coppe et al., 2008]. Ovarian surface epithelial cells within inclusion cysts have a more committed epithelial phenotype (E-Cadherin+, CA125+), presumed to be due to closer interactions with the mitogen rich stroma.

differentiation. In this present study, the effect of ageing stromal fibroblasts on epithelial transformation is explored.

In vivo, stromal fibroblasts play the central role in the structure of tissue architecture, though dynamic regulation of the extracellular matrix components (Figure 1.10). As an organism ages, the senescent fibroblasts accumulate in the tissue stroma, gradually replacing pre-senescent cells [Herbig et al., 2006]; [Jeyapalan et al., 2007]. Senescent cells are metabolically active, and the profile of secreted proteins has been demonstrated to be vastly different than their non-senescent counterparts [Coppe et al., 2006]. The induction of senescence induces a senescence-associated secretory phenotype (SASP); senescent fibroblasts secrete a myriad of growth factors (including VEGF), extracellular matrix proteins, proteases, chemo- and cyto-kines (Figure 1.10). This spectrum of molecules affects the phenotype of neighbouring epithelium directly and indirectly (through remodelling of the extracellular matrix or the effects on other cell types, such as endothelial cells) [Coppe et al., 2006]; [Coppe et al., 2006]. Furthermore, senescent cells have enhanced expression of proteins associated with an acute inflammatory response, such as matrix metalloproteinases (MMPs) [Parrinello et al., 2005]. *In vivo* xenograft modelling also suggests that the pro-tumourigenic effect of senescent fibroblasts may be due in part to the en-

hanced ability of senescent fibroblasts to illicit an inflammatory response compared to normal fibroblasts [Liu and Hornsby, 2007].

1.8 Aims of this study

Molecular events that occur during EOC initiation remain poorly understood. Progress in *in vitro* modelling of EOC tumourigenesis has been hindered by difficulties in culturing the normal cell precursor. Therefore, 3D models were hypothesised to be an approach of NOSE cell culture that may more closely reflect the cells *in vivo* than traditional 2D monolayer cultures. This is described in Chapter 3.

This study aimed to create an *in vitro* model of neoplastic transformation of the ovarian surface epithelium. Genes known to be involved in low-grade and high-grade serous EOCs and mucinous EOCs, namely *CMYC*, $KRAS^{G12V}$ and $BRAF^{V600E}$ were introduced into immortalised OSE cells to create a stepwise model of transformation (Chapter 4). The transformed phenotype associated with the expression of each gene/gene combination were analysed using a panel of *in vitro* assays. Gene expression profiles were generated to profile transcriptomic changes associated with *CMYC*, $KRAS^{G12V}$ and $BRAF^{V600E}$-driven transformation. In Chapter 4 novel genes are described that represent potential biomarkers of early-stage disease.

Finally, heterotypic models were developed, consisting of epithelial and fibroblastic cell lines. The effects of senescent and pre-senescent fibroblasts on the neoplastic phenotype of ovarian epithelial cells was assayed using 2D and 3D co-culture assays (Chapter 5). This final Chapter explores functional modelling of an epidemiological observation (most EOCs occur in older women), using an *in vitro* cell biology model.

2

Materials and Methods

2.1 Cell Culture & Establishment of Primary Cell Lines

2.1.1 General Equipment and Solutions

All cell culture was performed in a laminar-flow safety cabinet (Heraus), and cells were incubated in an Heracell incubator (Heraus) at 37 °C with 5% or 10% CO_2, according to the requirements of each cell line. Cells were grown in tissue-culture treated disposable 60mm, 100mm and 145mm dishes, 25 cm^2, 75 cm^2, 175 cm^2 flasks, or multiwell plates (all Greiner). Disposable 15ml or 50ml tubes (Greiner) were used to centrifuge cell suspensions. All glassware was cleaned and autoclaved by heating to 121^{o}C for 15 minutes at a pressure of 103kPa to sterilise.

2.1.2 General Tissue Culture Methods

Media and Solutions

All tissue culture media were stored at 4 °C. Antibiotic and growth factor solutions were stored at −20 °C. G418 (Sigma) and blasticidine S hydrochloride (Sigma) solutions were prepared in double distilled water (DDW) and filter sterilised through a 0.2μM filter. Puromycin solutions (Sigma) were prepared in methanol (Sigma). Zeocin (Invitrogen) and Hygromycin (Calbiochem) were purchased as solutions from the manufacturer and used as provided or diluted 1:10 in sterile DDW. Cells were washed with sterile 1X phosphate-buffered saline (PBS) (VWR). A 10X PBS solution was diluted 1:10 with DDW and the

1X solution was then autoclaved to sterilise.

Foetal bovine serum (FBS) was purchased from Invitrogen or Lonza and batch tested before use. Briefly, cells were selected which were known to be particularly sensitive to serum (normal ovarian fibroblasts or syrian hamster embryonic fibroblasts). Cells were mass cultured in the test serum for a minimum of 7 days before plating at clonal density (100 cells per well in a 6 well plate, in triplicate). Cultures were re-fed every 2-3 days and stained with crystal violet. To stain cells, cultures were fixed in 100% methanol (VWR) for 10 minutes and then rinsed with DDW. Cultures were then stained with 0.5% crystal violet (Sigma) solution (in DDW). After 10 minutes plates were rinsed extensively with DDW and allowed to air dry. Colonies were then counted. Colony formation efficiency (CFE) was calculated using the following formula.

$$\text{CFE } (\%) = \left[\frac{\text{Total Number of Colonies}}{\text{Inital Number of Cell Plated}}\right] * 100\%$$

Mass cultures were continued in parallel and observed under the light microscope for gross changes in culture morphology.

Passaging, Cryopreservation and Counting of Cells

To split or passage cells, cell monolayers were washed with 1X PBS and cells were detached using 1X Trypsin-EDTA (Invitrogen). After 2 to 5 minutes incubation at 37 °C, cells detached from the plastic flask or dish. Trypsin was then neutralised with an equal volume of complete media, and the cell suspension was collected and centrifuged at 1,500g for 5 minutes to pellet cells. The supernatant was then aspirated and the cell pellet resuspended in complete media for replating, or in a freezing solution for cryopreservation.

Freezing solutions were prepared using 10% DMSO (Sigma) in FBS or Newborn Calf Serum (NCS) (Invitrogen). 1ml of cells suspended in freezing solution was aliquotted into 1.8ml freezing vials (Nunc) and the vials were stored in a Mr Frosty container for at least 3 hours, to slowly cool at 1 °C per minute before cells were transferred into liquid nitrogen for storage at −196 °C.

To count cells, cells were detached from the tissue culture dish or flask by trypsinisation. Cell suspensions were centrifuged at 1,500g for 5 minutes with an equal volume of complete medium. The supernatant was aspirated and cell pellets flicked to loosen from the side of the tube. Cells were then completely resuspended in growth medium and counted using a

hemocytometer (Neubauer).

2.1.3 Mycoplasma Screening

Cell cultures were regularly tested for the presence of contaminating mycoplasma. Mycoplasma infections can persist in cell cultures without causing turbidity of the cell culture media. Such infections induce gene expression and phenotypic changes in host cells, and are difficult to eliminate from cultures once infected. Furthermore, mycoplasmas are often resistant to many of the antibiotics routinely used in tissue culture media.

Two methods of mycoplasma detection were used: Hoescht staining and polymerase chain reaction (PCR). Hoescht fluorescently stains DNA, and hence mycoplasma are visible with a fluorescent microscope. This method can detect mycoplasa at a concentration of $>10^6$cfu/ml, thus, prior to staining, cells were incubated for a minimum of two weeks in antibiotic-free media to allow any low-level infections to expand. Cell cultures, grown on coverslips, were fixed in freshly-made Carnoy's fixative (3:1 methanol:acetic acid, both Sigma) using the following protocol:

1. 3mls fixative was added to cell culture media, and incubated for 5 minutes at room temperature
2. Fixative solution was then aspirated, replaced with 5 mls fresh fixative and incubated for 5 minutes
3. Step 2. was repeated, and coverslips washed with DDW and air dried
4. 50μl Hoescht bisbenzimide 33258 solution (Sigma, 0.05μg/ml in DDW) was then added to coverslips, and cells were visualised by fluorescent microscopy. Positive cells can be identified by bright spotty cytoplasmic staining (mycoplasma DNA). In cultures that are free of contaminating mycoplasma, only the cell nuclei should be detected. For analysis of staining, positive and negative controls were stained in parallel.

For mycoplasma screening by PCR, 1ml medium was removed from cell cultures (pre-incubation without antibiotics is not required for this protocol). Media aliquots were spun at 13,000rpm for 30 minutes, and the majority of the supernatant removed (to leave 20μl remaining). Pellets were resuspended in 50μl of TE buffer (10mM Tris-HCl with 1mM EDTA) with added Proteinase K (Sigma, 200μg/ml final concentration), and incubated for 1h at 55 °C. Finally the enzyme was deactivated by incubation at $98 - 100$ °C for 10

min (both incubations were performed in dry heating blocks to avoid contamination risk of water baths).

The following primers detect of all members of Mollicutes class, which include all mycoplasmas (and also ureaplasmas and spiroplasmas). All different mycoplasma species can be detected with the following primers, targeting the 16S rRNA gene:

Forwards primer (MYCO-F): 5'-GGGAGCAAACAGGATTAGATACCCT-3'
Reverse primer (MYCO-R): 5'-TGCACCATCTGTCACTCTGTTAACCTC-3'

A standard PCR was run, with a negative control (water) and a mycoplasma contaminated cell line as a positive control.

Reagent	**Volume per reaction**
milliQ H_20	7.38μl
25mM $MgCl_2$	1.5μl
2.5mM dNTPs	1.5μl
10X buffer (Promega)	1.5μl
Forwards primer	1μl
Reverse primer	1μl
Taq Polymerase (Promega)	0.12μl
Sample	1.00μl

2.1.4 Culture Conditions: Non-Ovarian Cells

NIH3T3 Swiss mouse kidney fibroblast cells were grown in Dulbecco's Modified Eagle's Medium (DMEM, Sigma) supplemented with 10% NCS and 2mM L-Glutamine (Invitrogen). The cells were incubated at 37 °C, 10% CO_2.

BRM-1 human embryonic fibroblast cells were grown in DMEM supplemented with 15% FCS and 2mM L-Glutamine. The cells were incubated at 37 °C, 5% CO_2.

293T human embryonic kidney cells (gift from M.Anesti) were grown in DMEM supplemented with 15% FCS, 2mM L-Glutamine, 1X Non-Essential Amino Acids (NEAA) and 2mM Sodium Pyruvate (both Sigma). The cells were incubated at 37 °C, 5% CO_2.

Phi-Nx cells (Orbigen), a 293T-based packaging cell line, were grown in DMEM supplemented with 15% FCS and 2mM L-Glutamine. The cells were incubated at 37 °C, 10% CO_2.

MCF7 breast cancer cells were grown in DMEM supplemented with 10% FCS and 2mM

L-Glutamine. The cells were incubated at 37 °C, 10% CO_2.

When required, 1X Penicillin and Streptomycin (Invitrogen) were added although the use of antibiotics was avoided where possible.

2.1.5 Tissue Collection

All tissues were collected from University College Hospital. All tissues were collected with informed consent from donors, according to a protocol approved by the Joint UCL/UCLH Committees on the Ethics of Human Research (Committee Alpha).

For collection of primary tissue, 50μg/ml gentamicin sulphate (Sigma) was added to the collection medium. Ovarian surface brushings or stromal biopsies were collected in complete growth medium and taken immediately to the laboratory for processing, as described below.

2.1.6 Establishment of Normal Ovarian Surface Epithelial Cell Lines

A modified growth medium (NOSE-CM), is recommended for the culture of primary normal ovarian surface epithelial (NOSE) cell isolates [Li et al., 2004a]. This medium consists of MCDB105 and Medium 199 (both Sigma) in a 1:1 ratio and supplemented with 15% FBS, 34μg protein/μl bovine pituitary extract (BPE) (Invitrogen), 5μg/μl insulin, 10ng/μl epidermal growth factor (EGF), and 0.5μg/μl hydrocortisone (all Sigma). MCDB105 was purchased as a powder and prepared, according to manufacturers instructions, to pH6.5 and then filter sterilised into sterile bottles.

Normal ovarian surface epithelial cells were collected from patients with disease-free ovaries undergoing total laparoscopic/abdominal hysterectomy. The surface of the ovaries were gently scraped using a sterile Transwab brush swab (Medical Wire and Equipment Ltd) and the cells were plated in NOSE-CM by shaking the cytobrush in a tube of complete medium, and then transferring the medium in a 25cm^2 flask at 37 °C and 5% CO_2. Cultures were left undisturbed for 5-7 days, until the cells begin to colonise. The medium was then replaced every 2-3 days, and cells were incubated until flasks become around 50% confluent. Cells were then trypsinised as described above, and split in a ratio of 1:2-1:5, depending on the growth characteristics of each individual cell line.

2.1.7 Establishment of Normal Ovarian Fibroblast Cell Lines

Normal ovarian fibroblast cells were grown in MCDB105:Medium 199 in a 1:1 ratio, supplemented with 15% foetal bovine serum and 2mM L-glutamine. A piece of ovarian stroma was isolated by a Pathologist following removal of the specimen from the patient. Tissue was removed from the collection medium and washed twice with 1X PBS to remove loosely attached epithelial cells. Tissues were then placed into a P100 dish, and minced using sterile forceps and a scalpel. 20mls of medium was then added to the dish and cells were then incubated, undisturbed, for 7 days. Cultures were then refed every 2-3 days and the growth of fibroblastic colonies (swirling clone morphology, cells have an elongated morphology compared to OSE) was monitored using a light microscope.

Fibroblastic colonies were isolated using either ring cloning or cloning disks (Sigma). Clones were incubated in 6-well plates and stained for fibroblastic and epithelial markers (see below) before immortalisation.

2.1.8 Drug Dose Response Assays

A confluent P100 dish of cells was trypsinised and split equally into 10 P60 dishes. The following day the media was changed and varying concentrations of the drugs was added: Puromycin 0-1000 ng/ml, G418 0-1000 μg/ml, hygromycin B 0-100 units/ml, blasticidine S hydrochloride 0-10 μg/ml.

The cells were incubated undisturbed for 7 to 10 days, and the media was replaced every 3 to 4 days. After the 7 to 10 day incubation, plates were fixed and then stained with Coomaasie blue (Sigma), dissolved in DDW. To stain the cells the media was discarded and cells fixed with 5ml methanol for 10 minutes. Cells were washed with water and then stained with Coomaasie blue for 10 minutes. Excess dye was rinsed off with DDW and plates air dried and cell colonies were counted by naked eye or by light microscopy.

Kill curves were performed to obtain the optimal doses of selective antibiotics. 10-30U/ml hygromycin was used to isolated *hTERT*-expressing clones. Single mutant clones were selected with 400ng/ml puromycin or 125μg/ml G418. IOSE^{CMYC} cells were tolerant of much higher concentrations of G418 than the IOSE cell lines. IOSE11$^{CMYC.KRAS}$ clones were selected with 333μg/ml G418; IOSE19$^{CMYC.KRAS}$ clones were selected with 1mg/ml G418; and all IOSE$^{CMYC.BRAF}$ clones were selected with 400ng/ml puromycin.

2.1.9 Transfection with FuGene^{TM}6

Cells were plated at 50 to 80% confluency one day prior transfection with FuGene^{TM}6 (Roche) transfection reagent. On the day of transfection the reagent was prepared in serum free media (SFM) according to manufacturers instructions. To transfect a P100 dish at a 3:1 ratio of reagent to DNA, 18μl FuGene^{TM}6 transfection reagent was added to 582μl SFM in a sterile 1.5ml microcentrifuge tube, without allowing the reagent to touch the plastic sides of the tube. The mixture was then vortexed for one second and incubated at room temperature for 5 minutes. 6μg DNA was then added to the diluted reagent (keeping the total volume of added DNA solution to between 0.5 and 50μl). The mixture was then vortexed for 1 second to mix and incubated for 15 minutes minimum at room temperature. A control plate was transfected with reagent only, and DNA solution was substituted for SFM.

Cells to be transfected were then removed from the incubator. Removal of complete growth medium containing serum is not required. The contents of each microcentrifuge tube was then added dropwise to a P100 dish, and the medium was then swirled to distribute the transfection mixture throughout the dish. Cells were then returned to the incubator, passaged the following day, and antibiotic selection was begun on day 4.

2.1.10 Immunofluorescence Cytochemistry of Cultured Cells

Cells were grown on coverslips. The growth media was aspirated, and cells were washed with ice cold PBSAg (0.3% v/v fish skin gelatin (Sigma) in 1X PBS). Cells were then fixed for 10 minutes in cold 3% formaldehyde (VWR), the fixative was then aspirated and the cells rinsed well in PBSAg. Cells were then permeabilised by immersing the coverslips for 5 minutes at room temperature in 0.3% v/v Triton X-100 (Sigma) in PBSAg. Cells were rinsed in PBSAg and incubated for 10 minutes at room temperature in 50μl 1% v/v non-immune goat serum (Invitrogen). Serum was then gently aspirated off, and 50μl of optimally diluted primary antibody was immediately applied to the coverslips:

Anti-Ck7 (clone LP5K)	1:1000 dilution (CRUK)
Anti-fibronectin (FN-3)	1:1000 dilution (CRUK)
Anti-pan cytokeratin (clone AE1/AE3)	1:1000 dilution (Dako)
Anti-calretinin	1:1000 dilution (Dako)
Anti-BerEP4	1:1000 dilution (Dako)
Anti-CA125	1:1000 dilution (Dako)
Anti-E-Cadherin	1:2500 dilution (Cell Signalling)
Anti-FSP	1:1000 dilution (Sigma)
Anti-Factor 8 Related Antigen (clone F8/86)	1:1000 dilution (Lab Vision)

The cells were then incubated with antibody at room temperature for 1 hour, before the primary antibody was completely rinsed off with PBSAg and an Alexa Fluor-488 (1:2500 dilution, Invitrogen) secondary antibody applied. The cells were then incubated with the secondary antibody at room temperature for 30 minutes and protected from light. The cells were then rinsed in PBSAg and were incubated for 10mins in Evans Blue solution (Sigma), diluted in DDW 1% w/v . Coverslips were washed in 1X PBS and finally water before mounting onto a slide with mounting medium and 5μl DAPI (Vector Laboratories, Inc) was added before covering the cells with a coverslip. The mounted cells were then incubated for 30 minutes before viewing with an Olympus BX64 fluorescence microscope. Images were captured and analysed using Cytovision Genus 3.6 software.

2.1.11 Three-dimensional cell culture

Two protocols were tested for the generation of three-dimensional spheroids. Seeding densities, coating volumes and secondary assays for different 3D approaches are summarised in Table 2.1.

PolyHEMA coating of plastics

Poly-hydroxymethylacrylate (polyHEMA) solutions were prepared in 95% ethanol/5% distilled water. PolyHEMA solutions were incubated at 65 °C for 1-2 hours, until completely dissolved. Working within a tissue culture laminar flow safety hood, tissue culture plastics were then coated with the polyHEMA solution (4-5ml per P100 dish or F75 flask, also see Table 2.1). Coated plastics were then allowed to dry before a second coat was applied. Once completely dried, sterile coated plates were stored at ambient temperature until use.

To generate 3D cultures polyHEMA-coated plate/flask were washed with 1xPBS for 5 minutes. 2D monolayer cells were trypinised, pelleted and enumerated, as described above.

	polyHEMA or agarose solution volume	Approximate cell numbers (examples)	Recommended culture media volume	Examples of Secondary Assays
Rotary Cell Culture System				
RCCS 10mls	N/A	1-2 x 10^6	10mls	Immunohistochemistry; FACS; molecular analyses (gene/protein expression)
RCCS 50ml	N/A	3-5 x 10^6	50mls	
Static 3D cultures				
P100/F75	4-5mls	2-4 x 10^6	20mls	Immunohistochemistry; FACS; molecular analyses (gene/protein expression)
F175	15mls	6-8 x 10^6	50-80mls	
6-well plate	3mls	5-8 x 10^5	5-7mls	Confocal microscopy; electron microscopy
12-well plate	1.5mls	3-5 x 10^5	2mls	
24-well plate	500µl	1-2 x 10^5	1.5mls	Confocal microscopy; electron microscopy; moderate-throughput screens
48-well plate	250µl	5-8 x 10^4	500µl	*In vivo* xenografts; high-throughput screens
96-well plate	50µl	1-5 x 10^4	200µl	High-throughput screens; side population sphere formation assays

Table 2.1: Cell seeding densities and secondary assays for RCCS and polyHEMA 3D cultures. Volumes of polyHEMA coating solutions used are also shown.

Cell suspensions were then inoculated onto polyHEMA-coated plastics with an appropriate volume of complete medium (20mls for a P100 dish) Spheroid formation was be monitored by phase-contrast microscopy. To refeed 3D cultures, dishes or flasks were rested at an angle to allow spheroids to settle at one corner (such as by resting one side of the vessel on a pipette). After 10-20 mins, cultures were inspected to ensure the spheroids had completely settled before refeeding (longer resting periods were necessary for cultures that contain smaller spheroids). Up to 80% of the culture medium was carefully removed with a pipette. Fresh medium was then slowly added.

The rotary cell culture system

Sterile rotary cell culture vessels (Synthecon) were rehydrated with complete tissue culture medium for 10min. Medium was then removed. 2D monolayer cells were trypinised, pelleted and enumerated, as described above. Rotary cell culture vessels (10ml or 50mls) were inoculated with an appropriate number of cells (see Table

Cells were incubated undisturbed and refed twice a week. To refeed, rotation was stopped and the vessel was removed from the base and placed in tissue culture hood. The vessel was rested in an upright position with the filling hole at the top. After approximately 20 minutes, spheroids collected at the bottom of the vessel. Two-thirds of the medium was

then carefully removed and slowly replaced with fresh medium. Air bubbles were removed as above.

Fixing of 3D cultures and Processing for Immunohistochemistry

3D cultures were removed from the incubator and culture medium containing MCS was poured into 50ml v-bottomed tube. Spheroids were allowed to settle for 10-20 mins, cell culture medium was then removed and replaced with neutral-buffered formalin (VWR). At the University College Hospital Histology Services, samples were then processed into paraffin for immunohistochemistry. Immunohistochemistry was performed at University College Hospital Advanced Diagnostic Laboratory.

2.1.12 Heterotypic Culture Protocols

Fibroblast cultures were used at 80% confluency. Freshly prepared, filter sterilised hydrogen peroxide solutions were added to cell culture medium for 2 hours. Cells were then passaged at a ratio of 1:2 and stained for senescence associated β-galactosidase expression after 24 hours.

3D Co-culture Assays

Cells were grown as 3D dimensional multicellular spheroids on plastic dishes coated twice with a 1.5% solution of poly-2-hydroxyethyl methacrylate (polyHEMA) from Sigma, prepared in 95% ethanol (Sigma). Fibroblasts were plated onto polyHEMA coated plates and allowed to form spheroids for 7 days, before the culture was inoculated with epithelial cells at a ratio of 4:1 fibroblasts:epithelial cells. 3D heterotypic cultures were maintained in BM for two weeks and re-fed twice weekly, before multicellular aggregates were harvested, fixed in neutral-buffered formalin (VWR) and processed into paraffin (at the CR-UK Histology Service).

2.1.13 Electron Microscopy

For primary fixation: (note that for scanning EM cells were first washed in 1X PBS to remove proteins and the fixative was filtered before use). Samples were fixed for 1-2 hours in 2% fresh paraformaldyhyde, 1.5% glutaraldehyde in 0.1M cacodylate buffer, pH 7.3 (all Sigma). For 2D cells, cells were grown on coverslips, the media removed and replaced

with fixative. For 3D cultures: spheroids were spun down, the media removed and the spheroids resuspended in fixative. Fixed samples were then washed in 0.1M cacodylate buffer, then incubated in 1% OsO_4 (Sigma) in 0.1M cacodylate buffer, pH 7.3 for 1 hour in the fridge. Samples were then washed in 0.1M cacodylate buffer for 5 min, the washed in DDW for 5 min. Samples were incubated in 0.5% uranyl acetate in DDW for 20 min, then washed once more in DDW for 5 min. Samples were then dehydrated with increasing concentrations of ethanol: 25% ethanol/5 mins, 50% ethanol/5 mins, 70% ethanol/5 mins, 90% ethanol/5 mins, 100% ethanol/5 mins x 4 incubations.

Dehydrated samples were then embedded in resin. These steps were performed in a glass petri dish. 2 parts propylene oxide was mixed with 1 part resin mix, the mixture was added to samples and incubated for 1 hour. The resin mix was then replaced with a mix of 1 part propylene oxide and 1 part resin mix for 1 hour. Finally, this was replaced with 1 part propylene oxide:2 parts resin mix for 1 hour. Samples were then submerged in 100% resin mix overnight. Fresh resin was replaced the following day, and to create a block, a beem capsule was filled with resin so that there is a slight convex surface. A cover slip was then placed atop the resin of the beem capsule (all reagents for EM were obtained from Sigma).

The recipe for the epoxy resin mix (medium hardness) ie:

Agar resin:	Agar 100	12gm
	DDSA	8gm
	MNA	5gm
	DBMA	0.65gm

Epon:	Taab 812	19.2gm
	DDSA	7.6gm
	MNA	13.2gm
	DBMA	0.8gm

For scanning electron microscopy, samples were mounted on carbon stubs and gold-coated before viewing using a JEOL 7401 series FEGSEM. For transmission electron microscopy, samples were examined on a JEOL 1010 transmission electron microscope (both JEOL Ltd).

2.2 Preparation and Manipulation of Plasmid DNA

KRAS^{G12V} was cloned from the pcDNA3.1 vector into pLNCX (BD Biosciences) (Figure 2.1).

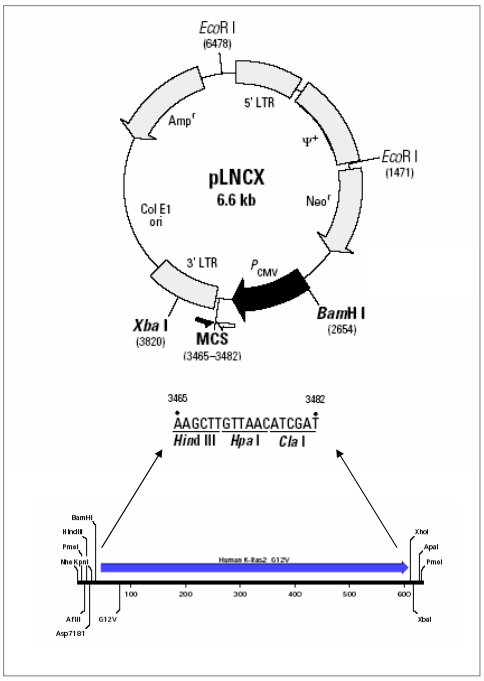

Figure 2.1: *KRAS*^{G12V} cDNA was cloned into the multiple cloning site (MCS) of the pLNCX retroviral vector.

The plasmids used in these experiments all contain an ampicillin resistance gene under the control of a bacterial promotor sequence, enabling selection with ampicillin for isolation of bacterial colonies containing the plasmid of interest. All bacteria will contain amplified, replicated plasmid DNA as well as the bacterial genome. The plasmid DNA can then be isolated.

2.2.1 Transformation of DH5α™T1® Competent *E.coli*

One Shot® MAX Efficiency Competent Cells DH5 α^{TM}T1® competent *E.coli* (Invitrogen) were used for preparation of plasmid stocks, according to the manufacturers protocol. DNA must be free from alcohol, detergent or protein contaminants that may remain following enzymatic manipulation of the DNA, as these will inhibit bacterial transformation. For each transformation experiment, one tube of bacterial cells was transformed with

pUC19 as a positive control, or no DNA as a negative control.

1-2μl of DNA was added to a tube containing 50μl DH5a^{TM}T1® competent *E.coli* on ice. The tube was then gently tapped to mix and the mixture was incubated on ice for 30 minutes. *E.coli* were then heat shocked by incubating for exactly 30 seconds at 42 °C. Cells were then placed on ice before 250μl of room temperature SOC medium was added. Tubes were then shaken at 37 °C for 1 hour at 225 rpm. 20 to 100 μl of the transformation reaction was plated onto LB-agar plates containing 100μg/ml ampicillin. The bacterial solutions were spread onto the plates using the quadrant streaking technique to achieve well spaced bacterial colonies. Plates were incubated inverted overnight at 37 °C.

LB agar plates were prepared using the following recipe:

5g	Tryptone	2.5g	NaCl
2.5g	Yeast Extract	1.5 %	Agar
	Distilled water to 500ml		

The solution was then sterilised by autoclaving and allowed to cool to below 60 °C before adding ampicillin (dissolved in 70% ethanol). The LB-agar with antibiotic was then poured into sterile 100mm petri dishes within a laminar flow hood, and allowed to cool and set before replacing the lid and storing at 4 °C.

2.2.2 Preparation of Plasmid DNA

Plasmid DNA was prepared using a QIAgen Maxi Plasmid DNA Isolation kit.

100ml of LB medium plus 100μg/ml ampicillin was inoculated with a discrete colony picked from a streaked plate using a sterile tip. The medium was then incubated at 37 °C overnight in a shaking incubator with shaking at 225rpm.

The following day bacterial cells were pelleted by centrifugation at 6,000g for 15 minutes at 4 °C in a Sorvall RC 5C Plus centrifuge. The supernatant was discarded and the cell pellet resuspended in 10mls of lysis buffer. The suspension was vortexed to ensure no cell clumps remained. 10mls of buffer was then added and the container was inverted 4 to 6 times to ensure complete mixing before the suspension was incubated for 5 minutes at room temperature. 10 mls of chilled buffer P3 was then added to precipitate cellular protein and the mixture was incubated on ice for 20 minutes. The cell suspension was then centrifuged twice for 30 minutes then 15 minutes at 20,000g at 4 °C to remove cell debris. A QIAgen filter tip 500 was equilibriated with buffer QBT and the bacterial

supernatant was then passed through the filter by gravity flow. Two 30ml washes with QC buffer were followed by elution with 15mls buffer QF. Isopropanol preciptation and ethanol precipitation was then used to clean up the DNA solution to remove any residual protein - 0.7vols room temperature isopropanol (Sigma) were added to the DNA solution, the tube was inverted to mix and centrifuged for 30 minutes at 15,000g at 4 °C. The supernatant was then carefully discarded and the resulting DNA pellet washed with 5 mls 70% ethanol and centrifuged for 10 minutes at 15,000g at 4 °C. The plasmid DNA pellet was then allowed to air dry at room temperature. The DNA was then dissolved in 1ml 10mM Tris-EDTA buffer.

A NanoDrop® Spectrophotometer determine the concentration and purity of DNA solutions.

2.2.3 Enzymatic Manipulation of Plasmid DNA

Restriction Enzyme Digests

KRAS was excised from pcDNA3.1 using BamH1 and Xho1. the pLNCX2 vector was opened by digestion of the multiple cloning site using BglII and Sal1. All enzymes were purchased from NEB. To ensure enzyme activity and to ensure there is no contamination of DNA other than sample DNA, two control digests are included in the experiment. The first contains sample DNA and no restriction enzyme, and the second contains no DNA and restriction enzyme is added. When the former control digest is run on an agarose gel, the uncut vector DNA should migrate faster than fully digested or nicked circular vector DNA. A two- to tenfold excess of restriction enzyme to substrate DNA was always used. When double digests were performed, 0.5μl of each enzyme was used so that the total volume of enzyme remained the same. When performing double digests it was ensured that both enzymes had sufficient activity in the buffer used in that reaction.

The following reagents were added to a 1.5ml microcentrifuge tube:

Reagent	Sample DNA	Uncut DNA	No DNA
	Volume (μl)		
RE 10X buffer	2.0	2.0	2.0
Acetylated BSA (10μg/μl)	0.2	0.2	0.2
DNA (1μg/μl)	1	1	0
Restriction enzyme	1.0	1.0	1.0
Sterile deionised water	Makes reaction volume up to 20μl		

Restriction enzyme were taken out of the freezer immediately before use and were added last to the reaction mixture. The complete digest mixture was then mixed by pipetting, and centrifuged at 13,000 rpm for a few seconds. The samples were then incubated for 1 to 4 hours at 37 °C. When required, enzymes were heat inactivated by incubation at 65 °C for 20 minutes.

Following incubation, digest products were separated by agarose gel electrophoresis, with the percentage of agarose in the gel adjusted according to the size of the fragments to be separated. The digested vector and insert fragments were identified by size, the corresponding bands were excised from the gel and the DNA was then purified using the QIAgen Gel Elution Kit (see 2.4.1). DNA's were eluted in 28μl Tris.Cl, pH 8.5, and quantified using a Nanodrop Spectrophotometer.

2.2.4 Ligation with NEB Quick Ligase^{TM}Kit

50ng of restriction enzyme (RE) digested vector (pLNCX2) were added to a 1.5ml microcentrifuge tube, along with 150ng of RE digested insert (*KRAS*) DNA, containing complementary sticky ends. A excess of insert DNA increases the efficiency of a ligation reaction. To increase the number of intermolecular reactions - vector DNA should always be <10ng/μl. DDW was added to make the DNA mixture up to a volume of 10μl. The following control reactions were also prepared in separate 1.5ml microcentrifuge tubes:

Uncut vector To test transformation efficiency and antibiotic resistance of that specific plasmid.

RE digested vector DNA + no insert + no enzyme This control checks for uncut vector in the ligation reaction. It may be necessary to purify open vectors by agarose gel electrophoresis as uncut vector will compete with ligated vector during bacterial transformation.

Vector DNA + no insert + Quick T4 DNA ligase This reaction will check the activity of the ligase enzyme and ensure the integrity of the sticky ends of the DNA. The number of transformed colonies obtained when transforming cells with this DNA should be around 60% of the number of colonies obtained when transforming cells using uncut vector DNA.

The DNA mixtures were then incubated at 65 °C for 5 minutes to break any unwanted insert-insert or vector-vector bonds. The samples were then centrifuged for 30 seconds

and cooled on ice. 10μl 2X Quick Ligation Reaction buffer (NEB) was then added to each tube and samples were mixed by pipetting the mixture up and down. 1μl Quick T4 DNA Ligase was then added to each tube and samples were mixed thoroughly. Tubes were then centrifuged briefly and incubated at room temperature for 5 mins.

Following the 5 minute incubation, samples were chilled on ice to stop the reaction. DNA was clean-up by standard ethanol precipitation or using a Qiagen QIAquick PCR Purification Kit spin column. This step will remove T4 DNA Ligase and PEG (in the ligase buffer) from the reaction as these both inhibit transformation of bacteria.

Cleaned-up ligation reaction products were then used to transform DH5a™T1® competent *E.coli* cells, as described above. 1μl is was sufficient to get transformed colonies. Transforming bacteria with too much DNA reduces transformation efficiency, as at higher concentrations of DNA (eg. 500ng instead of 20ng in a transformation) competition between transforming and non-transforming DNA (eg. linear vector, insert only) is higher.

2.2.5 Colony PCR

In order to screen for bacterial colonies that had been transformed by a complete vector:insert molecule, colony PCRs were performed. *E.coli* colonies were picked using a sterile pipette tip, inoculated into 1ml of LB medium containing 100μg/ml ampicillin and incubated at 37 °C with shaking for 5-6 hours.

The following mastermix was prepared and 14μl was aliquotted:

Reagent	**Volume per reaction**
dd H_20	7.38μl
25mM $MgCl_2$	1.5μl
2.5 mM dNTPs	1.5μl
10x buffer (Promega)	1.5μl
Forwards primer	1μl
Reverse primer	1μl
Taq Polymerase (Promega)	0.12μl
Sample	1.0μl

1μl of each *E.coli* solution was then aliquotted into each reaction, plus two control reactions: (i) the original vector from which the gene was cloned (ii) no DNA (water).

The PCR was run on the following program:

20 minutes at 95 °C to disrupt the bacterial wall
45 cycles of 95 °C/45 seconds, 58 °C*/1 minute, 72 °C/1 minute
72 °C/10 minutes, 4 °C/10 minutes

(*annealing temperature was optimised for each set of primer pairs.) PCR products were analysed on an agarose gel and products of the expected size were excised from the gel.

2.2.6 Sequencing

All vectors used in these experiments were sequenced to verify the cDNA sequences were complete and contained no mutations acquired during the cloning process. The presence of the $KRAS^{G12V}$ and $BRAF^{V600E}$ cell lines was confirmed.

2.2.7 Testing Oncogene Constructs in NIH3T3 Cells

In vitro transformation of NIH3T3 cells is well documented, and so oncogene constructs were tested for their transforming ability by expression in NIH3T3 cells. 600,000 NIH3T3 cells were plated per P100 dish the day before transfection with the cDNA constructs. Gene expression and *in vitro* tumourigenicity were assayed by RT-PCR and foci formation assays respectively.

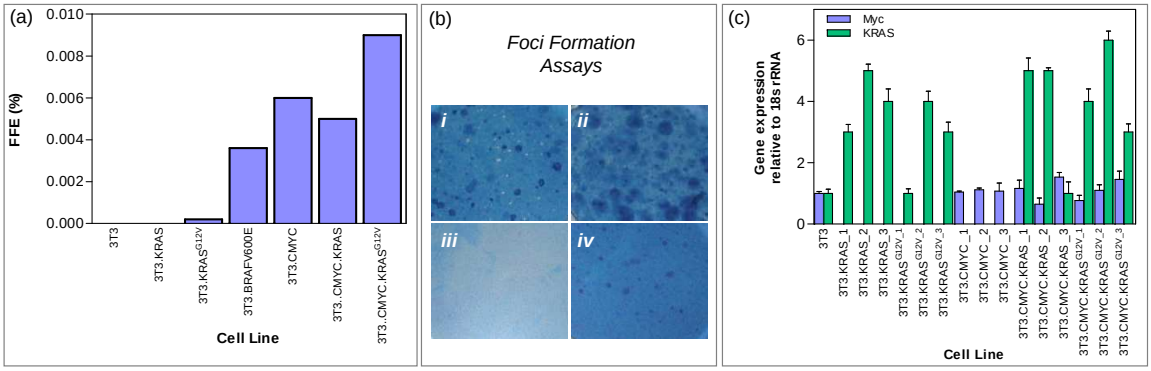

Figure 2.2: Neoplastic features are induced in NIH3T3 cells by the introduction of common oncogenes. (a) *C-MYC*, $KRAS^{G12V}$ and $BRAF^{V600E}$ confer different abilities to form foci in NIH3T3 cells. (b) (i) A clone expressing $KRAS^{G12V}$; (ii) A clone expressing $KRAS^{G12V}$ and *C-MYC*; (iii) Untransfected control cells; and (iv) cells transfected with *C-MYC* cDNA alone. Cells were stained with Coomaasie Blue and dark staining of foci can be clearly seen in (i,ii,iv) (arrows), where loss of contact inhibition allows cells to grow at high densities. (c) Gene expression of total *C-MYC* or *KRAS* in clones transfected with *C-MYC* +/− $KRAS^{G12V}$.

2.3 Gene Delivery by Retroviral Transduction

When working with sensitive primary cells, it is necessary to use a system for gene delivery that has a higher efficiency of gene delivery than transfection reagents. Natural retrovirus systems have been engineered to enable the generation of replication-deficient virions that deliver DNA into host cells at frequencies of over 90%. Upon infection of a cell, the virus will inject its RNA genome which is then reverse transcribed and the DNA molecule will integrate into the genome of the cell, hence enabling the generation of cell lines with stable expression of the gene of interest.

Firstly, the two packaging vectors contain expression cassettes for *gag*, *pol* and *env*. These genes contain the minimal requirements for the generation of a replication-deficient retrovirus capable of delivering DNA into a host cell. *Gag* is a gene encoding the proteins that comprise the internal structure of the virus, the *pol* gene encodes the enzymatic component of the virus, namely the reverse transcriptase and integrase, and the *env* gene contains the sequence for production of the virus envelope. In these experiments the pVPack system (Stratagene) was used for production of replication-deficient virion particles. This system is based on the Moloney Murine Leukemia Virus (MMLV). The pVPack-GP plasmid contains both the *gag* and *pol* sequences in a bicistronic expression cassette and pVPack-10A1 contains the *env* gene. This *env* protein recognises the same cell surface receptor as an amphotrophic MMLV virus, but in combination with a second receptor, hence gene delivery is even more efficient.

The third plasmid required contains the gene of interest cloned between two 600 bp long terminal repeat sequences (LTR). Within these sequences are the retroviral promotor/enhancer region (U3), the viral polyadenylation signal (R) and the sequences required for retroviral transcription (U5 and R). Upstream of the multiple cloning site (MCS) into which the gene of interest is ligated, is the viral packaging signal ($\psi+$) which is required for packaging of the RNA sequence between the two LTRs to be packaged into the head of the virus particle.

2.3.1 Production of Retrovirus

Extra care must be taken when working with retroviruses, in particular in these experiments where virions are designed for efficient delivery of oncogenes into human cells. This work falls within NIH Biosafety Level 2. All glassware and solutions used in viral work were not used for non-viral work and gloves and a lab coat worn at all times. The laminar flow hood and any pipettes used were UV irradiated for 1 hour following retroviral work.

The packaging cell line(s) were transfected using FuGene^{TM}6 (Roche) transfection reagent as described above, using a 3:1 ratio of transfection reagent to plasmid DNA. In these experiments the pVPack-GP and pVPack-10A1 packaging vectors were used plus the following plasmids containing the genes of interest: pLNCX.neo.KRAS$G12V$, pBabe.hygro.hTERT (Addgene), pWZL.Blast.CMYC (Addgene), pBabe.puro.BRAF (a kind gift from D. Peeper, Netherlands Cancer Institute). As three plasmids were used to transfect the cells, 2μg DNA of each was used per transfection. An outline of the protocol is shown in Figure 2.3. Cells were transfected at the end of day 1, and the media was replaced the following morning with 10mls of complete media per P100 dish. Cells were then incubated for 48 hours post-transfection before the media containing retrovirus was collected, aliquotted into sterile 15ml tubes, snap-frozen in liquid nitrogen and stored at $-80\,^{\circ}$C. The media was replaced and viral supernatant collected 72 hours post-transfection. This was repeated a third time to obtain viral supernatant 96 hours post-transfection. Packaging cells were then discarded.

Figure 2.3: Production of retrovirus and gene delivery into target cells, experimental overview

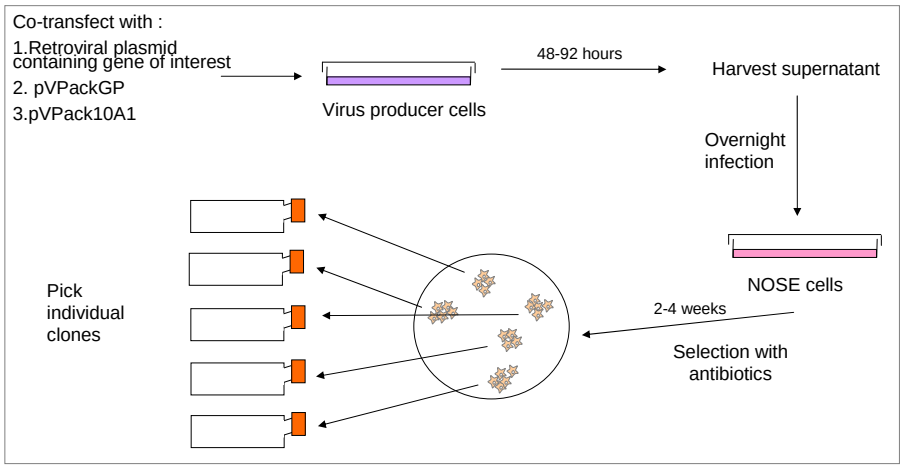

2.3.2 Optimisation of Infection Conditions

Retrovirions containing the lacZ reporter gene were produced from early passage 293T and Phi-Nx cells by transfection with pVPack-GP, pVPack-10A1 and pBMN-Z (Orbigen). A P100 plate of NIH3T3 cells was split 1:12 into a 6 well plate and six 15ml tubes, as shown in Figure 2.4.

Figure 2.4: Optimisation of packaging cell line and infection conditions, experimental overview. NIH3T3 cells have been previously shown to be susceptible to retroviral infection and so were used in the experiments optimising virus protocols

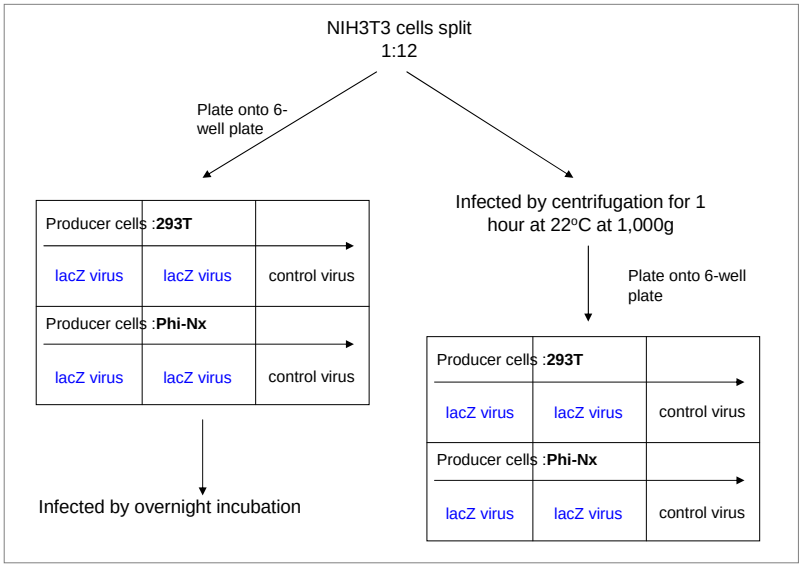

Infection by Overnight Incubation with Retrovirus

Cells were allowed to adhere overnight and at the end of the day the media was aspirated and 1ml of virus applied to each well in duplicate. The final wells were infected with 1ml 'empty virus'. 1ml of complete media containing 4μg/ml DEAE-dextran hydrochloride (Sigma). The cells were placed in the incubator overnight and the media replaced with 3ml complete media.

Infection by Gentle Centrifugation

Cells were trypsinised and pelleted and the media aspirated. Cell pellets were then re-suspended in 1ml of complete media containing 4μg/ml DEAE-dextran hydrochloride and 1ml of virus. The tubes were then spun for 1 hour at 22 °C at 1,000g. The viral supernatant was then removed, the cells were resuspended in complete media and transferred to a well of a 6-well plate, as shown diagrammatically in Figure 2.5.

Cells were incubated for two days and then assayed for lacZ expression as described below. As shown in Figure 2.5, there was no observable differences between the two infection methods described above. However, 293T cells produced retroviral supernatant which infected NIH3T3 cells with a higher efficiency than retrovirus produced by the Phi-Nx

packaging cell line (Figure 2.5 a-d).

Optimisation of Timepoint for Retrovirus Harvesting

Primary BRM-1 cells were infected with *hTERT* retrovirus in order to test the effects of increasing time between transfection of packaging cell line and collection of retroviral supernatant. BRM-1 cells were split equally onto 8 P60 plates and allowed to adhere overnight. The following day, the cells were infected (in duplicate) overnight. Selection with 10-20U/ml hygromycin was maintained for 3 weeks, before cells were fixed with methanol and stained with Coomaasise blue. 48 hours post-transfection was optimum for virus harvesting, as shown in Figure 2.5.

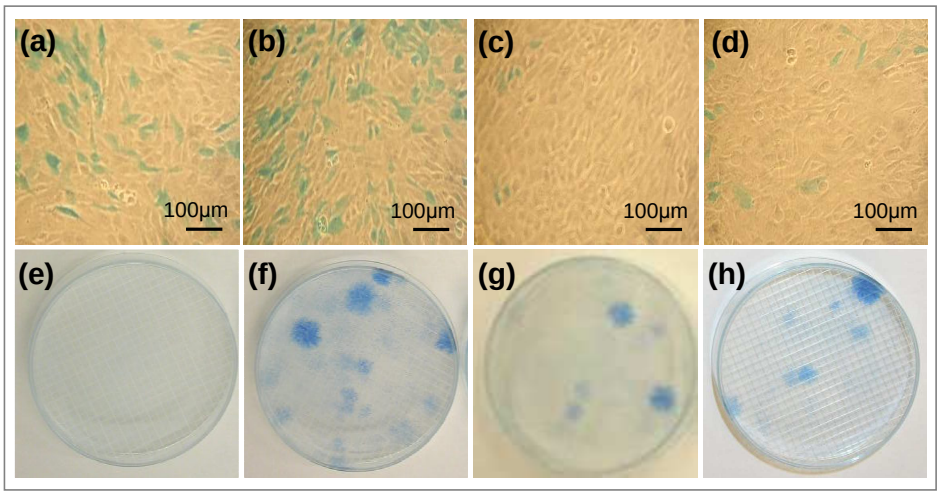

Figure 2.5: Optimisation of harvesting time-point and producer cells for retroviral production. (a,b) 293T cells produce retroviral supernatants that infect NIH3T3 cells with higher efficiency than Phi-Nx cells (c,b). Cells were infected by centrifugation (a,c) or overnight incubation (b,d). Infected cells are blue. (e-f) Increasing time between transfection and collection decreases infection efficiency. Primary human fibroblasts (BRM-1) cells were infected with either empty virus (e), or *hTERT* retroviral supernatants collected 48 (f), 72 (g) and 96 (h) hours post-transfection of the 293T virus producer cells. Colonies were stained 3 weeks post infection, following selection with hygromycin. Images show representative cultures.

2.4 *In Vitro* Assays for a Transformed Phenotype

2.4.1 *hTERT* Immortalisation of Primary Ovarian Cells

Early passage normal ovarian surface epithelial (NOSE) cells (n=3) or normal ovarian fibroblast (NOF) cells (n=1) were infected with *hTERT* retroviral supernatants. Following transduction, cells were left undisturbed in the incubator for 2 to 3 days before the medium was replaced with fresh complete medium containing a low dose of the appropriate selective antibiotic (10U/ml hygromycin). Media were then changed every 5-7 days, with all subsequent media containing a high dose of the selective antibiotic (hygromycin at 20U/ml for NOSE cultures, 30U/ml for NOF cultures). Following 2 to 3 weeks of selection, independent colonies were picked from plates and replated in a 25 cm^2 flask.

Isolation of Total Cellular DNA

A P100 plate of cells was taken at 80% confluency. Cells were trypsinised and pelleted and the DNA extracted with a QIAgen DNeasy kit, according to the manufacturer's protocol. Briefly, pelleted cells were resuspended in 200μl PBS and then lysed by incubation with proteinase K at 56 °C for 10 minutes. Buffer AL and 100% ethanol were added to each sample and the mixture pipetted into a QIAgen DNeasy mini spin column. The column was then spun at maximum speed for 1 minute and the flow through discarded. The column was then washed with wash buffer AW1 and then buffer AW2. To elute the DNA, up to 200μl of buffer AE or water was added to the column, and the column spun at maximum speed for 1 minute to collect the DNA into a fresh microcentrifuge tube.

2.4.2 Telomere Restriction Fragment Length Analysis

To detect telomere restriction fragment (TRF) length, the TeloTAGGG Telomere Length Assay (Roche) was performed, according the manufacturers instructions. Briefly, 1μg DNA from each cell line was digested by incubation for 2 hours at 37 °C with frequently cutting enzymes (Hinf1 and Rsa1). These enzymes restrict non-telomeric DNA into low molecular weight fragments, leaving sub-telomeric and telomeric regions of chromosomes intact. Restriction products were then separated by agarose gel electrophoresis, and Southern blotted, by overnight capillary transfer, onto a nylon membrane. DNAs were UV-crosslinked onto the membrane, and the membrane washed with 2xSSC (0.3M NaCl, 0.03M Sodium citrate, pH7.0). The membrane was prehybridised by incubation with for 1 hour with 25ml

DIG Easy Hyb Solution (provided in the kit) at 42 °C. Blotted fragments then hybridised for 3 hours with 1μl of a digoxigenin (DIG)-labelled telomere-specific probe per 5ml DIG Easy Hyb Solution. The membrane was then washed twice (5 mins) with 2xSSC/0.1% SDS at ambient temperature, then for 20mins with 0.2xSSC/0.1% SDS at 50 °C. The membrane was then washed with washing buffer and blocked for 30 mins with blocking solution (both in the kit). The blot was then incubated for 30 mins with anti-DIG-AP (alkaline phosphatase) diluted in blocking buffer. The membrane was then washed a final time in washing buffer and then incubated with detection solution for 5 mins. The membrane was then incubated for 3ml with ∼3mls chemiluminescent substrate solution and then exposed using a standard film developer. TRF lengths were calculated using a molecular weight marker run on the gel.

2.4.3 Analysis of Telomerase Activity

To detect telomerase activity, the TeloTAGGG Telomerase PCR ELISA^{PLUS} assay (Roche) was performed, according the manufacturers instructions. Cell extracts were prepared by pelleting 2x10^5 cells in a sterile eppendorf. Cells were washed once in 1X PBS. Pellets were resuspended in 200μl lysis buffer (in the kit) and incubated on ice for 30 mins. the lysates were centrifuged at 16,000g at 4 °C for 20 mins. The supernatant was then removed to a fresh tube for the telomeric repeat amplification protocol (TRAP) reaction. For each sample, 25μl reaction mixture and 5μl internal standard was pipetted into a PCR tube. Negative controls (heat-treated immortalised cell line extract to destroy telomerase activity, plus a lysis buffer only negative control) were included in each experiment. 1μl control template was pipetted into a separate PCR tube. Each tube was made up to 50μl with nuclease-free water. The tubes were then incubated in a thermal cycler (Applied Biosystems) and run on the following program:

25 °C/30 mins
30 cycles of 94 °C/30 secs, 50 °C/30 secs, 72 °C/90 secs
72 °C/10 mins
74 °C/hold

10μl denaturation solution was then added to 2 tubes per sample, 2.5μl sample was added to each and the reaction incubated at room temperature for 10 mins. Hybridisation buffer T was then added to one tube, and hybridisation buffer IS added to the other tube. Samples were vortexed and then 100μl of each transferred the MP modules provided in the kit. The modules were then covered in foil and incubated at 37 °C for 2 hours, with shaking at 200 rpm. The hybridisation solutions were then removed and the wells washed

3x with 250μl washing buffer (in the kit). 100μl Anti-DIG-HRP (horse-radish peroxidase coupled secondary antobody) was then added to each well and the plate incubated at 37 °C for 30 mins, with shaking at 200 rpm. The wells were then washed 5x with 250μl washing buffer and then 100μl TMB substrate solution was added to each well. The colour was allowed to develop for 20 mins before 100μl Stop reagent was added. The absorbance of each well at 450nm (with a reference of 690nm) was read using a Varioskan microplate platereader. Telomerase activity was calculated using the following formula:

$$\text{Relative Telomerase Activity (RTA)} = \left[\frac{(\text{A}_S\text{-A}_{S,O})/\text{A}_{S,IS}}{(\text{A}_{TS8}\text{-A}_{TS8,0})/\text{A}_{TS8,IS}}\right] * 100$$

A_S	absorbance of the sample
$\text{A}_{S,O}$	absorbance of heat-treated sample
$\text{A}_{S,IS}$	absorbance of internal standard of the sample
A_{TS8}	absorbance of control template
$\text{A}_{TS8,O}$	absorbance of lysis buffer
$\text{A}_{TS8,IS}$	absorbance of internal standard of the control template

2.4.4 Growth Curve Experiments

To assess the rate of population doubling for cell lines, cells were trypsinised, counted and 100,000 cells were plated in 60mm dishes in triplicate. After 7 days or when cells became over 80% confluent, cells were trypsinised, passaged at a ratio of 1:2-1:8 and counted.

The rate of population doubling (PD) was then calculated using the following formula:

$$\text{PD} = \log 2\left[\frac{\text{Total Number of Cells}}{\text{Inital Number of Cell Plated}}\right]$$

Cumulative population doublings were plotted, or average population doubling time calculated.

2.4.5 Analysis of Cellular Karyotype

Cell cultures were seeded at 60-80% confluency in complete medium in a F25cm^2 flask. Karyotypic analyses were performed at The Doctors Laboratory, 60 Whitfield Street, London W1T 4EU. Cytogenetic profiles were analysed by a Senior Cytogeneticist (Mr. Terry Ballard).

2.4.6 Foci Formation

$1x10^6$ cells were plated in a P100 cell culture dish. Cells were refed three times per week and stained with Coomaasie blue solution after 14 days.

The foci formation efficiency was calculated using the following formula:

$$\mathrm{FFE}(\%) = \left[\frac{\text{Total Number of Foci}}{\text{Inital Number of Cell Plated}}\right]$$

2.4.7 X-gal Staining for β-galactosidase Expression

For analysis of expression of the lacZ reporter gene: Cells were stained 24 hours post-infection. Media was aspirated from the cells and cells were fixed with 2mls 0.05% glutaraldehyde in 1x PBS and incubated at room temperature for 5 minutes. 0.05% glutaraldehyde was then discarded into proper waste and cells were washed in 2mls 1X PBS and then incubated in 2mls 1X PBS for 10 minutes at room temperature. PBS was aspirated before adding sufficient X-gal solution to cover cells. To make up X-gal solution: X-gal (Promega) was added to a final concentration of 1mg/ml X-Gal/5mM $K_4Fe(CN)_6.3H_2O$/5mM $K_3Fe(CN)_6$/1M $MgCl_2$/PBS. Cells were then incubated at 37 °C and 5% CO_2 for 2-24 hours before inspection under the light microscope. Positive cells turn blue.

For senescence-associated-β-galactosidase expression, the X-gal solution was prepared to pH6, and used as described above.

2.4.8 Flow cytometry

For analysis of externalization of phosphatidyl-serine (indicator of early apoptosis) cell cultures were trypsinised, centrifuged, and cell pellets resuspended in FACS buffer, with or without the anti-annexin-FITC antibody, according to manufacturers instructions (Roche, Basel, Switzerland). Samples were run on a Becton Dickinson FACS Scan (Franklin Lakes, NJ, USA) and the annexin-V-positive population measured. For cell cycle analysis, cells were incubated with 1mM 5-bromo-2-deoxyuridine (BrdU) (Sigma) for 2 hours. Cells were then washed in PBS and fixed by dropwise addition of 70% ethanol with constant agitation. Samples were incubated at 4 °C overnight before extraction of labeled nuclei using standard pepsin digestion protocols. Pelleted nuclei were incubated with an anti-BruU antibody (Beckton Dickinson), washed twice with IFA (10mM HEPES, pH 7.4; 150mM NaCl; 0.1%

sodium azide; (all Sigma); 4% fetal bovine serum (Lonza)) then incubated with an Alexa Flour488 coupled secondary antibody (Invitrogen). Washed nuclei were resuspended 100 g/mL propidium iodide (Sigma) diluted in PBS, and analysed as above.

2.4.9 Anchorage-Dependent Growth Assays

Cell cultures were trypsinised, pelleted and enumerated, as described above. Cell solutions were prepared (in complete growth medium) at 200 cells/ml, and P100 dishes were inoculated with 500μl cell solution. 14.5ml complete medium was then added to each P100 dish. Three to six replicates were performed for each experiment. Cells were allowed to attach for 24 hours, and the following day complete media were replaced with test media if required. Cultures were refed every 2-3 days, and, after 14 days, stained with Coomaasie blue solution as described above.

Colonies were counted and graphically represented. Alternatively, Colony Formation Efficiencies (CFE %) were calculated using the formula described in Section 2.1.2.

2.4.10 Anchorage-Independent Growth Assays

Assays for anchorage-independent growth were performed as follows. 100mg/ml bactopeptone solutions containing 3.3% or 6% Noble agar (both Sigma) were prepared in DDW, and sterilised by autoclaving. Liquid agar solutions were then incubated at 65 °C until required. In 6-well plates, a base layer of complete medium (pre-warmed to 37 °C) containing 0.6% Noble agar was prepared and allowed to set. Cells were then trypsinised, pelleted and enumerated, and solutions prepared in prewarmed, complete medium, at the appropriate concentration (in these experiments, 0.33-6.6x10^4 cells/ml were used to plate 0.01-2x10^4 cells/well). Cell suspensions were then inoculated with 1/10 vols of the 3.3% agar solution. 3ml of cell suspension/medium/agar solution were then added to each well and allowed to set before incubation at 37 °C, 5% CO_2. Three to five replicates were plated for each cell line. As control, anchorage independent growth was evaluated simultaneously for the TOV112D endometrioid ovarian cancer cell line. After 4 weeks, cells were fixed with methanol and stained overnight at 37 °C with 1% p-iodonitrotetrazolium violet (Sigma). Colony formation was observed and number of colonies counted. Colony forming efficiencies (CFE %) were calculated as described above.

2.4.11 Invasion Assays

24-well Chemicon QCM ECMatrix Flourimetric Invasion Assay kits were purchased from Millipore. Cells were trypsinised, pelleted and washed in 1X PBS. Cells were then resuspended in serum-free medium (SFM) and counted. Cell solutions were then prepared at a concentration of $0.5x10^6$. Meanwhile, 24-well flourimetric invasion chambers (Millipore) were brought to room temperature and rehydrated with 300μl SFM. After 30mins, 250μl of the rehydration medium was removed and replaced with 250μl of cell suspension. 500μl of medium containing 10% FBS was then added as a chemoattractant.

Assays were incubated for 24hrs at 37 °C, 5% CO_2. Invasion chambers were then removed from the plate and the medium within the chamber aspirated. The chambers were then placed into 225μl cell detachment buffer (in the kit) and incubated at 37 °C for 30 mins, with occasional rocking. Finally, 75μl of a 75:1 mixture of CyQuant Dye and lysis buffer was added to each well. After a 15mins incubation at ambient temperature, 200μl of solution was taken from each well and transferred to a 96-well plate for reading. In each experiment, control wells (no cells) were included.

Heterotypic Invasion and Migration Assays

Standard invasion and migration assays were modified to use normal and senescent ovarian fibroblasts as a chemoattractant. $9x10^4$ fibroblasts were plated in 24-well plates. The following day the cells w ere washed twice with PBS and then 500μl serum free media was added. Migration chambers (Greiner) or re-hydrated invasion chambers (Millipore) were placed atop the fibroblast monolayers and 3 $x10^4$ (for migration assays) and 12.5 $x10^4$ (for invasion assays) epithelial cells were plated within the chamber. Assays were incubated at 37 °C5% CO2 for 24 hours before detection of invaded/migrated cells. For invasion assays, invaded cells were detached from the membrane, lysed and a quantitative flourimetric dye added, using reagents from the 24-well Chemicon QCM ECMatrix Flourimetric Invasion Assay kit (Millipore). Relative fluorescence units were read on a Varikoscan platereader. For migration assays, migrated cells were quantified as above, or membranes were stained *in situ* with 1% crystal violet (Sigma) in 100% methanol, washed twice with distilled water, and air-dried. The migrated cells were counted in ten fields of view per membrane. In all experiments, 10% FBS as a chemoattractant was also plated.

2.4.12 2D and 3D Proliferation Assays

Alamar Blue (Promega) is a colourimetric reagent which can be used to measure proliferation of cells in 2D or 3D. Cell numbers were optimised to ensure the reagent would not become fully reduced during the course of the experiment. For the cell lines used in this thesis, the optimium cell number was 1000-5000 cells/ml. Cells were counted and plated in 48-well plated in complete medium containing 10% Alamar Blue. Medium alone and medium containing reagent but no cells were included as a control. At the desired timepoints, plates were read on a Varioskan Platereader.

2.5 Assaying Gene Expression

2.5.1 Isolation of Total Cellular RNA

RNA molecules are unstable and extremely vulnerable to degradation by RNase enzymes. Therefore the bench and all pipettes were cleaned with RNA-Zap (Ambion) prior to performing RNA extractions to remove any RNase enzymes present on the workstation. Also, all solutions were made up with RNase-free water and only tubes or plastics certified as RNase and DNase free were used. RNase-free water may be substituted with DDW containing 0.1% diethylpyrocarbonate (DEPC), as this chemical is a strong (but not absolute) inhibitor of RNase activity. Finally, all samples containing RNA were stored at $-80\,^{\circ}$C, and the number of times samples were freeze-thawed was kept to a minimum.

Isolation of total RNA from cells was performed using the QIAgen RNeasy Mini kit, according to the manufacturers protocol. This procedure uses a silica-based membrane and a series of high salt buffers that enable binding of up to 100μg of RNA (over 200 bases in length). Therefore the process effectively enriches for preparation of mRNA content, as most RNA smaller than 200 bases in length are excluded - such as tRNAs and 5M rRNA. Furthermore, the cells are lysed and homogenised in buffer that contains guanidine-thiocyanate and β-mercaptoethanol. This creates a denaturing environment that inactivates degradative RNase enzymes immediately.

Cells were grown until 80% confluency. The RNeasy spin columns have a RNA binding capacity of 100μg. Cells were trypsinised and pelleted as described above and the cell pellet was loosened by flicking the tube before addition of 600μl lysis buffer containing 10μl/ml β-mercaptoethanol. Cell lysates were then homogenised by pipetting the lysate through a QIAshredder spin column (QIAgen) and centrifuging at room temperature for

2 minutes at full speed. 1 volume of 70% ethanol was then added to the homogenised lysate and the solution was mixed by pipetting. The samples were then carefully applied to an RNeasy spin column, in 700μl aliquots and tubes were centrifuged for 15 seconds at $\geq$8,000g. The flow-through was discarded and the column washed with 700μl of buffer RW1 by spinning for 15 seconds at $\geq$8,000g. 500μl of buffer RPE was then carefully applied to the RNeasy spin column and the tube was then centrifuged for 2 minutes at $\geq$8,000g to wash the membrane. The spin column can be placed in a new 2 ml collection tube for an optional extra spin at full speed for 1 minute to reduce the chance of carryover of residual buffer.

The spin column, containing RNA bound to the silica-based membrane, was then placed into a new 1.5 ml microfuge tube and RNA was then eluted with 2 x 30μl RNase-free water, applied carefully to the membrane of the spin column. The samples were then centrifuged for 1 minute at $\geq$8,000g. Using a second elution step increases the overall RNA yield.

The quality and concentration of RNA samples was determined using the RNA 6000 Nano chip (Agilent).

2.5.2 DNase Treatment of Total RNA

To remove any genomic DNA contamination from the RNA preparations, the samples were treated either (i) subjected to on-column DNase treatment using QIagen DNase kit or (ii) post-extraction, treated with RQ1 RNase-free DNase (Promega). RNA was normalised to 1μg/μl in a RNase-free 1.5μl microcentrifuge tube. The following reaction was then set up and incubated at 37 °C for 1 hour:

Total RNA	15μl
DNase Buffer (transcription buffer)	10μl
RQ1 RNase free DNase	1μl
RNasin®	1 μl
RNase-free H_20	23μl
Total reaction vol	50μl

Following the 1 hour incubation, 50μl RNase-free H_20 was added to each tube. An equal volume of citrate-buffered phenol:chloroform (100μl) was then added before the mixture was vortexed for 10 seconds and centrifuged for 5 mins at 13,000 rpm. The upper, aqueous phase from each tube was then transferred to a new 1.5μl microcentrifuge tube and 1μl glycogen/tRNA (Promega) was added to each tube to act as a carrier during the RNA

precipitation. To precipitate RNA, 1:5 vol 10M ammonium acetate (Sigma) and 2.5 vol 100% ethanol was added, and the mixtures were incubated on on dry ice for 30 mins. Samples were then centrifuged for 15mins at 13,000rpm and the resulting supernatant was carefully poured off. RNA pellets were then washed with 1ml 75-80% ethanol (made up with RNase-free water). The pellets were centrifuged for 10 minutes at 13,000 rpm before ethanol supernatant was decanted and RNA pellets allowed to air-dry at room temperature. 15μl RNase-free water was then added to each pellet and tubes were incubated at 55 °C for 10 minutes to redissolve the RNA.

2.5.3 Reverse Transcription of mRNA

Random hexamers (Promega) were used as primer for the synthesis of cDNA by a viral reverse transcriptase enzyme. The first step of the procedure is as follows: the following reagents are added to a clean 1.5μl microcentrifuge tube, including DNase-treated RNA prepared as described above:

DNase treated RNA (1μg/1μl)	2μl
Random hexamers	2μl
RNase-free water	10μl (to a final volume of 14μl)

Samples were then incubated at 75 °C for 5 minutes and then cooled on ice for 5 minutes in order to denature the random hexamers and allow annealing of these primers to RNA.

The following reagents were then added to the reaction:

M-MLV Reaction Buffer (Promega)	5μl
Nucleotide pool (Promega)	5μl
M-MLV RT enzyme (Promega)	1μl

The samples were incubated at room temperature for 10 minutes, followed by an incubation at 50 °C for 50 minutes. The volume of the samples was then made up to 100μl with RNase-free water. Reverse transcribed samples can be stored at −20 °C.

2.5.4 Real-Time PCR

TaqMan^{TM}pre-designed and pre-optimised probes (AB) were used to perform Real-Time Polymerase Chain Reaction (RT-PCR) experiments. Real-Time PCR enables quantification of mRNA abundance by amplification of cDNA. In any PCR, the amount of PCR product theoretically doubles with every cycle - when DNA cycle number and the amount

of DNA are plotted on a logarithmic scale the relationship between the two variables is linear. PCR amplification of DNA is a logarithmic reaction. Since there are limited amounts of reagents in the PCR mastermix, the reaction will eventually reach a plateau phase. The point at which the exponential phase of the PCR reaction ceases and the reaction enters the plateau phase will vary considerably, even within replicates. Therefore, in RT-PCR, the PCR product is quantified during the logarithmic phase of the reaction.

The TaqMan^{TM}reaction uses a system of probes with a flourescent dye incorporated onto the 5' base of the oligonucleotide, usually FAM or VIC. A quenching dye, TAMRA, is incorporated onto the 3' base of the probe, and during the course of the PCR reaction the 5'exonuclease activity of the polymerase will cleave the probe, separating the 5'flourescent dye from the 3'quenching dye. This emits fluorescence, and the amount of flourescence emitted will be proportional to the amount of probe that has been cleaved within that cycle of the PCR.

In these experiments a $\delta\delta$-Ct method was employed to analyse RT-PCR data. Primers and probes for amplification of 18S rRNA were loaded into each reaction as an internal control. The change in mRNA expression levels for each target gene is normalised so that each value for the gene of interest is relative to the expression of an endogenous gene (18s rRNA). This is achieved by calculating the difference between the cycle threshold (Ct) value for 18S rRNA and the Ct value for the gene being tested. These *delta*-Ct values (δCt) are averaged for each sample. The average δCt values for each test cell line is then compared to the δCt of the control cell line.

The following pre-made primers and probes were used in this study: *BRAF*, Hs00269944-m1; *KRAS* , Hs00270666-m1; *C-MYC*, Hs00153408-m1; 18S RNA internal control (Applied Biosystems).

The following real-time PCR mastermix was prepared:

Reagent	Volume per sample (μl)
TaqMan^{TM}Universal PCR Master Mix	12.50
18S rRNA pre-made primer/probe	1.25
Gene of interest pre-made primer/probe	1.25
Water	8.00
cDNA sample	2.00
Total	25.0

The appropriate volume of PCR mastermix was prepared for each gene to be analysed and 23μl aliquotted into the correct number of wells in a 96-well plate. 2μl of cDNA were then

added to the plate in triplicate. The plate was then placed into an Applied Biosystems 7900HT Fast Real-Time PCR System and the samples were run on a program consisting of the following thermal cycling conditions:

50 °C/2 minutes, 95 °C/10 minutes
40 cycles of 95 °C/15 seconds, 60 °C/1 minute

Data analysis was performed using SDS software (Applied Biosystems).

2.5.5 RFLP PCR

For detection of the KRAS restriction fragment length polymorphism, PCR was performed using KRAS-F primer: 5'-GACTGAATATAAACTTGTGGTAGTTGGACCT-3' and KRAS-R primer 5'-TCCTCTTGACCTGCTGTGTCG-3', with the following PCR conditions:

72 °C/2 minutes
50 cycles of 95 °C/30 seconds, 58 °C/30 seconds, 72 °C/30 seconds
72 °C/10 minutes

1μg purified PCR product was then digested with BstN1 overnight at 60 °C as previously described [Sato et al., 2006]. Digested products were electrophoresed on a 3% agarose gel.

2.5.6 Western Blot Analysis

Cells were grown to 80% confluence, washed twice in ice cold 1X PBS, then lysed with lysis buffer: 1% NP40, 30mM Hepes pH7.4, 150mM NaCl, 1mM EDTA containing 17μg/mL aprotinin; 1μg/ml pepstatin; 1μg/ml leupeptin, 100μg/ml AEBSF, and 1X phosphatase inhibitor cocktails (all Sigma). Lysed cells were collected with a cell scraper (Greiner), transferred to a sterile microfuge tube and incubated on ice for 20 mins. Cellular debris was then cleared from the lysates by centrifugation at 14,000 rpm for 10 mins at 4 °C. Proteins were quantified using a Bradford assay (Pierce). Proteins were then reduced and denatured in Laemmli sample buffer by boiling for 5 min at 100C: 50mM Tris pH6.8, 10% (v/v) glycerol, 2% SDS (w/v), 0.1% (w/v) bromophenol blue, 2% β-mercaptoethanol (all Sigma).

1D SDS-polyacrylamide gels of an appropriate % were poured and 10μg protein loaded and electrophoresed. Gels were electro-blotted onto polyvinylidene fluoride (PVDF) membrane (Millipore) using a wet transfer tank in transfer buffer :(195 mM glyine, 25 mM Tris, 20%

(v/v) methanol). The membrane was soaked in methanol before placing onto the gel.

Membrane blocked for 1h with 5% (w/v) BSA in Tris buffered saline (50 mM Tris pH 8, 150 mM NaCl) with 0.05% Tween-20 (TBS-T). The membrane was then incubated for a minimum of 1h in a primary antibody solution, diluted in TBS-T. Antibody solution was removed and the membrane washed in TBS-T three times for 15 mins. The membrane was then probed with the appropriate horseradish peroxidase (HRP)-coupled secondary antibody for 1 hour before three final TBS-T washes. Immunoprobed proteins were visualised using enhanced chemiluminescence liquid (mixed 1:1) (Pierce) and the film exposed in dark room.

The following antibodies were used in these experiments:

anti-C-MYC, clone 9E10	1:500 dilution (CRUK)
anti-MAPK	1:5000 dilution (Promega)
anti-active-MAPK	1:5000 dilution (Promega)

2.6 Gene expression microarrays

Sample Preparation

RNA samples were prepared as described above. Again, great care was taken to avoid contamination with RNases. The work area, all pipettes and racks were cleaned with RNAZap (Ambion) prior to use for RNA work. Filter tips were used at all times and only double-autoclaved milliQ water used. Cell lines were grown for 14 days in 3D on polyHEMA coated plates (described above). Multi-cellular spheroids were harvested by centrifugation and washed with sterile 1X PBS. RNA was isolated with the QIAgen RNA extraction kit, as described above, but with an additional step during lysis, as spheroids had to be processed as a solid tissue specimen. Washed spheroids were transferred to a sterile 1.5ml eppendorf and 600μl RLT lysis buffer (containing 10μl/ml β-mercaptoethanol) added. Using a sterile 22-gauge needle attached to a sterile 2ml syringe, spheroids were mechanically disrupted by passing through the needle 20 times. Lysed samples were then applied to the QIAshredder column and RNA extracted as described above. RNA sample concentration and quality were assayed using the Agilent 2100 BioAnalyser (Agilent).

Reverse Transcription, Labelling and Array Hybridisation

All reverse transcription and labelling experiments were performed by the UCL Genomics Facility. Briefly, RNA was amplified and labelled using the Ambion Illumina TotalPrep RNA Amplification kit (Ambion), according to manufacturer's instructions. 500ng RNA was reverse transcribed to cDNA, then biotinylated NTPs were incorporated during *in vitro* transcription overnight to generate labelled cRNA. Hybridisation, staining and scanning was carried out according to the Illumina Whole-Genome Gene Expression Direct Hybridisation Protocol. 750ng of biotin-labelled cRNA was hybridised to the Illumina Human HT-12 Expression Beadchip (Illumina). Chips were incubated at 58 °C for 16-20 hours. Following hybridisation, chips were washed and then stained with Streptavidin-Cy3 dye. Chips were scanned in the Illumina iScan scanner and data produced via the Illumina GenomeStudio v1.0 software (both Illumina).

Data Analysis

Data were exported from the Illumina GenomeStudio software as '.txt' files without prior background subtraction or data normalisation. The R language and environment for statistical computing was used for all data analysis [R Development Core Team, 2009]. The 'lumi' package was used to perform data pre-processing, quality control and normalisation steps [Du et al., 2008]. The 'bgAdjust','forcePositive' background correction was used to correct background signal. This algorithm forces all values to be positive, this is achieved by adding an offet value. The offset value is calculated using the control probe data. This method of background correction prepares the data for transformation. A variance-stabalizing transformation step, was then performed to predict the confidence intervals of the data. This step is critical for calculating the significance of differentially expressed genes, in particular high fold-change in the low expression range. Data were normalised using the robust spline method. Data pre-processing, quality control, normalisation and analysis are also discussed in Chapters 1 & 4.

Normalised data were then analysed using the Linear Models of Microarray' or 'limma' package [Smyth, 2004]. Limma enables the simultaneous analysis of many RNA targets across arrays. To identify genes that were differentially expressed, data were first filtered to select (i) only expressed genes and (ii) only genes which showed statistically significant differences in gene expression relative to the control cell line (IOSE) ($P \leq 0.05$). Bayesian statistics in 'limma' were then used to fit pre-processed expression data to a linear model, using similar statistics to ANOVA or multiple regression, but with every gene being analysed simultaneously. The 'decideTests' function in limma was then be used to classify

the value for each probe as significantly different from zero or not. This method adjusts for multiple testing. 'Top' tables of differentially expressed genes were created from the 'decideTests' data matrix, and sorted by statistical significance. To plot the expression of individual genes, normalised but non-VST transformed expression data were exported from 'R' and analysed in excel to create 'bar-chart' representations of gene expression changes.

3

Three-Dimensional Modelling of the Ovarian Surface Epithelium

3.1 Introduction

Understanding the biological and molecular characteristics of the ovarian surface epithelium (OSE) and the earliest stages of ovarian tumour development has been hampered in the past by the lack of suitable *in vitro* models of normal OSE (NOSE). This is partly because primary OSE cells have proved difficult to establish in culture and have a short lifespan *in vitro*. Since the first description of OSE culture in 1984, optimisation of collection techniques and culture media has increased the *in vitro* lifespan of these cells [Auersperg et al., 1984]; [Auersperg et al., 1994]; [Li et al., 2004a]. However, there remain limitations to culturing NOSE cells as standard two-dimensional (2D) monolayers and NOSE cells still lose some of their epithelial characteristics, even when cultured in enriched media [Li et al., 2004a]; [Salamanca et al., 2004]. Cells demonstrate considerable plasticity and will respond dramatically to their environment. A transcriptome that promotes growth within an organism is unlikely to provide the cell with an optimal phenotype for growth in 2D. Three-dimensional (3D) culture of other difficult-to-culture cell types has lead to dramatic improvements in *in vitro* lifespan and maintenance of *in vivo* phenotypic features (discussed in more detail in Chapter 1). Therefore, I hypothesised that a 3D culturing system would represent a good *in vitro* model of the OSE, and that 3D cultures of the OSE may be biologically more similar to the OSE *in vivo* than traditional 2D cultures.

There are many different approaches that can be employed to grow cells in a 3D mod-

els, the most widely used being gels consisting of extracellular matrix (ECM) proteins. Commercially available gels typically consist of a single matrix protein, such as collagen, laminin or fibronectin; more complex gels consist of two to three different matrix proteins, although in these preparations the relative quantities of constituent proteins cannot be easily altered. In 3D models of breast epithelial cells it is well documented that varying the ECM substrate upon which cells are grown can dramatically alter the transformed phenotype and cell-ECM interactions are integral for organogenesis to occur (reviewed in [Fata et al., 2004]). *In vivo*, a complex admixture of ECM proteins makes up the structure of the ovary; hence, growing NOSE cells within commercially available matrices would not necessarily be a good representation of the tissue. In this study two 3D culturing techniques were compared. In both systems the cells lay down matrix protein that forms and stablises the 3D structure:

PolyHEMA-coating of tissue culture plastics Poly(2-hydroxyethyl methacrylate) is a hydrogel. Hydrogels are hydrophilic compounds and when prepared by thermal polymerization at 65 °C in 95% ethanol (at a concentration of 1.5%), polyHEMA dissolves and expands within the 5% water content to generate a sterile solution that can be used to coat tissue-culture plastics. Upon drying and evaporation, the solidified hydrogel coats the entire surface of the vessel, and the modified surface is an ultra-low/non-adherent surface, to which many cell types cannot attach. Thus, cells grow in suspension and many cell types will spontaneously aggregate in such conditions.

The Rotary Cell Culture System (RCCS) The RCCS was designed by NASA as an improvement on traditional spinner flasks. Spinner flasks are bottle-shaped and contain a magnetic paddle. Cultures are inoculated into the flask, and the flask is placed upon a stirrer within the cell culture incubator (see Figure 3.1a). The culture is stirred at 10-250 revolutions per minute (rpm) and constant movement of the medium maintains cells in suspension. Although this technique has been proved to be optimal for the culture of suspension cell lines (such as lymphoma cell lines) there are limitations to the applicability of this technique to the generation of 3D multicellular spheroids (MCS) of adherent cell lines. Primarily, the movement of the paddle generates high shear forces that may destroy loosely-formed cellular aggregates or easily disrupt the structure of mature spheroids. In the RCCS, (Figure 3.1b) the vessel constantly spins, thus preventing cells from adhering to the vessel to promote the formation of MCS [Navran, 2008]. Around 14 rpm is recommended for optimal spheroid formation [Becker and Blanchard, 2007]. RCCS vessels were designed to reduce minimal mechanical shear forces on the cells. All air bubbles are removed and

gas exchange occurs by diffusion through a specialised liquid-impermeable membrane on the back of the vessel.

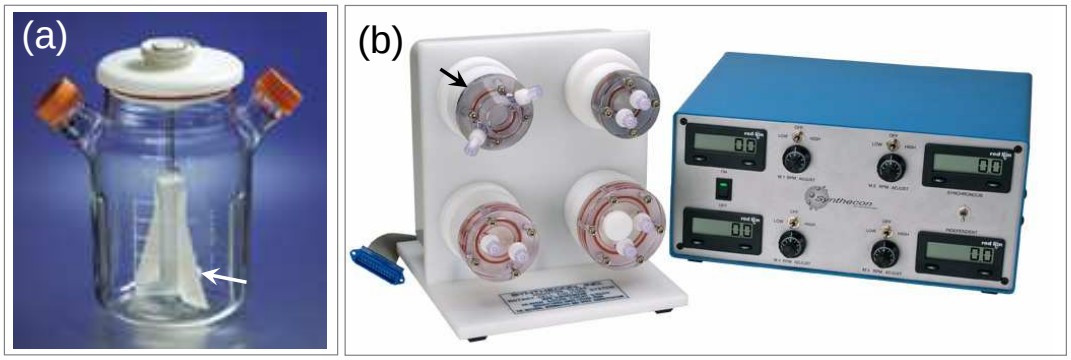

Figure 3.1: (a) In traditional spinner flasks, a magnetic paddle (white arrow) spins when the flask is placed atop a magnetic stirrer. (b) The rotary cell culture system (RCCS). Individual vessels (black arrow) are controlled by a powerpack. Revolutions per minute can be individually controlled. Images from (a) www.sigmaaldrich.com and (b) www.synthecon.com.

The working hypothesis for this Chapter is:

- Normal ovarian surface epithelial cells established as 3D *in vitro* models would more closely resemble OSE *in vivo* than the same cells cultured using traditional 2D monolayer techniques

The following objectives were designed to test this hypothesis:

- To isolate ovarian surface epithelial cells from normal ovaries and characterise the growth properties and marker expression of primary cultures
- To establish three-dimensional (3D) cultures of NOSE cells
- To characterise and compare the morphology, ultrastructure, ECM expression and apoptotic rate of OSE cells in 2D culture and 3D culture and compare to OSE *in vivo*

3.2 Isolating and Characterising Primary Normal Ovarian Surface Epithelial (NOSE) Cells

Primary normal ovarian surface epithelial (NOSE) cells were collected during gynaecological surgical procedures at University College Hospital. Patient information is listed in Table 3.1. OSE cells were harvested by gently brushing the surface of the ovary with a sterile cytobrush, as previously described [Li et al., 2004a]. Gross morphology of the ovaries was confirmed as normal in theatre, by the operating surgeon, and tissues were examined subsequently for abnormal features by a Gynaecological Pathologist (Dr E. Benjamin, UCL/UCH Department of Histopathology). Only ovaries that were confirmed as normal by gross morphology, initial Pathologists' inspection and subsequent histopathological examination (where available) were used in this study.

Following collection, NOSE cells were immediately transferred into a 25cm^2 flask and incubated undisturbed for 5-7 days before refeeding. Flasks were then examined by light microscopy for the growth of epithelial colonies (Figure 3.2). NOSE cells were isolated and maintained in growth factor rich NOSE-CM [Li et al., 2004a]. NOSE-CM is similar

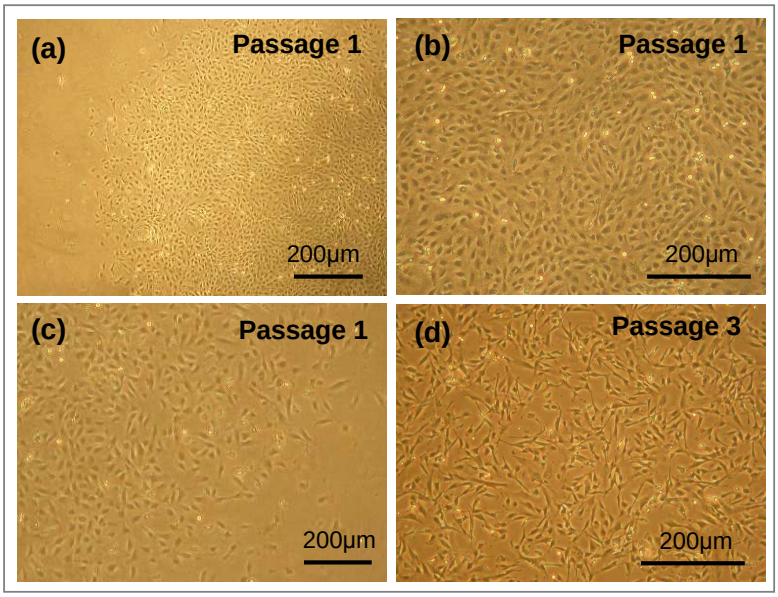

Figure 3.2: *In vitro* morphology of normal ovarian surface epithelial cells. (a) A passage 1 (p1) clone at low magnification, cells have a cuboidal morphology. (b) Cells have a regular 'cobblestone' morphology, are closely opposed and tightly packed at the centre of the clone. (c) NOSE cells with a more fibroblastic morphology, and cells are scattered. (d) Following passaging, all NOSE cell lines acquired a fibroblastic morphology.

Cell Line	Patient Age/Number	Pathology	Suitable for this Study?†
NOSE1/NOSE2	*NK*	*Lost through bacterial contamination*	*N/A*
NOSE 3/ **NOSE 4**	62	Endometrioid endometrial carcinoma grade I plus cervical clear cell carcinoma	✓
NOSE5	63	Endometrial mullerian-type tumour (very large) *Cells not collected from other ovary as was not grossly normal*	*N/A*
NOSE6/NOSE7	46	Enlarged uterus *Lost through bacterial contamination passage 1*	*N/A*
NOSE 9/ NOSE 10	61	Endometrial adenocarcinoma stage III	✓
NOSE 11/NOSE12	48	Hyperplasia of endometrium and ovarian stroma *NOSE12 lost through bacterial contamination*	✓
NOSE 13	Pa. no N14	Clear cell endometrial carcinoma	✓
NOSE 14R/ NOSE 15L	44	CIN Stage III with stromal microinvasion *(HepC+, patient has had radiotherapy)*	X
NOSE 16/ NOSE 17	32	Severe endometriosis *(cells exhibit anchorage independent growth)*	X
NOSE 18R/ **NOSE 19L**	39	Cervical carcinoma	✓
NOSE 20/ NOSE 21	Pa. no 154	Endometrial carcinoma	✓
NOSE 22/ NOSE 23	Pa. no 165	Endometrial carcinoma	✓
NOSE 24/ NOSE 25	Pa. no 169	Endometrial carcinoma	✓

Table 3.1: Primary NOSE cell line collection. Patient age/number and diagnosis. Cell lines highlighted in red were taken forwards for subsequent experiments. †Samples were suitable for the study if ovary was confirmed as normal and free of tumour by pathological examination. CIN = cervical intra-epithelial neoplasia. NK = not known.

to medium in its constituents to Mammary Epithelial Growth Medium (MEGM) in that it contains hydrocortisone, insulin, epidermal growth factor and bovine pituitary extract plus an additional 15% foetal bovine serum. MEGM has been demonstrated to dramatically increase yield and efficiency of collection of human mammary epithelial cells whilst maintaining a differentiated epithelial phenotype witn culturing (differentiated human mammary epithelial cells are characteristically cytokeratin (Ck) 14 and Ck18 positive, and Ck19 negative) [Hammond et al., 1984]. For the collection of NOSE cells described here, of 24 brushings taken from 13 patients, 5 were lost through bacterial contamination; thus efficiency of the collection protocol was 79%. At the first passage, a variety of different cell morphologies were observed, including cobblestone, cuboidal and fibroblastic morphologies (Figure 3.2). This is typical for NOSE cells, which characteristically

demonstrate phenotypic plasticity *in vivo* and *in vitro* [Auersperg et al., 1984].

Growth curves were established for five of the primary cell lines collected (Figure 3.3(a)). Cell cultures showed *in vitro* growth characteristics that were typical of NOSE cell cultures from other studies [Li et al., 2004a]. The *in vitro* lifespan of NOSE cells was under 60 days and cultures became increasingly senescent with passaging (enlarged, flattened morphologies, observed under the phase microscope, see Figure 3.4). Senescence was also induced when cells were split at too high a ratio (over > 1:5). This reinforced a need to immortalise cells in order to facilitate further studies of NOSE cells. Immortalisation of NOSE cells is described in Chapter 4.

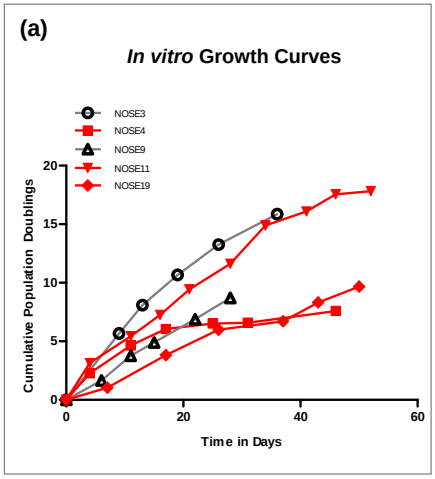

(b)

	ANTIBODY						
	AE1/AE3	Ck7	BerEP4	FN-3	FSP	CA125	Factor VIII
	Pan-cytokeratin	Cytokeratin 7	Epithelial cells	Fibronectin	Fibroblasts	Mucin 16	Endothelial cells
Positive control	EN-TRL 71T	EN-TRL 71T	EN-TRL 71T	1BR3.7	1BR3.7	EN-TRL 71T	HUVEC
NOSE 3	++	+	++	++	-	-	-
NOSE 4	+/-	++	+	+++	-	+/-	-
NOSE 9	++	+	++	+	-	-	-
NOSE 10	++	++	++	+++	+++	-	-
NOSE 11	+/-	+	+	+	+/-	-	-
NOSE 17	++	+++	nd	nd	-	++	-
NOSE18R3	++	+++	nd	nd	-	+	-
NOSE19L3	-	++	+	+	+	-	-

Figure 3.3: Characterisation of primary NOSE cell cultures. (a) Growth curves, lifespan of primary cultures is limited to under 60 days. (b) Immunoflourescent cytochemistry: NOSE cells are typically positive for epithelial markers (Ck7, AE1/AE3, BerEP4) and negative for markers of fibroblastic (FSP) and endothelial contaminants (Factor VIII). Cell lines highlighted in red were taken forward for further studies. Positive cell lines used were EN-TRL71T (endometrial cancer primary cell line), 1BR3.7(immortalised human skin fibroblast cell line) and HUVEC (human umbilical vein endothelial cell line), for staining images, see Chapter 4. nd = not done - no additional information would be provided by these markers.

Using immunoflourescent cytochemistry, eight NOSE cultures were characterised for the expression of epithelial markers or markers of contaminant cell types (Figure 3.3):

Anti-cytokeratin, clone: AE1/AE3 Identifies two epitopes present on most epithelial cytokeratin molecules.

Anti-cytokeratin, clone: 7 This cytokeratin molecule is known to be expressed in various epithelial and mesothelial cells.

BerEP4 An epithelial marker, also known as EPCAM, this antibody recognises two cytoplasmic and cell surface glycoproteins present in nearly all epithelial cells with few exceptions.

Anti-Fibroblast Surface Protein. Recognises an antigen present on the cell surface membrane and in lysosomes of fibroblasts, this marker was used to detect any fibroblastic contamination from the stroma. Although this antigen has been shown to be present on the surface of synovial, mammary, foreskin and thymic fibroblasts, its function is not yet known.

Anti-CA125 Cancer antigen 125 (CA125) is an antigen expressed highly in many epithelial ovarian cancers. This marker is used to test ovarian cells (and EOC patients blood sera) for malignancy, although normal ovarian surface epithelium can also stain positive for this marker. Differentiated Müllerian epithelia also express CA125.

Factor VIII This antibody binds to a cytoplasmic glycoprotein (F8 antigen) present in endothelial cells. This tests for any contamination of NOSE cultures by cells from blood vessels.

Negative controls (i.e. no primary antibody plus a negative cell line) were included in each experiment. Positive control cell lines were also used to assist in the interpretation of the staining (for reference see Figure 4.10 in Chapter 4). This was particularly important for fibroblast surface protein (FSP) since OSE cells typically show considerable phenotypic plasticity and often demonstrate weak-to-moderate positivity for this marker. One cell line demonstrated strong reactivity with FSP (NOSE10) and so was not selected for further study. No cell line tested stained positive for Factor VIII, suggesting that no cultures were contaminated by endothelial cells. Primary NOSE cell isolates all stained positive for epithelial markers (cytokeratin 7 or AE1/AE3) and negative for an ovarian cancer marker (E-Cadherin). Using immunoflourescent cytochemistry and also immunohistochemistry (described in Chapters 4 & 5) NOSE cells and their derivative cell lines repeatedly demonstrated more widespread staining with cytokeratin 7 than with pan-cytokeratin (AE1/AE3) suggesting Ck7 is a better marker of OSE cells *in vitro*. Finally, as previously reported in the literature, early passage normal OSE cultures can express CA125, which is also expressed by normal epithelia of the female reproductive tract [Auersperg et al., 1997].

3.3 Establishing Three-Dimensional NOSE Cell Cultures

From the panel of normal ovarian surface epithelial cell lines described above, three were selected (NOSE4, NOSE11, NOSE19L3, see Table 3.1 and Figure 3.3) to establish as three-dimensional (3D) models. Patient information and *in vitro* two-dimensional (2D) and three-dimensional (3D) phenotype data are summarised in Table 3.2. Soft agar assays were performed to verify that cell lines exhibited a non-tumourigenic phenotype. None of the cell lines displayed any ability to grow in an anchorage-independent manner ($2x10^5$ cells/well). The *in vitro* growth characteristics of each cell line were analysed by establishing long-term growth curve assays. NOSE11 cells had the shortest population doubling time and the longest lifespan of the three primary cell isolates. This may be because NOSE4 cells were derived from a post-menopausal woman and are therefore likely to have a reduced lifespan *in vitro* (Figures 3.3 and Table 3.2). NOSE19L3 was a clone isolated from a brushing, and thus originates from a smaller initial population, hence the reduced lifespan observed for this culture. Due to contamination of initial brushings by blood cells and other debris, it was not possible to start growth curve assays at passage 1, and so the true *in vitro* lifespan of NOSE cells exceeds the values calculated here.

	Patient Characteristics		Cells grown as 2D monolayers			3D multicellular spheroids
Primary Cell line	Age	Menopausal Status	PD Time[1] (hrs)	Max. No. PDs	CFE in Soft Agar[2]	Average MCS Diameter (μM) (range)[3]
NOSE4	62	Post	82.4	7.6	0	**78.25** (32.70-152.00) n=11
NOSE11	48	Peri	57.2	17.8	0	**91.053** (80.92-252.40) n=11
NOSE19L3	39	Pre	83.6	9.7	0	**171.98** (63.90-125.60) n=5

Table 3.2: [1]Population doubling (PD) times calculated from the exponential growth phase; [2]Colony forming efficiency (CFE); [3]Multicellular spheroids (MCSs) grown in 3D by polyHEMA coating of tissue culture plastics, size measured under the scanning electron microscope.

NOSE4, NOSE11 and NOSE19L3 were then established as three-dimensional (3D) cultures. The aim was to compare morphological and biological characteristics of the same cells grown as 2D cultures, and with primary ovarian tissues. Two approaches were employed to generate 3D cultures: (1) polyHEMA coating of plastic tissue-culture dishes/flasks

and (2) the Rotary Cell Culture System (RCCS). The MCF7 breast cancer cell line was plated on polyHEMA-coated plastics as a control [Ghosh et al., 2005]. All three NOSE cells lines formed multicellular spheroids (MCSs) using both techniques. Cells were cultured in 3D for 14 days. MCSs grown on polyHEMA-coated plates (PH-MCSs) were typically 70-170μm in diameter (Table 3.2). NOSE19L3 cells formed significantly larger PH-MCS than NOSE4 or NOSE11 cells (P<0.0001 and P=0.025 respectively, two-tailed unpaired T-test). MCSs formed in the RCCS (RCCS-MCS) grew to 1-2mm in diameter and were limited to 1-2 in number per vessel. MCSs appeared solid and smooth under the light microscope (Figure 3.4)

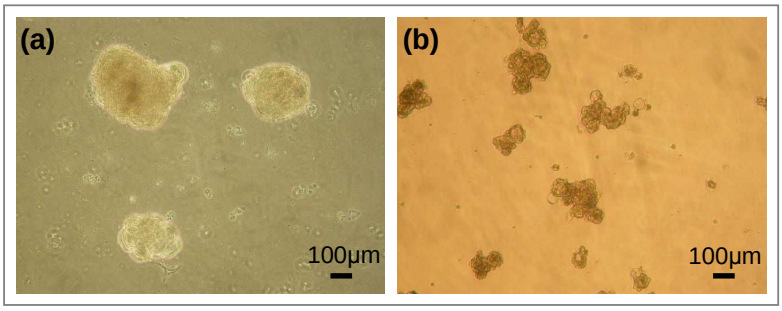

Figure 3.4: (a) NOSE4 in 3D culture, typical spheroids formed by culture on polyHEMA coated plastics. (b) The MCF7 breast carcinoma cell line, plated as a control, forms loose multicellular aggregates when cultured on polyHEMA coated plates [Ghosh et al., 2005].

The internal architecture of MCSs was examined following paraffin embedding, sectioning and staining with hematoxylin and eosin. For all three primary cell lines, PH-MCSs have a defined internal architecture: a central core of matrix protein, surrounded by aligned elongated cells (Figure 3.5a & b). The cells form a ring around the matrix core, often as a 'cap' to one side, which resembles papillary structures sometimes observed on the surface of normal ovaries *in vivo* (Figure 3.5e & f). The matrix core often contains degenerate nuclear debris. When cells were grown in the RCCS, the resulting MCSs had a less organised arrangement of cells. Cells within the centre of the RCCS spheroids tended to be more rounded, with a 1-2 cell deep layer of cells around the edge of the MCS that had an elongated morphology (Figure 3.5c & d).

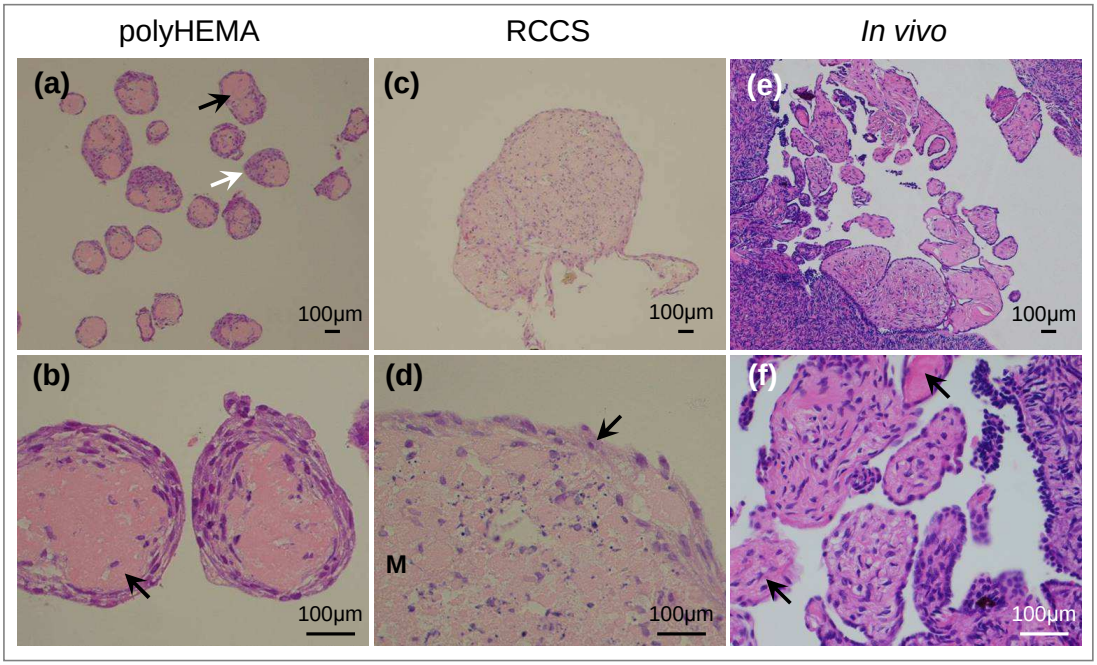

Figure 3.5: Hematoxylin and eosin stained sections of multicellular spheroids from 3D cultures. (a, b) NOSE cells form multiple small 3D multicellular structures when cultured on polyHEMA coated plates. The matrix cores of PH-MCS are clearly visible (black arrow); the cells form either a ring around the matrix or a cap on one side (white arrow). (c, d) When cultured in the RCCS, NOSE MCS were large and contained abundant ECM (M). Viable cells (arrow) surround the MCS, many degrading nuclei were distributed throughout the centre of the spheroids. (e, f) PH-MCSs show architectural resemblance to 3D structures observed on the surface of the ovary *in vivo*, where surface papillary projections consist of epithelial cells around stromal cores with matrix protein (black arrows).

3.4 Biological Characterisation of 3D NOSE Cell Cultures

3.4.1 Ultrastructure of PH-MCS

The polyHEMA-MCSs appeared architecturally interesting, and so both transmission and scanning electron microscopy (TEM and SEM) were used to study their ultrastructure compared to the same cells grown in 2D. Desmosomes, which are characteristic of epithelial cells, can be identified using TEM, and were present in all 2D and 3D cultures (Figure 3.6b).

Transmission electron microscopy revealed that in polyHEMA-MCSs, outer cells were often up to 8 cell layers thick but sometimes were only 1-2 cells thick. Outer cells were elongated and aligned. Peripheral cells were longer in shape compared to cells located towards the core of the spheroid, where cells were rounder and less densely packed (Figure 3.6c). Cells towards the centre of polyHEMA-MCS tended to have an extensive and dilated rough endoplasmic reticulum, well developed Golgi apparatus and an open nucleolus. Some central cells were observed to be secreting a discontinuous basement membrane and matrix-like material in the extracellular space. This extracellular matrix material was abundant in the core of the MCSs. Gap junctions and desmosomes connect neighbouring cells and indicate complex intercellular signalling within spheroids (Figure 3.6b & c)

When examined by SEM, 2D monolayers also had very few surface features; the cells were unremarkable, except that there were long surface projections extending between cells, similar to those seen on PH-MCSs (Figure 3.7a). Cells on the outer surface of the polyHEMA-MCS had flattened morphologies and very few surface features. Although microvilli were absent, there were often many surface projections connecting adjacent cells in the PH-MCS (Figure 3.7b &c). The absence of microvilli may be due to loss of polarisation as a result of culturing of the cells on glass. It may be possible to overcome this by growing NOSE cells with oestrogen for example, or a synthetic basement membrane in an attempt to maintain polarisation and microvilli formation [Saridogan et al., 1997]; [Bai et al., 2000]. Dead cells were observed both on the surface of the PH-MCS and in 2D cultures. Early-stage cell death was identifiable by the holes in the membrane and later-stage degraded cells were observed budding off the PH-MCSs and 2D cultures (Figure 3.7d).

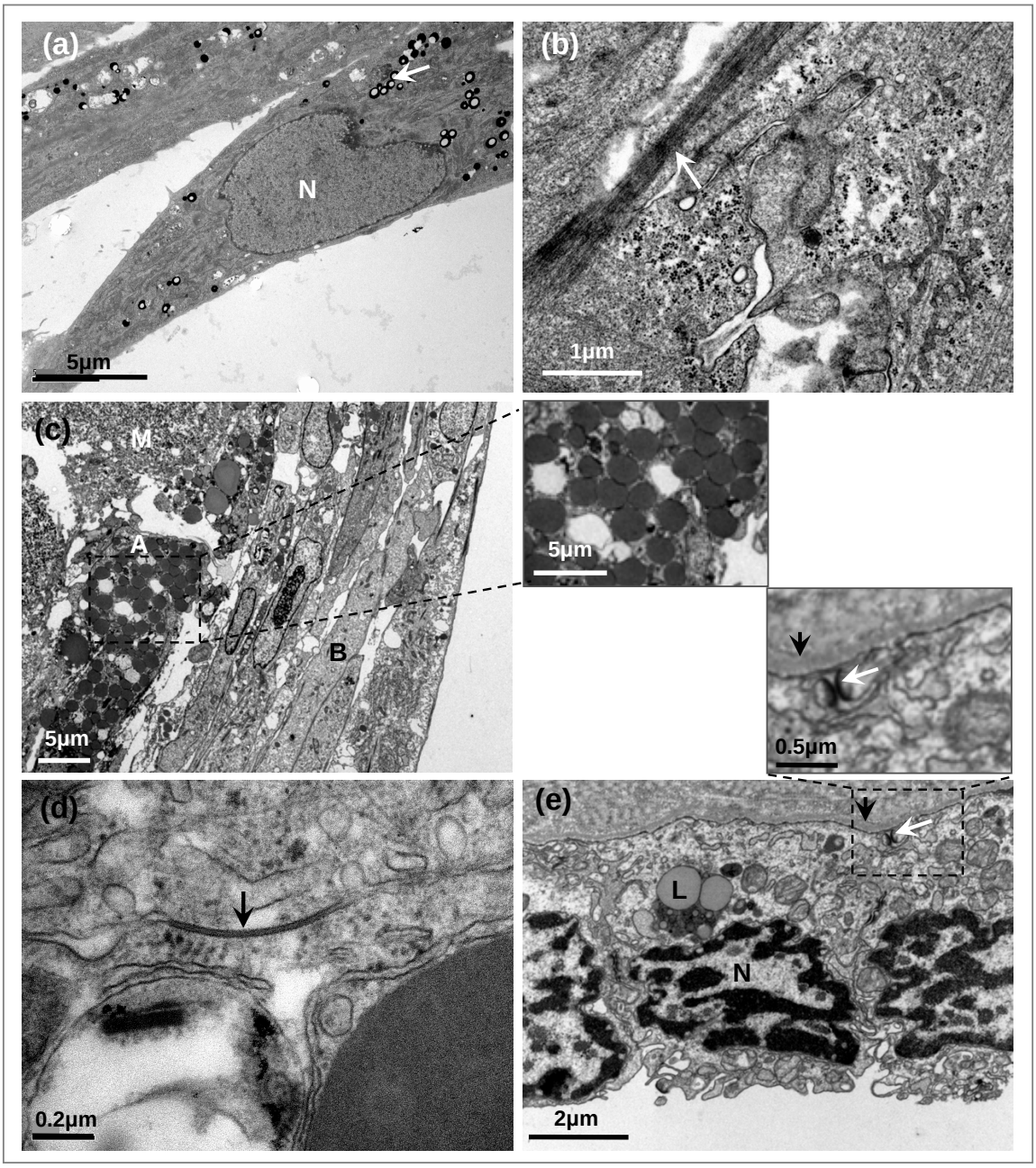

Figure 3.6: Transmission electron microscopy of NOSE cells in culture and from primary tissues. (a) NOSE cells in 2D. Cells are unpolarised and have lipid-rich vacuoles (white arrows). Cell nucleus is indicated (N). (b) In 3D cultures, desmosomes can be seen between adjacent cells (white arrow). (c) In PH-MCSs, flatter and closely opposed cells at the periphery form concentric rings (e.g. cell B). Cells within the inner region of the PH-MCS have a more rounded morphology and are less tightly packed (cell A). Cells towards the core of the MCS are full of electron dense vesicles (white arrow, inset), which may illustrate a trend to a more secretary phenotype towards the centre of the spheroids. Extracellular material (M) is abundant in the cores of PH-MCS. (d) Within the PH-MCS, gap junctions connect the cytoplasm of neighbouring cells. (e) Section of quiescent ovarian epithelium. Note the cuboidal shape of the cell, condensed chromatin within the nuclei (N), basement membrane (black arrow), desmosomes (white arrow, inset) and age related storage structures (lipofuscin, L).

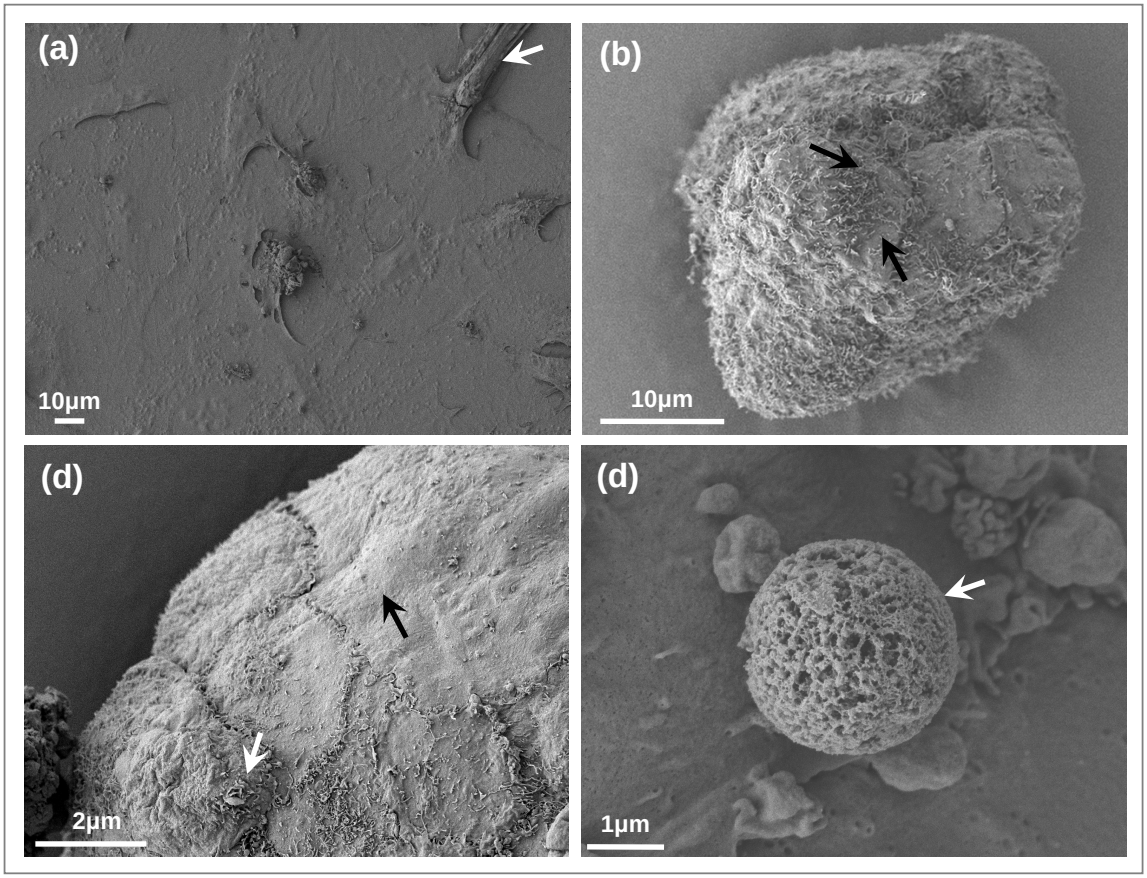

Figure 3.7: Scanning electron microscopy of NOSE cells in culture and from primary tissues. (a) 2D NOSE monolayers show few surface features, indeed cell boundaries are difficult to distinguish unless the cell is dividing (white arrow). (b) The surface morphology of PH-MCS. The flattened cells form a patchwork with no obvious orientation. Many surface projections between cells are visible on the surface of the MCS (black arrows). (c) High power SEM image illustrates the variation in the number of cellular projections often observed within a single spheroid, from few (black arrow) to many (white arrow). Surface cells have an enlarged, flattened morphology (also observed by TEM). (d) A dead cell budding of a polyHEMA spheroid. Many holes puncture the cell membrane, indicating late-stage apoptosis and degradation of the cell.

MARKER	NOSE 4			NOSE 11			NOSE 19L3			NORMAL
	2D	PH-MCS	RCCS-MCS	2D	PH-MCS	RCCS-MCS	2D	PH-MCS	RCCS-MCS	OSE *IN VIVO*
AE1/AE3										
Collagen IV					[2]					
Fibronectin[1]										
Laminin[1]										
Vimentin				[3]			[3]			

Table 3.3: Tabulated intensities of immunostaining data. Differential expression of pan-cytokeratin (AE1/AE3), laminin, vimentin and collagen IV, detected by immunohistochemistry in 2D and 3D cultures and in primary normal ovarian tissues. Graded shading denotes extent of staining. White denotes negative staining; crosshatched grey denotes weak or focal staining; light grey represents that 20-50% cells stain positive and dark grey shading indicates over 50% cells stain positive.[1]Secreted matrix material also shows positive staining for fibronectin and laminin. [2]Focal staining of collagen IV in NOSE11 PH-MCS. [3]NOSE11 and NOSE19L3 show limited focal staining for vimentin around mitoses in 2D.

3.4.2 Expression of Extracellular Matrix (ECM) Proteins in 2D and 3D Cultures

Previous studies have shown that culturing cells in 3D may alter cell-cell interactions, including the expression of extracellular matrix (ECM) proteins, receptors and corresponding degradative enzymes. NOSE cells produce a variety of ECM molecules *in vitro* [Kruk et al., 1994]. Therefore, immunohistochemical staining was performed to test whether any ECM proteins were differentially expressed between 2D and 3D cultures (Figure 3.8 and Table 3.3). Fibronectin was expressed in 2D and 3D cultures in all three cell lines. Vimentin staining was absent in 2D cultures, with the exception of weak focal vimentin staining around some mitoses (2/3 cell lines). However, strong positive vimentin staining characterised all 3D cultures and the OSE *in vivo*. Laminin and AE1/AE3 were not expressed in 2D cultures, but strong expression of these markers was observed in PH-MCSs, RCCS-MCSs and in the epithelium of normal ovarian tissues. Within spheroids, fibrous fibronectin, laminin and vimentin filaments were observed between cells, suggesting that these proteins play a role in maintaining the structure of MCSs.

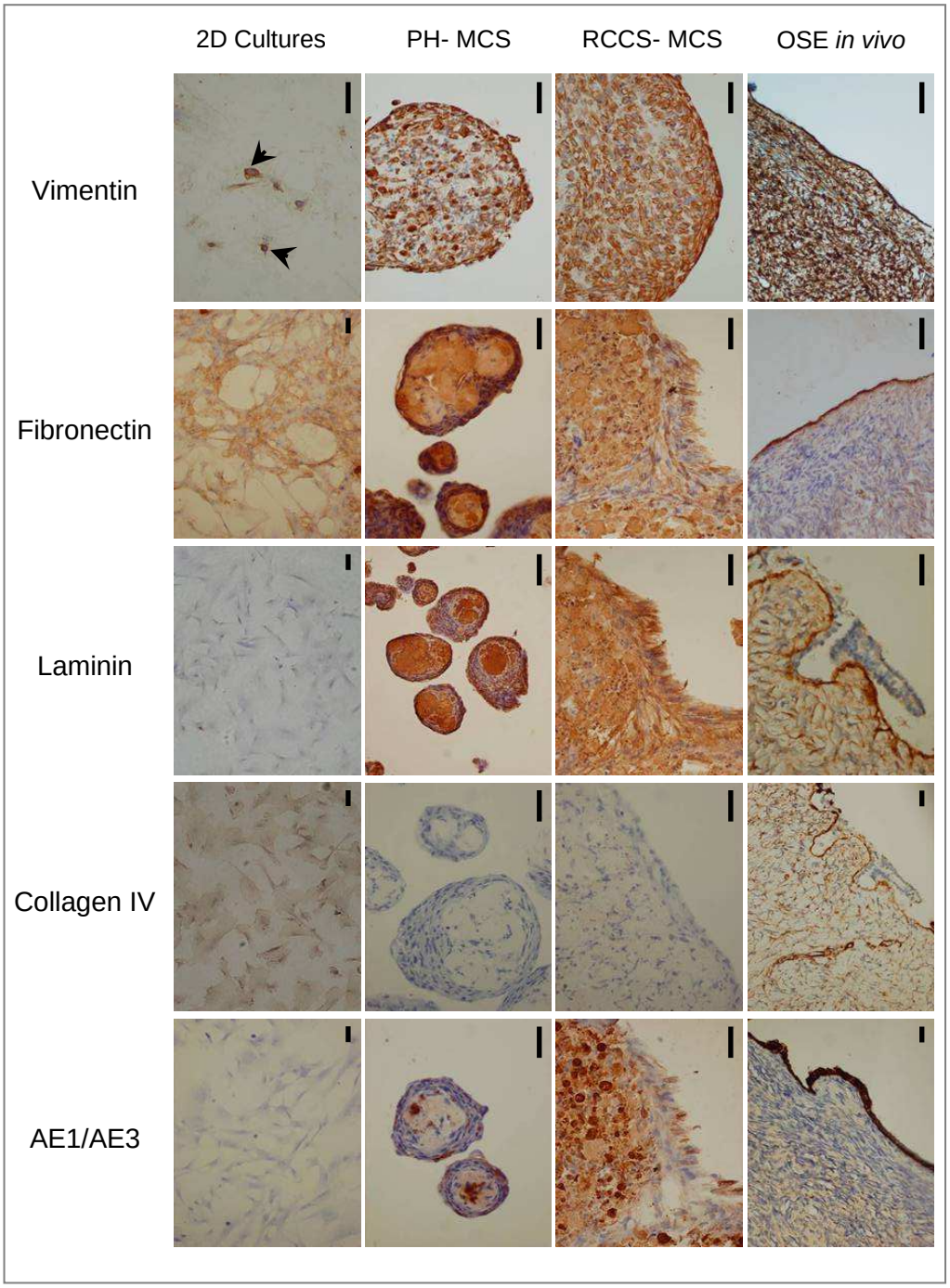

Figure 3.8: Expression analysis of pan-cytokeratin (AE1/AE3) and extracellular matrix proteins by immunohistochemistry of NOSE cells from representative 2D and 3D cultures and in primary NOSE from tissue sections of normal ovaries. Here, staining patterns demonstrate that primary NOSE from normal ovarian tissues express a range of extracellular matrix proteins (e.g. vimentin, fibronectin, laminin). Staining profiles of 3D cultures more closely resemble that of primary OSE than 2D cultures. Vimetin staining in 2D was absent, except some focal staining around mitoses (in 2/3 cell lines). Scale bars represent 100μm. PH = polyHEMA, RCCS = rotary cell culture system, MCS = multicellular spheroid

3.4.3 Apoptosis in 2D and 3D cultures

The proportion of apoptotic cells in the cultures was analysed using staining with an anti-annexin-V antibody and propidium iodide (PI), followed by flow cytometry (Figure 3.9). PI staining identifies the necrotic component of cell cultures; anti-annexin-V recognises externalised phosphatidylserine, which is an indicator of the early stages of apoptosis. In RCCS-MCSs, the proportion of cells that stained positive for annexin-V was at least 2.5-fold higher than the same cells grown in 2D cultures and PH-MCSs. For two cell lines, there was no significant difference in the proportion of apoptotic cells in PH-MCSs compared to 2D cultures. In NOSE19L3 there was more apoptosis in PH-MCSs (borderline significance, p= 0.047 using two-tailed paired T-test) compared to 2D cultures. This may be due to accumulation of apoptotic cells at later passages. There were significant differences in the proportion of annexin-V positive cells in RCCS-MCSs compared to 2D cultures and PH-MCSs for all three cell lines (NOSE4, p=0.0176; NOSE11, p=0.0164; and NOSE19L3, p= 0.0152 using two-tailed paired t-tests). For one cell line (NOSE11) a significantly larger necrotic component was also identified by PI staining in RCCS-MCSs compared to 2D and PH-MCSs (p= 0.0242, two-tailed paired t-test). Thus, for NOSE11 there was a statistically significant increase in the proportion of cells at all stages of apoptosis in RCCS cultures compared to cultures grown in 2D or on polyHEMA coated plates. Indeed, cells at all stages of apoptosis were distributed throughout the RCCS-MCSs (e.g. karyoretic nuclei, as indicated in Figure 3.9b). There was no observable pattern of apoptotic cell distribution related to spheroid size, or depth of the cell within a spheroid.

Untransformed epithelial cells undergo anoikis (programmed cell death) upon detachment from the basement membrane. Although there was a trend for more Annexin-V positive staining in the PH-MCS, no statistically significant increase in apoptosis was observed when polyHEMA spheroids were compared to 2D cultures, which suggests that the NOSE cells were not undergoing anoikis under these conditions. In both 3D systems, cells were plated at high densities and spheroids began to form within 24 hours. It thus appears that the process of aggregation was rapid enough to preventing anoikis.

3.5 Discussion

The aim of this Chapter was to establish and characterise a panel of normal ovarian surface epithelial (NOSE) cell lines and then to evaluate 3D methodologies for growing NOSE cells *in vitro* and compare with the phenotypes of the same cells grown in 2D.

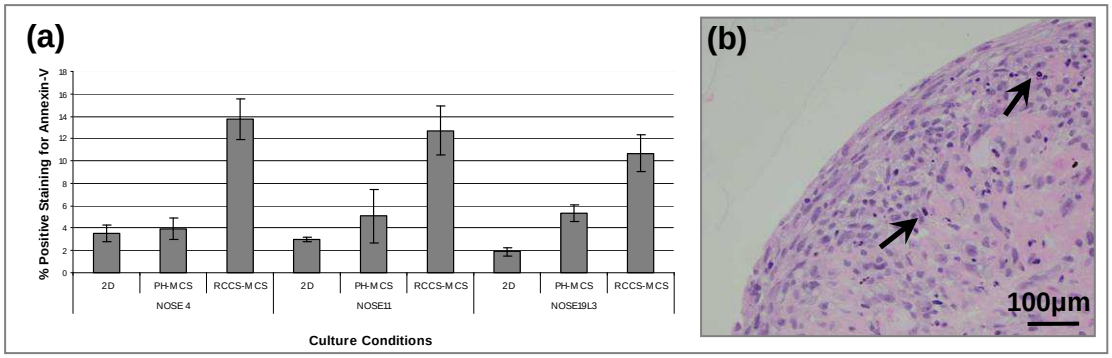

Figure 3.9: Apoptosis in 2D and 3D cultures. (a) Levels of apoptosis (as measured by annexin-V expression) are significantly higher in 3D cultures from the RCCS-MCS, compared to similar proportions of apoptotic cells detected in 2D and PH-MCS cultures. Error bars = standard error of the mean (S.E.M.) (b) Apoptotic cells (arrow) are distributed throughout the RCCS-MCS, identifiable by degrading nuclei.

The primary NOSE cell lines used in this study demonstrated typical staining and growth characteristics *in vitro*, as previously shown by other studies [Auersperg et al., 1984]; [Li et al., 2004a]. The *in vitro* lifespan of NOSE cultures maintained in a growth factor rich medium was less than 60 days. NOSE cells demonstrate phenotypic plasticity and can co-express epithelial and fibroblastic markers *in vitro* and *in vivo*. In highly mitogenic medium (NOSE-CM) NOSE cells have a fibroblastic morphology, which is promoted by the inclusion of hydrocortisone (HC) and epidermal growth factor (EGF) in the medium [Salamanca et al., 2004]; [Ahmed et al., 2007]. However, without HC and EGF, the growth potential of primary OSE cultures is reduced significantly, by around 2/3rds [Salamanca et al., 2004]. Thus all NOSE cultures and their derivatives were maintained in NOSE-CM for the experiments described in this thesis. Highly mitogenic NOSE-CM culture medium, however, is not optimal for reproducing the phenotype of a typically quiescent ovarian epithelial cell and may more closely reflect the phenotype of NOSE cells during wound repair, at the site of ovulation. In addition, NOSE-CM may contribute to tumourigenesis through incessant stimulation of pathways involved in growth and proliferation (including the MAPK pathway, discussed in Chapter 4).

The OSE is typically described as a monolayer of cells, but it nonetheless has a three-dimensional (3D) geometry that cannot be replicated by culturing primary NOSE cells in two-dimensional (2D) cultures on an adherent plastic surface. Thus, 3D cultures of NOSE cells were established to investigate whether 3D *in vitro* models were a closer representation of OSE *in vivo* than traditional 2D techniques. In these experiments, NOSE cells formed three-dimensional structures (multicellular spheroids; MCSs) when cells were prevented

from adhering to tissue culture surfaces either by chemical treatment of tissue culture vessels or by maintaining cells in constant rotation. In the rotary cell culture system (RCCS), NOSE cell clusters were larger and had a chaotic internal structure compared to cells grown on polyHEMA-coated plastics. NOSE cells grown in polyHEMA coated vessels formed concentric layers around a core of matrix protein. These data demonstrate that in a static microenvironment NOSE cells can spontaneously form organised three-dimensional multicellular structures.

Within each spheroid there exists a number of different microenvironments, and different selective pressures influence cellular phenotype depending on the part of the spheroid in which a cell is located. Other reports describing 3D cell aggregates of other cells types have observed two distinct regions within homotypic MCS - an inner area of cells that are smaller and less proliferative than surrounding cells on the periphery of MCS [Sutherland et al., 1986]; [Ghosh et al., 2005]. In one study, Freyer and Sutherland found that cells on the surface of MCSs formed from mouse mammary tumour cells were similar in size to an exponentially growing 2D cell culture, but with 60% fewer cells in S-phase [Freyer and Sutherland, 1980]. My observations of the structure of RCCS-MCSs (by light microscopy) and polyHEMA-MCSs (by light and transmission electron microscopy) are consistent with these findings; instead of a continual reduction in cell size from the outer to inner core of spheroids, there was a clear distinction in morphology observed between cells on the outer layers compared to cells within the spheroids. Cells within the MCS also had rounder morphologies compared to the elongated cells at the periphery.

Measurements of apoptosis in 2D and 3D cultures suggested that a greater proportion of cells grown in the RCCS are apoptotic compared to 2D and polyHEMA 3D cultures. This was confirmed by the observation of many apoptotic nuclei distributed throughout the RCCS-MCS (in H & E stained sections of paraffin embedded samples). The explanation for this is unclear; but it could be that the continual motion of spinning the cells in the RCCS causes mechanical damage to cells, which in turn induces apoptosis. Thus, the increased apoptosis levels observed in RCCS-MCSs may be an experimental artefact. Apoptosis is low in the ovarian epithelium *in vivo* since these cells are usually quiescent. Unlike cancer cell spheroids, a central core of extensive apoptosis and necrosis was not observed in NOSE spheroids. Conditions at the centre of the RCCS-MCS are unlikely to be hypoxic (which would induce cell death) in comparison to the *in vivo* microenvironment - the oxygen concentration in the pelvis is 5.5% (measured at the cervix) but cells were cultured in 20% oxygen in this present study [Juul et al., 2007]. Furthermore, cell death induced by hypoxia would result in a distinct distribution of apoptotic cells throughout the spheroids: cell death would be lowest near the surface and gradually increase towards the core. In largest spheroids, one would expect that chronic hypoxic conditions would

results in a necrotic central region. However, apoptotic cells were distributed throughout the spheroid, independently of spheroid size or cell depth within the spheroid, suggesting that in this system cell death was not induced by hypoxia. This suggests that the increased rates of apoptosis observed in RCCS-MCS are a consequence of mechanical damage. In this laboratory, it has been observed that prolonged culture in the RCCS results in spheroids that consist mainly of degenerated cells (observation, KL and B. Grun).

Examination under the transmission electron microscope enabled analysis of cellular and spheroid ultrastructure. PolyHEMA-MCS cells contained swollen endoplasmic reticulum and Golgi bodies and had an open nucleolus, which is indicative of active protein synthesis and transcription. Cells within central regions of polyHEMA-MCS were actively producing and appeared to be secreting a basement membrane-like matrix which was abundant in the core of MCSs. Extracellular matrix (ECM) molecules play a vital role in tissue architecture and are reporte to be essential for the formation of hepatoma spheroids [Lin et al., 2006]. Both RCCS- and PH-MCSs contained an abundance of the extracellular matrix (ECM) proteins laminin, fibronectin and vimentin, but did not express collagen IV. 2D cultures showed widespread expression of fibronectin and collagen IV but not laminin, and vimentin was only expressed focally at mitoses (2/3 cultures). Increased expression of vimentin and a concurrent decrease in expression of collagen IV in 3D could indicate an epithelial-to-mesenchymal transition. However, upregulation of pan-cytokeratin indicates a more epithelial phenotype. These patterns of protein expression reflect the phenotypic plasticity that is characteristic of NOSE cells: in both 2D and 3D cells show both epithelial and mesenchymal features.

The importance of the extracellular matrix cannot be understated, since dysregulation of cell-ECM interactions have been demonstrated to have a role in many critical processes in tumourigenesis beyond invasion and metastasis, including chemotherapeutic resistance and development of minimal residual disease [Damiano et al., 1999]; [Matsunaga et al., 2003]; [Sherman-Baust et al., 2003]. Remodelling of the basement membrane and stromal ECM proteins occur during during follicular maturation (in non-neoplastic ovaries) and the development of ovarian carcinomas [Capo-Chichi et al., 2002]; [Lind et al., 2006]. Downstream pathways of cancer cell interactions with the extracellular matrix may represent important therapeutic targets [Ahmed et al., 2007]. In NOSE spheroids, the complex ECM observed was synthesised autonomously by the NOSE cells, since no synthetic matrix proteins were introduced in the cultures. This is a significant advantage of both the RCCS and polyHEMA methods described here, since the heterogeneous ECM closely resembles the ECM of the organ.

Microenvironment - phenotype over genotype?

When suspended in laminin rich ECM gels, human mammary epithelial cells (HMECs) form organotypic acini structures and express milk proteins [Weir et al., 2006]. In contrast, breast carcinoma cell lines form disorganised aggregates in ECM gels, displaying a loss of tissue differentiation [Weaver et al., 1995]. However, acini structure can be re-established *in vitro*, and thus the malignant phenotype reversed, by altering carcinoma cell interactions with the extracellular matrix [Weaver et al., 1997]. This demonstrates that the microenvironment can dominate over cellular genotype to control a neoplastic phenotype, which has important implications for studying cell transformation. These models also offer a new approach for the development of therapeutic drugs which reverse the malignant phenotype as an alternative to inducing cancer cell death.

As with HMECs, 3D models of ovarian epithelial cells are likely to increase our understanding of the biology of normal and malignant cells *in vivo*. For example, the mechanisms of wound repair following follicular rupture remain poorly understood, yet could have implications for understanding the biology of EOC. Ovarian inclusion cysts develop from crypts formed following ovulation and appear to be the site of initiation of a large proportion of EOCs. It is known that remodelling of the ECM (and changes in the relative proportions of constituent proteins) preceeds ovulatory rupture [Lind et al., 2006]. By adding synthetic ECM proteins to the 3D spheroids, such changes could be replicated *in vitro* and the NOSE cell phenotype monitored. Additionally, wound healing requires an EMT and extensive proliferation of NOSE cells. Understanding the molecular mechanisms and microenvironmental signalling that governs these processes in normal tissues is likely to provide valuable insight into tumour development and EOC cell behaviour.

Implications for the Study of Epithelial Ovarian Cancer

Collection of primary normal ovarian surface epithelial cells is challenging and the number of cells that can be isolated from each ovary is small, as the OSE is a monolayer and the ovary is a small organ (1-2cm diameter). Normal OSE samples serve as necessary controls for many different studies, such as gene expression microarray profiling of normal and cancer tissues or biomarker validation by analysing mRNA or protein. Gene expression microarray studies have often used pooled ovarian brushings or pieces of whole ovary (the majority of which is stroma) as normal controls. The control used for comparisons of gene expression profiles of normal *versus* EOC cells will significantly affect the outcome of the analyses. Zorn and colleagues found limited overlap between the lists of differentially expressed genes when EOC gene expression profiles were compared to the profiles

of whole ovarian biopsies, OSE brushings, short-term OSE cultures, SV40-immortalised OSE or telomerase-immortalised OSE [Zorn et al., 2003]. 3D models of NOSE cells could be used as an alternative normal control for studies that require relatively large amounts of material e.g. analysis of the transcriptome and proteome. Another approach would be to use cores taken from formalin-fixed paraffin embedded (FFPE) 3D cultures in tissue-microarrays (TMAs) for analysis of biomarker expression by immunohistochemistry. Many commercially available FFPE normal ovaries and TMAs contain little or no epithelium, as it constitutes such a small portion of the organ and is loosely attached and therefore easily lost during processing.

The origin of EOCs has yet to be fully understood, and current *in vitro*, *in vivo* and histological evidence support multiple origins for ovarian tumours of different histotypes. However, what is not yet understood is whether EOCs in humans arise from a normal ovarian stem cell precursor. Wound repair of ovulatory sites in the murine ovary are repaired by a small population of slowly cycling progenitor 'stem-like' cells. To repair the site of follicular rupture, this population of cells undergoes rapid cell division to repopulate the lesion on the surface of the ovary [Szotek et al., 2008]. Whether ovulatory sites are repaired by stem-like progenitor cells in humans has yet to be elucidated. For EOCs there are data to suggest that populations of stem-like cells exist within tumours [Alvero et al., 2009]; [Curley et al., 2009]. However, markers of normal or malignant ovarian stem cells have yet to be confirmed. 3D models represent an organoid model for studying EOC origins and a role for stem cells in tumour initiation, development and metastases.

Conclusions

The next stages of my study, described in Chapters 4 & 5, require the use of an appropriate 3D modelling approach. Having tested the RCCS and polyHEMA methods for culturing NOSE cells in 3D, it was concluded that the RCCS would not be an appropriate model for the next stages of the study, as (1) elevated levels of apoptosis were observed in cells cultured in the RCCS, (2) only a small number of replicate experiments (n=5) can be performed simultaneously and (3) RCCS vessels are costly. The polyHEMA models tested and presented here were considered to represent a flexible tool for examining many different aspects of EOCs. In our laboratory, polyHEMA models are now being used to study NOSE cell transformation (Chapter 4), the biology of normal fallopian tube epithelial cells, stromal-epithelial interactions in cancer, chemoresistance and stem cell biology. The polyHEMA models were also subsequently employed in a functional study of a candidate ovarian cancer tumour suppressor gene [Dafou *et al.*, manuscript in preparation].

Finally, it was concluded that the 3D NOSE models could provide the basis for establishing more complex three-dimensional cultures. Heterotypic 3D models comprising ovarian stromal fibroblasts as well as epithelial cells may assist in developing an understanding of the role of stromal-epithelial interactions during epithelial tumourigenesis, this is explored in Chapter 5. Two major advantages of the polyHEMA approach to 3D spheroid formation are the low cost and the flexibilty of the technique - any tissue culture plastic can be used. An additional advantage of the polyHEMA (and also RCCS) over the popular gel-based 3D culturing methodologies is that the cells create the extracellular matrix autonomously, and the data presented here show that the ECM of the spheroids reflects the ECM of the ovary *in vivo*. Therefore, the polyHEMA technique was chosen for the further 3D modelling work described in the following chapters. it is hoped that this three-dimensional *in vitro* tool can provide a more biologically relevant model not only for modelling disease, as described in this thesis, but also for high-throughput screening of candidate biomarkers of disease, or for testing novel therapeutics. 3D models are likely to be more accurate at predicting efficiencies of novel therapeutic compounds than 2D systems, which often fail to translate in an *in vivo* or clinical setting [Friedrich et al., 2007].

4

In Vitro Transformation of the Ovarian Surface Epithelium

4.1 Introduction

The scarcity of tissues derived from early-stage epithelial ovarian cancers (EOC) means that little is known about the cellular molecular and phenotypic changes that occur early in the development of EOCs. In addition, progress in understanding the molecular features of early ovarian carcinogenesis has also been hindered by a shortage of good *in vitro* models of ovarian cancer. Previously established models introduced viral oncogenes into ovarian surface epithelial (OSE) cells to induce neoplastic transformation. The resulting cells formed tumours in mice that express cytokeratins and resemble epithelial ovarian tumours [Li et al., 2004b]; [Kusakari et al., 2003]. Recently, the first description of transformation of the OSE with defined genetic elements was reported [Sasaki et al., 2009].

Mutations in a handful of genes, including *BRCA1/2*, *KRAS*, *BRAF*, *PTEN*, *PIK3CA* and *β-catenin* occur in a subtype-specific manner in EOCs. Different subtypes of EOC differ in their histological features, biomarker expression, and prognoses. However, there are few descriptions of correlations between genetic mutation and *in vitro* phenotype of OSE cells. All *in vitro* studies to date have been performed using traditional 2D monolayer cultures. Additionally, molecular profiles associated with *KRAS/BRAF* mutation in the OSE have not been described in *in vitro* or in *in vivo* studies. This project aimed to investigate the role of specific genetic alterations in an *in vitro* model of early EOC development with the following hypothesis:

- *In vitro* neoplastic transformation of normal ovarian surface epithelial cells can be achieved through the introduction of defined oncogenic elements

The aims of this Chapter were to address the following questions:

1. Can stepwise transformation of NOSE cells be achieved by the introduction of *hTERT*, *C-MYC*, plus $KRAS^{G12V}$ or $BRAF^{V600E}$?
2. Are phenotypic differences detected *in vitro* that are induced by the different oncogenes?
3. Does 3-dimensional modelling reveal features of neoplastic transformation visible in tumour specimens but not detectable in traditional 2D cultures?
4. Do the gene expression profiles of 3D cultures at each stage of the transformation model reveal novel genes that are altered in synergy with the genes introduced, which may be candidate markers of early disease? Is there molecular heterogeneity associated with transformation mediated by the different oncogenes?

We hypothesised that features of transformation can be induced in normal ovarian surface epithelial cells by sequentially introducing alleles commonly found to be mutated or overexpressed in EOC specimens. Cellular phenotype can be monitored with a series of *in vitro* assays to measure the transformed phenotype. *In vitro* and *in vivo*, changes in the cellular phenotype observed as a cell becomes increasingly transformed may include: increased proliferation and anchorage-dependent growth; acquired anchorage-independent growth; up-regulation of pro-angiogenic factors; increased invasiveness; enhanced migrative ability; reduced apoptosis and increased dependence from growth factors. Changes in cellular metabolism may also occur. These changes can be monitored in vitro and a panel of assays can be selected according to the question being addressed.

4.2 Immortalisation of Primary NOSE Cells

One of the major origins of EOCs is the ovarian surface epithelium, a monolayer of epithelial-mesothelial cells covering the surface of the ovary [Auersperg et al., 1984]. Isolation and characterisation of primary normal ovarian surface epithelial (NOSE) cells is described in detail in Chapter 3. Primary normal ovarian surface epithelial (NOSE) cells have an average *in vitro* lifespan of only 10-15 population doublings. In 1965 Hayflick

first described what was coined the 'Hayflick Limit', which describes how explanted normal somatic cells have a limited lifespan *in vitro* before cells will undergo irreversible replicative senescence [Hayflick, 1965]. It was, therefore, necessary to extend the *in vitro* lifespan of NOSE cultures to enable the cells to bypass replicative senescence and thus facilitate the introduction of further genetic alterations. This was achieved by ectopically overexpressing the catalytic subunit of the human telomerase holoenzyme, *hTERT*.

Immortalisation of NOSE cells with *hTERT* has been previously described [Li et al., 2004a]. A cDNA encoding *hTERT* was delivered into cells by retroviral transduction. In these experiments, a retroviral system based on the Moloney Murine Leukemia Virus (MMLV) was employed. Retroviral supernatants harvested at 48-hours post-transfection of 293T cells and used to infect NOSE4, NOSE11 and NOSE19 cell lines. Optimisation of retroviral production and transduction protocols are described in Chapter 2. Transduced clones were selected using 10-30U/ml hygromycin, and clones were isolated by ring cloning 3-4 weeks post-infection. *hTERT*-clones were denoted 'immortalised ovarian surface epithelial' (IOSE) cells (e.g. IOSE4.1, to describe a clones from *hTERT* infection of NOSE4 cells, clone number 1).

In the first instance, a minimum of 2 clones per NOSE parental cell line were maintained in culture for up to 10 passages to ensure that the cells bypassed replicative senescence. The length of *in vitro* lifespan of NOSE and IOSE cell lines was measured. Growth characteristics of 2-3 clones per primary culture were analysed to assay growth characteristics over a period of 80 days. Not all clones that were analysed displayed extension of *in vitro* lifespan, suggesting that some clones were expressing levels of telomerase that were insufficient to maintain telomere length and bypass senescence (Figure 4.1).

IOSE4.1, IOSE11.1 and IOSE19.1 were maintained in culture as long-term growth curve experiments beyond day 80. From this point, that these cell lines are denoted IOSE4, IOSE11, IOSE19. Lifespan of NOSE cell lines was around 50 days, whereas the introduction of *hTERT* increased the lifespan of these 3 cell lines to over 200 days (Figure 4.2a). At this point the cell lines were considered to be "immortalised" and the growth experiments were discontinued. IOSE cells displayed a fibroblastic epithelial morphology when visualised by phase-contrast microscopy (Figure 4.2b). There were no changes in gross morphologies of cell cultures following immortalisation.

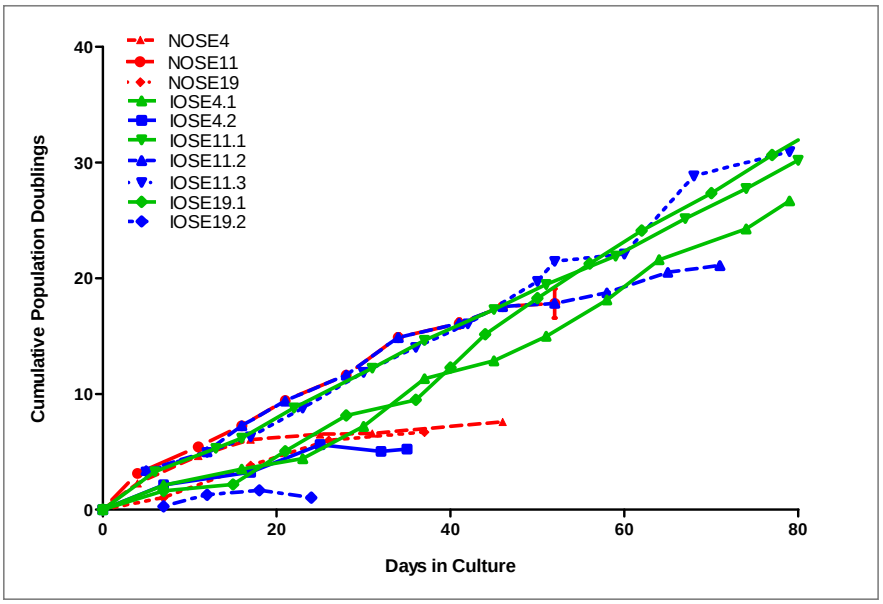

Figure 4.1: Immortalised ovarian surface epithelial (IOSE) cell lines: growth curves to assay *in vitro* lifespan. IOSE clones taken forwards for further experiments are indicated in green. NOSE cell lines are shown in red and other IOSE cell lines in blue. IOSE4.2 and IOSE19.2 did not bypass replicative senescence and grew slowly in culture. Error bars show standard deviation.

4.2.1 Fluorescent Immunocytochemistry

Primary NOSE and IOSE cells were examined for the expression of epithelial (cytokeratin-7, Ck7; pan-cytokeratin, AE1/AE3), mesothelial (calretinin), fibroblastic (fibroblast surface protein, FSP) and ovarian cancer markers (cancer antigen 125, CA125; E-Cadherin) (Figures 4.3, 4.4, 4.5, 4.6, 4.7 & 4.8 and summarised in Table 4.9). Positive control cell lines were included in each staining experiment; representative images of positive staining for each antigen can be found in Figure 4.10. NOSE and IOSE lines demonstrated very similar staining profiles when examined by flourescent immunocytochemistry. All NOSE and IOSE cultures stained positive for Ck7, and, to a lesser extent, AE1/AE3. Keratins are structural proteins in epithelial cells, and the staining detected in NOSE and IOSE cultures was correctly localised to the cytoplasm. Cytokeratin-7 was a more reliable marker than AE1/AE3 of the epithelial status of normal ovarian surface epithelial cells - 40-70% of cells stained positive for the Ck7 antigen. Some cross-reactivity was observed when cultures were stained for FSP, but FSP expression was absent or low when compared to a positive control cell line (a normal ovarian fibroblast cell line, INOF2 or a skin fibroblast cell line, 1BR3). Furthermore, extensive testing of this antibody within this laboratory has demonstrated that this antibody frequently cross-reacts with non-fibroblast cells. Weak

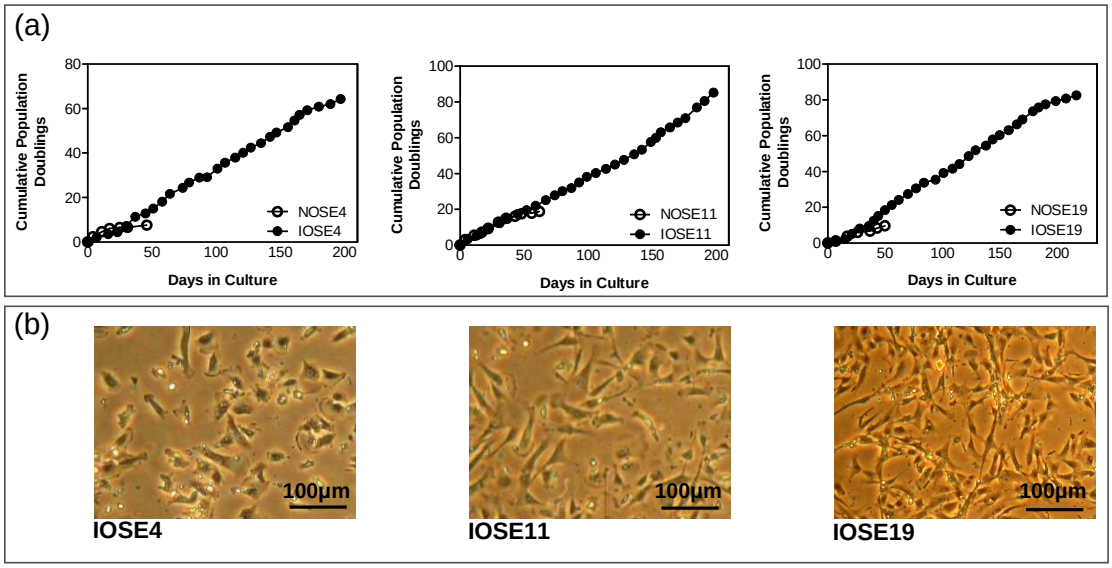

Figure 4.2: Immortalised ovarian surface epithelial (IOSE) cell lines: long-term growth curves and cell morphologies of 3 IOSE cell lines to be used in further experiments. (a) Lifespan of ovarian epithelial cultures cultures is extended to over 200 days following the introduction of the catalytically active subunit of human telomerase (*hTERT*). The lifespan of NOSE cultures is limited to under 60 days. (b) IOSE cell lines have an epithelial-fibroblastic morphology when visualised by phase-contrast microscopy.

staining of calretinin was observed in the majority of clones tested, suggesting NOSE and IOSE cells maintain some mesothelial characteristics *in vitro*. E-cadherin, often expressed in EOC specimens but absent in normal OSE cells *in vivo*, was not expressed in any of the NOSE or IOSE cultures tested. Staining profiles of NOSE and IOSE were consistent, suggesting that no gross changes in cell differentiation or neoplastic transformation were induced by immortalisation with *hTERT* (Table 4.9).

In some cell types, including human prostate epithelial cells and keratinocytes, inactivation of the *p16INK4a* is a pre-requisite for immortalisation; and so p16 expression was examined by fluorescent immunostaining. p16 expression was detected in nuclear and cytoplasmic regions of IOSE cells, suggesting that loss of this cell-cycle checkpoint was not required for immortalisation (Figures 4.3, 4.4, 4.5, 4.6, 4.7 & 4.8). This is similar to the observed p16 status after immortalisation of human mammary epithelial cells, embryonic lung fibroblasts and ovarian surface epithelial cells from other studies [Herbert et al., 2002]; [Darbro et al., 2006]; [Milyavsky et al., 2003]; [Li et al., 2007]; [Shao et al., 2008].

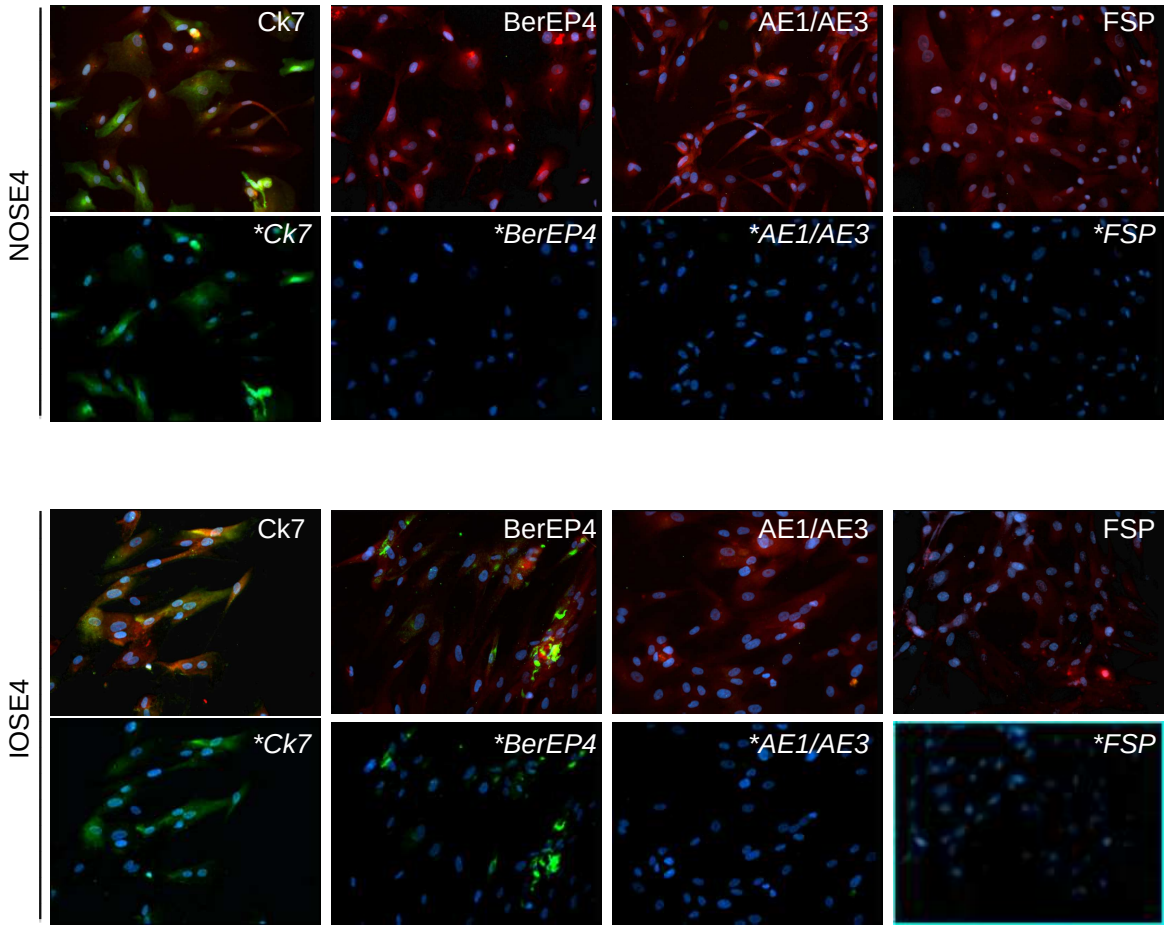

Figure 4.3: Fluorescent immunocytochemistry (NOSE4 part 1): staining profiles of NOSE4 and IOSE4 show that immortalisation does not induce changes in marker expression. Both cell lines stain positive for cytokeratin 7. Weaker positivity/absent staining with the BerEP4 antibody was detected; staining for pan-cytokeratin (AE1/AE3) epithelial marker was absent. No staining for FSP was observed. All images are 200X magnification and exposure times were consistent for each antigen. In the top panel for each cell line, Evans blue (red colour) staining of cellular cytoplasm is shown, green fluorescence indicates antigen positivity, nuclei are stained blue with DAPI. In the lower panel for each cell line, only the antigen of interest and nuclei are shown.

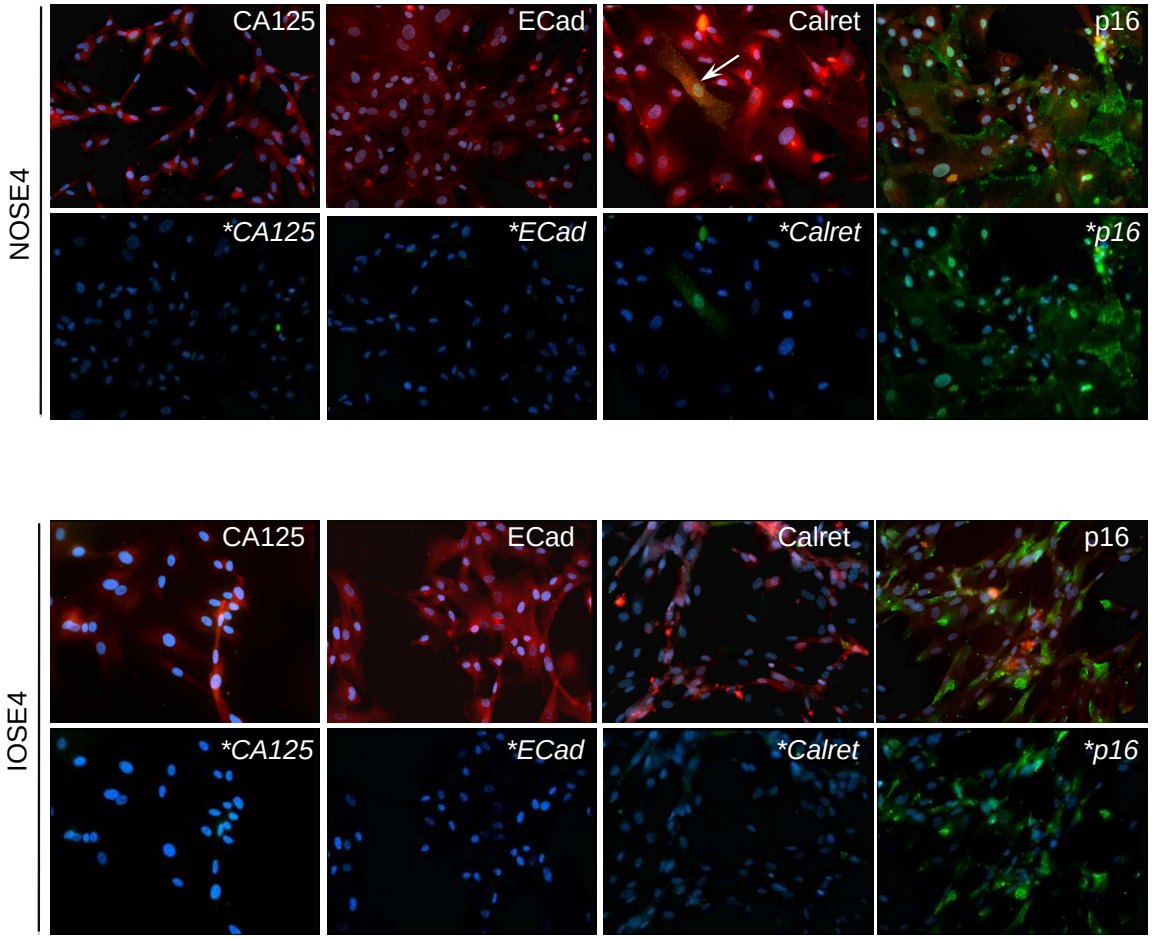

Figure 4.4: Fluorescent immunocytochemistry: staining profiles of NOSE4 & IOSE4, part 2. No expression of cancer-antigen 125 (CA125) or E-cadherin was detected. Discrete cells stain positive for mesothelial marker calretinin (arrow). Nuclear and cytoplasmic staining for p16 was detected in NOSE4 and IOSE4 cells. All images are 200X magnification and exposure times were consistent for each antigen. In the top panel for each cell line, Evans blue (red colour) staining of cellular cytoplasm is shown, green fluorescence indicates antigen positivity, nuclei are stained blue with DAPI. In the lower panel for each cell line, only the antigen of interest and nuclei are shown.

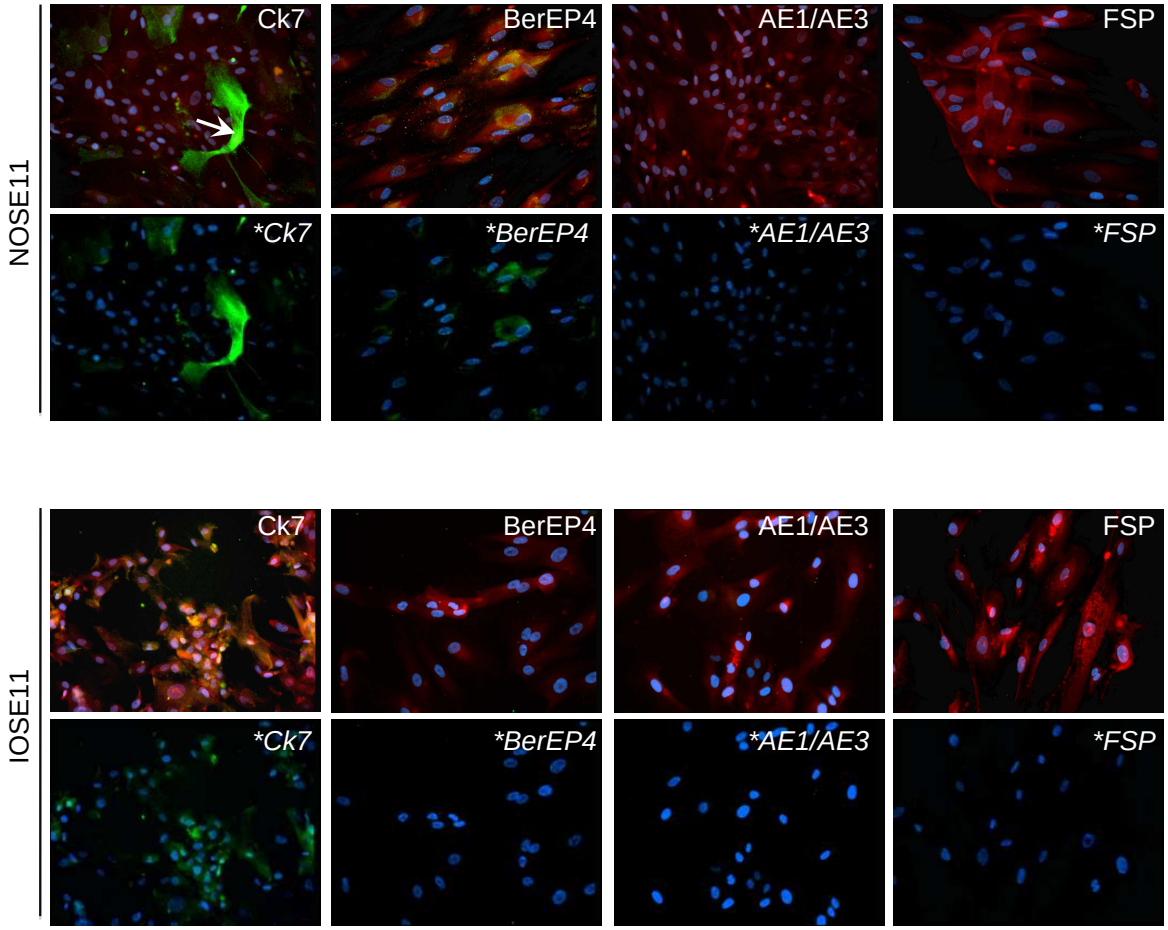

Figure 4.5: Fluorescent immunocytochemistry (NOSE11 part 1): staining profiles of NOSE11 and IOSE11 show that immortalisation does not induce changes in marker expression. Both cell lines stain positive for cytokeratin 7. Note that mitotic cells express higher levels of cytokeratin (white arrow). Weak positivity for BerEP4 was detected in NOSE11. Staining for pan-cytokeratin (AE1/AE3) epithelial marker was absent. No expression of fibroblast surface protein (FSP) was detected. All images are 200X magnification and exposure times were consistent for each antigen. In the top panel for each cell line, Evans blue (red colour) staining of cellular cytoplasm is shown, green fluorescence indicates antigen positivity, nuclei are stained blue with DAPI. In the lower panel for each cell line, only the antigen of interest and nuclei are shown.

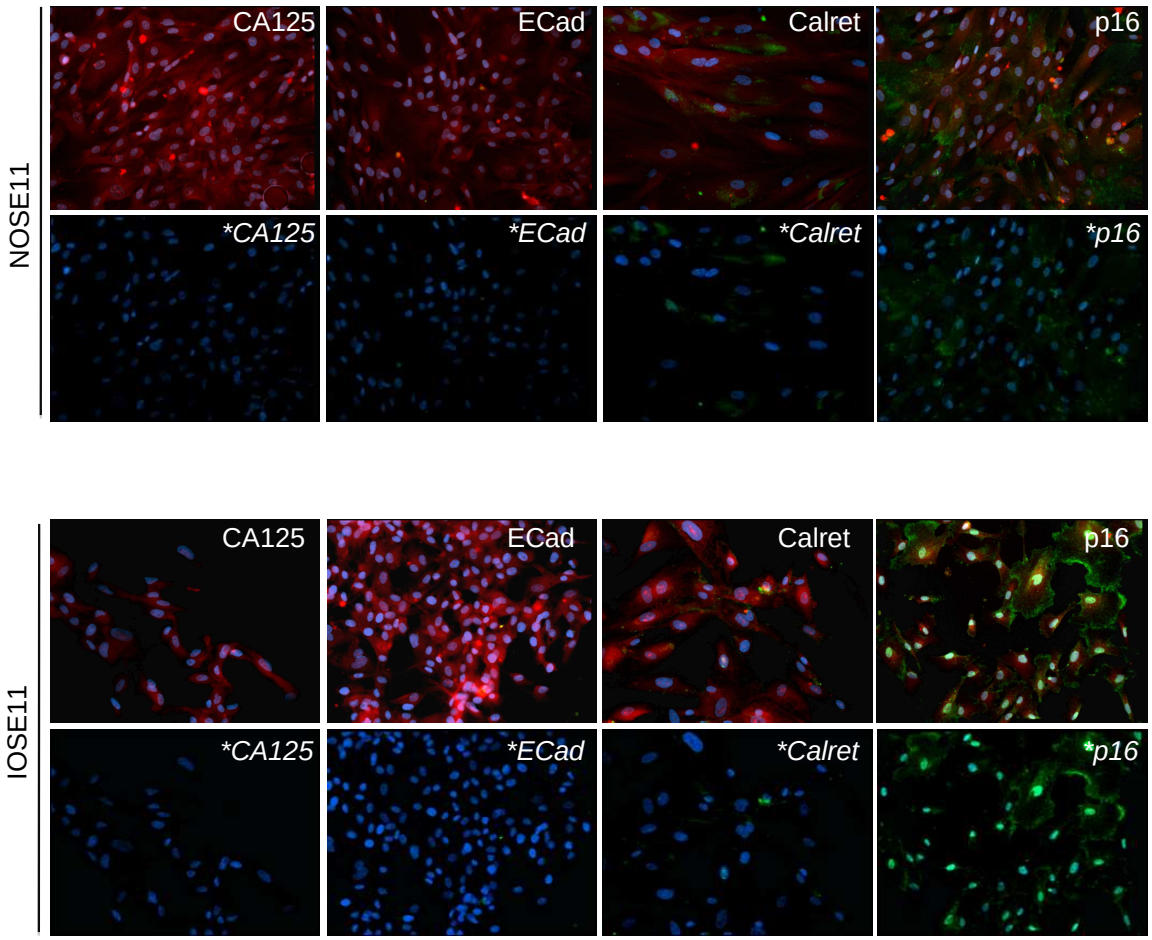

Figure 4.6: Fluorescent immunocytochemistry (NOSE11 part 2): staining profiles of NOSE11 and IOSE11 show that immortalisation does not induce changes in marker expression. No expression of cancer-antigen 125 (CA125), E-cadherin was detected. Nuclear and cytoplasmic staining for p16 was detected in NOSE11 and IOSE11 cells. All images are 200X magnification and exposure times were consistent for each antigen. In the top panel for each cell line, Evans blue (red colour) staining of cellular cytoplasm is shown, green fluorescence indicates antigen positivity, nuclei are stained blue with DAPI. In the lower panel for each cell line, only the antigen of interest and nuclei are shown.

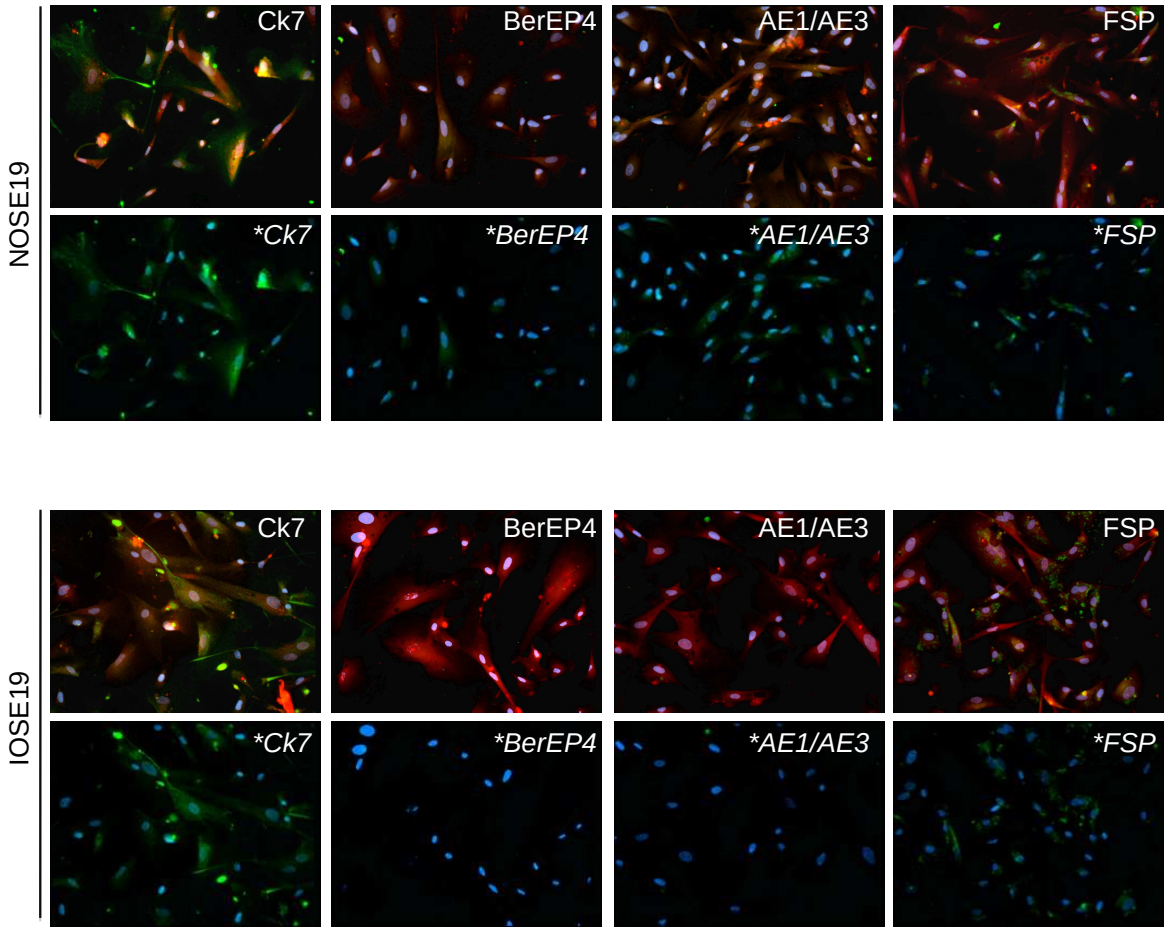

Figure 4.7: Fluorescent immunocytochemistry (NOSE19 part 1): staining profiles of NOSE19 and IOSE19 show that immortalisation does not induce changes in marker expression. Both cell lines stain positive for cytokeratin 7. Weak positivity for the BerEP4 and pan-cytokeratin (AE1/AE3) epithelial markers was also detected. Weak expression of fibroblast surface protein (FSP) was detected in NOSE and IOSE cultures. All images are 200X magnification and exposure times were consistent for each antigen. In the top panel for each cell line, Evans blue (red colour) staining of cellular cytoplasm is shown, green fluorescence indicates antigen positivity, nuclei are stained blue with DAPI. In the lower panel for each cell line, only the antigen of interest and nuclei are shown.

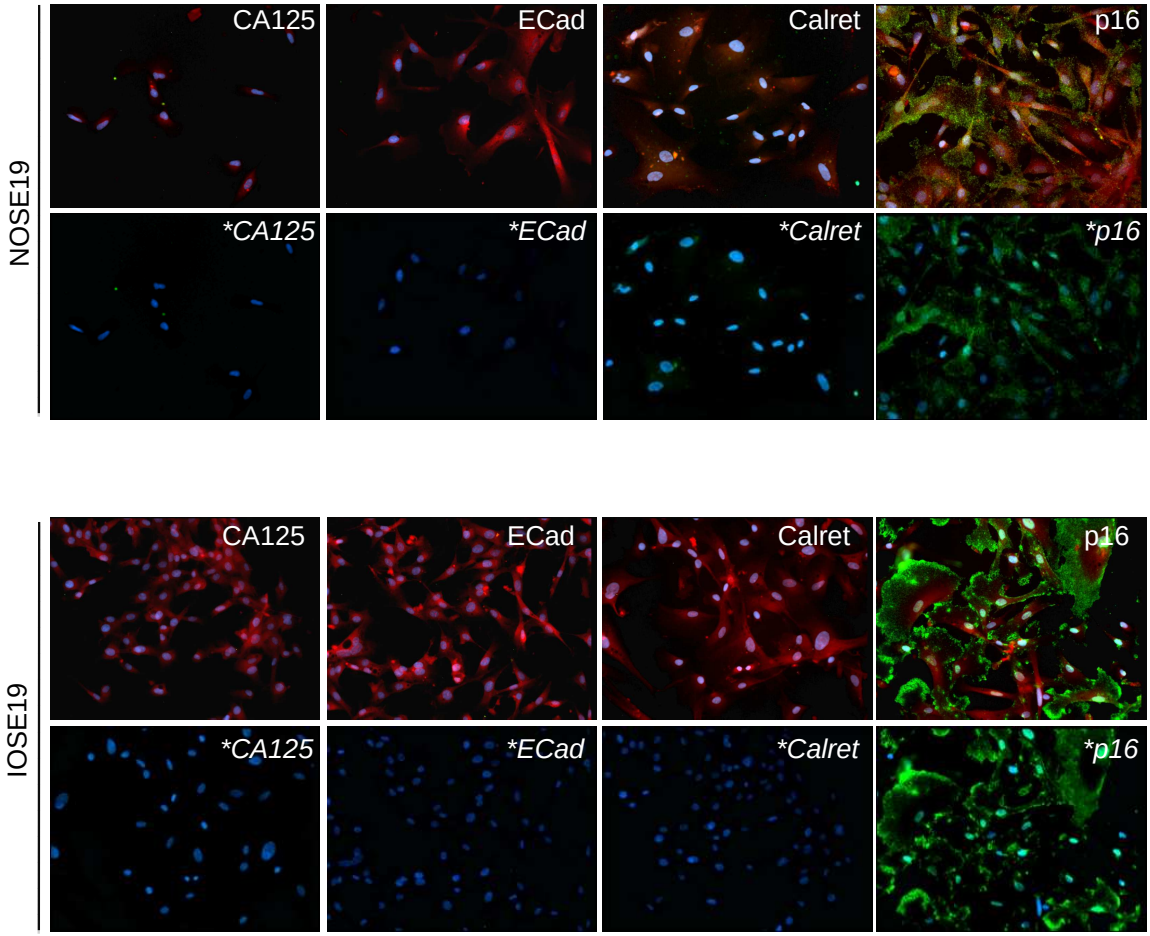

Figure 4.8: Fluorescent immunocytochemistry (NOSE19 part 2): staining profiles of NOSE19 and IOSE19 show that immortalisation does not induce changes in marker expression. No expression of cancer-antigen 125 (CA125) or E-cadherin was detected. Weak expression of calretinin (a mesothelial marker) was detected in NOSE and IOSE cultures. Nuclear and cytoplasmic staining for p16 was detected in NOSE19 and IOSE19 cells. All images are 200X magnification and exposure times were consistent for each antigen. In the top panel for each cell line, Evans blue (red colour) staining of cellular cytoplasm is shown, green fluorescence indicates antigen positivity, nuclei are stained blue with DAPI. In the lower panel for each cell line, only the antigen of interest and nuclei are shown.

ANTIBODY	Ck7	BerEP4	CA125	E-Cad	AE1/3	FSP	Calret	p16
Cell Line								
NOSE4	++	+	+/-	-	+/-	-	+	++
IOSE4	++	+	-	-	-	-	+/-	+++
IOSE4.2	++	+	-	-	+/-	-	+	*n.d.*
NOSE11	+	+	-	-	+/-	+/-	+	+
IOSE11.2	++	+	+/-	-	+/-	-	+	*n.d.*
IOSE11.3	++	+/-	-	-	+/-	-	+	*n.d.*
IOSE11	++	+	-	-	+/-	-	+	*n.d.*
IOSE11 (lp)	++	+	-	-	+/-	-	+	++
NOSE19	++	-	+	-	+	+/-	+	++
IOSE19.2	++	+	-	-	+/-	-	+/-	*n.d.*
IOSE19	++	+	-	-	-	-	+/-	+++

+++ 70-100% cells stain positive

++ 40-70% cells stain positive

\+ 10-40% cells stain positive

+/- Under 10% cells stain positive

\- No cells stain positive

Figure 4.9: Fluorescent immunocytochemistry summary - NOSE and IOSE clones derived from patients 4, 11 and 19 (Chapter 3). Cell lines that were taken forwards for further experiments are indicated in red. Cell lines were stained by fluorescent immunocytochemistry for epithelial, fibroblastic and ovarian cancer markers. Staining profiles of NOSE and IOSE are consistent for each patient, suggesting that immortalisation does not significantly affect cellular differentiation, nor does immortalisation induce neoplastic transformation or promote an epithelial-to-mesenchymal transition. n.d. = not done. lp = late passage

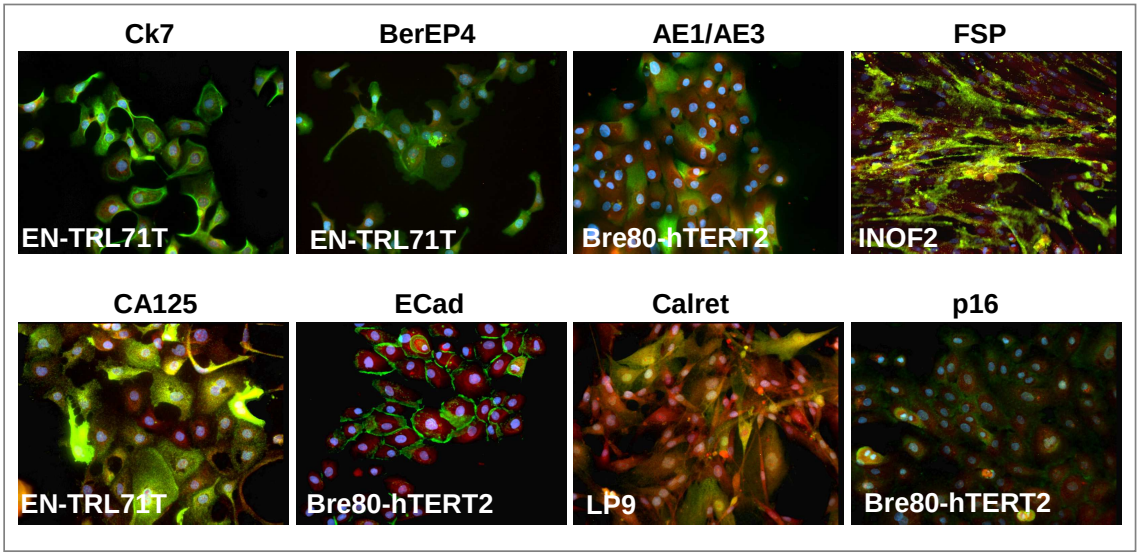

Figure 4.10: Fluorescent immunocytochemistry, staining of control cell lines. EN-TRL = an endometrial cancer cell line, Bre80-hTERT2 = an immortalised breast epithelial cell line, INOF2 = an immortalised normal ovarian fibroblast cell line. Nuclei are stained with DAPI (blue), cytoplasm is stained with Evan's Blue (red), test antigens are lebelled with a FITC-coupled secondary antibody (green). Cytokeratin (Ck7, AE1/AE3) and BerEP4 staining is cytoplasmic and membranous; CA125 and FSP staining is localised to the cell membrane. Positive staining for calretinin should be localised to the cytoplasm, E-cadherin staining localises to cell-cell adhesions, and p16 staining can be nuclear or cytoplasmic. In summary, staining of the control cell lines, as shown above, was used to score NOSE and IOSE staining, with attention paid to staining intensity and localisation.

4.2.2 Analysis of Telomere Length & Telomerase Activity

The telomere biology of IOSE4, IOSE11, IOSE19 was then analysed. It was necessary to identify (a) telomere length - telomere length should be maintained or increased following the ectopic expression of *hTERT*; and (b) that relative telomerase enzymatic activity was increased in *hTERT*-infected cells. Telomeric DNA preparations were Southern blotted onto a nylon membrane and detected using a digoxigenin (DIG)-labelled probe that recognises telomeric repeats (TTAGGG in all vertebrates). The mean telomere restriction fragment (TRF) length was calculated using the molecular weights of the DNA ladder as a reference. In the 3 primary samples, NOSE19 had the longest TRF length (7.26 kbp), (Figure 4.11 a & b). The patient from which this cell line originated was 39 years old, and the youngest of the 3 patients from which the three NOSE cell lines originated. NOSE4 and NOSE11 (patient ages 62 and 48 respectively) had TRF lengths of 3.5 kbp and 4.11 kbp respectively. This is consistent with the idea that telomeres shorten with advancing age.

All three IOSE cell lines have TRF lengths longer than the parental NOSE cultures. For NOSE4, TRF length was increased by 11.54 kbp in the immortalised cell line (IOSE4) relative to the primary cell lines. For NOSE11 and NOSE19 the increase in TRF lengths in the IOSEs clone tested were 6.13 kbp and 6.50 kbp repectively. This indicated that telomere length was increased in all IOSE cell lines relative to the NOSE cultures (Figure 4.11). To confirm that the increase in telomere length was due to transduction with telomerase and not due to activation of a telomerase-independent mechanism of telomere maintenance named alternative lengthening of telomeres (ALT), the levels of activity of the telomerase holoenzyme were assayed by PCR-ELISA. Telomerase activity was not detected in primary cultures but was present in all three immortalised cell lines (Figure 4.11c).

Transformed cells frequently display atypical karyotypes, and immortalisation of some cell types will induce karyotypic changes or genomic stability [Ramirez et al., 2004]. Thus, the karyotype of each NOSE and IOSE cell line was analysed. The predominant karyotype for each NOSE and IOSE cell line was 46,XX (Figure 4.12). Irregular karyotypes, detected in a subset of cells in 5/6 karyotypic analyses, were examined by a Clinical Cytogeneticist and designated as culturing artefacts. This suggested that culturing and immortalisation of NOSE cell lines did not induce genomic instability in these three cell lines.

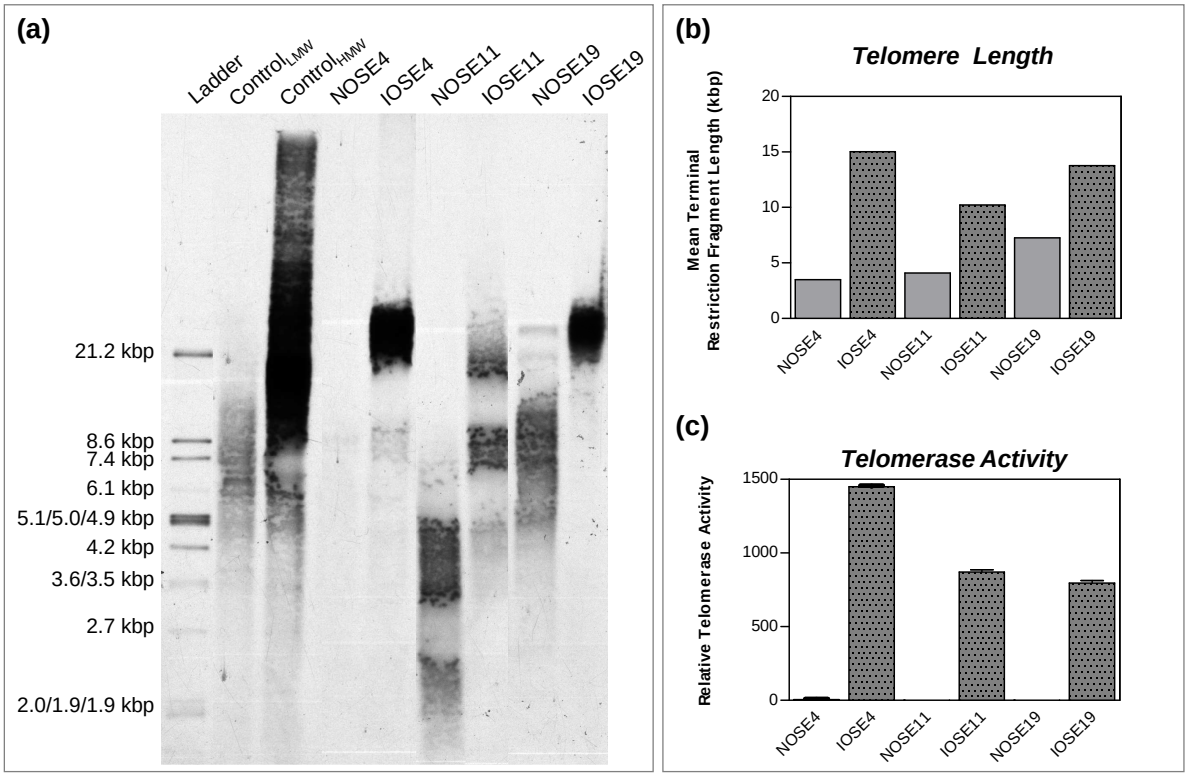

Figure 4.11: (a) Southern blot of telomere restriction fragments. The probe binds telomeric repeats. Included on the blot are a low molecular weight control (Control$_{LMW}$) and a high molecular weight control (Control$_{HMW}$) (some bleaching of the film was observed). (b) Mean telomere restriction fragment length is increased in immortalised OSE (IOSE) cell lines relative to normal OSE (NOSE) parental cell lines. (c) Telomerase activity, detected by PCR-ELISA, is absent in primary cultures but present in immortalised cell lines.

(a)

	Patient 4	Patient 11	Patient 19
NOSE	**46,XX (18 cells)** 46XX,t(5;8)(q11.1;q24.1) (1 cell) 45,XX,-14 (1 cell)	**46,XX (20 cells)** 46,XX,t(5;12),(?p10;?p10) (1 cell) 45,XX,-1 (1 cell) 45,XX,-18 (1 cell) 45,XX,-20 (1 cell) 45,XX,-6,-10 (1 cell)	**46,XX (9 cells)** 47,XX+?5 (1 cell)
IOSE	**46,XX (18 cells)** 46,XX,-8,-12 (1 cell)	**46,XX (20 cells)**	**46,XX (18 cells)** 45,XX,-6 (1 cell) 45,XX,-16 (1 cell)

(b)

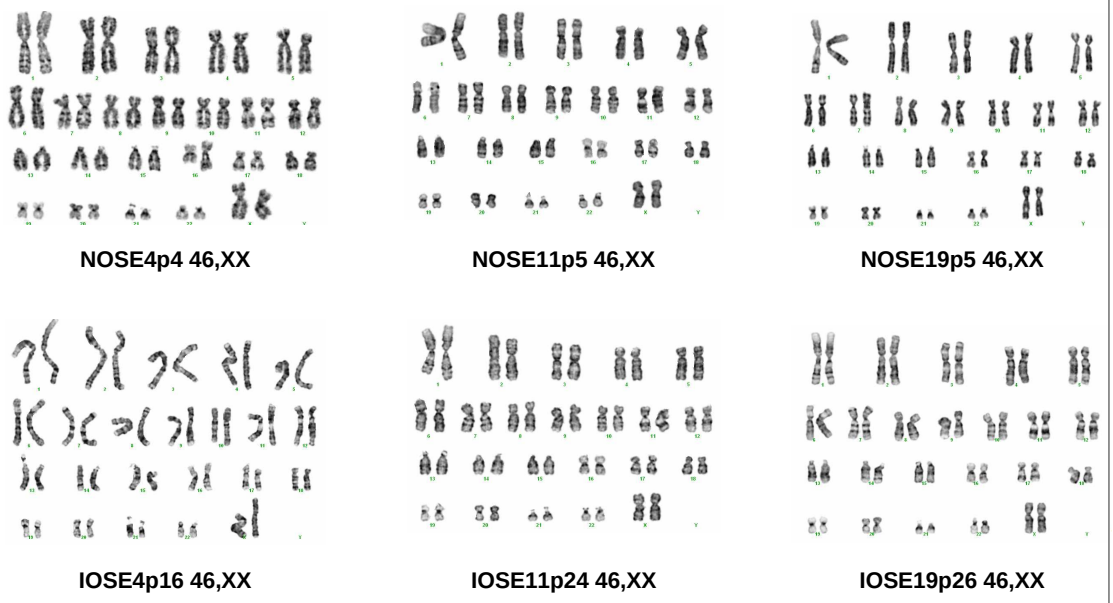

NOSE4p4 46,XX **NOSE11p5 46,XX** **NOSE19p5 46,XX**

IOSE4p16 46,XX **IOSE11p24 46,XX** **IOSE19p26 46,XX**

Figure 4.12: Karyotype analysis of primary and immortalised ovarian surface epithelial cell lines. (a) 20 karyotypes per cell line were analysed, except for NOSE19 where only 10 metaphase nuclei could be scored due to the restricted *in vitro* proliferation of this cell line. The modal karyotype for each NOSE and IOSE cell line is 46,XX (shown in bold). (b) A representative modal karyotype for each cell line is shown. p=passage number of the cell line

4.3 Expression of Individual Oncogenes in IOSE Cultures

4.3.1 Overexpression of *C-MYC* in IOSE Cultures

A full-length *C-MYC* cDNA clone was introduced into IOSE cells by retroviral transduction in an attempt to induce the early stages of neoplastic transformation. Clones were selected using 3μg/ml blasticidine-S-hydrochloride. Firstly, the anchorage-independent growth rates of all 3 IOSE and 9 IOSE^{CMYC} cell lines were tested. Colony formation efficiency (CFE, %) was calculated following 4-week culture of cells suspended in 0.33% Noble Agar gels. 7/9 IOSE^{CMYC} cell lines grew significantly more in anchorage-independent growth assays than the IOSE cell line from which they were derived ($P \leq 0.05$, two-tailed paired Student's T-Test) (Figure 4.13). At high densities (40,000 cells/well) some growth of IOSE11 and IOSE19 was observed. No IOSE cell line grew at densities <20,000 cells/well (in 6-well plates).

Clone morphologies were examined. The growing anchorage-independent colonies of all IOSE4^{CMYC} and IOSE11^{CMYC} cell lines were typically smooth on the surface and compact in appearance. However, anchorage-independent colonies of IOSE19^{CMYC} cell lines were large and had irregular morphologies. When plated at low densities (1000 cells/well), to better observe this characteristic, up to 50% of the clones were observed to have a peripheral region of cells which were invading out of the core of the clone and into the agar (Figure 4.13 (b, ii)). This phenotype was not observed for any of the IOSE4 or IOSE11 clones that overexpress *CMYC*, and has not previously been observed in this laboratory for any of the EOC cell lines tested [Dafou et al., 2009]; [Grun et al., 2009]. This suggested that IOSE19^{CMYC} clones have an aggressive *in vitro* phenotype in anchorage-independent growth assays. Indeed, the CFE of 2/3 IOSE19^{CMYC} cell lines were >15%, thus exceeding the reported CFEs of many ovarian cancer cell lines (TOV112D, CFE=6.50%; TOV21G CFE=8.35%; OV-TRL12B, CFE=3.07%) [Dafou et al., 2009]; [Grun et al., 2009].

From each IOSE cell line, the clone with the highest rate of anchorage-independent growth was selected and a broader panel of assays were performed to measure neoplastic progression. The clones selected were IOSE4^{CMYC1}, IOSE11^{CMYC2} and IOSE19^{CMYC3}. (From this point onwards the clones are denoted without the clone number - IOSE4^{CMYC}, IOSE11^{CMYC} and IOSE19^{CMYC}).

The expression of *C-MYC* mRNA and protein were analysed in the IOSE4, IOSE11 and IOSE19 and IOSE4^{CMYC}, IOSE11^{CMYC}, IOSE19^{CMYC}. Firstly, expression of *C-MYC* mRNA was analysed by real-time PCR. *C-MYC* mRNA expression levels were increased 80 to 501-fold relative to IOSE cells (Figure 4.14a). The differences in *C-MYC* mRNA ex-

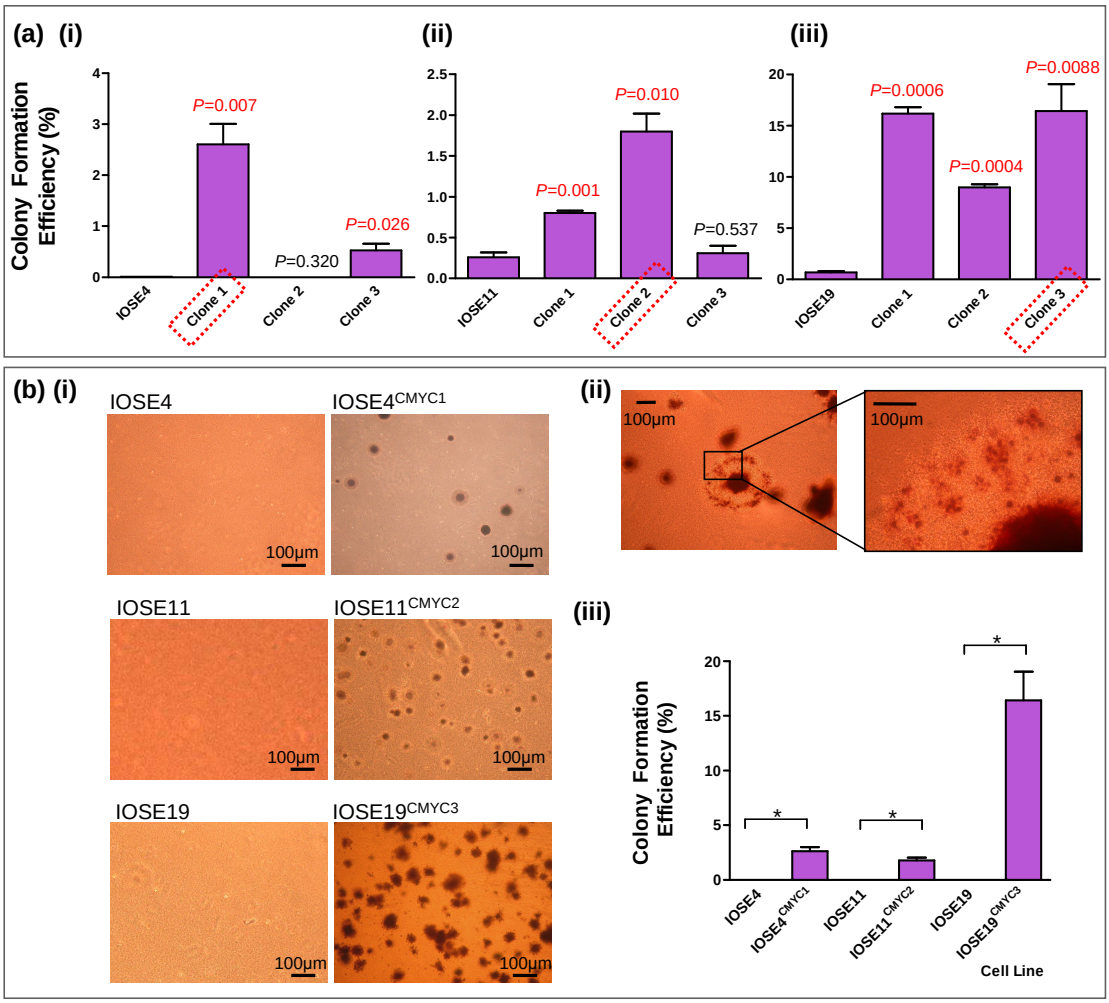

Figure 4.13: Overexpression of *C-MYC* in three IOSE cell lines increased colony formation efficiency in anchorage-independent growth assays in 7/9 clones. Three IOSE^{CMYC} clones per IOSE cell line were screened for anchorage-independent growth. (a)(i-iii) Colony formation efficiency (CFE) of IOSE and IOSE^{CMYC} cell lines, plated at high density (40,000 cells/well in a 6-well plate). Statistically significant differences in CFE, (significance level of $P \leq 0.01$), are highlighted in red. (a, i) In IOSE4, clones 1 and 3 grew significantly more in anchorage-independent growth assays than the parental IOSE cell line. (a, ii) In IOSE11, clones 1 and 2 grew significantly more in anchorage-independent growth assays than the parental IOSE cell line. (a, iii) In IOSE19, all 3 clones tested grew significantly more in anchorage-independent growth assays than the parental IOSE cell line. One IOSE^{CMYC} clone was selected per IOSE parental cell lines to take forwards for more detailed phenotypic analyses (indicated by red boxes). (b, i) Representative fields of view of anchorage-independent growth assays; 20,000 cells/well were plated. (b, ii) IOSE19^{CMYC} cells demonstrate an aggressive *in vitro* phenotype: anchorage independent growth efficiencies exceed many ovarian cancer cell lines and cells invade out of the colony and into the agar (arrow). Cells were plated at low density (1000 cells/well). (b, iii) Anchorage-independent growth rates of IOSE and IOSE^{CMYC} cell lines, plated at low density (1000 cell/well) at passage 28-30. (* $P \leq 0.01$)

pression levels were significantly elevated in IOSE^{CMYC} cells compared to parental IOSE lines. It was observed that in the parental lines, IOSE4 displayed significantly lower expression of endogenous *CMYC* mRNA than IOSE11 and IOSE19 (Figure 4.14b). IOSE19 also expressed the *CMYC* transcript at levels significantly higher than IOSE11. As described in this thesis, IOSE19 appeared to be more susceptible to neoplastic transformation *in vitro* than IOSE4 and IOSE11, this may be due in part, to the higher *CMYC* expression observed in this experiment. Secondly, western blotting of total cell lysates with an anti-*C-MYC* antibody was performed to see if increased levels of *C-MYC* protein could be detected. However, there were no visible differences detected in the expression of *C-MYC* protein (Figure 4.14b). This may be due to the short half-life of the *C-MYC* protein; proteins with a short half-life are difficult to detect by Western blotting as they can be degraded very rapidly during sample collection. Alternatively, the transforming effects observed may be mediated by the *CMYC* mRNA transcript.

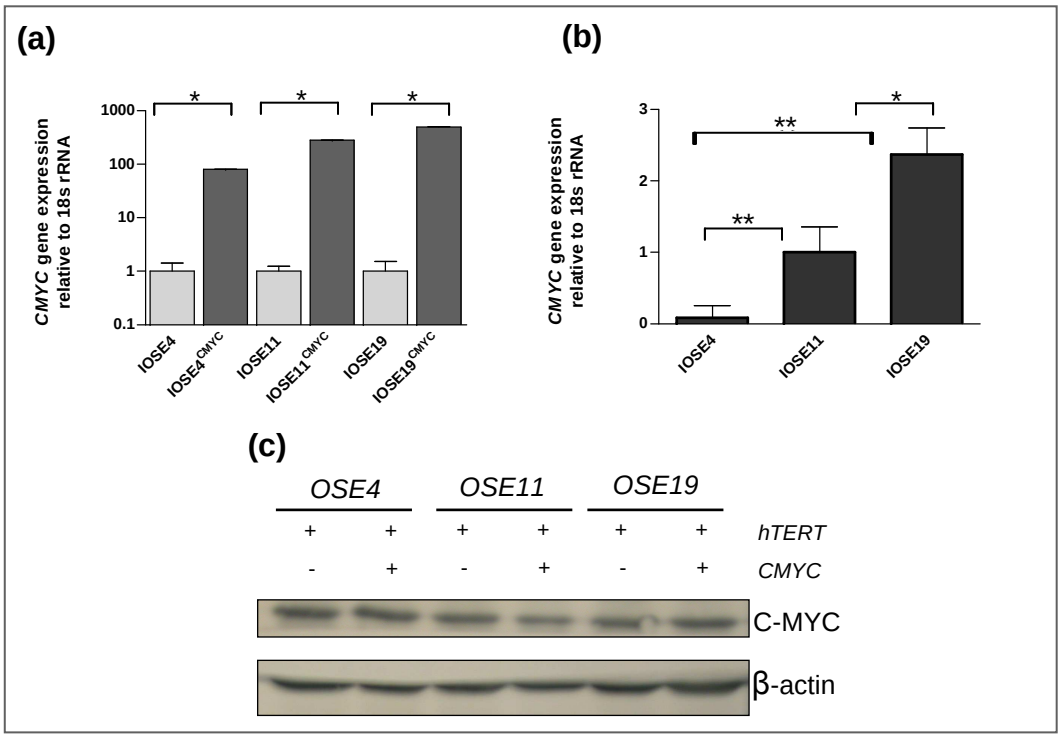

Figure 4.14: Detection of *C-MYC* overexpression in IOSE^{CMYC} cell lines. (a) Expression of *C-MYC* mRNA, relative to an 18s rRNA internal control. (b) Endogenous expression of *CMYC* mRNA is significantly higher in IOSE19 compared to IOSE11 and IOSE4. * $P \leq 0.05$, ** $P \leq 0.05$ (c) Western blot analysis of *C-MYC* protein expression in total cell lysates. β-actin represents a loading control.

IOSE cells that overexpress *C-MYC* also displayed altered cell morphology when visualised

by phase-contrast microscopy. Cell size was decreased and cell shape became more cuboidal and more classically epithelial than the characteristic fibroblastic morphology of IOSE clones when grown in growth-factor rich medium (Figure 4.15). NOSE cells typically show phenotypic plasticity, both *in vitro* and *in vivo*, and commitment to an epithelial phenotype is associated with ovarian cancer progression. Anchorage-dependent growth was tested to assay clonogenicity and proliferation of the IOSE cell lines compared to IOSE^{CMYC}. IOSE^{CMYC} cell lines formed significantly more colonies in anchorage-dependent growth assays than the IOSE cell lines ($P \leq 0.01$, paired T-Test) (Figure 4.16).

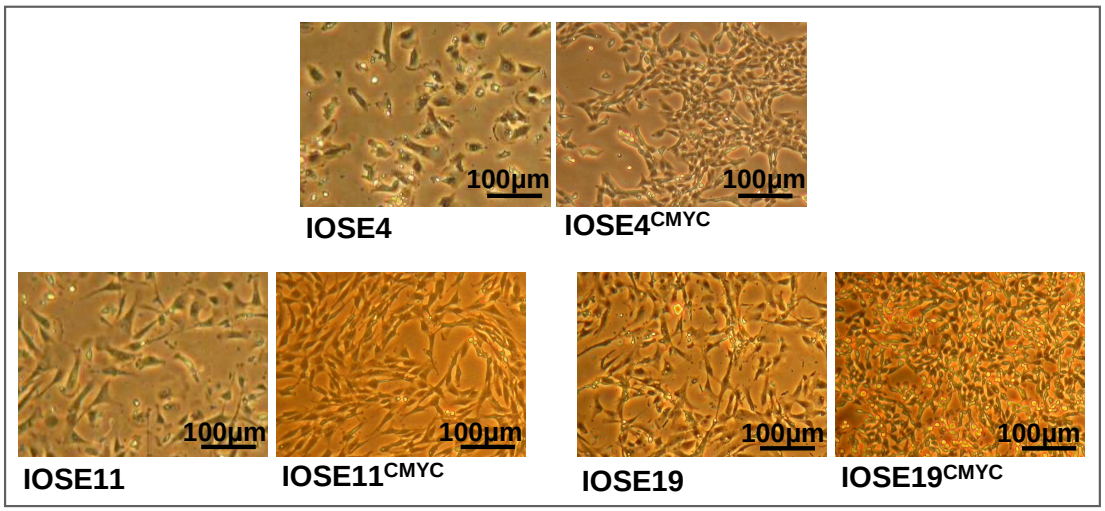

Figure 4.15: IOSE cultures overexpressing *C-MYC* have a more classic cuboidal-epithelial morphology than IOSE cell lines. The fibroblast-like elongated morphology of IOSE cultures changes to a more typically epithelial (cuboidal) morphology upon *C-MYC* overexpression. Commitment to an epithelial phenotype is a hallmark of epithelial ovarian cancer cells. OSE cells *in vitro* and *in vivo* are able to convert between epithelial, mesenchymal or mesothelial phenotypes. Cell size is also visibly reduced.

A hallmark of transformation is reduced apoptosis and increased independence from pro-apoptotic signals [Hanahan and Weinberg, 2000], thus the proportion of apoptotic cells was analysed. Cell suspensions were labelled with anti-annexin-V-FITC and the percentage of apoptotic cells analysed using flow cytometry. Anti-annexin-V labels externalised phosphatidyl-serine, a marker of cells which are undergoing early apoptosis. A statistically significant reduction in the percentage of apoptotic cells was observed in all three IOSE^{CMYC} cell lines compared to the IOSE cells ($P \leq 0.05$) (Figure 4.17 (a)). This suggested that IOSE^{CMYC} clones had reduced rates of apoptosis compared to the IOSE cell lines from which they were derived.

C-MYC is known to play a role in proliferation and progression through the cell cycle. Fur-

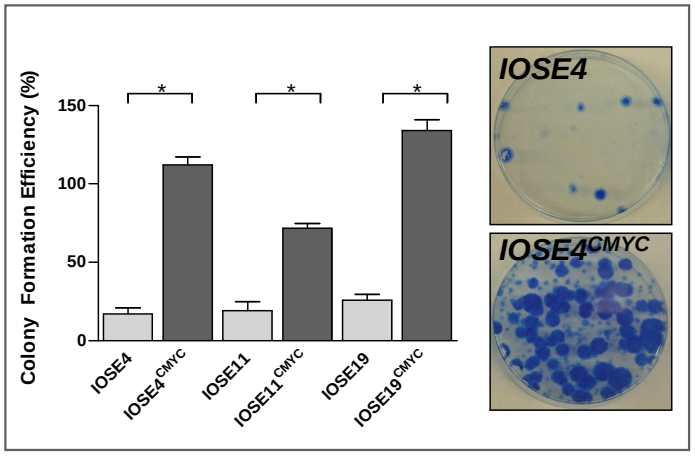

Figure 4.16: IOSE cultures overexpressing *C-MYC* show enhanced clonogenicity in anchorage-dependent growth assays (* $P \leq 0.05$). Representative plates with colonies stained with Coomaasie blue, are shown. In plates where CFE appears to exceed 100%, it was observed that confluent colonies shed cells into the medium, and it is hypothesised that these cells then form secondary colonies

thermore, transformed cells are often more proliferative than non-transformed cells *in vitro* and *in vivo*. Therefore, cell cycle analysis was performed using 5-bromo-2-deoxyuridine incorporation (Brd-U), followed by labelling and flow cytometry. Brd-U is a synthetic thymidine analogue and, when added to cell culture medium, becomes incorporated into cellular DNA during S-phase of the cell cycle. Nuclei can then be harvested from the cultures, and the relative proportion of cells in each phase of the cell cycle calculated by labelling Brd-U positive nuclei and total DNA with propidium iodide. For this experiment, the percentage of cells in G2 phase was tabulated to determine the proportion of cells that are approaching mitosis within the timeframe of Brd-U exposure. A significant increase in the proportion of cells in G2 phase of the cell cycle was observed in IOSE^{CMYC} cells, compared to IOSE parental cell lines ($P \leq 0.05$) (Figure 4.17). Therefore, these data suggest that an increase in the proliferative rate was associated with the introduction of *C-MYC* into IOSE cell lines. However, an alternative explanation could be that an increased in *CMYC* expression may affect timing of the cell cycle and induce a prologued G2 phase.

Finally, Pearsons' Rank analyses were performed to test for correlation between *C-MYC* mRNA expression and *in vitro* phenotype. Firstly, a test was performed to identify any significant correlation between relative fold-change (FC) in *C-MYC* mRNA expression levels and colony formation efficiency (CFE) in anchorage-independent growth experiments. These two variables, CFE and mRNA fold-change, were significantly correlated (r^2=0.8,

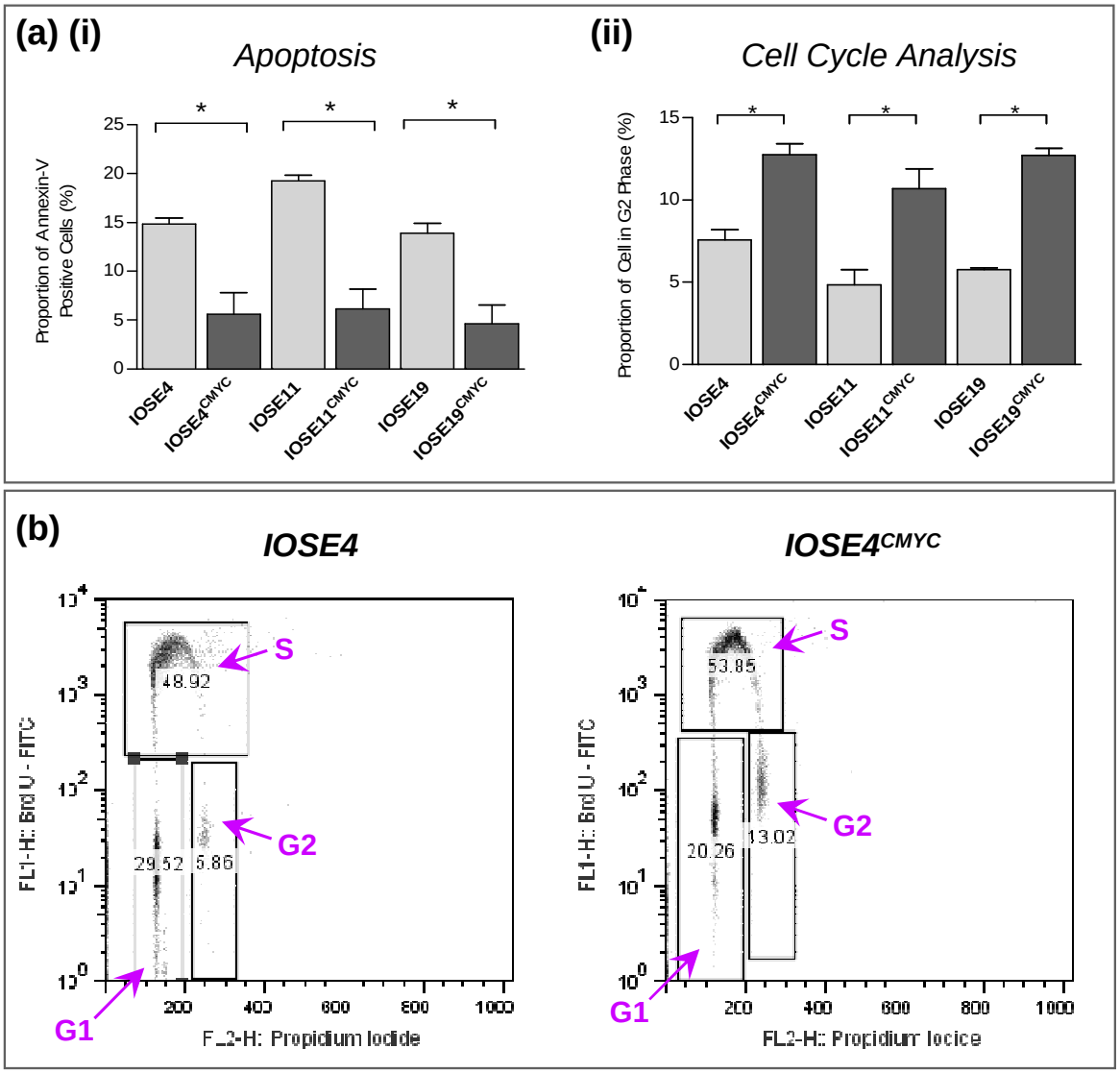

Figure 4.17: Analysis of apoptosis and cell cycle distribution in IOSE and IOSE^{CMYC} cell lines. (a)(i) IOSE cultures over-expressing *C-MYC* show reduced apoptosis and (ii) enhanced progression through the cell cycle, compared to parental IOSE cell lines. A minimum of three replicate samples were stained per cell line. (* P=0.05, paired T-test). (b) Representative scatter plots of IOSE4 and IOSE4^{CMYC} showing Brd-U staining (FL1-H) plotted against propidium iodide (PI) staining (FL2-H). Cells in G1 phase of the cell cycle have no Brd-U incorporated into cellular DNA, and 2n chromosomes; therefore staining by Brd-U is low/absent (below 10^1) and PI staining is half of that observed for cells in G2. Cells in S-phase of the cell cycle are actively undergoing DNA replication, and so a classic 'horse-shoe' plot is observed as DNA material is replicated and Brd-U is simultaneously incorporated. In G2 phase, chromosomes have been replicated and so staining with PI is double that of the cells in G1 phase. Cells in G2 phase also have high FL1 staining as Brd-U has become incorporated during DNA synthesis.

P=0.0156, α =0.05). Relative FC in *C-MYC* mRNA expression levels was also correlated to the percentage of apoptotic cells in the cultures (r^2=-0.5750, P=0.0333, α =0.05), but not to CFE in anchorage-dependent growth assays (r^2=0.6295, P=0.0596, α =0.05), or the proportion of cells in G2 phase of the cell cycle (r^2=0.5200, P= 0.1058, α =0.05). It may be that higher numbers of cell lines would need to be assayed to have the power to detect further correlations.

These tests suggest that increasing relative FC of *C-MYC* mRNA expression in these cell lines is correlated to rates of apoptosis and the degree of tumourigenicity in anchorage-independent growth assays. Correlation does not imply a 'cause' but a relationship between two variables and in this instance, this correlation suggests a trend in which increasing expression of *C-MYC* mRNA is positively correlated to colony formation efficiency in anchorage-independent growth assays and negatively correlated to the proportion of apoptotic cells in a culture. It can be inferred that *C-MYC* overexpression level may be proportionally related to the neoplastic phenotype. This trend could be validated and further investigated by increasing the total number of clones and thus increasing the number of data points for testing correlations. Also, shRNA/siRNAs targetting *C-MYC* could be used to knock-down expression of this gene and quantify any reversal of the transformed phenotype that is associated with subsequent depletion of the transcript.

4.3.2 Expression of Mutant *KRAS* and *BRAF* in IOSE Cell Lines

IOSE cell lines expressing $KRAS^{G12V}$ or $BRAF^{V600E}$ (the most common *RAS/RAF* mutations in EOC) were generated by transducing IOSE with retroviruses containing the sequences for these genes. Selection of these clones was achieved using an antibiotic selectable marker that confers resistance to G418 (for *KRAS*) or puromycin (for *BRAF*).

4.3.3 *KRAS/BRAF*-Associated Senescence in IOSE^{KRAS} Cell Lines

Expression of β-galactosidase (SA-β-gal) activity at pH6 is a marker of cellular senescence [Dimri et al., 1995]. *KRAS* and *BRAF* mutations classically induce senescence of normal cells in the absence of other pro-tumourigenic mutations [Denoyelle et al., 2006]. Therefore, clones that had been transduced with $KRAS^{G12V}$ or $BRAF^{V600E}$ were screened for expression of SA-β-gal and cell morphologies were closely observed.

In IOSE4, it was only possible to generate 2 IOSE4^{KRAS} cell lines that could be maintained in culture. These cell lines grew very slowly *in vitro* and cells displayed senescent

morphologies (enlarged size, vacuolated cytoplasm). Staining for senescence-associated-β-galactosidase (SA-β-gal) confirmed that 100% of cells were senescent in the two IOSE4^{KRAS} clones at passage 11. Only ~10% of cells were positive for SA-β-gal in IOSE4/IOSE4^{AP} (control cell line that expresses alkaline phosphatase) (Figure 4.18). Only ~1% of cells in the IOSE4^{CMYC} culture were senescent.

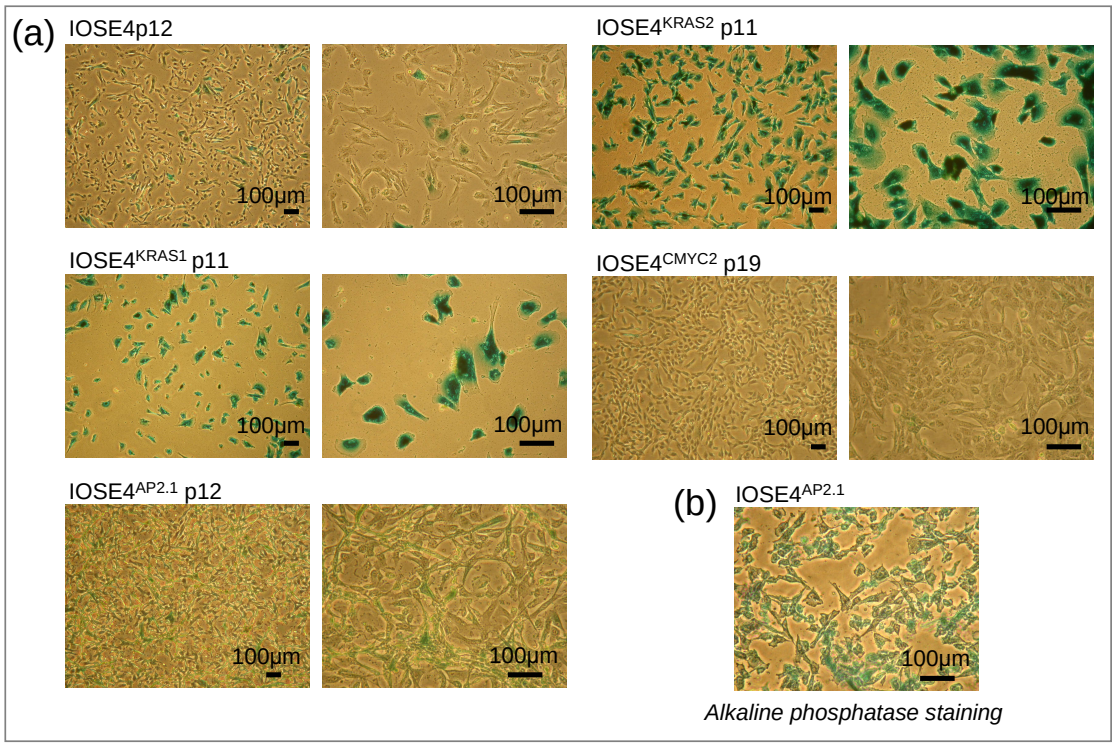

Figure 4.18: IOSE4 cultures expressing mutant *KRAS* stain positive for senesence-associated-β-galactosidase bioactivity, indicated by positive (blue) staining for β-galactosidase activity at pH6. (a) In two *KRAS* clones 100% of cells are senescent (blue). In IOSE4 and IOSE4^{AP}, around 10% of the cells are senescent. In IOSE^{CMYC}, the proportion of senescent cells is least, only around 1% of cells stain positive for β-galactosidase at pH6. IOSE4^{AP} = control cell line, transduced with the gene for alkaline phosphatase. (b) In the control cell lines 100% of cells stain positive (purple) for alkaline phosphatase (AP). Staining for AP was absent in all other cell lines.

However, from IOSE11 and IOSE19 transductions with *KRAS*^{G12V}, many clones were isolated that could be propagated in culture. Three clones from each cell line were assayed for SA-β-gal bioactivity. All of these clones were maintained in culture for over 20 passages. When stained for SA-β-gal, only IOSE11^{KRAS1} showed an elevated proportion of senescent cells (around 10%) compared to the parental IOSE11 cell line (around 1%).

It was not possible to generate clones that stably express *BRAF* from IOSE4 as all clones senesced at an early passage. Clones were generated from IOSE11 and IOSE19. In both

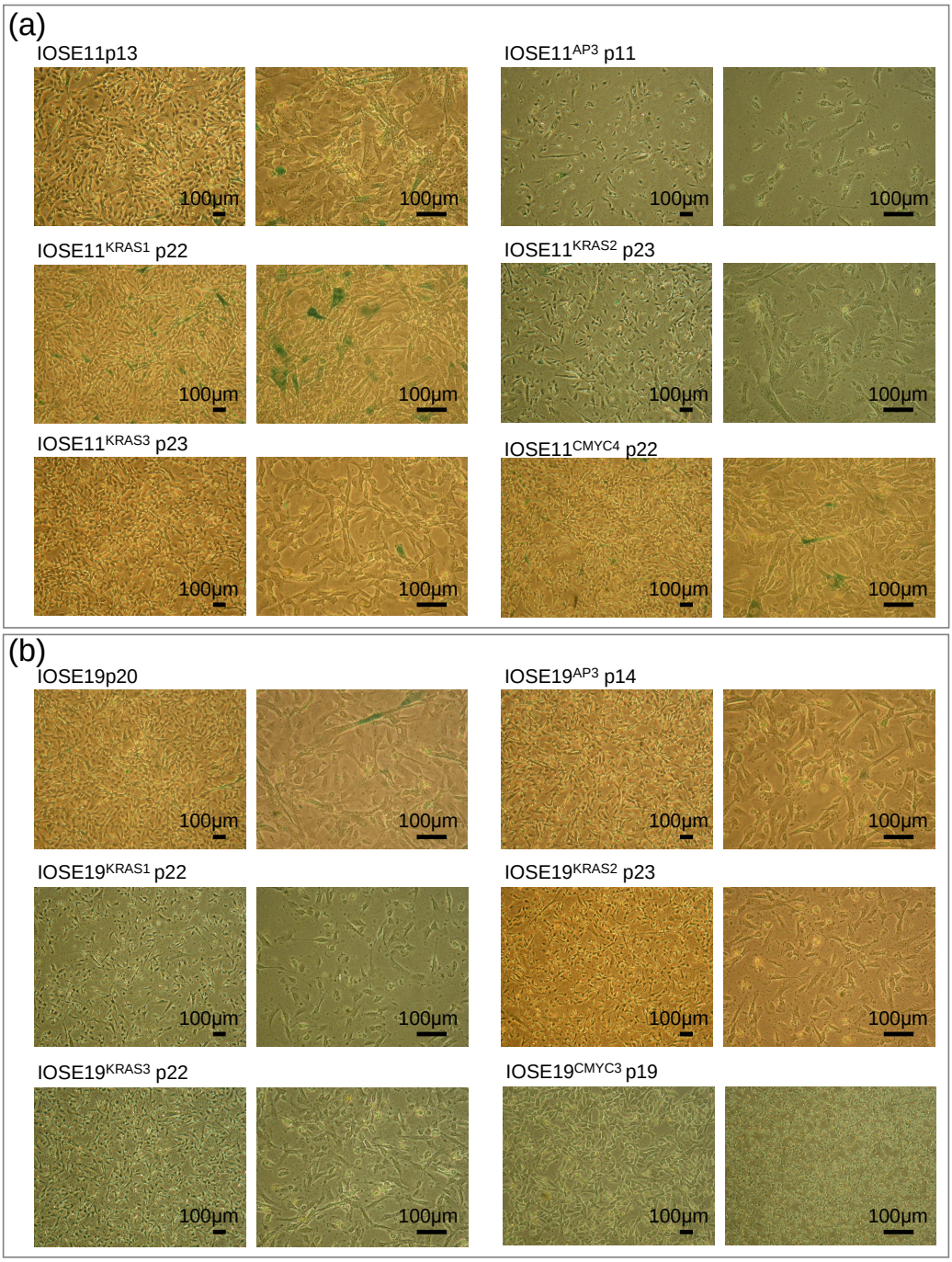

Figure 4.19: Senescence in IOSE11, IOSE19 and clones expressing $KRAS^{mut}$. Only one clone ($IOSE^{KRAS2}$) contained a higher proportion of senescent cells than the IOSE parental cell line or the control cell line ($IOSE^{AP}$). Blue cells indicate positive staining for SA-β-gal bioactivity

IOSE11 and IOSE19, $BRAF^{mut}$ induced higher rates of senescence than $KRAS^{mut}$. This strongly suggested that *BRAF* had been introduced into IOSE cell lines and was a more potent inducer of senescence than mutant *KRAS*. Control cell lines, expressing alkaline phosphatase (AP) did not show rates of senescence that were different to the IOSE parental cell lines. Three *BRAF* clones were derived from both IOSE11 and IOSE19. *BRAF* clones proliferated slowly in culture and rates of cellular senescence were observed that exceeded parental, control and $IOSE^{CMYC}$ cell lines (Figure 4.19 & 4.20).

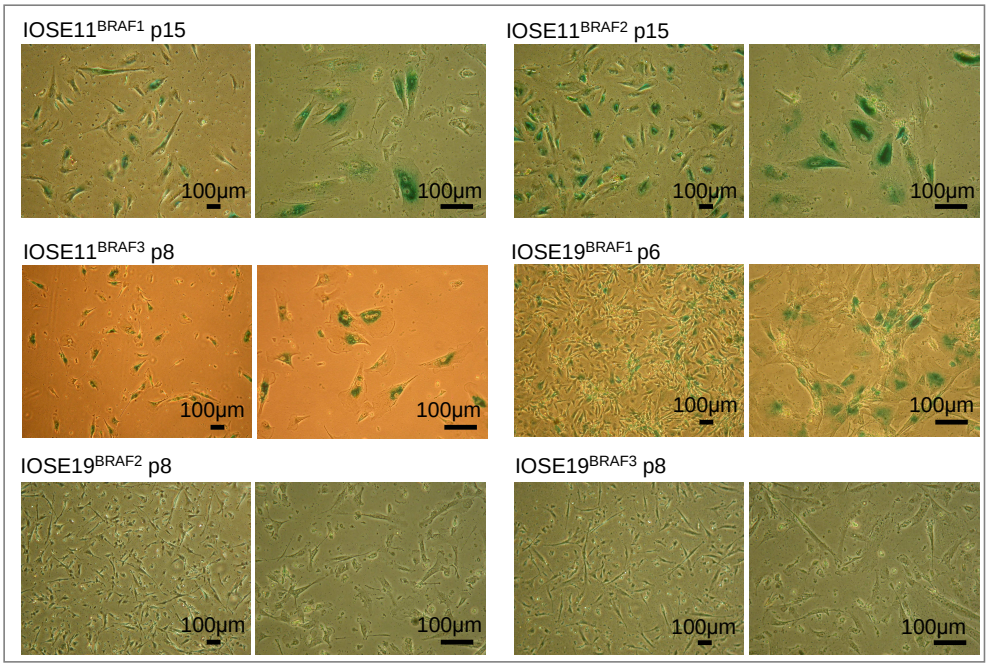

Figure 4.20: Senescence in IOSE11, IOSE19 and clones expressing $BRAF^{mut}$. All $IOSE^{BRAF}$ clones contained a higher proportion of senescent cells than the IOSE parental cell line.

4.3.4 Analysis of *KRAS/BRAF* Expression

To assay expression of the mutant *KRAS* alleles in the clones from IOSE11 and IOSE19, restriction fragment length polymorphism (RFLP) digests were performed on cDNA preparations [Sato et al., 2006]. RNA was isolated from selected clones, and reverse transcribed to create cDNA transcripts. A region spanning the $KRAS^{G12V}$ mutation was amplified by PCR. PCR-amplified cDNA fragments of $KRAS^{G12V}$ have lost a BstN1 restriction site that spans the G12V mutation. Therefore, RFLP analysis can be used to distinguish mutant and non-mutant strands of amplified cDNA. cDNA PCR products that carry the G12V mutation remain undigested by the BstN1 enzyme (see schematic in Figure 4.21a).

All 6 single mutant clones screened expressed mutant *KRAS* exclusively, or the majority of *KRAS* transcripts were the mutant allele (Figure 4.21b). Two IOSE19^{KRAS} clones (clone 1 and 2) co-expressed detectable, albeit low levels of non-mutant *KRAS*. However, the other 4 clones did not express levels of non-mutant *KRAS* mRNA that were detectable by this method (with the assumption that both transcripts are amplified with equal efficiencies). IOSE and control cell lines that express alkaline phosphatase (IOSE^{AP}) only expressed non-mutant *KRAS* transcripts. Since the transcriptional response the signalling down the MAPK pathway has a cell autonomous feedback component, it may be that when a constitutively active allele of *KRAS* is introduced into the cells, the endogeneous gene is then downregulated in response to elevated MAPK signalling [Schulze et al., 2001]; [Schulze et al., 2004]. It would be possible to test this hypothesis using a shRNA targetting mutant *KRAS* alleles, although such experiments were not within the aims of this project.

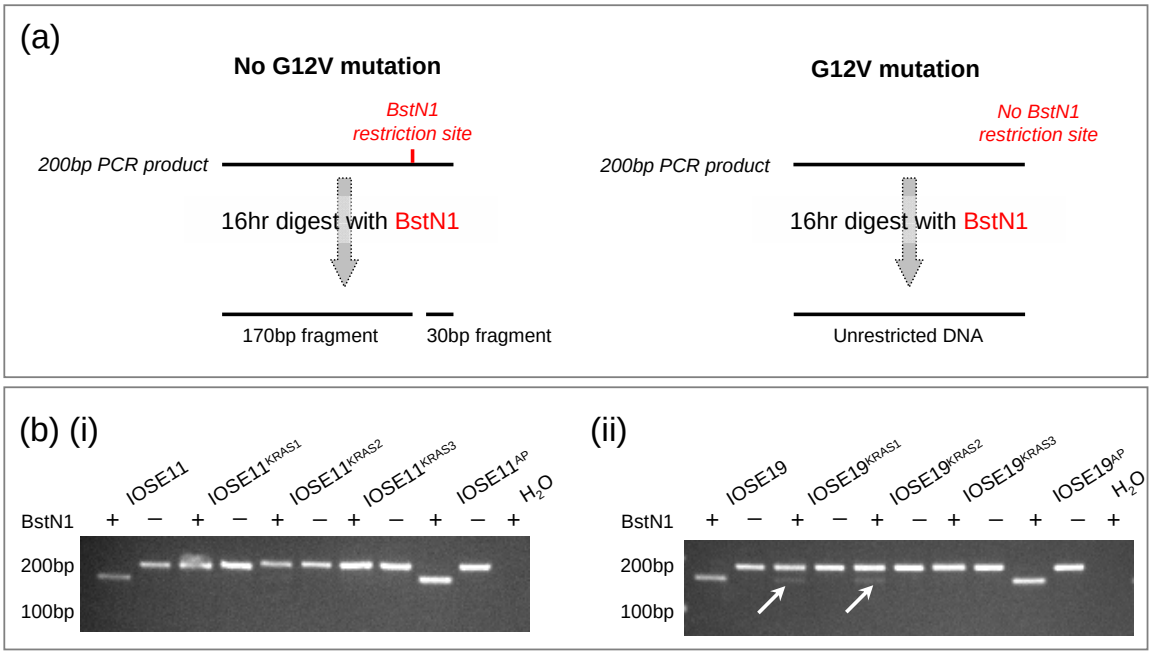

Figure 4.21: RFLP-PCR detection of *KRAS*^{mut} expression. (a) Non-mutant strands are digested by BstN1 to remove a 30bp fragment from the 5' end of the PCR product. (b) RFLP-PCR analysis of *KRAS* mutation status at codon 12 (i) IOSE11 and clones, (ii) IOSE19 and clones. Control cell lines expressing alkaline phosphatase (AP) do not express *KRAS*^{G12V}. IOSE19^{KRAS1} and IOSE19^{KRAS2} have detectable levels of expression of non-mutant *KRAS* cDNA (white arrows). These analyses are semi-quantitative.

Gene expression of total *KRAS* mRNA was assayed in all cell lines by real-time PCR. 3/6 IOSE11^{KRAS} and IOSE19^{KRAS} clones expressed relative levels of *KRAS* mRNA that were elevated 50- to 500-fold compared to the IOSE and IOSE^{AP} cell lines ($P \leq 0.01$ two-tailed

paired T-Tests) (Figure 4.22 a & b). This suggested that elevated MAPK signalling in IOSE^{KRAS} cell lines occurs via two mechanisms: (i) expression of a constitutively active *KRAS* allele and (ii) elevated expression of total *KRAS* (where the majority of transcripts are carrying the G12V mutation). These data indicate that IOSE11 and IOSE19, phenotypically normal cell lines, can tolerate expression of $KRAS^{G12V}$. IOSE^{KRAS2} was the clone with the highest expression of *KRAS* and also the clones with noticably increased rates of senescence, suggesting that there may be a correlation between high expression of $KRAS^{mut}$ and cellular senescence in IOSE11 clones. In IOSE19 cells, IOSE19^{KRAS1} expressed highest levels of *KRAS*, but there was no identifiable increase in cellular senescence. However, total *KRAS* expression was 1/10th of that detected in IOSE11^{KRAS2}.

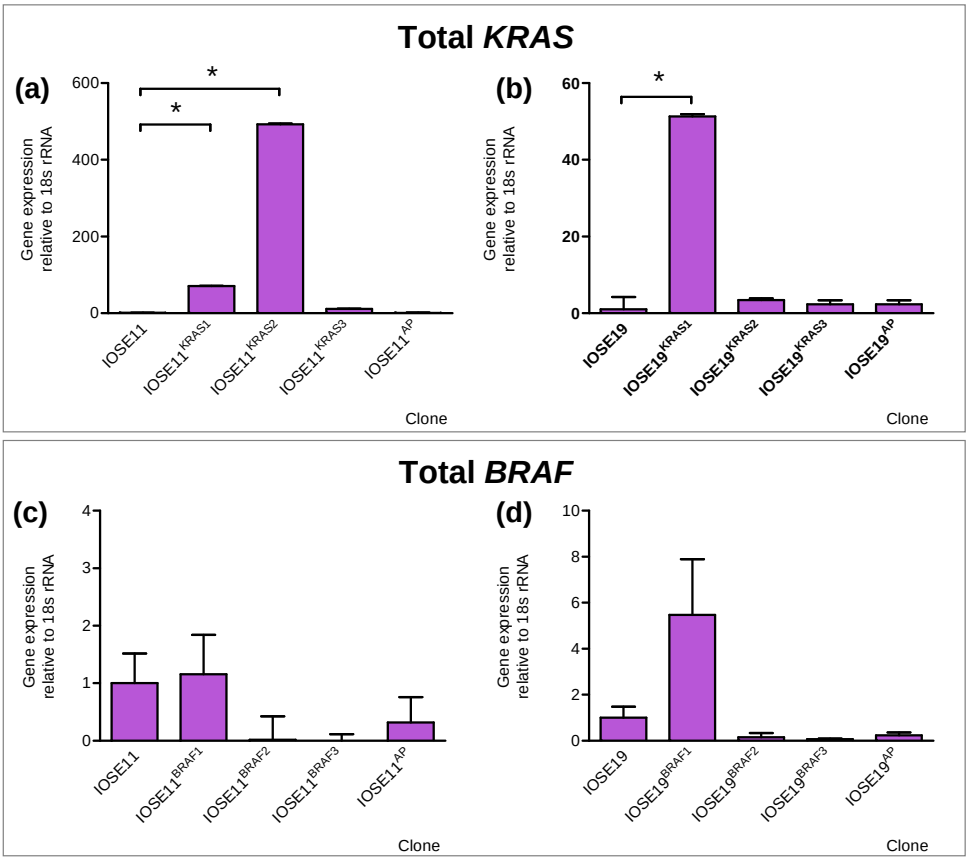

Figure 4.22: Real-time PCR analysis of (a,b) total *KRAS* or (c,d) total *BRAF* expression. mRNA from all cell lines was reverse-transcribed to cDNA and the expression of total *KRAS/BRAF* mRNA calculated, relative to an internal control (18s ribosomal RNA). Clonal variation in total gene expression in clones was observed. Error bars = standard deviation. $P \leq 0.01$.

Detection of $BRAF^{mut}$ by RFLP-PCR has been previously described [Watanabe et al., 2009]. However, even with extended incubation times (16 or 24 hours), digestions did not run

to completion. Varying protocol for the clean-up of PCR products (using QIAgen PCR clean-up kit, ethanol precipitation or drying with the vacuum centrifuge) did not improve the digest. However, the SA-β-gal results strongly suggest that these clones were expressing mutant *BRAF* alleles. Expression levels of total *BRAF* mRNA were not significantly different in transduced clones, parental cells and the control cell line (Figure 4.22), suggesting that $BRAF^{V600E}$ was a more potent inducer of cellular senescence than $KRAS^{G12V}$ in the three IOSE cell lines tested.

Finally, anchorage-independent growth assays were performed to measure any neoplastic phenotype that was induced by the expression of $KRAS^{G12V}$ and $BRAF^{V600E}$ in IOSE11 and IOSE19. IOSE19 $KRAS^{G12V}$ clones did show a significant increase in colony formation efficiency (Figure 4.23). *KRAS* expression levels did not correlate to CFE in anchorage-independent growth assays. Rates of anchorage-independent growth were low in all clones. Also, in both cell lines, 6/6 clones transduced with $BRAF^{V600E}$ had significantly lower rates of anchorage-independent growth than IOSE cell lines (plated at high density, 40,000 cells per well) ($P \leq 0.05$, paired Student's T-Test). This may be due to senescence-induced growth arrest reducing the proliferative ability of the transduced cell lines.

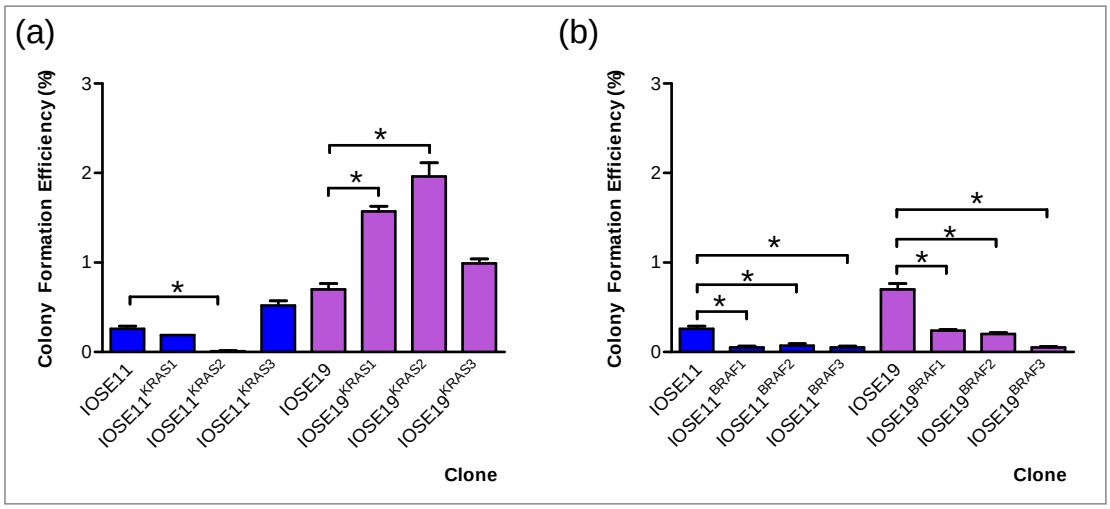

Figure 4.23: Anchorage-independent growth rates in IOSE cells transduced with (a) mutant *KRAS* or (b) *BRAF* alleles. Cells were seeded at a high density (40,000/well). * $P \leq 0.05$.

4.4 Co-expression of Oncogenes in IOSE Cell Lines

To investigate the phenotypic effects of combining oncogene expression, $KRAS^{G12V}$ and $BRAF^{V600E}$ were transfected into two $IOSE^{CMYC}$ clones, $IOSE11^{CMYC}$ and $IOSE19^{CMYC}$,

thus generating cell lines that stably overexpress *CMYC* and also express a mutant *KRAS/BRAF* allele. *KRAS/BRAF* mutations occur mutually exclusively in ovarian tumours, suggesting saturating effects of mutant alleles of these two genes [Singer et al., 2003]. Attempts to create double-mutant *KRAS/BRAF* lines were not successful.

Anchorage-independent growth assays were performed on three clones for each gene and for each cell line. This was to ensure that any differences observed were reproduced in more than one clone. Clonal variation was observed, but in 75% of clones there was a significant increase in anchorage-independent growth rates upon the introduction of $KRAS^{G12V}/BRAF^{V600E}$ into IOSE^{CMYC} cell line (Figure 4.24a). Colonies were typically smooth and regular in shape, with the largest colonies observed in IOSE11$^{CMYC.KRAS}$ clones. As with the IOSE19^{CMYC} cells, the IOSE19 clones co-expressing *C-MYC* plus mutant *KRAS/BRAF* displayed irregular morphologies that were often invasive (Figure 4.24d).

One clone per gene per cell line was taken forwards for further analyses: *KRAS* clone 2 and *BRAF* clone 3 from IOSE11^{CMYC}, and *KRAS* clone 2 and *BRAF* clone 3 from IOSE19^{CMYC}. From this point these cell lines shall be denoted IOSE11/19$^{CMYC.KRAS}$ and IOSE11/19$^{CMYC.BRAF}$. Expression of total *KRAS* and *BRAF* mRNA was assayed, relative to an internal 18s rRNA control. In IOSE11$^{CMYC.KRAS}$, total *KRAS* mRNA expression was increased by nearly 80-fold relative to IOSE. In IOSE19$^{CMYC.KRAS}$, total *KRAS* mRNA was increased 5.92 -fold, relative to IOSE. As with the 'single-oncogene' mutant cell lines, no significant differences in expression of total *BRAF* mRNA were detected.

Expression of mutant *KRAS* was detected by RFLP-PCR, as described above. Transcripts harbouring $KRAS^{G12V}$ mutations were detected in 3/3 IOSE11$^{CMYC.KRAS}$ and 3/3 IOSE19$^{CMYC.KRAS}$ clones. IOSE cell lines, IOSE^{CMYC} and IOSE$^{CMYC.AP}$ did not express mutant (undigested) KRAS mRNA.

BRAF expression of mutant/non-mutant alleles was not detectable by RFLP-PCR, so downstream extracellular-signal regulated kinase (ERK) activity was analysed by Western blotting. ERK1/2 are the first two kinases in the MAPK pathway. Phosphorylation of ERK1/2 was detected with a phosphorylation-specific antibody, as constitutively active alleles of *KRAS* and *BRAF* result in increased signalling down the MAPK pathway. IOSE11 cell line were starved of serum and growth factor supplements for 48 hours and then stimulated with epidermal growth factor (EGF). Lysates were collected at 0 mins, 2 mins, 10 mins and 30 mins. IOSE11 demonstrated rapid activation of MAPK signalling following stimulation with EGF, as indicated by increase phosphorylation of ERK (p-

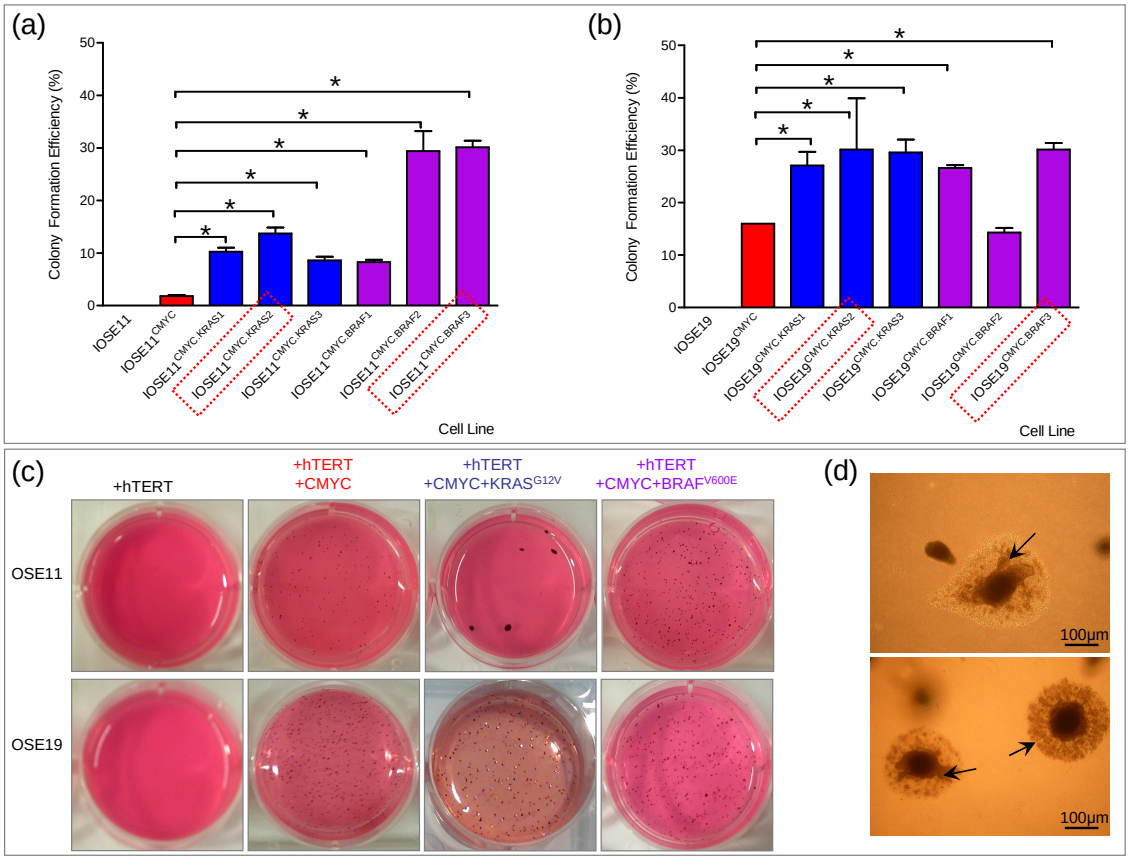

Figure 4.24: Anchorage independent growth of IOSE, IOSE^{CMYC}, IOSE$^{CMYC.KRAS}$ and IOSE$^{CMYC.BRAF}$. (a) IOSE11 and clones and (b) IOSE19 and clones. Cells were plated at a low density (1000 cells/well). * $P \leq 0.01$. (c) One clone per gene per cell line was taken forwards for further analyses (red boxes). Representative images of stained agar gels are shown. (d) IOSE19 double mutant cell lines have an invasive phenotype in anchorage-independent growth assays. IOSE19$^{CMYC.KRAS}$ cell lines are shown, with the invasive region indicated (arrows).

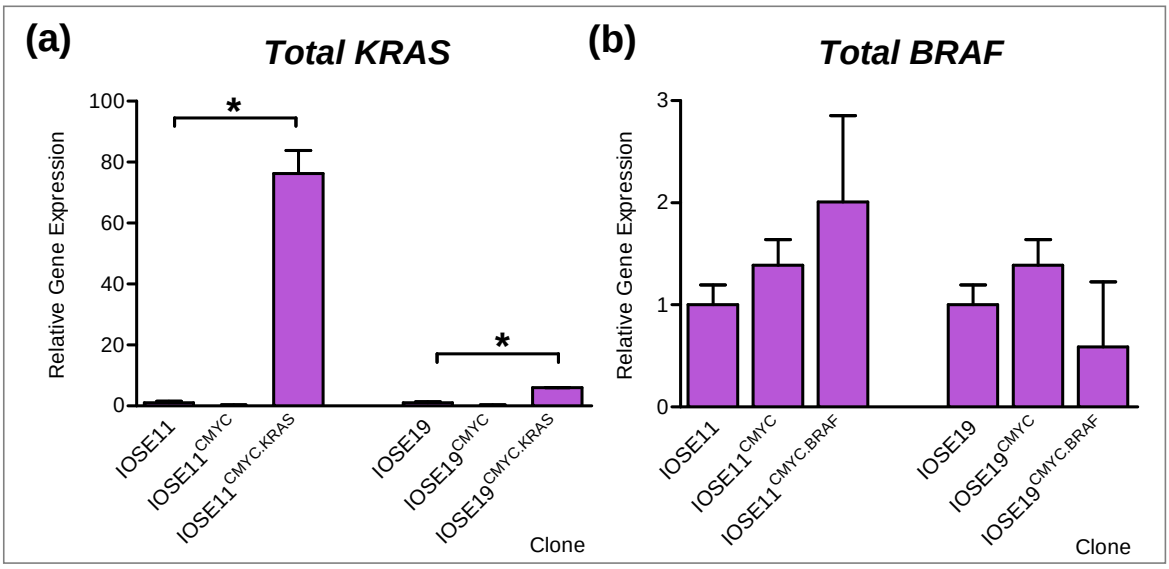

Figure 4.25: Relative expression of total *KRAS* and *BRAF* mRNA in IOSE$^{CMYC.KRAS}$ and IOSE$^{CMYC.BRAF}$ cell lines. Gene expression is calculated relative to an 18s ribosomal RNA internal control (by the $\delta\delta$Ct method)

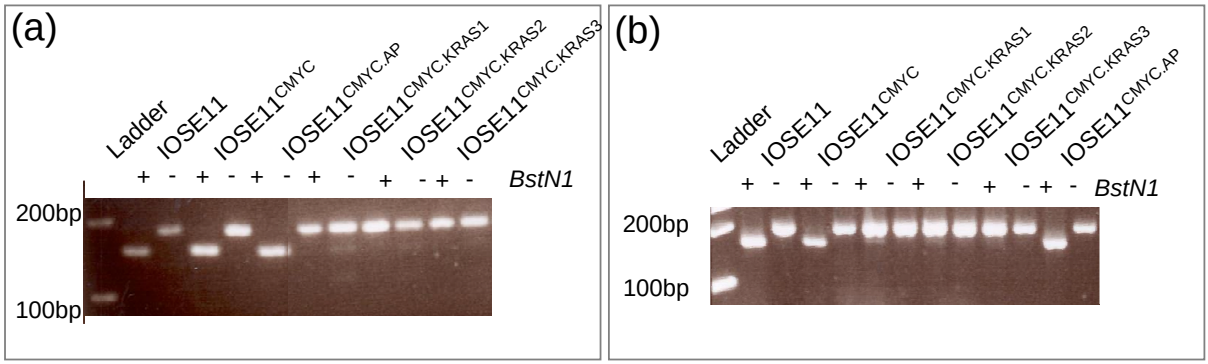

Figure 4.26: RFLP analysis of KRAS^{G12V} expression in IOSE11^{CMYC} and IOSE19^{CMYC}. KRAS^{G12V} mutations are detected in 3 IOSE11$^{CMYC.KRAS}$, 3 IOSE19$^{CMYC.KRAS}$ clones. IOSE cell lines, IOSE^{CMYC} and IOSE$^{CMYC.AP}$ (control cell line co-expressing alkaline phosphatase) did not express mutant (undigested) KRAS mRNA .

ERK1/2). Activation of MAPK signalling was sustained for over 30 mins (Figure 4.27a). Basal levels of p-ERK (timepoint 0 mins) in IOSE11 and IOSE11^{CMYC} were low, but there was strong expression of p-ERK in unstimulated IOSE11$^{CMYC.BRAF}$ cells. MAPK signalling at ERK was also elevated in IOSE11$^{CMYC.KRAS}$. Thus, IOSE19 and clones were tested for levels of basal pERK1/2 only and, as with IOSE11, IOSE19$^{CMYC.BRAF}$ had the highest expression of phosphorylated ERK1/2 (Figure 4.27b).

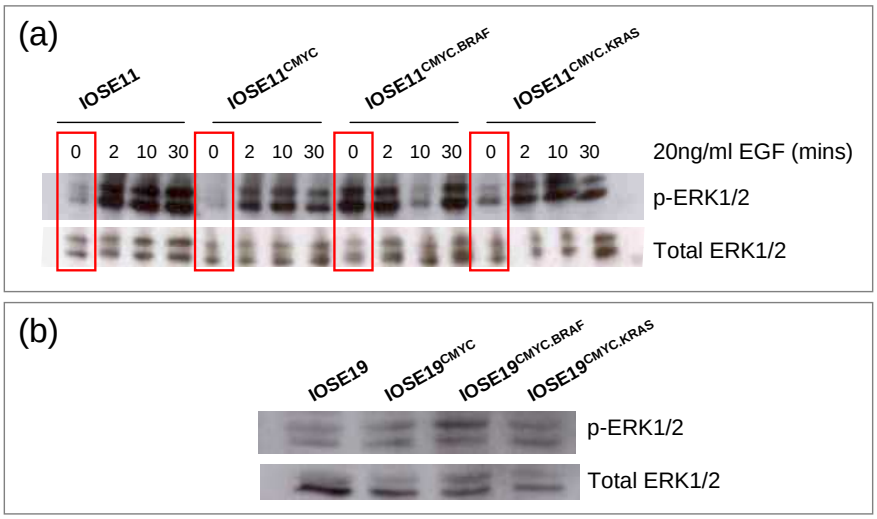

Figure 4.27: Western blot analysis of MAPK activation in oncogene-expressing cell lines. (a) With IOSE11 and derivative cell lines, an EGF timecourse was performed, starved cells were unstimulated (time=0 mins) or stimulated with epidermal growth factor (EGF) for 2, 10 or 30 mins. Activation of the MAPK pathway is indicated by phosphorylation of ERK1/2. Basal expression of phosphorylated ERk1/2 is visible in IOSE11$^{CMYC.KRAS/BRAF}$(b) IOSE19 and derivative cell lines, were tested for basal expression of pERK (timepoint = 0 mins)

The morphology of cell lines was observed by phase-contrast microscopy. Clones expressing mutant *KRAS* and mutant *BRAF* had a more regular, classically epithelial morphology than IOSE cells. Cell shape was more cuboidal than the elongated, fibroblastic-epithelial morphology of IOSE cells (Figure 4.28). Double-oncogene cell lines were tightly packed in the monolayer and did not show the cell scattering phenotype that was observed in IOSE cell lines. Cytokeratin-7 (Ck7) expression was analysed by immunofluorescence. Ck7 expression was detectable in up to 40-70% of IOSE cells, but expressed in 100% of IOSE$^{CMYC.KRAS}$ and IOSE$^{CMYC.BRAF}$ cells. This suggested a commitment to an epithelial phenotype had occurred in these cell lines. However, in 2D monolayer cultures all cell lines were negative for CA125 and E-Cadherin by immunofluorescence, thus all cell lines were lacking these features of differentiated Müllerian epithelial cells, markers which are expressed in many ovarian cancer specimens.

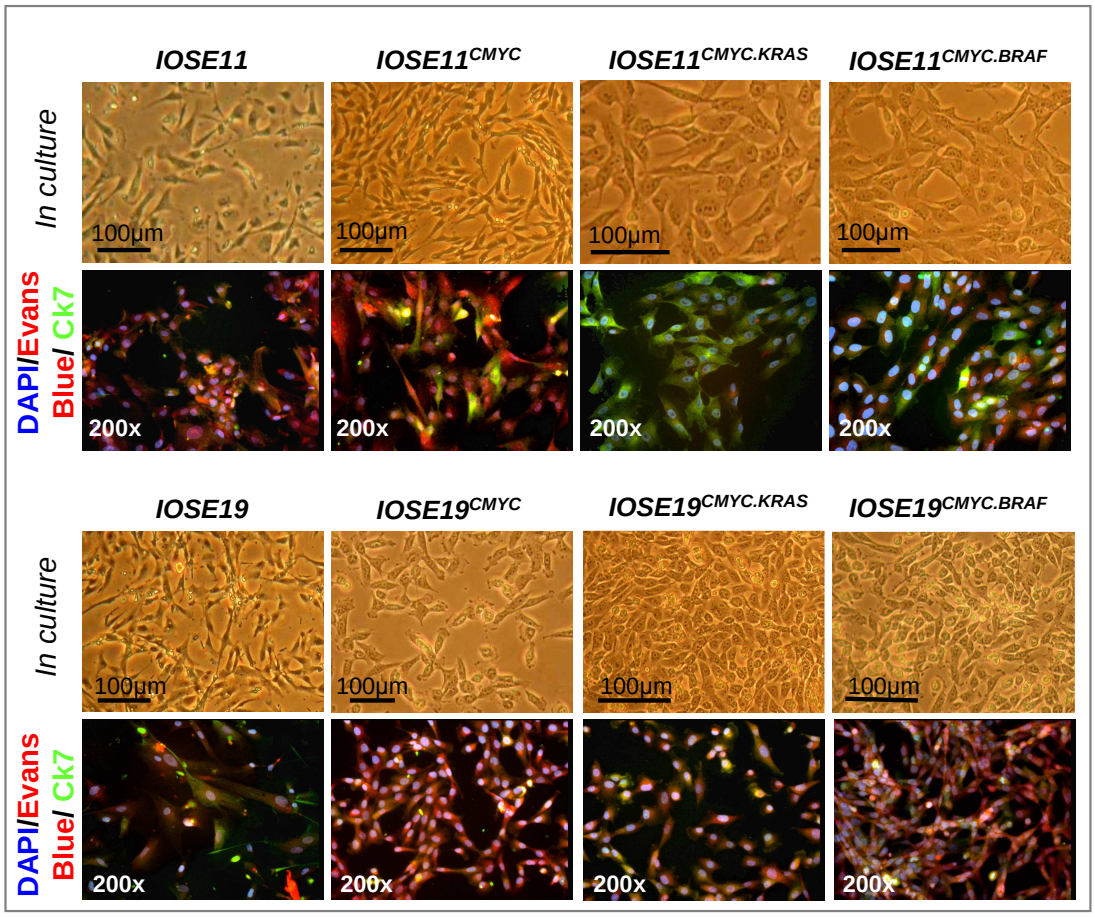

Figure 4.28: Cellular morphology and cytokeratin expression in IOSE, IOSE^{CMYC}, IOSE$^{CMYC.KRAS}$, IOSE$^{CMYC.BRAF}$, by phase-contrast and fluorescent microscopy. Cells have a progressively increasing epithelial morphology with increasing neoplastic phenotype. Cell size also decreases. All fluorescent images are 200X magnification and exposure times were consistent for each antigen.

Enhanced invasive ability is often associated with neoplastic transformation. Also, activation of the MAPK pathway has been shown to induce upregulation of genes involved in invasion [Schulze et al., 2001]. The invasiveness of all cell lines was compared. IOSE^{CMYC} cells were not significantly more invasive than IOSE parental cell lines, however, IOSE$^{CMYC.KRAS}$ and IOSE$^{CMYC.BRAF}$ were significantly more invasive than the IOSE parental cell line ($P \leq 0.05$, Student's paired T-Test).

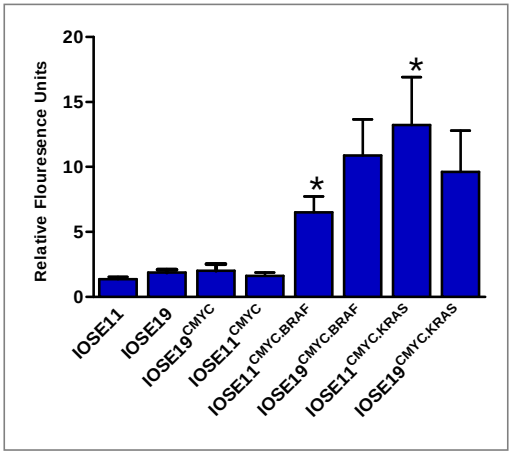

Figure 4.29: Transwell invasion assays reveal invasiveness is enhanced when *CMYC* is co-expressed with $KRAS^{G12V}$ or $BRAF^{V600E}$. Invaded cells were lysed and stained with a fluorescent dye, invasiveness is proportional to fluorescence emitted.

4.5 3D Models of Transformed IOSE Cell Lines

Optimisation of 3D modelling techniques for the growth of NOSE cell spheroids was described in Chapter 3 and have been published [Lawrenson et al., 2009a]. In this laboratory, 3D models of primary ovarian cancer cells have also been established and compared to the primary tumour and the same cells grown in 2D [Grun et al., 2009]. In both reports, it was observed that 3D models of ovarian epithelial cells are more representative of ovarian tissue *in vivo* than 2D monolayer cultures. Therefore, the cell lines described above were established as 3D spheroid models, by culturing cells on polyHEMA coated plastics.

Firstly, the proliferation of cell lines were compared between 2D and 3D models. In 2D, no significant differences were observed in cell proliferation rates for IOSE, IOSE^{CMYC}, and IOSE$^{CMYC.BRAF}$ cell lines. IOSE11/19$^{CMYC.KRAS}$ clones were significantly less proliferative in 2D monolayer than both parental IOSE cell lines (Figure 4.30). This suggests that expression of mutant *KRAS* was associated with a reduction in 2D proliferation.

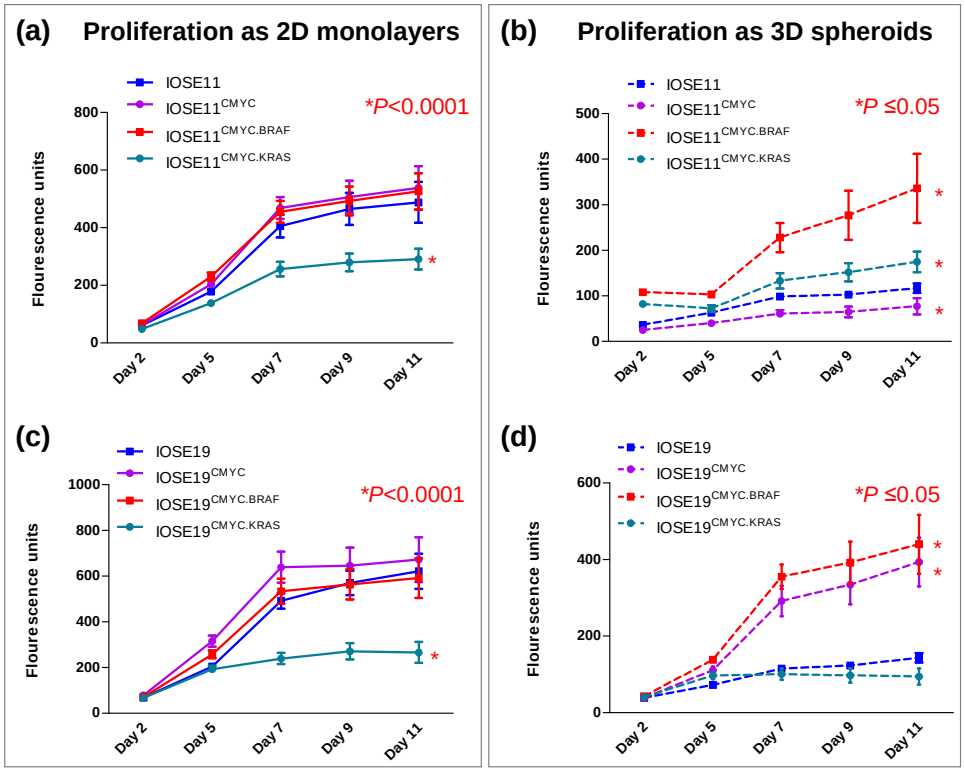

Figure 4.30: 2D and 3D proliferation of IOSE and oncogene-expressing cell lines. Clones expressing one or two oncogenes show enhanced growth in 3D proliferation assays, when compared to IOSE cell lines and 2D proliferation assays. Cell lines in 2D and 3D were incubated with 10% Alamar Blue and the fluorescence emitted recorded every 48 hours.

In 3D culture IOSE cell lines rapidly (within 4-5 days) underwent growth arrest and ceased proliferating in spheroid cultures. Overall, 6/8 cell lines were significantly less proliferative in 3D than 2D (Figure 4.31). The IOSE11$^{CMYC.BRAF}$ and IOSEaa$^{CMYC.KRAS}$ cell lines were not significantly less proliferative in 3D than 2D, although the trend was similar to that observed in the other cell lines. Specifically, cell lines overexpressing *C-MYC*, with or without mutant *KRAS/BRAF* were observed to have growth rates in 2D and 3D that were were less divergent than the 2D/3D growth rates of IOSE cell cultures (Figure 4.31). This suggested that the transformed cell lines did not undergo the growth arrest observed in IOSE cell lines, and that the cells continued to be highly proliferative even under non-adherent conditions. IOSE$^{CMYC.BRAF}$ cell lines were the most proliferative in spheroid cultures.

4.5.1 Histological Analysis of Spheroid Cultures

PolyHEMA-coated flasks were inoculated with 8x10^6 cells and allowed to form MCS. At this high density, spheroid formation was observed within 2-3 days of culture under non-adherent conditions. Dynamics of spheroid formation were monitored by phase-contrast microscopy (Figures 4.32 & 4.33). All cell lines formed loose aggregates within 24 hours of culture on polyHEMA coated plastics. Within 48 hours, spheroids became smooth in appearance and began to increase in size. After 48 hours, IOSE cultures remain static and no significant changes in spheroid morphology were observed during the remaining 12 days of 3D culture (Figure 4.32). This is consistent with the Alamar Blue data, which indicate that IOSE cells undergo growth arrest and become quiescent when cultured as spheroids. In oncogene-expressing clones however, spheroids continued to increase in number and size between day 3 and day 14. From day 4 onwards, the spheroids began to aggregate to form irregular poly-aggregate structures (Figure 4.33). The oncogene-expressing clones were highly proliferative in 3D spheroid culture.

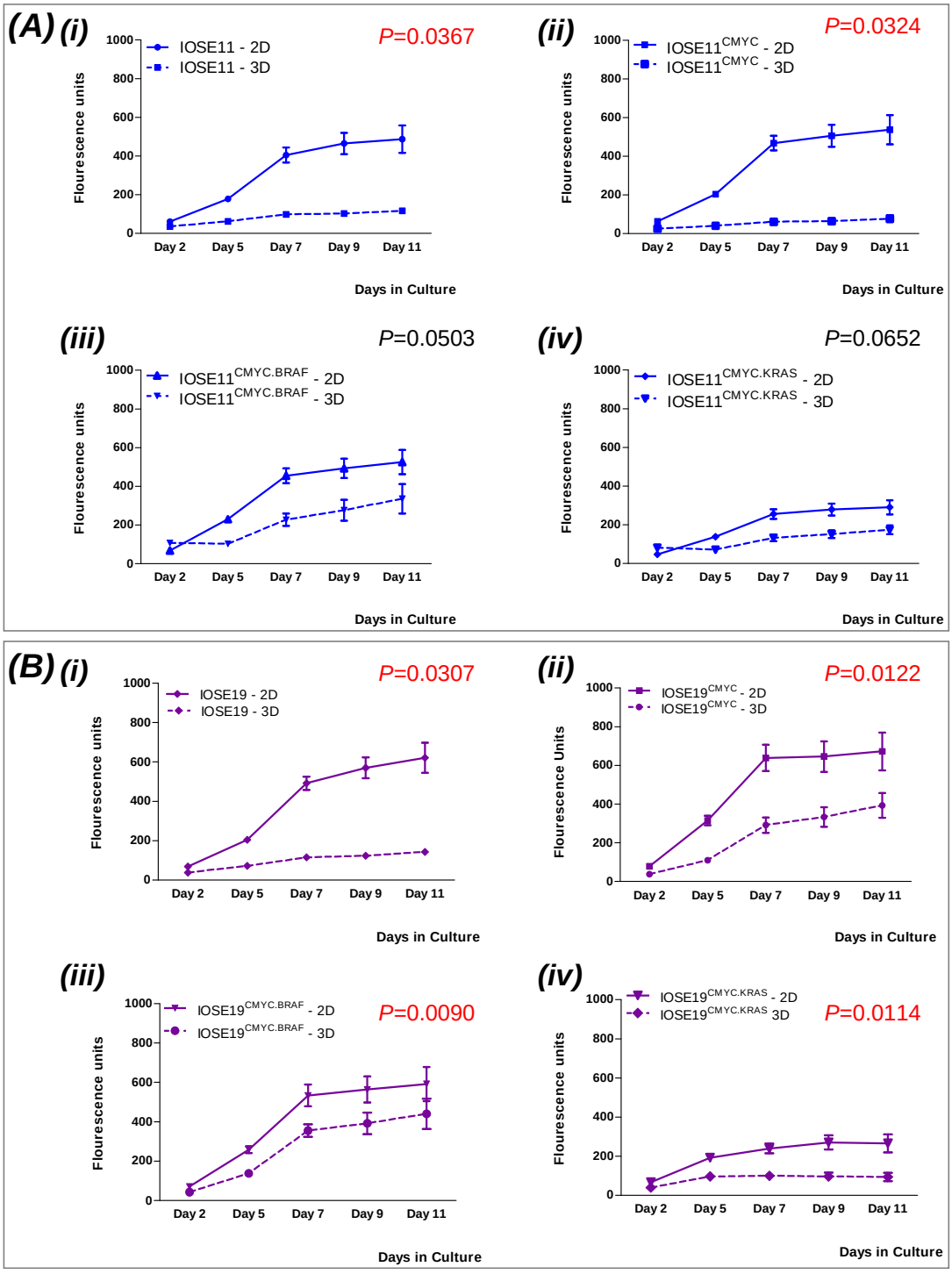

Figure 4.31: Growth characteristics of each cell line in 2D and 3D culture. Cell lines with more genetic alterations introduced tended to proliferate more in 3D culture than the parental IOSE cell lines. The growth rates in 2D and 3D or more transformed cell lines were less different than the 2D v 3D growth rates of IOSE cell cultures. Significant P values are indicated in red (significance level = 0.05).

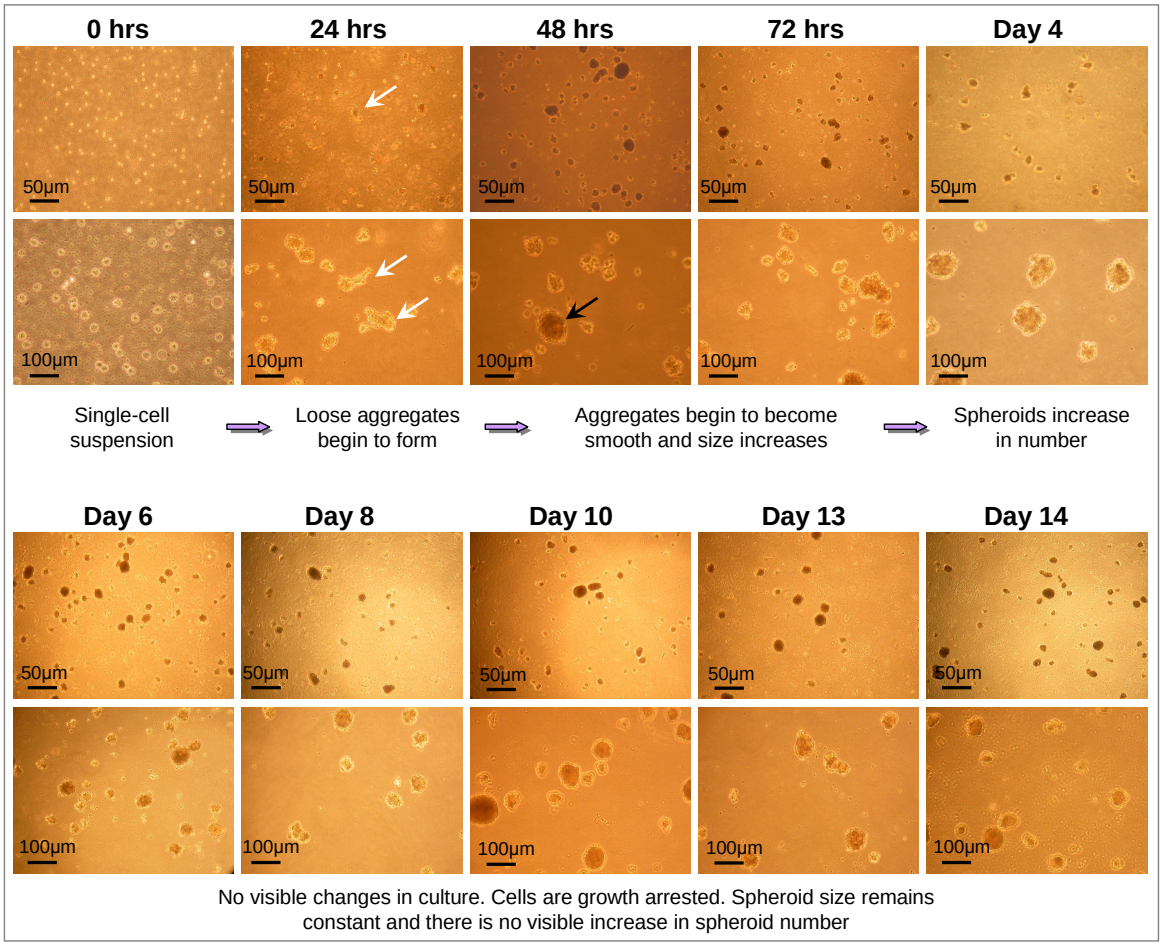

Figure 4.32: Spheroid formation of IOSE cells under low-adherent conditions, at time of seeding and 1-14 day timepoints. Loose aggregates start to form within 24 hours (white arrows) and smooth spheroids appear within 48 hours (black arrows). Once spheroid formation has occurred, appearance of the culture does not significantly alter during the remainder of the experiment.

Cell lines were cultured in 3D for 14 days before fixation with formalin and paraffin embedding. Sections were cut from the paraffin-embedded samples, and stained with hematoxylin and eosin (H&E) and for a panel of biomarkers by immunohistochemistry. Spheroids stained by H&E were examined by light microscopy to observe spheroid and cellular morphologies (Figure 4.34). IOSE cells form regular, rounded spheroids with uniform architectural features. IOSE spheroids contain small foci of matrix material and spheroids are mostly cellular. IOSE19 spheroids tended to be more cellular than IOSE11 (Figure 4.34). No central regions of apoptosis or necrosis were observed, which correlated with the the 3D NOSE cultures described in Chapter 3. In 3D spheroid cultures, IOSE cells have a spindled fibroblastic-epithelial morphology, also observed in 2D cultures of NOSE and IOSE cell lines.

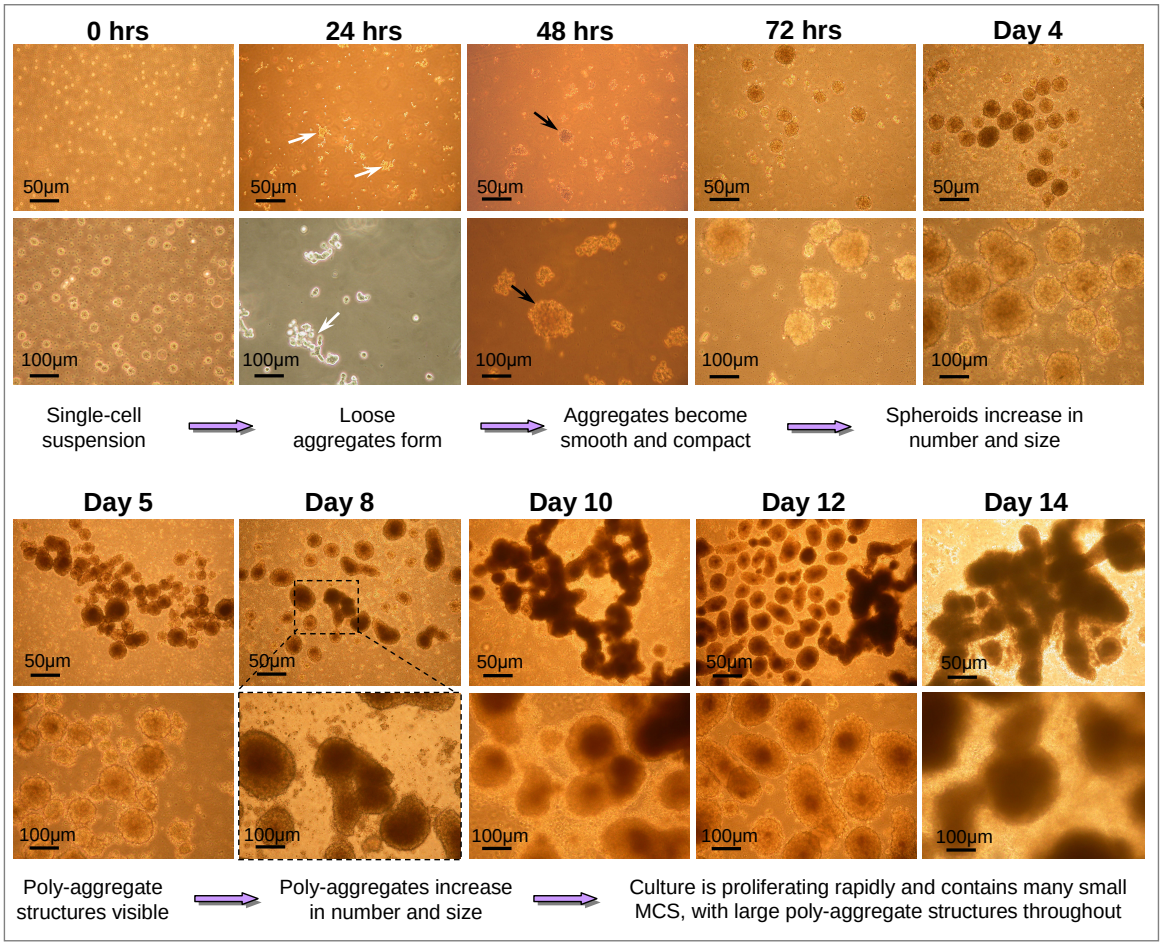

Figure 4.33: Spheroid formation of IOSE19$^{CMYC.BRAF}$, under low-adherent conditions, at time of seeding and 1-14 day timepoints. This is representative of all IOSE$^{CMYC.KRAS.BRAF}$ cell lines and IOSE19^{CMYC}. Aggregation begins within 24 hours (white arrows) and spheroids start to condense within 48 hours (black arrows). At day 5, spheroids begin to aggregate to form poly-aggregate structures which continued to grow in size and number until the 14 day endpoint.

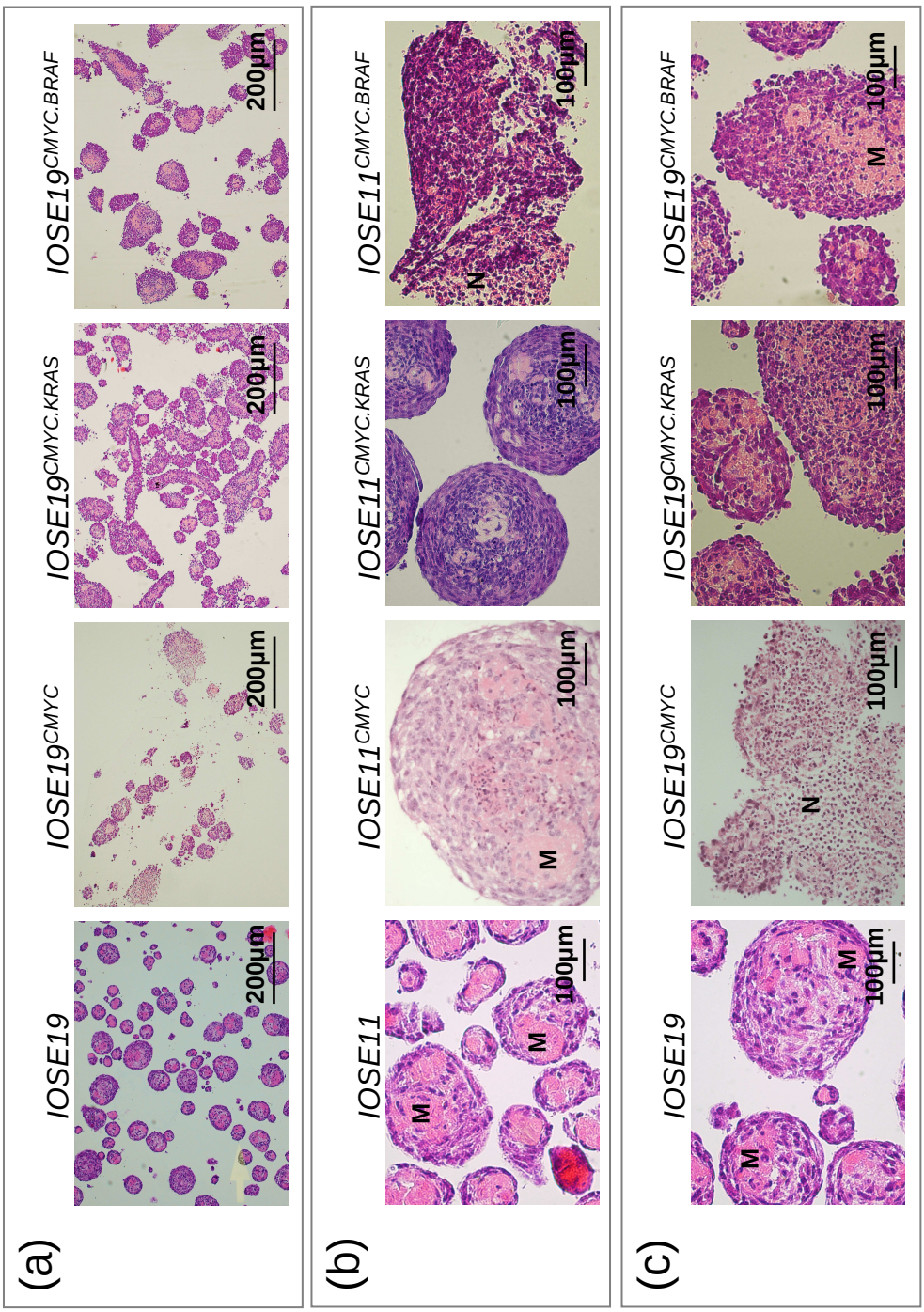

Figure 4.34: Cellular and spheroid morphology in 3D cultures. Sections of paraffin-embedded spheroids were stained with hematoxylin and eosin. (a) IOSE19 and derivation clones expressing oncogenes. Low power images, light microscopy. Note the regularity of spheroid architecture in the IOSE compared to the irregular, chaotic appearance of IOSE19^{CMYC}, IOSE19$^{CMYC.KRAS}$ and IOSE19$^{CMYC.BRAF}$ (b,c) IOSE11, IOSE19 and oncogene-expressing clones. IOSE cells are quiescent. Matrix desposition is observed (M) in greater abundance in IOSE cell lines than in the cell lines expressing *CMYC/KRAS/BRAF*. Cell lines expressing two oncogenes are more cellular, with areas of necrosis (N) and rapid proliferation visible.

IOSE clones overexpressing *CMYC* grew more numerous 3D structures than the IOSE parental cell lines. This was more striking for IOSE19^{CMYC} than for IOSE11^{CMYC}. Mitoses were observed in IOSE11/19^{CMYC}, indicating that the cultures were actively proliferating when harvested. Typically, the centre of larger aggregates had foci of apoptotic cells and these apoptotic foci were larger in the larger spheroids (Figure 4.34). Architectural features also included flattening of cells at the surface. The IOSE19^{CMYC} cell line in particular contained many regions of both extensive apoptosis and extensive proliferation. In this cell line some aggregates were necrotic at the core with 1-2 layers of active cells at the surface of the MCS. Syncytial cell structures were also visible (two nuclei with shared cytoplasm), indicative of rapid uncontrolled proliferation and aberrant cell division. In *CMYC*-overexpressing cell lines, prominent nucleoli were observed and nuclei were often pleomorphic or polygonal in shape (an irregular morphology for nuclei). Prominent nucleoli have been linked to *CMYC* amplifications in tumours where amplification of this gene is common (eg. neuroblastoma, lung cancer) [Kobayashi et al., 2005].

Cell lines overexpressing *CMYC*, in the absence or presence of *KRAS/BRAF* activation, formed spheroids with irregular architectures (Figure 4.34). Spheroids aggregated to form large irregular poly-aggregate structures (Figure 4.33). Cells expressing *CMYC* plus mutant *KRAS/BRAF* tended to have rounded morphologies. Cell lines expressing two oncogenes were very cellular, with areas of apoptosis and rapid proliferation visible (Figure 4.34). Expression of *BRAF* alleles tended to be associated with necrosis rather than apoptosis in the MCS, whereas little necrosis was observed in cell lines expressing *KRAS*^{G12V}. Mitoses were observed on the periphery of MCS. Cells in spheroids from IOSE11/19$^{CMYC.KRAS/BRAF}$ lines tended to contain large nucleoli.

H&E analysis of mass-cultures is a good way to observe morphological trends and gross appearance of cells grown in 3D. However, little other information can be gleaned from H&E-stained sections and few quantifiable characteristics can be measured using this approach. Therefore, sections of 3D spheroids were stained, by immunohistochemistry, for the epithelial markers (cytokeratin-18, Ck18 and cytokeratin-7, Ck7); the ovarian cancer markers CA125 and WT1; a proliferation marker (MIB1) and an apoptosis marker (Bcl2) (Figure **??**). All cell lines expressed Ck18 and Ck7 but did not express CA125. In IOSE cell lines, some staining of MIB1 was detected, and this was localised to peripheral regions of the MCS. In the peripheral regions, cells had a notably elongated mesenchymal morphology, whereas in the centre of MCS, cells had a plump, rounded cell morphology (Figures 4.35 and 4.36). This suggested a more fibroblastic morphology was associated with proliferation of IOSE cells in 3D spheroids, which reflects the phenotype of NOSE cells during wound repair (NOSE cells are more mesenchymal at post-ovulatory sites). IOSE19^{CMYC} and IOSE19$^{CMYC.KRAS/BRAF}$ cell lines were highly proliferative in 3D

spheroids, as indicated by the high proportion of nuclei staining positive for MIB1 (Figure 4.35). Although apoptotic regions of spheroids were detectable in the H & E stained sections, no staining for Bcl2 was observed in any of the cell lines tested. This indicated that apoptosis in the spheroids was not associated with expression of the Bcl2 apoptosis marker.

WT1 was expressed at low levels in IOSE19, and expression was increased in the transformed cell lines (Figures 4.35 and 4.36). WT1 is often expressed by ovarian carcinomas [Koebel et al., 2008]. WT1 was expressed in spheroid cultures of the IOSE11^{CMYC}, IOSE19^{CMYC} and IOSE19$^{CMYC.KRAS/BRAF}$ cell lines. WT1 is expressed in ovarian carcinomas, and interestingly, has previously been shown to be upregulated in 3D cultures of EOC cells [Hylander et al., 2006]; [Barbolina et al., 2008]. WT1 expression may also be associated with enhanced invasion and metastases and poorer patient prognoses [Netinatsunthorn et al., 2006]; [Barbolina et al., 2008].

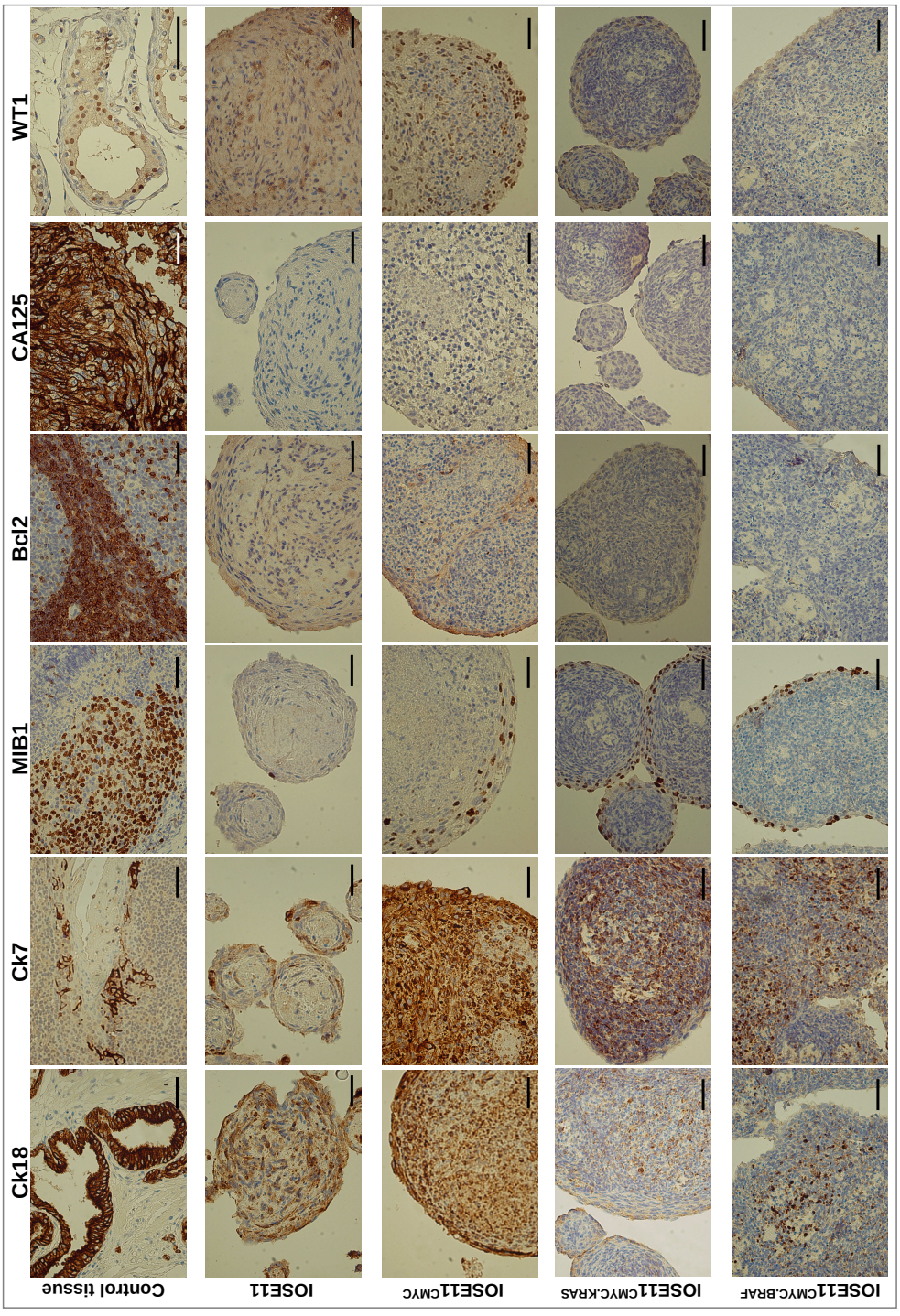

Figure 4.35: Biomarker expression in IOSE11 3D cultures. FFPE spheroids were stained by immunohistochemistry. All multicellular spheroids (MCS) stain positive for cytokeratins-18 and 7. The highest expression of these markers was in IOSE11^{CMYC}. IOSE11 MCS have a low proliferative index, few cells stain positive for MIB1. MIB1 expression in elevated in the cell lines expressing oncogenes. WT1 expression was observed in the nuclei of IOSE11^{CMYC}. No MCS stained positive for Bcl2 or CA125. Light microscopy, positive stain indicated by brown colour, counterstain is blue. Scale bars = 100μm

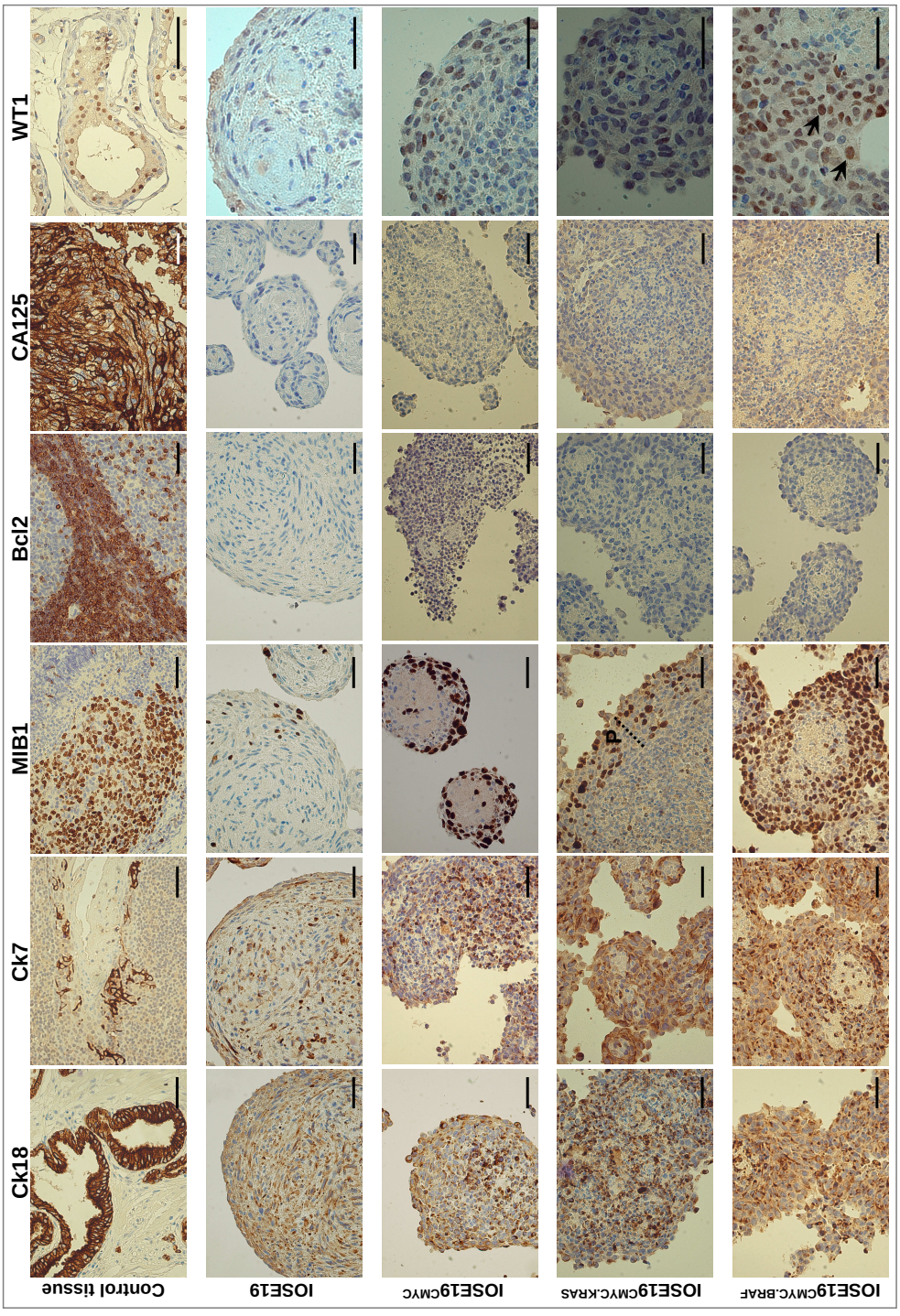

Figure 4.36: Biomarker expression in IOSE19 3D spheroid cultures, immunohistochemical staining of FFPE spheroids. IOSE19 culture were the least proliferative, as indicated by low MIB1 staining, note that the MIB1-positive proliferative cells are localised to a discrete peripheral region (P, indicated by a dashed line). All oncogene-expressing clones express WT1, with the highest expression observed in IOSE19$^{CMYC.BRAF}$ (arrows). No MCS stained positive for Bcl2 or CA125. Light microscopy, positive stain indicated by brown colour, counterstain is blue. Scale bars = 100μm

4.6 Profiling Transcriptomic Changes Associated with NOSE Cell Transformation

The aim of these experiments was to identify genes that were altered in synergy with the genetic alterations introduced in the step-wise genetic model of transformation of NOSE cells described above. The cell lines described have defined genetic alterations stably introduced, these array experiments aimed to analyse the transcriptome of each cell line. The hypothesis of these experiments was that gene expression microarray profiling would give insight into the transcriptomic effects of transformation mediated by the prolonged expression of specific genes/gene combinations in ovarian surface epithelial cells. As the model represents early transformation of NOSE cells, it was hypothesised that the genes identified in these experiments would be candidate biomarkers of the early stages of ovarian cancer.

Gene expression analyses were performed on two independent cell lines and three biological replicates. Profiles were generated for IOSE11, IOSE19, IOSE11^{CMYC}, IOSE19^{CMYC}, IOSE11$^{CMYC.KRAS}$, IOSE19$^{CMYC.KRAS}$, IOSE11$^{CMYC.BRAF}$ and IOSE19$^{CMYC.BRAF}$ cell lines. For detailed analysis of immediate transcriptional effects of a single gene, control vector cell lines represent a good reference cell line. However, as this is a model of progressive transformational changes it was decided that the profiles of IOSE cell lines would serve as an appropriate baseline control.

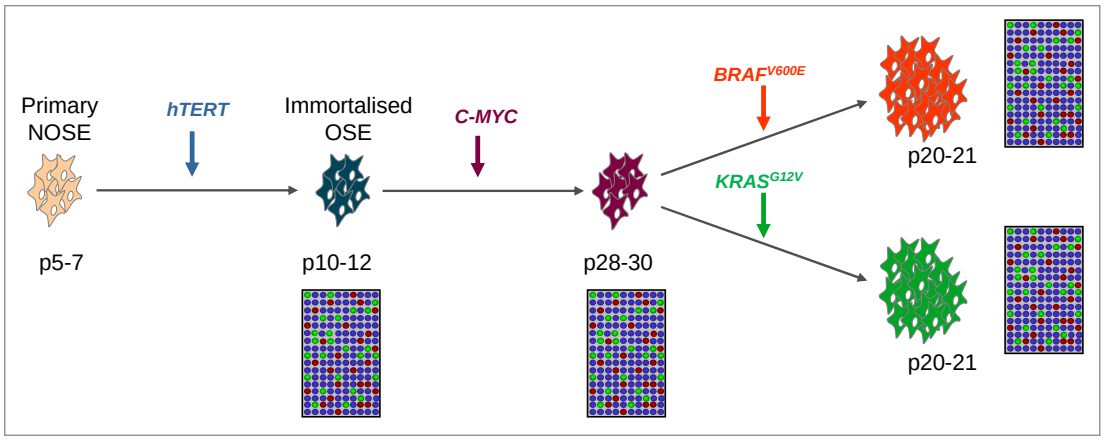

Figure 4.37: Schematic representation of genetic alterations introduced into NOSE cells and the corresponding passages (p) at which gene expression microarrays were performed

Cell lines were taken at a defined passage number: IOSE at passage 10-12, IOSE^{CMYC} at passage 28-30, and IOSE$^{CMYC.KRAS}$ and IOSE$^{CMYC.BRAF}$ at passage 20-21. Passage

numbers for derivative cell lines represent passages since genetic manipulation occurred (see Figure 4.37). The passage numbers also represent the point in the parental cell line at which the next genetic element was introduced, for example, *C-MYC* was introduced into IOSE at passage 10-12. Cell lines at the indicated passage number were grown in 3D cultures, in triplicate, for 14 days, and the RNA was then harvested. RNA samples were quantified, reverse-transcribed, labelled and hybridised to Illumina HT12 gene expression microarrays at the UCL Genomics Facility.

4.6.1 Data Analysis of Microarray Experiments

Data Pre-processing and Quality Control

A schema showing the workflow for data analysis of gene expression microarrays is shown in Figure 4.38. There are many approaches to data pre-processing, as discussed in Chapter 1. The first step was to analyse the quality control (QC) output for control probes on the array to check for consistency across the arrays in terms of (i) hybridisation efficiency, (ii) washing stringency, (iii) RNA labelling, (iv) background signal (v) signal to noise ratios. All arrays in this study showed consistent signals for the control probes.

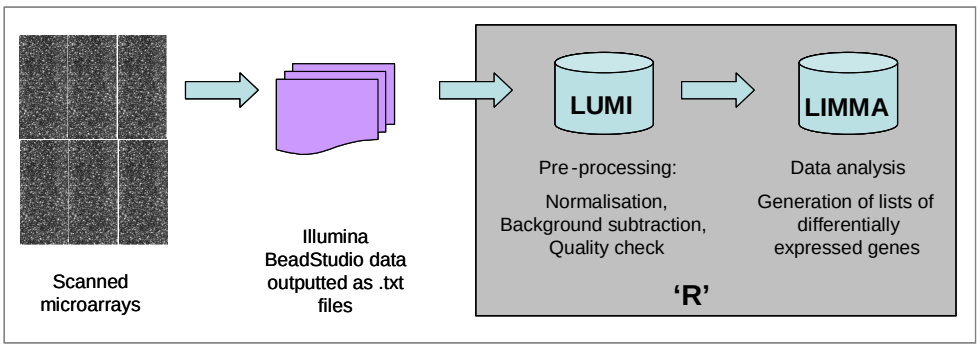

Figure 4.38: Microarray data analysis work flow, using the 'Lumi' and 'Limma' packages in 'R'

In these experiments, image analysis was performed by BeadStudio software, and raw data exported with no background subtraction or normalisation steps performed. This enabled these steps to be done in-house. Pre-processing steps were performed in 'R' using the 'lumi' package, designed for pre-processing of Illumina bead arrays [Du et al., 2008]. Boxplots and MA plots were created of the raw data, and background signal subtracted. Data were transformed using the variance-stabalisation normalisation algorithm and normalised to remove signal that is not due to differential gene expression but due to variation introduced

by technical variables such as spatial effects and differential biotinylation. The 'lumiN' robust spline normalisation technique used in these arrays had been previously validated using an *in vivo* mouse model of ovarian cancer [D. Sproul, personal communication].

Hierarchical Clustering of Gene Expression Profiles

Unsupervised hierarchical clustering was performed to test the relatedness of the cell lines. Outlier detection is based on the sample distance to the hypothetical 'centre'. The two IOSE cell lines are more closely related to each other than to the derivative IOSE^{CMYC} cell lines. This suggests that there are large transcriptional changes between the IOSE and IOSE^{CMYC} cell lines (Figure 4.39). Cell lines harbouring activating mutations in the MAPK pathway also cluster together, with IOSE11$^{CMYC.BRAF}$ clustering more closely to IOSE19$^{CMYC.KRAS/BRAF}$ than IOSE11$^{CMYC.KRAS}$.

4.6.2 Using Gene Expression Microarrays to Identify Genes Dysregulated in Early EOC Development

Normalised, transformed data were then analysed using the Linear Models of Microarray or 'limma' package [Smyth, 2004]. Details of data analysis steps can be found in Chapter 2. Numbers of differentially expressed genes induced by expression of oncogenes was analysed in each cell line. Control (IOSE) cell lines were first compared to IOSE^{CMYC} cell lines. IOSE^{CMYC} were subsequently compared to the IOSE$^{CMYC.KRAS/BRAF}$ cell lines to identify the numbers of genes which were differentially expressed in association with each oncogene. IOSE11 versus IOSE11^{CMYC} has 3253 genes which showed differential expression between the two cell lines (Figure 4.40). In total 1038 and 1023 of these genes overlapped with the changes observed in IOSE11$^{CMYC.BRAF}$ and IOSE11$^{CMYC.KRAS}$ respectively. A total of 2079 genes were in common in IOSE11$^{CMYC.KRAS}$ and IOSE11$^{CMYC.BRAF}$ comparisons with IOSE11^{CMYC}, which is unsurprising as it is known that *KRAS* and *BRAF* have many common transcriptional effects. All 3 groups showed upregulation of a core set of 2130 genes. Frequencies of differentially expressed genes were similar in the IOSE19 cell lines, except that the numbers of differentially expressed genes in the IOSE19$^{CMYC.KRAS}$ group were only 29% of that observed for IOSE11$^{CMYC.KRAS}$ (Figure 4.40).

A gene list was generated for each cell line of the top 30 most statistically significant changes (up- or downregulation) in gene expression, with genes sorted by P-value (Tables 4.1 & 4.2).

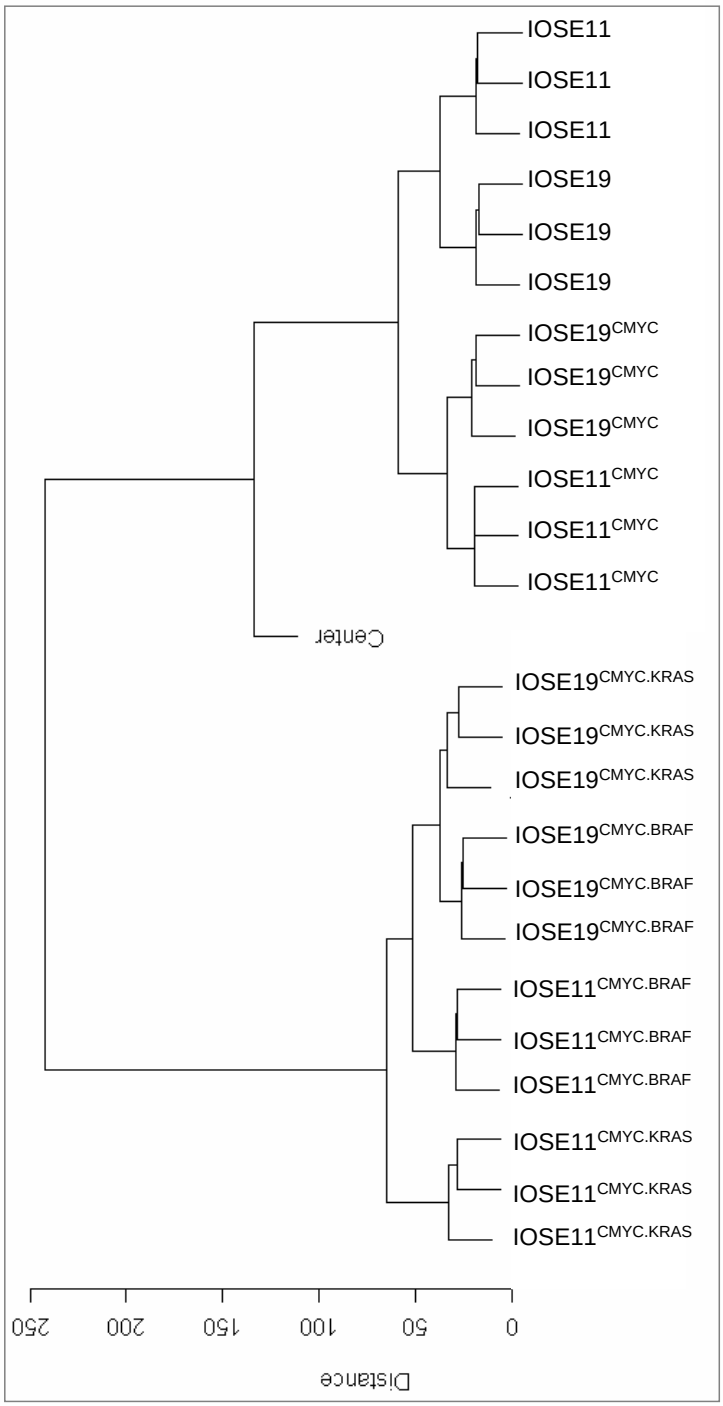

Figure 4.39: Unsupervised hierarchical clustering of normal and transformed cell lines using normalised gene expression microarray profiles. IOSE cell lines cluster together, as do IOSE^{CMYC} cell lines, suggesting that large differences in the transcriptional activity of IOSE cells is induced by the overexpression of *CMYC*. Cell lines with activation of the MAPK pathway cluster together. The IOSE19 'double-mutant' clones were more closely related than the IOSE11 'double-mutant' clones.

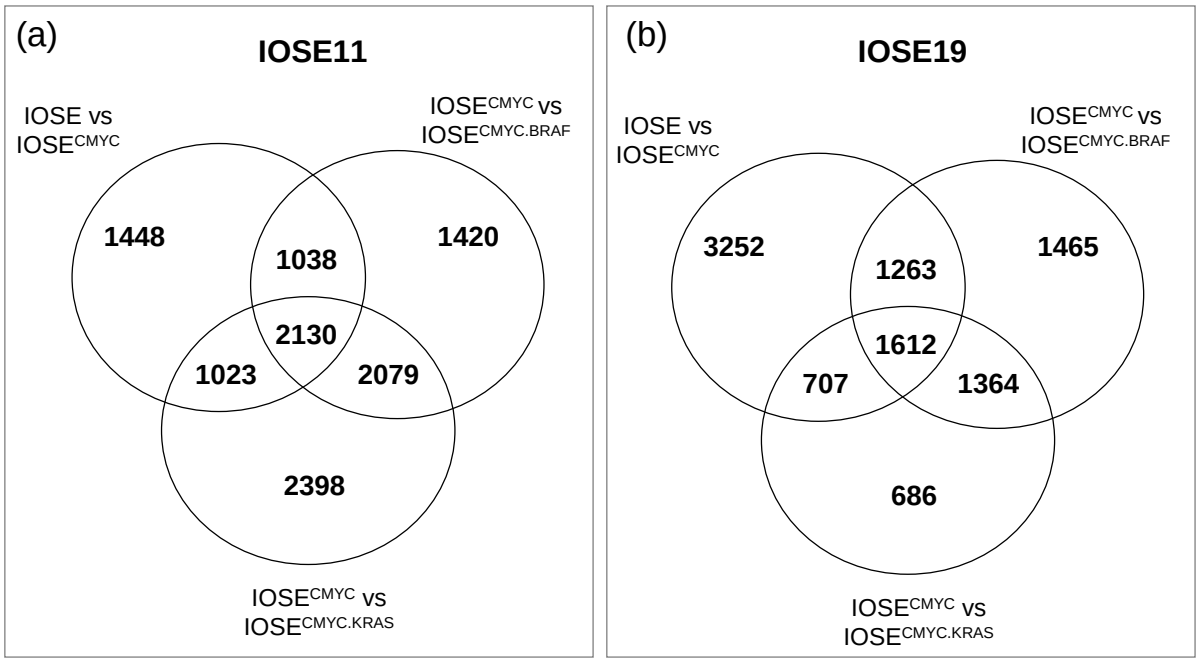

Figure 4.40: Venn diagram to show numbers of differentially expressed probes by oncogene expression in IOSE11 and IOSE19.

Eight genes were in common across the two cell lines. These genes were *THBS1*, *FEZ1*, *PITX1*, *RGS4*, *VGF*, *MOCOS*, *CTGF* and *HIST1H4C*. Thromobospondin-1 (*THBS1*) expression was reduced over 17-fold in the IOSE^{CMYC} cell lines relative to IOSE. In the cell lines also expressing mutant *KRAS* or *BRAF* the expression of *THBS1* was reduced 68.8-fold and 57.5-fold respectively. Expression of *FEZ1*, *RGS4* and *CTGF* was significantly reduced in the transformed cell lines, including the IOSE^{CMYC} cell lines (Figure 4.41). These 4 genes are interesting candidate tumour suppressor genes, expression of which may be lost early in the development of ovarian cancers. Three new candidate oncogenes have also been identified: *PITX1*, *MOCOS* and *HIST1H4C*. *VGF* was also present in the lists of genes for both IOSE11 and IOSE19, but exhibited opposite effects in the two cell lines: *VGF* was highly overexpressed in IOSE11^{CMYC}, IOSE19^{CMYC} and the IOSE19$^{CMYC.KRAS/BRAF}$ clones, but downregulated in IOSE11$^{CMYC.KRAS/BRAF}$ (Figure 4.41). The most interesting candidates are arguably those genes that show highly significant, correlated changes in gene expresison in both cell lines.

Illumina ID	logFC	adj.P.Val	Gene	Chr.	Function
ILMN_2199389	-4.01	3.75×10^{-12}	VIPR1	3	Homo sapiens vasoactive intestinal peptide receptor 1
ILMN_1779071	-2.68	1.02×10^{-11}	FEZ1	11	Homo sapiens fasciculation and elongation protein zeta 1 (zygin I), transcript variant 1
ILMN_1674386	3.44	1.14×10^{-11}	PITX1	5	Homo sapiens paired-like homeodomain transcription factor 1
ILMN_1720048	-2.12	1.37×10^{-11}	CCL2	17	Homo sapiens chemokine (C-C motif) ligand 2
ILMN_1758067	-2.64	1.44×10^{-11}	RGS4	1	Homo sapiens regulator of G-protein signalling 4
ILMN_1757497	3.11	2.28×10^{-11}	VGF	7	Homo sapiens VGF nerve growth factor inducible
ILMN_2197128	-2.57	2.64×10^{-11}	OSR1	2	Homo sapiens odd-skipped related 1 (Drosophila)
ILMN_2301083	2.31	3.20×10^{-11}	UBE2C	20	Homo sapiens ubiquitin-conjugating enzyme E2C, transcript variant 3
ILMN_1673522	2.98	5.09×10^{-11}	MOCOS	18	Homo sapiens molybdenum cofactor sulfurase
ILMN_2377385	-2.29	5.09×10^{-11}	SERPINA9	14	Homo sapiens serpin peptidase inhibitor, clade A (alpha-1 antiproteinase, antitrypsin), member 9, transcript variant B,
ILMN_1680925	-1.77	7.20×10^{-11}	SLC9A3R1	17	Homo sapiens solute carrier family 9 (sodium/hydrogen exchanger), member 3 regulator 1
ILMN_1686116	-3.49	9.22×10^{-11}	THBS1	15	Homo sapiens thrombospondin 1
ILMN_2115125	-2.17	1.06×10^{-10}	CTGF	6	Homo sapiens connective tissue growth factor
ILMN_1788874	2.70	1.44×10^{-10}	SERPINA3	14	Homo sapiens serpin peptidase inhibitor, clade A (alpha-1 antiproteinase, antitrypsin), member 3
ILMN_1654609	3.26	1.52×10^{-10}	TIGA1	5	Homo sapiens TIGA1
ILMN_1674696	-2.79	1.67×10^{-10}	OLAH	10	Homo sapiens oleoyl-ACP hydrolase, transcript variant 1
ILMN_1717934	-2.85	1.86×10^{-10}	SYT11	1	Homo sapiens synaptotagmin XI
ILMN_1693242	1.88	2.07×10^{-10}	ZNF342	19	Homo sapiens zinc finger protein 342
ILMN_1727200	1.70	2.19×10^{-10}	SLCO4A1	20	Homo sapiens solute carrier organic anion transporter family, member 4A1
ILMN_1785732	1.61	2.83×10^{-10}	TNFAIP6	2	Homo sapiens tumor necrosis factor, alpha-induced protein 6
ILMN_1754149	1.88	2.83×10^{-10}	LETMD1	12	Homo sapiens LETM1 domain containing 1, transcript variant 2
ILMN_1773079	2.31	2.88×10^{-10}	COL3A1	2	Homo sapiens collagen, type III, alpha 1 (Ehlers-Danlos syndrome type IV, autosomal dominant)
ILMN_1691476	-1.69	2.88×10^{-10}	MYLK	3	Homo sapiens myosin light chain kinase, transcript variant 8
ILMN_2188862	1.84	2.88×10^{-10}	GDF15	19	Homo sapiens growth differentiation factor 15
ILMN_2075334	1.88	3.83×10^{-10}	HIST1H4C	6	Homo sapiens histone cluster 1, H4c
ILMN_1752755	-1.26	3.86×10^{-10}	VWF	12	Homo sapiens von Willebrand factor
ILMN_1740426	-1.34	4.32×10^{-10}	RASD1	17	Homo sapiens RAS, dexamethasone-induced 1
ILMN_1753913	-2.40	4.73×10^{-10}	GPR177	1	Homo sapiens G protein-coupled receptor 177, transcript variant 1
ILMN_1714730	2.11	4.79×10^{-10}	UBE2C	20	Homo sapiens ubiquitin-conjugating enzyme E2C,, transcript variant 6
ILMN_1676728	1.68	4.79×10^{-10}	DLK2	6	Homo sapiens delta-like 2 homolog (Drosophila), transcript variant 2

Table 4.1: Top 30 differentially expressed genes in IOSE11 transformed cell lines. Genes were ranked by statistical significance. Genes highlighted in red were also found within the list of the top 30 differentially expressed genes for IOSE19. logFC = average log of fold change in gene expression (value is a log of the normalised signal intensity)

Illumina ID	Log FC	Adj. P Val	Gene	Chr	Function
ILMN_1686116	-5.79	$1.47x10^{-14}$	THBS1	15	Homo sapiens thrombospondin 1
ILMN_1699829	-3.489	$1.98x10^{-13}$	CTGF	6	Homo sapiens connective tissue growth factor
ILMN_1731206	3.909	$1.98x10^{-13}$	NKD2	5	Homo sapiens naked cuticle homolog 2 (Drosophila)
ILMN_1674386	3.59	$4.50x10^{-13}$	PITX1	5	Homo sapiens paired-like homeodomain transcription factor 1
ILMN_1758067	-3.49	$4.50x10^{-13}$	RGS4	1	Homo sapiens regulator of G-protein signalling 4
ILMN_2138765	-4.86	$4.50x10^{-13}$	ADFP	9	Homo sapiens adipose differentiation-related protein
ILMN_1778668	-5.18	$1.36x10^{-12}$	TAGLN	11	Homo sapiens transgelin transcript variant 2
ILMN_1707070	3.92	$1.72x10^{-12}$	PCOLCE	7	Homo sapiens procollagen C-endopeptidase enhancer
ILMN_1796316	3.69	$1.72x10^{-12}$	MMP9	20	Homo sapiens matrix metallopeptidase 9 (gelatinase B, 92kDa gelatinase, 92kDa type IV collagenase)
ILMN_2104356	-3.63	$1.72x10^{-12}$	COL1A2	7	Homo sapiens collagen, type I, alpha 2
ILMN_1779071	-2.85	$1.72x10^{-12}$	FEZ1	11	Homo sapiens fasciculation and elongation protein zeta 1 (zygin I), transcript variant 1
ILMN_1803073	3.58	$2.68x10^{-12}$	DNAJC12	10	Homo sapiens DnaJ (Hsp40) homolog, subfamily C, member 12, transcript variant 1
ILMN_1757497	3.19	$2.83x10^{-12}$	VGF	7	Homo sapiens VGF nerve growth factor inducible
ILMN_1673522	2.95	$4.52x10^{-12}$	MOCOS	18	Homo sapiens molybdenum cofactor sulfurase
ILMN_1695423	-2.30	$4.90x10^{-12}$	CD9	12	Homo sapiens CD9 molecule
ILMN_1769282	-2.40	$5.67x10^{-12}$	FRMD6	14	Homo sapiens FERM domain containing 6
ILMN_2400935	-3.08	$8.23x10^{-12}$	TAGLN	11	Homo sapiens transgelin, transcript variant 2
ILMN_1698732	-2.76	$8.23x10^{-12}$	PALLD	4	Homo sapiens palladin, cytoskeletal associated protein
ILMN_2307903	-2.63	$8.72x10^{-12}$	VCAM1	1	Homo sapiens vascular cell adhesion molecule 1, transcript variant 1
ILMN_1797776	-2.40	$1.04x10^{-11}$	PRSS23	11	Homo sapiens protease, serine, 23
ILMN_2075334	2.43	$1.12x10^{-11}$	HIST1H4C	6	Homo sapiens histone cluster 1, H4c
ILMN_2353161	-2.64	$1.13x10^{-11}$	MSLN	16	Homo sapiens mesothelin, transcript variant 2
ILMN_2315979	-1.88	$1.16x10^{-11}$	LBH	2	Homo sapiens limb bud and heart development homolog (mouse)
ILMN_1718866	-2.32	$1.43x10^{-11}$	MGC23985	5	Homo sapiens similar to AVLV472
ILMN_2115125	-3.40	$1.69x10^{-11}$	CTGF	6	Homo sapiens connective tissue growth factor
ILMN_1806040	2.69	$1.72x10^{-11}$	TYMS	18	Homo sapiens thymidylate synthetase
ILMN_2339835	-1.91	$1.80x10^{-11}$	PTGS1	9	Homo sapiens prostaglandin-endoperoxide synthase 1 (prostaglandin G/H synthase and cyclooxygenase)
ILMN_1654609	2.57	$2.16x10^{-11}$	TIGA1	5	Homo sapiens TIGA1
ILMN_2386973	-1.67	$2.45x10^{-11}$	PKP2	12	Homo sapiens plakophilin 2, transcript variant 2a
ILMN_1701827	-1.74	$3.12x10^{-11}$	CADM3	1	Homo sapiens cell adhesion molecule 3

Table 4.2: Top 30 differentially expressed genes in the IOSE19 transformation model, ranked by P-value. Genes highlighted in red were also found in the top 30 differentially expressed genes in IOSE11. logFC = average log of fold change

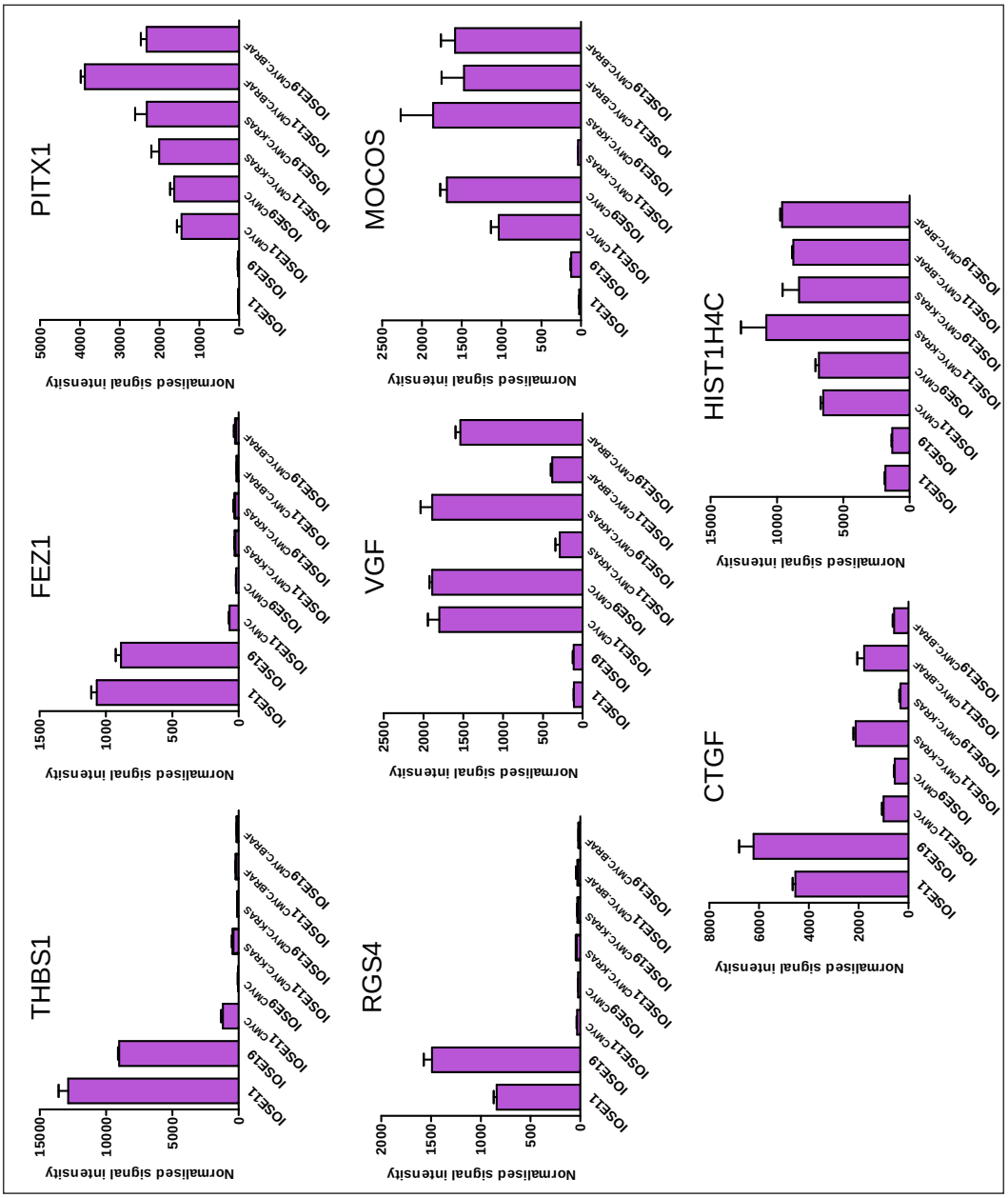

Figure 4.41: Expression of the 8 most significant genes differentially expressed in both cell lines. Normalised, background subtracted signal intensities are tabulated.

4.6.3 Expression of Genes Known to be Dysregulated in EOCs

The gene expression profiles for this transformation model were examined to analyse the expression of genes already known to be involved in ovarian cancer. These genes are described in detail in Chapter 1, and are components of main pathways in EOC: the DNA double-strand break (DSB) repair pathway, the mismatch repair (MMR) pathway, the mitogen-activated protein kinase (MAPK) pathway and the phosphatidylinositol 3-kinase (PI3K) pathway. All genes were analysed for expression across biological replicates, to ensure that any observed variation was reproducible between the two cell lines.

Expression of *BRCA1* and *BRCA2* was low in all transgenic cell lines. There is some evidence (in 2/4 probes) of enhanced *BRCA1* expression in the IOSE$^{CMYC.KRAS/BRAF}$ cell lines, and, relative to the IOSE^{CMYC} cell lines, *BRCA2* expression was reduced by 35% and 42% in IOSE$^{CMYC.KRAS}$ and IOSE$^{CMYC.BRAF}$ cell lines respectively. As TP53 is upregulated in response to DNA damage induced by loss of *BRCA1/2* function, expression of *p53* mRNA was also examined. *p53* expression was found to be upregulated by 1.8-fold in the IOSE11/19$^{CMYC.KRAS/BRAF}$ cell lines, relative to the IOSE/IOSE^{CMYC} cell lines. There were no significant changes in *p53* mRNA expression in the IOSE cell lines *versus* the IOSE^{CMYC} cells.

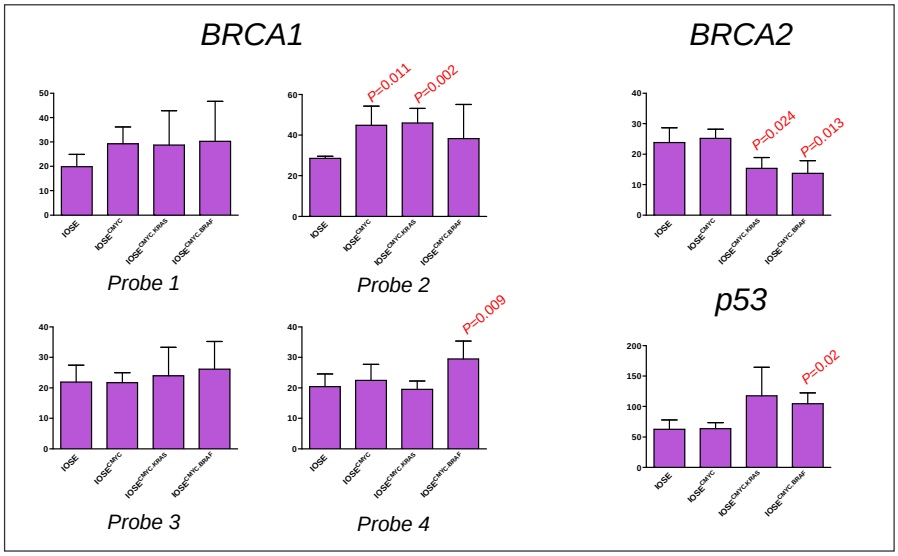

Figure 4.42: mRNA expression of genes involved in the double-stranded break repair pathway

Components of the MAPK pathway were also examined to identify any differential expression induced by the expression of *CMYC*+/-*KRAS*^{mut} and *BRAF*^{mut}. Firstly, expression of alternative *RAS*, *RAF* isoforms and receptor tyrosine kinases was exam-

ined. *ERBB2* and *HRAS* expression was significantly downregulated in the IOSE^{CMYC}, IOSE$^{CMYC.KRAS}$ and IOSE$^{CMYC.BRAF}$ cell lines, relative to the IOSE cultures. The most significant downregulation of these genes and of *CRAF* and *ARAF* occurred in the cell lines expressing mutant *KRAS* or *BRAF*, which suggests that cells downregulate endogenous MAPK signalling in an attempt to suppress the enhanced MAPK signal transduction. Results from both cell lines were highly correlated, as indicated by the low standard deviation observed. Downstream kinases in the pathway showed that heterogenous levels of expression were induced by the different oncogenes (e.g *MAPKAPK5*). There was some indication that *EGFR* expression was elevated in the IOSE$^{CMYC.BRAF}$ cell lines, which may indicate activation of the autonomous EGFR-dependent feedback look previously described as being associated with activation of this gene [Schulze et al., 2004].

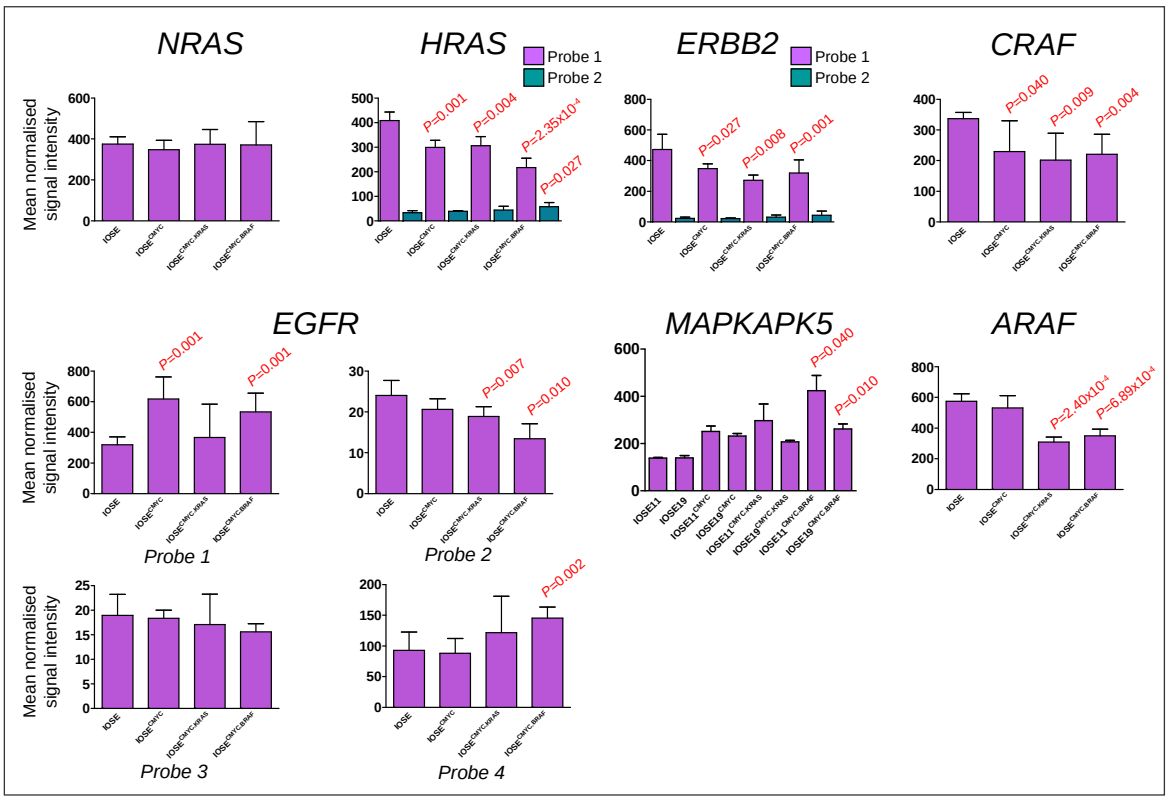

Figure 4.43: Gene expression of other *RAS* and *RAF* isoforms and receptor tyrosine kinases. Some probes, such as probe 1 for *HRAS* and *EGFR*, perform better than alternative probes included on the array (e.g. probe 2 for both of these genes).

The phosphatidyinositol 3-kinase pathway is commonly dysregulated in ovarian carcinomas. This pathway interacts closely with the MAPK signalling, as *RAS* also activates signalling down the PI3K pathway. *AKT2* did not show any differences in gene expression

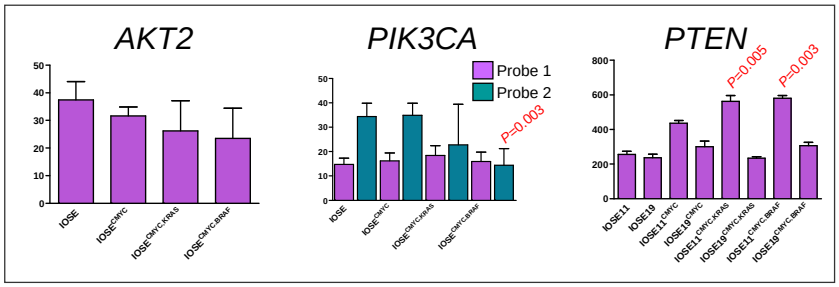

Figure 4.44: mRNA expression of genes in the PI3K pathway

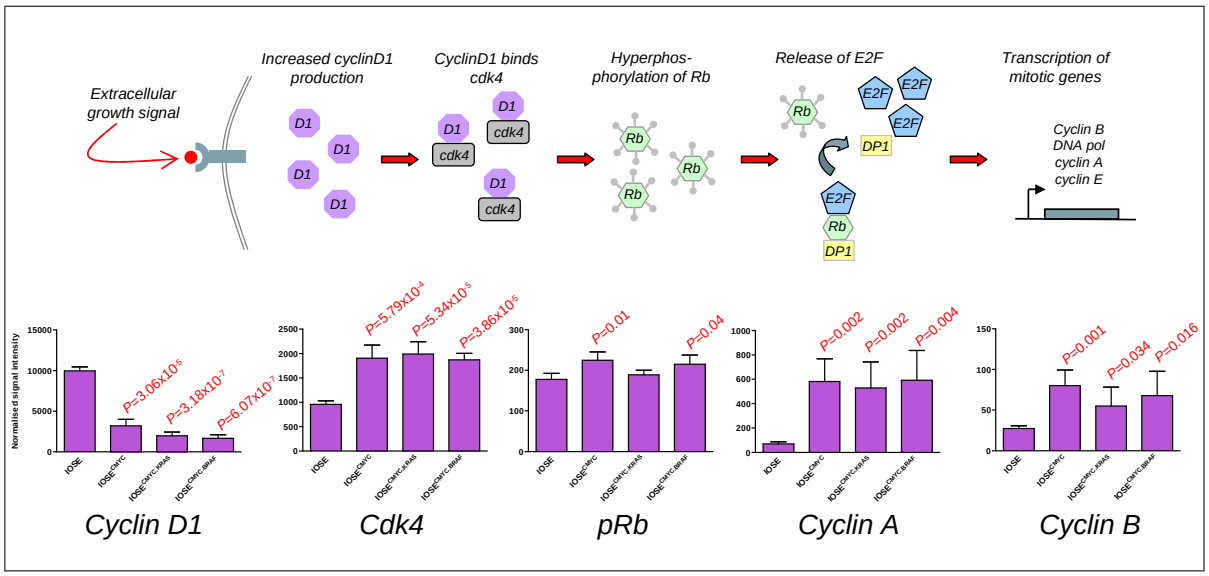

Figure 4.45: Genes involved in mitosis induction are differentially expressed in transformed cells. IOSE cells show enhanced responses to growth factors (indicated by elevated expression of *cyclin D1)*, but transformed cell lines have higher expression of genes involved in signal transduction and mitosis (*cdk4, cyclin A* and *cyclin E*).

in the normal and oncogene-expressing cell lines. *PTEN* negatively regulates signalling down the PI3K pathways, and was upregulated in the IOSE11 lines expressing mutant *KRAS/BRAF* alleles, suggesting that this is a negative feedback mechanism induced by enhanced transduction of growth signals.

Genes Involved in Cell Cycle Regulation

The gene expression microarray data were also examined for any changes in the expression of cell cycle regulation. Immortalised cell lines underwent rapid growth arrest in 3D culture, whereas the transformed cell lines continued to proliferate rapidly in 3D. When an external growth signal is received by a cell, levels of cyclin D1 increase rapidly. IOSE cells had an enhanced response to growth factor signalling (growth factors in the tissue culture medium), indicated by the high *cyclin D1* expression, despite the fact that the cells are in a growth arrested state (Figure 4.45). Whilst *cyclinD1* expression was lower in the transformed cell lines, these cell lines had high expression of downstream genes, including *cyclin A* and *cyclin E* (mitotic genes). *pRb* levels did not show any large changes across the cell lines, but activity of this protein is regulated mainly by changes in phosphorylation, not abundance.

4.6.4 Expression of Genes Associated with EOC Susceptibility

This laboratory recently led the first genome-wide association study (GWAS) for EOC and identified a panel of single nucleotide polymorphisms (SNPs) that are associated with ovarian cancer risk [Song et al., 2009] and [S.Gayther, unpublished data]. Susceptibility studies are designed with the hypothesis that some of the common natural somatic genetic variation that occurs in the general population can have small risk effects on individuals susceptibility to developing a disease. To identify low-penetrance susceptibility alleles, researchers analyse the SNP genotypes of thousands of cases and controls, usually using DNA isolated from peripheral blood samples. In recent years, GWASs have found genetic variants that alter a person's risk of many different diseases, including prostate, breast and ovarian cancer [Easton et al., 2007]; [Eeles et al., 2008]; [Ghoussaini et al., 2008]; [Song et al., 2009].

For ovarian cancer, the top 5 most significant loci are distributed throughout the genome at chromosomes 8q24, 9p22, 19p13, 2q31 and 3q25. However, only two out of the five SNPs fall within genes, and not one of the top SNPs lies in a coding region. SNPs represent a marker for a local haplotype block, in which a region of the genome is in linkage disequilibrium (LD). Homologous recombination within this LD block is restricted, and so a SNP within this region gives information about the genotype of other SNPs held in tight linkage disequilibrium with the identified susceptibility SNP. It is therefore very likely that a SNP identified in a GWAS is not the causal SNP, but is linked be association to the causal variant. It also follows that the gene of interest may not even be the nearest gene to the susceptibility SNP. The complexity is compounded by the likelihood that causal

Locus	Per-allele OR	P-trend
9p22	0.82	$6.9x10^{-20}$
8q24	0.85	$3x10^{-6}$
19p13	1.13	$7x10^{-5}$
2q31	1.15	$5x10^{-9}$
3q25	1.23	$7x10^{-8}$

Figure 4.46: The top five loci associated with ovarian cancer risk. Per-allele OR describes the odds ratio, or risk of developing disease in patients carrying the rare allele. Data are pooled in that genotype frequencies in all EOC patients are compared to genotype distributions in control women, who do not have ovarian cancer

SNPs in non-coding regions could be modifying the expression of distant genes, or even genes on other chromosomes.

Determining the functional effects of susceptibility SNPs is therefore immensely challenging, especially as effects are likely to be subtle. However, it is also true that even if the risk associated with a single SNP is small, it does not mean that that gene will not be important in disease. A good example of this can be found in the case of heart disease, in which enzyme CoA was identified as a risk locus. Although the risk associated with this gene was not large, the clinical impact of this gene is enormous, as illustated by the widespread use and efficacy of statins. It is likely that susceptibility SNPs have an effect early in disease development, therefore I identified genes in the regions spanning susceptibility loci and examined differential expression in the oncogene-expressing cell lines, using the model of OSE transformation described above.

One SNP was found at 8q24, ∼50 kbp distal to the *CMYC* gene. In this *in vitro* transformation model, *CMYC* was overexpressed the transformed cell lines, which was confirmed using the gene expression arrays data (Figure 4.47). There are few other genes in this region other than *CMYC*, although this region also includes *DDEF1*, *POUSF1B*, *GSDMC* and a handful of pseudogenes. *POUSF1B* did not show differential expression in the different cell lines tested. However, analysis of expression of two *DDEF1* probes from the array data indicated that this gene was significantly downregulated in the transformation model, suggesting that *DDEF1* may have a tumour suppressor role.

At 9p22, there are 4 genes within the 2800 Kbp region spanning the susceptibility SNP. These genes are *C9orf93*, *BNC2*, *CNTLN* and *SH3GL2*. Whilst expression of *C9orf93* and *SH3GL2* did not seem to be significantly different in the various transgenic cell lines, expression of *BNC2* was reduced in all oncogene expressing clones. *CNTLN* expression

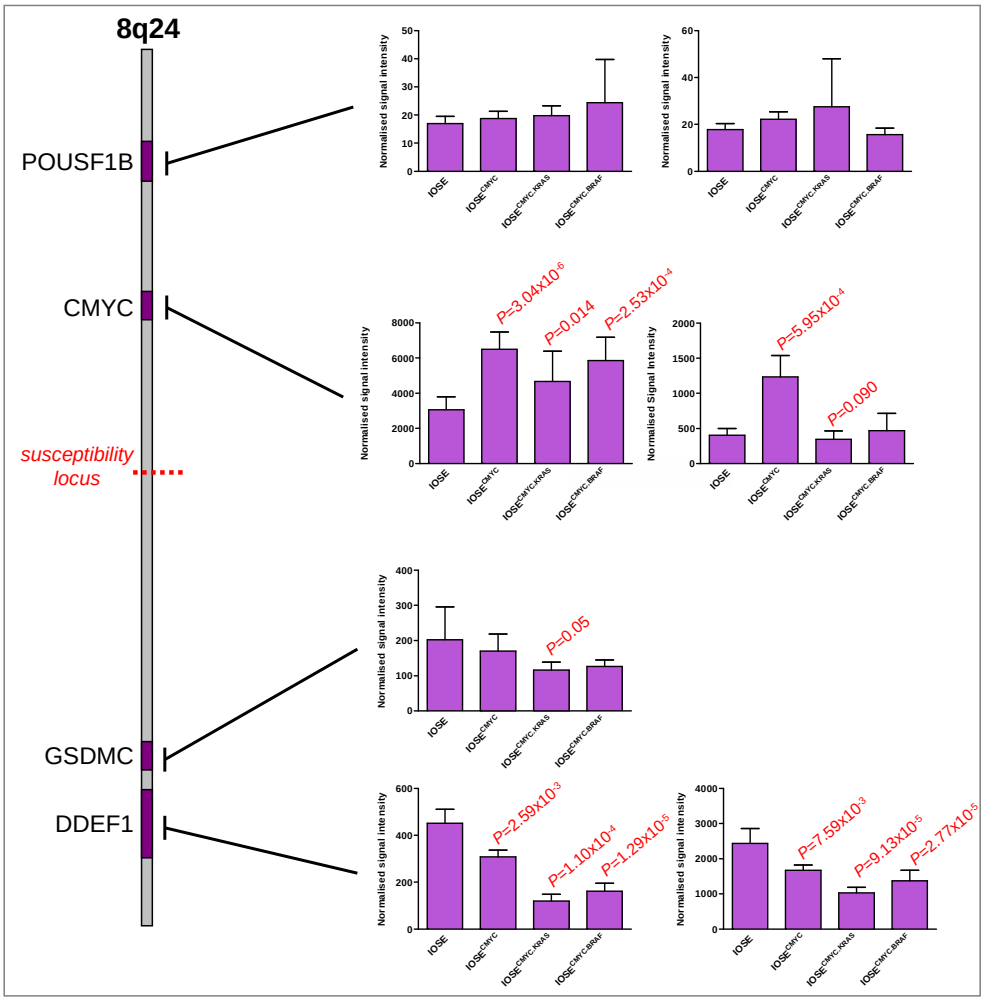

Figure 4.47: Expression of genes local to the 8q24 susceptibility locus. Few genes are located within the 2930 kbp spanning this susceptibility loci.

was significantly elevated in IOSE^{CMYC} cell lines and also in the cell lines over-expressing *CMYC* in combination with mutant *KRAS/BRAF*.

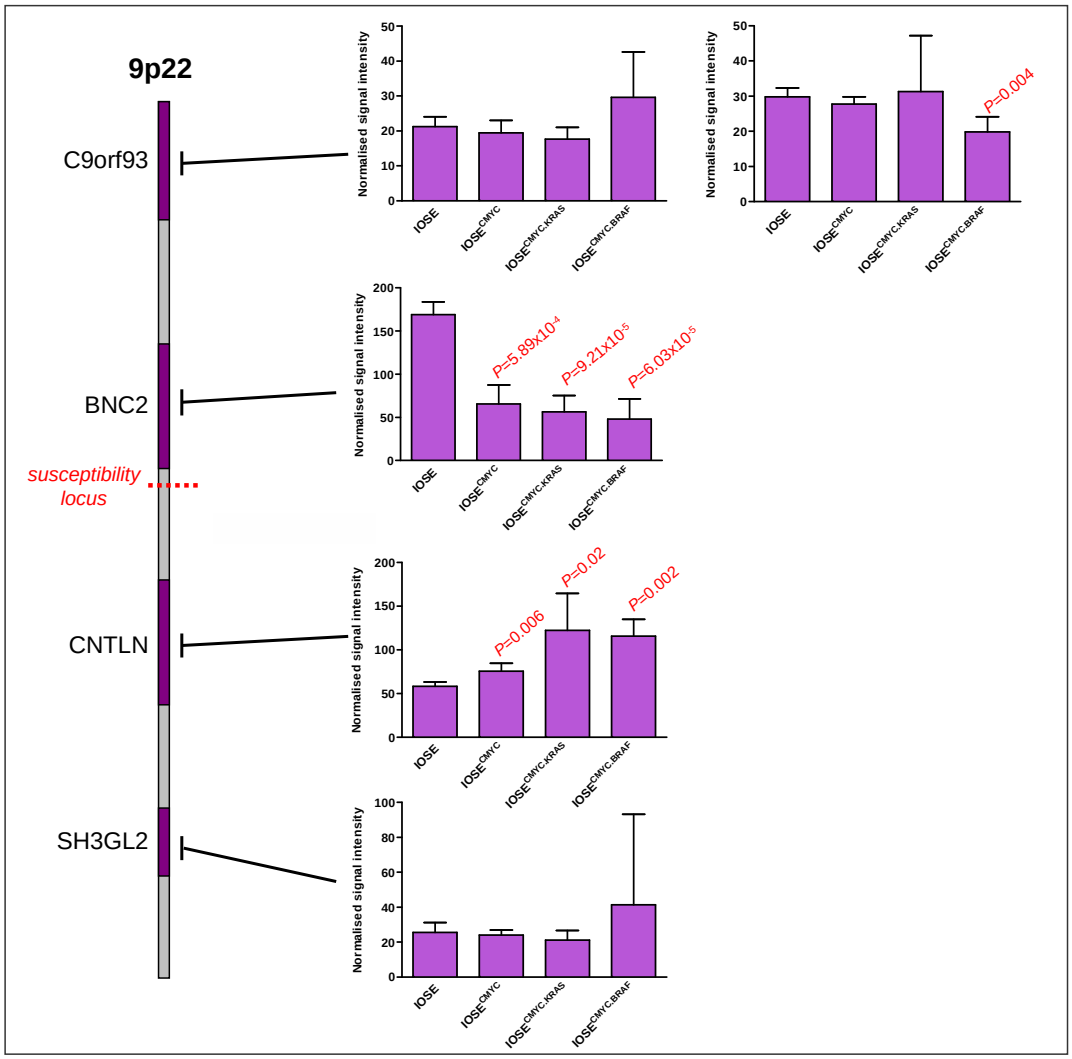

Figure 4.48: Expression of genes in the 2800 kbp spanning the 9p22 ovarian cancer susceptibility locus

At the chromosome 19p13 locus, the nearest genes, namely *MERIT40*, *ANKLE1* and *USHBP1* did not show any differential expression in this cellular transformation model. However, *NR2F6* and *MRPL34* were upregulated in both the IOSE$^{CMYC.KRAS}$ and IOSE$^{CMYC.BRAF}$ cell lines.

One region of the genome identified as a susceptibility locus for EOCs lies within a region on chromosome 2p31, which is dense with homeobox genes: *HOXD1*, *HOXD3*, *HOXD4*,

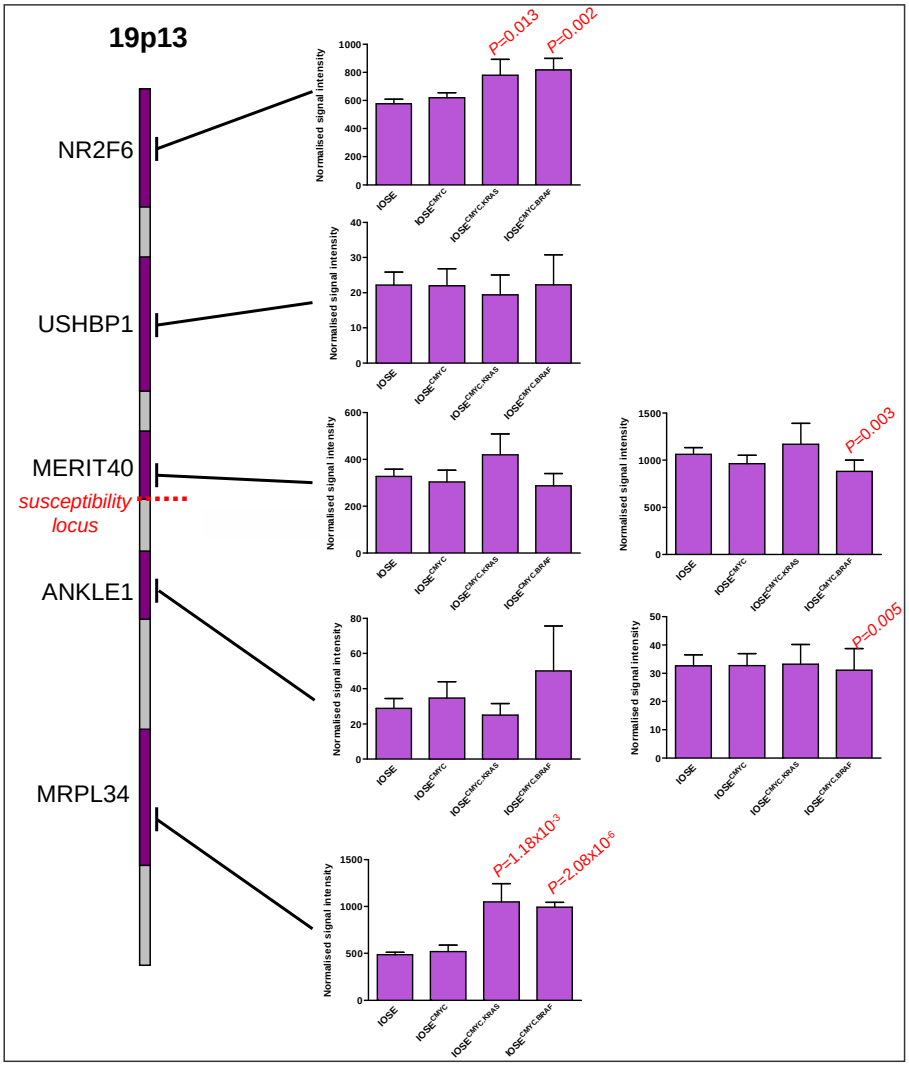

Figure 4.49: Expression of genes local to the 19p13 susceptibility locus

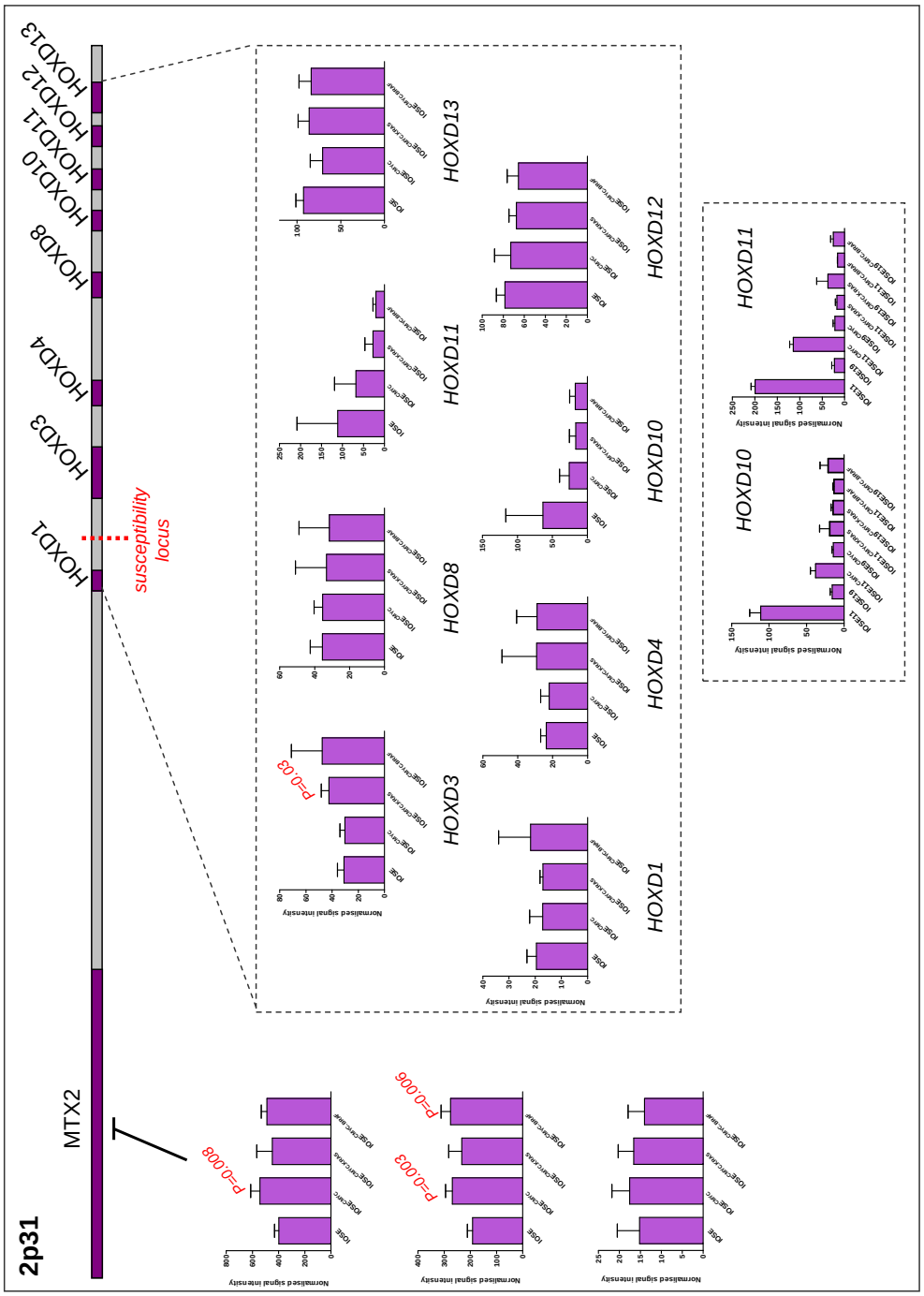

Figure 4.50: Expression of genes local to the 2p31 susceptibility locus. Grouped analyses are shown (all IOSE, all IOSE^{CMYC}, etc are analysed together). Analysis of individual cell lines expression of *HOXD10* and *HOXD11* are shown in the lower panel.

HOXD9-13. *HOX* genes are usually expressed temporally during development, and interest in *HOX* genes is fuelled by work in the field of cancer stem cells. In this cell model, overall expression of *HOX* genes was relatively low. There is some suggestion that *HOXD3* expression may be elevated in IOSE$^{CMYC.KRAS/BRAF}$ cell lines. *HOXD10-13* were more highly expressed than *HOXD1,3,4 & 8*. There was some evidence that expression of *HOXD10* and *HOXD11* was reduced in the transformed cell lines, relative to the IOSE cultures, but the large standard deviations observed in the grouped analyses suggested that the two cell lines were displaying different patterns of expression of this gene. Indeed, when cell lines were considered individually, it was observed that IOSE11 displayed highest levels of expression of both of these genes, and that expression was progressively reduced in the oncogene-expressing, neoplastically transformed cells.

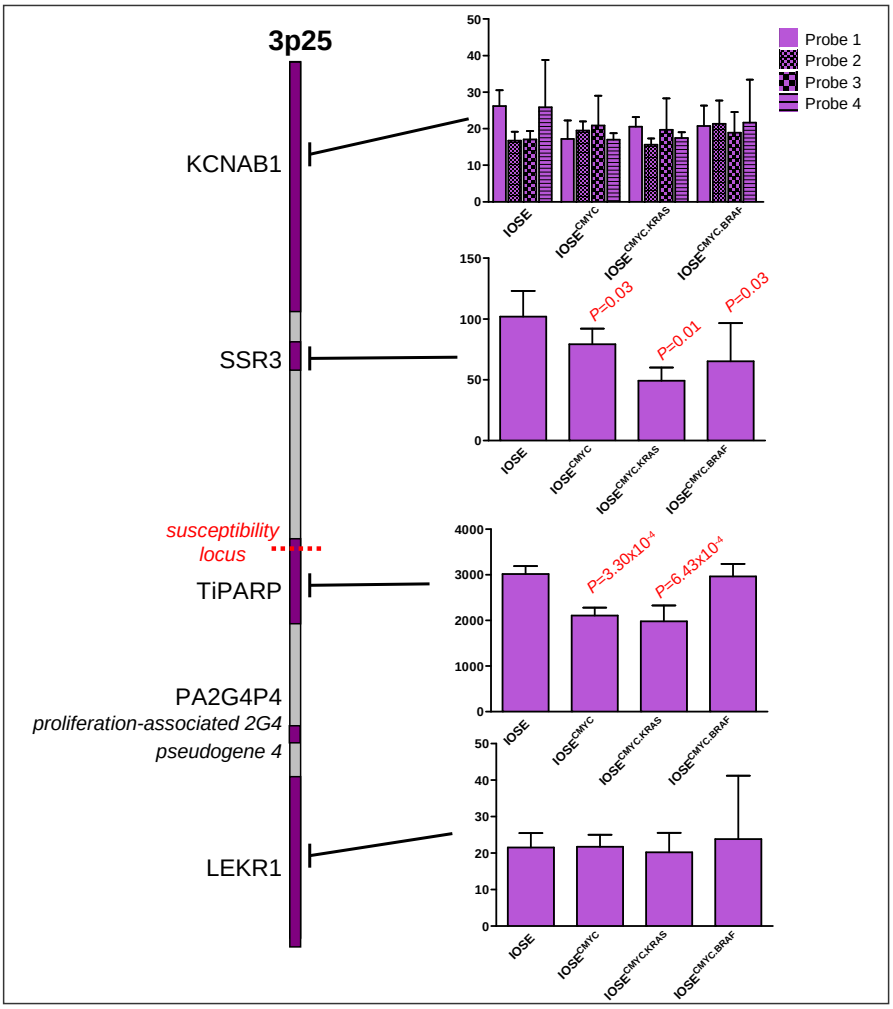

Figure 4.51: Gene expression of genes local to the 3q25 susceptibility locus

The final susceptibility locus is on chromosome 3p25. The gene nearest to the 3p25 susceptibility is *TiPARP*. In both independent cell lines, this gene was downregulated in IOSE^{CMYC} and IOSE$^{CMYC.KRAS}$ cell lines (Figure 4.51). *SSR3* was also significantly downregulated in all oncogene-expressing cell lines.

4.7 Conclusions and Discussion

Despite the discovery of the ovary-specific Müllerian inhibiting substance receptor type II, an *in vivo* model which accurately reflects epithelial ovarian cancer (EOC), a disease which is late-onset and histologically heterogeneous, has yet to be established. Therefore, in this Chapter, I describe an *in vitro* approach to modelling early ovarian neoplasia. Normal ovarian surface epithelial (NOSE) cells were isolated from patients with histologically normal ovaries and characterised to confirm the origin of the cells and the non-tumourigenic nature of the cell lines (Chapter 3). In this Chapter, the sequential introduction of defined genetic elements into NOSE cell lines is described, as an *in vitro* model of ovarian cancer development. Genes were selected that are known to be altered in EOC specimens, namely *hTERT*, *C-MYC*, *KRAS* and *BRAF*.

hTERT

The human telomerase gene (*hTERT*) is expressed in the majority of malignant EOCs [Brustmann, 2005]. However, ectopic expression of *hTERT* alone did not induce anchorage-independent growth or the expression of ovarian cancer markers (CA125 and E-Cadherin) in three independent NOSE cell lines. The immortalised NOSE cell lines (IOSE) also maintained a normal diploid karyotype post-immortalisation. Thus, although expression of *hTERT* extended the *in vitro* lifespan to over 200 days, telomerase expression not induce any other features of a transformed phenotype. This is consistent with previous models describing immortalisation of NOSE cells with *hTERT* alone or in combination with a small interfering RNA targetting *p53* or *pRb* [Li et al., 2007]; [Yang et al., 2007a]; [Yang et al., 2007b]. Recently, it has been reported that dysregulation of *cyclin D1* or *cdk4* alone or in combination with ectopic expression of *hTERT* was insufficient to immortalise OSE cells and that dysregulation of all 3 elements is required [Sasaki et al., 2009]. This is in contrast to the results reported here and by this laboratory previously [Li et al., 2007]. It may be that different culturing media have an influence on the potential to immortalise cells. Also, patient age was not reported in the study by Sasaki and colleagues; but cells from elderly patients do have a reduced *in vitro* lifespan and may perhaps be more difficult

to immortalise. In IOSE cells high levels of endogenous *cyclin D1* were observed, suggesting that IOSE cells were efficiently transducing extracellular growth signals. However, this signal did not result in enhanced entry into mitosis as levels of *cdk4*, *cyclin A* and *cyclin E* were lower in the IOSE than in the transformed cell lines. This suggests that IOSE cells exhibit more dependency on external growth factors for stimulating entry into mitosis than the transformed cell lines. Cell lines expressing oncogenes appeared to have a cell cycle signalling cascade which was activated in the absence of high levels of *cyclin D1*, suggesting the oncogene-expressing cells enter mitosis independently of external growth factor signalling.

IOSE cells are a good alternative model of primary normal ovarian surface epithelial cells, which can only be maintained *in vitro* as short-term cultures. It remains to be determined whether extended passaging *in vitro* will introduce karyotypic abnormalities and cause cells to acquire transformed characteristics, though *hTERT*-immortalised cell lines can undergo extensive passaging without signs of malignant transformation [MacKenzie et al., 2000].

hTERT is not expressed in normal adult somatic cells but is often expressed in cancer cells, and so has considerable potential as a therapeutic target that is specific for tumour cells. Inhibition of telomerase induces cell death of ovarian cancer cells *in vitro* [Saretzki et al., 2001]. Transgenic cell lines engineered to express *hTERT*, such as IOSE cell lines, offer a model system for the testing of gene-specific therapeutics in a tightly controlled *in vitro* system. Additionally, the *hTERT* promotor has been employed in the development of oncolytic viruses and was demonstrated to sensitize ovarian cancer cells to cisplatin in an *in vitro* model [Takakura et al., 2009]. Bilsland and colleagues utilised the *hTERT* promotor to drive bacterial nitroreductase (NTR) in an adenoviral suicide gene therapy model and were able to selectively sensitise cancer cells to a prodrug (CB1954, converted to a highly toxic compound by the NTR gene) [Bilsland et al., 2003].

C-MYC

Copy-number increases at 8q24 (the *C-MYC* locus) are common events in ovarian cancers and are found in 35−76% of malignant EOCs analysed by fluorescent *in situ* hybridization and comparative genomic hybridization [Dimova et al., 2006] (and references therein). *C-MYC* amplification occurs less frequently in benign/low malignant potential subgroups than in malignant EOCs [Dimova et al., 2006]. *C-MYC* amplification has also been correlated to platinum resistance [Wasenius et al., 1997]. Additionally murine models and *in vitro* models of EOC have demonstrated an important role for *C-MYC* [Orsulic et al., 2002]; [Sasaki et al., 2009]. Thus, the effect of overexpressing *C-MYC* in

phenotypically normal IOSE cell lines was tested. Overexpression of *C-MYC* in three IOSE cell lines (IOSE^{CMYC}) induced features of a neoplastic phenotype. IOSE^{CMYC} cells showed rates of anchorage-independent growth that exceeded or were comparable to ovarian cancer cell lines, and anchorage-independent growth was positively correlated to relative *C-MYC* mRNA expression. IOSE^{CMYC} were more proliferative than IOSE cell lines but were not more invasive. Therefore, IOSE^{CMYC} cell lines are partially transformed OSE cells. These cell lines are a novel tool for testing environmental factors that are suspected to have a role in EOC initiation or early development. Such factors that could be investigated include organismal ageing (described in Chapter 5), steroid hormones or chemical carcinogens. Similarly, by comparing the phenotypic effects of introducing or knocking down specific genes in IOSE and IOSE^{CMYC}, it would also be possible to investigate the role of novel genes that are suspected to play a role in EOC susceptibility or early tumourigenesis.

In normal human cells, there are few reports of anchorage-independent growth induction by expression of *hTERT* and *C-MYC* alone [Drayton et al., 2004]. This present study is the first to report that co-expression of *hTERT* and *CMYC* induces anchorage-independent growth in normal ovarian surface epithelial cells. This phenotype was observed in multiple cell lines (n=3) and multiple *CMYC*-overexpressing clones (n=7). Previous report have described the induction of anchorage-independent growth in the presence of other oncogenic elements [Sasaki et al., 2009]. The data described here suggests that NOSE cells are inherently more susceptible to transformation *in vitro* and *in vivo*, and this may be a hint as to why human ovarian tumours progress very rapidly. Divergent techniques used for immortalisation and transformation make it difficult to directly compare phenotypic data across different *in vitro* studies. Furthermore, protocols for *in vitro* and *in vivo* tumourigenicity assays vary significantly between studies (Table 4.3). To better understand the susceptibility of NOSE cells to transformation relative to other cell types, it would be necessary to transform different cell types using the same genetic elements, and to assay the transformed phenotype using consistent protocols. It is also true that this model represents NOSE cell transformation in a highly mitogenic microenvironment (see Chapter 3). The mitogenic culture environment of NOSE-CM reflects the conditions of OSE cells trapped within an inclusion cyst, with direct contact to the mitogenic ovarian stroma. To understand this more fully it would be necessary to isolate OSE in different types of culture medium, transform the cells *in vitro* with *hTERT*, *C-MYC* and *KRAS/BRAF* and compare the *in vitro* tumourigenicity with the data reported here. Indeed, Weinberg and colleagues isolated different types of normal mammary epithelial cells by culturing breast biopsies in two different types of cell culture medium. The primary cultures were maintained in the different media and transformed *in vitro* with *hTERT*+SV40t+*HRAS*,

and the resulting tumours in mice were of distinct histologies. Following *in vitro* transformation, one cell type was much more tumourigenic than the other: this cell type formed tumours when 10^4 fold fewer cells were injected into mice, and formed metastastic deposits [Ince et al., 2007]. This demonstrates that simply altering culture medium components can have profound effects on the outcome of *in vitro* models of transformation.

	Cell Type	Genetic elements introduced…		CFE† (%) in agar (cell no)	Growth *in vivo* (cell no)	Ref
		For immortalisation	For transformation			
Oncogenic virus models	HEK cells & BJ Fibroblasts	*hTERT* + *SV40 LT*	$HRAS^{mut}$	0.80/0.160 & 0.40/0.15 (10^3/10^4)	8/8 & 4/4 (2x10^6)	Hahn *et al.*, 1999
	HMECs	*hTERT* + *SV40 LT*	$HRAS^{mut}$	1.1-6.0 (5x10^3/5x10^4)	14/27-15/15 (2x10^6)	Elenbaas *et al.*, 2001
	Embronic lung & BJ fibroblasts	*hTERT* + *SV40 T/t,*	$HRAS^{G12V}$ + *CMYC*	0.10-0.22 (10^3)	*NR*	Boehm *et al.*, 2005
	BJ fibroblasts	*hTERT* + DN-p53 + *pRb*-shRNA + *PTEN*-shRNA	$HRAS^{G12V}$ + *CMYC*	0.09-0.18 (10^3)	3/6 & 5/6 (2x10^6)	Boehm *et al.*, 2005
	NOSE	*hTERT* + *SV40 LT*	$HRAS^{G12V}$ or *c-erbB-2*	0.22 or 0.43 (10^4)	4/10 or 5/10 (10^8)	Kusakari *et al.*, 2003
	NOSE	*hTERT* + *SV40 T/t*	$KRAS^{G12V}$ or $HRAS^{G12V}$	0.16-0.38 (10^5)	5/14 or 8/10 (5x10^6)	Lui *et al.*, 2004
Defined genetic elements	Leiden fibroblasts	*hTERT*	$HRAS^{mut}$ or *CMYC*	0.03 or 0.04 (10^4)	No	Drayton *et al.*, 2003
	Leiden fibroblasts	*hTERT*	$HRAS^{mut}$ + *CMYC*	0.04 (10^4)	5/16 (10^7)	Drayton *et al.*, 2003
	Oral keratinocytes	*cyclinD1* + DN-*p53* (ALT)	*EGFR*	0.08/0.15 (10^4/10^5)	No (2x10^6)	Goessel *et al.*, 2005
	Oral keratinocytes	*cyclinD1* + DN-*p53* (ALT)	*EGFR* + *CMYC*	0.06/0.016 (10^4/10^5)	10/10 (2x10^6)	Goessel *et al.*, 2005
	NOSE	*hTERT*	*CMYC*	2.61-16.43 (10^2/2x10^4/4x10^4)	?	This study
	NOSE	*hTERT*	*CMYC* + $KRAS^{G12V}$ or $BRAF^{V600E}$	13.70-29.40 (10^2)	?	This study

Table 4.3: Previous transformation models. Direct comparisons are difficult due to variation in genes used, and protocols for *in vitro* and *in vivo* tumourigenicity assays.† CFE = colony formation efficiency, where number of colonies was reported instead of CFE, the CFE was calculated using the formula described in the Materials and Methods. In brackets the number of cells plated/injected are indicated. DN-p53 = dominant negative p53 allele.

KRAS/BRAF

Expression of activated *RAS* or *RAF* in most normal cells will induce a tumour suppression pathway which triggers cellular senescence [Denoyelle et al., 2006]. Denoyelle and collegues investigated the mechanisms involved in senescence induced by infection of oncogenic *HRAS* and *BRAF* alleles into human melanocytes. Mutated forms of both these genes are frequently found in naevi (moles) and melanocytes harbouring *RAS* or *RAF* mutations senesce prematurely, thus suppressing the tumourigenic effects of these mutations. This study observed differences in the features of senescence initiated by these two genes - firstly $BRAF^{V600E}$-induced senescence took significantly longer to occur than senescence

induced by $HRAS^{G12V}$. Secondly, $HRAS^{G12V}$-induced senescence caused extensive disruption of the endoplasmic reticulum even before classical senescence markers, such as positive staining for β-galactosidase, are detectable. This response appeared to be in part due to activation of the ER-associated unfolded protein response (UPR). Despite activating a downstream target, ERK, to the same extent as $HRAS^{G12V}$, $BRAF^{V600E}$ does not induce an ER-associated UPR and hence different processes are involved in $BRAF^{V600E}$-induced cell senescence [Denoyelle et al., 2006].

In this present study, mutant alleles of *KRAS* and *BRAF* were introduced into IOSE and IOSE^{CMYC} cell lines. The most commonly found mutation in EOCs for each gene was selected (G12V for *KRAS*, V600E for *BRAF*). It was anticipated that both genes would induce senescence of phenotypically normal cells, as described above. However, surprisingly, 2/3 IOSE cell lines were able tolerate expression of mutant *KRAS* in multiple clones tested (n=6). In contrast, mutant *BRAF* alleles induced higher rates of senescence than $KRAS^{mut}$ in all 3 IOSE cell lines. This may suggest that an oncogene-induced senescence (OIS) response in IOSE cells is mediated mainly through *BRAF* and the MAPK pathway. Indeed, $BRAF^{V600E}$ expression did activate MAPK signalling more than upstream $KRAS^{G12V}$ as at *ERK1/2* was more elevated in *CMYC/BRAF* cell lines than *CMYC/KRAS* cell lines. This was in contrast to the observations of Denoyelle and colleagues, which suggests that *KRAS* and *HRAS* may have differing roles in cellular senescence. Expression levels of $BRAF^{V600E}$ mRNA were consistently lower than expression levels of $KRAS^{G12V}$ observed in selected clones, which suggests that elevated levels of $BRAF^{mut}$ were less tolerable than elevated levels of $KRAS^{mut}$ in the two IOSE cell lines tested. Double mutants expressing mutant *BRAF* also had the highest rates of anchorage-independent growth and 3D proliferation. In combination, these data suggest that in this model, expression of $BRAF^{V600E}$ was associated with more potent oncogenic signalling than $KRAS^{G12V}$.

cDNA microarrays have been used to demonstrate that immediate transcriptional responses to *RAS* includes not only activation of *RAF* and the MAPK pathway, but also other downstream effectors including the PI3K pathway and Ral-GDS (see Figure 4.52). In comparison, activated *RAF* in human mammary epithelial and OSE cells evokes a transcriptional response mediated almost entirely through MAPK pathway, with a significant involvement by autocrine signalling. Inhibition of the epidermal growth factor (EGF) receptor reduces cells transcriptional response to *RAF* activation by around one-half [Schulze et al., 2004]. In this present study, elevated expression of *EGFR* was observed in the IOSE$^{CMYC.BRAF}$ clones, which may be indicative of activation of an *EGFR*-dependent positive feedback mechanism. Activation of EGF-associated proteins appears to play a vital role in *RAF*-associated transformation, since autocrine-loop activated EGFR

was necessary for cells to evade a normal apoptotic response upon detachment from the extracellular matrix [Schulze et al., 2001]. Incessant stimulation of EGFR may therefore be acting in synergy with the expression of mutant *KRAS/BRAF* alleles in the NOSE transformation model, to promote the development of the neoplastic phenotype observed.

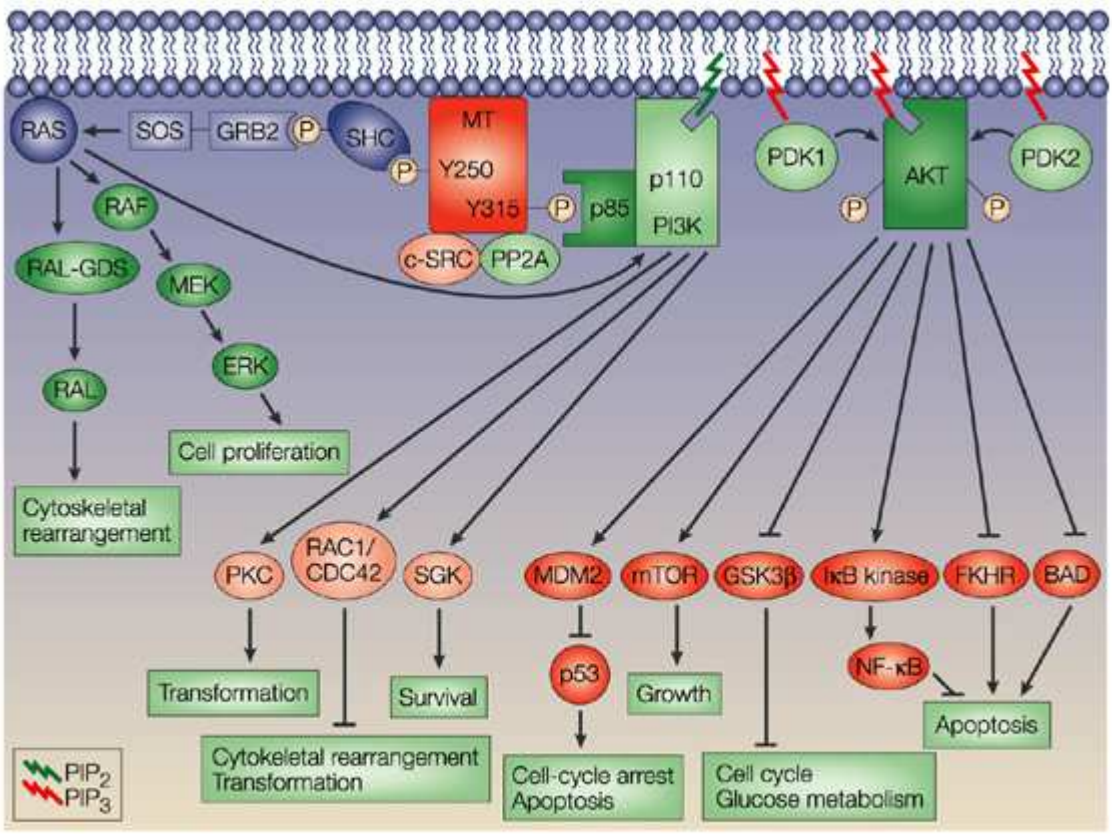

Figure 4.52: MAPK and PI3K pathways and downstream signalling, image from Dilworth [Dilworth, 2002]. The two pathways are closely interlinked, as *RAS* can activate PI3K, and thus also activated additional transformation pathways such as *PKC, RAC/cdc42* and *SGK*. The polyoma middle T antigen (MT, red); a potent viral inducer of neoplastic transformation in mammalian cells; can activate both the MAPK and PI3K pathways, via *son-of sevenless* (SOS) and the SH2 domain in the p85 subunit of PI3K.

KRAS/BRAF mutation status in EOCs could potentially be used to design tailored tumour therapies. In ovarian cancer cell lines harbouring mutations in *KRAS* or *BRAF* it has been demonstrated that inhibition of MEK results in increased rates of apoptosis and inhibition of growth [Pohl et al., 2005]. This response was absent in ovarian cancer cell lines with wild type *KRAS* and *BRAF*. This suggests that regardless of other pathways that are activated by a constitutively active allele of *KRAS*, the MAPK pathway is essential for the survival of the cells lines carrying mutations in either of these genes

[Pohl et al., 2005]. As it is known that the proliferative response to *RAS* is mediated through many other pathways such as the phosphatidylinositol 3-kinase (PI3K) pathway, these data are interesting from a clinical perspective, since targeted inhibition of a single pathway could inhibit tumour growth [Schulze et al., 2004]. Indeed, many components of the MAPK/PI3K pathways, particularly *mTOR*, are being investigated as therapeutic targets in clinical trials currently underway. The cell line models developed in this project could be used as a controlled system in which new drug therapies targetting the MAPK pathway could be developed and tested.

It is not uncommon for cancer cell lines harbouring *KRAS* mutations to be highly susceptible to inhibition of MAPK signalling or siRNA knockdown of the *KRAS* gene. This phenomenon is termed 'oncogene addiction' [Scholl et al., 2009]; [Singh et al., 2009]. As *KRAS* signalling is involved in many important metabolic pathways, inhibition of *KRAS* is likely to have high toxicity. RNAi screens testing for genes which are synthetic lethal in combination with a mutant *KRAS* alleles have identified enzymes involved in mitosis (including PLK1 and APC) and STK33 as candidate therapeutic targets for targetted induction of apoptosis. The synthetic lethal approach was used to identify PARP inhibition as targetted treatment for *BRCA1/2* patients with tumours that are deficient in DNA repair [Farmer et al., 2005]. PARP inhibitors proved to be highly effective therapies in clinical trials [Fong et al., 2009].

Mutant *RAS* and *RAF* activate distinct pathways in the cell and hence enable the cell to acquire different transformation-associated characteristics. Previous *in vitro* and *in vivo* models have employed effector-specific *RAS* allele to demonstrate that the many pathways activated by oncogenic *RAS* play distinct roles in tumour development [Gire et al., 2000]; [Janda et al., 2002]. $BRAF^{V600E}$ was a more potent inducer of senescence in IOSE cells, and MAPK signalling in $IOSE^{CMYC}$ cells. *BRAF* expression in $IOSE^{CMYC}$ cells was also associated with enhanced proliferation in 3D, relative to expression of mutant *KRAS*. Janda and colleagues have previously found that PI3K pathway activation was required to induce proliferation of mammary epithelial cells in 3D collagen gels [Janda et al., 2002]. However, in this study, reduced proliferation in 3D culture was associated with expression of $KRAS^{G12V}$. Phenotypic data described here suggests that in ovarian epithelial cells, *KRAS/BRAF* have distinct functional roles and induce different phenotypes *in vitro*. There is also, unsurprisingly, much cross-over in the phenotypic effects of these oncogenes as both genes enhanced features of transformation in $IOSE^{CMYC}$ cell lines in anchorage-independent growth and invasion assays. Furthermore, expression of mutant *KRAS* and *BRAF* both induced commitment to an epithelial phenotype in IOSE/$IOSE^{CMYC}$ cells, as measured by observation of cell morphology and cytokeratin-7 expression. Gene expression assays confirmed that there were distinct sets of genes and also many genes in

common in the transcriptional responses to prolonged (20 passages in culture) expression of $KRAS^{G12V}$ or $BRAF^{V600E}$.

4.7.1 Modelling Ovarian Cancer *In Vitro*

In 1999, Hahn and colleagues first created tumour cells *in vitro* by the introduction of viral and human oncogenes [Hahn et al., 1999]. Since that first study, the transformation of many other cell types has been reported, of which many are described in Table 4.3. For ovarian cancer, three studies to date have reported different approaches to modelling EOC development *in vitro* [Kusakari et al., 2003]; [Liu et al., 2004]; [Sasaki et al., 2009]. All three models use normal ovarian surface epithelial cells. Kusakari and colleagues immortalised OSE cells by expressing SV40T and *hTERT*. Subsequent overexpression of *ERBB2* or $HRAS^{mut}$ created cell lines that were more resistant to apoptosis induced serum-starvation than parental cell lines, and formed undifferentiated tumours in mice [Kusakari et al., 2003]. Liu and colleagues took OSE cells that had been immortalised by *hTERT* plus SV40t, and introduced mutant *HRAS* and *KRAS* alleles. Transformed cells formed tumours in mice that were positive for CA125. Transformed cells also displayed upregulated expression of a number of cytokines, and were sensitive to apoptosis induction by blocking antibodies against IL-1β and IL8 [Liu et al., 2004].

In these two models, cells displayed tumourigenic features *in vitro* and expressed epithelial and/or ovarian cancer markers *in vivo*. However, these models are limited by the fact that SV40 is not found to be involved in human EOCs, and the molecular effects of SV40 are not yet fully understood. In 2009, Sasaki and colleagues took a more biologically relevant approach to modelling EOCs *in vitro* and transformed OSE cell lines with oncogenic versions of genes that have been shown to be involved in EOCs. They included *p53* *AKT*, *PIK3CA*, *PTEN*, *C-MYC* and *KRAS*. In their model, OSE cells were immortalised with *cyclinD1*, *cdk4* and *hTERT*. This group found that the overexpression of *AKT*, or knockdown of *PIK3CA/PTEN*, conferred *in vivo* tumorigenic potential on IOSE cells that already express a dominant negative allele of *p53* in combination with $KRAS^{G12V}$ [Sasaki et al., 2009]. However, the tumours formed in mice were mainly sarcomatous or poorly differentiated. Although tumours were cytokeratin-18 positive, CA125 was not detected in culture supernatant, or in xenograft tumours.

This present study aimed to add to this body of work by looking specifically at the *MAPK* pathway. As with previous studies, this work has been performed using NOSE cells. However, it is now becoming widely accepted that EOCs are heterogeneous in origin and so in future, this will need to be incorporated into studies that model ovarian cancer develop-

ment *in vitro* (Table 4.4). For example, up to 40% of endometrioid and clear cell tumours are associated with endometrioitic plaques [de la Cuesta et al., 1996], and so a cell biology model of these subtypes would ideally focus on transforming endometrial epithelial cells in parallel to transformation of the OSE, using genes known to be altered in these subtypes, namely *PTEN* and mismatch repair genes [Martini et al., 2002]; [Dinulescu et al., 2005]. An as yet unquantified proportion of high-grade serous EOCs appear to arise as primary fallopian tube neoplasms [Jarboe et al., 2008] and so it would be valuable to transform fallopian tube epithelia and the OSE by altering *BRCA1/2* and *p53* to create an *in vitro* model of this subtype. By comparing all of these models, it may be possible to glean some much needed insight into the real origins of all EOC subtypes and to learn more about what genetic alterations may be involved in the earliest stages of tumour development for all EOC histotypes.

Histological Subtype	Cell(s) of Origin	Genetic alterations
High-grade serous	OSE, FTE	*BRCA1/2*, *TP53, HER2, HOXA9*
Low-grade/borderline serous	OSE	*KRAS*, *BRAF*
Mucinous	OSE	*KRAS, HOXA11*
Clear Cell	OSE, EEC	*PIK3CA, p16, MMR genes*
Endometrioid	OSE, EEC	*PTEN, β-catenin, HOXA10, p16, MMR genes*

Table 4.4: *In vitro* cell biology modelling of EOC subtypes may require distinct *in vitro* models. OSE = ovarian surface epithelium; FTE - fallopian tube epithelium; EEC = endometrial epithelial cells.

3D *in vitro* models are arguably a more biologically more relevant tool for studying transformation than traditional 2D monolayer cultures. Spheroids are thought to be reminiscent of earliest stages of tumour development, when small avascular nodules of transformed cells develop in the normal tissue [Sutherland and Durand, 1976]; [Ghosh et al., 2005]. In this study, transformed ovarian epithelial cell lines were grown as 3D spheroids and the proliferation rates were compared to the same cells grown in 2D. IOSE cell lines underwent growth arrest in 3D culture and proliferated slowly in spheroid cultures. This suggests that the IOSE cells in 3D are in a more functionally relevant state, as OSE cells *in vivo* are generally non-proliferative. However, the transformed cell lines had increased rates of 3D proliferation. This effects was not detected in 2D Alamar Blue proliferation assays. This may be due to the fact that parental IOSE cells proliferate rapidly in 2D and so it is not possible for derivative cell lines to exceed the proliferation rate of parental cell lines. Alternatively, the proliferative effect induced by *KRAS/BRAF* expression may

only be apparent in 3D spheroid cultures, as previously found for breast epithelial cells [Janda et al., 2002]. Significant differences in IOSE and IOSE^{CMYC} proliferation were detectable in 2D using BrdU incorporation, but were not detected by the Alamar Blue approach, suggesting Alamar Blue is a less sensitive method of detecting differences in cell proliferation between cell lines. However, the Alamar Blue technique has two major advantages over other, (endpoint) proliferation assays (such as MTT): (1) proliferative rates can be analysed over extended periods of time (2) proliferative rates of cells in 2D and 3D can be analysed.

4.7.2 Identification of Novel Genes Dysregulated During Neoplastic Progression of the OSE

Transcriptome profiling can be used to compare total gene expression profiles of two or more test groups (e.g. cancer versus normal; subtype X versus subtype Y; early stage versus late stage). A list of 'top' ranked differentially expressed genes (by fold change or significance) can then be identified. These genes are novel markers to distinguish the test groups. Often a gene expression signature is created in which the expression of a group of genes is used as a predictive or discriminatory tool. In ovarian cancer, gene expression microarray profiling has been used to identify genes associated with *BRCA1/2* status, molecular signatures of clinical outcome, chemotherapeutic response, tumour differentiation and histological subtype [Jazaeri et al., 2002]; [Jazaeri et al., 2003]; [Lu et al., 2004]; [Berchuck et al., 2005]; [Jazaeri et al., 2005]; [Tothill et al., 2008]; [Berchuck et al., 2009]. The genes that have been implicated in EOC, discovered through gene expression microarray studies are listed in Table 4.5. Each gene expression study has described genes that are significantly differentially expressed in each data set. Unfortunately, there is little cross-over between the reported genes between studies, and functional data to follow-up candidate genes is rarely reported. Genes reported as important in EOC include regulators of mitosis, genes in the MAPK pathway (particularly in the low grade tumours), regulators of proliferation, ECM components, β-catenin signalling molecules and genes involved in immune signalling. Reassuringly, we have observed some of these genes to be similarly dysregulated in our model, including *DUSP1*, *DUSP6*, *CCNE1*, and *UBE2C*.

Due to the rarity of early EOC specimens, there are few reports describing profiling of gene expression changes that occur during the early stages of tumourigenesis of the OSE [Marchini et al., 2008]. Therefore, in this study, the transcriptomic changes associated with early neoplastic progression in an *in vitro* model of ovarian cancer development were profiled. This is the first time that the transcriptomic consequences of *hTERT* plus *CMYC* +/- *KRAS*^{mut} or *BRAF*^{mut} have been profiled in NOSE cells. The gene expression

Samples compared	Observation	Gene(s) / Chromosomal Region(s)	Function	Ref.
BRCA1+, BRCA2+ founder mutation carriers; non-mutation carriers; IOSE culture	*BRCA1/2* associated tumours have distinct profiles	Xp11.23 (incl *WAS, PCTK1, UBE1*) *UBL-1, HE4* *WNT2/SFRP4* *RUNX1/AML1* *IFTIM1/2, HLA-DRB1/5, CD74, HLA-DRA, HLA-DPA, BRF2, SGK, FOS*	Many, including proteins involved in ubiquitination, chromosomal maintenance, and the endoplasmic reticulum Possible roles in homologous recombination and protease inhibition Wnt/β-catenin signalling Transcription factors, promote proliferation Interferon-inducible genes	Jazaeri *et al.* 2002
Grade I and Grade III serous papillary carcinomas	99 genes differentially expressed in Grade I and Grade III tumours	20q13 (incl. *STK15, MYBL2, UBE2C, RAE1, CCNE1, CCHB1, NEK2, BUB1, TOP2A*)	Centrosome-related genes, genes involved in progression through the cell cycle and mitotic checkpoints, Aurora-like/related proteins	Jazaeri *et al.* 2003
EOCs - various stage/grade/ subtype, OSE brushings	4 genes distinguished all EOCs from OSE	*NOTCH3, E2F, RAC-GAP1, HN1, CLDN3*	Included genes involved in the Notch, Rb and MAPK pathways and cell adhesions	Lu *et al.*, 2004
Primary chemosensitive, post-chemotherapy and chemoresistant tumours	760 genes differentially expressed in primary chemosensitive v post-chemotherapy. 230 genes in primary chemoresistant v post-chemotherapy. 85 genes in primary chemosensitive and chemoresistant tumours	*ADH1B, ADH1C, ALDH2, CDKN1C, ADAMTS1* *DOC1, CAV1, DUSP1, ITM2A, KLF4* *TOP1, TOP2A, ZWINT* *DCN, Col6A3, SPARC*	Oxidising enzymes and negative regulators of proliferation (higher in post-chemo) Genes involved in cell cycle progression, RTK and MAPK signalling, matrix assembly Topoisomerases, spindle formation ECM components/ ECM remodelling proteins	Jazaeri *et al.* 2005
EOC histotypes, NOSE brushings, FTE cells, colonic mucosa, normal endometrium	Profiles of serous EOCs resemble that of FTE cells, mucinous EOCs resemble colonic epithelia, endometrioid and clear cell resemble the endometrium	Mucinous:*TFF1, AGR2, LGALS4, CEACAM6, CTSE* Clear cell: *GPX3, GLRX, FXYD2, RBP4* Endometrioid: 16q31, 14q32 Serous: *AMY2B, CHI3L1*	Immune response, mucosal proteins, cell adhesion Oxidation/reduction, regulation of ATPases, retinol binding β-catenin signalling Amylase proteins	Marquez *et al.* 2005
Serous and endometrioid tumours of the ovary, peritoneum and fallopian tube	Six molecular subtypes identified, including a novel high-grade serous (HGS) subtype that has mesenchymal features	Low-grade serous:*DUSP4, DUSP6, SERPIN5A, MAP3K5, SPRY2* Low-grade endometrioid: *BMP4, CCND1, CD44, FGF9, EPHB3, MMP7, CST1* Novel HGS subtype: *HOXA7, -A9, -A10, -D10, HGMA2, CDH2/3, COL4A5, CLDN6*	MAPK-associated genes β-catenin signalling pathway associated genes Homeobox genes, N/P-Cadherins, β-catenin signalling pathway associated genes, ECM genes, proliferation genes	Tothill *et al. 2008*
Stage I and borderline serous tumours	Profiles relate to histology or differentiation	*CCNE1, MCM5*	Regulation of mitosis and DNA replication	Marchini *et al.*, 2008
Stage I, II, III, IV and low-malignant potential tumours	7 genes were independent predictors of poor survival	*MAL, APMCF1, PRPS2, L3MBTL, HNMT, RANBPM, DGCR2*	Incl. genes involved in T-cell signalling, ATP metabolism, proliferation, RNA processing, cell adhesion	Berchuck *et al.*, 2009

Table 4.5: Previous gene expression studies of EOC tumour specimens have identified many candidate markers of disease, as well as markers or profiles associated with differences in histology, tumour grade, differentiation and chemotherapeutic response.

array data were used to identify novel genes associated with early transformation of the OSE. The best candidates emerging from this model are: *THBS1*, *FEZ1*, *PITX1*, *RGS4*, *MOCOS*, *CTGF* and *HIST1H4C*. These genes were among the top 30 most significant changes observed in both IOSE11 and IOSE19 transformed with defined genetic elements. Furthermore, all of these genes showed some changes in expression associated with the expression of *CMYC* alone, suggesting these changes are characteristic of the earliest stages of transformation of the OSE.

Novel Tumour Suppressor Genes with a Role in Early EOC Development

Thromobospondin-1 (*THBS1*) expression was reduced up to 68.8-fold in the IOSE cell lines that expressed oncogenic elements. This suggests that *THBS1* is a candidate tumour suppressor gene for EOC . This gene has been identified as an inhibitor of angiogenesis in many types of cancers, including pancreatic and renal cell carcinomas [Laklai et al., 2009]; [Zubac et al., 2009]. *THBS1* is widely expressed in adult tissues, with the highest expression seen in bone and the mammary gland (Figure 4.53). *THBS1* is expressed in normal adult ovaries, and in tumour specimens, loss of *THBS1* is associated with enhanced tumour vasculature and poorer patient survival [Alvarez et al., 2001]; [Secord et al., 2007]; [Papadaki et al., 2009]; [Zubac et al., 2009]. *In vivo THBS1* null mice grow larger tumours than control mice injected with the same ovarian cancer cells [Greenaway et al., 2009].

Loss of *THBS1* expression may be associated with tumours harbouring aberrant MAPK signalling. One study employed chemical inhibition of the MAPK pathway, which selectively inhibited growth and increased apoptosis of EOC cell lines carrying mutant *KRAS* or *BRAF* alleles. *THBS1* was one of the genes that was significantly upregulated in treated cells [Pohl et al., 2005]. Furthermore, knockdown of *HER-2/neu* in breast and ovarian cancer cell lines resulted in restored expression of *THBS1*. In 2003, a study from Weinberg and colleagues observed that levels of *THBS1* and *VEGF* were correlated in an *in vivo* tumourigenicity assay with mammary epithelial cells and kidney cells that expressed the SV40 early region, *hTERT*, *CMYC* and $HRAS^{G12V}$. Knocking down *THBS1* in the less tumourigenic cell lines increased tumour formation in mice. Furthermore, overexpression of *CMYC* was essential for the repression of *THBS1* expression [Watnick et al., 2003].

THBS1 is an interesting gene for further study in *in vitro* models of ovarian cancer. Loss of *THBS1* in this model is an early event, but clinical studies have shown that loss of protein expression in tumours is correlated to late-stage disease behaviour and patient outcome. In invasive EOCs, *THBS-1* expression, detected by immunohistochemistry, was associated with increased survival compared to tumours not expressing this protein

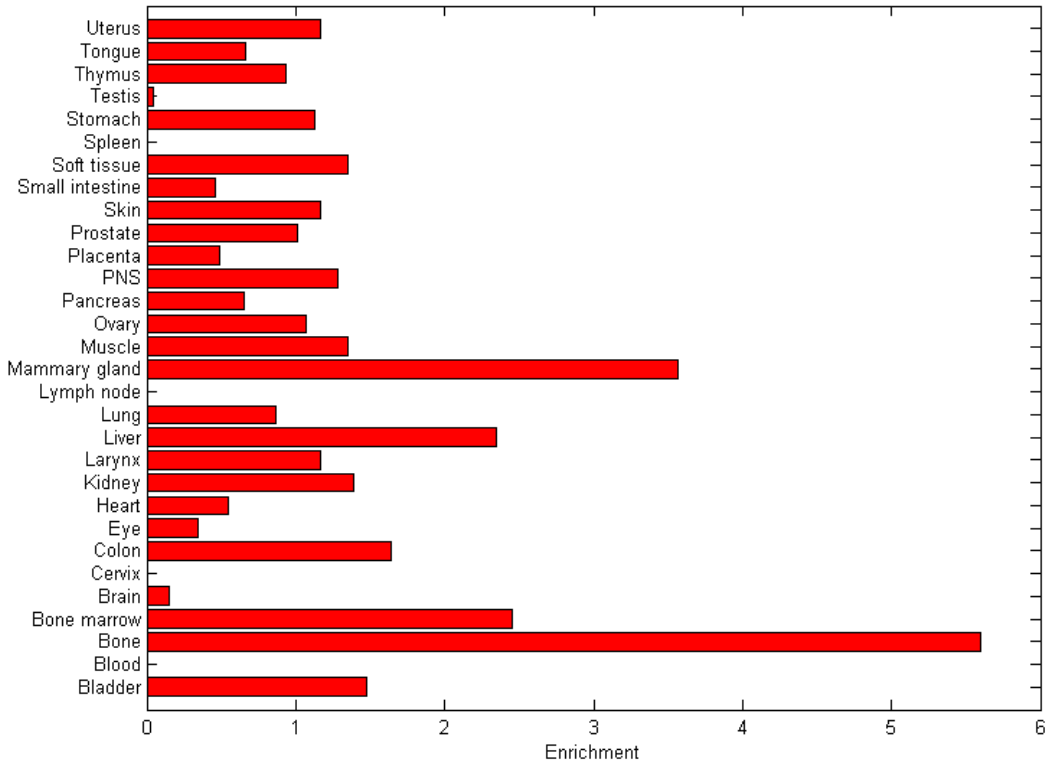

Figure 4.53: Thrombospondin-1 is expressed in a large number of normal adult tissues. *THBS1* is highly expressed in bone marrow, the mammary gland, liver and colon. The graph shows the ratio of observed number of expressed sequence tags (ESTs) to the expected number of ESTs for that tissue. Data were downloaded from the Tissue-specific Gene Expression and Regulation website http://bioinfo.wilmer.jhu.edu/tiger/

[Alvarez et al., 2001]; [Secord et al., 2007]. This information could be used clinically to identify the patients who may require the most aggressive therapy, or perhaps targetted therapy to inhibit angiogenesis. Indeed, therapeutic potential of *THBS1* has already been explored in an orthotopic model of ovarian cancer. A synthetic peptide ABT-510, mimics *THBS1* and treatment with this drug reduced tumour size and metastasis in *THBS1* null mice. The tumours in ABT-510-treated mice had less developed vasculature and reduced hypoxia [Greenaway et al., 2009].

Another candidate gene identified is *FEZ1*, on chromosome 8p22. This gene has not been widely studied in ovarian tumours, but one recent study found that expression of *FEZ1* is very low/absent in 38% of EOCs [Califano et al., 2009]. Generally, loss of 8p22 is commonly detected in cancers, and *FEZ1* may be lost in up to 60% of human epithelial tumours [Ishii et al., 1999]. Loss of *FEZ1* was associated with lymph node metastasis in breast cancer and may occur by promotor methylation or somatic mutation, resulting in loss of mRNA expression or truncation of the transcript respectively [Chen et al., 2009]; [Ishii et al., 1999]. *FEZ1*, or fasciculation and elongation protein zeta 1, is involved in regulation of cell growth; *FEZ1* hemizygous or null mice are more susceptible to spontaneous and chemical induced carcinogenesis [Vecchione et al., 2007]; [Baffa et al., 2008]; *FEZ1* null cells demonstrate altered progression through the cell cycle and appear to exit mitosis more rapidly thatn *FEZ1*+/+ cells; and loss of *FEZ1* results in lower Cdk1 levels, which subsequently results in missegregation of chromosomes during mitosis [Vecchione et al., 2007]. Therapeutically, *FEZ1* is also an interesting candidate. In cancer cells lacking this gene, re-expression of *FEZ1* reduces *in vivo* tumourigenicity and inhibits cell growth *in vitro* [Ishii et al., 2001]; [Vecchione et al., 2002].

A third candidate tumour suppressor was also identified in this study, namely *RGS4* (regulator of G-protein signaling 4). Loss of expression of *RGS4* has been shown to promote breast cancer migration and invasion [Xie et al., 2009]. In an orthotopic model of pancreatic cancer, *RGS4* expression was reduced at the invasive front and metastases, relative to primary tumours [Niedergethmann et al., 2007]. Breast cancer cell lines engineered to stably express *RGS4* demonstrate impaired tumour growth *in vivo*, due to the attenuated invasive capacity of the cells [Xie et al., 2009].

Finally, *CTGF* (connective tissue growth factor) was also identified as a candidate tumour suppressor gene in EOC. *CTGF* is expressed in a variety of adult tissues, including bone, bone marrow and small intestine, and also the adult ovary (Figure 4.54). In embryonic mice, *CTGF* is expressed predominantly in endothelial cells and blood vessels of the lung and cardiovascular system, and also in the brain [Friedrichsen et al., 2003]. Furthermore, in adult mice, strong expression of *CTGF* was observed in the mesenchyme surround-

ing ovarian follicles, suggesting that *CTGF* may have a role in follicular development [Friedrichsen et al., 2005].

This gene was expressed highly in IOSE cell lines, but expression was reduced by 86% in IOSE^{CMYC} cells, 77 and 78% in the IOSE$^{CMYC.KRAS/BRAF}$ cell lines (relative to IOSE). One previous study has found that reduced *CTGF* was associated with enhanced invasiveness of ovarian cancer cell lines *in vitro* [Barbolina et al., 2009]. Interestingly, these researchers also observed that *CTGF* expression was reduced in 3D cultures relative to the same cells grown in 2D. 100% of primary OSE samples expressed *CTGF*, whereas around 50% of ovarian cancer showed reduced expression of this gene [Barbolina et al., 2009]. *CTGF* is a mediator of tumour-stroma interactions, but the mechanisms by which *CTGF* modulates epithelial tumourigenicity is likely to be complex and appears to involve TGF-β signalling, which is pro- or anti-tumourigenic, depending on the context. In other types of epithelial carcinomas, increased *CTFG* has been shown to be associated with aggressive tumour behaviour, and is upregulated in invasive tumour models compared to non-invasive counterparts [Liu et al., 2008]; [Mazzocca et al., 2009]. In hepatocellular carcinoma, for example, *CTGF* expression is associated with increased invasiveness, and inhibition of the TGF-β receptor inhibits *CTGF* expression, tumour stroma development and metastasis [Mazzocca et al., 2010]. However, it is of note that the *in vitro* modelling described in this chapter did not incorporate a stromal component, and a heterotypic model plus stimulation with TGF-β would be a more appropriate model for studying this pathway.

Novel Oncogenes Associated with Early Ovarian Cancer Development

PITX1 (paired-like homeodomain transcription factor 1) mRNA expression was low in the IOSE but elevated in IOSE^{CMYC} and clones co-expressing mutant *KRAS/BRAF*. Previously, both overexpression and downregulation of this gene in tumours has been reported [Chen et al., 2008]. In a murine model of ovarian granulosa cell tumours, *PITX1* was overexpressed in transformed cells relative to normal ovarian samples [Boerboom et al., 2006]. Overexpression of this gene was found in 5/9 invasive pituitary tumours [Wierinckx et al., 2007]. Furthermore, *PITX1* has been identified as a potential suppressor of mutant *RAS* activity in prostate, bladder and colon cancer cells [Kolfschoten et al., 2005]. It may be that expression of this gene is an endogenous tumour suppressive mechanism to attempt to counteract the effects of ectopically enhanced MAPK signalling in partially transformed cell lines. Studies in larger numbers of ovarian tumours will be necessary to determine whether this gene is relevant in EOC.

MOCOS (molybdenum cofactor sulfurase) is a second candidate oncogene identified in

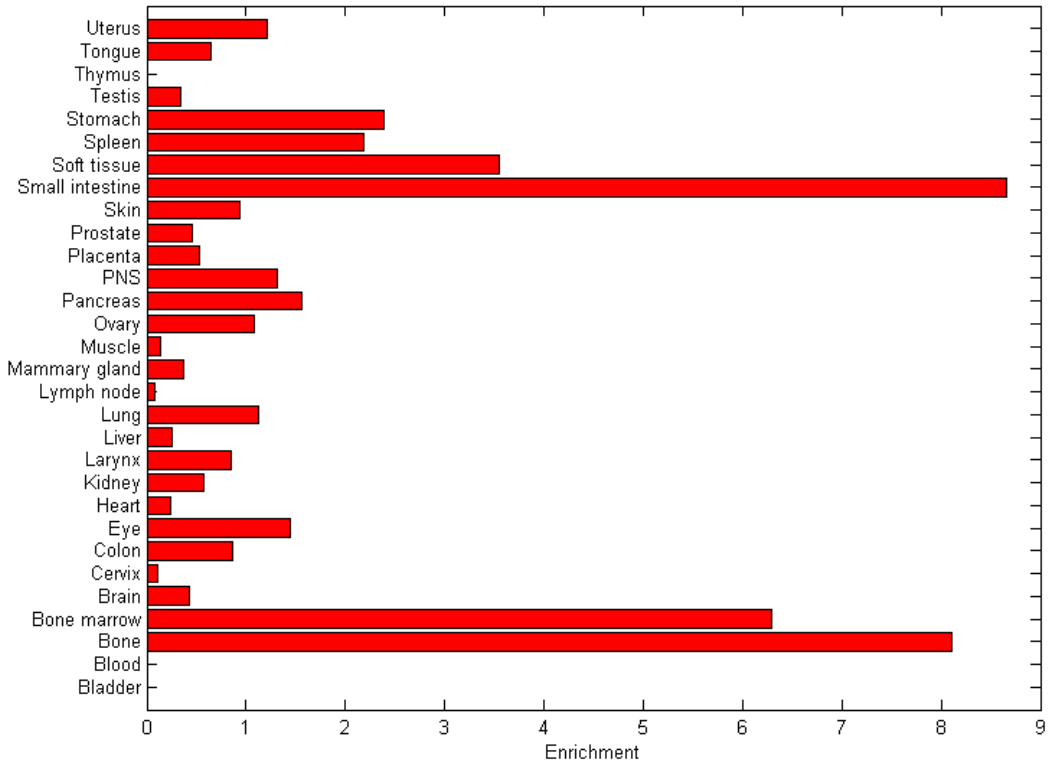

Figure 4.54: Connective tissue growth factor is expressed in a large number of normal adult tissues. *CTGF* is highly expressed in bone, bone marrow, small intestine, soft tissue, stomach and spleen. *CTGF* is expressed in the normal ovary. The graph shows the ratio of observed number of expressed sequence tags (ESTs) to the expected number of ESTs for that tissue. Data were downloaded from the Tissue-specific Gene Expression and Regulation website http://bioinfo.wilmer.jhu.edu/tiger/

this study. This gene was overexpressed in 5/6 cell lines expressing oncogene(s), relative to IOSE. This gene has not been widely described. The same is true for *HIST1H4C* (histone cluster 1, H4C) which has been identified as a susceptibility gene in therapy-related myeloid leukemia [Bogni et al., 2006]. Histone modifications can contribute to carcinogenesis by modulating transcription of local genes by affecting the strength of DNA-histone binding, and thus affecting access of DNA transcription machinery to the gene regions. Not interactions between *MOCOS* and *CMYC/RAS/RAF* have been reported to date.

It is of note that many of the most significant genes identified in this model are extracellular matrix genes (Thromobospondin-1, Collagen I and III subunits) and genes involved in recruitment of stromal cells (Thromobospondin-1) or genes involved in invasion of the local microenvironment (*RGS4*). It appears that many genes identified in this study are associated with the exploitation of the local microenvironment, which is perhaps not surprising as the 3D spheroid cultures are thought to represent tumour cell nodules preceeding the development of vasculature. Stromal components can be potent tumour therapies. The most effective drug therapies that aim to kill the cancer cells directly will always induce the strongest natural selection, and so inherently promote the development of a resistant population. However, natural selection acting on public goods, that is shared, stromal factors (e.g. angiogenesis promotors), will be lower, as only a small proportion of the tumour cell population need to make 'public goods' for the entire tumour to benefit. Thus, targetted inhibition of public goods is less likely to result in tumour resistance and therefore more likely to be an effective tumour therapy.

Gene expression microarrays offer a rapid way to characterise transcriptomic changes in cell biology models. Working with *in vitro* models removes the effect of sampling a small portion of a tumour, the gene expression profile of which may not represent changes found throughout the entire tumour. *In vitro* models can also be closely controlled to examine the effects of specific genetic alterations without the complexities of an *in vivo* system such as stromal contamination and inter-tumour heterogeneity. However, interesting changes in gene expression identified in *in vitro* model must be rigorously validated to ensure firstly that the effect is real in the model system and secondly, to test that the gene is differentially expressed in normal and malignant ovarian cells *in vivo*. Once differential expression in clinical specimens has been established, the next challenge is to establish that the gene is functionally relevant and elucidate the mechanisms by which the candidate gene acts. It would be of interest to see whether the candidate EOC TSGs and oncogenes described above are also dysregulated in 2D cultures of the same cells, to validate the hypothesis that culturing in 3D induces the expression of genes associated with recruitment of a tumour stroma.

4.7.3 Other Genes of Interest Deregulated in this Model

Although the focus of this study was to identify novel genes involved with transformation of the OSE, these data could be used in other studies e.g. by comparing the profiles with EOC cell lines/tumour profiles to identify additional oncogenes/tumour suppressor genes important in EOCs. One could also compare the profiles with fallopian tube lines (normal and transformed) to try and elucidate the true cellular origins of EOCs. Furthermore, one could use these data to further explore the molecular mechanisms by which *KRAS/BRAF* contribute to neoplastic transformation in this model. The pro-tumourigenic effects of *KRAS/BRAF* were enhanced in a *CMYC*-overexpression background, compared to when *KRAS/BRAF* mutant alleles were expressed in IOSE cell lines. In 2008, McMurray and colleagues described the importance of identifying those genes that are only deregulated when multiple oncogenes are expressed together, but the expression of this group of genes did not change when the oncogenic elements were expressed singly [McMurray et al., 2008]. In this present study, it was possible to identify those genes that were regulated by mutant *KRAS* or *BRAF* expression in a *CMYC* background. For *KRAS* these genes include: *CST3, BSG, CAMK1, CES2, CABC1* and *BBS2*. For *BRAF* these genes include: *HOXC8, SAMSN1, STX10, XAB2, SUZ12* and *CCS*. Whether these genes are expressed in IOSE lines expressing only mutant *KRAS/BRAF* is not yet known, but would be important to know to elucidate a role for these genes in the increased invasion and anchorage-independent growth observed in the double-mutant lines.

4.7.4 Expression of Genes Implicated in Genetic Susceptibility to Ovarian Cancer

This is a model of initiation and early-stage development of EOCs. Therefore, it follows that some of the genes dysregulated in this model are also candidate EOC susceptibility genes. Five regions have recently been identified as containing genetic susceptibility loci [Song et al., 2009] and [S.Gayther, personal communication]. One such susceptibility region for EOC is 8q24. The 8q24 region is a hotspot for single nucleotide polymorphisms (SNPs) that are associated with susceptibility to cancer. SNPs found within this region have been linked to breast, prostate, colorectal and ovarian cancer susceptibility (Figure 4.55) [Tomlinson et al., 2007]; [Eeles et al., 2008]; [Ghoussaini et al., 2008]; [Thomas et al., 2008]; [S.Gayther, personal communication]. The *CMYC* proto-oncogene is located in this region, and represents an enticing candidate gene as it is involved in many types of cancer and is commonly overexpressed or amplified. *CMYC* is known to be involved in EOC, as described above, and once the causal variant at this locus is identified,

and correlations between *CMYC* expression, genotype and phenotype could be readily assayed.

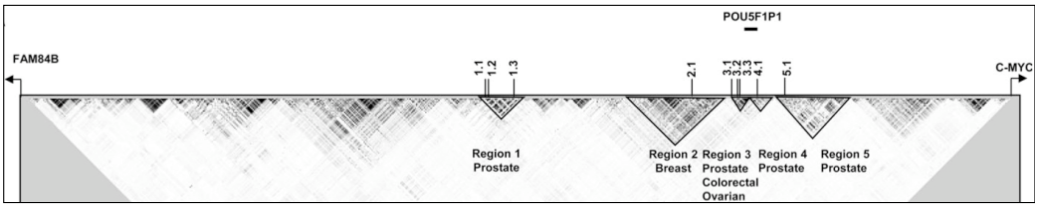

Figure 4.55: Chromosome 8q24 is a hotspot for cancer susceptibility loci.

DDEF1 at 8q24 was differentially expressed in the model of NOSE cell transformation. Both probes for this gene showed reduced expression in the cell lines expressing *CMYC* plus mutant alleles of *KRAS* or *BRAF*. *DDEF1* was also downregulated in IOSE^{CMYC} compared to IOSE cell lines. This suggests that both cell lines were behaving as tumour suppressor genes in this model. *DDEF1*, or development and differentiation enhancing factor 1 (also known as *ASAP1*), may have a role in cell growth and remodelling of the cytoskeleton by binding *SRC* and phosphatidylinositol biphospates (a key molecule in the PI3K pathway) [Ha et al., 2008]. This gene has been reported to be overexpressed in a panel of 25 high grade uveal melanomas, in which amplification of the 8q24 region is common [Ehlers et al., 2005]. These data contrast with the observations in this present study, although the effects of different genes are likely to vary between tissues, and expression of *DDEF1* in normal and malignant ovarian specimens has not yet be reported.

At the 9p22 locus, the gene nearest to a susceptibility association is *BNC2*. In a genome wide susceptibility study (GWAS), 12 SNPs showed genome-wide significance at this locus, some of which were located within the coding region of the *BNC2* (basonuclin 2) gene, as shown in Figure 4.56 [Song et al., 2009]. In the current study, *BNC2* expression was reduced by 62% in the cell lines overexpressing *CMYC*, and by 74% and 79% in the cell lines expressing mutant *KRAS* or *BRAF*. This suggests that loss of *BNC2* may be associated with cancer progression, and that *BNC2* may act as a tumour suppressor gene. *BNC2* has been previously identified as a putative tumour suppressor gene in glioblastoma and esophageal carcinoma [Nord et al., 2009]; [Akagi et al., 2009]. Work in this laboratory has also found that expression of *BNC2* is reduced in a panel of 23 ovarian cancer cell lines when compared to 42 normal ovarian surface epithelial cell lines [M. Notaridou, unpublished data]. *BNC2* is a nuclear protein, widely expressed in many different cell types and has multiple mRNA and protein isoforms. Functionally, this gene appears to have a role in mRNA processing within the nucleus, although the mechanistic role of this gene in carcinogenesis remains poorly understood [Vanhoutteghem and Djian, 2006];

[Vanhoutteghem and Djian, 2007].

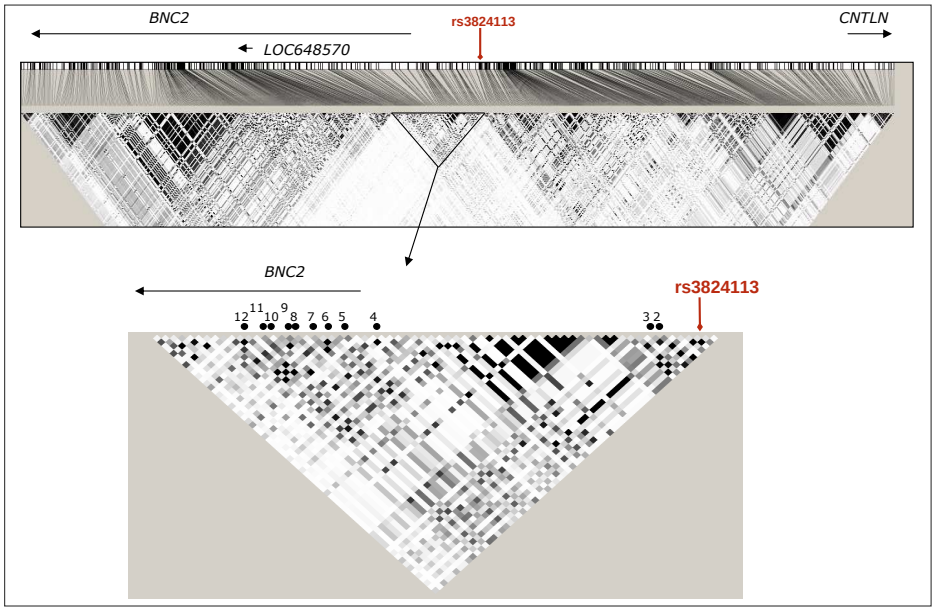

Figure 4.56: Many EOC susceptibility loci fall within or near to the *BNC2* gene. The SNP with the most significant association with ovarian cancer risk is shown in red. High linkage disequilibrium is indicated by dark shading in the haplotype map. From [Song et al., 2009]

Also at the 9p22 locus is the *CNTLN* gene. In this model, *CNTLN* was upregulated in IOSE^{CMYC}, IOSE$^{CMYC.KRAS/BRAF}$. *CNTLN* or centlein is a component of centrosomes; but so far work on this gene has not been published. More investigation is required to establish whether or not this gene is differentially expressed in normal ovarian epithelial cells compared to epithelial ovarian cancer cells. At the 9p22 locus, *BNC2* is currently the most interesting candidate gene for functional analysis.

At the chromosome 19p13 locus, the gene nearest to a susceptibility association is *MERIT40*. This gene did not appear to show differential expression in this transformation model, although it represents an interesting candidate gene for ovarian cancer as it interacts with *BRCA1* [Feng et al., 2009]; [Shao et al., 2009]; [Solyom et al., 2009]. Early investigations have suggested that this gene may be upregulated in ovarian cancer cell lines relative to primary normal ovarian surface epithelial cell lines [M. Notaridou, unpublished data]. At this locus, two other genes were dysregulated in the transformation model - *NR2F6* was upregulated in the cell lines expressing mutant *KRAS/BRAF* alleles in combination with *CMYC*, as was *MRPL34*. *NR2F6* is also an interesting candidate for EOC. This gene may have a role in the immune system [Hermann-Kleiter et al., 2008], but also appears to interact with steroid hormones (luteinizing hormone and oestrogen) in rat models

[Raccurt et al., 2005]; [Zhang and Dufau, 2000]. Interestingly, expression of this gene is elevated in pregnant rats, and the gene product binds a hormone-responsive element in the oxytocin promotor, antagonsising the action of oestrogen [Chu et al., 1998]. The role of steroid hormones in EOC development is strongly supported by epidemiological data, but the mechanisms by which hormones eventually cause EOC are poorly understood, particularly in the case of *BRCA1/2* tumours which are largely specific to hormone-responsive cells. *MRPL34* is a mitochondrial ribosomal protein, and there is little published information regarding this gene's specific function or role in cancer.

At the chromosome 3p25 locus, two genes nearby to the susceptibility SNP are down-regulated in the transformation model. These genes are *TiPARP* and *SSR3*. The *SSR3* gene is poorly characterised. This signal sequence receptor is an endoplasmic reticulum receptor with a role in protein trafficking. *TiPARP* is TCDD-inducible polyADP-ribose polymerase. PARP proteins catalyze the addition of polyADP-ribose groups onto other proteins, and *TiPARP* appears to selectively act on histones [Ma et al., 2001]; [Katoh and Katoh, 2003]. Little is known about this gene, but its role in DNA structure make it an exciting candidate for functional analyses. It has been shown that in breast and ovarian cells with mutant *BRCA1/2*, targetted inhibition of PARP can selectively kill the cancer cells. This synthetic lethality is due to the fact that cells deficient in functional BRCA1/2 protein can only repair DNA damage by a non-homologous recombination mechanism, in which PARP has an indispensable role [Farmer et al., 2005]. PARP inhibitors have been shown in clinical trials to be highly effective therapies for *BRCA1/2* breast and ovarian carcinomas [Fong et al., 2009]. Whether *PARP* and *TiPARP* interact directly or are part of a common pathway is unclear, and further studies are required to unravel the mechanism by which loss of *TiPARP* may contribute to tumourigenesis. However, it is known that altered histone ribosylation occurs during the repair of DNA strand breaks and chromatin remodelling during DNA replication. Increased DNA DSBs increases the ribosylation of histones by PARPs. PARP expression is also activated by DNA strand breaks [Boulikas, 1989]. Histone poly(ADP)-ribosylation is also required for chromatin unfolding during repair [Althaus et al., 1990]; [Boulikas, 1990]. The N-terminal zinc-finger domain of PARP molecules bind to the DNA strand breaks, thus activating the catalytic domain of the molecule. PARP molecules displace histones from the DNA, thus allowing DNA strand breaks to be repaired [Althaus et al., 1994]. Thus PARP down-regulation could contribute to tumourigenesis by preventing access of the cellular repair machinery to the site of DSBs, thus increasing the chance of cell division without complete repair of DNA DSBs.

Finally, a susceptibility association at chromosome 2p31 contains a cluster of *HOXD* genes. *HOXA* genes are a distinct family of homeobox genes that have been previously implicated

in ovarian cancer [Cheng et al., 2005]; [Ota et al., 2009]; [Widschwendter et al., 2009]. Dysregulation of *HOXD* genes in EOC has not yet been reported, but it is known that *HOXD* genes are involved in limb and digit development (in particular HOXD10-13) [Tsai et al., 1990]; [Sugie et al., 2009]. There was some suggestion that *HOXD3* is upregulated in the IOSE$^{CMYC.KRAS}$ cell lines relative to IOSE cultures. *HOXD3* has previously been shown to promote invasiveness, motility and metastatic activity of lung cancer cells by modulating the expression of adhesion molecules (integrin α-v β-3 and E-cadherin) [Ohta et al., 2006]. *HOXD3* has also been implicated as a promotor of angiogenesis and mediator of ECM remodelling during wound healing [Hansen et al., 2003]; [Boudreau and Varner, 2004]. However, in the present study, overall expression of most *HOX* genes was very low, and close to background signal, and so further investigation would be required to test expression levels of this gene in normal and malignant ovarian cells. Recent data from this laboratory confirm that *HOXD3* is not expressed at high levels in ovarian cell lines [M.Notaridou, unpublished data]. Transformation of IOSE11 was associated with reduced expression of *HOXD10* and *HOXD11*, suggesting loss of these genes could be implicated in transformation of the OSE. However, as this observation did not replicate the the IOSE19 model, further testing would be required to see if this is a real association.

The majority of the genes described above displayed high correlation of expression values across the technical and biological replicates. These results suggest that transformation models may be valuable tools in researching the functional effects of susceptibility genes that emerge from GWASs, particularly models which focus on early carcinogenesis, when it is most likely that susceptibility genes play a role. In the analyses described here, it is assumed that the functional effects of susceptibility SNPs in non-coding regions are mediated by a gene located immediately upstream or downstream of the locus. However, this is likely to be an incorrect assumption in many cases, as it is known that non-coding SNPs are likely to be modifiers, and that such elements can modify gene expression of genes located on any part of that chromosome, or indeed, throughout the genome.

It is notable that a high proportion of the genes at each loci are dysregulated in this cell transformation model. There were 794 genes were differentially expressed in cell lines expressing mutant *KRAS/BRAF* compared to the IOSE^{CMYC} cell lines. With the assumption that there are 20,000 genes in the human genome, this suggests that 0.04% of genes are dysregulated in this cell model. This equates to approximately 1 in every 25 genes which further suggests that there is a higher than average distribution of dysregulated genes at some susceptibility loci. This calculation does make many assumptions, as genes are not distributed evenly throughout the genome, but it may suggest that some susceptibility loci are transcriptional repressors or enhancers which affect many expression

of many nearby genes.

Limitations of the Model

In vitro cell biology modelling of disease has many limitations that may restrict the applicability of these approaches to understanding human disease. Primarily, the process of cell culture selects for cells that are able to grow in 2D, on tissue culture plastics, at concentrations of O_2 and nutrients that greatly exceed physiological levels. In this thesis I describe the use of 3D and heterotypic models (Chapter 5) to try and recreate some of the features of the tissue *in vivo* that are lost in 2D monocultures, such as O_2 and nutrient gradients, geometry and cell shape and heterogeneity of cell types. The 3D models could be improved further by including additional cell types for example, or by the use of synthetic scaffolds that can be engineered to release growth factors or hormones gradually.

A major limitation of this model in particular is that only a subset (∼20%) of ovarian cancers contain genetic alterations in *KRAS/BRAF*, and ovarian cancer itself is a relatively rare disease. Thus, arguably, any potential biomarkers that emerge from this study may only be applicable to the detection of a small proportion of ovarian tumours. However, the IOSE and IOSE^{CMYC} model represents a valid *in vitro* model of the earliest neoplastic changes in the OSE that is applicable across histotypes, as *C-MYC* amplification/overexpression may occur in up to 76% of EOC specimens and is not restricted to one subtype [Dimova et al., 2006]. Furthermore, *C-MYC* overexpression is more common in malignant tumours, which have the worst prognoses and so would benefit most from early detection.

A further limitation of this study is that the *in vivo* tumourigenicity of the transformed cell lines is not known. Xenografts of the spheroid cell lines into immuno-compromised mice would be an ideal way to study the early stages of transformation *in vivo* and study some of the complex processes that are difficult to model *in vitro* such as stromal recruitment and metastasis.

4.7.5 Implications for Epithelial Ovarian Cancer

In ovarian cancers, *BRAF* mutations are rarely found in high-grade tumours. *KRAS* mutations occur in high-grade and low-grade serous tumours, as well as the mucinous subgroup. We are currently investigating whether the gene expression profiles described here can be used to derive a gene expression signature that correlates to patient prognosis, as low-grade tumours have better prognoses than the high-grade counterparts [Shih and Kurman, 2004];

[Berchuck et al., 2009]. Furthermore, it appears that high-grade and low-grade tumours evolve via distinct molecular pathways, and a 'good-prognosis' signature could be used clinically to classify tumours with ambiguous histopathological features. As current treatments for EOC comprise aggressive surgery and platinum-based therapeutics, it would be of benefit to accurately classify the patients who could receive a milder but effective treatment regimen.

The current biomarker used in clinical practise for the detection of EOCs and monitoring of ovarian cancer patients is CA125. This is a marker of differentiated Müllerian epithelia, is frequently upregulated in ovarian cancers and detection of CA125 in blood sera is used clinically for EOC detection and monitoring ovarian cancer patients post-treatment. However, this is not a very reliable marker of EOC, and is not commonly expressed in mucinous ovarian cancers [Koebel et al., 2008]. Many ovarian tumours do not overexpress this marker, and as this is also a marker of other normal gynaecological epithelia, it can be elevated in blood serum of women with benign conditions. There is therefore a real need for novel biomarkers of early EOCs. Such biomarkers may be specific to a subtype, or may be applicable to the majority of EOCs. Although there is extensive disease heterogeneity, some biomarkers are expressed by all subtypes [Koebel et al., 2008]. This also appears to be reflected at the genetic level. Recent work in this and other laboratories has identified susceptibility loci that increase a woman's relative risk of developing EOC [Song et al., 2009]. Some of these loci are specific to the serous subtype; others however, appear to be applicable to all EOCs [Simon Gayther, personal communication].

The list of candidate genes identified in this study represents a panel of candidate biomarkers associated with early neoplastic development of the ovarian surface epithelium. Such biomarkers require thorough *in vitro* testing and validation. It is hoped that by using more functionally relevant 3D models, the biomarkers that emerge are more likely to translate to human disease, although this has yet to be fully evaluated. By using overexpression of *CMYC*, which is common in all EOCs and not restricted to one histotype, it is hoped that the candidate genes described here may be applicable to ovarian tumours of different histologies. It was also found that genes located near candidate susceptibility loci for EOC may be dysregulated early in EOC development. It is hoped that these *in vitro* tools will be of value in the functional follow-up of these susceptibility loci.

5

A Role for Senescent Fibroblasts in Early Transformation of the Ovarian Surface Epithelium

5.1 Introduction

Ovarian epithelial cells make up a small proportion of the organ, yet account for over 90% of all ovarian malignancies. The majority of the organ consists of the ovarian stroma, also called the ovarian cortex. Within the stroma there are many different cell types including fibroblasts, endothelial cells, pericytes; there are also many different extracellular matrix proteins; and, in pre-menopausal ovaries, developing follicles and the associated granulosa cells (the major producer of oestrogen in the ovary). In this Chapter I investigate the role of stromal cells in tumourigenesis of the epithelium, specifically the changes in the fibroblastic component that occur during ageing.

The ovary undergoes many changes with advancing age, particularly during the menopause. The organ shrinks in size and becomes quiescent, and no longer contains maturing follicles and granulosa cells. The regular cycle of ovulation, wound rupture and repair, ceases. Morphological changes in ovaries are more frequent with advancing age, including cortical inclusion cysts and deep invaginations of OSE into the ovarian cortex [Cai et al., 2006]. Additionally, throughout the body, cellular changes also occur that are associated with ageing, namely cellular senescence, either as a result of telomere shortening (replicative senescence, RS), oncogene activation (oncogene induced senescence, OIS) or other genotoxic stresses (stress-induced premature senescence, SIPS). Genotoxic stresses include ex-

posure to cytotoxic drugs, DNA damage and oxidative stress. Senescence has a protective, anti-tumourigenic effect in younger organisms, as a cellular response to oncogene activation/overexpression or other genotoxic stresses, yet there is a growing body of evidence demonstrating that senescent cells can have pro-tumourigenic properties and in fact promote tumourigenesis of neighbouring cells. Campisi and collegues succinctly describe this paradox as antagonistic pleiotropy: the senescence-response has a tumour-suppressive function early in life, but accumulation of senescent fibroblasts can promote epithelial tumour initiation in post-reproductive years [Krtolica et al., 2001].

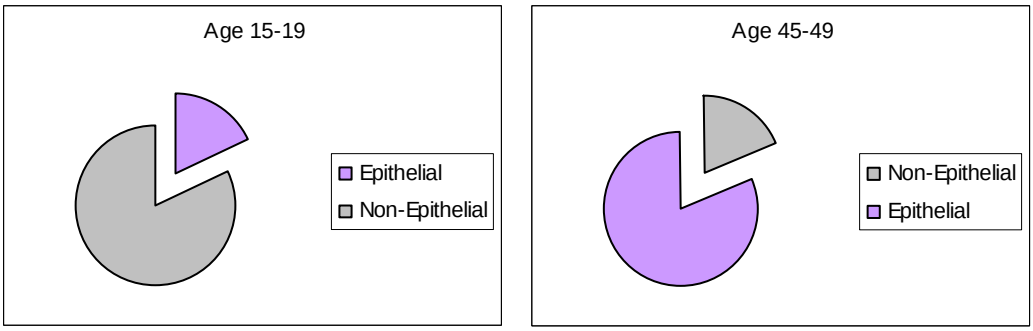

Figure 5.1: Incidence of epithelial tumours increases with age. Epithelial tumours are rare in children and young adults, but make up the majority of tumours diagnosed in adults.

Epidemiological evidence also supports the 'pro-tumourigenic senescent stroma' effect - epithelial tumours are rare in children but common in adults (Figure 5.1). Several *in vitro* and *in vivo* models have found that senescent fibroblasts can promote epithelial tumourigenesis. The initiating events in ovarian tumourigenesis are currently poorly understood, and most EOC cases are diagnosed in women over the age of 60. I thus hypothesised that:

- Senescent fibroblasts promote neoplastic transformation of the ovarian surface epithelium, relative to pre-senescent fibroblasts.

To address this hypothesis I proposed:

- To isolate fibroblasts from the normal ovary and generate a phenotypically normal immortalised ovarian fibroblast cell line
- To establish 2D heterotypic models and study the effect of pre-senescent and senescent ovarian fibroblasts on the invasion, migration, anchorage-independent growth and proliferation rates of partially transformed ovarian surface epithelial cells

- To establish heterotypic 3D cultures of ovarian stromal-epithelial cells to study proliferation of ovarian epithelial cells in 3D heterotypic spheroid cultures

5.2 Isolation and Immortalisation of Normal Ovarian Fibroblasts

There is limited published evidence of *in vitro* normal ovarian fibroblast (NOF) culture and immortalisation. Thus, primary NOF cultures were established and immortalised in order to facilitate the study of stromal-epithelial interactions in the normal ovary. Primary NOFs were isolated from normal ovarian tissue. A biopsy was taken from the centre of a normal ovary, the tissue was then placed into a P100 dish and minced using a sterile scalpel. Growth of colonies and explants was observed using phase-contrast microscopy. Fibroblastic colonies were identified by their characteristic elongated cellular morphology and scattered colony morphologies. Fibroblastic colonies were isolated by ring cloning and established as primary fibroblast cell lines. Immunofluorescent staining was performed with an anti-Fibroblast Surface Protein (FSP), anti-vimentin (VIM) and anti-cytokeratin-7 (Ck7) antibodies, to screen for pure fibroblast clones. One clone was selected, this cell line showed strong expression of FSP and vimentin, whereas Ck7 was not expressed, suggesting that the cells were fibroblastic in origin (Figure 5.2). It is possible that other stromal cell contaminants could have been present in the initial culture. The lack of endothelial cell contamination was confirmed by negative staining for FactorVIII. Granulosa cells could also have contaminated the fibroblast cell line. Granulosa cells are associated with developing oocytes and are major producers of steroid hormones and growth factors in the ovary, particularly during oocyte development. One could test for granulosa cell contamination by staining for inhibin, a glycoprotein commonly and specifically produced by ovarian granulosa cells and granulosa cell tumours [Lapphn et al., 1989]. However, as it would not be anticipated that granulosa cells would express FSP, it was concluded that there was no granulosa cell contamination in the NOF cell line.

The lifespan of primary NOFs was restricted to under 30 days. The limited *in vitro* lifespan of the primary NOF cell line was extended by the ectopic expression of the catalytic subunit of human telomerase (*hTERT*) as described in Chapter 4. The *hTERT*-expressing derivative cell line was maintained in culture for over 140 days without signs of replicative senescence (arrested cell division; a flattened and enlarged cellular morphology) (Figure 5.2a). By PCR-ELISA, NOFs showed no telomerase activity before the introduction of *hTERT*; but after *hTERT* infection, telomerase activity was detectable and telomere terminal restriction fragment lengths were increased by 2kbp (Figure 5.2b).

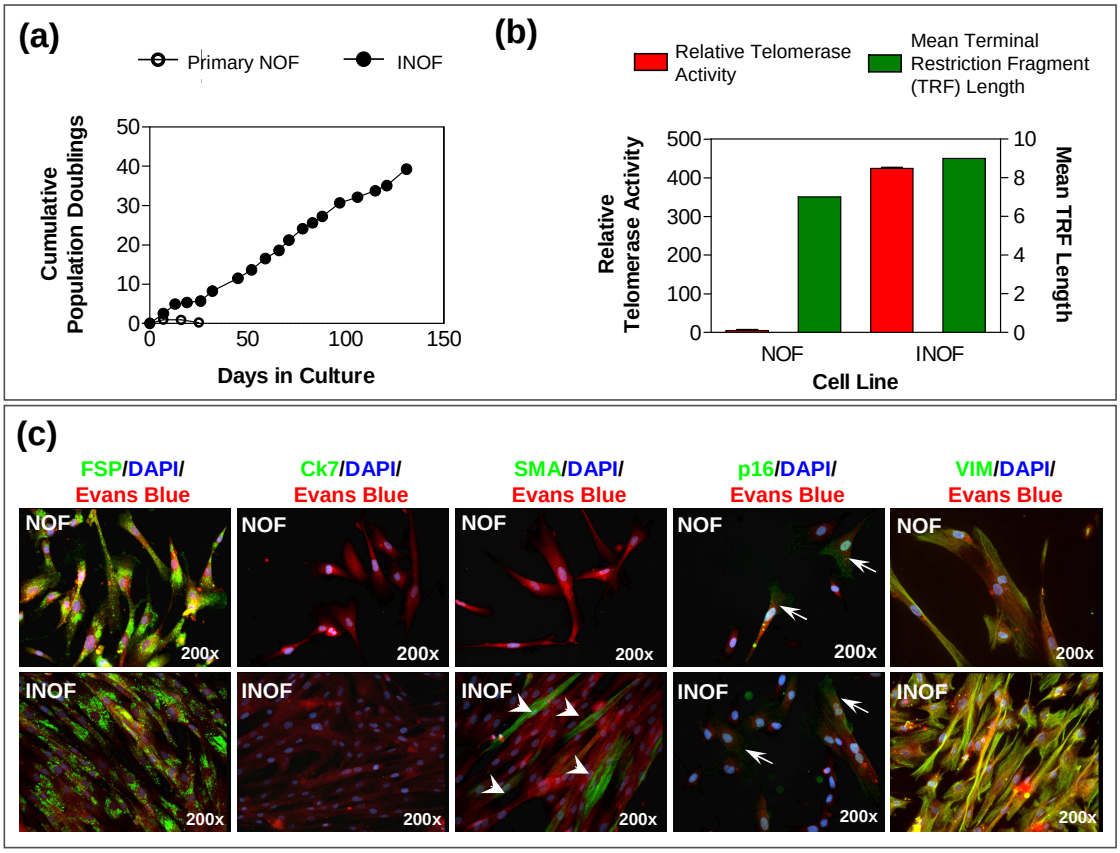

Figure 5.2: Extension of *in vitro* lifespan of primary normal ovarian fibroblasts (NOFs). (a) Ectopic expression of *hTERT* increased *in vitro* lifespan of NOFs from <30 days to >140 days. (b) Relative telomerase activity (relative to an internal positive control) is negligible in cell extracts from primary NOFs but elevated in immortalised NOFs (INOF) cultures, and telomere terminal restriction fragment length is increased by 2kb following introduction of *hTERT*. (c) NOFs and INOFs both exhibit characteristic 'spotty' staining with an anti-fibroblast surface protein (FSP) antibody. Both cell lines do not express cytokeratin 7 (Ck7). Smooth muscle actin (SMA) is expressed in approximately 30% of INOF cells (white arrowhead), indicating a transition towards an activated-fibroblast phenotype following immortalisation. Both NOF and INOF cells expressed p16 in the nucleus and cytoplasm (arrows). 100% of NOF and INOF cells express vimentin (VIM). DAPI (blue) stains cell nuclei, Evan's blue (red) stains the cell cytoplasm, and green fluorescence denotes positive staining. Exposure times were constant for each antigen. Note the elongated, spindled morphology of fibroblast cells compared to the more triangular/cuboidal morphology of ovarian epithelial cultures.

This suggested that NOFs had been immortalised. Neither NOFs nor immortalised NOFs (INOFs) showed evidence of tumourigenic transformation as shown by the absence of anchorage independent growth (20,000 cells/well).

Immunofluorescent staining of cells after *hTERT* immortalisation showed that INOFs

maintained expression of fibroblastic markers (FSP and vimentin) and did not express an epithelial cell marker (Ck7), showing that fibroblastic characteristics were maintained post-immortalisation. Around 30% of INOF cells expressed smooth-muscle actin (SMA), (which indicates an activated phenotype); but SMA expression was absent in the primary NOFs (Figure 5.2c). This is consistent with the findings of previous studies that show an activated phenotype in fibroblasts (from other organs) following immortalisation and exposure to serum during routine tissue culture [Iyer et al., 1999]; [Chang et al., 2004]. p16 expression was also examined by fluorescent immunostaining. INOFs maintained nuclear and cytoplasmic p16 expression, suggesting that loss of this cell-cycle checkpoint is not required for immortalisation.

5.2.1 Fibroblast Growth Medium Conditions

Normal ovarian fibroblast cultures were established in basic medium (BM: Medium 199: Medium MCDB105 with 15% foetal bovine serum and 1% L-glutamine) which has been used to culture epithelial and stromal cells isolated from endometrial and ovarian tumour specimens [Grun et al., 2009]. For the growth of NOF cells, basic medium was supplemented with fibroblast growth factor and insulin, and the morphology and colony formation ability of INOF cultures evaluated. Previous reports of *in vitro* fibroblast cultures have supplemented medium with these two supplements [Liu and Wu, 2009] [1].

The addition of insulin (5μg/ml) alone, or in combination with fibroblast growth factor (FGF, 10ng/ml) did not signifcantly affect colony formation of INOF cells relative to basic medium alone. The addition of FGF, alone or with insulin, visibly increased colony size; but when cultured with BM+FGF, INOF colony formation efficiency was significantly reduced (Figure 5.3 a,c). None of media tested had a visible effect on the morphology of INOF cells. Cells maintained an elongated morphology and colonies were characteristically 'swirly' in all media tested (Figure 5.3b). Since there were no significant improvements in the clonogenicity or morphology of the INOF cell line following supplementation of BM with insulin or FGF, INOFs were maintained in basic medium for all of the experiments described below. INOFs cells were susceptible to changes in the source of foetal bovine serum (Figure 5.3c), thus INOF cells were maintained in the same serum they had been originally isolated in, and all new batches of serum were quality checked before use.

[1] https://bcprd.lonza.com

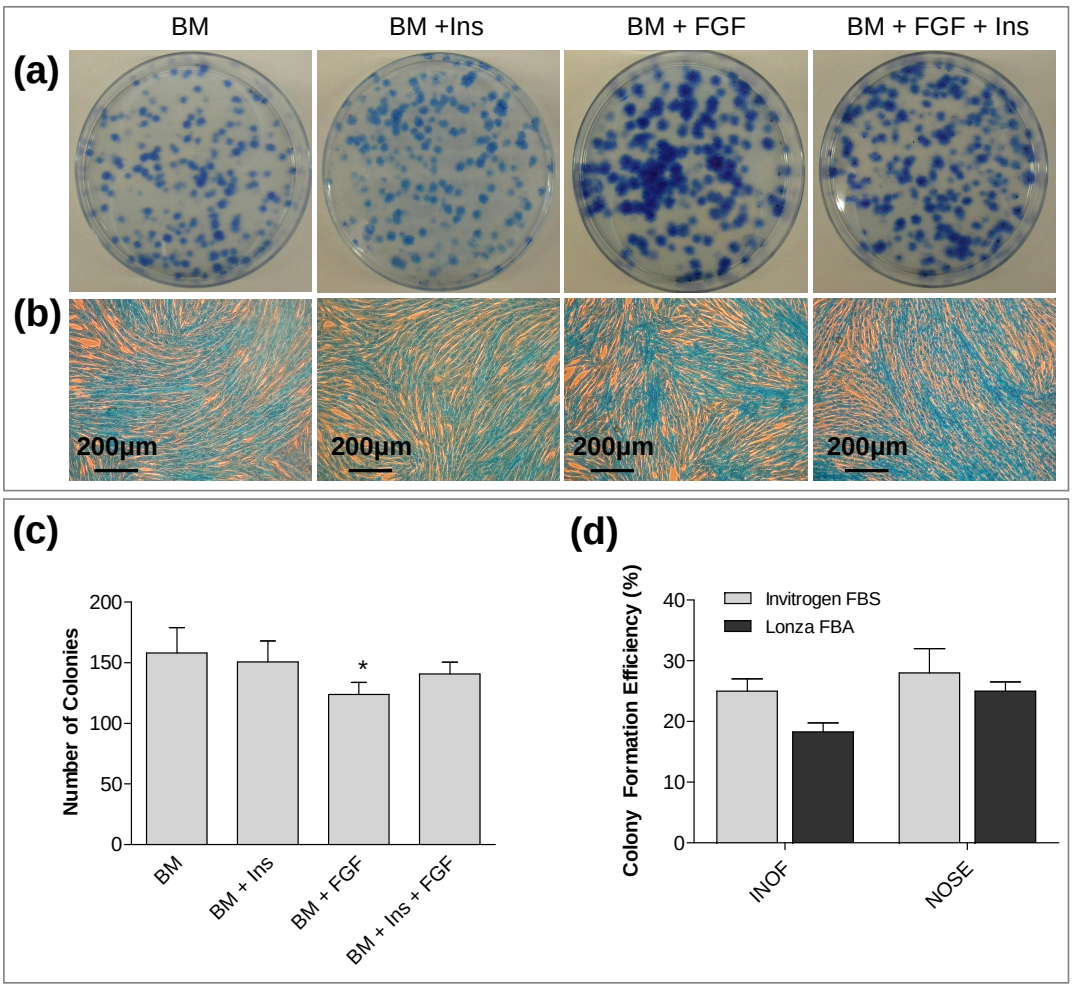

Figure 5.3: Supplementing fibroblast medium does not significantly improve INOF culture clonogenicity or morphology. (a) Colony formation efficiencies, one representative plate shown. Colonies are stained blue by Coomassie staining. Colonies were largest when fibroblast growth factor was added to the medium (b) Colony morphology was 'swirly' in each medium tested, and cell shape was elongated and characteristically mesenchymal. (c) Number of colonies formed in the four types of media tested. $^*P$=0.03. (d) INOF cells have a lower colony formation efficiency in Lonza foetal bovine serum (FBS) compared to Invitrogen FBS. NOSE cells were not susceptible to the change in FBS.

5.3 Senescent Fibroblasts Enhance the Transformed Phenotype of IOSE^{CMYC} cells

The purpose of these experiments was to model the effects of an ageing stromal microenvironment on the *in vitro* transformed phenotype of ovarian epithelial cells. The particular aspect of ageing that was of interest was cellular senescence and how the accumulation of

senescent fibroblasts may affect the neoplastic phenotype of epithelial cells. I hypothesised that either senescent fibroblasts create a pro-tumourigenic cue that can affect neighbouring epithelial cells, or that normal cells inhibit transformation of nearby epithelia and that this inhibitory effect is attenuated upon fibroblast senescence.

Immortalised cell lines, including the INOF cell line created for this study, are resistant to replicative senescence, and so it was necessary to artificially induce senescence. This can be achieved using two approaches (1) oncogene activation or (2) chemical exposure. In other cell types senescence is induced *in vitro* and *in vivo* by introducing mutant alleles of *KRAS*, *BRAF* or knocking-down expression of *p16INK4A* [Krtolica et al., 2001]; [Michaloglou et al., 2005]; [Denoyelle et al., 2006]. The response to these molecular alterations varies between cell type, thus I decided to use chemical exposure because senescence induction typically shows less cell-type-specific variation in effectiveness. Two chemical methods used to induce senescence are short-term exposure to bleomycin sulfate or hydrogen peroxide, the latter of which has been widely described and characterised in many cell types, and was therefore the agent I chose to use. Exposing normal cells to hydrogen peroxide (H_2O_2) induces a senescence response that is considered to be biologically similar to replicative senescence observed in ageing organisms [Krtolica et al., 2001]; [Bavik et al., 2006]. Senescence was induced in INOFs by exposing the cells to low dose (80μM), non-toxic levels of H_2O_2 (Figure 5.4). At this dose up to 80% of cells expressed senescence-associated-β-galactosidase (SA-β-gal) (Figure 5.4a). H_2O_2 exposure reduced proliferation of INOFs by 30%, suggesting that either SA-β-gal-positive cells were displaying early signs of senescence but were not yet fully growth arrested, or that the SA-β-gal-negative cells outgrew the SA-β-gal-positive cells during the course of the growth assay.

The effect of pre-senescent (PSN) and senescent (SEN) fibroblasts on the neoplastic phenotype of ovarian epithelial cell was then investigated. In these experiments, the three immortalised ovarian surface epithelial (IOSE) cell lines, plus the IOSE^{CMYC} cell lines (that stably overexpress *C-MYC*, described in Chapter 4) were used. These cell lines were selected because the hypothesis of these experiments is that the ageing microenvironment may contribute to earliest stages of tumour development, and these two groups of cell lines represent an *in vitro* model of early neoplastic changes in the ovarian surface epithelium. The following phenotypic assays were chosen to measure any changes in the neoplastic phenotype of the IOSE and IOSE^{CMYC} cell lines that may be induced by the two types of fibroblasts: (1) invasion assays, (2) migration assays, (3) anchorage-independent growth assays and (4) proliferation assays (in 2D and 3D).

Firstly, the invasive and migratory phenotypes of IOSE and IOSE^{CMYC} cells were mea-

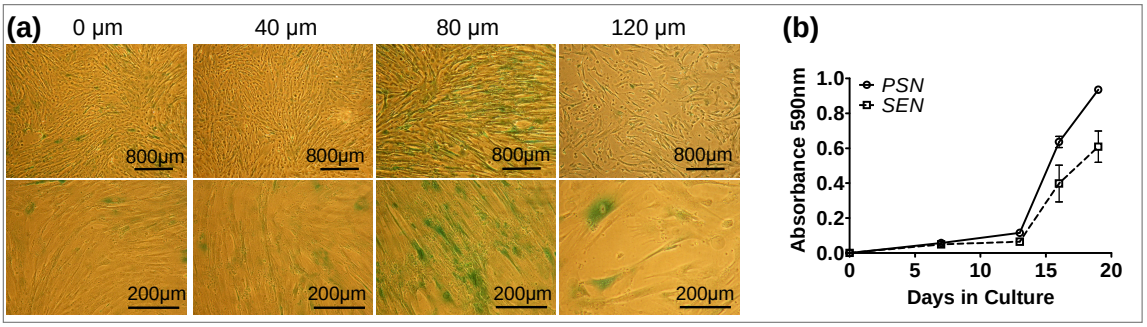

Figure 5.4: Induction of senescence in immortalised normal ovarian fibroblasts by exposure to hydrogen peroxide. (a) 80μM induced senescence-associated-β-galactosidase (SA-β-gal) expression in 70-80% of INOF cells without the toxicity observed at higher doses. When incubated with the X-gal substrate at pH6, cells expressing SA-β-gal become blue. (b) In a growth assay, the growth of INOFs is reduced by 30% following exposure to 80μM H_2O_2.

sured using untreated pre-senescent (PSN) and H_2O_2-treated senescent (SEN) fibroblasts as chemoattractants, with 10% serum included as a positive control. Firstly, assays were performed to identify any differences in IOSE migration and invasion when PSN or SEN fibroblasts were plated as a chemoattractant. In migration assays, the motility of one of the three IOSE cell lines (IOSE19) was inhibited by co-culturing with PSN or SEN fibroblasts, compared to the serum control (P=0.006 and 0.003 respectively, two-tailed paired T-test); but there were no differences in the ability of IOSE19 cells to migrate towards either a PSN or SEN fibroblast chemoattractant (P=0.934) (Figure 5.5a). Neither PSN nor SEN fibroblasts had any effect on the invasive properties of IOSE cells, the invasiveness of IOSE cell lines was not significantly different in co-cultures or the serum control (Figure 5.5b). The IOSE^{CMYC} cells were then tested in the same way, to see if migration and invasion of these cells would be affected by the different fibroblast chemoattractants. In contrast to the IOSE results, there was a 5.7 to 7.2-fold reduction in transwell migration of all three IOSE^{CMYC} cell lines in co-cultures with PSN fibroblasts, relative to the serum control ($P \leq 0.01$). Furthermore, IOSE^{CMYC} cells co-cultured with SEN fibroblasts showed 3.8 to 14.9-fold more migration than when cultured with PSN fibroblasts as a chemoattractant ($P \leq 0.01$). In one case migration was double that of the serum control (Figure 5.5 c,e). The effects of co-cultured fibroblasts on the invasive ability of IOSE^{CMYC} cells were less pronounced, although two of the three IOSE^{CMYC} cell lines were significantly more invasive when co-cultured with SEN compared to PSN fibroblasts ($P \leq 0.05$) (Figure 5.5d).

Conditioned medium (CM) was harvested from PSN and SEN fibroblast cultures used to establish anchorage-independent growth assays with the different epithelial cells. IOSE cells did not display any anchorage-independent growth in PSN or SEN fibroblast CM. CM

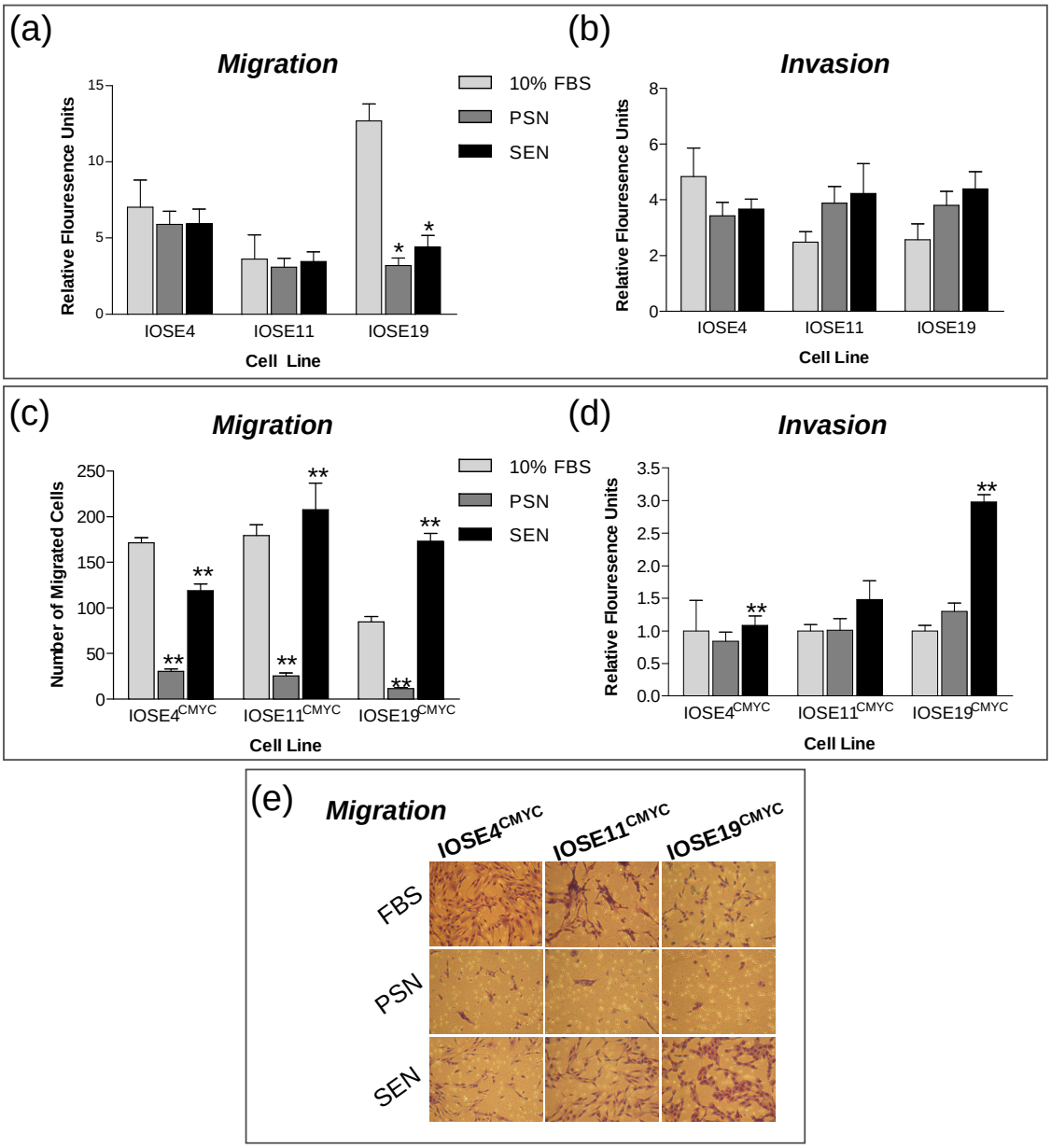

Figure 5.5: Pre-senescent (PSN) and senescent (SEN) fibroblasts differentially regulate the migratory and, to a lesser extent, invasive phenotype of IOSE^{CMYC} but not IOSE cells. 10% foetal bovine serum (FBS) was included as a positive control in all experiments. (a) PSN or SEN fibroblast chemoattractants both inhibited the migration of IOSE19. The other IOSE cell lines showed no significant differences in migratory ability. (b) PSN or SEN ovarian fibroblasts, when plated as a chemoattractant, do not affect the invasive ability of IOSE cell lines. (c) In migration assays, normal, PSN ovarian fibroblasts inhibited motility of all three IOSE^{CMYC} cell lines, relative to 10% FBS. SEN fibroblasts significantly enhanced migration of all *C-MYC*-overexpressing cell lines. (d) SEN fibroblasts significantly enhanced invasive ability of two *C-MYC*-overexpressing clones, relative to PSN fibroblast cells. (e) Stained migration assay membranes, representative fields of view. (*$P \leq 0.05$, ** $P \leq 0.01$, by two-tailed paired T-tests). Error bars = standard error of the mean.

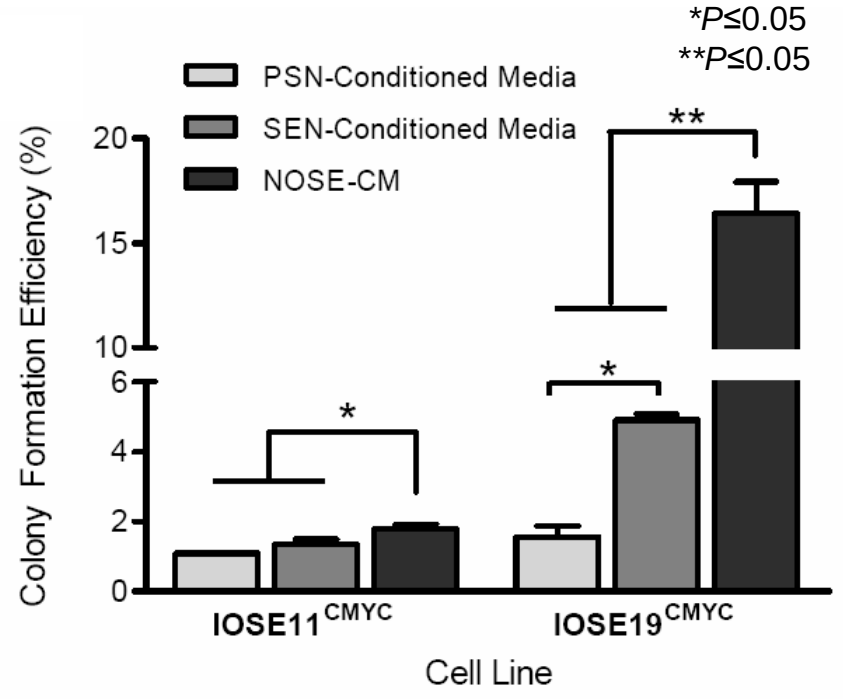

Figure 5.6: Anchorage-independent growth is enhanced when IOSE19^{CMYC} cell lines are grown in conditioned medium (CM) from senescent fibroblasts compared to CM from pre-senescent fibroblasts. 0.33% Noble agar gels were prepared using conditioned medium that had been filtered and then supplemented with NOSE-CM supplements. In conditioned medium, anchorage-independent growth rates were significantly lower than in NOSE-CM alone.

from SEN fibroblasts significantly enhanced anchorage-independent growth of IOSE19^{CMYC} ($P \leq 0.05$) (Figure 5.6). This observation was consistent with the previous findings that the neoplastic phenotype of IOSE19^{CMYC} cells is enhanced by SEN fibroblasts, relative to PSN fibroblasts. The invasion, migration and anchorage-independent growth data suggest that fibroblasts secrete soluble molecules that are chemoattractive to and can modulate growth of IOSE^{CMYC} cell lines. In conditioned medium, anchorage-independent growth rates of IOSE^{CMYC} cells were significantly lower that in NOSE-CM alone, suggesting that even conditioned medium from senescent fibroblasts contains factors which inhibit anchorage-independent proliferation of IOSE cells that overexpress *CMYC*. However, in IOSE19^{CMYC} and to some degree in IOSE11^{CMYC}, conditioned medium from SEN fibroblasts was less inhibitory to anchorage-independent growth than CM from PSN fibroblasts.

5.4 3D Heterotypic Models

In an ovary, particularly in an inclusion cyst, the OSE comes into close contact with the ovarian stroma. Thus, three-dimensional (3D) heterotypic models were created to mimic the close interactions of ovarian epithelial and stromal cells (Figure 5.7). Using the static 3D modelling approach described in Chapters 3 & 4, 3D multicellular INOF spheroids were generated by culturing fibroblasts on polyHEMA-coated tissue culture plastics. INOFs began to form spontaneous aggregates within 48 hours of culture in non-adherent conditions. 7-day multicellular INOF spheroids appeared robust and smooth when visualised by phase-constrast microscopy. A large range of spheroid sizes was observed in all cultures (Figure 5.8). Examination of formalin-fixed, paraffin embedded sections of INOF spheroids, stained with hematoxylin and eosin (H&E), revealed that central regions of spheroids contain abundant matrix protein (Figure 5.8b). Acellular hylanised nodules were also observed, with apoptotic cells distributed throughout a matrix-rich core. Peripherally, spindled cells with elongated nuclei and an eosinophilic cytoplasm, surrounded the spheroid. Pre-senescent and senescent fibroblast spheroids were indistinguishable by H&E staining (Figure 5.8). This is not surprising given that senescent cells *in vivo* are only identifiable by staining for specific senescence markers.

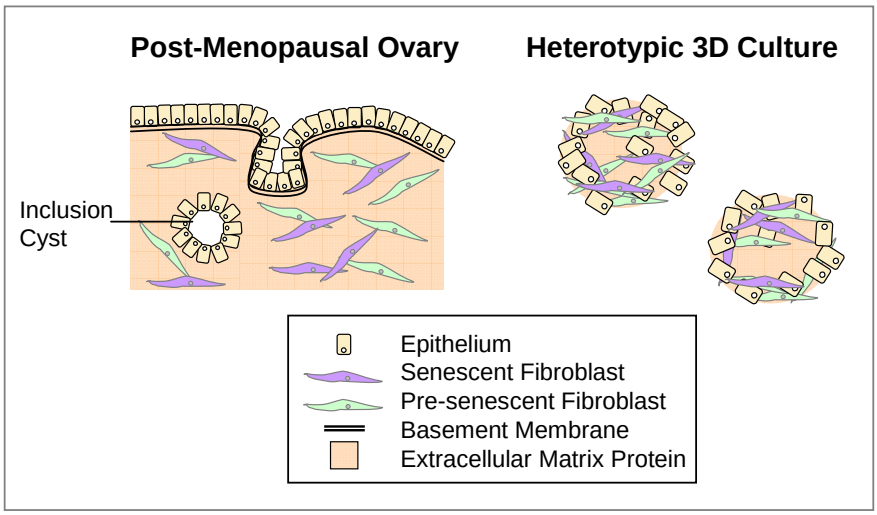

Figure 5.7: Heterotypic models aimed to mimic ovarian stromal-epithelial interactions. Within inclusion cysts in particular, ovarian epithelial and stromal cells are in close contact. Stromal cells are also responsible for the synthesis of the bulk of the extracellular matrix protein in the organ.

Spheroids were stained for vimentin, smooth muscle actin, cytokeratin 18 and collagen IV by immunohistochemistry, and compared to immortalised ovarian surface epithelial spheroids and normal ovarian tissue specimens. INOF spheroids expressed vimentin and

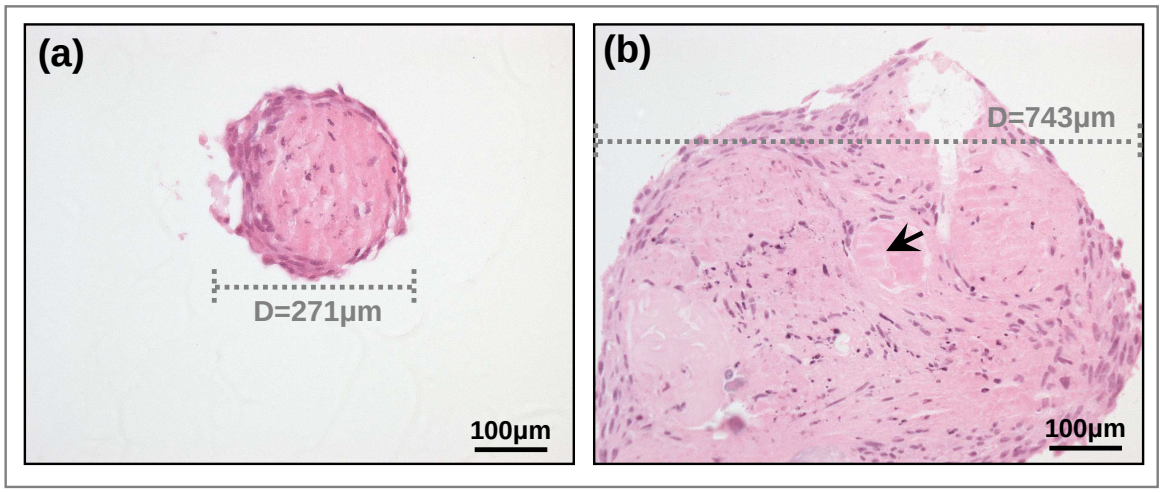

Figure 5.8: Three-dimensional (3D) models of INOF cells. Formalin-fixed, paraffin-embedded spheroids were stained by H&E for analysis of spheroid structure. Representative images of each culture are shown. (a) A small PSN and (b) a large SEN fibroblast monoculture spheroids consist of spindled cells and abundant matrix protein. Hylanised nodules of matrix protein (arrow) and apoptotic cells are visible within central regions of larger spheroids. For both SEN and PSN fibroblasts, a wide range of spheroid sizes is observed when 3D cultures are generated using this technique (D=diameter).

collagen IV, and did not express cytokeratin-18. (Figure 5.9). This was reflective of the ovarian stroma in ovarian tissue specimens. A subset of INOF cells in spheroids also expressed smooth-muscle actin (SMA), but only expressed at low levels *in vivo* and also expressed by $\sim 1/3$ INOF cells in 2D (see above). The aim of this experiment was to find good markers to distinguish epithelial and fibroblastic populations in heterotypic cultures; but only cytokeratin-18 (Ck18) reliably distinguished ovarian fibroblasts and epithelial cells. A commonly described fibroblastic marker, vimentin, was not discriminatory between epithelial cells and fibroblasts in samples of normal ovarian tissue or in 3D spheroid cultures. Desmin and fibroblast surface protein (FSP) were also tested, but did not reliably distinguish between IOSE and INOF due to cross-reactivity with IOSE cells, or poor staining of INOF spheroids. *In vitro* and *in vivo* OSE cells exhibit epithelial and mesenchymal characteristics, makes it difficult to distinguish OSE cells from fibroblasts (Chapter 3 and references therein). No marker was identified that could reliably and efficiently stain ovarian fibroblasts but not OSE *in vitro* or *in vivo* by immunohistochemistry, thus, dual staining of Ck18 plus the marker of interest would be the appropriate approach for analysis of heterotypic cultures.

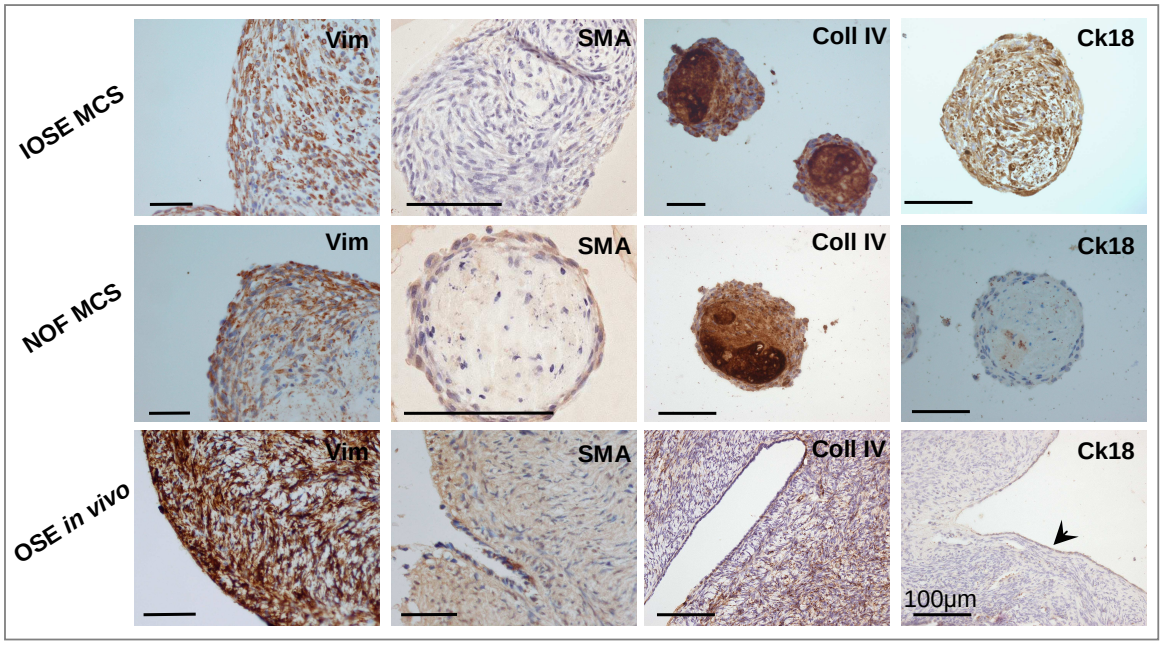

Figure 5.9: Immunohistochemical staining of immortalised ovarian surface epithelial (IOSE) and immortalised normal ovarian fibroblast (INOF) spheroids and normal ovarian tissue. IOSE and INOF spheroids express vimentin (Vim). OSE cells and ovarian stroma are also positive for this matrix protein. INOF spheroids and ovarian stroma are both positive for smooth muscle actin (SMA), but IOSE do not express this antigen. However, under 50% of INOF cells express SMA and staining is weak-moderate, suggesting this is not a good marker to distinguish INOF from IOSE cells. Epithelial cells and fibroblasts express collagen IV in 3D and *in vivo*. Finally, cytokeratin-18 (Ck18) was expressed by IOSE spheroids and OSE *in vivo* (arrowhead), but not detected in INOF spheroids or the ovarian stroma *in vivo*.

5.4.1 Senescent Fibroblasts Promote Epithelial Proliferation in 3D Heterotypic Models

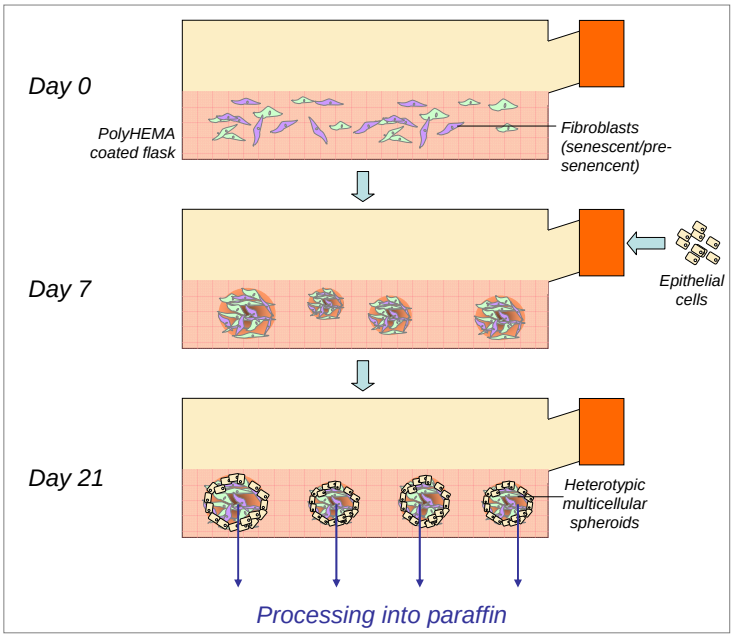

Figure 5.10: Schematic of heterotypic co-culture experiment plan. Fibroblast spheroids were created by culturing cells on polyHEMA coated plastics. After 7 days, epithelial cells were inoculated into the culture. The heterotypic cultures were then grown for a further 14 days before the spheroids were harvested and processed into paraffin.

To create heterotypic 3D models of ovarian fibroblast and epithelial cells, 7-day old spheroid cultures of INOFs were inoculated with IOSE cells at a ratio of 4:1 INOF:IOSE cells (see schematic, Figure 5.10). After 14 days of co-culture, spheroids were formalin-fixed and paraffin embedded. The paraffin-embedded samples were then sectioned. One section was stained with H&E and spheroid structures were examined (Figure 5.11). Central hylanised regions of abundant matrix protein were seen in all heterotypic 3D cultures. Spheroids consisted of two morphologically distinct populations of cells, with either spindled or plump cell morphologies, although the boundaries between the two populations were not distinct. When IOSE cells were cultured with SEN fibroblasts (n=3), nuclear atypia was observed within the population of plump, peripheral cells (Figure 5.11). Features such as prominent nucleoli and irregular or enlarged nuclear shape and 'giant' mononuclear cells budding off the spheroids were observed. These atypical features were not present when IOSE cells were cultured with PSN fibroblasts (n=3) (Figure 5.11a). There was also a trend for more numerous prominent nucleoli and mitoses in the plump cell populations when IOSE^{CMYC} and SEN fibroblasts were co-cultured, com-

pared to IOSE^{CMYC} co-cultures with PSN fibroblasts (Figure 5.11b & d). Finally, when IOSE11^{CMYC} and IOSE19^{CMYC} were co-cultured with PSN fibroblasts, there was marked apoptosis in the central regions of spheroids; these regions were absent in co-cultures with SEN fibroblasts.

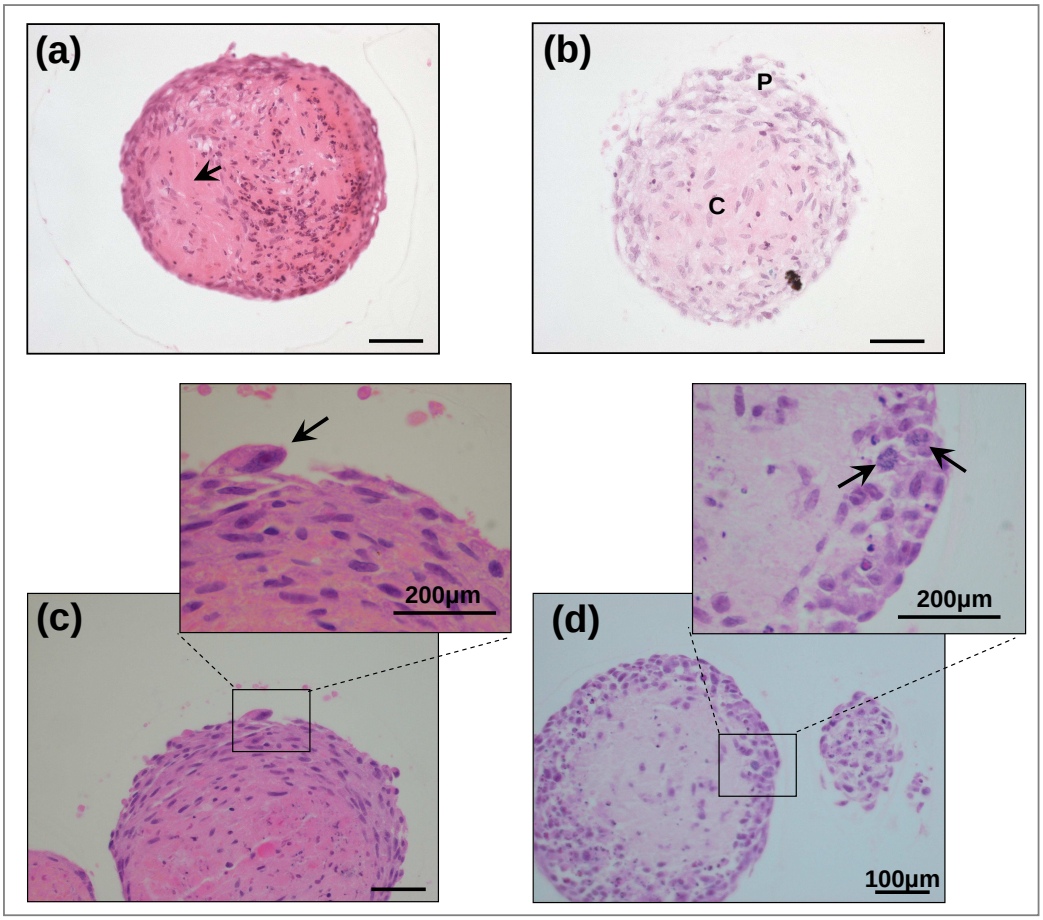

Figure 5.11: 3D models of ovarian stromal-epithelial interactions, paraffin-embedded spheroids stained by hematoxylin and eosin. Representative images of each culture are shown. (a) IOSE19/PSN co-culture. The spheroid is mainly cellular, with some regions of matrix accumulation. There is no visible boundary between the two cell types. (b) IOSE4^{CMYC}/PSN heterotypic culture. In the periphery (P), cells are have reduced matrix protein and are loosely attached. Cells in this region are likely to be the IOSE4^{CMYC} cells. In the core (C), it is likely that the cells are predominantly fibroblasts. Extracellular matrix deposition is observed (acellular eosinophilic regions). (c) IOSE11/SEN fibroblast 3D co-culture. Note the 'giant' cell (arrow) budding off the surface of the spheroid (inset). (d) IOSE19^{CMYC}/SEN fibroblast 3D co-culture. The large peripheral region of plump cells contain some mitotic figures (arrows).

In IOSE/INOF spheroids, epithelial cells were identified by positive staining for Ck18. Ck18-positive cells formed a peripheral region surrounding the fibroblast 'core' (see Figure 5.12). Dual immunohistochemical staining for Ck18 and the proliferation marker MIB-1

enabled identification of the actively proliferating epithelial proportion of the culture. The proliferating epithelial population was measured and calculated as a ratio of proliferating cells in the total epithelial population (Figure 5.13). This was compared to a 2D indirect co-culture proliferation assay. In this assay, epithelial cells and fibroblasts were co-cultured for 14 days, with fibroblasts cultured inside a permeable insert (pore size 1μm). In 3D co-cultures, IOSE^{CMYC} cells were 0.03-12.8-fold more proliferative than parental IOSE cells. In heterotypic spheroids established with SEN fibroblasts there was a statistically significant, 1.4-4.7-fold increase in the relative percentage of dual positive Ck18+/MIB-1 cells for IOSE^{CMYC} cell lines (n=3) compared to IOSE^{CMYC}/PSN co-cultures ($P \leq 0.05$). There was also a trend for an increase (1% to 6% increase) in the proliferation of IOSE cells in co-culture with PSN fibroblasts, although this did not reach statistical significance. In 2D proliferation assays there were no significant differences in the proliferation of IOSE or IOSE^{CMYC} cell lines when cultured with PSN or SEN fibroblasts. This suggests that fibroblast regulation of IOSE proliferation may require direct cell-cell interactions of the two cell types.

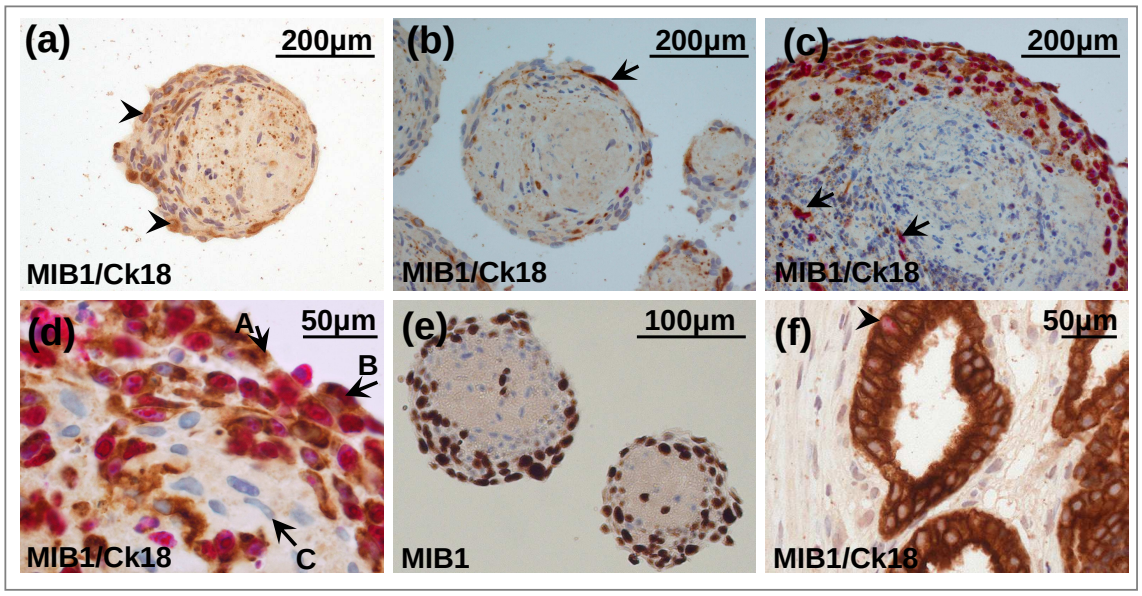

Figure 5.12: Three-dimensional (3D) modelling of stromal-epithelial interactions - analysis of proliferation in the epithelial component by dual staining for MIB1 (pink nuclear stain) and cytokeratin-18 (CK18, brown cytoplasmic stain). Unstained cells are counterstained blue. (a) IOSE11/PSN co-culture. Cytokeratin-positive cells are located at the peripheral region of the spheroid (arrowhead). Note: Non-specific staining of matrix protein does occur but can be distinguished by the absence of cellular structure. (b) IOSE11/SEN co-culture. Note Ck18+ epithelial cells located peripherally within spheroids. A single Ck18+/MIB1+ dual positive cell (arrow) is visible in this section (arrow). (c) IOSE19/SEN co-culture. The central Ck18- population and peripherally located Ck18+ cells within the spheroid are apparent. Some peripheral Ck18+ (epithelial) cells dual stain for MIB1 (pink nuclei). Some Ck18+ cells are located in central regions of the spheroid (arrows), indicating that IOSE19^{CMYC} cells may be capable of invading into fibroblast spheroids. (f) Ck18- cells (fibroblasts, C) closely interact with the population of Ck18+ cells (epithelial cells, A, B). Note the spindled morphology and elongated nucleus of Ck18- cells, (e.g. cell C), compared to the plump morphology and rounded nuclei of Ck18+ cells. Cell A is positive for Ck18 and negative for MIB1; cell B is dual Ck18+/MIB1+ positive. (d) IOSE19^{CMYC}/PSN spheroids, stained only for MIB1 (here MIB1 positive cells have brown nuclei) illustrate how it is not possible to determine the cell type of each positive nuclei, thus necessitating the use of dual staining. (e) Control tissue, dual stained for MIB1 and Ck18. A dual positive cell is visible (arrowhead).

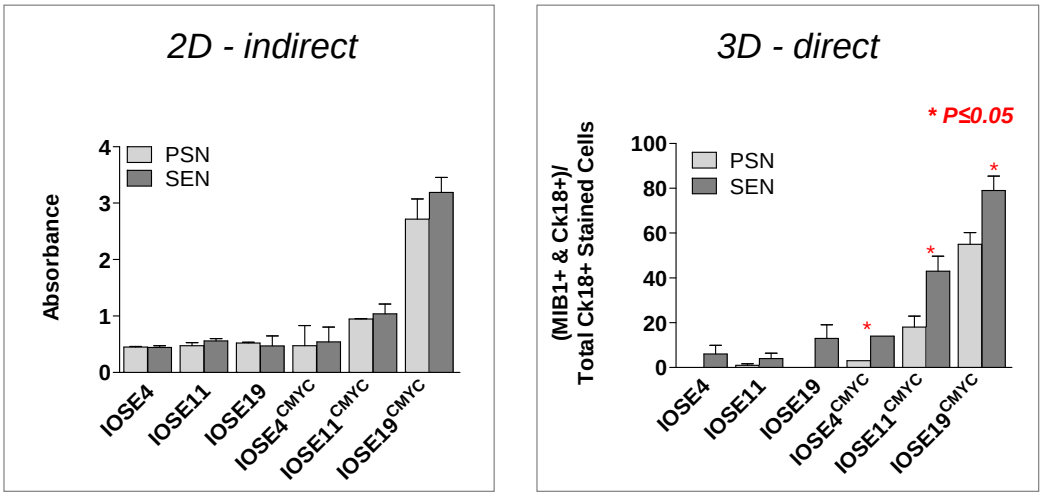

Figure 5.13: Proliferation of epithelial cell lines in 2D and 3D co-culture assays. (a) 2D proliferation assay. Epithelial cells were co-cultured with pre-senescent (PSN) or senescent (SEN) ovarian fibroblasts for 14 days, and then total cell numbers were determined using crystal violet staining. No significant differences in proliferation were detected in co-culture with PSN or SEN fibroblasts (α=0.01). (b) 3D co-culture; measurements of proliferative epithelial proportion of 14-day heterotypic spheroid cultures. Analysis of dual stained Ck18+/MIB1 cells reveals enhanced proliferation in epithelial cell lines when co-cultured in 3D with SEN or PSN fibroblasts, this was statistically significant for the three IOSE^{CMYC} cell lines. The proportion of MIB1 cells is calculated relative to the total Ck18+ population of the culture.

5.5 Discussion

As early as 1889, it was recognised that even highly aggressive tumour cells would only thrive in a permissive microenvironment [Paget, 1889] and many studies have since demonstrated that the phenotype of cancer cells can be modulated by the environment. In more recent years, researchers have begun to focus on the role of the local microenvironment in the earliest stages of carcinogenesis: in tumour initiation. Epithelial ovarian cancers are most commonly diagnosed in post-menopausal women. The life-history of the most common subtype (high-grade serous) suggests that these tumours progress rapidly [Brown and Palmer, 2009]. Two of the most well described risk factors for epithelial ovarian cancer are the protective effect of pregnancy and oral contraceptive use [Pike et al., 2004]; [Purdie et al., 2003]. It is hypothesised that this is due to the reduction in the number of ovulations, and thus repeated rupture and repair of the ovarian surface epithelium (OSE). A reduced number of ovulations over a lifetime equates to a reduced number of opportunities for the OSE to be exposed to the mitogenic, hormone-rich milieu of the ovarian stroma [Fathalla, 1971]. However, the majority of ovarian carcinomas occur in women at least ten years after menopause, and the natural history of high-grade serous tumours (the most common histopathological subtype) points to rapid, aggressive tumour growth.

This poses the question: does a trigger exist in the ovarian stroma of postmenopausal women that plays a role in the development of ovarian surface epithelial tumours? A main contender for this trigger would be hormonal factors; yet the post-menopausal ovary is no longer a major producer of steroid hormones. Not only do post-menopausal ovaries no longer produce oestrogen (due to the loss of granulosa cells), but androgen production also declines [Couzinet et al., 2001]. Therefore, the ovarian stroma no longer contains high levels of the major mitogenic hormones found in pre-menopausal ovaries. It has been postulated that elevated levels of gonadotrophin detected in post-menopausal women may stimulate proliferation of the OSE [Landen et al., 2008]; [Smith and Xu, 2008]. However, epidemiological, *in vitro* and *in vivo* data exploring a role for gonadotrophins are contradictory. This may be due difficulties in distinguishing the effects of gonadotrophins from the effects of repeated ovulation (gonadotrophins released from the pituitary gland trigger ovulation).

Age-related changes in gross morphology are observed in post-menopausal ovaries (increased number of inclusion cysts and deep invaginations of OSE into the ovarian stroma) and have been hypothesised to play a role in transformation [Cai et al., 2006]. In this present study, it was hypothesised that age-related changes in ovarian stromal fibroblasts

may be providing a molecular pro-tumourigenic cue in the post-menopausal ovary. This trigger may act in synergy with early tumourigenic events in epithelial cells (e.g. tumour suppressor gene inactivation, the activation of proto-oncogenes) but may have no effect on normal ovarian surface epithelial (OSE) cells. Here the earliest stages of OSE transformation were modelled using non-neoplastic *hTERT*-immortalised ovarian surface epithelial (IOSE) cells, and partially transformed IOSE^{CMYC} cell lines (overexpressing *C-MYC*). IOSE and IOSE^{CMYC} cells were co-cultured with pre-senescent and senescent ovarian fibroblasts. Senescent fibroblasts were able to promote migration of all the IOSE^{CMYC} cell lines tested but not the IOSE cells. A motile phenotype is associated with neoplastic transformation, and does not require the additional ability to degrade the extracellular matrix which is required for increased invasion. Indeed, senescent fibroblasts only increased the invasive ability of the IOSE^{CMYC} clones with the most aggressive *in vitro* phenotype. Furthermore, anchorage-independent growth was enhanced in IOSE19^{CMYC} cells when cultured in conditioned media from senescent fibroblast cells, in comparison with conditioned media from non-senescent fibroblasts. Thus, in three independent cell lines, senescent fibroblasts were able to promote different features of the neoplastic phenotype of IOSE^{CMYC} cells, relative to the pre-senescent counterparts. Since pre-senescent/senescent fibroblasts did not differentially affect the migration, invasion, 2D/3D proliferation or anchorage-independent growth of IOSE cells, it was concluded that the pro-tumourigenic effect of senescent fibroblasts is conditional on, and only has an effect in synergy with, oncogenic mutation in the epithelium. These data also suggest that the regulation of neoplastic epithelial cells by senescent fibroblasts is mediated, in part, by soluble, secreted factors that are chemoattractive to partially transformed ovarian epithelial cells.

In three-dimensional heterotypic cultures, senescent fibroblasts significantly enhanced proliferation of IOSE^{CMYC} cell lines relative to co-cultures with pre-senescent cells. Parental IOSE cell lines were not regulated in this way, although there was a trend for more MIB1-positive epithelial cells to be observed in co-culture with PSN fibroblasts. Further experiments, with larger numbers of replicates, would need to be performed to validate whether or not PSN/SEN fibroblasts can significantly differentially regulate IOSE proliferation in 3D spheroid co-cultures. Interestingly, nuclear atypia was observed in IOSE cells cultured with senescent fibroblasts, but these features were absent in the same cells cultured with pre-senescent fibroblasts. This may suggest that even the earliest neoplastic changes in the OSE (modelled here by the IOSE cells) may be susceptible to the pro-tumourigenic cue provided by the ovarian stroma, although it may be necessary to culture fibroblasts and primary OSE to investigate this further. The effects are also likely to be very subtle and thus challenging to detect. Since invasion and migration of IOSE were not regulated by fibroblasts, it can be concluded that IOSE cell invasion and migration is not influenced

by the ageing stromal microenviroment in this *in vitro* model.

The experiments described above provide *in vitro* evidence that senescence of normal ovarian stromal fibroblasts can enhance features of a neoplastic phenotype in partially transformed ovarian surface epithelial (OSE) cells. The data also provides *in vitro* evidence that normal (pre-senescent) fibroblasts may be inhibitory to neoplastic transformation of the OSE. This model is summarised in Figure 5.14. The interactions between epithelial and stromal cells are dynamic and bi-directional [Yang et al., 2006] and are likely to be essential for tumour initiation and maintenance. They therefore represent new sources of discovery for novel therapeutic targets for epithelial ovarian carcinomas.

The effects of fibroblasts on epithelial cells observed in this study reflect previous findings by groups working on different types of cancer. Previous reports have shown that

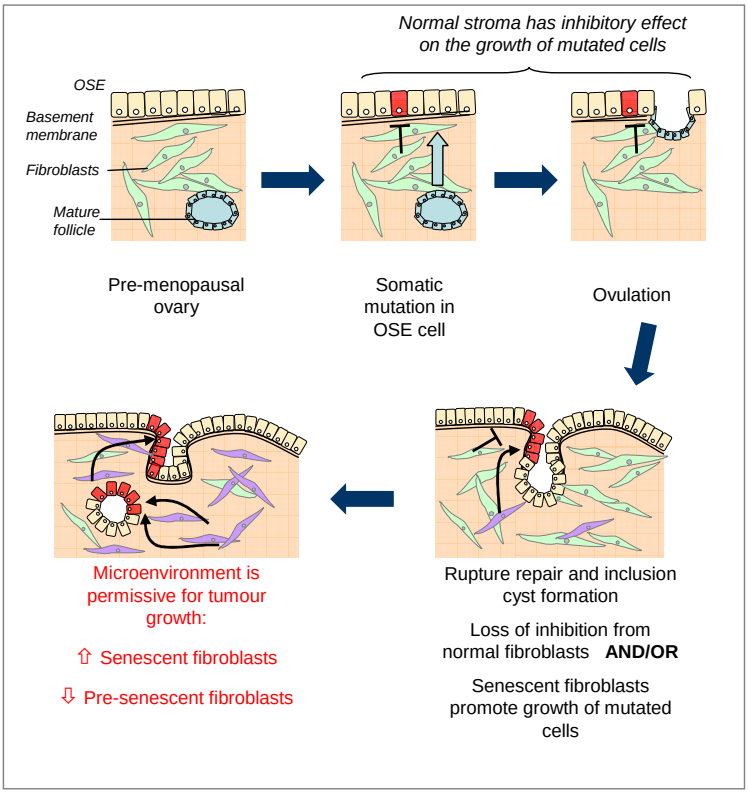

Figure 5.14: A model of the role of the ageing microenvironment in EOC development. Somatic mutations in the OSE may arise pre-menopausally, following the repeated cycles of rupture and repair associated with repeated ovulation. However, in the younger ovary, pre-senescent fibroblasts (green) inhibit proliferation and further neoplastic progression of the mutant cell. Ovulation also promotes inclusion cyst formation. During ageing, senescent fibroblasts (purple), secreting pro-tumourigenic factors, gradually replace pre-senescent fibroblasts, eventually creating a microenvironment that is permissive for tumour initiation.

normal fibroblasts and a normal tissue microenvironment can inhibit early tumourigenesis, and that fibroblast senescence results in a loss of inhibition of tumourigenesis or promotion of epithelial transformation [Olumi et al., 1999]; [Parrinello et al., 2005]; [Studebaker et al., 2008]. Krtolica *et al.*, demonstrated that senescent fibroblasts could enhance *in vitro* proliferation and induce *in vivo* tumour formation of premalignant and malignant human and murine epithelial cell xenografts [Krtolica et al., 2001]. Some of the factors that can mediate the differential effects of normal and senescent ovarian fibroblasts have been identidied. A recent study of senescent foreskin fibroblasts, by Pazolli *et al.*, identified osteopontin as a mediator of *in vitro* and *in vivo* growth stimulation [Pazolli et al., 2009]. Other molecules to have been identified in senescent fibroblasts as effectors of the pro-neoplastic phenotype include MMP-3, VEGF, AREG, HGF and IL-6 (summarised in Table 5.1) [Parrinello et al., 2005]; [Bavik et al., 2006]; [Coppe et al., 2006]; [Studebaker et al., 2008].

Whether or not the pro-oncogenic factors released by senescent fibroblasts will vary by tissue has yet to be determined. However, the morphological hallmarks of senescence (flattened morphology and β-galactosidase expression) are universal, suggesting there may be overlap in the molecular features of senescence between organs. Recent profiling of proteins secreted by senescent fibroblasts, using antibody and gene expression arrays, found many of the factors produced by senescent fibroblasts are also involved in inflammation and tissue remodelling [Coppe et al., 2008]; [Pazolli et al., 2009]. Senescent fibroblasts may be a mediator of the 'wound that does not heal' theory of carcinogenesis, which links inflammation and related changes in tissue structure to tumour formation, since many of the phenotypic changes associated with transformation are also associated with wound healing (e.g. ectopic proliferation, production of pro-angiogenic factors, increased invasion and migration). Sites of chronic wounds and inflammation have a high proportion of senescent cells and are prone to neoplastic transformation. In early neoplasia, the development of a 'wound-healing-like' or 'activated' stroma may be stimulated by epithelial signalling but could also be due to inherent biological changes in the stroma itself.

Furthermore, the pathways activated in the epithelial cells in response to exposure to senescent fibroblasts are not yet known. Senescent fibroblasts may stimulate one or multiple growth/oncogenic signalling pathways in the epithelial cells, and so a candidate approach could be used in which single pathways are inhibited with chemical inhibitors or blocking antibodies. In this study it could be of interest to examine whether the MAPK pathway is involved in the increased migration and proliferation of the IOSE^{CMYC} cell lines, since it is described in Chapter 4 that activation of the MAPK pathway can promote neoplastic transformation of IOSE cells in combination with overexpression of *CMYC*. One could test this hypothesis by incubating the cells with an EGFR blocking antibody or an ERK

inbibitor e.g. U0126. One could screen multiple signalling pathways in this way, though in co-cultures such an approach would also inhibit the same pathways in the fibroblasts. To avoid this, dominant-negative constructs could be used to target specific candidate pathways.

Model		*In vitro* Assays	*In vivo* Assays	Genes	References
Target cell	Fibroblasts				
Keratinocytes, Breast epithelia (non-malignant and malignant)	Foetal lung, foreskin and breast fibroblast cell lines	***Co-culture (direct and indirect) proliferation assays*** Normal epithelia were not regulated differentially by PF/SF. Preneoplastic cell growth stimulated by SF 2 to 7-fold, compared to PF.	SF induced/enhanced tumour formation in preneoplastic/ malignant epithelial cells	N/A	Krtolica et al., 2001
Mammary epithelial cells	Foetal lung	***Acini formation/ branching assays*** Oncogenic conversion of epithelia *in vivo* results in a loss of acini formation *in vitro* due to EMT. Co-culture with SF increases size and reduces organisation of alveoli. SFs stimulate epithelial branching through MMP-3 ***Invasion*** Oncogenic conversion of epithelia *in vivo* enhanced invasive ability	N/A	MMP3	Parrinello et al., 2004
Prostate epithelial cells	Prostate stromal fibroblasts	***Proliferation*** Fibroblasts from older patients were more growth enhancing in epithelial proliferation assays ***Transcriptome analysis*** CXCL12 (SDF-1) identified as a mediator of senescence-associated stimulation of epithelial proliferation	N/A	CXCL12 CXCR4	Begley et al., 2005
Prostate epithelial cells	Prostate stromal fibroblasts	***Transciptome analysis*** AERG identified as a mediator of senescence-associated stimulation of epithelial proliferation ***Co-culture (direct and indirect) proliferation assays*** SFs enhance epithelial proliferation	N/A	AERG	Bavik et al., 2006
Mammary epithelial cells Endothelial cells (HUVECs)	Foetal lung/foreskin fibroblasts	***Angiogenesis*** HUVEC invasion/migration enhanced by conditioned medium from SFs	SFs increased tumour size and vessel formation	VEGF	Coppé et al., 2006
Transformed ovarian epithelial cells	Ovarian/ Mammary	N/A	SFs promote tumour growth	GRO-1	Yang et al., 2006
Premalignant mammary epithelia	Foetal lung, foreskin; adult mammary	***Protein profiling*** Characterisation of the Senescence-Associated Secretory Phenotype ***Epithelial scattering, invasion*** of a pre-malignant cell line enhanced by SF, due to an EMT mediated largely though IL-6/-8	N/A	IL-6,-7,-8 GRO HGF MCP-2 IGFBPs	Coppé et al., 2008
Premalignant keratinocytes	Foreskin fibroblasts	***Direct co-culture*** SFs induce growth of premalignant cells	SFs enhance xenograft growth	OPN	Pazolli et al., 2009

Table 5.1: Senescent fibroblasts in epithelial tumourigenesis: A review of the literature SF= senescent fibroblasts

Although it is widely accepted that oncogene-induced senescence, replicative senescence and stress-induced premature senescence occur *in vitro* and *in vivo*, there are few studies to date that quantify the effect *in vivo*. Two studies analysed skin biopsies from baboons and found that around 15% of cells in ageing primates were senescent [Herbig et al., 2006]; [Jeyapalan et al., 2007]. However, the proportion of senescent cells that accumulate in the stroma of different human organs has yet to be determined. As part of these studies, antibodies against β-galactosidase and *p16* were tested extensively to try and quantify the proportion of senescent fibroblasts in formalin-fixed, paraffin-embedded ovarian specimens from women of different ages. However, neither approach was successful in identifying the senescent stromal component of ageing ovaries. β-galactosidase antibodies that have efficiencies comparable to the β-galactosidase bioactivity assay, or a new alternative marker that is specific to senescent cells and can be applied to paraffin-embedded tissue are much

needed for the quantification of actual rates of senescence in human tissues.

Implications for Epithelial Ovarian Cancer

This is the first time that the role of senescent fibroblasts in early ovarian cancer development has been investigated. An *in vitro* transformation model of epithelial ovarian cancer has previously identified a secreted molecule, Gro-1, which in turn induces senescence of the fibroblasts *in vitro*. Gro-1 was shown to induce senescence in ovarian and mammary fibroblasts and increased *in vivo* tumourigenicity of co-injected OSE cells expressing SV40 large-T antigen [Yang et al., 2006]. This model illustrates a role for senescent stromal fibroblasts in tumour maintenance and demonstrates the ability of transformed epithelial cells to signal to the neighbouring stroma to induce remodelling of the local microenvironment to support neoplasic progression. This study also found that senescent fibroblasts were commonly located adjacent to malignant ovarian cancer epithelial cells. It appears that, once again, ovarian cancers are an exception to the 'norm', in other epithelial cancers, senescent cells are common in benign tumours but rare in malignant carcinomas [Collado et al., 2005].

In this Chapter, I have described the creation of a phenotypically normal ovarian fibroblast (NOF) cell line. The primary fibroblast cell line had a restricted *in vitro* lifespan (under 30 days). This was around half that observed for the *in vitro* lifespan of NOSE cell lines described in Chapter 3. The restricted lifespan may be due to the population bottleneck caused by sub-cloning, although NOSE19 was generated by sub-cloning and yet could still be maintained in culture for over 50 days and 9.7 population doublings. Alternatively, this may be a cell-type specific effect, or due to the differences in the growth medium. It was therefore necessary to immortalise the primary NOFs, thus creating a novel immortalised normal ovarian fibroblast (INOF) cell line. This cell line also remained fibroblastic and phenotypically non-transformed during passaging *in vitro*. With the exception of the study by Yang and colleagues, described above, all other reports of stromal-epithelial interactions in ovarian cancer have utilised fibroblasts from other organs [Wang-Johanning et al., 2007]; [Noskova et al., 2009]. The Yang *et al.* study does not describe details of fibroblast isolation and immortalisation, and so this present study is the first to do so. The application of an INOF cell line to the study of stromal-epithelial interactions in epithelial ovarian cancer demonstrated here represents an organotypic model for the investigation of heterotypic interactions in normal and malignant ovaries. Staining for the expression of extracellular matrix (ECM) protein markers in 3D ovarian fibroblast cultures was consistent with the profile of the ovarian stroma in normal tissue specimens. This suggests, therefore, that culturing ovarian fibroblasts by this technique has an ad-

vantage over commercially available gels in that it more closely mimics the complex and heterogeneous extracellular matrix of the organ.

This Chapter describes stromal-epithelial interactions in a model of early neoplastic transformation of ovarian epithelial cells. Within ovarian cortical inclusion cysts, epithelial cells are in close contact with the hormone-rich milieu of the ovarian stroma, since there is no longer the barrier of the basement membrane beneath the OSE. These close interactions were imitated by establishing three-dimensional co-cultures of pre-senescent and senescent ovarian fibroblasts, and OSE cells that overexpress the *CMYC* oncogene. There is still dispute in the literature regarding the cell of origin for epithelial ovarian carcinomas; current data suggest that for the most common EOC subtype, high-grade serous, the ovarian surface epithelium (OSE) or the epithelia at the fallopian tube fimbrae are both sites of ovarian tumour initiation, particularly in BRCA mutation carriers [Callahan et al., 2007]; [Callahan et al., 2007]; [Roh et al., 2009]; [Hirst et al., 2009]. However, the bias towards finding occult primary tumours in the fallopian tubes of prophylactic-oophorectomy specimens from *BRCA1/2* mutation carriers may be due to the fact that the fallopian tubes of this high-risk group are examined more rigorously than those in non-mutation carriers. Epithelial cells from other Müllerian epithelia have also been suggested as possible origins of EOC (e.g. cells lining inclusion cysts and the subsequent tumours that arise at these sites), although empirical data to support this hypothesis have yet to be found [Dubeau, 1999]; [Dubeau, 2008]. Heterotypic three-dimensional models, as described here, provide an ideal basis for studying interactions between ovarian stroma and OSE, or ectopically located endometrial or tubal epithelia in order to understand more fully the true origins of invasive ovarian carcinomas.

By mimicking the processes of early ovarian tumour development in a microenvironment that closely resembles this process *in vivo*, it is hoped that such models can ultimately be used to identify new markers associated with tumour initiation and progression. By trying to replicate specific biological features of disease, such as dimensionality and heterogenity of cell types, the candidate biomarkers that emerge from such models may be of relevance to human disease. Currently, over 40% of EOCs are diagnosed at a late stage (III or IV), and for these patients five-year survival rates are ∼30%. Only a minority of epithelial ovarian tumours are diagnosed when disease is restricted to the ovary, but for this group, five-year survival rates are much higher (over 70%) (Thames Cancer Registry, 1992-1996). Mortality from ovarian cancer could be reduced by the discovery of biomarkers of the disease at its earliest stages; however, the molecular events that occur during early stages of tumourigenesis of the ovarian surface epithelium are still poorly understood. This model has demonstrated a role for senescent ovarian fibroblasts in tumourigenesis of the ovarian surface epithelium, and could readily be manipulated to test the role of senescent fibrob-

lasts at later stages of tumour development. Cell context is proving increasingly important in governing cell behaviour, and interactions at the interface of tumour epithelium and tumour stroma or transformed and non-transformed epithelial cells are a resource for the discovery of new therapeutic targets [Hogan et al., 2009]. It is hoped that an increased understanding of the signalling between ovarian epithelial cells and senescent fibroblasts in tumour initiation and maintenance may ultimately provide a novel approach for the development of novel biomarkers and therapeutic targets.

6

Conclusions & Future Directions

Understanding of molecular events that occur during the early stages of epithelial ovarian cancer (EOC) has been hindered by both the shortage of early-stage tumour specimens, and the lack of good *in vitro* models of disease. Understanding EOC development is all the more challenging when one considers that the disease is relatively rare and extremely heterogeneous, necessitating stratification of tumours (there are 4 main subtypes). Additionally, difficulties in the culture of primary ovarian cells has hindered *in vitro* studies.

Most *in vitro* models of EOC have utilised viral oncoproteins to induce malignant transformation of the ovarian surface epithelium (OSE). This present study, therefore, aimed to create a more biologically relevant model of OSE transformation. To do this, there were three important features of the project:

1. To develop three-dimensional modelling tools as a more biologically relevant model of the OSE and of ovarian tumourigenesis
2. To transform ovarian surface epithelial cells with oncogenes that are known to be altered in ovarian tumour specimens
3. To consider the contribution of the stromal microenvironment to the development of epithelial ovarian cancers

This project has demonstrated, for the first time, that NOSE cells and NOSE cells harbouring defined genetic alterations can be established as three-dimensional models. Three-dimensional *in vitro* models more closely recreate *in vitro* the geometry and the complex cell-cell, cell-ECM interactions of tissue *in vivo*. This thesis details the establishment of

models of neoplastic progression in epithelial ovarian cancer. Firstly, a step-wise model of transformation of normal ovarian surface epithelial cells was developed using genes that are known to be altered in ovarian tumour specimens. This model represents an *in vitro* model of early ovarian cancer development. Phenotypic heterogeneity was detectable *in vitro* and observed to be associated with the introduction of different genes. In 3D, features of tumourigenic cells *in vivo* were detected - such features were not identifiable in traditional 2D monolayer cultures. Gene expression microarrays were then used to examine the transcriptional changes associated with transformation driven by the different oncogenes. Molecular heterogeneity was observed, and a gene lists generated that represent novel candidate biomarkers of early EOC development. Genes of interest for further study include *THBS-1*, *CTGF*, *PITX1*, *MOCOS*, *RGS4* and *FEZ1*. Some of these genes have already been studied in EOC tumour specimens or in *in vitro* models, all represent biologically interesting candidates for validation of the functional roles in EOC development. Furthermore, some genes located within EOC susceptibility loci were also dysregulated in the IOSE cell lines that expressed *CMYC* +/- mutant *KRAS/BRAF* alleles, suggesting that genes such as *BNC2* and *TiPARP* are involved in early development of EOCs.

Additionally, a 3D heterotypic model were developed using a new immortalised ovarian fibroblast cell line. This model was used to demonstrate that age-related stromal changes may have a role in ovarian epithelial tumourigenesis, linking an epidemiological observation (most EOCs occur in post-menopausal, older women) to a functional effect modelled *in vitro*. The models presented here represent novel *in vitro* tools for the study of specific genes that are thought to have a role in EOC development, or for the development and validation of novel therapeutic agents or targets. The results also provide some much-needed insight into the early events that occur during EOC development *in vivo*, and also how the molecular and phenotypic heterogeneity observed in EOC specimens may correlate to the specific genetic alterations that drive tumour initiation and progression.

Major emphases on the establishment of new cell lines and organotypic techniques characterise this body of work. Consequently, the reagents described here could readily be applied to many of the remaining unanswered questions surrounding EOC development. For example: what proportion of high-grade serous EOCs originate in the OSE, and what proportion originate in the fallopian tube epithelia? How does the hormonal microenvironment affect stromal-epithelial interactions anf transformation of the OSE? How would different genetic alterations (e.g. loss of *BRCA1/2*) affect transformation of the OSE? Do low-moderate susceptibility alleles affect the stromal microenvironment? Do different genetic alterations in the OSE differentially alter susceptibility to the influence of the stroma?

The gene expression profiles described in Chapter 4 may provide some insight into the molecular biology of early transformation of NOSE cells. Such genes (e.g. thrombospondin-1) may be candidate therapeutic targets that may be specific for tumours harbouring those specific genetic alterations, which could be tested in the 3D polyHEMA modelling system described in this thesis. Moderate-throughput screens could be performed using the cell lines generated in this model and ovarian cancer cell lines that are genotyped for *KRAS/BRAF* mutations or *C-MYC* amplification. Lentiviral gene delivery would ensure the highest rates of transduction, and using a 3D screen would enhance the likelihood of identifying potentially therapeutic genes (for gene therapy) or gene/pathway targets (for drug development).

6.0.1 Future Directions

The list of candidate genes identified in this study represents a panel of candidate biomarkers associated with early stages of tumour progression. These genes are also potential biomarkers for the early detection of the disease and/or novel therapeutic targets. Such markers would require rigorous validation *in vitro* and *in vivo*. This work is part of a large body of work ongoing in the Department of Gynaecology at UCL. Genomic and proteomic tools are being used to identify novel candidate biomarkers of early ovarian cancer using both patient tumour/serum samples and *in vitro* modelling approaches. The best candidate biomarkers will ultimately be validated in serum samples from preceeding a diagnosis ovarian cancer, using the unique UKCTOCS cohort of over 200,000 women.

Bibliography

[Aasen et al., 2008] Aasen, T., Raya, A., Barrero, M. J., Garreta, E., Consiglio, A., Gonzalez, F., Vassena, R., Bili?, J., Pekarik, V., Tiscornia, G., Edel, M., Bou, S., and Belmonte, J. C. I. (2008). Efficient and rapid generation of induced pluripotent stem cells from human keratinocytes. *Nat Biotechnol*, 26(11):1276–1284.

[Abdollahi et al., 1997a] Abdollahi, A., Godwin, A. K., Miller, P. D., Getts, L. A., Schultz, D. C., Taguchi, T., Testa, J. R., and Hamilton, T. C. (1997a). Identification of a gene containing zinc-finger motifs based on lost expression in malignantly transformed rat ovarian surface epithelial cells. *Cancer Res*, 57(10):2029–2034.

[Abdollahi et al., 1997b] Abdollahi, A., Roberts, D., Godwin, A. K., Schultz, D. C., Sonoda, G., Testa, J. R., and Hamilton, T. C. (1997b). Identification of a zinc-finger gene at 6q25: a chromosomal region implicated in development of many solid tumors. *Oncogene*, 14(16):1973–1979.

[Ahmed et al., 2007] Ahmed, A. A., Mills, A. D., Ibrahim, A. E. K., Temple, J., Blenkiron, C., Vias, M., Massie, C. E., Iyer, N. G., McGeoch, A., Crawford, R., Nicke, B., Downward, J., Swanton, C., Bell, S. D., Earl, H. M., Laskey, R. A., Caldas, C., and Brenton, J. D. (2007). The extracellular matrix protein tgfbi induces microtubule stabilization and sensitizes ovarian cancers to paclitaxel. *Cancer Cell*, 12(6):514–527.

[Akagi et al., 2009] Akagi, T., Ito, T., Kato, M., Jin, Z., Cheng, Y., Kan, T., Yamamoto, G., Olaru, A., Kawamata, N., Boult, J., Soukiasian, H. J., Miller, C. W., Ogawa, S., Meltzer, S. J., and Koeffler, H. P. (2009). Chromosomal abnormalities and novel disease-related regions in progression from Barrett's esophagus to esophageal adenocarcinoma. *Int. J. Cancer*, 125:2349–2359.

[Allen et al., 2000] Allen, H. J., DiCioccio, R. A., Hohmann, P., Piver, M. S., and Tworek, H. (2000). Microsatellite instability in ovarian and other pelvic carcinomas. *Cancer Genet Cytogenet*, 117(2):163–166.

[Althaus et al., 1994] Althaus, F. R., Hfferer, L., Kleczkowska, H. E., Malanga, M., Naegeli, H., Panzeter, P. L., and Realini, C. A. (1994). Histone shuttling by poly adp-ribosylation. *Mol Cell Biochem*, 138(1-2):53–59.

[Althaus et al., 1990] Althaus, F. R., Naegeli, H., Realini, C., Mathis, G., Loetscher, P., and Mattenberger, M. (1990). The poly-adp-ribosylation system of higher eukaryotes: a protein shuttle mechanism in chromatin? *Acta Biol Hung*, 41(1-3):9–18.

[Altomare et al., 2004] Altomare, D. A., Wang, H. Q., Skele, K. L., Rienzo, A. D., Klein-Szanto, A. J., Godwin, A. K., and Testa, J. R. (2004). Akt and mtor phosphorylation is frequently detected in ovarian cancer and can be targeted to disrupt ovarian tumor cell growth. *Oncogene*, 23(34):5853–5857.

[Alvarez et al., 2001] Alvarez, A. A., Axelrod, J. R., Whitaker, R. S., Isner, P. D., Bentley, R. C., Dodge, R. K., and Rodriguez, G. C. (2001). Thrombospondin-1 expression in epithelial ovarian carcinoma: association with p53 status, tumor angiogenesis, and survival in platinum-treated patients. *Gynecol Oncol*, 82(2):273–278.

[Alvero et al., 2009] Alvero, A. B., Chen, R., Fu, H.-H., Montagna, M., Schwartz, P. E., Rutherford, T., Silasi, D.-A., Steffensen, K. D., Waldstrom, M., Visintin, I., and Mor, G. (2009). Molecular phenotyping of human ovarian cancer stem cells unravels the mechanisms for repair and chemoresistance. *Cell Cycle*, 8(1):158–166.

[Arroyo and Hahn, 2005] Arroyo, J. D. and Hahn, W. C. (2005). Involvement of pp2a in viral and cellular transformation. *Oncogene*, 24(52):7746–7755.

[Auersperg et al., 1995] Auersperg, N., Maines-Bandiera, S., Booth, J. H., Lynch, H. T., Godwin, A. K., and Hamilton, T. C. (1995). Expression of two mucin antigens in cultured human ovarian surface epithelium: influence of a family history of ovarian cancer. *Am J Obstet Gynecol*, 173(2):558–565.

[Auersperg et al., 1997] Auersperg, N., Maines-Bandiera, S. L., and Dyck, H. G. (1997). Ovarian carcinogenesis and the biology of ovarian surface epithelium. *J Cell Physiol*, 173(2):261–265.

[Auersperg et al., 1994] Auersperg, N., Maines-Bandiera, S. L., Dyck, H. G., and Kruk, P. A. (1994). Characterization of cultured human ovarian surface epithelial cells: phenotypic plasticity and premalignant changes. *Lab Invest*, 71(4):510–518.

[Auersperg et al., 2002] Auersperg, N., Ota, T., and Mitchell, G. W. E. (2002). Early events in ovarian epithelial carcinogenesis: progress and problems in experimental approaches. *Int J Gynecol Cancer*, 12(6):691–703.

[Auersperg et al., 1999] Auersperg, N., Pan, J., Grove, B. D., Peterson, T., Fisher, J., Maines-Bandiera, S., Somasiri, A., and Roskelley, C. D. (1999). E-cadherin induces mesenchymal-to-epithelial transition in human ovarian surface epithelium. *Proc Natl Acad Sci U S A*, 96(11):6249–6254.

[Auersperg et al., 1984] Auersperg, N., Siemens, C. H., and Myrdal, S. E. (1984). Human ovarian surface epithelium in primary culture. *In Vitro*, 20(10):743–755.

[Auersperg et al., 2001] Auersperg, N., Wong, A. S., Choi, K. C., Kang, S. K., and Leung, P. C. (2001). Ovarian surface epithelium: biology, endocrinology, and pathology. *Endocr Rev*, 22(2):255–288.

[Baffa et al., 2008] Baffa, R., Fassan, M., Sevignani, C., Vecchione, A., Ishii, H., Giarnieri, E., Iozzo, R. V., Gomella, L. G., and Croce, C. M. (2008). Fez1/lzts1-deficient mice are more susceptible to n-butyl-n-(4-hydroxybutil) nitrosamine (bbn) carcinogenesis. *Carcinogenesis*, 29(4):846–848.

[Bai et al., 2000] Bai, W., Oliveros-Saunders, B., Wang, Q., Acevedo-Duncan, M. E., and Nicosia, S. V. (2000). Estrogen stimulation of ovarian surface epithelial cell proliferation. *In Vitro Cell Dev Biol Anim*, 36(10):657–666.

[Barbolina et al., 2009] Barbolina, M. V., Adley, B. P., Kelly, D. L., Shepard, J., Fought, A. J., Scholtens, D., Penzes, P., Shea, L. D., and Stack, M. S. (2009). Downregulation of connective tissue growth factor by three-dimensional matrix enhances ovarian carcinoma cell invasion. *Int J Cancer*, 125(4):816–825.

[Barbolina et al., 2008] Barbolina, M. V., Adley, B. P., Shea, L. D., and Stack, M. S. (2008). Wilms tumor gene protein 1 is associated with ovarian cancer metastasis and modulates cell invasion. *Cancer*, 112(7):1632–1641.

[Bates and Mercurio, 2005] Bates, R. C. and Mercurio, A. M. (2005). The epithelial-mesenchymal transition (emt) and colorectal cancer progression. *Cancer Biol Ther*, 4(4):365–370.

[Bavik et al., 2006] Bavik, C., Coleman, I., Dean, J. P., Knudsen, B., Plymate, S., and Nelson, P. S. (2006). The gene expression program of prostate fibroblast senescence modulates neoplastic epithelial cell proliferation through paracrine mechanisms. *Cancer Res*, 66(2):794–802.

[Becker and Blanchard, 2007] Becker, J. L. and Blanchard, D. K. (2007). Characterization of primary breast carcinomas grown in three-dimensional cultures. *J Surg Res*, 142(2):256–262.

[Berchuck et al., 2005] Berchuck, A., Iversen, E. S., Lancaster, J. M., Pittman, J., Luo, J., Lee, P., Murphy, S., Dressman, H. K., Febbo, P. G., West, M., Nevins, J. R., and Marks, J. R. (2005). Patterns of gene expression that characterize long-term survival in advanced stage serous ovarian cancers. *Clin Cancer Res*, 11(10):3686–3696.

[Berchuck et al., 2009] Berchuck, A., Iversen, E. S., Luo, J., Clarke, J. P., Horne, H., Levine, D. A., Boyd, J., Alonso, M. A., Secord, A. A., Bernardini, M. Q., Barnett, J. C., Boren, T., Murphy, S. K., Dressman, H. K., Marks, J. R., and Lancaster, J. M. (2009). Microarray analysis of early stage serous ovarian cancers shows profiles predictive of favorable outcome. *Clin Cancer Res*, 15(7):2448–2455.

[Bilsland et al., 2003] Bilsland, A. E., Anderson, C. J., Fletcher-Monaghan, A. J., McGregor, F., Evans, T. R. J., Ganly, I., Knox, R. J., Plumb, J. A., and Keith, W. N. (2003). Selective ablation of human cancer cells by telomerase-specific adenoviral suicide gene therapy vectors expressing bacterial nitroreductase. *Oncogene*, 22(3):370–380.

[Blackmore, 1966] Blackmore, D. K. (1966). The clinical approach to tumours in cage birds. i. the pathology and incidence of neoplasia in cage birds. *J Small Anim Pract*, 7(3):217–223.

[Bodnar et al., 1998] Bodnar, A. G., Ouellette, M., Frolkis, M., Holt, S. E., Chiu, C. P., Morin, G. B., Harley, C. B., Shay, J. W., Lichtsteiner, S., and Wright, W. E. (1998). Extension of life-span by introduction of telomerase into normal human cells. *Science*, 279(5349):349–352.

[Boehm et al., 2005] Boehm, J. S., Hession, M. T., Bulmer, S. E., and Hahn, W. C. (2005). Transformation of human and murine fibroblasts without viral oncoproteins. *Mol Cell Biol*, 25(15):6464–6474.

[Boerboom et al., 2006] Boerboom, D., White, L. D., Dalle, S., Courty, J., and Richards, J. S. (2006). Dominant-stable beta-catenin expression causes cell fate alterations and wnt signaling antagonist expression in a murine granulosa cell tumor model. *Cancer Res*, 66(4):1964–1973.

[Bogni et al., 2006] Bogni, A., Cheng, C., Liu, W., Yang, W., Pfeffer, J., Mukatira, S., French, D., Downing, J. R., Pui, C.-H., and Relling, M. V. (2006). Genome-wide approach to identify risk factors for therapy-related myeloid leukemia. *Leukemia*, 20(2):239–246.

[Bond et al., 2004] Bond, J., Jones, C., Haughton, M., DeMicco, C., Kipling, D., and Wynford-Thomas, D. (2004). Direct evidence from sirna-directed "knock down" that

p16(ink4a) is required for human fibroblast senescence and for limiting ras-induced epithelial cell proliferation. *Exp Cell Res*, 292(1):151–156.

[Bonome et al., 2005] Bonome, T., Lee, J.-Y., Park, D.-C., Radonovich, M., Pise-Masison, C., Brady, J., Gardner, G. J., Hao, K., Wong, W. H., Barrett, J. C., Lu, K. H., Sood, A. K., Gershenson, D. M., Mok, S. C., and Birrer, M. J. (2005). Expression profiling of serous low malignant potential, low-grade, and high-grade tumors of the ovary. *Cancer Res*, 65(22):10602–10612.

[Boudreau and Varner, 2004] Boudreau, N. J. and Varner, J. A. (2004). The homeobox transcription factor hox d3 promotes integrin alpha5beta1 expression and function during angiogenesis. *J Biol Chem*, 279(6):4862–4868.

[Boulikas, 1989] Boulikas, T. (1989). Dna strand breaks alter histone adp-ribosylation. *Proc Natl Acad Sci U S A*, 86(10):3499–3503.

[Boulikas, 1990] Boulikas, T. (1990). Poly(adp-ribosylated) histones in chromatin replication. *J Biol Chem*, 265(24):14638–14647.

[Brown and Palmer, 2009] Brown, P. O. and Palmer, C. (2009). The preclinical natural history of serous ovarian cancer: defining the target for early detection. *PLoS Med*, 6(7):e1000114.

[Brown et al., 1997] Brown, R., Hirst, G. L., Gallagher, W. M., McIlwrath, A. J., Margison, G. P., van der Zee, A. G., and Anthoney, D. A. (1997). hmlh1 expression and cellular responses of ovarian tumour cells to treatment with cytotoxic anticancer agents. *Oncogene*, 15(1):45–52.

[Brustmann, 2005] Brustmann, H. (2005). Immunohistochemical detection of human telomerase reverse transcriptase (htert) and c-kit in serous ovarian carcinoma: a clinicopathologic study. *Gynecol Oncol*, 98(3):396–402.

[Buller et al., 2001] Buller, R. E., Shahin, M. S., Holmes, R. W., Hatterman, M., Kirby, P. A., and Sood, A. K. (2001). p53 mutations and microsatellite instability in ovarian cancer: Yin and yang. *Am J Obstet Gynecol*, 184(5):891–902; discussion 902–3.

[Burleson et al., 2006] Burleson, K. M., Boente, M. P., Pambuccian, S. E., and Skubitz, A. P. N. (2006). Disaggregation and invasion of ovarian carcinoma ascites spheroids. *J Transl Med*, 4:6.

[Burleson et al., 2004a] Burleson, K. M., Casey, R. C., Skubitz, K. M., Pambuccian, S. E., Oegema, T. R., and Skubitz, A. P. N. (2004a). Ovarian carcinoma ascites spheroids

adhere to extracellular matrix components and mesothelial cell monolayers. *Gynecol Oncol*, 93(1):170–181.

[Burleson et al., 2004b] Burleson, K. M., Hansen, L. K., and Skubitz, A. P. N. (2004b). Ovarian carcinoma spheroids disaggregate on type i collagen and invade live human mesothelial cell monolayers. *Clin Exp Metastasis*, 21(8):685–697.

[Buz'Zard and Lau, 2007] Buz'Zard, A. R. and Lau, B. H. S. (2007). Pycnogenol reduces talc-induced neoplastic transformation in human ovarian cell cultures. *Phytother Res*, 21(6):579–586.

[Cai et al., 2006] Cai, K. Q., Klein-Szanto, A., Karthik, D., Edelson, M., Daly, M. B., Ozols, R. F., Lynch, H. T., Godwin, A. K., and Xu, X.-X. (2006). Age-dependent morphological alterations of human ovaries from populations with and without brca mutations. *Gynecol Oncol*, 103(2):719–728.

[Califano et al., 2009] Califano, D., Pignata, S., Pisano, C., Greggi, S., Laurelli, G., Losito, N. S., Ottaiano, A., Gallipoli, A., Pasquinelli, R., Simone, V. D., Cirombella, R., Fusco, A., and Chiappetta, G. (2009). Fez1/lzts1 protein expression in ovarian cancer. *J Cell Physiol*.

[Callahan et al., 2007] Callahan, M. J., Crum, C. P., Medeiros, F., Kindelberger, D. W., Elvin, J. A., Garber, J. E., Feltmate, C. M., Berkowitz, R. S., and Muto, M. G. (2007). Primary fallopian tube malignancies in brca-positive women undergoing surgery for ovarian cancer risk reduction. *J Clin Oncol*, 25(25):3985–3990.

[Campbell et al., 2004] Campbell, I. G., Russell, S. E., Choong, D. Y. H., Montgomery, K. G., Ciavarella, M. L., Hooi, C. S. F., Cristiano, B. E., Pearson, R. B., and Phillips, W. A. (2004). Mutation of the pik3ca gene in ovarian and breast cancer. *Cancer Res*, 64(21):7678–7681.

[Capo-Chichi et al., 2002] Capo-Chichi, C. D., Smith, E. R., Yang, D.-H., Roland, I. H., Vanderveer, L., Cohen, C., Hamilton, T. C., Godwin, A. K., and Xu, X.-X. (2002). Dynamic alterations of the extracellular environment of ovarian surface epithelial cells in premalignant transformation, tumorigenicity, and metastasis. *Cancer*, 95(8):1802–1815.

[Castagnola and Giaretti, 2005] Castagnola, P. and Giaretti, W. (2005). Mutant kras, chromosomal instability and prognosis in colorectal cancer. *Biochim Biophys Acta*, 1756(2):115–125.

[Catass et al., 2004] Catass, L., Bussaglia, E., Rodrguez, I., Gallardo, A., Pons, C., Irving, J. A., and Prat, J. (2004). Molecular genetic alterations in endometrioid carcinomas of

the ovary: similar frequency of beta-catenin abnormalities but lower rate of microsatellite instability and pten alterations than in uterine endometrioid carcinomas. *Hum Pathol*, 35(11):1360–1368.

[Chang et al., 2004] Chang, H. Y., Sneddon, J. B., Alizadeh, A. A., Sood, R., West, R. B., Montgomery, K., Chi, J.-T., van de Rijn, M., Botstein, D., and Brown, P. O. (2004). Gene expression signature of fibroblast serum response predicts human cancer progression: similarities between tumors and wounds. *PLoS Biol*, 2(2):E7.

[Chen et al., 2009] Chen, L., Zhu, Z., Sun, X., Dong, X.-Y., Wei, J., Gu, F., Sun, Y.-L., Zhou, J., Dong, J.-T., and Fu, L. (2009). Down-regulation of tumor suppressor gene fez1/lzts1 in breast carcinoma involves promoter methylation and associates with metastasis. *Breast Cancer Res Treat*, 116(3):471–478.

[Chen et al., 2008] Chen, Y.-N., Chen, H., Xu, Y., Zhang, X., and Luo, Y. (2008). Expression of pituitary homeobox 1 gene in human gastric carcinogenesis and its clinicopathological significance. *World J Gastroenterol*, 14(2):292–297.

[Cheng et al., 1992] Cheng, J. Q., Godwin, A. K., Bellacosa, A., Taguchi, T., Franke, T. F., Hamilton, T. C., Tsichlis, P. N., and Testa, J. R. (1992). Akt2, a putative oncogene encoding a member of a subfamily of protein-serine/threonine kinases, is amplified in human ovarian carcinomas. *Proc Natl Acad Sci U S A*, 89(19):9267–9271.

[Cheng et al., 2005] Cheng, W., Liu, J., Yoshida, H., Rosen, D., and Naora, H. (2005). Lineage infidelity of epithelial ovarian cancers is controlled by hox genes that specify regional identity in the reproductive tract. *Nat Med*, 11(5):531–537.

[Chodankar et al., 2005] Chodankar, R., Kwang, S., Sangiorgi, F., Hong, H., Yen, H.-Y., Deng, C., Pike, M. C., Shuler, C. F., Maxson, R., and Dubeau, L. (2005). Cell-nonautonomous induction of ovarian and uterine serous cystadenomas in mice lacking a functional brca1 in ovarian granulosa cells. *Curr Biol*, 15(6):561–565.

[Chu et al., 1998] Chu, K., Boutin, J. M., Breton, C., and Zingg, H. H. (1998). Nuclear orphan receptors COUP-TFII and Ear-2: presence in oxytocin-producing uterine cells and functional interaction with the oxytocin gene promoter. *Mol. Cell. Endocrinol.*, 137:145–154.

[Collado et al., 2005] Collado, M., Gil, J., Efeyan, A., Guerra, C., Schuhmacher, A. J., Barradas, M., Bengura, A., Zaballos, A., Flores, J. M., Barbacid, M., Beach, D., and Serrano, M. (2005). Tumour biology: senescence in premalignant tumours. *Nature*, 436(7051):642.

[Connolly et al., 2003] Connolly, D. C., Bao, R., Nikitin, A. Y., Stephens, K. C., Poole, T. W., Hua, X., Harris, S. S., Vanderhyden, B. C., and Hamilton, T. C. (2003). Female mice chimeric for expression of the simian virus 40 tag under control of the misiir promoter develop epithelial ovarian cancer. *Cancer Res*, 63(6):1389–1397.

[Consortium et al., 2006] Consortium, M. A. Q. C., Shi, L., Reid, L. H., Jones, W. D., Shippy, R., Warrington, J. A., Baker, S. C., Collins, P. J., de Longueville, F., Kawasaki, E. S., Lee, K. Y., Luo, Y., Sun, Y. A., Willey, J. C., Setterquist, R. A., Fischer, G. M., Tong, W., Dragan, Y. P., Dix, D. J., Frueh, F. W., Goodsaid, F. M., Herman, D., Jensen, R. V., Johnson, C. D., Lobenhofer, E. K., Puri, R. K., Schrf, U., Thierry-Mieg, J., Wang, C., Wilson, M., Wolber, P. K., Zhang, L., Amur, S., Bao, W., Barbacioru, C. C., Lucas, A. B., Bertholet, V., Boysen, C., Bromley, B., Brown, D., Brunner, A., Canales, R., Cao, X. M., Cebula, T. A., Chen, J. J., Cheng, J., Chu, T.-M., Chudin, E., Corson, J., Corton, J. C., Croner, L. J., Davies, C., Davison, T. S., Delenstarr, G., Deng, X., Dorris, D., Eklund, A. C., hui Fan, X., Fang, H., Fulmer-Smentek, S., Fuscoe, J. C., Gallagher, K., Ge, W., Guo, L., Guo, X., Hager, J., Haje, P. K., Han, J., Han, T., Harbottle, H. C., Harris, S. C., Hatchwell, E., Hauser, C. A., Hester, S., Hong, H., Hurban, P., Jackson, S. A., Ji, H., Knight, C. R., Kuo, W. P., LeClerc, J. E., Levy, S., Li, Q.-Z., Liu, C., Liu, Y., Lombardi, M. J., Ma, Y., Magnuson, S. R., Maqsodi, B., McDaniel, T., Mei, N., Myklebost, O., Ning, B., Novoradovskaya, N., Orr, M. S., Osborn, T. W., Papallo, A., Patterson, T. A., Perkins, R. G., Peters, E. H., Peterson, R., Philips, K. L., Pine, P. S., Pusztai, L., Qian, F., Ren, H., Rosen, M., Rosenzweig, B. A., Samaha, R. R., Schena, M., Schroth, G. P., Shchegrova, S., Smith, D. D., Staedtler, F., Su, Z., Sun, H., Szallasi, Z., Tezak, Z., Thierry-Mieg, D., Thompson, K. L., Tikhonova, I., Turpaz, Y., Vallanat, B., Van, C., Walker, S. J., Wang, S. J., Wang, Y., Wolfinger, R., Wong, A., Wu, J., Xiao, C., Xie, Q., Xu, J., Yang, W., Zhang, L., Zhong, S., Zong, Y., and Slikker, W. (2006). The microarray quality control (maqc) project shows inter- and intraplatform reproducibility of gene expression measurements. *Nat Biotechnol*, 24(9):1151–1161.

[Coppe et al., 2006] Coppe, J.-P., Kauser, K., Campisi, J., and Beausjour, C. M. (2006). Secretion of vascular endothelial growth factor by primary human fibroblasts at senescence. *J Biol Chem*, 281(40):29568–29574.

[Coppe et al., 2008] Coppe, J.-P., Patil, C. K., Rodier, F., Sun, Y., Muoz, D. P., Goldstein, J., Nelson, P. S., Desprez, P.-Y., and Campisi, J. (2008). Senescence-associated secretory phenotypes reveal cell-nonautonomous functions of oncogenic ras and the p53 tumor suppressor. *PLoS Biol*, 6(12):2853–2868.

[Couzinet et al., 2001] Couzinet, B., Meduri, G., Lecce, M. G., Young, J., Brailly, S., Loosfelt, H., Milgrom, E., and Schaison, G. (2001). The postmenopausal ovary is not a major androgen-producing gland. *J Clin Endocrinol Metab*, 86(10):5060–5066.

[Crijnen et al., 2005] Crijnen, T. E. M., Janssen-Heijnen, M. L. G., Gelderblom, H., Morreau, J., Nooij, M. A., Kenter, G. G., and Vasen, H. F. A. (2005). Survival of patients with ovarian cancer due to a mismatch repair defect. *Fam Cancer*, 4(4):301–305.

[Curley et al., 2009] Curley, M. D., Therrien, V. A., Cummings, C. L., Sergent, P. A., Koulouris, C. R., Friel, A. M., Roberts, D. J., Seiden, M. V., Scadden, D. T., Rueda, B. R., and Foster, R. (2009). Cd133 expression defines a tumor initiating cell population in primary human ovarian cancer. *Stem Cells*.

[Cvetkovic et al., 2004] Cvetkovic, D., Pisarcik, D., Lee, C., Hamilton, T. C., and Abdollahi, A. (2004). Altered expression and loss of heterozygosity of the lot1 gene in ovarian cancer. *Gynecol Oncol*, 95(3):449–455.

[Dafou et al., 2009] Dafou, D., Ramus, S. J., Choi, K., Grun, B., Trott, D. A., Newbold, R. F., Jacobs, I. J., Jones, C., and Gayther, S. A. (2009). Chromosomes 6 and 18 induce neoplastic suppression in epithelial ovarian cancer cells. *Int J Cancer*, 124(5):1037–1044.

[Damiano et al., 1999] Damiano, J. S., Cress, A. E., Hazlehurst, L. A., Shtil, A. A., and Dalton, W. S. (1999). Cell adhesion mediated drug resistance (cam-dr): role of integrins and resistance to apoptosis in human myeloma cell lines. *Blood*, 93(5):1658–1667.

[Darbro et al., 2006] Darbro, B. W., Lee, K. M., Nguyen, N. K., Domann, F. E., and Klingelhutz, A. J. (2006). Methylation of the p16(ink4a) promoter region in telomerase immortalized human keratinocytes co-cultured with feeder cells. *Oncogene*, 25(56):7421–7433.

[Davies et al., 2003] Davies, B. R., Steele, I. A., Edmondson, R. J., Zwolinski, S. A., Saretzki, G., von Zglinicki, T., and O'Hare, M. J. (2003). Immortalisation of human ovarian surface epithelium with telomerase and temperature-sensitive sv40 large t antigen. *Exp Cell Res*, 288(2):390–402.

[de la Cuesta et al., 1996] de la Cuesta, R. S., Eichhorn, J. H., Rice, L. W., Fuller, A. F., Nikrui, N., and Goff, B. A. (1996). Histologic transformation of benign endometriosis to early epithelial ovarian cancer. *Gynecol Oncol*, 60(2):238–244.

[Dehari et al., 2007] Dehari, R., Kurman, R. J., Logani, S., and Shih, I.-M. (2007). The development of high-grade serous carcinoma from atypical proliferative (borderline) serous tumors and low-grade micropapillary serous carcinoma: a morphologic and molecular genetic analysis. *Am J Surg Pathol*, 31(7):1007–1012.

[Denoyelle et al., 2006] Denoyelle, C., Abou-Rjaily, G., Bezrookove, V., Verhaegen, M., Johnson, T. M., Fullen, D. R., Pointer, J. N., Gruber, S. B., Su, L. D., Nikiforov, M. A., Kaufman, R. J., Bastian, B. C., and Soengas, M. S. (2006). Anti-oncogenic role of the endoplasmic reticulum differentially activated by mutations in the mapk pathway. *Nat Cell Biol*, 8(10):1053–1063.

[DePinho, 2000] DePinho, R. A. (2000). The age of cancer. *Nature*, 408(6809):248–254.

[Dilworth, 2002] Dilworth, S. M. (2002). Polyoma virus middle t antigen and its role in identifying cancer-related molecules. *Nat Rev Cancer*, 2(12):951–956.

[Dimova et al., 2006] Dimova, I., Raitcheva, S., Dimitrov, R., Doganov, N., and Toncheva, D. (2006). Correlations between c-myc gene copy-number and clinicopathological parameters of ovarian tumours. *Eur J Cancer*, 42(5):674–679.

[Dimri et al., 1995] Dimri, G. P., Lee, X., Basile, G., Acosta, M., Scott, G., Roskelley, C., Medrano, E. E., Linskens, M., Rubelj, I., and Pereira-Smith, O. (1995). A biomarker that identifies senescent human cells in culture and in aging skin in vivo. *Proc Natl Acad Sci U S A*, 92(20):9363–9367.

[Dinulescu et al., 2005] Dinulescu, D. M., Ince, T. A., Quade, B. J., Shafer, S. A., Crowley, D., and Jacks, T. (2005). Role of k-ras and pten in the development of mouse models of endometriosis and endometrioid ovarian cancer. *Nat Med*, 11(1):63–70.

[Drayton et al., 2004] Drayton, S., Brookes, S., Rowe, J., and Peters, G. (2004). The significance of p16ink4a in cell defenses against transformation. *Cell Cycle*, 3(5):611–615.

[Drayton et al., 2003] Drayton, S., Rowe, J., Jones, R., Vatcheva, R., Cuthbert-Heavens, D., Marshall, J., Fried, M., and Peters, G. (2003). Tumor suppressor p16ink4a determines sensitivity of human cells to transformation by cooperating cellular oncogenes. *Cancer Cell*, 4(4):301–310.

[Du et al., 2008] Du, P., Kibbe, W. A., and Lin, S. M. (2008). lumi: a pipeline for processing illumina microarray. *Bioinformatics*, 24(13):1547–1548.

[Dubeau, 1999] Dubeau, L. (1999). The cell of origin of ovarian epithelial tumors and the ovarian surface epithelium dogma: does the emperor have no clothes? *Gynecol Oncol*, 72(3):437–442.

[Dubeau, 2008] Dubeau, L. (2008). The cell of origin of ovarian epithelial tumours. *Lancet Oncol*, 9(12):1191–1197.

[Dyck et al., 1996] Dyck, H. G., Hamilton, T. C., Godwin, A. K., Lynch, H. T., Maines-Bandiera, S., and Auersperg, N. (1996). Autonomy of the epithelial phenotype in human ovarian surface epithelium: changes with neoplastic progression and with a family history of ovarian cancer. *Int J Cancer*, 69(6):429–436.

[Easton et al., 2007] Easton, D. F., Pooley, K. A., Dunning, A. M., Pharoah, P. D. P., Thompson, D., Ballinger, D. G., Struewing, J. P., Morrison, J., Field, H., Luben, R., Wareham, N., Ahmed, S., Healey, C. S., Bowman, R., collaborators, S. E. A. R. C. H., Meyer, K. B., Haiman, C. A., Kolonel, L. K., Henderson, B. E., Marchand, L. L., Brennan, P., Sangrajrang, S., Gaborieau, V., Odefrey, F., Shen, C.-Y., Wu, P.-E., Wang, H.-C., Eccles, D., Evans, D. G., Peto, J., Fletcher, O., Johnson, N., Seal, S., Stratton, M. R., Rahman, N., Chenevix-Trench, G., Bojesen, S. E., Nordestgaard, B. G., Axelsson, C. K., Garcia-Closas, M., Brinton, L., Chanock, S., Lissowska, J., Peplonska, B., Nevanlinna, H., Fagerholm, R., Eerola, H., Kang, D., Yoo, K.-Y., Noh, D.-Y., Ahn, S.-H., Hunter, D. J., Hankinson, S. E., Cox, D. G., Hall, P., Wedren, S., Liu, J., Low, Y.-L., Bogdanova, N., Schrmann, P., Drk, T., Tollenaar, R. A. E. M., Jacobi, C. E., Devilee, P., Klijn, J. G. M., Sigurdson, A. J., Doody, M. M., Alexander, B. H., Zhang, J., Cox, A., Brock, I. W., MacPherson, G., Reed, M. W. R., Couch, F. J., Goode, E. L., Olson, J. E., Meijers-Heijboer, H., van den Ouweland, A., Uitterlinden, A., Rivadeneira, F., Milne, R. L., Ribas, G., Gonzalez-Neira, A., Benitez, J., Hopper, J. L., McCredie, M., Southey, M., Giles, G. G., Schroen, C., Justenhoven, C., Brauch, H., Hamann, U., Ko, Y.-D., Spurdle, A. B., Beesley, J., Chen, X., kConFab, Group, A. O. C. S. M., Mannermaa, A., Kosma, V.-M., Kataja, V., Hartikainen, J., Day, N. E., Cox, D. R., and Ponder, B. A. J. (2007). Genome-wide association study identifies novel breast cancer susceptibility loci. *Nature*, 447(7148):1087–1093.

[Edmondson and Monaghan, 2001] Edmondson, R. J. and Monaghan, J. M. (2001). The epidemiology of ovarian cancer. *Int J Gynecol Cancer*, 11(6):423–429.

[Eeles et al., 2008] Eeles, R. A., Kote-Jarai, Z., Giles, G. G., Olama, A. A. A., Guy, M., Jugurnauth, S. K., Mulholland, S., Leongamornlert, D. A., Edwards, S. M., Morrison, J., Field, H. I., Southey, M. C., Severi, G., Donovan, J. L., Hamdy, F. C., Dearnaley, D. P., Muir, K. R., Smith, C., Bagnato, M., Ardern-Jones, A. T., Hall, A. L., O'Brien, L. T., Gehr-Swain, B. N., Wilkinson, R. A., Cox, A., Lewis, S., Brown, P. M., Jhavar, S. G., Tymrakiewicz, M., Lophatananon, A., Bryant, S. L., Collaborators, U. K. G. P. C. S., of Urological Surgeons' Section of Oncology, B. A., Collaborators, U. K. P. S., Horwich, A., Huddart, R. A., Khoo, V. S., Parker, C. C., Woodhouse, C. J., Thompson, A., Christmas, T., Ogden, C., Fisher, C., Jamieson, C., Cooper, C. S., English, D. R., Hopper, J. L., Neal, D. E., and Easton, D. F. (2008). Multiple newly identified loci associated with prostate cancer susceptibility. *Nat Genet*, 40(3):316–321.

[Ehlers et al., 2005] Ehlers, J. P., Worley, L., Onken, M. D., and Harbour, J. W. (2005). Ddef1 is located in an amplified region of chromosome 8q and is overexpressed in uveal melanoma. *Clin Cancer Res*, 11(10):3609–3613.

[Elenbaas et al., 2001] Elenbaas, B., Spirio, L., Koerner, F., Fleming, M. D., Zimonjic, D. B., Donaher, J. L., Popescu, N. C., Hahn, W. C., and Weinberg, R. A. (2001). Human breast cancer cells generated by oncogenic transformation of primary mammary epithelial cells. *Genes Dev*, 15(1):50–65.

[Elmasry and Gayther, 2006] Elmasry, K. and Gayther, S. A. (2006). Ovarian cancer aetiology: facts and fiction. *J Fam Plann Reprod Health Care*, 32(2):82–86.

[Eskenazi and Warner, 1997] Eskenazi, B. and Warner, M. L. (1997). Epidemiology of endometriosis. *Obstet Gynecol Clin North Am*, 24(2):235–258.

[Esteller et al., 1998] Esteller, M., Levine, R., Baylin, S. B., Ellenson, L. H., and Herman, J. G. (1998). Mlh1 promoter hypermethylation is associated with the microsatellite instability phenotype in sporadic endometrial carcinomas. *Oncogene*, 17(18):2413–2417.

[Faleiro-Rodrigues et al., 2004] Faleiro-Rodrigues, C., Macedo-Pinto, I., Pereira, D., Ferreira, V. M., and Lopes, C. S. (2004). Association of e-cadherin and beta-catenin immunoexpression with clinicopathologic features in primary ovarian carcinomas. *Hum Pathol*, 35(6):663–669.

[Farmer et al., 2005] Farmer, H., McCabe, N., Lord, C. J., Tutt, A. N. J., Johnson, D. A., Richardson, T. B., Santarosa, M., Dillon, K. J., Hickson, I., Knights, C., Martin, N. M. B., Jackson, S. P., Smith, G. C. M., and Ashworth, A. (2005). Targeting the dna repair defect in brca mutant cells as a therapeutic strategy. *Nature*, 434(7035):917–921.

[Fata et al., 2004] Fata, J. E., Werb, Z., and Bissell, M. J. (2004). Regulation of mammary gland branching morphogenesis by the extracellular matrix and its remodeling enzymes. *Breast Cancer Res*, 6(1):1–11.

[Fathalla, 1971] Fathalla, M. F. (1971). Incessant ovulation–a factor in ovarian neoplasia? *Lancet*, 2(7716):163.

[Fearon and Vogelstein, 1990] Fearon, E. R. and Vogelstein, B. (1990). A genetic model for colorectal tumorigenesis. *Cell*, 61(5):759–767.

[Feng et al., 2009] Feng, L., Huang, J., and Chen, J. (2009). MERIT40 facilitates BRCA1 localization and DNA damage repair. *Genes Dev.*, 23:719–728.

[Fong et al., 2009] Fong, P. C., Boss, D. S., Yap, T. A., Tutt, A., Wu, P., Mergui-Roelvink, M., Mortimer, P., Swaisland, H., Lau, A., O'Connor, M. J., Ashworth, A., Carmichael, J., Kaye, S. B., Schellens, J. H. M., and de Bono, J. S. (2009). Inhibition of poly(adp-ribose) polymerase in tumors from brca mutation carriers. *N Engl J Med*, 361(2):123–134.

[Forbes et al., 2006] Forbes, S., Clements, J., Dawson, E., Bamford, S., Webb, T., Dogan, A., Flanagan, A., Teague, J., Wooster, R., Futreal, P. A., and Stratton, M. R. (2006). Cosmic 2005. *Br J Cancer*, 94(2):318–322.

[Freyer and Sutherland, 1980] Freyer, J. P. and Sutherland, R. M. (1980). Selective dissociation and characterization of cells from different regions of multicell tumor spheroids. *Cancer Res*, 40(11):3956–3965.

[Friedrich et al., 2007] Friedrich, J., Ebner, R., and Kunz-Schughart, L. A. (2007). Experimental anti-tumor therapy in 3-d: spheroids–old hat or new challenge? *Int J Radiat Biol*, 83(11-12):849–871.

[Friedrichsen et al., 2005] Friedrichsen, S., Heuer, H., Christ, S., Cuthill, D., Bauer, K., and Raivich, G. (2005). Gene expression of connective tissue growth factor in adult mouse. *Growth Factors*, 23(1):43–53.

[Friedrichsen et al., 2003] Friedrichsen, S., Heuer, H., Christ, S., Winckler, M., Brauer, D., Bauer, K., and Raivich, G. (2003). Ctgf expression during mouse embryonic development. *Cell Tissue Res*, 312(2):175–188.

[Fujita et al., 2003] Fujita, M., Enomoto, T., and Murata, Y. (2003). Genetic alterations in ovarian carcinoma: with specific reference to histological subtypes. *Mol Cell Endocrinol*, 202(1-2):97–99.

[Garson et al., 2005] Garson, K., Shaw, T. J., Clark, K. V., Yao, D.-S., and Vanderhyden, B. C. (2005). Models of ovarian cancer–are we there yet? *Mol Cell Endocrinol*, 239(1-2):15–26.

[Gayther et al., 1999] Gayther, S. A., Russell, P., Harrington, P., Antoniou, A. C., Easton, D. F., and Ponder, B. A. (1999). The contribution of germline brca1 and brca2 mutations to familial ovarian cancer: no evidence for other ovarian cancer-susceptibility genes. *Am J Hum Genet*, 65(4):1021–1029.

[Geisler et al., 2003] Geisler, J. P., Goodheart, M. J., Sood, A. K., Holmes, R. J., Hatterman-Zogg, M. A., and Buller, R. E. (2003). Mismatch repair gene expression defects contribute to microsatellite instability in ovarian carcinoma. *Cancer*, 98(10):2199–2206.

[Gemignani et al., 2003] Gemignani, M. L., Schlaerth, A. C., Bogomolniy, F., Barakat, R. R., Lin, O., Soslow, R., Venkatraman, E., and Boyd, J. (2003). Role of kras and braf gene mutations in mucinous ovarian carcinoma. *Gynecol Oncol*, 90(2):378–381.

[Geyer et al., 2009] Geyer, J. T., Lpez-Garca, M. A., Snchez-Estevez, C., Sarri, D., Moreno-Bueno, G., Franceschetti, I., Palacios, J., and Oliva, E. (2009). Pathogenetic pathways in ovarian endometrioid adenocarcinoma: a molecular study of 29 cases. *Am J Surg Pathol*, 33(8):1157–1163.

[Ghosh et al., 2005] Ghosh, S., Spagnoli, G. C., Martin, I., Ploegert, S., Demougin, P., Heberer, M., and Reschner, A. (2005). Three-dimensional culture of melanoma cells profoundly affects gene expression profile: a high density oligonucleotide array study. *J Cell Physiol*, 204(2):522–531.

[Ghoussaini et al., 2008] Ghoussaini, M., Song, H., Koessler, T., Olama, A. A. A., Kote-Jarai, Z., Driver, K. E., Pooley, K. A., Ramus, S. J., Kjaer, S. K., Hogdall, E., DiCioccio, R. A., Whittemore, A. S., Gayther, S. A., Giles, G. G., Guy, M., Edwards, S. M., Morrison, J., Donovan, J. L., Hamdy, F. C., Dearnaley, D. P., Ardern-Jones, A. T., Hall, A. L., O'Brien, L. T., Gehr-Swain, B. N., Wilkinson, R. A., Brown, P. M., Hopper, J. L., Neal, D. E., Pharoah, P. D. P., Ponder, B. A. J., Eeles, R. A., Easton, D. F., Dunning, A. M., of Urological Surgeons' Section of Oncology, U. K. G. P. C. S. C. A., and Collaborators, U. K. P. S. (2008). Multiple loci with different cancer specificities within the 8q24 gene desert. *J Natl Cancer Inst*, 100(13):962–966.

[Gire et al., 2000] Gire, V., Marshall, C., and Wynford-Thomas, D. (2000). Pi-3-kinase is an essential anti-apoptotic effector in the proliferative response of primary human epithelial cells to mutant ras. *Oncogene*, 19(19):2269–2276.

[Godwin et al., 1992] Godwin, A. K., Testa, J. R., Handel, L. M., Liu, Z., Vanderveer, L. A., Tracey, P. A., and Hamilton, T. C. (1992). Spontaneous transformation of rat ovarian surface epithelial cells: association with cytogenetic changes and implications of repeated ovulation in the etiology of ovarian cancer. *J Natl Cancer Inst*, 84(8):592–601.

[Goodchild, 1969] Goodchild, W. M. (1969). Adenocarcinoma of the oviduct in laying hens. *Vet Rec*, 84(5):122.

[Gourley et al., 2002] Gourley, C., Al-Nafussi, A., Abdulkader, M., Smyth, J. F., and Gabra, H. (2002). Malignant mixed mesodermal tumours: biology and clinical aspects. *Eur J Cancer*, 38(11):1437–1446.

[Gowen et al., 1996] Gowen, L. C., Johnson, B. L., Latour, A. M., Sulik, K. K., and Koller, B. H. (1996). Brca1 deficiency results in early embryonic lethality characterized by neuroepithelial abnormalities. *Nat Genet*, 12(2):191–194.

[Gras et al., 2001] Gras, E., Catasus, L., Argelles, R., Moreno-Bueno, G., Palacios, J., Gamallo, C., Matias-Guiu, X., and Prat, J. (2001). Microsatellite instability, mlh-1 promoter hypermethylation, and frameshift mutations at coding mononucleotide repeat microsatellites in ovarian tumors. *Cancer*, 92(11):2829–2836.

[Greenaway et al., 2009] Greenaway, J., Henkin, J., Lawler, J., Moorehead, R., and Petrik, J. (2009). Abt-510 induces tumor cell apoptosis and inhibits ovarian tumor growth in an orthotopic, syngeneic model of epithelial ovarian cancer. *Mol Cancer Ther*, 8(1):64–74.

[Grun et al., 2009] Grun, B., Benjamin, E., Sinclair, J., Timms, J. F., Jacobs, I. J., Gayther, S. A., and Dafou, D. (2009). Three-dimensional in vitro cell biology models of ovarian and endometrial cancer. *Cell Prolif*, 42(2):219–228.

[Ha et al., 2008] Ha, V. L., Bharti, S., Inoue, H., Vass, W. C., Campa, F., Nie, Z., de Gramont, A., Ward, Y., and Randazzo, P. A. (2008). Asap3 is a focal adhesion-associated arf gap that functions in cell migration and invasion. *J Biol Chem*, 283(22):14915–14926.

[Haga et al., 2007] Haga, K., ichi Ohno, S., Yugawa, T., Narisawa-Saito, M., Fujita, M., Sakamoto, M., Galloway, D. A., and Kiyono, T. (2007). Efficient immortalization of primary human cells by p16ink4a-specific short hairpin rna or bmi-1, combined with introduction of htert. *Cancer Sci*, 98(2):147–154.

[Hahn et al., 1999] Hahn, W. C., Counter, C. M., Lundberg, A. S., Beijersbergen, R. L., Brooks, M. W., and Weinberg, R. A. (1999). Creation of human tumour cells with defined genetic elements. *Nature*, 400(6743):464–468.

[Hammond et al., 1984] Hammond, S. L., Ham, R. G., and Stampfer, M. R. (1984). Serum-free growth of human mammary epithelial cells: rapid clonal growth in defined medium and extended serial passage with pituitary extract. *Proc Natl Acad Sci U S A*, 81(17):5435–5439.

[Hanahan and Weinberg, 2000] Hanahan, D. and Weinberg, R. A. (2000). The hallmarks of cancer. *Cell*, 100(1):57–70.

[Hansen et al., 2003] Hansen, S. L., Myers, C. A., Charboneau, A., Young, D. M., and Boudreau, N. (2003). Hoxd3 accelerates wound healing in diabetic mice. *Am J Pathol*, 163(6):2421–2431.

[Hayflick, 1965] Hayflick, L. (1965). The limited in vitro lifetime of human diploid cell strains. *Exp Cell Res*, 37:614–636.

[Heinzelmann-Schwarz et al., 2006] Heinzelmann-Schwarz, V. A., Gardiner-Garden, M., Henshall, S. M., Scurry, J. P., Scolyer, R. A., Smith, A. N., Bali, A., Bergh, P. V., Baron-Hay, S., Scott, C., Fink, D., Hacker, N. F., Sutherland, R. L., and O'Brien, P. M. (2006). A distinct molecular profile associated with mucinous epithelial ovarian cancer. *Br J Cancer*, 94(6):904–913.

[Helleman et al., 2006] Helleman, J., van Staveren, I. L., Dinjens, W. N. M., van Kuijk, P. F., Ritstier, K., Ewing, P. C., van der Burg, M. E. L., Stoter, G., and Berns, E. M. J. J. (2006). Mismatch repair and treatment resistance in ovarian cancer. *BMC Cancer*, 6:201.

[Herbert et al., 2002] Herbert, B.-S., Wright, W. E., and Shay, J. W. (2002). p16(ink4a) inactivation is not required to immortalize human mammary epithelial cells. *Oncogene*, 21(51):7897–7900.

[Herbig et al., 2006] Herbig, U., Ferreira, M., Condel, L., Carey, D., and Sedivy, J. M. (2006). Cellular senescence in aging primates. *Science*, 311(5765):1257.

[Hermann-Kleiter et al., 2008] Hermann-Kleiter, N., Gruber, T., Lutz-Nicoladoni, C., Thuille, N., Fresser, F., Labi, V., Schiefermeier, N., Warnecke, M., Huber, L., Villunger, A., Eichele, G., Kaminski, S., and Baier, G. (2008). The nuclear orphan receptor NR2F6 suppresses lymphocyte activation and T helper 17-dependent autoimmunity. *Immunity*, 29:205–216.

[Hirst et al., 2009] Hirst, J. E., Gard, G. B., McIllroy, K., Nevell, D., and Field, M. (2009). High rates of occult fallopian tube cancer diagnosed at prophylactic bilateral salpingo-oophorectomy. *Int J Gynecol Cancer*, 19(5):826–829.

[Ho et al., 2004] Ho, C.-L., Kurman, R. J., Dehari, R., Wang, T.-L., and Shih, I.-M. (2004). Mutations of braf and kras precede the development of ovarian serous borderline tumors. *Cancer Res*, 64(19):6915–6918.

[Hogan et al., 2009] Hogan, C., Dupr-Crochet, S., Norman, M., Kajita, M., Zimmermann, C., Pelling, A. E., Piddini, E., Baena-Lpez, L. A., Vincent, J.-P., Itoh, Y., Hosoya, H., Pichaud, F., and Fujita, Y. (2009). Characterization of the interface between normal and transformed epithelial cells. *Nat Cell Biol*, 11(4):460–467.

[Hogdall et al., 2003] Hogdall, E. V. S., Christensen, L., Kjaer, S. K., Blaakaer, J., Bock, J. E., Glud, E., Nrgaard-Pedersen, B., and Hgdall, C. K. (2003). Distribution of her-2

overexpression in ovarian carcinoma tissue and its prognostic value in patients with ovarian carcinoma: from the danish malova ovarian cancer study. *Cancer*, 98(1):66–73.

[Howlett et al., 1995] Howlett, A. R., Bailey, N., Damsky, C., Petersen, O. W., and Bissell, M. J. (1995). Cellular growth and survival are mediated by beta 1 integrins in normal human breast epithelium but not in breast carcinoma. *J Cell Sci*, 108 (Pt 5):1945–1957.

[Hylander et al., 2006] Hylander, B., Repasky, E., Shrikant, P., Intengan, M., Beck, A., Driscoll, D., Singhal, P., Lele, S., and Odunsi, K. (2006). Expression of wilms tumor gene (wt1) in epithelial ovarian cancer. *Gynecol Oncol*, 101(1):12–17.

[Ince et al., 2007] Ince, T. A., Richardson, A. L., Bell, G. W., Saitoh, M., Godar, S., Karnoub, A. E., Iglehart, J. D., and Weinberg, R. A. (2007). Transformation of different human breast epithelial cell types leads to distinct tumor phenotypes. *Cancer Cell*, 12(2):160–170.

[Ishii et al., 1999] Ishii, H., Baffa, R., Numata, S. I., Murakumo, Y., Rattan, S., Inoue, H., Mori, M., Fidanza, V., Alder, H., and Croce, C. M. (1999). The fez1 gene at chromosome 8p22 encodes a leucine-zipper protein, and its expression is altered in multiple human tumors. *Proc Natl Acad Sci U S A*, 96(7):3928–3933.

[Ishii et al., 2001] Ishii, H., Vecchione, A., Murakumo, Y., Baldassarre, G., Numata, S., Trapasso, F., Alder, H., Baffa, R., and Croce, C. M. (2001). Fez1/lzts1 gene at 8p22 suppresses cancer cell growth and regulates mitosis. *Proc Natl Acad Sci U S A*, 98(18):10374–10379.

[Israeli et al., 2003] Israeli, O., Gotlieb, W. H., Friedman, E., Goldman, B., Ben-Baruch, G., Aviram-Goldring, A., and Rienstein, S. (2003). Familial vs sporadic ovarian tumors: characteristic genomic alterations analyzed by cgh. *Gynecol Oncol*, 90(3):629–636.

[Iyer et al., 1999] Iyer, V. R., Eisen, M. B., Ross, D. T., Schuler, G., Moore, T., Lee, J. C., Trent, J. M., Staudt, L. M., Hudson, J., Boguski, M. S., Lashkari, D., Shalon, D., Botstein, D., and Brown, P. O. (1999). The transcriptional program in the response of human fibroblasts to serum. *Science*, 283(5398):83–87.

[Janda et al., 2002] Janda, E., Litos, G., Grnert, S., Downward, J., and Beug, H. (2002). Oncogenic ras/her-2 mediate hyperproliferation of polarized epithelial cells in 3d cultures and rapid tumor growth via the pi3k pathway. *Oncogene*, 21(33):5148–5159.

[Jarboe et al., 2008] Jarboe, E., Folkins, A., Nucci, M. R., Kindelberger, D., Drapkin, R., Miron, A., Lee, Y., and Crum, C. P. (2008). Serous carcinogenesis in the fallopian tube: a descriptive classification. *Int J Gynecol Pathol*, 27(1):1–9.

[Jazaeri et al., 2005] Jazaeri, A. A., Awtrey, C. S., Chandramouli, G. V. R., Chuang, Y. E., Khan, J., Sotiriou, C., Aprelikova, O., Yee, C. J., Zorn, K. K., Birrer, M. J., Barrett, J. C., and Boyd, J. (2005). Gene expression profiles associated with response to chemotherapy in epithelial ovarian cancers. *Clin Cancer Res*, 11(17):6300–6310.

[Jazaeri et al., 2003] Jazaeri, A. A., Lu, K., Schmandt, R., Harris, C. P., Rao, P. H., Sotiriou, C., Chandramouli, G. V. R., Gershenson, D. M., and Liu, E. T. (2003). Molecular determinants of tumor differentiation in papillary serous ovarian carcinoma. *Mol Carcinog*, 36(2):53–59.

[Jazaeri et al., 2002] Jazaeri, A. A., Yee, C. J., Sotiriou, C., Brantley, K. R., Boyd, J., and Liu, E. T. (2002). Gene expression profiles of brca1-linked, brca2-linked, and sporadic ovarian cancers. *J Natl Cancer Inst*, 94(13):990–1000.

[Jeyapalan et al., 2007] Jeyapalan, J. C., Ferreira, M., Sedivy, J. M., and Herbig, U. (2007). Accumulation of senescent cells in mitotic tissue of aging primates. *Mech Ageing Dev*, 128(1):36–44.

[Jiang et al., 1999] Jiang, X. R., Jimenez, G., Chang, E., Frolkis, M., Kusler, B., Sage, M., Beeche, M., Bodnar, A. G., Wahl, G. M., Tlsty, T. D., and Chiu, C. P. (1999). Telomerase expression in human somatic cells does not induce changes associated with a transformed phenotype. *Nat Genet*, 21(1):111–114.

[Jordan et al., 2006] Jordan, S., Green, A., and Webb, P. (2006). Benign epithelial ovarian tumours-cancer precursors or markers for ovarian cancer risk? *Cancer Causes Control*, 17(5):623–632.

[Juul et al., 2007] Juul, N., Jensen, H., Hvid, M., Christiansen, G., and Birkelund, S. (2007). Characterization of in vitro chlamydial cultures in low-oxygen atmospheres. *J Bacteriol*, 189(18):6723–6726.

[Katoh and Katoh, 2003] Katoh, M. and Katoh, M. (2003). Identification and characterization of human TIPARP gene within the CCNL amplicon at human chromosome 3q25.31. *Int. J. Oncol.*, 23:541–547.

[Kerner et al., 2005] Kerner, R., Sabo, E., Gershoni-Baruch, R., Beck, D., and Ben-Izhak, O. (2005). Expression of cell cycle regulatory proteins in ovaries prophylactically removed from jewish ashkenazi brca1 and brca2 mutation carriers: correlation with histopathology. *Gynecol Oncol*, 99(2):367–375.

[Khaoustov et al., 1999] Khaoustov, V. I., Darlington, G. J., Soriano, H. E., Krishnan, B., Risin, D., Pellis, N. R., and Yoffe, B. (1999). Induction of three-dimensional assembly

of human liver cells by simulated microgravity. *In Vitro Cell Dev Biol Anim*, 35(9):501–509.

[Knuechel et al., 1990] Knuechel, R., Keng, P., Hofstaedter, F., Langmuir, V., Sutherland, R. M., and Penney, D. P. (1990). Differentiation patterns in two- and three-dimensional culture systems of human squamous carcinoma cell lines. *Am J Pathol*, 137(3):725–736.

[Kobayashi et al., 2005] Kobayashi, C., Monforte-Munoz, H. L., Gerbing, R. B., Stram, D. O., Matthay, K. K., Lukens, J. N., Seeger, R. C., and Shimada, H. (2005). Enlarged and prominent nucleoli may be indicative of mycn amplification: a study of neuroblastoma (schwannian stroma-poor), undifferentiated/poorly differentiated subtype with high mitosis-karyorrhexis index. *Cancer*, 103(1):174–180.

[Koebel et al., 2008] Koebel, M., Kalloger, S. E., Boyd, N., McKinney, S., Mehl, E., Palmer, C., Leung, S., Bowen, N. J., Ionescu, D. N., Rajput, A., Prentice, L. M., Miller, D., Santos, J., Swenerton, K., Gilks, C. B., and Huntsman, D. (2008). Ovarian carcinoma subtypes are different diseases: implications for biomarker studies. *PLoS Med*, 5(12):e232.

[Kolasa et al., 2006] Kolasa, I. K., Rembiszewska, A., Janiec-Jankowska, A., Dansonka-Mieszkowska, A., Lewandowska, A. M., Konopka, B., and Kupryja?czyk, J. (2006). Pten mutation, expression and loh at its locus in ovarian carcinomas. relation to tp53, k-ras and brca1 mutations. *Gynecol Oncol*, 103(2):692–697.

[Kolfschoten et al., 2005] Kolfschoten, I. G. M., van Leeuwen, B., Berns, K., Mullenders, J., Beijersbergen, R. L., Bernards, R., Voorhoeve, P. M., and Agami, R. (2005). A genetic screen identifies pitx1 as a suppressor of ras activity and tumorigenicity. *Cell*, 121(6):849–858.

[Krtolica et al., 2001] Krtolica, A., Parrinello, S., Lockett, S., Desprez, P. Y., and Campisi, J. (2001). Senescent fibroblasts promote epithelial cell growth and tumorigenesis: a link between cancer and aging. *Proc Natl Acad Sci U S A*, 98(21):12072–12077.

[Kruk et al., 1994] Kruk, P. A., Uitto, V. J., Firth, J. D., Dedhar, S., and Auersperg, N. (1994). Reciprocal interactions between human ovarian surface epithelial cells and adjacent extracellular matrix. *Exp Cell Res*, 215(1):97–108.

[Kusakari et al., 2003] Kusakari, T., Kariya, M., Mandai, M., Tsuruta, Y., Hamid, A. A., Fukuhara, K., Nanbu, K., Takakura, K., and Fujii, S. (2003). C-erbb-2 or mutant haras induced malignant transformation of immortalized human ovarian surface epithelial cells in vitro. *Br J Cancer*, 89(12):2293–2298.

[Kwong et al., 2009] Kwong, J., Chan, F. L., kwok Wong, K., Birrer, M. J., Archibald, K. M., Balkwill, F. R., Berkowitz, R. S., and Mok, S. C. (2009). Inflammatory cytokine tumor necrosis factor alpha confers precancerous phenotype in an organoid model of normal human ovarian surface epithelial cells. *Neoplasia*, 11(6):529–541.

[Laklai et al., 2009] Laklai, H., Laval, S., Dumartin, L., Rochaix, P., Hagedorn, M., Bikfalvi, A., Guellec, S. L., Delisle, M.-B., Schally, A. V., Susini, C., Pyronnet, S., and Bousquet, C. (2009). Thrombospondin-1 is a critical effector of oncosuppressive activity of sst2 somatostatin receptor on pancreatic cancer. *Proc Natl Acad Sci U S A*, 106(42):17769–17774.

[Landen et al., 2008] Landen, C. N., Birrer, M. J., and Sood, A. K. (2008). Early events in the pathogenesis of epithelial ovarian cancer. *J Clin Oncol*, 26(6):995–1005.

[Lapphn et al., 1989] Lapphn, R. E., Burger, H. G., Bouma, J., Bangah, M., Krans, M., and de Bruijn, H. W. (1989). Inhibin as a marker for granulosa-cell tumors. *N Engl J Med*, 321(12):790–793.

[Lawrenson et al., 2009a] Lawrenson, K., Benjamin, E., Turmaine, M., Jacobs, I., Gayther, S., and Dafou, D. (2009a). In vitro three-dimensional modelling of human ovarian surface epithelial cells. *Cell Prolif*.

[Lawrenson et al., 2009b] Lawrenson, K., Ramus, S. J., and Gayther, S. A. (2009b). *Somatic Genetic Development in Epithelial Ovarian Cancer. In: The Role of Genetics in Breast and Reproductive Cancers*. Springer Science & Business Media and Humana Press, New York, NY, USA.

[Lee and Reddy, 1999] Lee, C. M. and Reddy, E. P. (1999). The v-myc oncogene. *Oncogene*, 18(19):2997–3003.

[Lee et al., 2008] Lee, J., Cuddihy, M. J., and Kotov, N. A. (2008). Three-dimensional cell culture matrices: state of the art. *Tissue Eng Part B Rev*, 14(1):61–86.

[Levine et al., 2005] Levine, D. A., Bogomolniy, F., Yee, C. J., Lash, A., Barakat, R. R., Borgen, P. I., and Boyd, J. (2005). Frequent mutation of the pik3ca gene in ovarian and breast cancers. *Clin Cancer Res*, 11(8):2875–2878.

[Li et al., 2007] Li, N. F., Broad, S., Lu, Y. J., Yang, J. S., Watson, R., Hagemann, T., Wilbanks, G., Jacobs, I., Balkwill, F., Dafou, D., and Gayther, S. A. (2007). Human ovarian surface epithelial cells immortalized with htert maintain functional prb and p53 expression. *Cell Prolif*, 40(5):780–794.

[Li et al., 2004a] Li, N. F., Wilbanks, G., Balkwill, F., Jacobs, I. J., Dafou, D., and Gayther, S. A. (2004a). A modified medium that significantly improves the growth of human normal ovarian surface epithelial (ose) cells in vitro. *Lab Invest*, 84(7):923–931.

[Li et al., 2004b] Li, W., Lee, J., Vikis, H. G., Lee, S.-H., Liu, G., Aurandt, J., Shen, T.-L., Fearon, E. R., Guan, J.-L., Han, M., Rao, Y., Hong, K., and Guan, K.-L. (2004b). Activation of fak and src are receptor-proximal events required for netrin signaling. *Nat Neurosci*, 7(11):1213–1221.

[Liang and Slingerland, 2003] Liang, J. and Slingerland, J. M. (2003). Multiple roles of the pi3k/pkb (akt) pathway in cell cycle progression. *Cell Cycle*, 2(4):339–345.

[Liang et al., 2009] Liang, S., Yang, N., Pan, Y., Deng, S., Lin, X., Yang, X., Katsaros, D., Roby, K. F., Hamilton, T. C., Connolly, D. C., Coukos, G., and Zhang, L. (2009). Expression of activated pik3ca in ovarian surface epithelium results in hyperplasia but not tumor formation. *PLoS One*, 4(1):e4295.

[Lin et al., 2006] Lin, R.-Z., Chou, L.-F., Chien, C.-C. M., and Chang, H.-Y. (2006). Dynamic analysis of hepatoma spheroid formation: roles of e-cadherin and beta1-integrin. *Cell Tissue Res*, 324(3):411–422.

[Lind et al., 2006] Lind, A.-K., Weijdegrd, B., Dahm-Khler, P., Mlne, J., Sundfeldt, K., and Brnnstrm, M. (2006). Collagens in the human ovary and their changes in the perifollicular stroma during ovulation. *Acta Obstet Gynecol Scand*, 85(12):1476–1484.

[Liu and Wu, 2009] Liu, C.-H. and Wu, K.-W. (2009). Synergistic effects of basic fibroblast growth factor and insulin on chinese hamster ovary cells under serum-free conditions. *J Biosci Bioeng*, 107(3):312–317.

[Liu and Hornsby, 2007] Liu, D. and Hornsby, P. J. (2007). Senescent human fibroblasts increase the early growth of xenograft tumors via matrix metalloproteinase secretion. *Cancer Res*, 67(7):3117–3126.

[Liu et al., 2004] Liu, J., Yang, G., Thompson-Lanza, J. A., Glassman, A., Hayes, K., Patterson, A., Marquez, R. T., Auersperg, N., Yu, Y., Hahn, W. C., Mills, G. B., and Bast, R. C. (2004). A genetically defined model for human ovarian cancer. *Cancer Res*, 64(5):1655–1663.

[Liu et al., 2008] Liu, L.-Y., Han, Y.-C., Wu, S.-H., and Lv, Z.-H. (2008). Expression of connective tissue growth factor in tumor tissues is an independent predictor of poor prognosis in patients with gastric cancer. *World J Gastroenterol*, 14(13):2110–2114.

[Lu et al., 2004] Lu, K. H., Patterson, A. P., Wang, L., Marquez, R. T., Atkinson, E. N., Baggerly, K. A., Ramoth, L. R., Rosen, D. G., Liu, J., Hellstrom, I., Smith, D., Hartmann, L., Fishman, D., Berchuck, A., Schmandt, R., Whitaker, R., Gershenson, D. M., Mills, G. B., and Bast, R. C. (2004). Selection of potential markers for epithelial ovarian cancer with gene expression arrays and recursive descent partition analysis. *Clin Cancer Res*, 10(10):3291–3300.

[Ma et al., 2001] Ma, Q., Baldwin, K. T., Renzelli, A. J., McDaniel, A., and Dong, L. (2001). TCDD-inducible poly(ADP-ribose) polymerase: a novel response to 2,3,7,8-tetrachlorodibenzo-p-dioxin. *Biochem. Biophys. Res. Commun.*, 289:499–506.

[Mabuchi et al., 2007] Mabuchi, S., Altomare, D. A., Cheung, M., Zhang, L., Poulikakos, P. I., Hensley, H. H., Schilder, R. J., Ozols, R. F., and Testa, J. R. (2007). Rad001 inhibits human ovarian cancer cell proliferation, enhances cisplatin-induced apoptosis, and prolongs survival in an ovarian cancer model. *Clin Cancer Res*, 13(14):4261–4270.

[MacKenzie et al., 2000] MacKenzie, K. L., Franco, S., May, C., Sadelain, M., and Moore, M. A. (2000). Mass cultured human fibroblasts overexpressing htert encounter a growth crisis following an extended period of proliferation. *Exp Cell Res*, 259(2):336–350.

[Malander et al., 2006] Malander, S., Rambech, E., Kristoffersson, U., Halvarsson, B., Ridderheim, M., Borg, A., and Nilbert, M. (2006). The contribution of the hereditary nonpolyposis colorectal cancer syndrome to the development of ovarian cancer. *Gynecol Oncol*, 101(2):238–243.

[Malpica et al., 2004] Malpica, A., Deavers, M. T., Lu, K., Bodurka, D. C., Atkinson, E. N., Gershenson, D. M., and Silva, E. G. (2004). Grading ovarian serous carcinoma using a two-tier system. *Am J Surg Pathol*, 28(4):496–504.

[Marchini et al., 2008] Marchini, S., Mariani, P., Chiorino, G., Marrazzo, E., Bonomi, R., Fruscio, R., Clivio, L., Garbi, A., Torri, V., Cinquini, M., Dell'Anna, T., Apolone, G., Broggini, M., and D'Incalci, M. (2008). Analysis of gene expression in early-stage ovarian cancer. *Clin Cancer Res*, 14(23):7850–7860.

[Marquez et al., 2005] Marquez, R. T., Baggerly, K. A., Patterson, A. P., Liu, J., Broaddus, R., Frumovitz, M., Atkinson, E. N., Smith, D. I., Hartmann, L., Fishman, D., Berchuck, A., Whitaker, R., Gershenson, D. M., Mills, G. B., Bast, R. C., and Lu, K. H. (2005). Patterns of gene expression in different histotypes of epithelial ovarian cancer correlate with those in normal fallopian tube, endometrium, and colon. *Clin Cancer Res*, 11(17):6116–6126.

[Martini et al., 2002] Martini, M., Ciccarone, M., Garganese, G., Maggiore, C., Evangelista, A., Rahimi, S., Zannoni, G., Vittori, G., and Larocca, L. M. (2002). Possible involvement of hmlh1, p16(ink4a) and pten in the malignant transformation of endometriosis. *Int J Cancer*, 102(4):398–406.

[Matsunaga et al., 2003] Matsunaga, T., Takemoto, N., Sato, T., Takimoto, R., Tanaka, I., Fujimi, A., Akiyama, T., Kuroda, H., Kawano, Y., Kobune, M., Kato, J., Hirayama, Y., Sakamaki, S., Kohda, K., Miyake, K., and Niitsu, Y. (2003). Interaction between leukemic-cell vla-4 and stromal fibronectin is a decisive factor for minimal residual disease of acute myelogenous leukemia. *Nat Med*, 9(9):1158–1165.

[Mayr et al., 2006] Mayr, D., Hirschmann, A., Lhrs, U., and Diebold, J. (2006). Kras and braf mutations in ovarian tumors: a comprehensive study of invasive carcinomas, borderline tumors and extraovarian implants. *Gynecol Oncol*, 103(3):883–887.

[Mazzocca et al., 2009] Mazzocca, A., Fransvea, E., Dituri, F., Lupo, L., Antonaci, S., and Giannelli, G. (2009). Down-regulation of connective tissue growth factor by inhibition of transforming growth factor beta blocks the tumor-stroma cross-talk and tumor progression in hepatocellular carcinoma. *Hepatology*.

[Mazzocca et al., 2010] Mazzocca, A., Fransvea, E., Dituri, F., Lupo, L., Antonaci, S., and Giannelli, G. (2010). Down-regulation of connective tissue growth factor by inhibition of transforming growth factor beta blocks the tumor-stroma cross-talk and tumor progression in hepatocellular carcinoma. *Hepatology*, 51(2):523–534.

[McMurray et al., 2008] McMurray, H. R., Sampson, E. R., Compitello, G., Kinsey, C., Newman, L., Smith, B., Chen, S.-R., Klebanov, L., Salzman, P., Yakovlev, A., and Land, H. (2008). Synergistic response to oncogenic mutations defines gene class critical to cancer phenotype. *Nature*, 453(7198):1112–1116.

[Michaloglou et al., 2005] Michaloglou, C., Vredeveld, L. C. W., Soengas, M. S., Denoyelle, C., Kuilman, T., van der Horst, C. M. A. M., Majoor, D. M., Shay, J. W., Mooi, W. J., and Peeper, D. S. (2005). Brafe600-associated senescence-like cell cycle arrest of human naevi. *Nature*, 436(7051):720–724.

[Milyavsky et al., 2003] Milyavsky, M., Shats, I., Erez, N., Tang, X., Senderovich, S., Meerson, A., Tabach, Y., Goldfinger, N., Ginsberg, D., Harris, C. C., and Rotter, V. (2003). Prolonged culture of telomerase-immortalized human fibroblasts leads to a premalignant phenotype. *Cancer Res*, 63(21):7147–7157.

[Miotti et al., 2005] Miotti, S., Tomassetti, A., Facetti, I., Sanna, E., Berno, V., and Canevari, S. (2005). Simultaneous expression of caveolin-1 and e-cadherin in ovarian

carcinoma cells stabilizes adherens junctions through inhibition of src-related kinases. *Am J Pathol*, 167(5):1411–1427.

[Modugno et al., 2001] Modugno, F., Ness, R. B., and Wheeler, J. E. (2001). Reproductive risk factors for epithelial ovarian cancer according to histologic type and invasiveness. *Ann Epidemiol*, 11(8):568–574.

[Monaghan and Williams, 2003] Monaghan, H. and Williams, A. R. W. (2003). Brenner tumour with carcinoma in situ: evidence for a spectrum from benign to malignant. *Histopathology*, 43(5):502–504.

[Morales et al., 1999] Morales, C. P., Holt, S. E., Ouellette, M., Kaur, K. J., Yan, Y., Wilson, K. S., White, M. A., Wright, W. E., and Shay, J. W. (1999). Absence of cancer-associated changes in human fibroblasts immortalized with telomerase. *Nat Genet*, 21(1):115–118.

[Nakayama et al., 2006] Nakayama, K., Nakayama, N., Kurman, R. J., Cope, L., Pohl, G., Samuels, Y., Velculescu, V. E., Wang, T.-L., and Shih, I.-M. (2006). Sequence mutations and amplification of pik3ca and akt2 genes in purified ovarian serous neoplasms. *Cancer Biol Ther*, 5(7):779–785.

[Nasi et al., 2001] Nasi, S., Ciarapica, R., Jucker, R., Rosati, J., and Soucek, L. (2001). Making decisions through myc. *FEBS Lett*, 490(3):153–162.

[Navran, 2008] Navran, S. (2008). The application of low shear modeled microgravity to 3-d cell biology and tissue engineering. *Biotechnol Annu Rev*, 14:275–296.

[Netinatsunthorn et al., 2006] Netinatsunthorn, W., Hanprasertpong, J., Dechsukhum, C., Leetanaporn, R., and Geater, A. (2006). Wt1 gene expression as a prognostic marker in advanced serous epithelial ovarian carcinoma: an immunohistochemical study. *BMC Cancer*, 6:90.

[Niedergethmann et al., 2007] Niedergethmann, M., Alves, F., Neff, J. K., Heidrich, B., Aramin, N., Li, L., Pilarsky, C., Grtzmann, R., Allgayer, H., Post, S., and Gretz, N. (2007). Gene expression profiling of liver metastases and tumour invasion in pancreatic cancer using an orthotopic scid mouse model. *Br J Cancer*, 97(10):1432–1440.

[Nord et al., 2009] Nord, H., Hartmann, C., Andersson, R., Menzel, U., Pfeifer, S., Piotrowski, A., Bogdan, A., Kloc, W., Sandgren, J., Olofsson, T., Hesselager, G., Blomquist, E., Komorowski, J., von Deimling, A., Bruder, C. E., Dumanski, J. P., and Daz de Sthl, T. (2009). Characterization of novel and complex genomic aberrations in glioblastoma using a 32K BAC array. *Neuro-oncology*.

[Noskova et al., 2009] Noskova, V., Ahmadi, S., Asander, E., and Cassln, B. (2009). Ovarian cancer cells stimulate upa gene expression in fibroblastic stromal cells via multiple paracrine and autocrine mechanisms. *Gynecol Oncol*, 115(1):121–126.

[Obata et al., 1998] Obata, K., Morland, S. J., Watson, R. H., Hitchcock, A., Chenevix-Trench, G., Thomas, E. J., and Campbell, I. G. (1998). Frequent pten/mmac mutations in endometrioid but not serous or mucinous epithelial ovarian tumors. *Cancer Res*, 58(10):2095–2097.

[Ohta et al., 2006] Ohta, H., ichi Hamada, J., Tada, M., Aoyama, T., Furuuchi, K., Takahashi, Y., Totsuka, Y., and Moriuchi, T. (2006). Hoxd3-overexpression increases integrin alpha v beta 3 expression and deprives e-cadherin while it enhances cell motility in a549 cells. *Clin Exp Metastasis*, 23(7-8):381–390.

[Okamura and Katabuchi, 2001] Okamura, H. and Katabuchi, H. (2001). Detailed morphology of human ovarian surface epithelium focusing on its metaplastic and neoplastic capability. *Ital J Anat Embryol*, 106(2 Suppl 2):263–276.

[Oliva et al., 2006] Oliva, E., Sarri, D., Brachtel, E. F., Snchez-Estvez, C., Soslow, R. A., Moreno-Bueno, G., and Palacios, J. (2006). High frequency of beta-catenin mutations in borderline endometrioid tumours of the ovary. *J Pathol*, 208(5):708–713.

[Olumi et al., 1999] Olumi, A. F., Grossfeld, G. D., Hayward, S. W., Carroll, P. R., Tlsty, T. D., and Cunha, G. R. (1999). Carcinoma-associated fibroblasts direct tumor progression of initiated human prostatic epithelium. *Cancer Res*, 59(19):5002–5011.

[Orsulic et al., 2002] Orsulic, S., Li, Y., Soslow, R. A., Vitale-Cross, L. A., Gutkind, J. S., and Varmus, H. E. (2002). Induction of ovarian cancer by defined multiple genetic changes in a mouse model system. *Cancer Cell*, 1(1):53–62.

[Ota et al., 2009] Ota, T., Klausen, C., Salamanca, M. C., Woo, H. L., Leung, P. C. K., and Auersperg, N. (2009). Expression and function of hoxa genes in normal and neoplastic ovarian epithelial cells. *Differentiation*, 77(2):162–171.

[Paget, 1889] Paget, S. (1889). The distribution of secondary growths in cancer of the breast. 1889. *Cancer Metastasis Rev*, 8(2):98–101.

[Papadaki et al., 2009] Papadaki, C., Mavroudis, D., Trypaki, M., Koutsopoulos, A., Stathopoulos, E., Hatzidaki, D., Tsakalaki, E., Georgoulias, V., and Souglakos, J. (2009). Tumoral expression of txr1 and tsp1 predicts overall survival of patients with lung adenocarcinoma treated with first-line docetaxel-gemcitabine regimen. *Clin Cancer Res*, 15(11):3827–3833.

[Parrinello et al., 2005] Parrinello, S., Coppe, J.-P., Krtolica, A., and Campisi, J. (2005). Stromal-epithelial interactions in aging and cancer: senescent fibroblasts alter epithelial cell differentiation. *J Cell Sci*, 118(Pt 3):485–496.

[Pazolli et al., 2009] Pazolli, E., Luo, X., Brehm, S., Carbery, K., Chung, J.-J., Prior, J. L., Doherty, J., Demehri, S., Salavaggione, L., Piwnica-Worms, D., and Stewart, S. A. (2009). Senescent stromal-derived osteopontin promotes preneoplastic cell growth. *Cancer Res*, 69(3):1230–1239.

[Petersen et al., 1992] Petersen, O. W., Rnnov-Jessen, L., Howlett, A. R., and Bissell, M. J. (1992). Interaction with basement membrane serves to rapidly distinguish growth and differentiation pattern of normal and malignant human breast epithelial cells. *Proc Natl Acad Sci U S A*, 89(19):9064–9068.

[Petitjean et al., 2007] Petitjean, A., Mathe, E., Kato, S., Ishioka, C., Tavtigian, S. V., Hainaut, P., and Olivier, M. (2007). Impact of mutant p53 functional properties on tp53 mutation patterns and tumor phenotype: lessons from recent developments in the iarc tp53 database. *Hum Mutat*, 28(6):622–629.

[Pike et al., 2004] Pike, M. C., Pearce, C. L., Peters, R., Cozen, W., Wan, P., and Wu, A. H. (2004). Hormonal factors and the risk of invasive ovarian cancer: a population-based case-control study. *Fertil Steril*, 82(1):186–195.

[Pohl et al., 2005] Pohl, G., Ho, C.-L., Kurman, R. J., Bristow, R., Wang, T.-L., and Shih, I.-M. (2005). Inactivation of the mitogen-activated protein kinase pathway as a potential target-based therapy in ovarian serous tumors with kras or braf mutations. *Cancer Res*, 65(5):1994–2000.

[Pullen and Thomas, 1997] Pullen, N. and Thomas, G. (1997). The modular phosphorylation and activation of p70s6k. *FEBS Lett*, 410(1):78–82.

[Purdie et al., 2003] Purdie, D. M., Bain, C. J., Siskind, V., Webb, P. M., and Green, A. C. (2003). Ovulation and risk of epithelial ovarian cancer. *Int J Cancer*, 104(2):228–232.

[R Development Core Team, 2009] R Development Core Team (2009). *R: A Language and Environment for Statistical Computing*. R Foundation for Statistical Computing, Vienna, Austria. ISBN 3-900051-07-0.

[Raccurt et al., 2005] Raccurt, M., Smallwood, S., Mertani, H. C., Devost, D., Abbaci, K., Boutin, J. M., and Morel, G. (2005). Cloning, expression and regulation of chicken ovalbumin upstream promoter transcription factors (COUP-TFII and EAR-2) in the rat anterior pituitary gland. *Neuroendocrinology*, 82:233–244.

[Ramirez et al., 2004] Ramirez, R. D., Sheridan, S., Girard, L., Sato, M., Kim, Y., Pollack, J., Peyton, M., Zou, Y., Kurie, J. M., Dimaio, J. M., Milchgrub, S., Smith, A. L., Souza, R. F., Gilbey, L., Zhang, X., Gandia, K., Vaughan, M. B., Wright, W. E., Gazdar, A. F., Shay, J. W., and Minna, J. D. (2004). Immortalization of human bronchial epithelial cells in the absence of viral oncoproteins. *Cancer Res*, 64(24):9027–9034.

[Ramus et al., 1999] Ramus, S. J., Bobrow, L. G., Pharoah, P. D., Finnigan, D. S., Fishman, A., Altaras, M., Harrington, P. A., Gayther, S. A., Ponder, B. A., and Friedman, L. S. (1999). Increased frequency of tp53 mutations in brca1 and brca2 ovarian tumours. *Genes Chromosomes Cancer*, 25(2):91–96.

[Ramus and Gayther, 2009] Ramus, S. J. and Gayther, S. A. (2009). The contribution of brca1 and brca2 to ovarian cancer. *Mol Oncol*, 3(2):138–150.

[Ramus et al., 2003] Ramus, S. J., Pharoah, P. D. P., Harrington, P., Pye, C., Werness, B., Bobrow, L., Ayhan, A., Wells, D., Fishman, A., Gore, M., DiCioccio, R. A., Piver, M. S., Whittemore, A. S., Ponder, B. A. J., and Gayther, S. A. (2003). Brca1/2 mutation status influences somatic genetic progression in inherited and sporadic epithelial ovarian cancer cases. *Cancer Res*, 63(2):417–423.

[Richardson et al., 2004] Richardson, C. J., Schalm, S. S., and Blenis, J. (2004). Pi3-kinase and tor: Piktoring cell growth. *Semin Cell Dev Biol*, 15(2):147–159.

[Risch et al., 1996] Risch, H. A., Marrett, L. D., Jain, M., and Howe, G. R. (1996). Differences in risk factors for epithelial ovarian cancer by histologic type. results of a case-control study. *Am J Epidemiol*, 144(4):363–372.

[Roh et al., 2009] Roh, M. H., Kindelberger, D., and Crum, C. P. (2009). Serous tubal intraepithelial carcinoma and the dominant ovarian mass: clues to serous tumor origin? *Am J Surg Pathol*, 33(3):376–383.

[Roskelley and Bissell, 2002] Roskelley, C. D. and Bissell, M. J. (2002). The dominance of the microenvironment in breast and ovarian cancer. *Semin Cancer Biol*, 12(2):97–104.

[Russell et al., 2000] Russell, P. A., Pharoah, P. D., Foy, K. D., Ramus, S. J., Symmonds, I., Wilson, A., Scott, I., Ponder, B. A., and Gayther, S. A. (2000). Frequent loss of brca1 mrna and protein expression in sporadic ovarian cancers. *Int J Cancer*, 87(3):317–321.

[Russell and McCluggage, 2004] Russell, S. E. H. and McCluggage, W. G. (2004). A multistep model for ovarian tumorigenesis: the value of mutation analysis in the kras and braf genes. *J Pathol*, 203(2):617–619.

[Salamanca et al., 2004] Salamanca, C. M., Maines-Bandiera, S. L., Leung, P. C. K., Hu, Y.-L., and Auersperg, N. (2004). Effects of epidermal growth factor/hydrocortisone on the growth and differentiation of human ovarian surface epithelium. *J Soc Gynecol Investig*, 11(4):241–251.

[Saretzki et al., 2001] Saretzki, G., Ludwig, A., von Zglinicki, T., and Runnebaum, I. B. (2001). Ribozyme-mediated telomerase inhibition induces immediate cell loss but not telomere shortening in ovarian cancer cells. *Cancer Gene Ther*, 8(10):827–834.

[Saridogan et al., 1997] Saridogan, E., Djahanbakhch, O., Kervancioglu, M. E., Kahyaoglu, F., Shrimanker, K., and Grudzinskas, J. G. (1997). Placental protein 14 production by human fallopian tube epithelial cells in vitro. *Hum Reprod*, 12(7):1500–1507.

[Sasaki et al., 2009] Sasaki, R., Narisawa-Saito, M., Yugawa, T., Fujita, M., Tashiro, H., Katabuchi, H., and Kiyono, T. (2009). Oncogenic transformation of human ovarian surface epithelial cells with defined cellular oncogenes. *Carcinogenesis*, 30(3):423–431.

[Sato et al., 2006] Sato, M., Vaughan, M. B., Girard, L., Peyton, M., Lee, W., Shames, D. S., Ramirez, R. D., Sunaga, N., Gazdar, A. F., Shay, J. W., and Minna, J. D. (2006). Multiple oncogenic changes (k-ras(v12), p53 knockdown, mutant egfrs, p16 bypass, telomerase) are not sufficient to confer a full malignant phenotype on human bronchial epithelial cells. *Cancer Res*, 66(4):2116–2128.

[Sato et al., 2000] Sato, N., Tsunoda, H., Nishida, M., Morishita, Y., Takimoto, Y., Kubo, T., and Noguchi, M. (2000). Loss of heterozygosity on 10q23.3 and mutation of the tumor suppressor gene pten in benign endometrial cyst of the ovary: possible sequence progression from benign endometrial cyst to endometrioid carcinoma and clear cell carcinoma of the ovary. *Cancer Res*, 60(24):7052–7056.

[Scartozzi et al., 2003] Scartozzi, M., Nictolis, M. D., Galizia, E., Carassai, P., Bianchi, F., Berardi, R., Gesuita, R., Piga, A., Cellerino, R., and Porfiri, E. (2003). Loss of hmlh1 expression correlates with improved survival in stage iii-iv ovarian cancer patients. *Eur J Cancer*, 39(8):1144–1149.

[Schlosshauer et al., 2003] Schlosshauer, P. W., Cohen, C. J., Penault-Llorca, F., Miranda, C. R., Bignon, Y.-J., Dauplat, J., and Deligdisch, L. (2003). Prophylactic oophorectomy: a morphologic and immunohistochemical study. *Cancer*, 98(12):2599–2606.

[Scholl et al., 2009] Scholl, C., Frhling, S., Dunn, I. F., Schinzel, A. C., Barbie, D. A., Kim, S. Y., Silver, S. J., Tamayo, P., Wadlow, R. C., Ramaswamy, S., Dhner, K.,

Bullinger, L., Sandy, P., Boehm, J. S., Root, D. E., Jacks, T., Hahn, W. C., and Gilliland, D. G. (2009). Synthetic lethal interaction between oncogenic kras dependency and stk33 suppression in human cancer cells. *Cell*, 137(5):821–834.

[Schulze et al., 2001] Schulze, A., Lehmann, K., Jefferies, H. B., McMahon, M., and Downward, J. (2001). Analysis of the transcriptional program induced by raf in epithelial cells. *Genes Dev*, 15(8):981–994.

[Schulze et al., 2004] Schulze, A., Nicke, B., Warne, P. H., Tomlinson, S., and Downward, J. (2004). The transcriptional response to raf activation is almost completely dependent on mitogen-activated protein kinase kinase activity and shows a major autocrine component. *Mol Biol Cell*, 15(7):3450–3463.

[Scully, 1995] Scully, R. E. (1995). Pathology of ovarian cancer precursors. *J Cell Biochem Suppl*, 23:208–218.

[Secord et al., 2007] Secord, A. A., Darcy, K. M., Hutson, A., Lee, P. S., Havrilesky, L. J., Grace, L. A., Berchuck, A., and study, G. O. G. (2007). Co-expression of angiogenic markers and associations with prognosis in advanced epithelial ovarian cancer: a gynecologic oncology group study. *Gynecol Oncol*, 106(1):221–232.

[Shao et al., 2008] Shao, G., Balajee, A. S., Hei, T. K., and Zhao, Y. (2008). p16ink4a downregulation is involved in immortalization of primary human prostate epithelial cells induced by telomerase. *Mol Carcinog*, 47(10):775–783.

[Shao et al., 2009] Shao, G., Patterson-Fortin, J., Messick, T. E., Feng, D., Shanbhag, N., Wang, Y., and Greenberg, R. A. (2009). MERIT40 controls BRCA1-Rap80 complex integrity and recruitment to DNA double-strand breaks. *Genes Dev.*, 23:740–754.

[Sherman-Baust et al., 2003] Sherman-Baust, C. A., Weeraratna, A. T., Rangel, L. B. A., Pizer, E. S., Cho, K. R., Schwartz, D. R., Shock, T., and Morin, P. J. (2003). Remodeling of the extracellular matrix through overexpression of collagen vi contributes to cisplatin resistance in ovarian cancer cells. *Cancer Cell*, 3(4):377–386.

[Shih and Kurman, 2004] Shih, I.-M. and Kurman, R. J. (2004). Ovarian tumorigenesis: a proposed model based on morphological and molecular genetic analysis. *Am J Pathol*, 164(5):1511–1518.

[Shih and Kurman, 2005] Shih, I.-M. and Kurman, R. J. (2005). Molecular pathogenesis of ovarian borderline tumors: new insights and old challenges. *Clin Cancer Res*, 11(20):7273–7279.

[Shivji and Venkitaraman, 2004] Shivji, M. K. K. and Venkitaraman, A. R. (2004). Dna recombination, chromosomal stability and carcinogenesis: insights into the role of brca2. *DNA Repair (Amst)*, 3(8-9):835–843.

[Singer et al., 2003] Singer, G., Oldt, R., Cohen, Y., Wang, B. G., Sidransky, D., Kurman, R. J., and Shih, I.-M. (2003). Mutations in braf and kras characterize the development of low-grade ovarian serous carcinoma. *J Natl Cancer Inst*, 95(6):484–486.

[Singer et al., 2005] Singer, G., Sthr, R., Cope, L., Dehari, R., Hartmann, A., Cao, D.-F., Wang, T.-L., Kurman, R. J., and Shih, I.-M. (2005). Patterns of p53 mutations separate ovarian serous borderline tumors and low- and high-grade carcinomas and provide support for a new model of ovarian carcinogenesis: a mutational analysis with immunohistochemical correlation. *Am J Surg Pathol*, 29(2):218–224.

[Singh et al., 2009] Singh, A., Greninger, P., Rhodes, D., Koopman, L., Violette, S., Bardeesy, N., and Settleman, J. (2009). A gene expression signature associated with "k-ras addiction" reveals regulators of emt and tumor cell survival. *Cancer Cell*, 15(6):489–500.

[Smith and Xu, 2008] Smith, E. R. and Xu, X.-X. (2008). Ovarian ageing, follicle depletion, and cancer: a hypothesis for the aetiology of epithelial ovarian cancer involving follicle depletion. *Lancet Oncol*, 9(11):1108–1111.

[Smyth, 2004] Smyth, G. K. (2004). Linear models and empirical bayes methods for assessing differential expression in microarray experiments. *Stat Appl Genet Mol Biol*, 3:Article3.

[Solyom et al., 2009] Solyom, S., Patterson-Fortin, J., Pylks, K., Greenberg, R. A., and Winqvist, R. (2009). Mutation screening of the MERIT40 gene encoding a novel BRCA1 and RAP80 interacting protein in breast cancer families. *Breast Cancer Res. Treat.*

[Son et al., 2004] Son, B. H., Ahn, S. H., Ko, C. D., Ka, I. W., Gong, G. Y., and Kim, J. C. (2004). Significance of mismatch repair protein expression in the chemotherapeutic response of sporadic invasive ductal carcinoma of the breast. *Breast J*, 10(1):20–26.

[Song et al., 2009] Song, H., Ramus, S. J., Tyrer, J., Bolton, K. L., Gentry-Maharaj, A., Wozniak, E., Anton-Culver, H., Chang-Claude, J., Cramer, D. W., DiCioccio, R., Drk, T., Goode, E. L., Goodman, M. T., Schildkraut, J. M., Sellers, T., Baglietto, L., Beckmann, M. W., Beesley, J., Blaakaer, J., Carney, M. E., Chanock, S., Chen, Z., Cunningham, J. M., Dicks, E., Doherty, J. A., Drst, M., Ekici, A. B., Fenstermacher, D., Fridley, B. L., Giles, G., Gore, M. E., Vivo, I. D., Hillemanns, P., Hogdall, C., Hogdall, E., Iversen, E. S., Jacobs, I. J., Jakubowska, A., Li, D., Lissowska, J., Lubi?ski, J.,

Lurie, G., McGuire, V., McLaughlin, J., Medrek, K., Moorman, P. G., Moysich, K., Narod, S., Phelan, C., Pye, C., Risch, H., Runnebaum, I. B., Severi, G., Southey, M., Stram, D. O., Thiel, F. C., Terry, K. L., Tsai, Y.-Y., Tworoger, S. S., Berg, D. J. V. D., Vierkant, R. A., Wang-Gohrke, S., Webb, P. M., Wilkens, L. R., Wu, A. H., Yang, H., Brewster, W., Ziogas, A., Study, A. C. O., Group, A. O. C. S., Consortium, O. C. A., Houlston, R., Tomlinson, I., Whittemore, A. S., Rossing, M. A., Ponder, B. A. J., Pearce, C. L., Ness, R. B., Menon, U., Kjaer, S. K., Gronwald, J., Garcia-Closas, M., Fasching, P. A., Easton, D. F., Chenevix-Trench, G., Berchuck, A., Pharoah, P. D. P., and Gayther, S. A. (2009). A genome-wide association study identifies a new ovarian cancer susceptibility locus on 9p22.2. *Nat Genet*, 41(9):996–1000.

[Sowter and Ashworth, 2005] Sowter, H. M. and Ashworth, A. (2005). Brca1 and brca2 as ovarian cancer susceptibility genes. *Carcinogenesis*, 26(10):1651–1656.

[Stewart et al., 2004] Stewart, S. L., Querec, T. D., Ochman, A. R., Gruver, B. N., Bao, R., Babb, J. S., Wong, T. S., Koutroukides, T., Pinnola, A. D., Klein-Szanto, A., Hamilton, T. C., and Patriotis, C. (2004). Characterization of a carcinogenesis rat model of ovarian preneoplasia and neoplasia. *Cancer Res*, 64(22):8177–8183.

[Strathdee et al., 1999] Strathdee, G., MacKean, M. J., Illand, M., and Brown, R. (1999). A role for methylation of the hmlh1 promoter in loss of hmlh1 expression and drug resistance in ovarian cancer. *Oncogene*, 18(14):2335–2341.

[Studebaker et al., 2008] Studebaker, A. W., Storci, G., Werbeck, J. L., Sansone, P., Sasser, A. K., Tavolari, S., Huang, T., Chan, M. W. Y., Marini, F. C., Rosol, T. J., Bonaf, M., and Hall, B. M. (2008). Fibroblasts isolated from common sites of breast cancer metastasis enhance cancer cell growth rates and invasiveness in an interleukin-6-dependent manner. *Cancer Res*, 68(21):9087–9095.

[Sugie et al., 2009] Sugie, Y., Sugie, H., Fukuda, T., and Osawa, J. (2009). Study of hoxd genes in autism particularly regarding the ratio of second to fourth digit length. *Brain Dev.*

[Sundfeldt et al., 1997] Sundfeldt, K., Piontkewitz, Y., Ivarsson, K., Nilsson, O., Hellberg, P., Brnnstrm, M., Janson, P. O., Enerback, S., and Hedin, L. (1997). E-cadherin expression in human epithelial ovarian cancer and normal ovary. *Int J Cancer*, 74(3):275–280.

[Sutherland and Durand, 1976] Sutherland, R. M. and Durand, R. E. (1976). Radiation response of multicell spheroids–an in vitro tumour model. *Curr Top Radiat Res Q*, 11(1):87–139.

[Sutherland et al., 1986] Sutherland, R. M., Sordat, B., Bamat, J., Gabbert, H., Bourrat, B., and Mueller-Klieser, W. (1986). Oxygenation and differentiation in multicellular spheroids of human colon carcinoma. *Cancer Res*, 46(10):5320–5329.

[Syed et al., 2001] Syed, V., Ulinski, G., Mok, S. C., Yiu, G. K., and Ho, S. M. (2001). Expression of gonadotropin receptor and growth responses to key reproductive hormones in normal and malignant human ovarian surface epithelial cells. *Cancer Res*, 61(18):6768–6776.

[Szotek et al., 2008] Szotek, P. P., Chang, H. L., Brennand, K., Fujino, A., Pieretti-Vanmarcke, R., Celso, C. L., Dombkowski, D., Preffer, F., Cohen, K. S., Teixeira, J., and Donahoe, P. K. (2008). Normal ovarian surface epithelial label-retaining cells exhibit stem/progenitor cell characteristics. *Proc Natl Acad Sci U S A*, 105(34):12469–12473.

[Takahashi et al., 2006] Takahashi, A., Ohtani, N., Yamakoshi, K., ichi Iida, S., Tahara, H., Nakayama, K., Nakayama, K. I., Ide, T., Saya, H., and Hara, E. (2006). Mitogenic signalling and the p16ink4a-rb pathway cooperate to enforce irreversible cellular senescence. *Nat Cell Biol*, 8(11):1291–1297.

[Takahashi et al., 2007] Takahashi, K., Tanabe, K., Ohnuki, M., Narita, M., Ichisaka, T., Tomoda, K., and Yamanaka, S. (2007). Induction of pluripotent stem cells from adult human fibroblasts by defined factors. *Cell*, 131(5):861–872.

[Takakura et al., 2009] Takakura, M., Nakamura, M., Kyo, S., Hashimoto, M., Mori, N., Ikoma, T., Mizumoto, Y., Fujiwara, T., Urata, Y., and Inoue, M. (2009). Intraperitoneal administration of telomerase-specific oncolytic adenovirus sensitizes ovarian cancer cells to cisplatin and affects survival in a xenograft model with peritoneal dissemination. *Cancer Gene Ther*.

[Tanner et al., 1998] Tanner, B., Hengstler, J. G., Luch, A., Meinert, R., Kreutz, E., Arand, M., Wilkens, C., Hofmann, M., Oesch, F., Knapstein, P. G., and Becker, R. (1998). C-myc mrna expression in epithelial ovarian carcinomas in relation to estrogen receptor status, metastatic spread, survival time, figo stage, and histologic grade and type. *Int J Gynecol Pathol*, 17(1):66–74.

[Thomas et al., 2008] Thomas, G., Jacobs, K. B., Yeager, M., Kraft, P., Wacholder, S., Orr, N., Yu, K., Chatterjee, N., Welch, R., Hutchinson, A., Crenshaw, A., Cancel-Tassin, G., Staats, B. J., Wang, Z., Gonzalez-Bosquet, J., Fang, J., Deng, X., Berndt, S. I., Calle, E. E., Feigelson, H. S., Thun, M. J., Rodriguez, C., Albanes, D., Virtamo, J., Weinstein, S., Schumacher, F. R., Giovannucci, E., Willett, W. C., Cussenot, O.,

Valeri, A., Andriole, G. L., Crawford, E. D., Tucker, M., Gerhard, D. S., Fraumeni, J. F., Hoover, R., Hayes, R. B., Hunter, D. J., and Chanock, S. J. (2008). Multiple loci identified in a genome-wide association study of prostate cancer. *Nat Genet*, 40(3):310–315.

[Tomlinson et al., 2007] Tomlinson, I., Webb, E., Carvajal-Carmona, L., Broderick, P., Kemp, Z., Spain, S., Penegar, S., Chandler, I., Gorman, M., Wood, W., Barclay, E., Lubbe, S., Martin, L., Sellick, G., Jaeger, E., Hubner, R., Wild, R., Rowan, A., Fielding, S., Howarth, K., Consortium, C. O. R. G. I., Silver, A., Atkin, W., Muir, K., Logan, R., Kerr, D., Johnstone, E., Sieber, O., Gray, R., Thomas, H., Peto, J., Cazier, J.-B., and Houlston, R. (2007). A genome-wide association scan of tag snps identifies a susceptibility variant for colorectal cancer at 8q24.21. *Nat Genet*, 39(8):984–988.

[Tothill et al., 2008] Tothill, R. W., Tinker, A. V., George, J., Brown, R., Fox, S. B., Lade, S., Johnson, D. S., Trivett, M. K., Etemadmoghadam, D., Locandro, B., Traficante, N., Fereday, S., Hung, J. A., Chiew, Y.-E., Haviv, I., Group, A. O. C. S., Gertig, D., DeFazio, A., and Bowtell, D. D. L. (2008). Novel molecular subtypes of serous and endometrioid ovarian cancer linked to clinical outcome. *Clin Cancer Res*, 14(16):5198–5208.

[Treeck et al., 2006] Treeck, O., Wackwitz, B., Haus, U., and Ortmann, O. (2006). Effects of a combined treatment with mtor inhibitor rad001 and tamoxifen in vitro on growth and apoptosis of human cancer cells. *Gynecol Oncol*, 102(2):292–299.

[Tsai et al., 1990] Tsai, Y. C., Nichols, P. W., Hiti, A. L., Williams, Z., Skinner, D. G., and Jones, P. A. (1990). Allelic losses of chromosomes 9, 11, and 17 in human bladder cancer. *Cancer Res*, 50(1):44–47.

[Vaisman et al., 1998] Vaisman, A., Varchenko, M., Umar, A., Kunkel, T. A., Risinger, J. I., Barrett, J. C., Hamilton, T. C., and Chaney, S. G. (1998). The role of hmlh1, hmsh3, and hmsh6 defects in cisplatin and oxaliplatin resistance: correlation with replicative bypass of platinum-dna adducts. *Cancer Res*, 58(16):3579–3585.

[Vanhoutteghem and Djian, 2006] Vanhoutteghem, A. and Djian, P. (2006). Basonuclins 1 and 2, whose genes share a common origin, are proteins with widely different properties and functions. *Proc. Natl. Acad. Sci. U.S.A.*, 103:12423–12428.

[Vanhoutteghem and Djian, 2007] Vanhoutteghem, A. and Djian, P. (2007). The human basonuclin 2 gene has the potential to generate nearly 90,000 mRNA isoforms encoding over 2000 different proteins. *Genomics*, 89:44–58.

[Vecchione et al., 2007] Vecchione, A., Baldassarre, G., Ishii, H., Nicoloso, M. S., Belletti, B., Petrocca, F., Zanesi, N., Fong, L. Y. Y., Battista, S., Guarnieri, D., Baffa, R., Alder, H., Farber, J. L., Donovan, P. J., and Croce, C. M. (2007). Fez1/lzts1 absence impairs cdk1/cdc25c interaction during mitosis and predisposes mice to cancer development. *Cancer Cell*, 11(3):275–289.

[Vecchione et al., 2002] Vecchione, A., Ishii, H., Baldassarre, G., Bassi, P., Trapasso, F., Alder, H., Pagano, F., Gomella, L. G., Croce, C. M., and Baffa, R. (2002). Fez1/lzts1 is down-regulated in high-grade bladder cancer, and its restoration suppresses tumorigenicity in transitional cell carcinoma cells. *Am J Pathol*, 160(4):1345–1352.

[Wang et al., 2004] Wang, C., Horiuchi, A., Imai, T., Ohira, S., Itoh, K., Nikaido, T., Katsuyama, Y., and Konishi, I. (2004). Expression of brca1 protein in benign, borderline, and malignant epithelial ovarian neoplasms and its relationship to methylation and allelic loss of the brca1 gene. *J Pathol*, 202(2):215–223.

[Wang et al., 2005] Wang, Y., Helland, A., Holm, R., Kristensen, G. B., and Brresen-Dale, A.-L. (2005). Pik3ca mutations in advanced ovarian carcinomas. *Hum Mutat*, 25(3):322.

[Wang-Johanning et al., 2007] Wang-Johanning, F., Huang, M., Liu, J., Rycaj, K., Plummer, J. B., Barnhart, K. F., Satterfield, W. C., and Johanning, G. L. (2007). Sheep stromal-epithelial cell interactions and ovarian tumor progression. *Int J Cancer*, 121(10):2346–2354.

[Wasenius et al., 1997] Wasenius, V. M., Jekunen, A., Monni, O., Joensuu, H., Aebi, S., Howell, S. B., and Knuutila, S. (1997). Comparative genomic hybridization analysis of chromosomal changes occurring during development of acquired resistance to cisplatin in human ovarian carcinoma cells. *Genes Chromosomes Cancer*, 18(4):286–291.

[Watanabe et al., 2009] Watanabe, R., Hayashi, Y., Sassa, M., Kikumori, T., Imai, T., Kiuchi, T., and Murata, Y. (2009). Possible involvement of brafv600e in altered gene expression in papillary thyroid cancer. *Endocr J*, 56(3):407–414.

[Watnick et al., 2003] Watnick, R. S., Cheng, Y.-N., Rangarajan, A., Ince, T. A., and Weinberg, R. A. (2003). Ras modulates myc activity to repress thrombospondin-1 expression and increase tumor angiogenesis. *Cancer Cell*, 3(3):219–231.

[Watson and Lynch, 2001] Watson, P. and Lynch, H. T. (2001). Cancer risk in mismatch repair gene mutation carriers. *Fam Cancer*, 1(1):57–60.

[Weaver et al., 1995] Weaver, V. M., Howlett, A. R., Langton-Webster, B., Petersen, O. W., and Bissell, M. J. (1995). The development of a functionally relevant cell culture model of progressive human breast cancer. *Semin Cancer Biol*, 6(3):175–184.

[Weaver et al., 1997] Weaver, V. M., Petersen, O. W., Wang, F., Larabell, C. A., Briand, P., Damsky, C., and Bissell, M. J. (1997). Reversion of the malignant phenotype of human breast cells in three-dimensional culture and in vivo by integrin blocking antibodies. *J Cell Biol*, 137(1):231–245.

[Wei et al., 1999] Wei, S., Wei, S., and Sedivy, J. M. (1999). Expression of catalytically active telomerase does not prevent premature senescence caused by overexpression of oncogenic ha-ras in normal human fibroblasts. *Cancer Res*, 59(7):1539–1543.

[Weir et al., 2006] Weir, M. L., Oppizzi, M. L., Henry, M. D., Onishi, A., Campbell, K. P., Bissell, M. J., and Muschler, J. L. (2006). Dystroglycan loss disrupts polarity and beta-casein induction in mammary epithelial cells by perturbing laminin anchoring. *J Cell Sci*, 119(Pt 19):4047–4058.

[Welcsh and King, 2001] Welcsh, P. L. and King, M. C. (2001). Brca1 and brca2 and the genetics of breast and ovarian cancer. *Hum Mol Genet*, 10(7):705–713.

[Werness et al., 2000] Werness, B. A., Ramus, S. J., Whittemore, A. S., Garlinghouse-Jones, K., Oakley-Girvan, I., Dicioccio, R. A., Tsukada, Y., Ponder, B. A., and Piver, M. S. (2000). Histopathology of familial ovarian tumors in women from families with and without germline brca1 mutations. *Hum Pathol*, 31(11):1420–1424.

[Whittemore et al., 2004] Whittemore, A. S., Balise, R. R., Pharoah, P. D. P., Dicioccio, R. A., Oakley-Girvan, I., Ramus, S. J., Daly, M., Usinowicz, M. B., Garlinghouse-Jones, K., Ponder, B. A. J., Buys, S., Senie, R., Andrulis, I., John, E., Hopper, J. L., and Piver, M. S. (2004). Oral contraceptive use and ovarian cancer risk among carriers of brca1 or brca2 mutations. *Br J Cancer*, 91(11):1911–1915.

[Whittemore et al., 1992] Whittemore, A. S., Harris, R., and Itnyre, J. (1992). Characteristics relating to ovarian cancer risk: collaborative analysis of 12 us case-control studies. ii. invasive epithelial ovarian cancers in white women. collaborative ovarian cancer group. *Am J Epidemiol*, 136(10):1184–1203.

[Widschwendter et al., 2009] Widschwendter, M., Apostolidou, S., Jones, A. A., Fourkala, E. O., Arora, R., Pearce, C. L., Frasco, M. A., Ayhan, A., Zikan, M., Cibula, D., Iyibozkurt, C. A., Yavuz, E., Hauser-Kronberger, C., Dubeau, L., Menon, U., and Jacobs, I. J. (2009). Hoxa methylation in normal endometrium from premenopausal

women is associated with the presence of ovarian cancer: a proof of principle study. *Int J Cancer*, 125(9):2214–2218.

[Wierinckx et al., 2007] Wierinckx, A., Auger, C., Devauchelle, P., Reynaud, A., Chevallier, P., Jan, M., Perrin, G., Fvre-Montange, M., Rey, C., Figarella-Branger, D., Raverot, G., Belin, M.-F., Lachuer, J., and Trouillas, J. (2007). A diagnostic marker set for invasion, proliferation, and aggressiveness of prolactin pituitary tumors. *Endocr Relat Cancer*, 14(3):887–900.

[Willner et al., 2007] Willner, J., Wurz, K., Allison, K. H., Galic, V., Garcia, R. L., Goff, B. A., and Swisher, E. M. (2007). Alternate molecular genetic pathways in ovarian carcinomas of common histological types. *Hum Pathol*, 38(4):607–613.

[Wong and Auersperg, 2003] Wong, A. S. T. and Auersperg, N. (2003). Ovarian surface epithelium: family history and early events in ovarian cancer. *Reprod Biol Endocrinol*, 1:70.

[Wu et al., 2007] Wu, R., Hendrix-Lucas, N., Kuick, R., Zhai, Y., Schwartz, D. R., Akyol, A., Hanash, S., Misek, D. E., Katabuchi, H., Williams, B. O., Fearon, E. R., and Cho, K. R. (2007). Mouse model of human ovarian endometrioid adenocarcinoma based on somatic defects in the wnt/beta-catenin and pi3k/pten signaling pathways. *Cancer Cell*, 11(4):321–333.

[Wu et al., 2005] Wu, X., Groves, F. D., McLaughlin, C. C., Jemal, A., Martin, J., and Chen, V. W. (2005). Cancer incidence patterns among adolescents and young adults in the united states. *Cancer Causes Control*, 16(3):309–320.

[Wu et al., 2004] Wu, Y., Soslow, R. A., Marshall, D. S., Leitao, M., and Chen, B. (2004). Her-2/neu expression and amplification in early stage ovarian surface epithelial neoplasms. *Gynecol Oncol*, 95(3):570–575.

[Xie et al., 2009] Xie, Y., Wolff, D. W., Wei, T., Wang, B., Deng, C., Kirui, J. K., Jiang, H., Qin, J., Abel, P. W., and Tu, Y. (2009). Breast cancer migration and invasion depend on proteasome degradation of regulator of g-protein signaling 4. *Cancer Res*, 69(14):5743–5751.

[Yancik, 1993] Yancik, R. (1993). Ovarian cancer. age contrasts in incidence, histology, disease stage at diagnosis, and mortality. *Cancer*, 71(2 Suppl):517–523.

[Yang et al., 2007a] Yang, G., Rosen, D. G., Colacino, J. A., Mercado-Uribe, I., and Liu, J. (2007a). Disruption of the retinoblastoma pathway by small interfering rna and ectopic expression of the catalytic subunit of telomerase lead to immortalization of human ovarian surface epithelial cells. *Oncogene*, 26(10):1492–1498.

[Yang et al., 2007b] Yang, G., Rosen, D. G., Mercado-Uribe, I., Colacino, J. A., Mills, G. B., Bast, R. C., Zhou, C., and Liu, J. (2007b). Knockdown of p53 combined with expression of the catalytic subunit of telomerase is sufficient to immortalize primary human ovarian surface epithelial cells. *Carcinogenesis*, 28(1):174–182.

[Yang et al., 2006] Yang, G., Rosen, D. G., Zhang, Z., Bast, R. C., Mills, G. B., Colacino, J. A., Mercado-Uribe, I., and Liu, J. (2006). The chemokine growth-regulated oncogene 1 (gro-1) links ras signaling to the senescence of stromal fibroblasts and ovarian tumorigenesis. *Proc Natl Acad Sci U S A*, 103(44):16472–16477.

[Zhang and Dufau, 2000] Zhang, Y. and Dufau, M. L. (2000). Nuclear orphan receptors regulate transcription of the gene for the human luteinizing hormone receptor. *J. Biol. Chem.*, 275:2763–2770.

[Zietarska et al., 2007] Zietarska, M., Maugard, C. M., Filali-Mouhim, A., Alam-Fahmy, M., Tonin, P. N., Provencher, D. M., and Mes-Masson, A.-M. (2007). Molecular description of a 3d in vitro model for the study of epithelial ovarian cancer (eoc). *Mol Carcinog*, 46(10):872–885.

[Zorn et al., 2003] Zorn, K. K., Jazaeri, A. A., Awtrey, C. S., Gardner, G. J., Mok, S. C., Boyd, J., and Birrer, M. J. (2003). Choice of normal ovarian control influences determination of differentially expressed genes in ovarian cancer expression profiling studies. *Clin Cancer Res*, 9(13):4811–4818.

[Zubac et al., 2009] Zubac, D. P., Bostad, L., Kihl, B., Seidal, T., Wentzel-Larsen, T., and Haukaas, S. A. (2009). The expression of thrombospondin-1 and p53 in clear cell renal cell carcinoma: its relationship to angiogenesis, cell proliferation and cancer specific survival. *J Urol*, 182(5):2144–2149.

Appendix A: Top 100 Genes Up- or Down-regulated in IOSE11, IOSE19 and Derivative Clones

Top 100 genes differentially expressed in IOSE11$^{CMYC.KRAS/BRAF}$ compared to control cell lines, ranked by statistical significance.

Gene	Log FC	Adjusted P Val	Gene Name
VIPR1	-4.01	3.75E-12	vasoactive intestinal peptide receptor 1 (VIPR1).
FEZ1	-2.68	1.02E-11	fasciculation and elongation protein zeta 1 (zygin I) (FEZ1), transcript variant 1.
PITX1	3.44	1.14E-11	paired-like homeodomain transcription factor 1 (PITX1).
CCL2	-2.12	1.37E-11	chemokine (C-C motif) ligand 2 (CCL2).
RGS4	-2.64	1.44E-11	regulator of G-protein signalling 4 (RGS4).
VGF	3.11	2.28E-11	VGF nerve growth factor inducible (VGF).
OSR1	-2.57	2.64E-11	odd-skipped related 1 (Drosophila) (OSR1).
UBE2C	2.31	3.20E-11	ubiquitin-conjugating enzyme E2C (UBE2C), transcript variant 3.
MOCOS	2.98	5.09E-11	molybdenum cofactor sulfurase (MOCOS).
SERPINA9	-2.29	5.09E-11	serpin peptidase inhibitor, clade A (alpha-1 antiproteinase, antitrypsin), member 9 (SERPINA9), transcript variant B
SLC9A3R1	-1.77	7.20E-11	solute carrier family 9 (sodium/hydrogen exchanger), member 3 regulator 1 (SLC9A3R1).
THBS1	-3.49	9.22E-11	thrombospondin 1 (THBS1).
CTGF	-2.17	1.06E-10	connective tissue growth factor (CTGF).
SERPINA3	2.70	1.44E-10	serpin peptidase inhibitor, clade A (alpha-1 antiproteinase, antitrypsin), member 3 (SERPINA3).
TIGA1	3.26	1.52E-10	TIGA1 (TIGA1).
OLAH	-2.79	1.67E-10	oleoyl-ACP hydrolase (OLAH), transcript variant 1.
SYT11	-2.85	1.86E-10	synaptotagmin XI (SYT11).
ZNF342	1.88	2.07E-10	zinc finger protein 342 (ZNF342).
SLCO4A1	1.70	2.19E-10	solute carrier organic anion transporter family, member 4A1 (SLCO4A1).
TNFAIP6	1.61	2.83E-10	tumor necrosis factor, alpha-induced protein 6 (TNFAIP6).
LETMD1	1.88	2.83E-10	LETM1 domain containing 1 (LETMD1), transcript variant 2.
COL3A1	2.31	2.88E-10	collagen, type III, alpha 1 (Ehlers-Danlos syndrome type IV, autosomal dominant) (COL3A1).
MYLK	-1.69	2.88E-10	myosin light chain kinase (MYLK), transcript variant 8.
GDF15	1.84	2.88E-10	growth differentiation factor 15 (GDF15).
HIST1H4C	1.88	3.83E-10	histone cluster 1, H4c (HIST1H4C).
VWF	-1.26	3.86E-10	von Willebrand factor (VWF).
RASD1	-1.34	4.32E-10	RAS, dexamethasone-induced 1 (RASD1).
GPR177	-2.40	4.73E-10	G protein-coupled receptor 177 (GPR177), transcript variant 1.
UBE2C	2.11	4.79E-10	ubiquitin-conjugating enzyme E2C (UBE2C), transcript variant 6.
DLK2	1.68	4.79E-10	delta-like 2 homolog (Drosophila) (DLK2), transcript variant 2.
CABC1	2.03	4.81E-10	chaperone, ABC1 activity of bc1 complex homolog (CABC1), nuclear gene encoding mitochondrial protein.
GPM6B	1.98	4.94E-10	glycoprotein M6B (GPM6B), transcript variant 1.
TAGLN	-3.59	4.94E-10	transgelin (TAGLN), transcript variant 2.

LOC645688	1.52	5.72E-10	PREDICTED: similar to 60S ribosomal protein L12 (LOC645688).
PCDH18	1.63	5.87E-10	protocadherin 18 (PCDH18).
MAD2L1	1.98	5.95E-10	MAD2 mitotic arrest deficient-like 1 (yeast) (MAD2L1).
GAL	1.21	6.33E-10	galanin prepropeptide (GAL).
FBL	1.56	6.60E-10	fibrillarin (FBL).
ITGAV	-1.75	6.60E-10	integrin, alpha V (vitronectin receptor, alpha polypeptide, antigen CD51) (ITGAV).
LOC650298	1.58	6.71E-10	PREDICTED: similar to 40S ribosomal protein S26 (LOC650298).
DLEU1	1.59	6.72E-10	deleted in lymphocytic leukemia, 1 (DLEU1) on chromosome 13.
CTGF	-2.11	6.86E-10	connective tissue growth factor (CTGF).
LOC651894	1.96	6.89E-10	PREDICTED: similar to ribosomal protein S12 (LOC651894).
LOC728554	1.48	7.14E-10	PREDICTED: similar to THO complex 3 (LOC728554).
IL27RA	1.39	7.24E-10	interleukin 27 receptor, alpha (IL27RA).
HBEGF	-1.46	7.31E-10	heparin-binding EGF-like growth factor (HBEGF).
GJB2	-2.03	8.04E-10	gap junction protein, beta 2, 26kDa (GJB2).
MAPK13	-1.68	8.19E-10	mitogen-activated protein kinase 13 (MAPK13).
GABBR2	-1.91	8.66E-10	gamma-aminobutyric acid (GABA) B receptor, 2 (GABBR2).
PTGES	2.28	8.72E-10	prostaglandin E synthase (PTGES).
VAMP8	-2.83	8.87E-10	vesicle-associated membrane protein 8 (endobrevin) (VAMP8).
SERPINB2	-1.49	9.88E-10	serpin peptidase inhibitor, clade B (ovalbumin), member 2 (SERPINB2).
YZ87G11	-1.93	1.24E-09	(insert cDNA clone YZ87G11)
EIF2A	1.66	1.24E-09	eukaryotic translation initiation factor 2A, 65kDa (EIF2A).
TMEFF2	2.03	1.24E-09	transmembrane protein with EGF-like and two follistatin-like domains 2 (TMEFF2).
GPR4	-1.32	1.24E-09	G protein-coupled receptor 4 (GPR4).
KCTD10	-1.51	1.28E-09	potassium channel tetramerisation domain containing 10 (KCTD10).
NUAK1	-1.55	1.36E-09	NUAK family, SNF1-like kinase, 1 (NUAK1).
PRC1	1.70	1.46E-09	protein regulator of cytokinesis 1 (PRC1), transcript variant 2.
CPS1	1.42	1.54E-09	carbamoyl-phosphate synthetase 1, mitochondrial (CPS1).
CYGB	1.25	1.60E-09	cytoglobin (CYGB).
IGFBP5	-1.79	1.60E-09	insulin-like growth factor binding protein 5 (IGFBP5).
ADAMTS9	-2.22	1.64E-09	ADAM metallopeptidase with thrombospondin type 1 motif, 9 (ADAMTS9).
HMGB2	1.87	1.76E-09	high-mobility group box 2 (HMGB2).
LOC127295	1.51	1.76E-09	PREDICTED: similar to 60S ribosomal protein L36 (LOC127295).
PPAPDC1A	-1.37	1.88E-09	phosphatidic acid phosphatase type 2 domain containing 1A (PPAPDC1A).
CCNA1	-1.93	2.28E-09	cyclin A1 (CCNA1).
TMEM38B	1.15	2.64E-09	transmembrane protein 38B (TMEM38B).
ITGB1	-1.58	2.80E-09	integrin, beta 1 (fibronectin receptor, beta polypeptide, antigen CD29 includes MDF2, MSK12) (ITGB1)
LOC91561	1.88	2.80E-09	PREDICTED: similar to ribosomal protein S2, transcript variant 3 (LOC91561).
KRT17	1.57	2.80E-09	keratin 17 (KRT17).
MYBPC1	1.78	2.80E-09	myosin binding protein C, slow type (MYBPC1), transcript variant 4.

IL1RAPL1	-1.31	2.82E-09	interleukin 1 receptor accessory protein-like 1 (IL1RAPL1).
IMPDH2	1.83	3.04E-09	IMP (inosine monophosphate) dehydrogenase 2 (IMPDH2).
CCNB1IP1	2.01	3.04E-09	cyclin B1 interacting protein 1 (CCNB1IP1), transcript variant 2.
RAB3IL1	1.17	3.22E-09	RAB3A interacting protein (rabin3)-like 1 (RAB3IL1).
C20orf75	-1.34	3.36E-09	chromosome 20 open reading frame 75 (C20orf75).
GPR56	-1.84	3.43E-09	G protein-coupled receptor 56 (GPR56), transcript variant 2.
MLLT11	-1.55	3.48E-09	myeloid/lymphoid or mixed-lineage leukemia (trithorax homolog, Drosophila); translocated to, 11 (MLLT11).
H19	2.40	3.48E-09	H19, imprinted maternally expressed transcript (H19) on chromosome 11.
BMP2	-1.76	3.56E-09	bone morphogenetic protein 2 (BMP2).
TAGLN	-2.90	3.56E-09	transgelin (TAGLN), transcript variant 2.
FEZ1	-1.00	3.57E-09	fasciculation and elongation protein zeta 1 (zygin I) (FEZ1), transcript variant 2.
FOXQ1	2.86	3.60E-09	forkhead box Q1 (FOXQ1).
RPS26L	2.18	3.97E-09	PREDICTED: 40S ribosomal protein S26-like (RPS26L), misc RNA.
MFAP4	2.10	4.24E-09	microfibrillar-associated protein 4 (MFAP4).
RMND1	0.92	4.49E-09	required for meiotic nuclear division 1 homolog (S. cerevisiae) (RMND1).
SLITRK4	-1.67	4.49E-09	SLIT and NTRK-like family, member 4 (SLITRK4).
DNAJC12	2.36	4.79E-09	DnaJ (Hsp40) homolog, subfamily C, member 12 (DNAJC12), transcript variant 1.
PAPPA	-2.45	4.79E-09	pregnancy-associated plasma protein A, pappalysin 1 (PAPPA).
TMEM5	1.22	4.79E-09	transmembrane protein 5 (TMEM5).
GPR56	-1.68	4.86E-09	G protein-coupled receptor 56 (GPR56), transcript variant 3.
SLFN11	2.29	4.95E-09	schlafen family member 11 (SLFN11).
PTTG1	2.37	4.95E-09	pituitary tumor-transforming 1 (PTTG1).
CTSC	-1.15	4.95E-09	cathepsin C (CTSC), transcript variant 1.
LIAS	1.04	4.95E-09	lipoic acid synthetase (LIAS), nuclear gene encoding mitochondrial protein, transcript variant 1.
NAT10	0.92	4.97E-09	N-acetyltransferase 10 (NAT10).
IL1RL1	2.05	5.49E-09	interleukin 1 receptor-like 1 (IL1RL1), transcript variant 2.
SHMT1	1.04	5.68E-09	serine hydroxymethyltransferase 1 (soluble) (SHMT1), transcript variant 1.
CXCL6	-2.76	5.68E-09	chemokine (C-X-C motif) ligand 6 (granulocyte chemotactic protein 2) (CXCL6).

Top 100 genes differentially expressed in IOSE19$^{CMYC.KRAS/BRAF}$ compared to control cell lines, ranked by statistical significance.

Gene	Log FC	Adjusted P Val	Gene Name
THBS1	-5.79	1.47E-14	thrombospondin 1 (THBS1).
CTGF	-3.48	1.98E-13	connective tissue growth factor (CTGF).
NKD2	3.90	1.98E-13	naked cuticle homolog 2 (Drosophila) (NKD2).
PITX1	3.59	4.50E-13	paired-like homeodomain transcription factor 1 (PITX1).
RGS4	-3.49	4.50E-13	regulator of G-protein signalling 4 (RGS4).
ADFP	-4.86	4.50E-13	adipose differentiation-related protein (ADFP).
TAGLN	-5.18	1.36E-12	transgelin (TAGLN), transcript variant 2.
PCOLCE	3.92	1.72E-12	procollagen C-endopeptidase enhancer (PCOLCE).
MMP9	3.69	1.72E-12	matrix metallopeptidase 9 (gelatinase B, 92kDa gelatinase, 92kDa type IV collagenase) (MMP9).
COL1A2	-3.63	1.72E-12	collagen, type I, alpha 2 (COL1A2).
FEZ1	-2.85	1.72E-12	fasciculation and elongation protein zeta 1 (zygin I) (FEZ1), transcript variant 1.
DNAJC12	3.58	2.68E-12	DnaJ (Hsp40) homolog, subfamily C, member 12 (DNAJC12), transcript variant 1.
VGF	3.19	2.83E-12	VGF nerve growth factor inducible (VGF).
MOCOS	2.95	4.52E-12	molybdenum cofactor sulfurase (MOCOS).
CD9	-2.30	4.90E-12	CD9 molecule (CD9).
FRMD6	-2.40	5.67E-12	FERM domain containing 6 (FRMD6).
TAGLN	-3.08	8.23E-12	transgelin (TAGLN), transcript variant 2.
PALLD	-2.76	8.23E-12	palladin, cytoskeletal associated protein (PALLD).
VCAM1	-2.63	8.72E-12	vascular cell adhesion molecule 1 (VCAM1), transcript variant 1.
PRSS23	-2.40	1.04E-11	protease, serine, 23 (PRSS23).
HIST1H4C	2.43	1.12E-11	histone cluster 1, H4c (HIST1H4C).
MSLN	-2.64	1.13E-11	mesothelin (MSLN), transcript variant 2.
LBH	-1.88	1.16E-11	limb bud and heart development homolog (mouse) (LBH).
MGC23985	-2.32	1.43E-11	similar to AVLV472 (MGC23985).
CTGF	-3.40	1.69E-11	connective tissue growth factor (CTGF).
TYMS	2.69	1.72E-11	thymidylate synthetase (TYMS).
PTGS1	-1.91	1.80E-11	prostaglandin-endoperoxide synthase 1 (prostaglandin G/H synthase and cyclooxygenase) (PTGS1), transcript variant 2.
TIGA1	2.57	2.16E-11	TIGA1 (TIGA1).
PKP2	-1.67	2.45E-11	plakophilin 2 (PKP2), transcript variant 2a.
CADM3	-1.74	3.12E-11	cell adhesion molecule 3 (CADM3).
UBE2C	3.54	3.12E-11	ubiquitin-conjugating enzyme E2C (UBE2C), transcript variant 3.
OLAH	-2.05	3.34E-11	oleoyl-ACP hydrolase (OLAH), transcript variant 1.
PLAT	-2.28	3.34E-11	plasminogen activator, tissue (PLAT), transcript variant 1.
F2R	-1.81	3.48E-11	coagulation factor II (thrombin) receptor (F2R).

GABBR2	-2.83	4.00E-11	gamma-aminobutyric acid (GABA) B receptor, 2 (GABBR2).
ADFP	-3.06	4.04E-11	adipose differentiation-related protein (ADFP).
FBLN5	-2.44	4.19E-11	fibulin 5 (FBLN5).
OSR1	-2.71	4.45E-11	odd-skipped related 1 (Drosophila) (OSR1).
PYCARD	-1.76	4.80E-11	PYD and CARD domain containing (PYCARD), transcript variant 1.
MAD2L1	2.89	5.14E-11	MAD2 mitotic arrest deficient-like 1 (yeast) (MAD2L1).
PRICKLE1	-2.42	5.14E-11	prickle homolog 1 (Drosophila) (PRICKLE1).
GPM6B	1.85	5.14E-11	glycoprotein M6B (GPM6B), transcript variant 1.
MXRA5	-2.11	5.14E-11	matrix-remodelling associated 5 (MXRA5).
PRC1	2.68	6.06E-11	protein regulator of cytokinesis 1 (PRC1), transcript variant 2.
FBLN5	-2.27	6.06E-11	fibulin 5 (FBLN5).
MYLK	-2.24	8.27E-11	myosin light chain kinase (MYLK), transcript variant 8.
DARC	-1.96	8.74E-11	Duffy blood group, chemokine receptor (DARC), transcript variant 2.
RRM2	1.63	8.89E-11	ribonucleotide reductase M2 polypeptide (RRM2).
CDKN2A	-1.31	9.16E-11	cyclin-dependent kinase inhibitor 2A (melanoma, p16, inhibits CDK4) (CDKN2A), transcript variant 1.
VIPR1	-2.44	9.52E-11	vasoactive intestinal peptide receptor 1 (VIPR1).
ITM2A	-2.16	1.02E-10	integral membrane protein 2A (ITM2A).
IL1B	1.90	1.20E-10	interleukin 1, beta (IL1B).
GPR177	-2.60	1.26E-10	G protein-coupled receptor 177 (GPR177), transcript variant 2.
RASL11B	1.90	1.26E-10	RAS-like, family 11, member B (RASL11B).
PTGS2	2.50	1.28E-10	prostaglandin-endoperoxide synthase 2 (prostaglandin G/H synthase and cyclooxygenase) (PTGS2).
ANXA8	-1.78	1.29E-10	annexin A8 (ANXA8).
SLFN11	2.06	1.42E-10	schlafen family member 11 (SLFN11).
HMMR	1.66	1.49E-10	hyaluronan-mediated motility receptor (RHAMM) (HMMR), transcript variant 2.
CSF3	2.49	1.53E-10	colony stimulating factor 3 (granulocyte) (CSF3), transcript variant 1.
FN1	-1.94	1.53E-10	fibronectin 1 (FN1), transcript variant 3.
GINS2	1.65	1.56E-10	GINS complex subunit 2 (Psf2 homolog) (GINS2).
	1.46	1.56E-10	AGENCOURT_14354957 NIH_MGC_191 cDNA clone IMAGE:30413554 5 sequence
OSAP	-1.93	1.56E-10	ovary-specific acidic protein (OSAP).
HTRA1	-1.51	1.56E-10	HtrA serine peptidase 1 (HTRA1).
TK1	1.65	1.77E-10	thymidine kinase 1, soluble (TK1).
OIP5	1.71	1.86E-10	Opa interacting protein 5 (OIP5).
SYNCRIP	-1.48	1.86E-10	synaptotagmin binding, cytoplasmic RNA interacting protein (SYNCRIP).
DNAJC12	3.20	2.01E-10	DnaJ (Hsp40) homolog, subfamily C, member 12 (DNAJC12), transcript variant 2.
LOC652846	-1.79	2.05E-10	PREDICTED: similar to Annexin A8 (Annexin VIII) (Vascular anticoagulant-beta) (VAC-beta) (LOC652846).
DBNL	-1.52	2.05E-10	drebrin-like (DBNL), transcript variant 2.
DKK3	-2.51	2.06E-10	dickkopf homolog 3 (Xenopus laevis) (DKK3), transcript variant 1.
EXTL2	-1.55	2.21E-10	exostoses (multiple)-like 2 (EXTL2), transcript variant 1.
WDR51A	1.68	2.21E-10	WD repeat domain 51A (WDR51A).

SHMT1	1.40	2.40E-10	serine hydroxymethyltransferase 1 (soluble) (SHMT1), transcript variant 1.
KIAA0101	3.68	2.50E-10	KIAA0101 (KIAA0101), transcript variant 1.
PTTG1	2.87	2.50E-10	pituitary tumor-transforming 1 (PTTG1).
IL1A	1.72	2.50E-10	interleukin 1, alpha (IL1A).
UBE2C	3.24	2.50E-10	ubiquitin-conjugating enzyme E2C (UBE2C), transcript variant 6.
LOC644029	1.44	2.53E-10	PREDICTED: similar to 60S ribosomal protein L7a (LOC644029).
SGSH	-1.73	2.83E-10	N-sulfoglucosamine sulfohydrolase (sulfamidase) (SGSH).
WDR1	-1.17	3.30E-10	WD repeat domain 1 (WDR1), transcript variant 1.
SVIL	-1.71	3.41E-10	supervillin (SVIL), transcript variant 1.
KLF2	-1.71	3.68E-10	Kruppel-like factor 2 (lung) (KLF2).
PTPN2	1.19	3.78E-10	protein tyrosine phosphatase, non-receptor type 2 (PTPN2), transcript variant 2.
PGCP	-1.56	3.86E-10	plasma glutamate carboxypeptidase (PGCP).
PLOD2	-2.07	3.95E-10	procollagen-lysine, 2-oxoglutarate 5-dioxygenase 2 (PLOD2), transcript variant 1.
PTGES	3.20	3.98E-10	prostaglandin E synthase (PTGES).
MELK	1.81	4.32E-10	maternal embryonic leucine zipper kinase (MELK).
CTXN1	-1.70	4.32E-10	cortexin 1 (CTXN1).
C11orf1	1.35	4.38E-10	chromosome 11 open reading frame 1 (C11orf1).
TEAD4	1.48	4.53E-10	TEA domain family member 4 (TEAD4), transcript variant 3.
IL11	2.27	4.89E-10	interleukin 11 (IL11).
ITGB1	-1.77	4.89E-10	integrin, beta 1 (fibronectin receptor, beta polypeptide, antigen CD29 includes MDF2, MSK12) (ITGB1), transcript variant 1D.
PLTP	1.48	4.94E-10	phospholipid transfer protein (PLTP), transcript variant 2.
GAL	2.02	4.94E-10	galanin prepropeptide (GAL).
GIPC1	-1.14	5.06E-10	GIPC PDZ domain containing family, member 1 (GIPC1), transcript variant 3.
LOC645688	1.45	5.16E-10	PREDICTED: similar to 60S ribosomal protein L12 (LOC645688).
RFC4	1.65	5.51E-10	replication factor C (activator 1) 4, 37kDa (RFC4), transcript variant 1.
KCNK6	-1.39	5.66E-10	potassium channel, subfamily K, member 6 (KCNK6).
LOC148915	1.21	5.77E-10	PREDICTED: similar to Nonhistone chromosomal protein HMG-17 (High-mobility group nucleosome binding domain 2) (LOC148915).

Appendix B: Manuscripts Published and In Press

.1 *In vitro* Three-Dimensional Modelling of Human Ovarian Surface Epithelial Cells.

Cell Prolif. 2009, **42**, 385–393 doi: 10.1111/j.1365-2184.2009.00604.x

In vitro three-dimensional modelling of human ovarian surface epithelial cells

K. Lawrenson*, E. Benjamin†, M. Turmaine‡, I. Jacobs*, S. Gayther* and D. Dafou*

**Gynaecological Cancer Research Laboratories, UCL Elizabeth Garrett Anderson Institute for Women's Health, University College London, London, UK, †Department of Histopathology, Royal Free/UCL Medical School, London, UK, and ‡Department of Anatomy and Developmental Biology, University College London, London, UK*

Received 30 March 2008; revision accepted 15 July 2008

Abstract

Objectives: Ninety percent of malignant ovarian cancers are epithelial and thought to arise from the ovarian surface epithelium (OSE). We hypothesized that biological characteristics of primary OSE cells would more closely resemble OSE *in vivo* if established as three-dimensional (3D) cultures.

Materials and methods: OSE cells were cultured as multicellular spheroids (MCS) (i) in a rotary cell culture system (RCCS) and (ii) on polyHEMA-coated plastics. The MCSs were examined by electron microscopy and compared to OSE from primary tissues and cells grown in 2D. Annexin V FACS analysis was used to evaluate apoptosis and expression of extracellular matrix (ECM) proteins was analysed by immunohistochemical staining.

Results: On polyHEMA-coated plates, OSE spheroids had defined internal architecture. RCCS MCSs had disorganized structure and higher proportion of apoptotic cells than polyHEMA MCSs and the same cells grown in 2D culture. In 2D, widespread expression of AE1/AE3, laminin and vimentin were undetectable by immunohistochemistry, whereas strong expression of these proteins was observed in the same cells grown in 3D culture and in OSE on primary tissues.

Conclusions: Physiological and biological features of OSE cells grown in 3D culture more closely resemble characteristics of OSE cells *in vivo* than when grown by classical 2D approaches. It is likely that establishing *in vitro* 3D OSE models will lead to greater understanding of the mechanisms of neoplastic transformation in epithelial ovarian cancers.

Corresponding author: Simon A. Gayther: Gynaecological Cancer Research Laboratories, UCL Elizabeth Garrett Anderson Institute for Women's Health, University College London, London, UK. Tel: 020 3108 2009; Fax: 020 3108 2010 Email: s.gayther@ucl.ac.uk

Introduction

Human ovaries are covered with a monolayer of flat/cuboidal mesothelial-type cells referred to as the ovarian surface epithelium (OSE). These cells are widely considered to be the origin of epithelial ovarian cancers, which represent about 90% of all malignant ovarian tumours (1–3). Understanding biological and molecular characteristics of OSE and the earliest stages of ovarian tumour development has been hampered in the past by lack of a suitable *in vitro* model of normal OSE (NOSE). This is partly because primary OSE cells have proved difficult to establish in culture and have a short lifespan *in vitro*. Since the first description of OSE cultures in 1984, optimization of collection techniques and culture media has increased *in vitro* lifespan of these cells (4–6). However, there remain limitations to culturing NOSE cells as standard two-dimensional (2D) monolayers. For example, NOSE cells can lose some of their epithelial characteristics, even when cultured in enriched media (6). Primary NOSE cell cultures show considerable phenotypic plasticity and can exhibit both epithelial (for example, presence of desmosomes; collagen IV, laminin and cytokeratin production) and mesenchymal characteristics (collagen I, collagen III and vimentin production) (5,7).

Three-dimensional (3D) culture systems enable the propagation of cells in a microenvironment that resembles *in vivo* conditions more closely than traditional 2D cultures. *In vivo*, epithelial cells are surrounded by a complex extracellular matrix (ECM). They contact and communicate with a host of different cell types through receptors distributed throughout the entire cell surface. However, in 2D monocultures, clonally derived cells only communicate along a small proportion of their membrane. Cells that are traditionally difficult to culture in 2D, such as primary hepatocytes, can often be maintained *in vitro* for longer periods when grown in 3D cultures (8). There is now substantial evidence to suggest that 3D cultures more closely resemble the *in vivo* microenvironment than 2D cultures, and that culturing cells in 3D can cause phenotypic and molecular changes that reflect *in vivo* biology of the cells more closely than 2D (9–11).

Several different approaches can be used to establish 3D cell culture models. For example, cells can be grown in 3D using ECM protein gel scaffolds (such as collagen gels). Other techniques prevent cell adherence to tissue culture plastics and hence, encourage cells to adhere to each other; such systems include the rotary cell culture system (RCCS) or poly-2-hydroxyethyl methacrylate (polyHEMA)-coated tissue culture plastics. However, few studies have directly compared different 3D culture techniques. In one study, Ghosh *et al*. cultured melanoma cells in collagen gels and found that gene expression profiles were similar to those of cells in 2D; yet when cells were grown on polyHEMA-coated plates, they observed differential expression of > 150 genes (10) and many of the genes upregulated in polyHEMA 3D cultures were consistent with their upregulation *in vivo* (10). Hence, different 3D culture techniques are not equivalent in their effectiveness.

To date, there are no reports describing 3D culturing of NOSE cells. There are some reports of culturing ovarian cancer cells in 3D, in particular, tumour cell aggregates derived from ascites (11–13). The purpose of the current study was to evaluate biological effects of two different 3D culturing techniques on culture of primary normal ovarian surface epithelial cells and to establish a 3D model of NOSE cells that could be used to study the earliest stages of neoplastic transformation in epithelial ovarian cancer. In evaluating these 3D models, we compared morphological and biological characteristics of cells with the same cells grown in 2D cultures and of NOSE from primary tissue samples. We hypothesized that by allowing NOSE cells to form 3D structures, we would maintain a phenotype that more closely resembles NOSE cells *in vivo* than in 2D culture.

Materials and methods

Tissue samples

Primary NOSE cells were collected and established as previously described (6). Two primary cell isolates (NOSE4 and NOSE11) were established from cells obtained during total laparoscopic hysterectomy with bilateral salpingo-oophorectomy procedures. NOSE4 cells were from a 62-year-old-woman diagnosed with endometrioid endometrial cancer stage I and cervical clear cell carcinoma; NOSE11 cells were from a 49-year-old-woman with ovarian stromal and endometrial hyperplasia. Another line, NOSE19L3 was derived from cells from an ovarian cytobrushing from a 39-year old patient undergoing total abdominal hysterectomy for cervical cancer. In all cases, ovarian epithelia were verified as histologically normal with no evidence of hyperplasia nor neoplasia.

Cell culture and reagents

All NOSE cell cultures were maintained in medium (NOSE-CM) comprising MCDB105:Medium 199 (1 : 1) supplemented with 15% foetal bovine serum, 10 ng/ml epidermal growth factor, 0.5 mg/ml hydrocortisone, 5 mg/ml insulin, and 34 mg protein/ml bovine pituitary extract, (all Sigma, St Louis, MO, USA). Primary NOSE cells were collected by brushing the surface of normal ovaries with a sterile cytobrush, which was then agitated in 5 ml of NOSE-CM to release the cells. Suspensions were plated into 25-cm^2 tissue culture flasks and left for 7 days to allow cells to grow. Cell culture medium was changed every 2–3 days until cultures reached 80–90% confluence, at which point they were subcultured. Cells were grown as 3D multicellular spheroids (MSC) either in RCCS (Synthecon, Houston, TX, USA) or in plastic dishes coated with 2.5% solution of polyHEMA (Sigma), prepared in 95% ethanol, also from Sigma.

In vitro phenotypic analysis of cell cultures

Population doubling rates were measured for 1×10^5 cells, in triplicate. Cultures were passaged and population doublings (PD) calculated using the following formula:

$$PD = \log(\text{total cell number at each passage/initial cell number})/\log 2.$$

Assays for anchorage independent growth were performed by plating 2×10^4 cells in complete medium containing 0.3% Noble Agar (Sigma) over a base layer of complete medium containing 0.6% Noble Agar. Five replicates were plated for each primary NOSE cell line. As control, anchorage independent growth was evaluated simultaneously for the TOV112D endometrioid ovarian cancer cell line. After 4 weeks, cells were fixed with methanol and stained with 1% p-iodonitrotetrazolium violet (Sigma). Colony formation was observed and number of colonies containing > 50 cells were counted. Colony forming efficiencies (CFE %) were calculated using the following formula:

$$CFE = [(\text{number of colonies counted})/(\text{number of cells plated})] \times 100\%.$$

Immunoflourescent cytochemistry/immunohistochemistry

All three primary cell isolates (NOSE4, NOSE11 and NOSE19L3) were confirmed as epithelial by immunofluorescent cytochemistry, performed using standard protocols. The following antibodies were used (all diluted 1 : 1000): AE1/AE3 (Dako Corporation, Carpinteria, CA,

USA), cytokeratin 7 (CRUK, London, UK), BerEp4 (Dako), CA125 (Dako), E-cadherin (Cell Signaling, Danvers, MA, USA), FSP (Sigma), and Factor VIII (Lab Vision, Fremont, CA, USA). All cell cultures tested were found to express epithelial markers (AE1/AE3, BerEP4, ck7), and did not express endothelial cell (Factor VIII) and fibroblast (FSP) markers. Cells were weakly positive for ovarian cancer-associated marker CA125. This observation is consistent with findings of another study: 50% of NOSE cell cultures express CA125 in the first few passages (14). Staining for CA125 was also observed in primary ovaries from which NOSE4 and NOSE11 were derived. Immunohistochemistry for 2D and 3D cultures was performed using standard protocols at the CRUK Histology Service.

Apoptosis assays

MCSs from 3D cell clusters were washed in phosphate-buffered saline and trypsinized at 37 °C to create single cell suspensions; 2D cultures were trypsinized and centrifuged, and cell pellets resuspended in FACS buffer, according to manufacturer's instructions (Roche, Basel, Switzerland). Samples were run on a Becton Dickinson FACS Scan (Franklin Lakes, NJ, USA) and the annexin V-positive cell population was measured.

Transmission electron microscopy/scanning electron microscopy

Cells were either grown on glass coverslips or, for 3D cultures, cell clusters were harvested and media aspirated. Cells were washed once with phosphate-buffered saline from VWR (West Chester, PA, USA) then fixed with 2% paraformaldehyde, 1.5% glutaraldehyde in 0.1 M cacodylate buffer (pH 7.3) for 1–2 h (all from Sigma). Samples were then washed in 0.1 M cacodylate buffer and post-fixed with 1% osmium tetroxide (Sigma) in 0.1 M cacodylate buffer (pH 7.3) for 1 h at 4 °C, before washing twice in 0.1 M cacodylate buffer, then water for 5 min. Samples were stained with 0.5% uranyl acetate (Sigma) for 20 min then washed in water before dehydration with increasing concentrations of ethanol. Samples were then embedded in agar resin, sectioned and examined on a JEOL (JEOL Ltd, Tokyo, Japan) 1010 transmission electron microscope. For scanning electron microscopy, samples were fixed as for transmission electron microscopy, post-fixed with 1% osmium tetroxide in 0.1 M cacodylate buffer (pH 7.3) for 45 min at 4 °C and dehydrated with increasing concentrations of ethanol. Samples were then critically point dried, mounted on carbon stubs and gold-coated before viewing using a JEOL 7401 series FEGSEM.

Results

The aim of this study was to establish 3D *in vitro* models of NOSE cells and to compare morphological and biological characteristics with the same cells grown as 2D cultures, and with primary ovarian tissues. We first established and characterized three primary NOSE cell isolates (NOSE4, NOSE11, NOSE19L3) grown as 2D monolayers. Cell cultures *in vitro* had growth characteristics typical of NOSE cell cultures (Table 1) (6). NOSE11 cells had the shortest population doubling time and the longest lifespan of the three primary cell isolates. This may be because NOSE4 cells were derived from a postmenopausal woman and, therefore, are likely to have reduced lifespan *in vitro*. NOSE19L3 was a clone isolated from cell brushing thus, originates from a smaller initial population, hence the reduced lifespan observed in this culture.

Table 1. Patient information and growth characteristics of normal primary ovarian epithelial cells (OSE)

	Patient characteristics		Cells grown as 2D monolayers			3D multicellular spheroids
Primary cell line	Age	Menopausal status	PD time[a] (hours)	Maximum no. of PDs	CFE in soft agar[b]	Average MCS diameter (μm) (range)[c]
NOSE4	62	Post	82.4	7.6	0	78.25 (32.70–152.00) $n = 11$
NOSE11	48	Peri	57.2	17.8	0	91.053 (80.92–252.40) $n = 11$
NOSE19L3	39	Pre	83.6	9.7	0	171.98 (63.90–125.60) $n = 5$

[a]Population doubling (PD) times calculated from the exponential growth phase; [b]colony forming efficiency (CFE); [c]multicellular spheroids (MCS) grown in 3D by polyHEMA coating of tissue culture plastics, size measured under the scanning electron microscope.

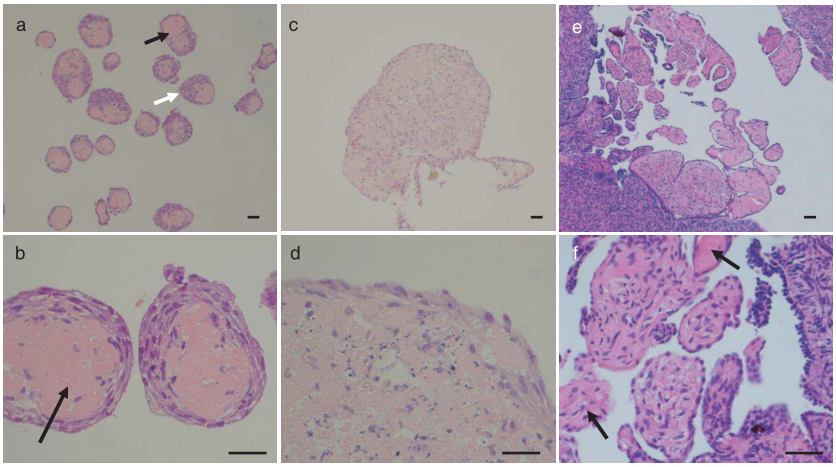

Figure 1. Haematoxylin and eosin-stained sections of multicellular spheroids from three-dimensional (3D) cultures. Normal ovarian surface epithelium (NOSE) cells form smaller 3D multicellular structures when cultured on polyHEMA-coated plates (PH-MCSs) (a,b) compared to culturing in the rotary cell culture system (RCCS-MCSs) (c,d). The matrix cores of PH-MCS are clearly visible (black arrows); cells form either a ring around the matrix or a 'cap' on one side (white arrow). PH-MCSs show architectural resemblance to 3D structures observed on the surface of the ovary *in vivo* (e,f), where surface papillary projections consist of epithelial cells around stromal cores with matrix protein (black arrows). Scale bars represent 0.1 mm.

Table 2. Differential expression of pan-cytokeratin (AE1/AE3), laminin, vimentin and collagen IV, detected by immunohistochemistry in two- (2D) and three-dimensional (3D) cultures and in primary normal ovarian tissues. Graded shading denotes extent of staining. White denotes negative staining; crosshatched grey denotes weak or focal staining; light grey represents that 20–50% cells stain positive; and dark grey shading indicates over 50% cells stain positive.

Marker	NOSE 4			NOSE 11			NOSE 19L3			Normal OSE
	2D	PH-MCS	RCCS-MCS	2D	PH-MCS	RCCS-MCS	2D	PH-MCS	RCCS-MCS	*In vivo*
AE1/AE3										
Collagen IV					[2]					
Fibronectin[1]										
Laminin[1]										
Vimentin				[3]			[3]			

[1]Secreted matrix material also shows positive staining for fibronectin and laminin.

[2]Focal staining of collagen IV in NOSE11 PH-MCS.

[3]NOSE11 and NOSE19L3 show limited focal staining for vimentin around mitoses in 2D.

Establishing and characterizing 3D NOSE cell cultures

All three primary cell isolates formed MCSs when cultured for 14 days either on polyHEMA-coated plates or in the Rotary Cell Culture System (Fig. 1). MCSs appeared solid and smooth by light microscopy. MCSs grown on polyHEMA-coated plates (PH-MCSs) were typically 70–170 µm in diameter (Table 1). NOSE19L3 cells formed significantly larger PH-MCS than NOSE4 or NOSE11 cells ($P < 0.0001$ and $P = 0.025$, respectively; two-tailed unpaired *t*-test). MCSs formed in the RCCS (RCCS-MCS) grew to 1–2 mm in diameter.

We examined the internal architecture of MCSs following paraffin wax embedding, sectioning, and staining with haematoxylin and eosin. For all three primary cell cultures, PH-MCSs had defined internal architecture: a central core of matrix protein, surrounded by aligned elongated cells. The cells formed a ring around the matrix core, often with a 'cap' to one side, with resemblance to papillary structures sometimes observed on the surface of

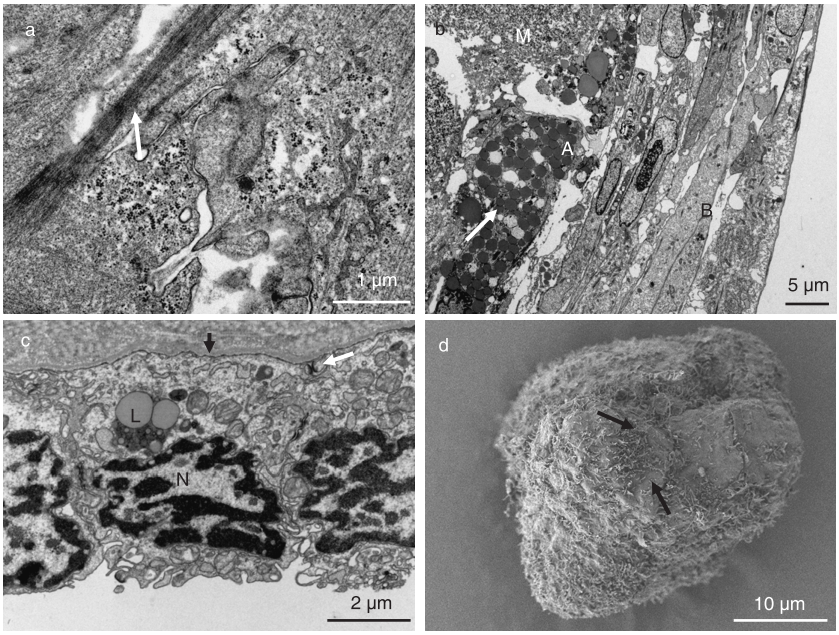

Figure 2. Transmission and scanning electron micrographs of normal ovarian surface epithelium (NOSE) cells in culture and from primary tissues. (a) A high-power electron micrograph of two-dimensional (2D) NOSE cultured cells. Bundles of intermediate filaments can be seen, with the formation of desmosomes between adjacent cells (white arrow). (b) A low-power electron micrograph of multicellular structures cultured on poly-HEMA-coated plates (PH-MCS) showing the flatter and closely opposed cells at the periphery forming concentric rings (such as cell B). Cells within the inner region of the PH-MCS have a more rounded morphology and are less tightly packed (cell A). Note the cells towards the core of the MCS are full of electron dense vesicles (white arrow), which may illustrate a trend to a more secretary phenotype towards the centre of the multicellular clusters. Extracellular material (M) is abundant in the cores of PH-MCS. (c) Section of quiescent ovarian epithelium. Note the cuboidal shape of cell, condensed chromatin within the nuclei (N), basement membrane (black arrow), desmosomes (white arrow) and age-related storage: lipofuscin (L). *In vivo* NOSE cells are mostly quiescent (unless at the site of follicular rupture, following ovulation). (d) A low power SEM image of a PH-MCS showing surface morphology. The flattened surface cells form a patchwork with no obvious orientation. The number of surface protrusions varied from a few to many between cells (black arrows).

normal ovaries *in vivo* (Fig. 1). The matrix core often contained degenerate nuclear debris. When cells were grown in RCCS, resulting MCSs had a less organized arrangement of cells. Cells within RCCS spheroids tended to be more rounded with a 1–2 cell deep layer of cells around the edge of the clusters which had an elongated morphology (Fig. 1).

Ultrastructure of PH-MCS

PH-MCS were architecturally interesting, so we used transmission and scanning electron microscopy to study their ultrastructure and of the same cells grown in 2D. Desmosomes, which are characteristic of epithelial cells, were present in all 2D and 3D cultures (Fig. 2a). In PH-MCSs, outer cells (up to 8 cell layers but sometimes only 1–2 cells thick) were elongated and aligned. Peripheral cells were also longer in shape compared to cells located towards the core of the spheroid, where cells were rounder and less densely packed (Fig. 2b). Transmission electron microscopy of PH-MCSs revealed that cells towards the centre tended to have extensive and dilated rough endoplasmic reticulum, well-developed Golgi apparatus and open nucleolus. Some cells appeared to have formed a discontinuous basement membrane and matrix-like material in the extracellular space. This ECM material was abundant in the core of the MCSs.

When examined by scanning electron microscopy (SEM), cells on the outer surface of PH-MCS had a flattened morphology and very few surface features. Although microvilli were absent, there were often many surface projections connecting adjacent cells amongst PH-MCS. Two-dimensional monolayers also had very few surface features; cells were unremarkable, with the exception of long surface projections extending between cells, similar to those seen on PH-MCSs. Absence of microvilli may have been due to loss of polarization as a result of culturing the cells on glass. It may be possible to overcome this by growing NOSE cells with oestrogen, ovarian stromal fibroblasts or on collagen or fibronectin-coated plates to attempt to maintain polarization and microvilli formation (15,16). Dead cells were observed both on the surface of

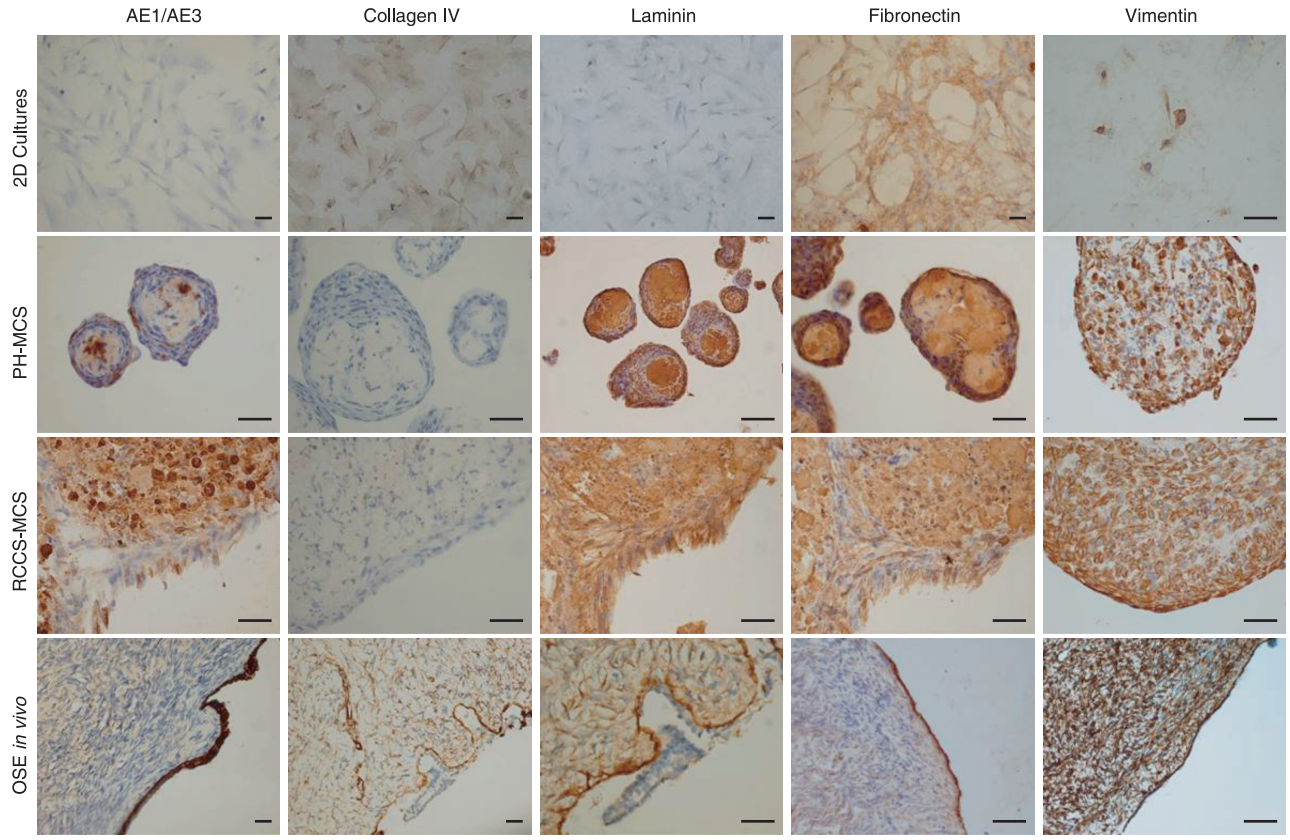

Figure 3. Expression analysis of candidate markers by immunohistochemistry of normal ovarian surface epithelium (NOSE) cells from representative two- (2D) and three-dimensional (3D) cultures and in primary NOSE from tissue sections of normal ovaries. A summary of the results of these analyses are given in Table 2. Here, staining patterns suggest that primary NOSE from normal ovarian tissues express a range of extracellular matrix proteins (e.g. vimentin, fibronectin, laminin). Staining profiles of 3D cultures more closely resemble that of primary OSE than 2D cultures. Scale bars represent 0.1 mm.

the PH-MCS and in 2D cultures. Early-stage cell death was identifiable by holes in the membrane and later-stage degraded cells were observed budding off the PH-MCSs and 2D cultures.

Expression of ECM proteins in 2D and 3D cultures

Previous studies have shown that culturing cells in 3D may alter cell–cell interactions, including expression of ECM proteins, receptors and corresponding degradative enzymes. NOSE cells reportedly produce a variety of ECM molecules *in vitro* (17). Therefore, we used immunohistochemistry to determine whether any of these proteins were differentially expressed between 2D and 3D cultures (Fig. 3). Fibronectin was expressed in 2D and 3D cultures in all three cell cultures. For 2 out of the 3 cell cultures, weak focal vimentin staining was observed in 2D cultures around some mitoses. However, strong positive vimentin characterized all 3D cultures and OSE *in vivo*. Laminin and AE1/AE3 were not expressed in 2D cultures, but strong expression of these markers was observed PH-MCSs, RCCS-MCSs and in epithelium of normal ovarian tissue. Fibrous fibronectin, laminin and vimentin filaments were observed between cells, suggesting that these proteins play a role in maintaining the structure of MCSs. For the markers tested, staining intensity did not vary according to spheroid size.

Apoptosis in 2D and 3D cultures

We characterized the proportion of apoptotic cells in the cultures using annexin V and propidium iodide staining, followed by FACS analysis (Fig. 4). Propidium iodide staining identifies the necrotic component of cell cultures; annexin V recognizes externalized phosphatidylserine, which is a measure of early stages of apoptosis. In RCCS-MCSs, the proportion of cells positive for annexin V was at least 2.5-fold that of 2D cultures and PH-MCSs. For

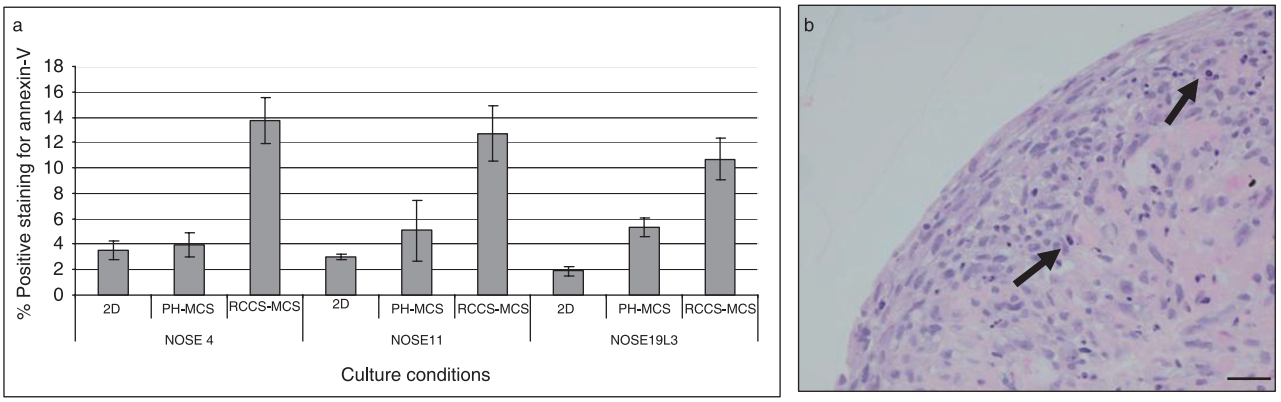

Figure 4. Variation in levels of apoptosis in two- (2D) and three-dimensional (3D) cultures. (a) Levels of apoptosis (as measured by annexin V expression) are significantly higher in 3D multicellular spheroids (MCS) grown in the rotary cell culture system (RCCS-MCS) compared to 2D cultures and MCS grown on polyHEMA-coated plates (PH-MCS). Error bars = standard error of the mean (SEM). (b) Apoptotic cells (arrow) are visible throughout the RCCS-MCS, and are not localized to a necrotic 'core' of MCSs. Scale bar represents 0.1 mm.

two cell cultures, we did not observe any significant difference in proportion of apoptotic cells in PH-MCSs compared to 2D cultures. For one primary cell isolate (NOSE19L3), there was significantly more apoptosis in PH-MCS ($P = 0.0470$ using two-tailed paired *t*-test) compared to 2D cultures. This may be due to the shorter population doubling time for this culture or due to loss of apoptotic cells from 2D cultures during washing and harvesting. We found significant differences in proportions of annexin V-positive cells in RCCS-MCSs compared to 2D cultures and PH-MCS for all three cell cultures (NOSE4, $P = 0.0176$; NOSE11, $P = 0.0164$; and NOSE19L3, $P = 0.0152$, using two-tailed paired *t*-tests). For one culture (NOSE11), we observed by propidium iodide staining, a significantly larger necrotic component in RCCS-MCSs compared to 2D and PH-MCSs ($P = 0.0242$, two-tailed paired *t*-test). Thus, for this culture there was a statistically significant increase in the proportion of cells at all stages of apoptosis in RCCS cultures compared to cultures grown in 2D or on polyHEMA-coated plates. Indeed, cells at all stages of apoptosis were distributed throughout the RCCS-MCSs (Fig. 4).

Discussion

To the best of our knowledge, this paper describes for the first time the development and characterization of a 3D model of normal ovarian surface epithelial cells. The OSE is typically described as a monolayer of cells, but it nonetheless has a 3D architecture that cannot be replicated by culturing primary NOSE cells in 2D on adherent plastic surfaces. In this study, we show that NOSE cells form 3D structures (MCSs) when cells are prevented from adhering to tissue culture surfaces either by chemical treatment of tissue culture vessels or by maintaining cells in constant rotation. In the RCCS, NOSE cell clusters were larger and had a chaotic internal structure compared to cells grown on polyHEMA-coated plastics. NOSE cells grown in polyHEMA-coated vessels formed concentric layers around a core of matrix protein. These data suggest that in a static microenvironment, NOSE cells spontaneously form organized 3D multicellular structures.

There are other reports describing 3D cell aggregates of other cell types in which two distinct regions of cells are observed: an inner area of cells that are smaller and less proliferative than surrounding cells on the periphery of MCS (10,18). In one study, Freyer and Sutherland found that cells on the surface of MCSs formed from mouse mammary tumour cells were similar in size to an exponentially growing 2D cell culture, but with 60% less cells in S phase (19). Our observations of the structure of RCCS-MCSs (by light microscopy) and PH-MCSs (by light and transmission electron microscopy) are consistent with these findings: instead of a continual reduction in cell size from the outer to inner core of spheroids, we found clear distinction in morphology between cells on the outer layers compared to cells within the spheroids. Cells within MCS also appeared to be rounder in shape compared to elongated cells at the periphery. Other studies have found differences in cell size and morphology at different regions of MCSs (10,19).

Measurements of apoptosis between 2D and 3D cultures suggest a greater proportion of cells grown in the RCCS are apoptotic when compared to 2D and polyHEMA 3D cultures. This was confirmed by the observation of many apoptotic nuclei distributed throughout the RCCS-MCS. An explanation for this is unclear, but it could be that the continual motion of spinning the cells in

the RCCS causes mechanical damage which in turn induces apoptosis. Thus, increased levels of apoptosis observed in RCCS-MCSs may be an experimental artefact. Apoptosis is generally low in the ovarian epithelium *in vivo* since these cells are usually quiescent (except immediately after rupture of a mature follicle). Unlike some cancer cell spheroids, extensive apoptosis and necrosis is not localized to the cores of the clusters. Conditions at the centre of the RCCS-MCS are unlikely to be hypoxic in comparison to the *in vivo* microenvironment – the oxygen concentration in the pelvis is 5.5% (measured at the cervix) and cells were cultured in 20% oxygen (20), further suggesting that increased rates of apoptosis observed in RCCS-MCS were a consequence of mechanical damage. Indeed, we have observed that prolonged culture in the RCCS can result in spheroids that consist only of cells that have degenerated (unpublished data).

Transmission electron microscopy of PH-MCSs revealed that cells contained swollen endoplasmic reticulum and Golgi apparatus and had an open nucleolus. Cells within PH-MCS were actively producing and appeared to be secreting a basement-membrane-like matrix, which was abundant in the core of the MCSs. ECM molecules play a vital role in tissue architecture and are vital for the formation of hepatoma spheroids (21). Both RCCS-MCSs and PH-MCSs produced an abundance of ECM proteins laminin, fibronectin and vimentin, but did not express collagen IV. Two-dimensional cultures showed widespread expression of fibronectin and collagen IV but not laminin, and vimentin was only expressed focally at mitoses in 2 out of the 3 primary cell cultures. These patterns of protein expression reflect the phenotypic plasticity that is characteristic of NOSE cells: in both 2D and 3D, cells show both epithelial (collagen IV, laminin, cytokeratin) and mesenchymal (vimentin) features.

In general, cells demonstrate considerable plasticity and have an ability to respond dramatically to their environment. A transcriptome that promotes growth within an organism is unlikely to provide the cell with an optimal phenotype for growth in 2D. Since the 1970s, 3D culture techniques have been considered to be an invaluable tool for studying cancer cell growth. Some studies have suggested that multicellular tumour spheroids grown either in spinner flasks or on polyHEMA-coated plates are representative of the early stages of tumour growth prior to vascular involvement (10,22). Furthermore, many studies point to the downstream pathways of cancer cell interactions with the ECM as important therapeutic targets (23). Thus, 3D models, such as those presented here, are likely to represent useful tools to examine the roles of different genes involved in the earliest stages of tumorigenesis. More complex, heterotypic cultures containing ovarian stromal fibroblasts and endothelial cells will assist in developing our understanding of the role of interactions between different cell types during epithelial tumourigenesis. There is a need for more biologically relevant *in vitro* models of epithelial ovarian cancer since *in vivo* modelling of this disease has had limited success (24,25). Despite the discovery of ovary-specific Mullerian-inhibiting substance receptor type II, an *in vivo* model that accurately reflects epithelial ovarian cancer: a disease that is late-onset and histologically heterogeneous, has yet to be established. By mimicking the processes of early ovarian tumour development in an microenvironment that closely resembles this process *in vivo*, it may be possible to identify new proteins associated with tumour progression that represent biomarkers for early detection of disease and/or novel therapeutic targets.

Acknowledgements

This work is supported by an Medical Research Council studentship (Kate Lawrenson), the Eve Appeal Gynaecology Cancer Research Fund and the Rosetrees Trust (via The Eve Appeal). We also thank Ken Choi for his help with fluorescence activated cell sorting analysis.

References

1 Scully RE (1995) Pathology of ovarian cancer precursors. *J. Cell. Biochem*. **23**, 208–218.
2 Auersperg N, Wong AS, Choi KC, Kang SK, Leung PC (2001) Ovarian surface epithelium: biology, endocrinology, and pathology. *Endocr. Rev*. **22**, 255–288.
3 Okamura H, Katabuchi H (2001) Detailed morphology of human ovarian surface epithelium focusing on its metaplastic and neoplastic capability. *Ital. J. Anat. Embryol*. **106**(2 Suppl. 2), 263–276.
4 Auersperg N, Siemens CH, Myrdal SE (1984) Human ovarian surface epithelium in primary culture. *In Vitro* **20**, 743–755.
5 Auersperg N, Maines-Bandiera SL, Dyck HG, Kruk PA (1994) Characterization of cultured human ovarian surface epithelial cells: phenotypic plasticity and premalignant changes. *Lab. Invest*. **71**, 510–518.
6 Li NF, Wilbanks G, Balkwill F, Jacobs IJ, Dafou D, Gayther SA (2004) A modified medium that significantly improves the growth of human normal ovarian surface epithelial (OSE) cells *in vitro*. *Lab. Invest*. **84**, 923–931.
7 Dyck HG, Hamilton TC, Godwin AK, Lynch HT, Maines-Bandiera S, Auersperg N (1996) Autonomy of the epithelial phenotype in human ovarian surface epithelium: changes with neoplastic progression and with a family history of ovarian cancer. *Int. J. Cancer* **69**, 429–436.
8 Khaoustov VI, Darlington GJ, Soriano HE, Krishnan B, Risin D, Pellis NR *et al*. (1999) Induction of three-dimensional assembly of human liver cells by simulated microgravity. *In. Vitro. Cell Dev. Biol. Anim*. **35**, 501–509.
9 Knuechel R, Keng P, Hofstaedter F, Langmuir V, Sutherland RM, Penney DP (1990) Differentiation patterns in two- and three-dimensional culture systems of human squamous carcinoma cell lines. *Am. J. Pathol*. **137**, 725–736.
10 Ghosh S, Spagnoli GC, Martin I, Ploegert S, Demougin P, Heberer M *et al*. (2005) Three-dimensional culture of melanoma cells profoundly

affects gene expression profile: a high density oligonucleotide array study. *J. Cell. Physiol*. **204**, 522–531.
11 Zietarska M, Maugard CM, Filali-Mouhim A, Alam-Fahmy M, Tonin PN, Provencher DM *et al*. (2007) Molecular description of a 3D *in vitro* model for the study of epithelial ovarian cancer (EOC). *Mol. Carcinog*. **46**, 872–885.
12 Burleson KM, Casey RC, Skubitz KM, Pambuccian SE, Oegema TR Jr, Skubitz AP (2004) Ovarian carcinoma ascites spheroids adhere to extracellular matrix components and mesothelial cell monolayers. *Gynecol. Oncol*. **93**, 170–181.
13 Burleson KM, Boente MP, Pambuccian SE, Skubitz AP (2006) Disaggregation and invasion of ovarian carcinoma ascites spheroids. *J. Transl. Med*. **4**, 6.
14 Auersperg N, Maines-Bandiera SL, Dyck HG (1997) Ovarian carcinogenesis and the biology of ovarian surface epithelium. *J. Cell. Physiol*. **173**, 261–265.
15 Saridogan E, Djahanbakhch O, Kervancioglu ME, Kahyaoglu F, Shrimanker K, Grudzinskas JG (1997) Placental protein 14 production by human Fallopian tube epithelial cells *in vitro*. *Hum. Reprod*. **12**, 1500–1507.
16 Bai W, Oliveros-Saunders B, Wang Q, Acevedo-Duncan ME, Nicosia SV (2000) Estrogen stimulation of ovarian surface epithelial cell proliferation. *In. Vitro. Cell Dev. Biol. Anim*. **36**, 657–666.
17 Kruk PA, Uitto VJ, Firth JD, Dedhar S, Auersperg N (1994) Reciprocal interactions between human ovarian surface epithelial cells and adjacent extracellular matrix. *Exp. Cell. Res*. **215**, 97–108.
18 Sutherland RM, Sordat B, Bamat J, Gabbert H, Bourrat B, Mueller-Klieser W (1986) Oxygenation and differentiation in multicellular spheroids of human colon carcinoma. *Cancer Res*. **46**, 5320–5329.
19 Freyer JP, Sutherland RM (1980) Selective dissociation and characterization of cells from different regions of multicell tumor spheroids. *Cancer Res*. **40**, 3956–3965.
20 Juul N, Jensen H, Hvid M, Christiansen G, Birkelund S (2007) Characterization of *in vitro* chlamydial cultures in low-oxygen atmospheres. *J. Bacteriol*. **189**, 6723–6726.
21 Lin RZ, Chou LF, Chien CC, Chang HY (2006) Dynamic analysis of hepatoma spheroid formation: roles of E-cadherin and β1-integrin. *Cell Tissue Res*. **324**, 411–422.
22 Sutherland RM, Durand RE (1976) Radiation response of multicell spheroids – an *in vitro* tumour model. *Curr. Top. Radiat. Res. Q* **11**, 87–139.
23 Ahmed AA, Mills AD, Ibrahim AE, Temple J, Blenkiron C, Vias M *et al*. (2007) The extracellular matrix protein TGFBI induces microtubule stabilization and sensitizes ovarian cancers to paclitaxel. *Cancer Cell* **12**, 514–527.
24 Connolly DC, Bao R, Nikitin AY, Stephens KC, Poole TW, Hua X *et al*. (2003) Female mice chimeric for expression of the simian virus 40 TAg under control of the MISIIR promoter develop epithelial ovarian cancer. *Cancer Res*. **63**, 1389–1397.
25 Garson K, Shaw TJ, Clark KV, Yao DS, Vanderhyden BC (2005) Models of ovarian cancer – are we there yet? *Mol. Cell. Endocrinol*. **239**, 15–26.

.2 Senescent Fibroblasts Promote Neoplastic Transformation of Ovarian Epithelial Cells in a Three-Dimensional Model of Early Stage Ovarian Cancer, submitted to Neoplasia

NEOPLASIA
www.neoplasia.com

Volume 12 Number 4 April 2010 pp. 317–325 317

Senescent Fibroblasts Promote Neoplastic Transformation of Partially Transformed Ovarian Epithelial Cells in a Three-dimensional Model of Early Stage Ovarian Cancer[1,2]

Kate Lawrenson*[,3], Barbara Grun*, Elizabeth Benjamin†, Ian J. Jacobs*, Dimitra Dafou* and Simon A. Gayther*

*Gynaecological Cancer Research Laboratories, UCL EGA Institute for Women's Health, University College London, London, UK; †Department of Histopathology, Royal Free/UCL Medical School, Rockefeller Building, London, UK

Abstract

Most epithelial ovarian cancers are diagnosed postmenopausally, although the well-established epidemiological risk factors (parity, oral contraceptive use) are premenopausal. We hypothesized that accumulation of senescent fibroblasts, together with concomitant loss of presenescent fibroblasts within the ovarian cortex, promotes initiation and early development of ovarian cancer from ovarian surface epithelial (OSE) cells. To test this, we established immortalized OSE (IOSE) cell lines that mimic early neoplastic transformation by overexpressing the *CMYC* oncogene ($IOSE^{CMYC}$) and normal ovarian presenescent (PSN) and senescent (SEN) fibroblast cell lines. We then evaluated the ability of PSN and SEN fibroblasts to transform IOSE and $IOSE^{CMYC}$ after coculture. SEN fibroblasts significantly enhanced neoplastic development of $IOSE^{CMYC}$ cells; there was an up to 15-fold increase in migration of $IOSE^{CMYC}$ cells cocultured with SEN fibroblasts compared with PSN fibroblasts. Conditioned medium from SEN fibroblasts promoted anchorage-independent growth of $IOSE^{CMYC}$ cells. We studied fibroblast-epithelial cell interactions in heterotypic three-dimensional spheroid models. Dual immunohistochemical staining of spheroids for a proliferation marker (MIB-1) and cytokeratin-18 indicated that SEN fibroblasts induce approximately a five-fold increase in proliferation of $IOSE^{CMYC}$ cells relative to cocultures with PSN fibroblasts. SEN, but not PSN fibroblasts, also induced nuclear atypia in epithelial cells in three-dimensional spheroids. These data suggest for the first time that the accumulation of senescent, or loss of presenescent fibroblasts, can promote neoplastic development of partially transformed OSE cells *in vitro* and illustrates the power of using three-dimensional heterotypic modeling to gain better insights into the etiology underlying the development of epithelial ovarian cancer.

Neoplasia (2010) 12, 317–325

Introduction

More than 80% of all epithelial ovarian cancers (EOCs) are diagnosed in postmenopausal women older than 60 years [1,2]. However, the strongest epidemiological risk factors for EOC are premenopausal factors (oral contraceptive pill use and parity) [3,4]. High-grade serous tumors are the most common histopathologic subtype of the disease but are rarely diagnosed at an early stage, suggesting that these tumors progress rapidly. One hypothesis to explain postmenopausal disease development is that some as yet unknown microenvironmental trigger initiates proliferation in dormant epithelial cells that harbor somatic mutation(s). One possible trigger could be age-related changes (senescence) occurring in ovarian stromal fibroblasts, which work in synergy with early genetic changes in the epithelium to promote EOC development.

Abbreviations: NOF, normal ovarian fibroblast; INOF, immortalized NOF; SEN, senescent NOF; PSN, presenescent NOF; OSE, ovarian surface epithelium; IOSE, immortalized ovarian surface epithelium

Address all correspondence to: Kate Lawrenson, PhD, MRC Laboratory for Molecular Cell Biology, University College London, Gower Street, London, WC1E 6BT, UK.
E-mail: kate.lawrenson@ucl.ac.uk

[1]This work was funded by Medical Research Council studentships (K.L. and B.G.), the Eve Appeal Gynaecology Cancer Research Fund, the Rosetrees Trust, and by a charitable donation from UCLH special trustees.

[2]This article refers to supplementary material, which is designated by Figure W1 and is available online at www.neoplasia.com.

[3]Current address: MRC Laboratory for Molecular Cell Biology, University College London, Gower Street, London, WC1E 6BT, UK.

Received 23 November 2009; Revised 26 January 2010; Accepted 27 January 2010

DOI 10.1593/neo.91948

As an organism ages, senescent fibroblasts accumulate in the tissue stroma, gradually replacing presenescent cells [5,6]. *In vitro* and *in vivo* models have demonstrated that normal fibroblasts in a normal tissue microenvironment can inhibit early tumorigenesis but that fibroblast senescence results in a loss of inhibition of tumorigenesis and/or promotion of epithelial transformation [7–9]. For example, senescent fibroblasts enhance epithelial neoplastic progression *in vitro* and promote the formation of tumor xenografts *in vivo* in models of mammary, prostate, and keratinocyte tumors [10–13]. Senescent cells do not divide but remain metabolically active, and the profile of secreted proteins in senescent cells differs substantially from their nonsenescent counterparts [14]. The induction of senescence induces a senescence-associated secretory phenotype; senescent fibroblasts secrete a multitude of growth factors (including vascular endothelial growth factor), extracellular matrix proteins, proteases, chemokines, and cytokines [14,15]. It is likely that these molecules act in paracrine to affect the phenotype of neighboring epithelium, directly and indirectly, through remodeling of the extracellular matrix and/or through interaction with other cell types (e.g., inflammatory or endothelial cells) [8,16].

The aim of the current study was to investigate the role of aging fibroblasts in the initiation and development of EOCs, using a three dimensional model of cellular transformation of the ovarian surface epithelium (OSE). We have previously established three-dimensional cell culture models of normal, primary OSE cells and demonstrated their biological similarities to primary tissues [17]. In the current study, we created a three-dimensional heterotypic model of ovarian stromal-epithelial cell interactions, and of the earliest stages of OSE transformation, to test the hypothesis that accumulation of senescent fibroblasts, with concomitant loss of presenescent stromal cells, contributes to transformation of ovarian epithelial cells. The results imply a role for senescent fibroblasts in promoting early tumorigenesis of OSE and further suggest that the ovarian stromal microenvironment may have a crucial role in the development of EOCs.

Materials and Methods

Cell Culture, Retroviral Production, and Transduction

Primary normal ovarian surface epithelial (NOSE) cell isolates NOSE4, NOSE11, and NOSE19L3 have been previously described [17]. All ovarian epithelial cell cultures were maintained in NOSE medium (NOSE-CM) [17]. Normal ovarian fibroblast (NOF) cells were isolated from a patient undergoing total abdominal hysterectomy for endometrial carcinoma. The ovary was confirmed as free of disease by a gynecological pathologist (E.B.). A tissue sample was excised from the ovary and washed twice with phosphate-buffered saline (PBS; from VWR, Lutterworth, UK) to remove loosely attached epithelial cells. Tissue was then minced and incubated at 37°C/5% CO_2 for 7 to 14 days to allow colony growth. Colonies with fibroblastic morphologies were isolated. Fibroblast cultures were maintained in basic medium MCDB105/Medium 199 (1:1 ratio; both Sigma, St Louis, MO), 15% fetal bovine serum (FBS), and 1% L-glutamine (both Invitrogen, Paisley, UK). To induce senescence, cells were exposed for 2 hours to 80 μM of hydrogen peroxide solutions (VWR) diluted in culture medium. β-Galactosidase bioactivity assays were performed as previously described [18]. Senescent fibroblasts were freshly prepared for replicate experiments.

293T cells at 70% confluence were cotransfected with the pVPack10A1, pVPackGP, and pBabe.hygro.hTERT/ pWZL.Blast. CMYC (Addgene) vectors using FuGene6 transfection reagent (Roche, Basel, Switzerland) at ratio of 3:1, reagent/DNA. The medium was replaced 16 hours after transfection, and cultures were incubated for a further 48 hours before retroviral supernatants were harvested and stored at −80°C. To infect recipient cells, 3 ml of supernatant and 4 μg/ml DEAE-dextran (Sigma) were added to NOSE/NOF cells at 30% to 50% confluence. Cells were split the following day, and positive cells were selected with 10 to 30 U/ml hygromycin B (Merck, Darmstadt, Germany)/2 to 3 μg/ml blasticidin (Sigma).

Immunofluorescent Cytochemistry and Immunohistochemistry

Immunofluorescent cytochemistry was performed using standard protocols. The following antibodies were used at 1:1000 dilutions: AE1/AE3 (Dako Corporation, Carpinteria, CA), cytokeratin 7 (CR-UK, London, UK), BerEp4 (Dako), CA-125 (Dako), E-cadherin (Cell Signaling, Danvers, MA), and fibroblast surface protein (FSP; Sigma). Alexa Fluor 488–coupled secondary antimouse or antigoat antibodies (Invitrogen) were used for antigen detection. Cells were counterstained with Evans Blue (Sigma) diluted in H_2O. Immunohistochemistry of three-dimensional cultures was performed using standard protocols at the UCL Advanced Diagnostics Laboratory. For analysis of MIB-1 and cytokeratin 18 (Ck18) dual staining, the proportion of MIB-1^+/$Ck18^+$ cells were calculated relative to the total $Ck18^+$ population of the culture, using the following formula: relative % dual positive cells = (number of MIB-1^+/$Ck18^+$ cells)/(total number of $Ck18^+$ cells)] × 100%.

Telomere Length and Telomerase Activity Assays, In Vitro *Analysis of Tranduced Clones*

To detect telomere length and telomerase activity, the Telo*TAGGG* Telomere Length Assay and Telomerase PCR ELISA^{PLUS} from Roche were used according to the manufacturer's protocols. For calculation of relative telomerase activity, an *hTERT*-immortalized fibroblast cell line (1BR3) was included as a positive control. Population doubling rates were measured for 1×10^5 cells, in triplicate. Cultures were passaged, and population doublings (PD) were calculated using the following formula: PD = log (total cell number at each passage/initial cell number)/$\log_2$. Anchorage-independent growth assays were performed as previously described [17]. Anchorage-dependent growth was assayed by plating 100 cells in six replicates onto 100-mm plates. Cells were refed three times a week for 2 weeks and then fixed with methanol and stained with Coomassie blue (Sigma). Colonies containing more than 10 cells were counted, and colony formation efficiencies were calculated using the following formula: colony-forming efficiency (CFE) = [(number of colonies counted)/(number of cells plated)] × 100%.

Real-time Polymerase Chain Reaction

RNA extractions were performed using the QIAgen RNA extraction kit with on-column DNase treatment. Samples were quantified and reverse-transcribed using random hexamer primers, according to standard protocols. For real-time polymerase chain reaction (PCR), samples were run according to manufacturer's protocols: a FAM-labeled real-time probe for *CMYC* (HS00153349_m1; Applied Biosystems, Carlsbad, CA) was used with 18S rRNA probe as an internal control. Samples were analyzed on an ABI 7900HT Fast Real-time PCR System (Applied Biosystems) and analyzed using the $\Delta\Delta C_t$ relative quantification method.

Flow Cytometry

Cell cultures were trypsinized and centrifuged, and cell pellets were resuspended in FACS buffer, with or without an anti–Annexin-FITC–labeled antibody, according to the manufacturer's instructions (Roche).

Samples were run on a Becton Dickinson FACS Scan (Franklin Lakes, NJ), and the Annexin V–positive population was measured. For cell cycle analysis, cells were incubated with 1 mM 5-bromo-2-deoxyuridine (BrdU; Sigma) for 2 hours. Cells were then washed in PBS and fixed by dropwise addition of 70% ethanol with constant agitation. Samples were incubated at 4°C overnight before extraction of nuclei using standard pepsin digestion protocols. Pelleted nuclei were incubated with an anti-BrdU antibody (Becton Dickinson), washed twice with IFA (10 mM HEPES pH 7.4, 150 mM NaCl, 0.1% sodium azide [all Sigma]; 4% FBS [Lonza, Basel, Switzerland]) and then incubated with an Alexa Fluor 488–coupled secondary antibody (Invitrogen). Washed nuclei were resuspended 100 μg/ml propidium iodide (Sigma) in PBS and analyzed as above.

Heterotypic Assays (Invasion, Migration, and Three-dimensional Cell Culture)

Standard invasion and migration assays were modified to use presenescent and senescent ovarian fibroblasts as a chemoattractant. A total of 9×10^4 fibroblasts were plated in 24-well plates. The following day, the cells were washed twice with PBS, and then 500 μl of serum-free medium was added. Migration chambers (Greiner, Frickenhausen, Germany) or rehydrated invasion chambers (Millipore, Billerica, MA) were placed atop the fibroblast monolayers, and 3×10^4 (for migration assays) and 12.5×10^4 (for invasion assays) epithelial cells were plated within the chamber. Assays were incubated at 37°C/5% CO_2 for 24 hours before detection of invaded/migrated cells. For invasion assays, invaded cells were detached from the membrane and lysed, and a quantitative fluorimetric dye was added, using reagents from the 24-well Chemicon QCM ECMatrix fluorimetric Invasion Assay Kit (Millipore). Relative fluorescence units were read on a Varioskan Flash plate reader (Thermo Scientific, Waltham, MA), and average values of a negative control (no cells) were deduced from each test well. For migration assays, migrated cells were quantified as above, or membranes were stained *in situ* with 1% crystal violet (Sigma) in 100% methanol, washed twice with distilled water, and air-dried. The migrated cells were counted in 10 fields of view per membrane. In all experiments, 10% FBS as a chemoattractant was also plated as a positive control.

Cells were grown as three-dimensional multicellular spheroids on plastic dishes coated twice with a 1.5% solution of poly-2-hydroxyethyl methacrylate (polyHEMA) from Sigma, prepared in 95% ethanol (also Sigma). Fibroblasts were plated onto polyHEMA-coated plates and allowed to form spheroids for 7 days before the culture was inoculated with epithelial cells at a ratio of 4:1 fibroblasts-epithelial cells. Three-dimensional heterotypic cultures were maintained in basic medium for 2 weeks and fed twice weekly before multicellular aggregates were harvested, fixed in neutral-buffered formalin (VWR), processed into paraffin, and stained by standard immunohistochemical techniques (at the CR-UK Histology Service). For two-dimensional indirect coculture assays, epithelial cells were plated into 24-well plates, and fibroblasts were seeded into permeable tissue culture inserts (Greiner) at a ratio of 4:1 fibroblasts-epithelial cells. After 24 hours, the two cell types were cocultured and maintained for 14 days with twice-weekly refeeding. Epithelial cells were then fixed with methanol and stained with crystal violet (5 mg/ml in 2% ethanol), and cells lysed with 2% SDS/dH_2O. Absorbance was then read at 595 nm on a Varioskan Flash plate reader.

Statistical Analysis

Where indicated, 2-tailed paired Student's *t*-tests were performed.

Results

Normal Ovarian Fibroblasts Can Be Immortalized by the Ectopic Expression of hTERT

Primary NOFs have a limited proliferative capacity *in vitro*. To address this, we used ectopic overexpression of the catalytic subunit of human telomerase (*hTERT*) to extend the life span of primary NOF cells beyond 100 days without signs of replicative senescence (Figure 1*A*). *hTERT* infected NOFs expressed telomerase, whereas primary NOFs showed no telomerase activity, suggesting that NOFs had been immortalized (INOFs; Figure 1*B*). Neither NOFs nor INOFs showed any evidence of tumorigenic transformation, evaluated by anchorage-independent growth. INOFs maintain expression of vimentin and FSP and did not express the epithelial cell marker Ck7 (Figure 1*C*). There was no expression of smooth muscle actin (SMA) in primary NOFs, but SMA expression in INOFs indicated an activated phenotype, which is consistent with other studies that show fibroblasts from other organs become activated after *hTERT* immortalization (Figure 1*C*) [19,20]. INOFs also maintained p16 expression, suggesting that loss of this cell cycle checkpoint is not required for immortalization. Similar observations have been reported after immortalization of human mammary epithelial cells, embryonic lung fibroblasts, and ovarian surface epithelial (OSE) cells [21–25]. As part of this study, we also *hTERT*-immortalized OSE (IOSE) cells derived from three different, normal, primary OSE cultures (IOSE4, IOSE11, and IOSE19) using previously described methods [17,24]. We confirmed that the primary OSE and IOSE cells used in this study exhibit both epithelial and nonneoplastic characteristics (Figure W1).

CMYC *Overexpression Induces Neoplastic Transformation of IOSE Cells*

A complementary DNA encoding full-length *CMYC* was introduced into IOSE cells by retroviral transduction to induce the early stages of neoplastic transformation. *CMYC* messenger RNA expression levels were increased 80 to 500-fold in CMYC-infected IOSE cell lines ($IOSE4^{CMYC}$, $IOSE11^{CMYC}$, and $IOSE19^{CMYC}$). $IOSE^{CMYC}$ cells displayed altered cell morphology with cell size decreased, cell shape more cuboidal, and cells more classically epithelial than IOSE cells. $IOSE^{CMYC}$ cells were tightly packed into a monolayer in traditional two-dimensional cultures and lost the mesenchymal scattering phenotype that is characteristic of IOSE cells (Figure 2*A*). $IOSE^{CMYC}$ cells also showed increased CFEs in anchorage-dependent and anchorage-independent growth assays ($P \le .01$; Figure 2, *B* and *C*). *CMYC* messenger RNA levels correlated with anchorage-independent CFE (Pearson's coefficient test, $r^2 = 0.8$, $P = .0156$, $\alpha = 0.05$). Flow cytometry showed significant reductions in the percentage of apoptotic cells in $IOSE^{CMYC}$ cell lines compared with the IOSE cell lines ($P \le .05$; Figure 2*D*). A significantly greater proportion of $IOSE^{CMYC}$ cells was in G_2 phase of the cell cycle ($P \le .05$; Figure 2*E*). These characteristics are all consistent with the suggestion that $IOSE^{CMYC}$ cells had undergone neoplastic transformation, although neither IOSE nor $IOSE^{CMYC}$ cells expressed the ovarian cancer markers E-cadherin and CA-125, suggesting that $IOSE^{CMYC}$ cells were only partially transformed.

Senescent Fibroblasts Enhance the Neoplastic Phenotype of $IOSE^{CMYC}$ Cells

We induced senescence in INOF cells by exposing the cells to low dose levels of hydrogen peroxide (H_2O_2). H_2O_2 exposure reduced proliferation of INOFs by approximately 30% and induced senescence,

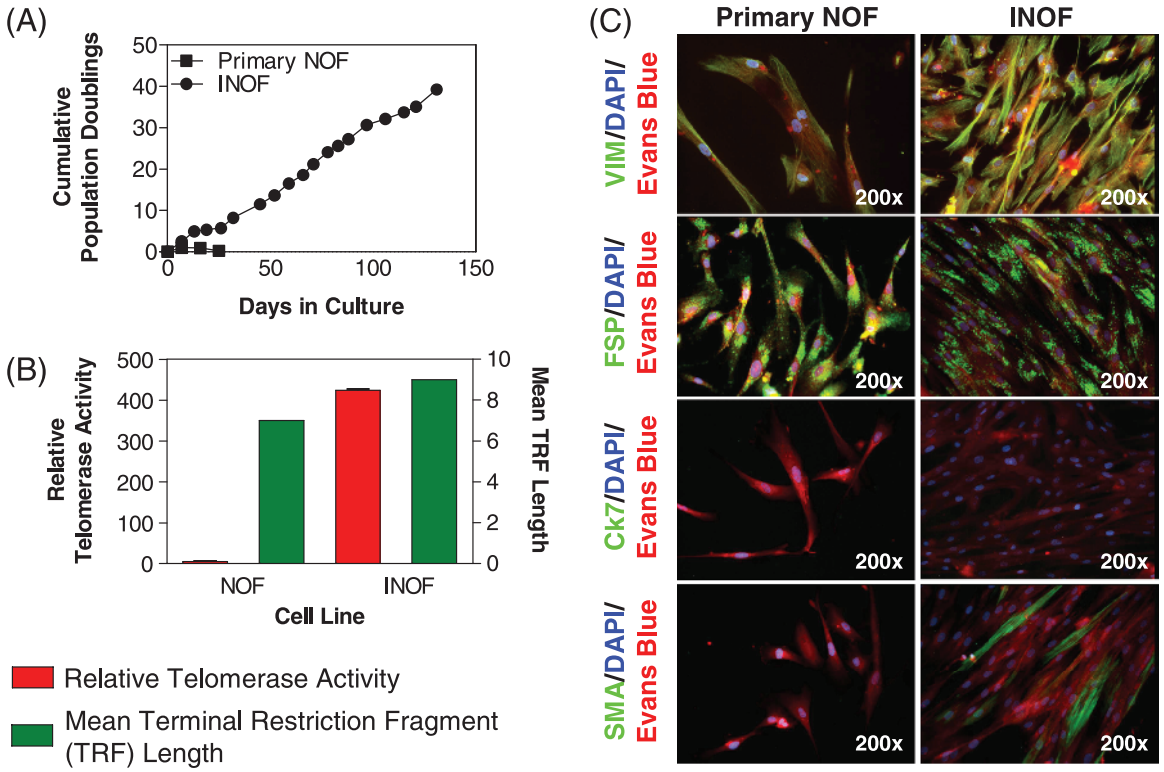

Figure 1. Extended life span of primary NOFs after *hTERT* immortalization. (A) Ectopic expression of *hTERT* increases the number of PDs of NOFs to more than 30 PDs in INOFs. (B) Telomerase activity (relative to an internal positive control) is negligible in cell extracts from primary NOFs but elevated in INOF cultures, and telomere terminal restriction fragment lengths are increased by approximately 2 kb after introduction of *hTERT*. (C) NOFs and INOFs both exhibit "spotty" positive staining with an anti-FSP antibody, which is characteristic of fibroblasts. Both cell lines stain negative for Ck7. SMA is expressed in approximately 30% of INOF cells indicating a transition toward an activated fibroblast phenotype with immortalization. Primary NOF cells did not express SMA, and this was independent of cell density. Both NOF and INOF cells express p16 in the nucleus and cytoplasm (arrows). 4′,6-Diamidino-2-phenylindole (blue) stains cell nuclei, Evan's blue (red) stains the cell cytoplasm, and green fluorescence denotes positive staining. Note the spindled morphology of fibroblast cells. Exposure times for immunofluorescent images were constant for each antigen. Error bars, SEM.

as shown by β-galactosidase expression (Figure 3*A*). We compared the effects of H_2O_2-treated senescent fibroblasts (SEN) and untreated presenescent fibroblasts (PSNs) on the invasive and migratory phenotypes of IOSE and IOSE^{CMYC} cells. There was a 5.7- to 7.2-fold reduction in transwell migration for all three IOSE^{CMYC} cell lines cocultured with PSN fibroblasts relative to a serum control ($P \leq .01$). In contrast, migration levels increased 3.8- to 14.9-fold compared with serum controls when IOSE^{CMYC} cells were cocultured with SEN fibroblasts (Figure 3*B*). SEN fibroblasts also increased the invasive ability of IOSE^{CMYC} cells compared with PSN fibroblasts ($P \leq .05$; Figure 3*C*). Neither PSN nor SEN fibroblasts had any significant effects on the invasive or migratory properties of IOSE cells. Finally, when we used conditioned medium (CM) from cultured SEN fibroblasts in anchorage-independent growth assays, we found that it increased the tumorigenic phenotype of IOSE19^{CMYC} cells relative to the same cells grown in CM from PSN fibroblasts ($P \leq .05$). Colony formation efficiencies of IOSE^{CMYC} cells grown in PSN-CM or SEN-CM were significantly reduced relative to cells grown in standard growth medium (NOSE-CM, $P \leq .05$; Figure 3*D*).

Senescent Fibroblasts Enhance Epithelial Proliferation in Three-dimensional Heterotypic Culture Models

Three-dimensional spheroid models of INOFs were generated by culturing cells on polyHEMA-coated tissue culture plastics. INOFs formed spontaneous aggregates within 48 hours of culture in nonadherent conditions. Examination of formalin-fixed, paraffin-embedded sections of 7-day-old INOF spheroids, stained with hematoxylin and eosin (H&E), revealed that the central regions of spheroids contain predominantly acellular hyalinized nodules with apoptotic cells distributed throughout a matrix-rich core. Peripherally, spindled cells with elongated nuclei and an eosinophilic cytoplasm surround the spheroid. PSN and SEN fibroblast spheroids were indistinguishable by H&E staining.

Seven-day-old INOF spheroid cultures were inoculated with IOSE cells (INOF/IOSE cells ratio of 4:1) to establish three-dimensional fibroblast-epithelial cell models. H&E examination of stained sections of these heterotypic three-dimensional cultures showed central hyalinized cores of abundant matrix protein (Figure 4, *A* and *B*). Spheroids consisted of two morphologically distinct populations of cells, with either spindled or plump cell morphologies. When IOSE cells were cultured with SEN fibroblasts, we observed nuclear atypia within populations of plump, peripheral cells and features such as irregular/enlarged nuclei, prominent nucleoli and "giant" mononuclear cells within peripheral regions of the spheroids (Figure 4*A*). These atypical features were not present in spheroids generated from IOSE cells cultured with PSN fibroblasts. There were also more prominent nucleoli and mitoses in the plump cell populations from SEN-IOSE^{CMYC} cocultures compared with PSN-IOSE^{CMYC} cocultures (Figure 4*B*). Finally, when IOSE^{CMYC} cells were cocultured with PSN fibroblasts, we saw marked apoptosis

in the central regions of spheroids, which was not present in SEN-IOSE^{CMYC} cocultures (data not shown).

IOSE/INOF spheroids were compared with normal ovarian tissues after staining for several epithelial and fibroblast markers. Only cytokeratin 18 (Ck18) reliably distinguished between ovarian fibroblasts and epithelial cells. The fibroblastic markers vimentin, desmin, and proline-4-hydroylase did not accurately discriminate between epithelial cells and fibroblasts in normal ovarian tissue samples and spheroid cultures (data not shown). In IOSE/INOF spheroids, epithelial cells could be identified by Ck18 staining; IOSE cells formed a single cell layer surrounding the fibroblast "core," reminiscent of the OSE monolayer *in vivo* (Figure 4*C*). However, in INOF-IOSE^{CMYC} cocultures, IOSE^{CMYC} cells formed multiple cell layers surrounding the fibroblast core, with some Ck18^{+} cells invading into the central regions of the spheroid (Figure 4, *E* and *F*). Dual immunohistochemical staining for Ck18 and the proliferation marker MIB-1 highlighted the actively proliferating epithelial proportion of culture (Figure 4, *C*–*F*). In three-dimensional cocultures, IOSE^{CMYC} cells were 0.03- to 12.8-fold more proliferative than IOSE cells. In SEN-IOSE^{CMYC} spheroids, there was a 1.4- to 4.7-fold increase in the relative percentage of IOSE^{CMYC} cell staining positive for both Ck18 and MIB-1 relative to PSN-IOSE^{CMYC} cocultures (Figure 4*G*). SEN/PSN fibroblasts did not significantly affect the proliferation of epithelial cells in two-dimensional cocultures (Figure 4*H*).

Discussion

The two most well-described risk factors for EOCs are the protective effects conferred by pregnancy and oral contraceptive use [3,4]. It has been postulated that both act by reducing the number of ovulations throughout a woman's lifetime, thus limiting the extent of rupture and repair of the OSE [26]. However, ovarian cancer usually occurs several years after menopause, and the natural history of high-grade serous tumors (the most common histopathologic subtype) suggests rapid and aggressive tumor growth. The microenvironmental trigger for this is unlikely to be hormonal factors, given that postmenopausal ovaries no longer produce mitogenic steroid hormones (neither estrogens nor androgens) [27]. Postmenopausal ovaries often show age-related histopathologic changes, such as increased numbers of inclusion cysts and deep invaginations of OSE into ovarian stroma, and it has been hypothesized that these may be associated with neoplastic transformation [28]. We hypothesized that loss of presenescent stromal fibroblasts and/or an accumulation of metabolically active but senescent fibroblasts

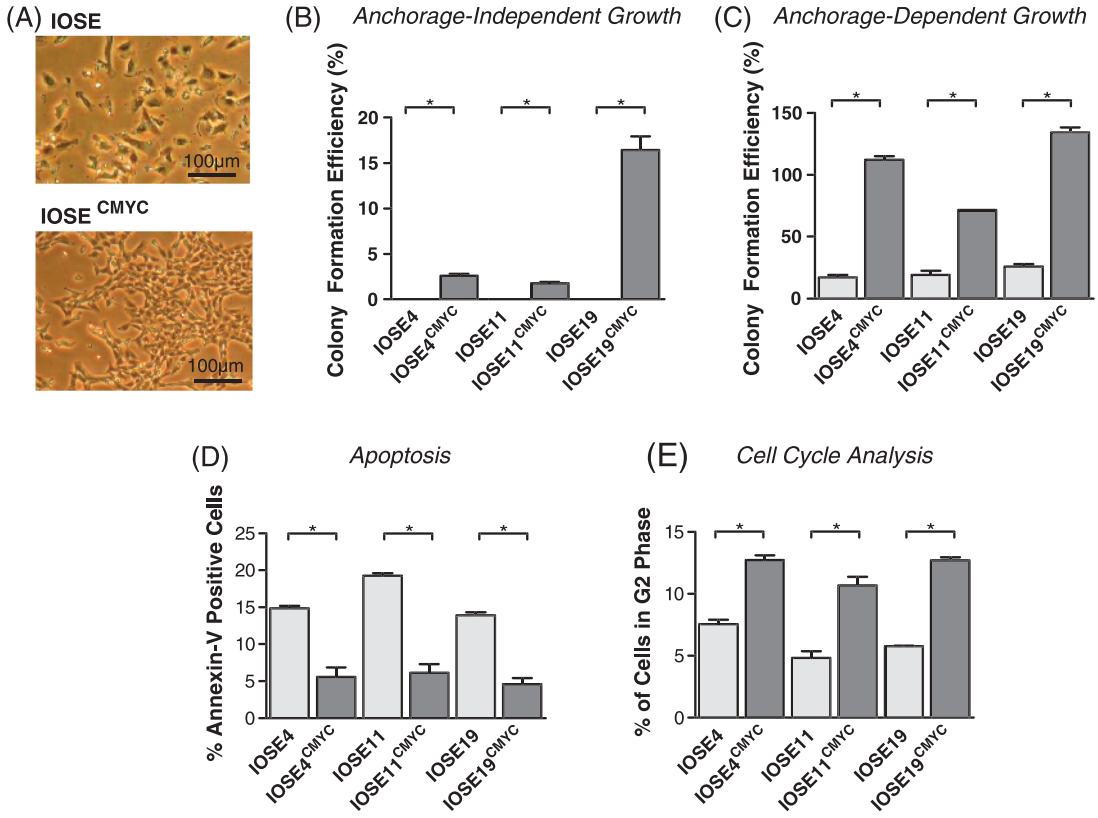

Figure 2. Immortalized OSE (IOSE) cell cultures overexpressing *CMYC* (IOSE^{CMYC} cells) show features of neoplastic transformation. (A) The fibroblast-like elongated morphology of IOSE cultures changes to a more typically epithelial (cuboidal) morphology on *CMYC* overexpression. Commitment to an epithelial phenotype is a hallmark of EOC cells. OSE cells *in vitro* and *in vivo* are able to switch among epithelial, mesenchymal, and mesothelial phenotypes. (B) Overexpression of *CMYC* increases colony formation efficiency in both anchorage-independent growth assays and in anchorage-dependent colony formation assays (C). (D) Staining with an anti–annexin V antibody followed by flow cytometry analysis reveals significantly fewer apoptotic cells in IOSE^{CMYC} cultures compared with parental cell lines. (E) Cells were incubated with BrdU, and nuclei were stained with anti-BrdU. In *CMYC*-overexpressing cultures, there were significantly larger proportions of cells in the G_2 phase of the cell cycle compared with IOSE counterparts. In panels B to E, the differences for each phenotypic assay between IOSE and IOSE^{CMYC} cells were statistically significant ($P \leq .05$). Error bars, SEM.

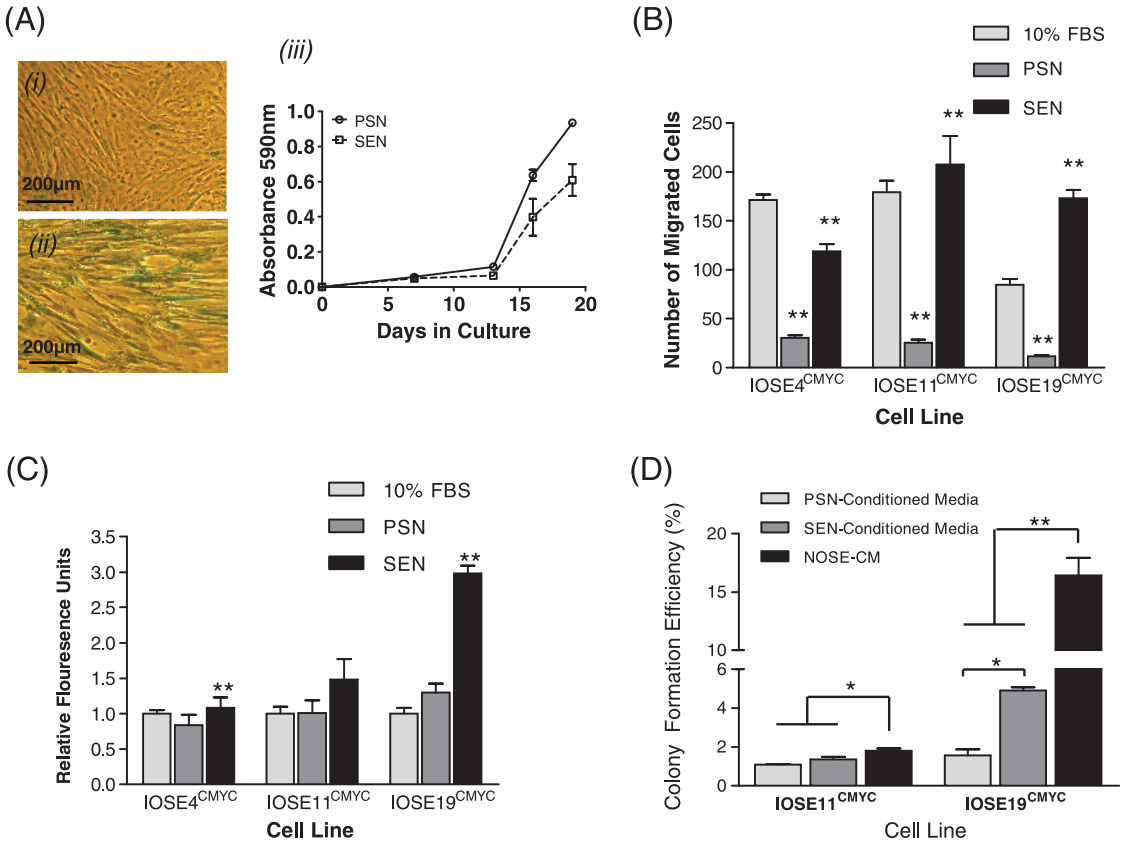

Figure 3. Effects of PSN and SEN fibroblasts on the phenotype of IOSE^{CMYC} cells. (A) Exposing INOFs to hydrogen peroxide (H_2O_2) induces a senescence response that is biologically similar to replicative senescence observed in aging organisms. β-Galactosidase bioactivity confirms senescence induction in INOFs: (*i*) 60% to 80% of SEN stain blue, (*ii*) untreated PSN fibroblasts do not stain, and (*iii*) crystal violet growth assay (absorbance at 595 nm is relative to cell number) show that PSN fibroblasts are more proliferative than SEN fibroblasts. (B) In a migration assay, PSN fibroblasts inhibited motility of IOSE^{CMYC} clones relative to 10% FBS. SEN fibroblasts significantly enhanced migration of all *CMYC* clones relative to a PSN fibroblast chemoattractant. (C) SEN fibroblasts enhanced invasive ability of IOSE^{CMYC} clones relative to PSN fibroblast cells. (D) IOSE19^{CMYC} cells proliferate significantly more in an anchorage-independent growth assay when incubated with conditioned medium from SEN fibroblasts relative to PSN fibroblast conditioned medium. In both SEN/PSN–conditioned media, colony formation efficiency of IOSE^{CMYC} cell lines was reduced relative to standard growth medium (NOSE-CM) (*$P \leq .05$,**$P \leq .01$ by Student's paired *t*-test). Error bars, SEM.

within the ovary create a microenvironment that can trigger neoplastic transformation of dormant, partially transformed ovarian epithelial cells, and that this is a possible explanation for the late-stage development of ovarian cancers from an otherwise inactive organ. In support of this hypothesis, we show for the first time that cellular changes in ovarian stromal fibroblasts can promote neoplastic transformation of OSE cells. This paracrine trigger acts in synergy with early genetic events in partially transformed OSE cells but has little or no effect on untransformed OSE cells.

We modeled the earliest stages of OSE transformation by overexpressing the *CMYC* oncogene in *hTERT*-immortalized OSE cells (IOSE^{CMYC}) because both *hTERT* and *CMYC* are commonly overexpressed in EOCs [29,30]. IOSE^{CMYC} cell lines show evidence of anchorage-independent growth but not invasion, confirming that they are only partially transformed. We observed some variability in the response of different cell lines to *CMYC* overexpression, although the phenotypic trends were the same for all three cell lines; this variation may be the result of subtle differences in the underlying genetic background of the individuals from which the different cell lines were established, influencing the phenotype. When we tested the effects of coculturing IOSE and IOSE^{CMYC} cells with PSN and SEN fibroblasts, we found that SEN fibroblasts had a significant effect on increasing neoplastic transformation of IOSE^{CMYC} cells compared with PSN fibroblasts; neither PSN nor SEN fibroblasts appeared to transform IOSE cells. In anchorage-independent growth assays, we also found that conditioned medium taken from cultured SEN fibroblasts had the ability to promote the neoplastic phenotype of IOSE^{CMYC} cells relative to the conditioned medium harvested from PSN fibroblasts. Taken together, these data suggest that the regulation of neoplastic epithelial cells by PSN/SEN fibroblasts is mediated, at least in part, by soluble, secreted factors.

Key to performing these studies was our ability to generate and characterize an immortalized NOF (INOF) cell line. To our knowledge, this represents the first report detailing the generation of such a line. We were able to confirm the normal, nontransformed, and fibroblastic nature of this cell line, suggesting that it is a relevant model of NOFs. Senescent fibroblasts were also created from the same INOF cell line after exposure to hydrogen peroxide, and so it is unlikely that any of the experimental differences we see between SEN and PSN fibroblasts are the result of differences in the genetic background of cells taken from different individuals.

Inducing senescence-like growth arrest after exposure to hydrogen peroxide has been described previously, and senescent cells have subsequently been shown to exhibit many of the features that are in common with replicative senescence (e.g., β-galactosidase expression, G_1 arrest, enlarged morphology, transcriptomic changes) [12,23,31]. Other mechanisms of inducing cellular senescence can be considered including exposure to bleomycin sulfate, but there is no evidence in the literature to suggest that bleomycin offers an advantage over hydrogen peroxide [12]. The limited life span of primary ovarian fibroblasts meant that their immortalization using *hTERT* was a necessary step, but immortalized cells bypass replicative senescence, hence the need to perform chemically induced senescence. This study therefore has its limitations because it is unclear how closely stress-induced premature senescence *in vitro*, such as that induced by hydrogen peroxide, reflects age-related senescence *in vivo*.

We were able to examine the morphological and biological characteristics of epithelial-fibroblast interactions and to confirm the neoplastic-promoting effects of senescent fibroblasts after creating a three-dimensional heterotypic model of the ovary. This is the first time that a heterotypic three-dimensional model of the normal ovary has been described. In three-dimensional cultures, senescent fibroblasts enhanced proliferation and nuclear atypia in IOSE^{CMYC} cells relative to presenescent and, to a lesser extent, the proliferation of IOSE cell lines.

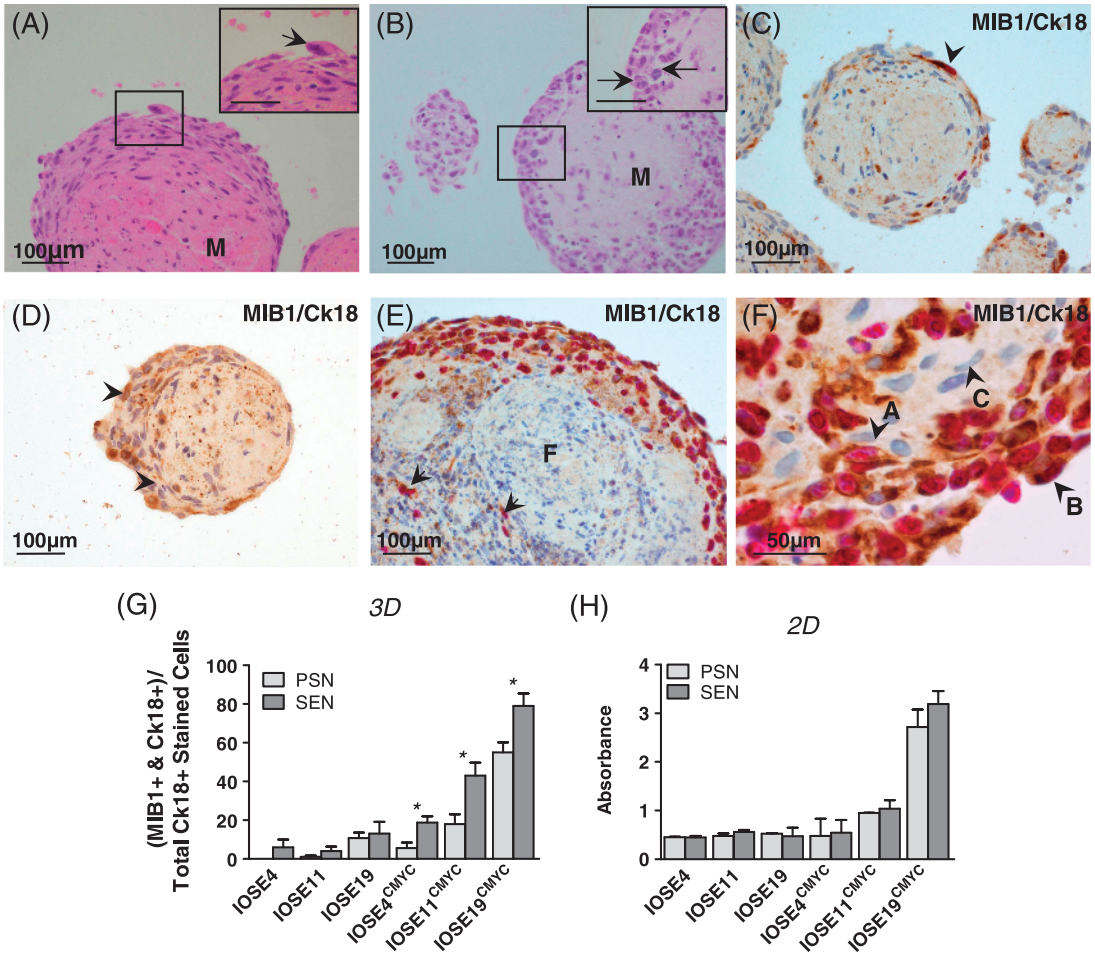

Figure 4. Three-dimensional (3D) *in vitro* modeling of stromal-epithelial interactions. (A) In SEN-IOSE three-dimensional cocultures, "giant" cells (arrow) were observed within peripheral regions of the spheroids. Spheroids contained abundant matrix protein "**M**." (B) In SEN-IOSE^{CMYC} three-dimensional coculture, there was a large peripheral region of plump cells containing some mitotic figures (arrows). (C–F) INOF-IOSE cocultures dual stained for MIB-1 (pink nuclear stain, proliferation marker) and Ck18 (brown cytoplasmic stain). Unstained cells are counterstained with hematoxylin (blue). (C) In SEN-IOSE cocultures, cytokeratin-positive cells are located in the peripheral region of the spheroid (arrowhead). A Ck18$^+$/MIB-1$^+$ dual-positive cell (arrow) is visible in the largest spheroid. (D) In PSN-IOSE cocultures, nonspecific staining of matrix protein can be distinguished by the absence of cellular structure. (E) SEN-IOSE^{CMYC} three-dimensional coculture viewed at low magnification shows the central Ck18-negative staining fibroblastic population "**F**" and peripherally located Ck18-positive stained cells within the spheroid. Some peripheral Ck18-positive stained cells, dual stained for MIB-1 (pink nuclei), can also be seen. (F) In SEN-IOSE^{CMYC} three-dimensional cocultures negative Ck18 stain fibroblasts "**C**" closely interact with the population of Ck18-positive staining epithelial cells "**A**" and "**B**." Note the spindled morphology and elongated nucleus of Ck18-negative cells (e.g., cell **C**) compared with the plump morphology and rounded nuclei of Ck18-positive cells. Cell **A** is positive for Ck18 and negative for MIB-1; cell **B** is positive for both Ck18 and MIB-1. (G) Analysis of dual-stained Ck18/MIB-1–positive cells reveals enhanced proliferation in IOSE^{CMYC} cells when cocultured three-dimensionally with SEN fibroblasts compared with PSN fibroblasts (*$P \leq .05$, Student's paired *t*-test). The proportion of MIB-1 cells is calculated as a ratio of the total Ck18$^+$ population of the culture. (H) Two-dimensional (2D) indirect coculture; crystal violet staining. Epithelial cells do not show significant differences in rates of proliferation when cocultured with SEN or PSN fibroblasts.

This suggests that even the earliest neoplastic changes in normal ovarian epithelia may render cells susceptible to a tumor-promoting trigger from the microenvironment. Our data also suggest that the synergistic relationship between senescent fibroblasts and epithelial cells may continue as tumorigenesis progresses. This is consistent with studies by Yang et al. [32] who have shown that inducing senescence in fibroblasts increases the *in vivo* tumorigenicity of coinjected OSE cells expressing SV40 large-T antigen.

If the results of these studies are real, and the accumulation of metabolically active senescent fibroblasts does act as the microenvironmental trigger for ovarian cancer development, then it raises the question, "what are the secretary factors responsible for epithelial cell transformation?" Some candidates have been identified from previous studies, including osteopontin, stromal cell–derived factor (SDF-1), vascular endothelial growth factor, amphiregulin, hepatocyte growth factor, and interleukin-6, all of which have been shown to act as mediators of the differential paracrine effects of presenescent and senescent fibroblasts [9,11–13,15]. The tumor-promoting effects of the conditioned medium from SEN-IOSE^{CMYC} cocultures compared with the medium from PSN-IOSE^{CMYC} cocultures suggest a possible biological comparison that could be used to identify such factors in the future.

In conclusion, we have used an *in vitro* model of early-stage neoplastic transformation of normal ovarian epithelial cells to test the hypothesis that the accumulation of senescent fibroblasts in aging ovaries can act as a trigger to the rapid development of ovarian cancers—this is consistent with many well-established epidemiological risk factors for ovarian cancer. These effects may be due to the loss of an inhibitory factor, secreted by normal fibroblasts, which inhibits carcinogenesis of epithelial cells harboring mutation(s). Thus, loss of this inhibitory signal on fibroblast senescence may create a microenvironment that is permissive for tumor development. Alternatively, senescent fibroblasts may produce factors that promote transformation of neoplastically transformed epithelia. Support for this hypothesis has come from the analysis of human ovarian tumors, which have been shown to contain a large number of senescent fibroblasts within the tumor stroma; this may also suggest a role for senescent fibroblasts in the maintenance of ovarian tumors [32]. However, testing such a hypothesis *in vivo* in normal ovaries is challenging. There are no reports of the rates of cellular senescence in human ovaries and to study this would probably require mass sectioning and analysis of large numbers of normal ovaries to identify senescent cells. This may be possible using a β-galactosidase bioactivity assay, which enables sensitive detection of senescent cells in frozen tissue specimens. Another way to address the hypothesis, and a focus of future studies, is to evaluate the tumorigenic phenotype of three-dimensional heterotypic models of senescent and presenescent fibroblasts with partially transformed normal ovarian epithelial cells after implantation into immunosuppressed mice.

Acknowledgments

The authors thank the staff at UCLH, the patients who kindly consent to partake in our studies, and John F. Timms for critical review of the manuscript.

References

[1] Yancik R (1993). Ovarian cancer. Age contrasts in incidence, histology, disease stage at diagnosis, and mortality. *Cancer* **71**(2 suppl), 517–523.

[2] Smith ER and Xu XX (2008). Ovarian ageing, follicle depletion, and cancer: a hypothesis for the aetiology of epithelial ovarian cancer involving follicle depletion. *Lancet Oncol* **9**(11), 1108–1111.

[3] Purdie DM, Bain CJ, Siskind V, Webb PM, and Green AC (2003). Ovulation and risk of epithelial ovarian cancer. *Int J Cancer* **104**(2), 228–232.

[4] Pike MC, Pearce CL, Peters R, Cozen W, Wan P, and Wu AH (2004). Hormonal factors and the risk of invasive ovarian cancer: a population-based case-control study. *Fertil Steril* **82**(1), 186–195.

[5] Herbig U, Ferreira M, Condel L, Carey D, and Sedivy JM (2006). Cellular senescence in aging primates. *Science* **311**(5765), 1257.

[6] Jeyapalan JC, Ferreira M, Sedivy JM, and Herbig U (2007). Accumulation of senescent cells in mitotic tissue of aging primates. *Mech Ageing Dev* **128**(1), 36–44.

[7] Olumi AF, Grossfeld GD, Hayward SW, Carroll PR, Tlsty TD, and Cunha GR (1999). Carcinoma-associated fibroblasts direct tumor progression of initiated human prostatic epithelium. *Cancer Res* **59**(19), 5002–5011.

[8] Parrinello S, Coppe JP, Krtolica A, and Campisi J (2005). Stromal-epithelial interactions in aging and cancer: senescent fibroblasts alter epithelial cell differentiation. *J Cell Sci* **118**(Pt 3), 485–496.

[9] Studebaker AW, Storci G, Werbeck JL, Sansone P, Sasser AK, Tavolari S, Huang T, Chan MW, Marini FC, Rosol TJ, et al. (2008). Fibroblasts isolated from common sites of breast cancer metastasis enhance cancer cell growth rates and invasiveness in an interleukin-6–dependent manner. *Cancer Res* **68**(21), 9087–9095.

[10] Krtolica A, Parrinello S, Lockett S, Desprez PY, and Campisi J (2001). Senescent fibroblasts promote epithelial cell growth and tumorigenesis: a link between cancer and aging. *Proc Natl Acad Sci USA* **98**(21), 12072–12077.

[11] Begley L, Monteleon C, Shah RB, Macdonald JW, and Macoska JA (2005). CXCL12 overexpression and secretion by aging fibroblasts enhance human prostate epithelial proliferation *in vitro*. *Aging Cell* **4**(6), 291–298.

[12] Bavik C, Coleman I, Dean JP, Knudsen B, Plymate S, and Nelson PS (2006). The gene expression program of prostate fibroblast senescence modulates neoplastic epithelial cell proliferation through paracrine mechanisms. *Cancer Res* **66**(2), 794–802.

[13] Pazolli E, Luo X, Brehm S, Carbery K, Chung JJ, Prior JL, Doherty J, Demehri S, Salavaggione L, Piwnica-Worms D, et al. (2009). Senescent stromal-derived osteopontin promotes preneoplastic cell growth. *Cancer Res* **69**(3), 1230–1239.

[14] Coppé JP, Patil CK, Rodier F, Sun Y, Muñoz DP, Goldstein J, Nelson PS, Desprez PY, and Campisi J (2008). Senescence-associated secretory phenotypes reveal cell-nonautonomous functions of oncogenic RAS and the p53 tumor suppressor. *PLoS Biol* **6**(12), 2853–2868.

[15] Coppé JP, Kauser K, Campisi J, and Beauséjour CM (2006). Secretion of vascular endothelial growth factor by primary human fibroblasts at senescence. *J Biol Chem* **281**(40), 29568–29574.

[16] Liu D and Hornsby PJ (2007). Senescent human fibroblasts increase the early growth of xenograft tumors via matrix metalloproteinase secretion. *Cancer Res* **67**(7), 3117–3126.

[17] Lawrenson K, Benjamin E, Turmaine M, Jacobs IJ, Gayther SA, and Dafou D (2009). *In vitro* three-dimensional modelling of human ovarian surface epithelial cells. *Cell Prolif* **42**(3), 385–393.

[18] Dimri GP, Lee X, Basile G, Acosta M, Scott G, Roskelley C, Medrano EE, Linskens M, Rubelj I, Pereira-Smith O, et al. (1995). A biomarker that identifies senescent human cells in culture and in aging skin *in vivo*. *Proc Natl Acad Sci USA* **92**(20), 9363–9367.

[19] Iyer VR, Eisen MB, Ross DT, Schuler G, Moore T, Lee JC, Trent JM, Staudt LM, Hudson J Jr, Boguski MS, et al. (1999). The transcriptional program in the response of human fibroblasts to serum. *Science* **283**, 83–87.

[20] Chang HY, Sneddon JB, Alizadeh AA, Sood R, West RB, Montgomery K, Chi JT, van de Rijn M, Botstein D, and Brown PO (2004). Gene expression signature of fibroblast serum response predicts human cancer progression: similarities between tumors and wounds. *PLoS Biol* **2**(2), e7.

[21] Herbert BS, Wright WE, and Shay JW (2002). p16(INK4a) inactivation is not required to immortalize human mammary epithelial cells. *Oncogene* **21**(51), 7897–7900.

[22] Darbro BW, Lee KM, Nguyen NK, Domann FE, and Klingelhutz AJ (2006). Methylation of the p16(INK4a) promoter region in telomerase immortalized human keratinocytes co-cultured with feeder cells. *Oncogene* **25**(56), 7421–7433.

[23] Milyavsky M, Shats I, Erez N, Tang X, Senderovich S, Meerson A, Tabach Y, Goldfinger N, Ginsberg D, Harris CC, et al. (2003). Prolonged culture of

telomerase-immortalized human fibroblasts leads to a premalignant phenotype. *Cancer Res* **63**(21), 7147–7157.

[24] Li NF, Broad S, Lu YJ, Yang JS, Watson R, Hagemann T, Wilbanks G, Jacobs I, Balkwill F, Dafou D, et al. (2007). Human ovarian surface epithelial cells immortalized with hTERT maintain functional pRb and p53 expression. *Cell Prolif* **40**(5), 780–794.

[25] Shao G, Balajee AS, Hei TK, and Zhao Y (2008). $p16^{INK4a}$ downregulation is involved in immortalization of primary human prostate epithelial cells induced by telomerase. *Mol Carcinog* **47**(10), 775–783.

[26] Fathalla MF (1971). Incessant ovulation—a factor in ovarian neoplasia? *Lancet* **2**(7716), 163.

[27] Couzinet B, Meduri G, Lecce MG, Young J, Brailly S, Loosfelt H, Milgrom E, and Schaison G (2001). The postmenopausal ovary is not a major androgen-producing gland. *J Clin Endocrinol Metab* **86**(10), 5060–5066.

[28] Cai KQ, Klein-Szanto A, Karthik D, Edelson M, Daly MB, Ozols RF, Lynch HT, Godwin AK, and Xu XX (2006). Age-dependent morphological alterations of human ovaries from populations with and without *BRCA* mutations. *Gynecol Oncol* **103**(2), 719–728.

[29] Brustmann H (2005). Immunohistochemical detection of human telomerase reverse transcriptase (*hTERT*) and c-kit in serous ovarian carcinoma: a clinicopathologic study. *Gynecol Oncol* **98**(3), 396–402.

[30] Dimova I, Raitcheva S, Dimitrov R, Doganov N, and Toncheva D (2006). Correlations between c-*myc* gene copy-number and clinicopathological parameters of ovarian tumours. *Eur J Cancer* **42**(5), 674–679.

[31] Bladier C, Wolvetang EJ, Hutchinson P, de Haan JB, and Kola I (1997). Response of a primary human fibroblast cell line to H_2O_2: senescence-like growth arrest or apoptosis? *Cell Growth Differ* **8**(5), 589–598.

[32] Yang G, Rosen DG, Zhang Z, Bast RC Jr, Mills GB, Colacino JA, Mercado-Uribe I, and Liu J (2006). The chemokine growth–regulated oncogene 1 (*Gro-1*) links RAS signaling to the senescence of stromal fibroblasts and ovarian tumorigenesis. *Proc Natl Acad Sci USA* **103**(44), 16472–16477.

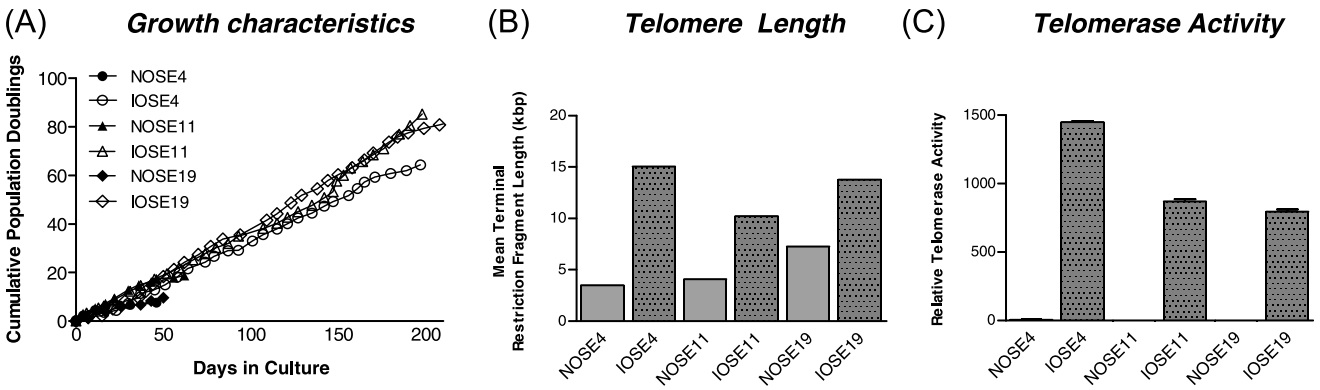

(D)

CELL LINE	ANTIBODY: Ck7	BerEP4	CA125	E-Cadherin	AE1/AE3	FSP	Calretinin
NOSE4	++	++	+/-	-	+	-	+
IOSE4	+++	+	+/-	-	++	-	+/-
NOSE11	+++	++	+	-	++	+/-	++
IOSE11	++	+	-	-	++	-	+
NOSE19	++	-	+	-	++	+/-	+
IOSE19	+++	+	-	-	+/-	-	+/-

+++ 70-100% cells stain positive
++ 40-70% cells stain positive
+ 10-40% cells stain positive
+/- Under 10% cells stain positive
- No cells stain positive

Figure W1. Immortalization of primary NOSE cells. The three IOSE cell lines have been maintained in culture for more than 200 days without signs of transformation: the cells do not grow in anchorage-independent growth assays and do not stain for CA-125 or E-cadherin, which is commonly expressed in ovarian epithelial tumors. (A) *In vitro* life span of primary NOSE cells is typically around 50 days. Immortalized OSE (IOSE) cells have been passaged for more than 200 days to date. Primary cells were immortalized by the ectopic expression of *hTERT*. (B) Telomere terminal restriction fragment length is increased in IOSE cell lines compared with parental NOSE cultures. (C) Telomerase activity, detected by PCR-ELISA, is absent in primary cultures but present in immortalized cell lines. (D) Staining for cytokeratin (Ck7), BerEP4, CA-125, E-cadherin, pan-cytokeratin (AE1/AE3), FSP, and calretinin by fluorescent immunocytochemistry reveals that primary NOSE and IOSE have similar staining profiles.